

UNIVERSITÀ DEGLI STUDI DI PADOVA

Dipartimento di Fisica e Astronomia “Galileo Galilei”

Master Degree in Physics

Final Dissertation

Diagrammatic Effective Field Theory Approach to Coalescing Binary Systems in General Relativity and Gravitational Waves Phenomenology

Thesis supervisor

Prof. Pierpaolo Mastrolia

Thesis co-supervisor

Prof. Nicola Bartolo

Dr. Angelo Ricciardone

Candidate

Matteo Pegorin

Academic Year 2022/2023

Abstract

In this thesis we study the dynamics of a gravitationally bound binary system composed of two spinless compact objects, which could be black holes or neutron stars, in the post-Newtonian (PN) approximation scheme of general relativity. The predictions obtained within this scheme have already been fundamental for the observation of gravitational waves by the LIGO-Virgo-KAGRA collaboration, yet an improvement of their accuracy will be of uttermost importance to match the precision of future gravitational wave observatories, such as Einstein Telescope, Cosmic Explorer and LISA.

Specifically in this work we employ an effective field theory approach to the gravitational dynamics, applying modern diagrammatic techniques to address the computation of the post-Newtonian corrections: these techniques have been first developed in the context of quantum field theory for the evaluation of elementary particles scattering amplitudes, yet recently they have been successfully applied also to the study of coalescing binary systems in general relativity.

Using these techniques we thoroughly derive the corrections to the Lagrangian of the binary system up to the 2.5PN order (v^5), i.e. at next-to-next-to-leading order in the conservative sector and at leading order in the dissipative sector. The former sector includes corrections to the binding energy of the binary system, whereas the latter encodes radiation-reaction effects. From these results then we analytically compute the observable gravitational wave.

To evaluate the conservative diagrams we have also developed a `Mathematica` code, which we apply as well to evaluate some selected conservative diagrams first contributing at 7PN order (v^{14}), so N^7 LO corrections to the Newtonian potential.

Finally, we perform a Fisher matrix forecast on the precision with which the future space-based LISA gravitational wave observatory will be able to constrain possible deviations from general relativity during the early inspiral phase of compact binary systems. In particular we introduce a parametric deformation of the post-Newtonian expression for the phase of the emitted gravitational waves, finding that it may be possible to constrain relative deviations from the post-Newtonian coefficients ranging from $\mathcal{O}(0.1)$ for the 2PN coefficients to $\mathcal{O}(0.001)$ for the leading order one.

Throughout this thesis we review many of the needed topics and explicitly evaluate most of the necessary results, with the aim of presenting an accessible and self-contained exposition, spanning from the derivation of the post-Newtonian corrections to their application in a phenomenological analysis. The approach presented in this thesis could possibly be extended to modified theories of gravity as well.

CONTENTS

Introduction	ix
Notation	xiii
1 General relativity and gravitational waves	1
1.1 General relativity	1
1.2 Gravitational waves in general relativity	3
1.2.1 Historical overview	3
1.2.2 Gravitational waves phenomenology	4
1.3 Linearized general relativity and gravitational waves	7
1.3.1 Linearized general relativity	7
1.3.2 Propagation of gravitational waves	10
1.3.3 Energy-momentum tensor of gravitational waves	12
1.3.4 Generation of gravitational waves	15
1.4 Compact binaries evolution and radiation in linearized theory	21
1.4.1 Gravitational radiation from non-relativistic point particles	21
1.4.2 Quadrupole radiation from a circular binary system	22
1.4.3 Evolution of self-gravitating binary systems	24
1.4.4 Regime of validity of the approximations employed	29
1.5 Gravitational waves detectors	30
1.5.1 Interaction of gravitational waves in linearized theory	33
1.6 Beyond the linearized theory	35
1.6.1 The post-Newtonian formalism	38
2 Effective theories and multi-loop techniques in quantum field theory	43
2.1 Quantum field theory and effective theories	43
2.1.1 Partition function and generating functionals in quantum field theory	43
2.1.2 Integrating out fields and effective action	44
2.1.3 Effective field theories	45
2.1.4 In-in formalism	47
2.2 Multi-loop techniques in quantum field theory	49
2.2.1 Dimensional regularization	49
2.2.2 Tensor decomposition	50
2.2.3 Scalar integrals algebraic manipulation	52
2.2.4 Reduction to Master Integrals	53
2.2.5 Master integrals evaluation	55
3 Effective field theory for the inspiral of a compact binary system	59
3.1 Scalar gravity toy model	60
3.1.1 Evaluation via the diagrammatic approach	61

3.2	Effective theory for a compact binary system	64
3.2.1	Key ideas and outline of the construction procedure of the effective theory	64
3.2.2	Worldline effective theory	67
3.2.3	Near zone potential effective theory	69
3.2.4	Far zone radiation effective theory	82
3.2.5	Physical observables in the EFT for a binary system	86
3.3	Newtonian potential in the effective theory for binary systems	91
4	Post-Newtonian conservative corrections	97
4.1	Evaluation procedure for the conservative sector	97
4.1.1	Relevant diagrams generation	97
4.1.2	Symmetry factor of a diagram	100
4.2	Einstein–Infeld–Hoffmann Lagrangian - 1 PN order	101
4.2.1	Corrections to the two-body potential at 1PN order	108
4.3	General procedure to evaluate a conservative diagram	109
4.3.1	Example of the evaluation procedure	111
4.3.2	Evaluation of the integrals in the spatial components of the momenta	115
4.4	Mathematica code for the automatic evaluation of conservative diagrams	121
4.5	Conservative contributions to the potential at 2PN order	123
4.5.1	Contribution of order 2PN to the conservative two-body Lagrangian	127
4.6	Subset of conservative contributions at 7PN	128
5	Dissipative radiation corrections	133
5.1	Power loss in the far zone effective theory	133
5.2	Far away gravitational field and gravitational waveform	139
6	Post-Newtonian corrections to observables	145
6.1	Post-Newtonian corrections to the binary dynamics	145
6.1.1	Quasi-circular orbit approximation and energy balance equation	146
6.1.2	Binding energy of the binary system	147
6.1.3	Power loss of the binary system	153
6.1.4	Power balance equation and time evolution of the orbital phase	154
6.2	Analytic expression of the gravitational waveform	156
6.2.1	Gravitational waveform in the time domain	156
6.2.2	Fourier transform of the gravitational waveform	158
7	Observational constraints from future GW observatories	161
7.1	Parametrizing deviations from the post-Newtonian predictions	161
7.1.1	Observation cut-off to limit the systematic error	163
7.1.2	Suitability of gravitational wave observatories to perform the test	165
7.2	The LISA observatory	167
7.2.1	Modeling of the LISA interferometer	167
7.2.2	Noise power spectral density	171
7.3	Fisher matrix for observational forecasts	172
7.4	Analysis and results	174
7.4.1	Details of the analysis	174
7.4.2	Results and discussion	175
	Conclusions	183
A	Derivation of the Feynman rules	189

A.1	Propagators of the gravitational fields	190
A.1.1	Non-relativistic expansion of the propagators	194
A.2	Near zone Feynman rules for the conservative sector	195
A.2.1	Worldline-gravitational fields interaction vertices	195
A.2.2	Gravitational potential fields self-interaction vertices	201
A.3	Far zone Feynman rules for the dissipative sector	207
A.3.1	Feynman rules for bulk vertices involving radiation vertex	207
A.3.2	Worldline-radiation vertex	209
B	Common mathematical functions	221
B.1	Gamma function $\Gamma(z)$	221
B.2	Beta function $B(a, b)$	222
C	Evaluation of recurring scalar integrals	223
C.1	Evaluation of the scalar integral $I_S(d, a, b)$	223
C.2	Evaluation of 1-loop and 2-loop scalar integrals $I_{S,1L}$	224
C.2.1	Evaluation of the 1-loop master integral $I_{S,1L}(d, a, b)$	224
C.2.2	Evaluation of the 2-loop master integral $I_{S,2La}$	225
C.2.3	Evaluation of the 2-loop master integral $I_{S,2Lb}$	226
C.3	Evaluation of the scalar Fourier integral $I_F(d, a)$	226
C.3.1	Tensorial generalization of the integral $I_F(d, a)$	230
C.3.2	Generalization $I_{F,sp}(d, a, b)$ of the integral $I_F(d, a)$ with scalar products	231
C.4	Evaluation of the $I_R(d, a, b)$ scalar integral	232
C.5	Example of scalar integral evaluation using multi-loop techniques	234
C.5.1	Reduction to master integrals using integration-by-parts identities	234
C.5.2	Master integral evaluation using the differential equations method	237
C.5.3	Fourier integrals evaluation using tensor decomposition	240
D	Extracts from the Mathematica code	241
	Bibliography	245

INTRODUCTION

Ever since Einstein formulated its theory of general relativity in 1915 there has been a steady interest in the study of the new phenomena predicted by this new theory, the most renowned of them being gravitational waves. Gravitational waves are perturbations of the spacetime which can propagate indefinitely: this novel prediction, at first almost controversial, spurred a lot of interest, both as a way to either confirm or refute the theory of general relativity, and on its own, since gravitational waves represented a new potential probe to explore the cosmos, similar but complementary to electromagnetic waves.

In fact the spacetime is so stiff that only the most energetic events in the universe can produce gravitational waves with an amplitude large enough to possibly be observed; yet once produced they can travel almost undisturbed, up to us. For this reason gravitational waves may be employed to observe extreme phenomena which cannot be studied by any other means, such as the coalescence of compact binary systems which comprise black holes and neutron stars, among many others. These observations can scrutinize our fundamental physical theories in regimes otherwise unattainable, looking for possible deviations from them and for hints toward new physics.

This motivated the great experimental effort, which went on for several decades, to build ever so sensitive detectors capable of detecting gravitational waves. This exceptional endeavor finally culminated in 2015 with the first direct observation of a gravitational wave signal by the LIGO-Virgo collaboration [1, 2]: the exquisite sensitivity of the interferometric detectors allowed to measure the gravitational waves produced by the coalescence of two black holes, an extreme event which took place more than a billion years ago. Since then more than 90 events have been observed during three observing runs with ever increasing sensitivity [3–5], and already over 30 candidates have been observed during the first three months of the currently ongoing fourth (O4) run [6].

Nonetheless such accomplishments are based also on a significant amount of theoretical work. The theory of general relativity is non-linear and can be solved exactly in very few instances, therefore suitable approximation schemes are necessary to obtain quantitative predictions for realistic and physically relevant scenarios: this is also the case for the gravitational waves emitted by coalescing binary systems.

To study this problem then several different and complementary formalism have been introduced, each tailored to study a specific phase in the evolution of the binary system. Specifically, among the several methods used to study the stage prior to the coalescence of the two compact objects, which is denoted as the *inspiral phase*, there are the *post-Minkowskian* formalism [7–11], which performs a perturbative expansion in the strength of the gravitational field $\frac{Gm}{c^2 r} \ll 1$, related to the gravitational constant G ; the *post-Newtonian* formalism [12–23], which performs an expansion both in $\frac{Gm}{c^2 r} \ll 1$ and in the velocity $\frac{v^2}{c^2} \ll 1$ of the compact objects; and the *gravitational self-force* formalism [24, 25], which is akin to an expansion in the mass ratio $\frac{m_2}{m_1} \ll 1$, since it treats the second lighter compact object as a perturbation of the exact general relativistic solution for the first object. Other techniques are able to describe also the *merger phase*, when the two compact objects

coalesce; among them *numerical relativity* [26–29], which solves numerically Einstein’s equations; and the *Effective-One-Body* formalism [30, 31], which is a semi-analytical method that employs the results from the other formalism by properly resumming them. Finally other methods, such as black-hole perturbation theory [32–35], are used to study the last stage after the coalescence, which is denoted as the *ringdown phase*.

In particular in this thesis work we will focus on one of the historically most studied approximation schemes, the *post-Newtonian formalism*, which is well suited to describe the dynamics of compact binary systems during the long inspiral phase which precedes their merger, where the velocities v of the compact objects are still low enough. In fact this formalism evaluates the general relativistic dynamics of the binary system as a perturbative expansion in the parameter $\frac{v^2}{c^2} \sim \frac{Gm}{c^2 r} \ll 1$, obtaining a series of corrections to the classical Newtonian result. The post-Newtonian formalism has been introduced by Einstein himself, and the next-to-leading order 1PN dynamics have been computed already 1917 by Droste and Lorentz [13] and in 1938 by Einstein, Infeld and Hoffmann [12]. Despite this, the evaluation of higher orders corrections proved to be more difficult, presenting several subtleties and requiring a huge effort over the last century; currently the 4PN order has been addressed and cross-checked using a variety of approaches [36–39].

Among these methods, recently it has been put forward also an effective field theory approach to the study of the dynamics of binary systems in general relativity, which since then has allowed for a great and steady progress in the computation of post-Newtonian corrections, and which will be the focus of this thesis work. While in the past this problem had already been considered from a field theoretical and diagrammatic point of view [40–42], this method was formalized in 2004 in the seminal paper [43]. One of its main strengths is that the effective field theory framework is able to take advantage of the hierarchy of scales which is present in the two body problem to reduce the complexity of the computations: roughly speaking it handles the gravitational field as if it was composed of potential gravitons, mediating the gravitational force between the two compact objects, and radiation gravitons, representing the gravitational waves. Additionally this method allows for a systematic inclusion also of spin and finite size effects, which are needed to accurately model realistic binary systems.

The turning point in the application of this method however has been the introduction, a few years later, of a diagrammatic viewpoint regarding the evaluation of the post-Newtonian perturbative corrections: in reference [44] it was established a map between diagrams involving potential gravitons and multi-loop Feynman integrals in massless quantum field theories. This allows to employ multi-loop quantum field theory techniques, such as integration-by-parts identities [45–47] and the method of difference [48, 49] and differential equations [50–56], which were first developed in the context of particle physics, to address the computation of the post-Newtonian corrections. Since then, using these modern techniques, approaches based on Feynman diagrams [44, 57–65] and scattering amplitudes [66–76] have allowed to efficiently evaluate higher order corrections; while still yielding fully classical results. The synergy between this approaches enabled to achieve partial results up to 6PN for spinless and featureless systems [59, 64, 65, 77, 78], yet advancing the state of the art also regarding corrections due to spin [79–82] and finite size effects [83, 84]; still even higher order corrections will be needed to fully exploit the capabilities of next generation gravitational wave detectors.

A great effort is in fact underway in order to develop the next third generation of gravitational wave observatories, such as the ground based Einstein Telescope [85–87] and Cosmic Explorer [88–90], and the space based LISA [91]: they will greatly improve over the sensitivity of the current detectors, exploring also new frequencies bands, promising to unveil many scientific discoveries in the next decades.

Motivated by these future prospects, in the second part of this thesis work we will forecast the

capabilities of future gravitational wave observatories to constrain possible deviations from general relativity. In particular we will be interested in assessing the precision with which it will be possible to measure relative deviations from the predictions of the post-Newtonian theory, based solely on the observation of the early inspiral phase of compact binary systems; we will find LISA to be the observatory best suited for this task. We will then proceed by parametrizing the deviations from general relativity by introducing several deformation parameters in the expression for the phase of the observed gravitational wave signal, performing a test similar to the one already carried out in references [92–96].

Outline of the thesis work

The thesis is structured as follows:

- In chapter 1 we overview the theory of general relativity and the standard treatment of gravitational waves in linearized general relativity. In particular we explore how the linearized theory can be used to describe the generation of gravitational waves and their propagation, focusing then on gravitational waves generated by compact binary systems. Next we briefly introduce some notions about gravitational wave detectors. Finally we discuss the regime of validity of the linearized theory, and outline other approaches (such as the post-Newtonian approximation) which are able to overcome these limits, pointing out their complementarity as well.
- In chapter 2 we overview the frameworks of effective theories and of quantum field theory in the path integral formalism. We then present some modern evaluation techniques which are employed to evaluate multi-loop integrals appearing in quantum field theories.
- In chapter 3 we overview the construction of an effective theory which yields the post-Newtonian corrections to the dynamics of compact binary systems. In particular we first outline some key concepts using a toy model, presenting then the actual construction of the effective theory. In the end we explicitly show how the classical Newtonian gravitational potential follows from this construction.
- In chapter 4 we obtain the post-Newtonian corrections to the binary dynamics. In particular we start by outlining the evaluation procedure for diagrams which result in conservative contributions to the binary dynamics; then we explicitly evaluate all the next-to-leading order (1PN) corrections to the conservative sector; finally we generalize this procedure. We then present the `Mathematica` code which we wrote in order to automatize the evaluations of these conservative diagrams; and proceed by reporting the next-to-next-to-leading order (2PN) corrections to the conservative sector. Then, to illustrate the flexibility of the aforementioned code, we evaluate a few contributions which are N^7LO (7PN) corrections to the Newtonian potential, beyond the present state of the art.
- In chapter 5 we evaluate the leading order diagrams entering in the dissipative sector, obtaining the leading order power loss for the compact binary system due to gravitational waves emission. We conclude by evaluating also the leading order gravitational waveform directly in the effective theory, using the in-in formalism.
- In chapter 6 we present how to derive observables from the results obtained in chapter 4 and 5: complementing them with other results present in the literature we explicitly obtain the analytical expression for the gravitational waveform in the post-Newtonian theory.
- In chapter 7 we perform an observational forecast on the precision with which the future space-based gravitational wave detector LISA will be able to constrain possible deviations from the theory of general relativity. We discuss the parametrization employed to quantify

these deviations, estimating also the optimal trade off between statistical and systematic errors. Then we briefly introduce the modelization of the LISA instrument and the Fisher matrix formalism. In the end we present and discuss the results obtained for the forecast.

Finally in the **Conclusions** we summarize the main results of this thesis work, discussing also about possible extensions.

Furthermore some additional discussions and evaluations are presented in the appendices:

- In appendix **A** we outline the procedure to derive the Feynman rules for the effective theory presented in chapter **3**, and then proceed to explicitly evaluate the needed expressions.
- In appendix **B** we report the definitions and properties of some recurring mathematical functions.
- In appendix **C** we explicitly evaluate the integrals which were needed to obtain the results presented in chapter **4**. Furthermore we also show the application of the evaluation methods presented in chapter **2**.
- In appendix **D** we report some extracts from the **Mathematica** code and an example of its use.

NOTATION

The notation and a list of conventions adopted throughout this thesis are presented hereafter.

Physical constants and units

We define the reduced Planck mass as $m_{Pl} \equiv \sqrt{\frac{\hbar c}{32\pi G}}$, which is a factor of two smaller than the more widely used definition.

In chapter 1 the Planck constant \hbar and the speed of light c will be written explicitly, while in the rest of the thesis we'll frequently adopt $\hbar = c = 1$ units; the solar mass is denoted by M_{\odot} .

Space-time, metric, indices and vectors

The dimension of space-time is $3 + 1$; nonetheless when needed dimensional regularization will be adopted, in which case the dimension of space-time will be taken to be $d + 1$, with $d \rightarrow 3$ at the end of calculations.

For most of the work we will adopt a mostly minus metric signature, so for $d = 3$ it means $\eta_{\mu\nu} = \text{diag}(+, -, -, -)$. Only in chapter 1, in the end of chapter 6 and in chapter 7 we will employ the opposite, mostly plus metric signature $\eta_{\mu\nu} = \text{diag}(-, +, +, +)$, as it is customarily used when dealing with observables.

We employ Einstein summation notation, where summation over contracted indices is understood. We use letters from the Greek alphabet to denote space and time components, e.g. $\mu = 0, 1, 2, 3$; while we use letters from the Latin alphabet to denote spatial components only, e.g. $i = 1, 2, 3$.

The contravariant components of four-vectors are denoted by x^{μ} , their spatial part only by x^i ; the latter in vectorial form is denoted by \mathbf{x} ; therefore the coordinates are $x^{\mu} = (x^0, \mathbf{x})$, where $x^0 = ct$. The notation kx understands a contraction between the two four-vectors, as $kx \equiv g_{\mu\nu}k^{\mu}x^{\nu} = k_{\mu}x^{\mu} = +k^0x^0 - k^i x^i$; in particular we define $k^i x^i \equiv \sum_{i=1}^3 k^i x^i = \mathbf{k} \cdot \mathbf{x}$, that is, two spatial vectors with same spatial upper index are understood to be summed over that index via the Kronecker delta δ_{ij} .

We define the Lagrangian density \mathcal{L} via

$$S = \int dt d^3\mathbf{x} \sqrt{-g} \mathcal{L} = \frac{1}{c} \int d^4x \sqrt{-g} \mathcal{L} , \quad (\text{N1})$$

with $g \equiv \det(g_{\mu\nu}) < 0$ is the determinant of the covariant metric tensor.

Symbols and tensorial quantities

The Christoffel symbol is

$$\Gamma_{\mu\nu}^{\rho} = \frac{1}{2} g^{\rho\alpha} (\partial_{\mu} g_{\nu\alpha} + \partial_{\nu} g_{\mu\alpha} - \partial_{\alpha} g_{\mu\nu}) . \quad (\text{N2})$$

The Riemann tensor is defined as

$$R^\mu{}_{\nu\rho\sigma} = \partial_\rho \Gamma_{\nu\sigma}^\mu - \partial_\sigma \Gamma_{\nu\rho}^\mu + \Gamma_{\alpha\rho}^\mu \Gamma_{\nu\sigma}^\alpha - \Gamma_{\alpha\sigma}^\mu \Gamma_{\nu\rho}^\alpha , \quad (\text{N3})$$

the Ricci tensor is

$$R_{\mu\nu} = R^\alpha{}_{\mu\alpha\nu} , \quad (\text{N4})$$

while the Ricci scalar is

$$R = g^{\alpha\beta} R_{\alpha\beta} . \quad (\text{N5})$$

The Levi-Civita symbol is the totally antisymmetric tensor $\epsilon^{\mu\nu\rho\sigma}$, with $\epsilon^{0123} = +1$; or when restricting to $d = 3$ space, the totally antisymmetric tensor ϵ^{ijk} with $\epsilon^{123} = +1$.

Tensor (anti)symmetrization

We use round brackets to denote symmetrization of the corresponding indices, and instead square brackets to denote their anti-symmetrization, for example:

$$A^{(\mu\nu)} = \frac{1}{2} (A^{\mu\nu} + A^{\nu\mu}) , \quad A^{[\mu\nu]} = \frac{1}{2} (A^{\mu\nu} - A^{\nu\mu}) . \quad (\text{N6})$$

If the indices are not contiguous we employ a vertical bar to delimit them, for example:

$$A^{(\mu|\nu\rho|\sigma)} = \frac{1}{2} (A^{\mu\nu\rho\sigma} + A^{\sigma\nu\rho\mu}) , \quad A^{\mu[\nu|\rho|\sigma]} = \frac{1}{2} (A^{\mu\nu\rho\sigma} - A^{\mu\sigma\rho\nu}) . \quad (\text{N7})$$

Fourier transform

The general d -dimensional Fourier transform conventions, in the mostly minus signature, are:

$$f(k) = \int d^d x f(x) e^{ikx} \quad (\text{N8})$$

$$f(x) = \int \frac{d^d k}{(2\pi)^d} f(k) e^{-ikx} \quad (\text{N9})$$

$$(2\pi)^d \delta^{(d)}(k) = \int d^d x e^{ikx} \quad (\text{N10})$$

$$(2\pi)^d \delta^{(d)}(x) = \int d^d k e^{-ikx} ; \quad (\text{N11})$$

while in chapter 1, 6 and 7 the sign in the exponential is opposite, due to the mostly plus signature. In particular, when we will be working in $d + 1$ dimensions with the mostly minus Minkowski background metric, these conventions will explicitly read:

$$f(k) = \int d^{d+1} x f(x) e^{ikx} = \int d^{d+1} x f(x) e^{i(k^0 x^0 - \mathbf{k} \cdot \mathbf{x})} \quad (\text{N12})$$

$$f(x) = \int \frac{d^{d+1} k}{(2\pi)^{d+1}} f(k) e^{-ikx} = \int \frac{d^{d+1} k}{(2\pi)^{d+1}} f(k) e^{-i(k^0 x^0 - \mathbf{k} \cdot \mathbf{x})} \quad (\text{N13})$$

$$(2\pi)^{d+1} \delta^{(d+1)}(k) = \int d^{d+1} x e^{ikx} \quad (\text{N14})$$

$$(2\pi)^{d+1} \delta^{(d+1)}(x) = \int d^{d+1} k e^{-ikx} . \quad (\text{N15})$$

Integral compact notation

To streamline the calculations in $d + 1$ dimensions we will sometimes employ the shorthand notation for integrals

$$\int_{k,q,\dots} \equiv \int \frac{d^{d+1} k}{(2\pi)^{d+1}} \frac{d^{d+1} q}{(2\pi)^{d+1}} \dots \quad (\text{N16})$$

GENERAL RELATIVITY AND GRAVITATIONAL WAVES

In this chapter we review the theory of general relativity and the mathematical description of gravitational waves in the linearized theory.

In particular in section 1.1 we briefly present the theory of General Relativity; in section 1.2 we present gravitational waves and outline some related phenomenology; in section 1.3 we introduce the mathematical description of gravitational waves in linearized general relativity, specializing it in section 1.4 to the case of compact binary systems; in section 1.5 we proceed to discuss the gravitational wave detectors and their response to incoming gravitational waves; finally in section 1.6 we discuss several formalism which go beyond the linearized general relativity, with a particular focus on the post-Newtonian formalism.

1.1 | General relativity

The theory of *general relativity* was developed by Albert Einstein, who published it in 1915 [97, 98].

General relativity is based on a geometrical interpretation of the theory of gravitation: it posits that what was previously regarded as the gravitational force is actually just the effect on matter and energy of the specific geometry of spacetime, and in turn that geometry is dictated by those same matter and energy components which are present in the spacetime.

This geometrical view also allows general relativity to naturally embody Einstein's *equivalence principle*, which states that for each point of the spacetime it's possible to find an appropriate coordinate system for which, in a small enough region around that point, the laws of physics reduce to those of special relativity, if we neglect gravitational tidal effects [99–102].

To formalize mathematically such ideas, general relativity is formulated in the language of differential geometry. Therefore spacetime is a Lorentzian manifold, while physical quantities are expressed by means of tensor fields defined on it. Such a framework allows us to automatically satisfy the equivalence principle, as formulae with a proper tensorial structure guarantee general covariance: that is, those formulae are invariant in form under coordinate transformations specified by a diffeomorphism, where a diffeomorphism is a function which is differentiable, invertible, and with a differentiable inverse. In particular, it is always possible to construct local inertial coordinates in which the metric is locally Minkowski, up to tidal effects [101]. This also implies that all coordinate frames related by a diffeomorphism describe the same physics equivalently, and so that general relativity has a huge local gauge invariance under the group of arbitrary diffeomorphism [103].

General relativity can be formulated resorting to the principle of least action: to do so one starts by assuming the gravitational action to be given by the *Einstein-Hilbert action* [100, 103]

$$S_{EH} = \frac{c^3}{16\pi G} \int d^4x \sqrt{-g} R, \quad (1.1)$$

where $g \equiv \det(g_{\mu\nu}) < 0$ is the determinant of the covariant metric tensor.

One may also couple gravity to matter fields by introducing the matter action S_M , which is usually obtained starting from a flat space Lagrangian \mathcal{L} and employing the minimal coupling principle, according to which the metric becomes generic $\eta_{\mu\nu} \rightarrow g_{\mu\nu}(x)$, ordinary derivatives are substituted with covariant derivatives $\partial_\mu \rightarrow \nabla_\mu$, while the volume element for the integration over spacetime is taken to be $dV = c^{-1} d^4x \sqrt{-g}$ to be consistent with convention (N1); therefore:

$$S_M = \frac{1}{c} \int d^4x \sqrt{-g} \mathcal{L}. \quad (1.2)$$

From the last expression follows also the definition of the *energy-momentum tensor* $T_{\mu\nu}$ [103]

$$T_{\mu\nu} \equiv \frac{2c}{\sqrt{-g}} \frac{\delta S_M}{\delta g^{\mu\nu}}. \quad (1.3)$$

Finally, varying the full action $S = S_{EH} + S_M$ with respect to the inverse metric $g^{\mu\nu}$, we get *Einstein's equations* [99–101, 103, 104]:

$$R_{\mu\nu} - \frac{1}{2} g_{\mu\nu} R = \frac{8\pi G}{c^4} T_{\mu\nu}, \quad (1.4)$$

where $G = 6.674\,30(15) \text{ m}^3 \text{ kg}^{-1} \text{ s}^{-2}$ is the Newtonian constant of gravitation [105], $R_{\mu\nu}$ is the Ricci tensor (N4) and R the Ricci scalar (N5). The left hand side of equation (1.4) is also called the Einstein tensor $G_{\mu\nu}$, which identically satisfies the Bianchi identities $\nabla^\mu G_{\mu\nu} = 0$ [100, 101].

The vacuum Einstein's equations, that is, with $T_{\mu\nu}(x) = 0$, can be cast into a well posed system of nonlinear hyperbolic partial differential equations [106]. We can also notice that Einstein's equations are ten, due to the fact that the tensors in them are symmetric under the exchange of the μ and ν indices. Actually, due to the Bianchi identities, four equations are constraints on the initial conditions, while only six are dynamical second order differential equations. Further, this means that to unambiguously evolve Einstein's equations, one should provide four conditions which fix the coordinate system [99]. Nonetheless, as we'll see in section 1.3.2, in general relativity there are only two radiative degrees of freedom.

Such differential equations are however generically too difficult to be solved analytically, especially when general relativity is coupled to matter fields or the physical setting presents few or no space-time symmetries; this is actually what happens in most realistic scenarios. In fact, few exact analytical solutions of Einstein's equations are known. For example, aside from the *Minkowski metric*, the most known asymptotically flat vacuum stationary solutions are the *Schwarzschild metric*, which describes the metric outside a spherically symmetric body which posses only mass; the *Kerr metric*, which describes a massive rotating axially symmetric body; the *Reissner–Nordström metric*, which describes a spherically symmetric massive charged body, once we add electromagnetism as a matter field in (1.2); and the *Kerr–Newman metric*, which describes an axially symmetric rotating massive charged body [100, 101, 104, 107]. Another widely known solution, of interest in cosmology, is the *Robertson–Walker metric*, which describes a spatially homogeneous and isotropic expanding spacetime, eventually with a non zero spatial curvature [99, 108, 109]. Therefore, apart from the aforementioned idealized cases, one has to resort to perturbative schemes or numerical methods to study realistic physical scenarios in general relativity: in fact we'll do so, starting with linearized general relativity in section 1.3.1, and later on presenting in section 1.6 some approximation schemes which go beyond it.

1.2 | Gravitational waves in general relativity

Gravitational waves may be defined as perturbations of space-time, that propagate through it. In particular we will make this statement more quantitative in section 1.3 in the framework of linearized general relativity: there we will see that, given the right assumptions, gravitational waves can be treated as small perturbations $h_{\mu\nu}$ of the background metric $g_{\mu\nu}$, and these small perturbations satisfy wave equations similar for example to the one electromagnetic waves abide to. In this framework then gravitational waves are produced by the acceleration of masses (more precisely by a source with a non vanishing second time derivative of the mass quadrupole moment at leading order, as we'll see), and propagate away as a warpage of space-time at the speed of light.

1.2.1 — Historical overview

The existence of gravitational waves was inferred by Einstein himself already in 1916, one year after having postulated the theory of General Relativity [1, 110–113]. Nevertheless, due to the large gauge group of general relativity, which is invariant under generic space-time diffeomorphism, the issue of whether gravitational waves were real or just an artifact of the theory was a subject of debates for a long time: at one point even Einstein himself erroneously asserted the possibility of their non-existence [112].

Only at the Chapel Hill conference, which took place in January 1957, theoretical consensus was reached about the reality of gravitational waves [1, 112, 114]. In particular Pirani pointed out that the components of the Riemann tensor (N3) are related to the relative physical accelerations of neighboring free particles, which are experimentally measurable quantities, for example employing a gravity gradiometer [104], and therefore let us overcome the gauge issue [112, 114]. Furthermore, at the same conference, Feynman presented his famous *sticky bead argument*: if at each opposite end of a bar one places a ring of sticky beads, when a gravitational waves passes transversely to the bar, it will generate tidal forces on the system; especially, it will generate a longitudinal compressive stress on the bar [112]. This will make the beads and the end of the bar accelerate differently, and therefore move one with respect to the other: therefore in the sticky point of contact between the bar and the beads there will be friction, and therefore heat. This means that gravitational waves must carry energy, as they were the only source of energy in the system that could have produced that heat in first place [112].

Incidentally, the first attempts to actually detect gravitational waves were carried out by Weber in the 1960s: the principle was to look for mechanical oscillations induced in large metal cylinders, called *resonant bars*, by the passage of a gravitational wave [103, 112, 115]. Over four decades, they were improved to reach almost useful sensitivity, and a network of them was built; there were also claims of the discovery of gravitational waves [116], but they turned out to be erroneous due to an ill-defined statistical treatment of coincidences [112, 117]. The big drawback of resonant-mass detectors is that they're high frequency, low bandwidth detectors: this seriously hindered their ability to detect astrophysical sources [103].

In 1974, Hulse and Taylor detected the PSR B1913+16 binary pulsar [118]. Over the years this system has been carefully tracked and its orbital dynamics precisely reconstructed: this allowed for very precise tests of the theory of gravitation [119]. In particular it allowed them to probe the existence of gravitational radiation, due to the fact that the measured change in the binary orbital period was in excellent agreement with the one predicted by general relativity [103]. Even though this observation didn't directly detect gravitational waves, the fact that accelerated mass radiated gravitational energy pointed to their existence [112].

Gravitational waves from a binary black hole merger were finally observed by the LIGO and Virgo collaborations in 2015 [1], using the two LIGO *gravitational waves interferometers* in the United

States. This strengthened once again the evidence in favor of the validity of general relativity, and opened up a new, and sometimes unique, probe to explore the universe and many astro-physical phenomena. In particular the strength of these interferometric detectors is that they're sensitive to gravitational wave signals with frequency from a few tens to few hundreds of Hz: therefore their bandwidth is quite large and can be made to coincide with the frequencies relevant in the inspiral and merger of astrophysical compact object binaries, as we will see also in section 1.5.

After two years of upgrades, a new signal was detected in both the Advanced LIGO and also the European Advanced Virgo detector [120], allowing for more detailed tests about the nature of gravitational waves. Shortly after came also the first joint detection of gravitational and electromagnetic waves produced by a binary neutron star merger [121], which ushered in the multi-messenger astrophysics era. In the next future the ever-increasing sensitivity of these detectors, in combination with the inclusion in the gravitational wave detectors network of KAGRA in Japan and of LIGO-India [122, 123], will allow for almost daily detections [124]: this will make more detailed studies of general relativity and astrophysical phenomena possible, also in a statistical framework due to the expected large number of events.

Regarding the near future, the third generation of gravitational wave observatories is already under development, for example with plans to build Einstein Telescope in Europe [85–87] and Cosmic Explorer in the United States [88–90]. They will be much more sensitive than current detectors, potentially enabling a new host of discoveries. Nonetheless, ground-based interferometers are intrinsically limited to be sensitive only at frequency above about one Hz, due to the Newtonian and seismic noise: in order to explore the gravitational wave spectrum at lower frequencies there are several plans for space-based gravitational observatories, to be launched already starting in the 2030s. This is the case for the Laser Interferometer Space Antenna (LISA) [91]: it was proposed in the 1990s, but only recently it has entered the final mission study stage, which precede mission adoption that will lead to the spacecraft construction, with an expected launch date in 2037 [125]. These projects have also the potential to study quantities and phenomena of interest in cosmology [86, 126], such as the presence of a cosmological stochastic gravitational wave background: among other things they could probe gravitational waves produced in some inflationary scenarios [127, 128] in a complementary way with respect to the usual study of the B modes of the CMB [129].

1.2.2 — Gravitational waves phenomenology

In this section we'll briefly outline some phenomenology related to the field of gravitational waves.

In particular in this work we will be mostly interested in studying binary systems made of two *compact objects* orbiting each other under their mutual gravitational attraction. In fact such systems are one of the main mechanism by virtue of which gravitational waves are copiously produced: presently we've directly detected gravitational waves produced only via this mechanism.

Indeed in such systems, as we will discuss in section 1.4.3, the motion of the bodies in the binary produces gravitational waves, which carries away energy from the system, forcing the two bodies to get closer and closer in what's called the *inspiral* phase. In particular the amplitude of the gravitational waves is higher for more massive systems, and the gravitational radiation emitted increase in amplitude and frequency as the two bodies get closer, in what's called a *chirp signal*. If the bodies are compact enough, which in turn is possible only if they're heavy enough to start with, they will eventually get so close that strong general relativistic effects will become dominant, disrupting the orbital motion into a *plunge* phase, after which the two bodies will undergo the *merger* phase. The result of the merger is a single compact body, which will start from an excited state due to the violent process from which it was created, and hence will lose energy via gravitational wave emission, during the *ringdown* phase, until it settles into its ground state.

Nonetheless these systems are usually so far away from us, hence the gravitational wave amplitude so faint, that we may hope to detect the signal produced in the *coalescence* of the bodies only for very massive systems, once they get really close to each other; that is, towards the end of the long inspiral phase and in the subsequent merger and ringdown phases. This inspiral phase is actually extremely long, and the initial evolution proceeds really slowly: in fact, considering binary systems with mass of a few M_\odot , and an age comparable to the one of their host galaxy, then these system could have coalesce by today only if their initial orbital period was less than a day [103]. In figure 1.1 are depicted the last phases for the evolution of the first binary black hole system ever observed coalescing.

The characteristic length at which strong general-relativistic effect are dominant, and where roughly happens the transition between inspiral and plunge phases, is given by

$$R_s \equiv \frac{2Gm}{c^2} \approx 2.95 \text{ km} \left(\frac{m}{M_\odot} \right), \quad (1.5)$$

which is the *Schwarzschild radius* associated to the mass m [100, 101]; here $M_\odot = 1.98841(4) \cdot 10^{30} \text{ kg}$ is the solar mass [130]. In particular R_s is the value of the radial coordinate of the Schwarzschild metric where the future *event horizon* of a non-charged, non-rotating and spherically symmetric black hole is located [100, 101, 107]; nonetheless its numerical value gives an order of magnitude estimate for the distance at which general relativity must be taken into account also when used in the Newtonian mechanics calculations [103]. Let us also recall that a black hole is actually defined as a compact object with a future event horizon, that is, an hypersurface within which future-directed time-like or null geodesics (read an observer or a light ray) may enter, but never escape [101, 107].

From this discussion we can see that the binary systems we may hope to detect are made of heavy and compact objects, where now we can more precisely specify the latter adjective as those objects with a characteristic length comparable with their Schwarzschild radius: this compactness allows them get extremely close to each other before merging or being tidally disrupted. The astrophysical objects which satisfy such conditions are either *neutron stars* (NS) or *black holes* (BH), and the binary system they may form are denoted as *Binary Neutron Star* (BNS), *Binary Black Hole* (BBH) or *Neutron Star-Black Hole binary* (NSBH) systems.

Still it must be noted that what we've just described is not the only mechanism of production of gravitational waves: among others also rotating neutron stars may produce gravitational waves if

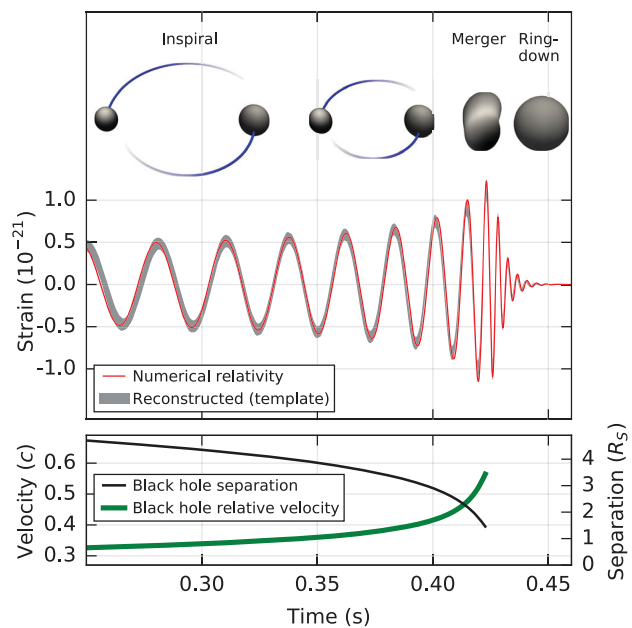


FIGURE 1.1 — Plots depicting the time evolution of the binary black hole (BBH) system which was discovered with event GW150914, the first direct gravitational waves detection [1, 2]. The top panel shows the expected strain that the gravitational wave induced in the LIGO Hanford observatory, as reconstructed either via an ad hoc numerical relativity simulation (red line) or template waveforms (grey band), with parameters tuned to the most likely ones, as obtained by the analysis of the recorded signal. In the upper part we can see also a depiction of the subsequent phases which the black holes went through: the inspiral which brought them closer, followed by the merger and the ringdown, which produced the new, final black hole; furthermore we can see that the amplitude of the detected signal peaks around the moment of merger. In the panel below are represented the Keplerian effective relative distance $\frac{R}{R_s}$, in units of Schwarzschild radii R_s , as defined in equation (1.5), and the Keplerian effective relative velocity $\frac{v}{c}$, evaluated using the formulae that will be presented in section 1.4.3. Figure taken from [1] under the license conditions.

their shape is asymmetric enough, for example due to small bumps or overdensities on their surface; similarly also supernovae may produce copious amounts of gravitational waves if the explosion is asymmetrical enough; furthermore we expect the universe to be permeated by a stochastic gravitational wave background due to the superposition of gravitational waves produced by a plethora of phenomena. For the latter of great interest is the cosmological stochastic background due to gravitational waves produced in the early universe, for example by inflation, but possibly also by phase transitions or more exotic phenomena such as cosmic strings [132, 133].

Regarding this aspect, recently the NANOGrav collaboration, using pulsar-timing arrays, was able to collect evidence for a stochastic gravitational wave background, probably due to the superposition of gravitational waves emitted by many supermassive black hole binaries, although it's possible for this signal to be of cosmological origin or of even more exotic nature [134].

Furthermore the observation of compact binary system via gravitational waves can give a lot of astrophysical informations about the evolution of their progenitors: just as an example, if future gravitational waves observatories were to observe mergers at redshift $z \gtrsim 30$, so before the first population III stars formed, then this would give a strong evidence for the existence of *primordial black holes*. Restricting instead to compact objects of astrophysical origin, and overlooking possible exotic compact objects, we can study their mass distribution (see also figure 1.2) and their merger rate. In particular we have that due to the stellar evolution the lower mass expected for a neutron star is of order $M_{NS,min} \approx 1.2 M_{\odot}$ [132, 135]; while for stellar black holes it is of order $M_{BH,min} \approx 3 \sim 5 M_{\odot}$ [136–138]. The upper bounds on the mass of a neutron star is instead given by the Tolman–Oppenheimer–Volkoff limit, and it's estimated to be $M_{NS,max} \approx 2.2 \sim 2.6 M_{\odot}$ [101,

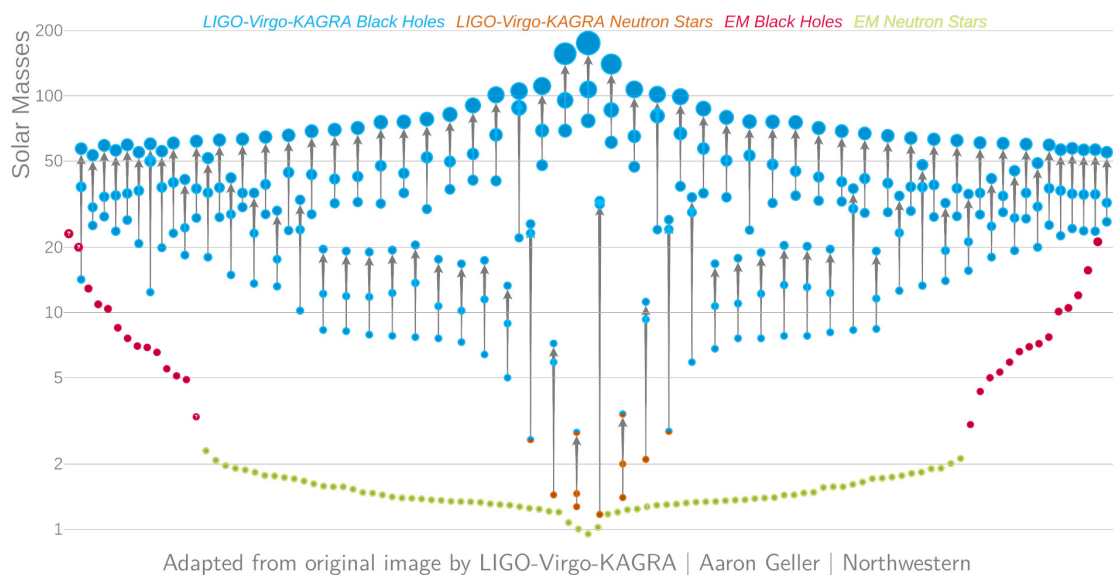


FIGURE 1.2 — Figure depicting the masses of the black holes and the neutron stars known so far, either through electromagnetic or gravitational wave observations. In particular, regarding the compact objects discovered thanks gravitational wave events, in the plot are depicted both the initial bodies and the resulting ones after merger, connected via an arrow. To produce this plots the events up to the end of the O3 run, with $p_{astro} > 0.5$, were used; where the p_{astro} statistic quantifies the probability of astrophysical origin of such events [131]. We can see that as the detector become more sensitive, and so the number of detected events increases, it becomes possible to perform studies about the compact objects population. Nonetheless it's important to recognize that there is a *selection bias* due to the fact that the detectors are most sensitive only at certain frequency, and so systems with specific parameters are more readily detected than others: this explains also why in the plot we have $m < \mathcal{O}(100) M_{\odot}$. Figure adapted from *Masses in the Stellar Graveyard: GWTC-3*, credits of the original image: LIGO-Virgo / Aaron Geller / Northwestern University.

139]; black holes instead could undergo several mergers and could have masses in a wide range, depending on several factors. In fact it is expected that the center of the galaxies should host a supermassive black hole (SMBH), which may have masses also of the order $M_{SMBH} \approx 10^6 \sim 10^9 M_\odot$ [140]; the observation of gravitational waves produced by the coalescence of (super)massive black holes binaries, also denoted as (S)MBHBs, are actually a scientific goal of future low-frequency gravitational wave missions, such as LISA [91].

Since we've already observed several compact binary coalescences, we can infer their merger rate from these observations: in particular the latest LIGO-Virgo data [141] finds the binary neutron star merger rate to be $R_{BNS} = (10 \sim 1700) \text{ Gpc}^{-3} \text{ yr}^{-1}$, the neutron star-black hole merger rate to be $R_{NSBH} = (7.8 \sim 140) \text{ Gpc}^{-3} \text{ yr}^{-1}$, and the binary black hole merger rate to be $R_{BBH} = (17.9 \sim 44) \text{ Gpc}^{-3} \text{ yr}^{-1}$. In particular this merger rate is found to evolve as a function of redshift, as well as a function of the component masses: there seems to be some mass gaps, i.e. the merger rate seems to be strongly suppressed in correspondence of specific mass values, and this could be due to astrophysical phenomena. On the other hand the merger rate strongly decreases for systems with total mass exceeding $100M_\odot$. In fact most of the binary systems directly observed up until now have a total mass $m < 100 M_\odot$, and there are astrophysical evidences for the existence of super massive black holes with masses $m > 10^6 M_\odot$ [37, 142]; instead much less is known for intermediate mass black holes (IMBHs), with masses in the range $10^2 M_\odot < m < 10^5 M_\odot$ [37, 143].

1.3 | Linearized general relativity and gravitational waves

As outlined in section 1.1, to study general relativity one usually has to resort to some approximation scheme. In particular in the following we'll present the linearization of Einstein's equations (1.4) around the Minkowski flat metric: this procedure allows to obtain linear partial differential equations, which are very well understood, and it allows to describe general physical scenarios, under the only assumption of having a weak gravitational field. As we'll see, this limit in most cases is not restrictive, and is actually very well suited to study gravitational waves in general relativity.

This section is based mostly on [103]; other references include [99–101, 104].

1.3.1 — Linearized general relativity

Linearized general relativity is a theory which approximates general relativity in the regime where the gravitational field is weak and the spacetime is almost flat. To do so it perturbs the metric tensor $g_{\mu\nu}(x)$ around the flat Minkowski one $\eta_{\mu\nu}$, and linearizes Einstein's equations (1.4) in that perturbation.

Specifically, one assumes that the metric can be written as:

$$g_{\mu\nu}(x) = \eta_{\mu\nu} + h_{\mu\nu}(x) , \text{ with } |h_{\mu\nu}(x)| \ll 1 . \quad (1.6)$$

This is equivalent to requiring the existence of at least one coordinate frame where the metric can be written as a small perturbation around the flat Minkowski metric [103, 104].

Having done so, it's now possible to expand the equations of motion (1.4) keeping only terms of order $O(h)$, while neglecting all terms of higher order. As a consequence, in the linearized theory the convention is that indices are raised and lowered using only $\eta_{\mu\nu}$, and not the full metric $g_{\mu\nu}$, as the difference would be of order $O(h^2)$ [103]; while the inverse metric at linear order is given by $g^{\mu\nu} = \eta^{\mu\nu} - h^{\mu\nu}$.

To elaborate further on condition (1.6), let us notice that due to the equivalence principle, and effectively by constructing the Riemann or Fermi normal coordinates [103], the metric can always be chosen to be exactly $g_{\mu\nu}(\bar{x}) = \eta_{\mu\nu}$ in a specific spacetime point \bar{x} and a small perturbation

of $g_{\mu\nu}(x) = \eta_{\mu\nu} + O(\partial_\rho \partial_\sigma g_{\mu\nu}(\bar{x}))$ around it [101]. Hence we can recognize that the magnitude of $(\partial_\rho \partial_\sigma g_{\mu\nu}(\bar{x}))^{-\frac{1}{2}}$ sets a characteristic length-scale: this gives us the order of magnitude of the extension of the spacetime region over which we may consider the metric to be flat enough, as required by (1.6). Moreover, to get a sense of the physical scenarios in which $|h_{\mu\nu}| \ll 1$ may be satisfied, let us first recall the *Newtonian limit*: if we can choose coordinates in which the metric is stationary, for a weak gravitational field and slowly moving particles it holds $g_{00} = (1 + 2\frac{\Phi}{c^2})$, where $\Phi = -\frac{Gm}{r}$ is the usual Newtonian gravitational potential [101]. From this last relation we can then see that $h_{00} c^2 \sim \Phi \sim -\frac{GM}{r}$, and therefore even at the surface of stars it holds $h \sim 10^{-5}$: this means that, as mentioned above, the weak field is an excellent approximation in many physical situations [101, 104].

It must be noted however that condition (1.6) does not uniquely fix the coordinate frame, or equivalently the gauge, because we could perform the following gauge transformation (coordinate frame redefinition):

$$x'^{\mu} = x^{\mu} + \xi^{\mu}(x) \quad (1.7)$$

with the constraint

$$|\partial_{\nu} \xi^{\mu}(x)| \sim O(h) \ll 1 \quad (1.8)$$

and still fulfill the aforementioned condition, as will be shown below. Let us notice also that (1.8) is a requirement concerning only on the derivatives of the field $\xi^{\mu}(x)$, which therefore by itself could assume also a large value and is only required to be slowly varying, both in space and time.

To show such a redundancy, let us start by recalling that under a generic diffeomorphism the metric, which is a rank 2 covariant symmetric tensor field, becomes

$$g'_{\mu\nu}(x') = \frac{\partial x^{\alpha}}{\partial x'^{\mu}} \frac{\partial x^{\beta}}{\partial x'^{\nu}} g_{\mu\nu}(x) = \frac{\partial x^{\alpha}}{\partial x'^{\mu}} \frac{\partial x^{\beta}}{\partial x'^{\nu}} (\eta_{\alpha\beta} + h_{\alpha\beta}(x)) , \quad (1.9)$$

with (1.7) implying

$$\frac{\partial x^{\alpha}}{\partial x'^{\mu}} = \delta^{\alpha}_{\mu} - \frac{\partial \xi^{\alpha}}{\partial x'^{\mu}} , \quad (1.10)$$

and therefore (1.6) becomes

$$\begin{aligned} g'_{\mu\nu}(x') &= \frac{\partial x^{\alpha}}{\partial x'^{\mu}} \frac{\partial x^{\beta}}{\partial x'^{\nu}} (\eta_{\alpha\beta} + h_{\alpha\beta}(x)) \\ &= \eta_{\mu\nu} - \frac{\partial \xi_{\mu}}{\partial x'^{\nu}} - \frac{\partial \xi_{\nu}}{\partial x'^{\mu}} + h_{\mu\nu}(x) + O(h^2) ; \\ &= \eta_{\mu\nu} + h'_{\mu\nu}(x') \end{aligned} \quad (1.11)$$

where we recalled condition (1.8), while the last line is just the definition of $h'_{\mu\nu}$, as in (1.6). Finally this implies that the tensor field $h_{\mu\nu}(x)$, under the gauge transformation (1.7), transforms as:

$$h'_{\mu\nu}(x') = h_{\mu\nu}(x) - (\partial_{\nu} \xi_{\mu} + \partial_{\mu} \xi_{\nu}) , \quad (1.12)$$

where we neglected terms of order $O(h^2)$ as by hypothesis we're working in linearized general relativity. We can now recognize that, as long as the condition (1.8) on the smallness of $\partial_{\mu} \xi_{\nu}$ is satisfied, the transformation (1.7) does not spoil condition (1.6), which specified to the new tensor reads $O(h'_{\mu\nu}(x')) \sim O(h_{\mu\nu}(x)) \ll 1$; therefore this new coordinate frame is equivalent to the previous one.

One can also notice that the set of transformations which are a symmetry of linearized general relativity comprises translations $\xi^{\mu} = a^{\mu}$ with $a^{\mu} = \text{const}$, spatial rotations, and generically slowly varying diffeomorphism, while for example boosts may spoil the $h_{\mu\nu} \ll 1$ requirement [103].

To obtain the equations of motion for the field $h_{\mu\nu}(x)$ in linearized general relativity, first one has to linearize the expression of the Riemann curvature tensor. To do so one has to replace the metric $g_{\mu\nu}(x)$ with the expansion (1.6) in the Christoffel symbols (N2) and in the Riemann tensor (N4), keeping only terms at most linear in $h_{\mu\nu}$. Doing so one obtains [101, 103]:

$$R_{\mu\nu\rho\sigma} = \frac{1}{2} (\partial_\nu \partial_\rho h_{\mu\sigma} + \partial_\mu \partial_\sigma h_{\nu\rho} - \partial_\mu \partial_\rho h_{\nu\sigma} - \partial_\nu \partial_\sigma h_{\mu\rho}) . \quad (1.13)$$

In particular this expression is invariant under gauge transformations in linearized general relativity, thanks to the properties of the Riemann tensor under exchange of its indices [103].

It is also customary to define the quantities:

$$h \equiv \eta^{\mu\nu} h_{\mu\nu} \quad (1.14)$$

$$\bar{h}_{\mu\nu} \equiv h_{\mu\nu} - \frac{1}{2} \eta_{\mu\nu} h , \quad (1.15)$$

from which follows also

$$\bar{h} \equiv \eta^{\mu\nu} \bar{h}_{\mu\nu} = h - 2h = -h . \quad (1.16)$$

Recalling (1.13) and adopting the previous definitions, it is now possible to compute the linearization of equations (1.4), to obtain the *linearized Einstein's equations* [101, 103, 104]:

$$\square \bar{h}_{\mu\nu} + \eta_{\mu\nu} \partial^\rho \partial^\sigma \bar{h}_{\rho\sigma} - \partial^\rho \partial_\nu \bar{h}_{\mu\rho} - \partial^\rho \partial_\mu \bar{h}_{\nu\rho} = -\frac{16\pi G}{c^4} T_{\mu\nu} , \quad (1.17)$$

where $\square = \eta^{\mu\nu} \partial_\mu \partial_\nu$ is the usual flat space d'Alembertian.

To further simplify the equations (1.17), we can take advantage of the gauge freedom (1.12). In particular we may choose the so called *harmonic gauge*, also known as De Donder gauge, which generically reads

$$\partial_\mu (g^{\mu\nu} \sqrt{-g}) = 0 , \quad (1.18)$$

and that at linear order reduces to the *Lorentz gauge* [103]:

$$\partial_\nu \bar{h}^{\mu\nu} = 0 . \quad (1.19)$$

Applying a gauge transformation (1.12) to (1.15) we obtain

$$\bar{h}_{\mu\nu} \rightarrow \bar{h}'_{\mu\nu} = \bar{h}_{\mu\nu} - \underbrace{(\partial_\mu \xi_\nu + \partial_\nu \xi_\mu - \eta_{\mu\nu} \partial_\rho \xi^\rho)}_{\equiv \xi_{\mu\nu}} . \quad (1.20)$$

Due to the fact that $\partial^\nu \xi_{\mu\nu} = \square \xi_\mu$, the same gauge transformation applied on (1.19) acts as

$$\partial_\nu \bar{h}^{\mu\nu} \rightarrow (\partial_\nu \bar{h}^{\mu\nu})' = \partial_\nu \bar{h}^{\mu\nu} - \square \xi^\mu . \quad (1.21)$$

This means that, even if we start from in generic coordinate frame, we can go to the one in which the Lorentz gauge is satisfied by means of a slowly varying diffeomorphism $\xi^\mu(x)$ given by $\square \xi_\mu = \partial^\nu \bar{h}_{\mu\nu}$. In particular this is always possible because, denoting with $G(x)$ the Green's function of the flat d'Alembertian operator, such that $\square_x G(x-y) = \delta^{(4)}(x-y)$, such a diffeomorphism is explicitly given by [103]

$$\xi_\mu(x) = \int d^4 y G(x-y) (\partial^\nu \bar{h}_{\mu\nu})(y) . \quad (1.22)$$

Evaluating (1.17) in Lorentz gauge we obtain the much simpler expression

$$\square \bar{h}_{\mu\nu} = -\frac{16\pi G}{c^4} T_{\mu\nu} , \quad (1.23)$$

which with the same Lorentz condition (1.19) implies the conservation of the energy-momentum tensor in the linearized theory:

$$\partial^\nu T_{\mu\nu} = 0 . \quad (1.24)$$

Equation (1.23) is the formula which generically describes the generation of gravitational waves in linearized general relativity, as we'll see in section 1.3.4, and their propagation and interaction with test masses: however, as explained in section 1.3.2 and 1.5.1 these last two scenarios can be more easily studied in the transverse-traceless gauge.

1.3.2 — Propagation of gravitational waves

It is customary to study the propagation of gravitational waves in linearized general relativity, due to the small amplitude expected, and in vacuum, defined as the regions of spacetime where $T_{\mu\nu}(x) = 0$: in this case, requiring also to be in Lorentz gauge (1.19), the linearized Einstein's equations (1.23) reduce to the usual flat space wave equation

$$\square \bar{h}_{\mu\nu} = 0 . \quad (1.25)$$

In this scenario which we chose, outside the source where $T_{\mu\nu}(x) = 0$, there is a residual gauge freedom, because the Lorentz gauge condition (1.19) doesn't fix completely the coordinate frame. In particular, starting from a frame which is in Lorentz gauge, we can perform an additional coordinate transformation given by $x'^\mu \rightarrow x''^\mu = x'^\mu + \xi'^\mu(x')$. Therefore, recalling the transformation property (1.21) of the $\bar{h}_{\mu\nu}$ tensor, we have that if we choose the gauge transformation $\xi'^\mu(x')$ such that $\square \xi'^\mu(x') = 0$, then the new gauge will still satisfy the Lorentz gauge condition $\partial_\nu \bar{h}''^{\mu\nu} = 0$. The tensor $\bar{h}'_{\mu\nu}$ transforms accordingly, as in (1.20); and due to the fact that $\square \xi'^\mu = 0$ implies $\square \xi'^{\mu\nu} = 0$, we have that the linearized Einstein's equations (1.25) in this new gauge still read $\square \bar{h}'_{\mu\nu} = 0$.

This gauge fixing procedure let us single out the real radiative degrees of freedom of general relativity. In fact, starting from a generic frame, we can choose four $\xi^\mu(x)$ functions, explicitly given in (1.22), to move to the Lorentz gauge. Its gauge condition (1.19), which we're imposing, is a constraint on four components of $\bar{h}_{\mu\nu}(x)$; therefore the number of independent components of $\bar{h}_{\mu\nu}$ is lowered from ten to six [103]. Where the energy-momentum tensor is also vanishing $T_{\mu\nu}(x) = 0$, we have an additional residual gauge freedom, that we can fix choosing four additional functions $\xi'^\mu(x')$ which satisfy $\square \xi'^\mu = 0$, as explained above. Specifically, we can choose the four functions $\xi'^\mu(x')$ to impose four additional conditions on the $\bar{h}_{\mu\nu}$ tensor, or equivalently on $h_{\mu\nu}$. This shows that the real propagating degrees of freedom of general relativity are only two [103].

We may apply the previous procedure to simplify the generic redundant expression of $h_{\mu\nu}$, in particular we may choose ξ'^μ such as to fix $\bar{h} = 0$, obtaining $\bar{h}_{\mu\nu} = h_{\mu\nu}$, and imposing $h_{0i} = 0$ [103]. Finally the $\mu = 0$ Lorentz gauge condition implies that h_{00} is constant in time, which corresponds to the static part of the gravitational interaction, and we may set it to zero if we're concerned only with propagating time-varying gravitational waves; while the $\mu = i$ spatial Lorentz gauge constraints read $\partial^i h_{ij} = 0$ [103].

Such choices define the *transverse-traceless gauge*, or TT gauge, in which the conditions

$$h_{0\mu} = 0 \quad \text{Vanishing-non spatial components} \quad (1.26a)$$

$$\partial^i h_{ij} = 0 \quad \text{Transverse} \quad (1.26b)$$

$$\delta^{ij} h_{ij} = 0 \quad \text{Traceless} \quad (1.26c)$$

hold [103], and we recognize that these conditions require the $h_{\mu\nu}$ tensor to be transverse and traceless, with vanishing non-spatial components. In particular the perturbation of the metric

tensor in TT gauge is usually denoted as h_{ij}^{TT} , where it suffices now to specify only its spatial (i, j) components.

We underline that we can choose the TT gauge only outside the sources. This is because if $T_{\mu\nu} \neq 0$, we have $\square \bar{h}_{\mu\nu} \neq 0$; and even though we may still perform a gauge transformation with $\square \xi^\mu = \square \xi^{\mu\nu} = 0$, we cannot use such a transformation to set the components of $\bar{h}_{\mu\nu}$ to zero [103]. To see this, for definiteness let us choose $\mu = \nu = 0$: recalling (1.20) we have that $\bar{h}'_{00} = \bar{h}_{00} - \xi_{00}$, nonetheless $\square \bar{h}'_{00} = \square \bar{h}_{00} - \square \xi_{00} = \square \bar{h}_{00} \neq 0$, therefore \bar{h}'_{00} cannot be identically constant.

After having imposed the TT gauge in vacuum, plane waves $h_{ij}^{TT}(x) = e_{ij}(\mathbf{k})e^{ikx}$ are solutions of the linearized Einstein's equation (1.25), where $k^\mu = (\frac{\omega}{c}, \mathbf{k})$ with $|\mathbf{k}| = \frac{\omega}{c} = \frac{(2\pi f)}{c}$, and $e_{ij}(\mathbf{k})$ is called the *polarization tensor*; still one need to take care of taking the real part only at the end of calculations. If we denote with $\hat{\mathbf{n}}$ the direction of propagation of the plane wave, such that $k^\mu = |\mathbf{k}|(1, \hat{\mathbf{n}})$ and $\delta^{ij}n_in_j = 1$, the condition (1.26b) becomes $n^i h_{ij} = 0$, so that we recognize the condition of transversality with respect to the direction of propagation $\hat{\mathbf{n}}$.

The expression of a generic solution $h_{ij}^{TT}(x)$ of (1.25) in TT gauge can be written as [103]

$$h_{ij}^{TT}(x) = \int \frac{d^3\mathbf{k}}{(2\pi)^3} \left(\mathcal{A}_{ij}(\mathbf{k}) e^{ikx} + \mathcal{A}_{ij}^*(\mathbf{k}) e^{-ikx} \right), \quad (1.27)$$

where the addition of the complex conjugate assures us that $h_{ij}^{TT}(x)$ will be a real quantity.

We may also introduce a generic orthonormal frame with axes $(\hat{\mathbf{u}}, \hat{\mathbf{v}}, \hat{\mathbf{n}})$, and consider a wave propagating along the third spatial axis, so in direction of $\hat{\mathbf{n}}$, to obtain the explicit expression [103]

$$h_{ij}^{TT}(t, z) = \begin{pmatrix} h_+ & h_\times & 0 \\ h_\times & -h_+ & 0 \\ 0 & 0 & 0 \end{pmatrix}_{ij} \cos\left(\omega\left(t - \frac{z}{c}\right)\right); \quad (1.28)$$

where we made explicit the amplitude h_+ of the *plus polarization*, and the amplitude h_\times of the *cross polarization*, which are the two polarization of the gravitational waves defined respectively with respect to the plus and cross polarization tensors [103]:

$$e_{ij}^+(\hat{\mathbf{n}}) = \hat{\mathbf{u}}_i \hat{\mathbf{u}}_j - \hat{\mathbf{v}}_i \hat{\mathbf{v}}_j, \quad (1.29a)$$

$$e_{ij}^\times(\hat{\mathbf{n}}) = \hat{\mathbf{u}}_i \hat{\mathbf{v}}_j + \hat{\mathbf{v}}_i \hat{\mathbf{u}}_j. \quad (1.29b)$$

Due to the fact that gravitational waves are described by a rank 2 tensor, we have that under spatial rotations of angle ψ around the propagation axis $\hat{\mathbf{n}}$, the amplitudes h_+ and h_\times mix into each other with a rotation matrix of angle 2ψ [103]; so for example they get swapped, up to a sign, by a rotation of $\frac{\pi}{4}$ radians.

With these definitions we may also specialize the generic solution (1.27) to a gravitational wave, once produced by a far away localized source, and now propagating along a well defined $\hat{\mathbf{n}}$ direction. In particular, defining $\tilde{h}_+(f)$ and $\tilde{h}_\times(f)$ via $\left(\tilde{h}_+(f) e_{ij}^+(\hat{\mathbf{n}}) + \tilde{h}_\times(f) e_{ij}^\times(\hat{\mathbf{n}})\right) \delta^{(2)}\left(\frac{\mathbf{k}}{|\mathbf{k}|} - \hat{\mathbf{n}}\right) \equiv \frac{f^2}{c^3} \mathcal{A}_{ij}(\mathbf{k})$, we obtain:

$$h_{ij}^{TT}(x)_{\hat{\mathbf{n}}} = \int_{-\infty}^{+\infty} df \left(\tilde{h}_+(f) e_{ij}^+(\hat{\mathbf{n}}) + \tilde{h}_\times(f) e_{ij}^\times(\hat{\mathbf{n}}) \right) e^{-i2\pi f(t - \frac{1}{c}\hat{\mathbf{n}}\cdot\mathbf{x})}. \quad (1.30)$$

On the other hand, starting from a plane wave solution $\bar{h}_{\mu\nu}(x)$ in Lorentz gauge of the linearized Einstein's (1.23), in the vacuum regions it's possible to find the components of the corresponding tensor in TT gauge $h_{\mu\nu}^{TT}(x)$ without the need to find explicitly the required coordinate transformation. To do so for a plane wave propagating in direction $\hat{\mathbf{n}}$, one defines the symmetric and transverse projector [103]:

$$P_{ij}(\hat{\mathbf{n}}) = \delta_{ij} - n_in_j. \quad (1.31)$$

From this we can define the so called Lambda tensor [103]

$$\Lambda_{ij,kl}(\hat{\mathbf{n}}) = P_{ik}(\hat{\mathbf{n}})P_{jl}(\hat{\mathbf{n}}) - \frac{1}{2}P_{ij}(\hat{\mathbf{n}})P_{kl}(\hat{\mathbf{n}}) ; \quad (1.32)$$

which is transverse on each index (e.g. $n^i \Lambda_{ij,kl}(\hat{\mathbf{n}}) = 0$), traceless ($\Lambda_{ii,kl}(\hat{\mathbf{n}}) = \Lambda_{ij,kk}(\hat{\mathbf{n}}) = 0$) and symmetric under the exchange of $(i, j) \leftrightarrow (k, l)$. Thanks to these properties, the Lambda tensor can be used to extract the transverse (with respect to $\hat{\mathbf{n}}$) and traceless part of any symmetric tensor S_{kl} , as $S_{ij}^{TT} = \Lambda_{ij,kl}(\hat{\mathbf{n}})S_{kl}$. Therefore, given a plane wave $\bar{h}_{\mu\nu}(x) \sim e^{ikx}$ in Lorentz gauge propagating along $\hat{\mathbf{n}} = \frac{\mathbf{k}}{|\mathbf{k}|}$, the corresponding spatial components in TT gauge are given by [103]

$$h_{ij}^{TT} = \Lambda_{ij,kl}(\hat{\mathbf{n}})\bar{h}_{kl} = \Lambda_{ij,kl}(\hat{\mathbf{n}})h_{kl} , \quad (1.33)$$

whereas the non spatial components are set to zero. If we have a generic solution $\bar{h}_{\mu\nu}(x)$ in Lorentz gauge, to obtain the corresponding expression in TT gauge we'd have to apply the aforementioned procedure in Fourier space to each mode $\bar{h}_{ij}(\mathbf{k})$ individually, with $\hat{\mathbf{n}} = \frac{\mathbf{k}}{|\mathbf{k}|}$ [104].

The properties under rotation of the h_+ and h_\times amplitudes, as in (1.28), which are consequences of the fact that $h_{\mu\nu}$ is a rank 2 tensor, carry over to the characteristics of the quanta of the gravitational field, the *graviton*. Indeed, the fact that it has spin 2 is related to the fact that the combinations $h_\times \mp ih_+$ acquire the phase $e^{\mp 2i\psi}$ after a spatial rotation by an angle ψ around the propagation axis, and therefore those combinations are helicity eigenstates with helicities ± 2 [99, 103]. Furthermore the graviton is massless, as could be seen for example by the fact that classical equation of motion $\square h_{ij}^{TT} = 0$ is a Klein-Gordon equation with $m_g^2 = 0$; which also tells us that the gravitons, or equivalently gravitational waves, travel at the speed of light, as $\square = \eta^{\mu\nu}\partial_\mu\partial_\nu = \frac{1}{c^2}\partial_t^2 - \nabla^2$ [103]. Experimentally these properties have never been falsified yet: actually stringent upper bounds exist on the mass as $m_g \lesssim 10^{-22}$ eV [144], while the speed of gravitational waves has been directly measured to be equal to the one of light, up to a relative difference $\frac{|\Delta v|}{v_{EM}} \lesssim 3 \cdot 10^{-15}$ [145].

1.3.3 — Energy-momentum tensor of gravitational waves

As we heuristically outlined in section 1.2.1, gravitational waves carry energy and momentum.

We should hence be able to associate an energy momentum tensor to gravitational waves, but this is not as straightforward as it may seem: to say that gravitational waves carry energy and momentum means that they can curve the spacetime, but therefore to study this phenomenon we should allow the background metric to be generic and spacetime dependent as $\bar{g}_{\mu\nu}(x)$, with $g_{\mu\nu}(x) = \bar{g}_{\mu\nu}(x) + h_{\mu\nu}(x)$, $|h_{\mu\nu}(x)| \ll 1$ [103]. However this now leads to an ambiguity in our definition of what are gravitational waves: we could move any perturbation from $\bar{g}_{\mu\nu}(x)$ to $h_{\mu\nu}(x)$ and viceversa, as only the total $g_{\mu\nu}(x)$ has a physical meaning.

This issue actually cannot be solved in general, as the separation of the metric we performed is artificial, and can be considered to be well defined only when there is a clear separation between the scales on which the background metric $\bar{g}_{\mu\nu}(x)$ and the gravitational waves perturbation $h_{\mu\nu}(x)$ vary: for example we can single out gravitational waves if the spatial scale over which $\bar{g}_{\mu\nu}(x)$ varies is much larger than the wavelength of the gravitational wave $h_{\mu\nu}(x)$, or if, at a given position, the Fourier transform of $\bar{g}_{\mu\nu}(f)$ comprises a set of frequency which is lower and does not overlap with the frequencies which make up the gravitational waves $h_{\mu\nu}(f)$ [103]. Let us observe that the latter condition is what actually is fulfilled for gravitational wave detectors [103].

This shows us as well that it's not meaningful to talk about gravitational waves of arbitrary amplitude, as it would become impossible to distinguish the gravitational waves from the background [103]. To be precise, actually, there exist exact wave solutions in general relativity [104], but it

would be too cumbersome to use them to describe gravitational waves emitted by generic bodies [103]. On the other hand, strictly speaking the gravitational wave solution of the linearized theory are not solutions of the full theory, as the non linearities in Einstein's equations will produce back-scattering and tails due to the interaction of the gravitational waves with the curvature produced by themselves [104]; moreover it's not possible to systematize linearized general relativity to higher orders, as we'd need to allow for a generic non-flat background metric just to accommodate for the curvature due to the perturbation $h_{\mu\nu}$ itself [103].

Having analyzed the limits of validity of our approximations, to find the explicit expression for the gravitational waves energy tensor, which we denoted by $t^{\mu\nu}(x)$, we'll actually resort to the field-theoretical approach of treating linearized gravity, so $h_{\mu\nu}(x)$, as a classical field theory over Minkowski spacetime, where one can apply Noether's theorem to obtain $t^{\mu\nu}(x)$ thanks to the symmetry of the theory under space-time translations [103].

This procedure still cannot overcome the intrinsic issues outlined above, which manifest themselves by the fact that the energy-momentum tensor obtained via Noether's theorem is not well defined per se, but has as a physically meaningful interpretation only once integrated over a finite spacetime region, if the field configuration vanish sufficiently fast on the boundaries [103]. In fact we may add a total four-divergence $\mathcal{L}' = \mathcal{L} + \partial_\mu K^\mu(h)$ to the original Lagrangian without modifying the equations of motion, but this would instead modify the mathematical expression of the Noether currents, and could affect also the Noether charges if boundary terms could not be neglected [103].

Furthermore in general relativity it's not even meaningful to try to find an expression of $t^{\mu\nu}(x)$, which is a Noether current, such that for example in each spacetime point $t^{00}(x)$ could have the physical interpretation of the energy density of gravitational waves: this is because at a given point, resorting to Einstein's equivalence principle as seen in section 1.3.1, we could always make the gravitational field vanish with a suitable coordinate transformation. Therefore the local energy density of gravitational waves is not gauge invariant, hence is not a physical quantity that could be measured [103].

Thus, in a similar way with respect to the separation of scales outlined above, the solution is to define the energy-momentum tensor of gravitational waves as a spatial average over several reduced wavelengths, which is denoted by $\langle \dots \rangle$; for plane waves equivalently one could take the temporal average over several periods [103]. Actually this procedure is required not only in general relativity, as the energy density of a wave-packet cannot be exactly localized neither classically, due to the Fourier transform properties, neither quantum-mechanically, due to the uncertainty principle [103].

Thus, the energy momentum tensor of a wave-packet will be given by [103]

$$t^{\mu\nu} = \left\langle -\frac{\partial \mathcal{L}}{\partial(\partial_\mu h_{\alpha\beta})} \partial^\nu h_{\alpha\beta} + \eta^{\mu\nu} \mathcal{L} \right\rangle, \quad (1.34)$$

where the spatial or temporal average $\langle \dots \rangle$ is understood to be taken in a region large enough such that value of $h_{\mu\nu}$ on the boundary is negligible; such an expression is conserved as $\partial_\mu t^{\mu\nu} = 0$ for the field configurations $h_{\mu\nu}(x)$ which satisfies the classical equations of motion.

In such an approach, the Lagrangian which governs the dynamic of the field $h_{\mu\nu}(x)$ can be obtained by expanding the Einstein-Hilbert action (1.1) to quadratic order in $h_{\mu\nu}(x) = g_{\mu\nu}(x) - \eta_{\mu\nu}$. By evaluating the algebra and integrating some terms by parts one obtains [103]

$$\mathcal{L} = -\frac{c^4}{64\pi G} (\partial_\mu h_{\nu\rho} \partial^\mu h^{\nu\rho} - \partial_\mu h \partial^\mu h + 2\partial_\mu h^{\mu\nu} \partial_\nu h - 2\partial_\mu h^{\mu\nu} \partial_\rho h^\rho_\nu) + O(h^3) \quad (1.35)$$

where $h = \eta^{\mu\nu} h_{\mu\nu}$ is the usual trace of $h_{\mu\nu}$. Such a Lagrangian is related to the Pauli-Fierz one by an appropriate rescaling of $h_{\mu\nu}$ [103].

We are now able to evaluate the explicit expression of the energy-momentum tensor $t^{\mu\nu}$ associated to gravitational waves, by specializing formula (1.34) to (1.35). To simplify calculations we choose the gauge [103]

$$\partial^\mu h_{\mu\nu} = 0, \quad h = 0, \quad (1.36)$$

and we perform an integration by parts, possible thanks to the average $\langle \dots \rangle$ [103], of a remaining term $\partial_\gamma h_{\alpha\beta} \partial^\gamma h^{\alpha\beta} \sim -h_{\alpha\beta} \square h^{\alpha\beta}$, which vanishes on the equation of motion $\square h_{\mu\nu} = 0$ which we assume to be fulfilled by our field configuration. In this way we obtain the expression of $t^{\mu\nu}$ we were looking for [103]:

$$t^{\mu\nu} = \frac{c^4}{32\pi G} \langle \partial^\mu h^{\alpha\beta} \partial^\nu h_{\alpha\beta} \rangle. \quad (1.37)$$

From this expression we can evaluate the energy emitted via gravitational waves by a source localized inside a volume V . Recalling that $t^{\mu\nu}$ is a Noether current, which therefore is conserved as $\partial_\mu t^{\mu\nu} = 0$ for on-shell $h_{\mu\nu}$ configurations, we define the gravitational wave energy inside the volume as

$$E_V = \int_V d^3\mathbf{x} t^{00}, \quad (1.38)$$

therefore, assuming all functions to be well behaved and applying Stokes' theorem, this translates into

$$\frac{dE_V}{dt} = -c \int d^3\mathbf{x} \partial_t t^{0i} = -c \int_{\partial V} dA n_i t^{0i}, \quad (1.39)$$

with dA surface element on the boundary ∂V of the integration volume V , and n^i normal vector to the surface [103].

To simplify such an expression, we take ∂V to be a sphere centered on the source, such that $dA = r^2 d\Omega$ and $\hat{n} = \hat{r}$ the radial direction; hence (1.39) becomes

$$\frac{dE_V}{dt} = -\frac{c^5 r^2}{32\pi G} \int d\Omega \langle \partial^0 h_{ij}^{TT} \partial^r h_{ij}^{TT} \rangle = +\frac{c^4 r^2}{32\pi G} \int d\Omega \langle \partial_t h_{ij}^{TT} \partial_r h_{ij}^{TT} \rangle. \quad (1.40)$$

Assuming the gravitational waves, at a large distance, to be propagating out radially outward in the void, we can impose the TT gauge and the metric tensor perturbation takes the form [103]

$$h_{ij}^{TT}(t, r) = \frac{1}{r} f_{ij} \left(t - \frac{r}{c} \right). \quad (1.41)$$

with f_{ij} a function of the retarded time $t_{ret} = t - \frac{r}{c}$, as in electromagnetism. From this last fact it also holds that we exchange the radial partial derivative with the temporal one via the chain rule, therefore expression (1.40) becomes [103]

$$\frac{dE_V}{dt} = -\frac{c^3 r^2}{32\pi G} \int d\Omega \langle \dot{h}_{ij}^{TT} \dot{h}_{ij}^{TT} \rangle + O\left(\frac{1}{r}\right) \quad (1.42)$$

where we have denoted the temporal derivative with the dot, as $\dot{h}_{ij}^{TT} \equiv \partial_t h_{ij}^{TT}$.

Finally, the fact that the energy E_V associated with the gravitational waves inside the volume V decreases, means that there is a flux of gravitational waves which are propagating outward from that volume. In particular the energy carried away by gravitational waves per unit time, as measured at the volume surface, is approximately given by

$$\frac{dE}{dt} = \frac{c^3 r^2}{32\pi G} \int d\Omega \langle \dot{h}_{ij}^{TT} \dot{h}_{ij}^{TT} \rangle. \quad (1.43)$$

A similar expression can be found for the momentum carried away by gravitational waves [103]:

$$\frac{dP^k}{dt} = -\frac{c^3 r^2}{32\pi G} \int d\Omega \langle \dot{h}_{ij}^{TT} \partial^k h_{ij}^{TT} \rangle . \quad (1.44)$$

Furthermore, because the theory is also invariant under spatial rotations, we can define the angular momentum conserved current and charge. As shown in [103], one finds that gravitational waves carry angular momentum too, with contributions both from the orbital angular momentum and from the spin operator: this was to be expected, as gravitons are massless quanta with helicities ± 2 .

1.3.4 — Generation of gravitational waves

In this section we discuss the generation of gravitational waves in the linearized theory: this means we'll consider the gravitational field due to the source to be weak enough, such that the spacetime can still be approximated as flat.

First we'll present the weak-field expansion, which actually doesn't impose any requirements on the velocities into play. Nonetheless later we would like to introduce a low-velocity expansion in powers of $\frac{v}{c}$ to describe the dynamics of non relativistic systems, in order to simplify the setup. Yet the case we're ultimately interested in is of *self-gravitating* binary systems: that is, of bound systems of two bodies evolving under the reciprocal gravitational force. In such cases from Newtonian dynamics it follows [103]

$$\frac{v^2}{c^2} = \frac{Gm}{c^2 r} , \quad (1.45)$$

with m total mass of the system and v the reciprocal velocity between the two bodies. Therefore for such systems the low-velocity expansion in powers of $\frac{v}{c}$ is not independent with respect to the expansion of in powers of G , and so it's not possible to consistently compute corrections beyond the lowest order in $\frac{v}{c}$ while working in the flat space of the linearized theory. This point will be discussed further in section 1.6.

■ Weak-field expansion

In this approximation scheme one assumes that the gravitational field produced by the source is sufficiently weak, such that the background metric can be taken to be flat [103].

To study the generation of gravitational waves in this setting we put ourselves in Lorentz gauge (1.19), where we recall that that the energy-momentum tensor is conserved in the flat space-time sense (1.24), and look for solutions of the linearized Einstein's equations (1.23). Such differential equations are linear in $\bar{h}_{\mu\nu}$ and therefore also in $h_{\mu\nu}$, therefore we can employ the Green's function method to solve them.

The Green's function $G(x)$ is formally the inverse of the differential operator \square , in the sense that it is the solution of

$$\square_x G(x - y) = \delta^{(4)}(x - y) . \quad (1.46)$$

From this follows that

$$\bar{h}_{\mu\nu}(x) = -\frac{16\pi G}{c^4} \int d^4y G(x - y) T_{\mu\nu}(y) \quad (1.47)$$

is a solution of (1.23) [103]. The specific expression of $G(x - y)$ depends on the boundary conditions we wish to impose on the solution, which in turn are related to the physical setting we're trying to describe. In particular, because we want to evaluate the radiation produced by a localized source at

a specific time, we'll impose the Kirchoff-Sommerfeld *no-incoming-radiation* boundary conditions, which single out the so called *retarded Green's function* [103]

$$G(x - y) = -\frac{1}{4\pi|\mathbf{x} - \mathbf{y}|} \delta(x_{ret}^0 - y^0) ; \quad (1.48)$$

where we have defined the *retarded time* as

$$t_{ret}(x, \mathbf{y}) = t - \frac{|\mathbf{x} - \mathbf{y}|}{c} , \quad (1.49)$$

which in flat space time, once chosen a specific reference frame, can be seen as the time at which a light-like signal has to be produced in (t_{ret}, \mathbf{y}) to be seen by an observer in (t, \mathbf{x}) .

As usually one is interested in evaluating the produced radiation in a point outside and far away from the source, that is, in the void, we can simplify the solution (1.47) by putting ourselves in TT gauge (1.26). If furthermore we're far enough with respect to the characteristic length scale of the source, we may also approximate the incoming waterfronsts as plane waves, and therefore the components of $h_{\mu\nu}$ after such a gauge transformation are easily obtained via projection with the Lambda tensor (1.32), as explained before in section 1.3.2. Therefore we obtain

$$h_{ij}^{TT}(t, \mathbf{x}) = \frac{4G}{c^4} \Lambda_{ij,kl}(\hat{\mathbf{n}}) \int d^3\mathbf{y} \frac{1}{|\mathbf{x} - \mathbf{y}|} T_{kl} \left(t - \frac{|\mathbf{x} - \mathbf{y}|}{c}, \mathbf{y} \right) \quad (1.50)$$

where we recall (1.33), and that the direction of propagation of the gravitational plane wave is $\hat{\mathbf{n}} = \frac{\mathbf{x}}{r}$, with $r = |\mathbf{x}|$, as can be seen from figure 1.3 once we choose the origin of our reference frame to be localized inside the source. The fact that only the spatial components of $T_{\mu\nu}$ are needed to find the general solution is due to the energy-momentum tensor conservation (1.24), which is actually a constraint on four components [103].

■ Multipole expansion

The *multipole expansion* lets us express the radiation seen far away from the source as a function of moments of the mass-energy distribution of the source, in such a way to significantly simplify the previous (1.50) expression in the *low-velocity* limit.

To do so, it breaks down the generally complicated integral (1.50) into a sum of simpler terms, each of which encode information about the radial and angular distribution of the source, with higher order moments describing finer details. Nonetheless, for gravitational waves emitted by non relativistic compact binaries, the radiation has a wavelength which is longer than the size of the binary systems, therefore its emission doesn't depend on the finest details of the source internal structure [103]: hence only the first few moments of the multipole expansion, which describe the coarse-grained source distribution, are needed to describe the emission of radiation. This fact lets

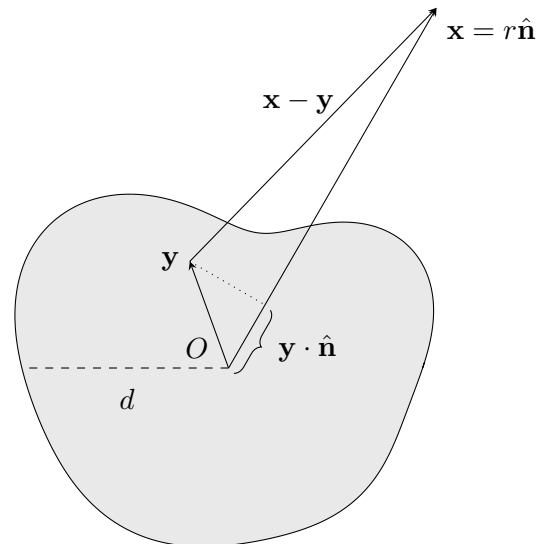


FIGURE 1.3 — A scheme of the quantities employed in the multipole expansion. The origin of the reference frame is denoted with the letter O , the typical length scale of the source with d , the position of the observer with \mathbf{x} , the position, inside the source, over which we're integrating with \mathbf{y} . Figure based on [103].

us simplify some calculations, but from observational point of view it means that using gravitational waves as a probe we may resolve only few internal details of the system, also because the gravitational wave signal at present cannot be measured with a signal-to-noise ratio much higher than a few dozen at most [5]. In the following therefore we'll retain only the first multipoles needed to obtain the desired accuracy.

As we'll see shortly, given a localized source with a typical length scale d , that we could take to be its maximum length, the multipole expansion converges if the source is localized near the origin O of the reference frame, that is $|\mathbf{y}| \lesssim d$; while simultaneously the observer is located far away from it, e.g. at a distance $r = |\mathbf{x}| \gg d$. Furthermore, it is customary to assume that the source is slowly varying, so for example that the compact objects of a binary system are moving at a *non relativistic* speed $\frac{v}{c} \ll 1$: in such a way the typical frequency of the emitted radiation will be of order $\omega \sim \frac{v}{d}$, and corresponding wavelength $\lambda = 2\pi \frac{c}{\omega} \sim \frac{c}{v} d \gg d$, as discussed before. In the following we'll assume such conditions to hold, as outlined in figure 1.3.

The first condition restricts the integration in (1.50) only to the region $|\mathbf{y}| \lesssim d$, as outside the integrand vanishes due to $T_{kl}(\mathbf{y}) = 0$ in the void; the second condition instead is needed to let us expand the distance $|\mathbf{x} - \mathbf{y}|$ in Taylor series:

$$|\mathbf{x} - \mathbf{y}| = r \sqrt{1 - 2 \frac{\hat{\mathbf{n}} \cdot \mathbf{y}}{r} + \frac{\mathbf{y} \cdot \mathbf{y}}{r^2}} = r - \hat{\mathbf{n}} \cdot \mathbf{y} + O\left(\frac{d^2}{r}\right), \quad (1.51)$$

with $\mathbf{x} = r\hat{\mathbf{n}}$ the position of the observer in this reference frame. Substituting the previous expansion in the retarded time definition (1.49), for large distance $|\mathbf{x}| = r \gg 1$ we obtain

$$t_{ret}(x, \mathbf{y}) = t - \frac{|\mathbf{x} - \mathbf{y}|}{c} = t - \frac{r}{c} + \frac{\hat{\mathbf{n}} \cdot \mathbf{y}}{c} + O\left(\frac{d^2}{cr}\right). \quad (1.52)$$

The condition of non relativistic source $v \ll c$, that is, of a energy-momentum tensor $T_{kl}(t_{ret}, \mathbf{y})$ slowly varying in time, let us perform an expansion of the Fourier transformed energy-momentum tensor in (1.50) [103], which is equivalent to Taylor expanding the time argument of $T_{kl}(t_{ret}, \mathbf{y})$ around $s = 0$, as:

$$T_{kl}(t_{ret}, \mathbf{y}) = T_{kl}\left(t - \frac{r}{c} + \frac{s}{c}, \mathbf{y}\right) = \sum_{p=0}^{+\infty} \frac{1}{p!} \left(\frac{s}{c}\right)^p (\partial_t^p T_{kl})\left(t - \frac{r}{c}, \mathbf{y}\right) \quad (1.53)$$

where we defined $s = r - |\mathbf{x} - \mathbf{y}| = \hat{\mathbf{n}} \cdot \mathbf{y} + O\left(\frac{d^2}{r}\right)$, which is of order $s \sim d$, and therefore $\frac{s}{r} \ll 1$.

Substituting all of these expressions in (1.50), keeping only terms up to $o\left(\frac{1}{r}\right)$, we finally obtain:

$$\begin{aligned} h_{ij}^{TT}(t, \mathbf{x}) &= \frac{4G}{c^4} \Lambda_{ij,kl}(\hat{\mathbf{n}}) \int d^3\mathbf{y} \frac{1}{r-s} \sum_{p=0}^{+\infty} \frac{1}{p!} \left(\frac{s}{c}\right)^p (\partial_t^p T_{kl})\left(t - \frac{r}{c}, \mathbf{y}\right) \\ &= \frac{4G}{c^4} \Lambda_{ij,kl}(\hat{\mathbf{n}}) \int d^3\mathbf{y} \frac{1}{r} \left(\sum_{m=0}^{+\infty} \left(\frac{s}{r}\right)^m\right) \left(\sum_{p=0}^{+\infty} \frac{1}{p!} \left(\frac{s}{c}\right)^p (\partial_t^p T_{kl})\left(t - \frac{r}{c}, \mathbf{y}\right)\right) \\ &= \frac{4G}{c^4} \frac{1}{r} \Lambda_{ij,kl}(\hat{\mathbf{n}}) \sum_{p=0}^{+\infty} \frac{1}{p! c^p} n^{i_1} \dots n^{i_p} \int d^3\mathbf{y} y^{i_1} \dots y^{i_p} (\partial_t^p T_{kl})\left(t - \frac{r}{c}, \mathbf{y}\right) + O\left(\frac{1}{r^2}\right) \end{aligned} \quad (1.54)$$

where in the last line we kept only the term with $m = 0$, as $m > 0$ would give terms of order $O(r^{-1-m})$; we traded s for $\hat{\mathbf{n}} \cdot \mathbf{y} = n^i y^i$, as the term $O\left(\frac{d^2}{r}\right)$ produces in the end terms of order at

least $O(\frac{1}{r^2})$, due to the leading $\frac{1}{r}$ factor out of the integral; and we assumed the integrand function to be well behaved as to allow the integral and the series to be swapped. Finally it is understood that $n^{i_1} \dots n^{i_p} = \prod_{q=1}^p n^{i_q}$, to let us explicitly show the contractions in $(\hat{\mathbf{n}} \cdot \mathbf{y})^p = (n^i y^i)^p = \prod_{q=1}^p n^{i_q} y^{i_q} = n^{i_1} \dots n^{i_p} y^{i_1} \dots y^{i_p}$.

Starting from the spatial components of the energy-momentum tensor T_{ij} , also called the stress tensor, it is useful to define its *momenta* $S^{ij, q_1 \dots q_p}$ as [103]:

$$S^{ij, q_1 \dots q_p}(t) \equiv \int d^3 \mathbf{y} y^{q_1} \dots y^{q_p} T^{ij}(t, \mathbf{y}) \quad (1.55)$$

where we can notice that they are position independent, depending only on time, and that they're symmetric in the (i, j) indices, and symmetric under the exchange of any pair of $q_1 \dots q_p$ indices. Therefore, assuming the observer distance r to not depend on time, equation (1.54) becomes:

$$\begin{aligned} h_{ij}^{TT}(t, \mathbf{x}) &= \frac{4G}{c^4} \frac{1}{r} \Lambda_{ij}{}^{kl}(\hat{\mathbf{n}}) \sum_{p=0}^{+\infty} \frac{1}{p! c^p} n^{i_1} \dots n^{i_p} \partial_t^p S^{lk, i_1 \dots i_p} \left(t - \frac{r}{c}, \mathbf{y} \right) \\ &= \frac{4G}{c^4} \frac{1}{r} \Lambda_{ij}{}^{kl}(\hat{\mathbf{n}}) \left(S^{kl} \left(t - \frac{r}{c}, \mathbf{y} \right) + \frac{1}{c} n^q \dot{S}^{kl, q} \left(t - \frac{r}{c}, \mathbf{y} \right) + \frac{1}{2c^2} n^q n^r \ddot{S}^{kl, qr} \left(t - \frac{r}{c}, \mathbf{y} \right) + \dots \right), \end{aligned} \quad (1.56)$$

where each dot over the S^{kl} tensor denotes a temporal derivative, and from now on we'll understand the $O(\frac{1}{r^2})$ subleading term. From this expression we can notice that each additional q index in (1.55) bring an additional $O(d)$ factor, while each time derivative acting on S^{kl} in Fourier space can be seen as a $\omega_s \sim \frac{v}{d}$ factor, which is the characteristic time over which the source varies significantly. Therefore the term of order p in (1.56) is of order $O((\frac{v}{c})^p)$ with respect the leading S^{kl} term [103].

For actual calculations it is easier to employ the *momenta of the energy density* T^{00} , defined as [103]:

$$M^{q_1 \dots q_p}(t) \equiv \frac{1}{c^2} \int d^3 \mathbf{y} y^{q_1} \dots y^{q_p} T^{00}(t, \mathbf{y}) \quad (1.57)$$

where the factor c^{-2} actually gives M the dimension of a mass. Let us notice that the energy density in T^{00} comprises all types of energy: for example the one due to the mass of the source components, due to their kinetic and potential energy, due to the gravitational binding energy [103]. In a similar fashion it's customary to introduce also the momenta of the momentum density $T^{0i} c^{-1}$ as [103]

$$P^{i, q_1 \dots q_p}(t) \equiv \frac{1}{c} \int d^3 \mathbf{y} y^{q_1} \dots y^{q_p} T^{0i}(t, \mathbf{y}) . \quad (1.58)$$

Starting from the flat space energy-momentum tensor conservation (1.24) valid in the weak-field linearized theory, assuming the source distribution to be well behaved and localized in space inside a spatial volume V , and employing Stokes' theorem, we obtain the relations:

$$\begin{aligned} \int_V d^3 \mathbf{y} y^{q_1} \dots y^{q_p} \partial_0 T^{0\mu}(t, \mathbf{y}) &= - \int_V d^3 \mathbf{y} y^{q_1} \dots y^{q_p} \partial_i T^{i\mu}(t, \mathbf{y}) \\ &= - \int_V d^3 \mathbf{y} \partial_i (y^{q_1} \dots y^{q_p} T^{i\mu}(t, \mathbf{y})) + \int_V d^3 \mathbf{y} \partial_i (y^{q_1} \dots y^{q_p}) T^{i\mu}(t, \mathbf{y}) \\ &= - \underbrace{\int_{\partial V} dS^i y^{q_1} \dots y^{q_p} T^{i\mu}(t, \mathbf{y})}_{=0} + \int_V d^3 \mathbf{y} (\delta_i^{q_1} y^{q_2} \dots y^{q_p} + y^{q_1} \delta_i^{q_2} y^{q_3} \dots y^{q_p} + \dots) T^{i\mu}(t, \mathbf{y}) , \end{aligned} \quad (1.59)$$

where we used the fact that $T^{i\mu}(\mathbf{y}) = 0$ on the surface boundary by hypothesis. From these explicitly we get:

$$\dot{M} = 0 , \quad (1.60a)$$

$$\dot{P}^i = 0, \quad (1.60b)$$

$$\dot{M}^i = P^i, \quad \dot{M}^{ij} = P^{i,j} + P^{j,i}, \quad \dot{M}^{ijk} = P^{i,jk} + P^{j,ki} + P^{k,ij}, \quad \dots, \quad (1.60c)$$

$$\dot{P}^{i,j} = S^{ij}, \quad \dot{P}^{i,jk} = S^{ij,k} + S^{ik,j}, \quad \dot{P}^{i,jkl} = S^{ij,kl} + S^{ik,lj} + S^{il,jk}, \quad \dots. \quad (1.60d)$$

The physical meaning of (1.60a) and (1.60b) is respectively that of total mass and total momentum conservation of the system. This actually holds only in the weak-field linearized theory, as such identities are valid only as long as we're neglecting the back-action of gravitational waves on the source [103], which are present in the non-linear full theory and we'd need to take into account at higher order. Similarly $\dot{P}^{i,j} - \dot{P}^{j,i} = 0$ gives the conservation of the total angular momentum of the source [103].

Finally we can employ relations (1.60c) and (1.60d) between the moments of the energy M , momentum P and stress S tensors to express the solution (1.56) as a function of the mass M and momentum P moments only [103]:

$$h_{ij}^{TT}(t, \mathbf{x}) = \frac{4G}{c^4} \frac{1}{r} \Lambda_{ij}{}^{kl}(\hat{\mathbf{n}}) \left[\frac{1}{2} \ddot{M}^{kl} \left(t - \frac{r}{c}, \mathbf{y} \right) + \frac{n^q}{6c} \left(\ddot{M}^{klq} + 2 \left(\ddot{P}^{k,lq} + \ddot{P}^{l,qk} - 2\ddot{P}^{q,kl} \right) \right) \left(t - \frac{r}{c}, \mathbf{y} \right) + \dots \right]. \quad (1.61)$$

This last expression can be evaluated more easily with respect to (1.56), and actually for a set of gravitationally bound point masses it allows to neglect, at order $O\left(\frac{v^2}{c^2}\right)$, the contributions of the gravitational potential and relativistic corrections [103].

From the expression (1.61) we can see that to produce gravitational waves in the weak-field linearized theory we need non vanishing second order or higher time derivatives of the moments of the energy M or momentum P density; also no monopole nor dipole moments of M or P enter in the solution: we can conclude that in the linearized theory there is neither monopole nor dipole radiation for gravitational waves.

These properties show some features which are actually valid beyond the approximations we employed. For example, due to *Birkhoff's theorem*, if the geometry of a given region of spacetime is spherically symmetric and satisfies the full Einstein's equation (1.4) in vacuum, then the geometry must be a piece of the *Schwarzschild metric* [101, 104]. It follows that a source distribution that changes over time, but does so preserving its spherical symmetry, will not emit any gravitational waves; in particular this result is exact in the full theory, and so for example an exactly spherically symmetric star that pulses radially cannot emit any gravitational signal into the surrounding void spacetime [101]. Besides, even in a more general setting, no source distribution can produce monopole or dipole radiation, even in the full theory: this follows from analysis of the non linear theory, but can be understood equivalently by the fact that gravitons are massless particles with helicities ± 2 , hence they cannot be put in states with total angular momentum $j < 2$; therefore we cannot have monopole nor dipole radiation, since they are respectively a collection of quanta with $j = 0$ and $j = 1$ [103].

■ Mass quadrupole radiation

The leading term in (1.61) gives the so called mass quadrupole radiation, as

$$h_{ij}^{TT}(t, \mathbf{x}) = \frac{2G}{c^4} \frac{1}{r} \Lambda_{ij}{}^{kl}(\hat{\mathbf{n}}) \ddot{M}^{kl} \left(t - \frac{r}{c}, \mathbf{y} \right); \quad (1.62)$$

with the mass quadrupole term given by (1.57), so explicitly

$$M^{kl}(t) = \frac{1}{c^2} \int d^3\mathbf{y} y^k y^l T^{00}(t, \mathbf{y}). \quad (1.63)$$

To lowest order in $\frac{v}{c}$ we may neglect kinetic, potential and alike contributions to the energy-momentum tensor: in such a case we can equate $T^{00} \approx \rho c^2$, where ρ is the mass density [103].

To simplify further expression (1.63) one may notice that the symmetric tensor M^{kl} , under the group of spatial rotations, decomposes into irreducible representations as [103]:

$$M^{kl} = \underbrace{\left(M^{kl} - \frac{1}{3} \delta^{kl} M^{ii} \right)}_{\equiv Q^{kl}} + \frac{1}{3} \delta^{kl} M^{ii}, \quad (1.64)$$

where M^{ii} is the trace of M^{kl} , which is a scalar under rotations, whereas Q^{kl} is called the *quadrupole moment*, which is a traceless pure spin-2 operator [103]. Therefore in equation (1.62) we may substitute the \ddot{M}^{kl} tensor with \ddot{Q}^{kl} , as after the contraction with the $\Lambda_{ij,kl}$ tensor only the traceless contribution will be non vanishing.

To explicitly evaluate equation (1.62), let us fix a coordinate frame (x, y, z) and consider a gravitational waves propagating in a generic direction $\hat{\mathbf{n}}$, with components

$$n^i = (\sin(\theta) \sin(\phi), \sin(\theta) \cos(\phi), \cos(\theta)). \quad (1.65)$$

One could then directly compute the $\Lambda_{ij,kl}$ tensor, but it's actually easier to go to a reference frame where the gravitational wave is propagating along a definite axis, to evaluate the quantities and to transform back the tensors via the appropriate rotation matrix, as shown in reference [103]. In particular, introducing such an auxiliary frame with coordinate axis parallel to the orthonormal basis $(\hat{\mathbf{u}}, \hat{\mathbf{v}}, \hat{\mathbf{n}})$, as shown in figure 1.4, while evaluating the M^{kl} tensor in our initial (x, y, z) frame, the amplitudes h_+ and h_\times of the gravitational wave propagating in direction $\hat{\mathbf{n}}$ read [103]

$$h_+(t, \theta, \phi) = \frac{1}{r} \frac{G}{c^4} \left[\ddot{M}_{11} (\cos^2(\phi) - \sin^2(\phi) \cos^2(\theta)) + \ddot{M}_{22} (\sin^2(\phi) - \cos^2(\phi) \cos^2(\theta)) - \ddot{M}_{33} \sin^2(\theta) - \ddot{M}_{12} \sin(2\phi) (1 + \cos^2(\theta)) + \ddot{M}_{13} \sin(\phi) \sin(2\theta) + \ddot{M}_{23} \cos(\phi) \sin(2\theta) \right] \Big|_{t_{ret}}, \quad (1.66a)$$

$$h_\times(t, \theta, \phi) = \frac{1}{r} \frac{G}{c^4} \left[(\ddot{M}_{11} - \ddot{M}_{22}) (\sin(2\phi) \cos(\theta)) + 2\ddot{M}_{12} \cos(2\phi) \cos(\theta) - 2\ddot{M}_{13} \cos(\phi) \sin(\theta) + 2\ddot{M}_{23} \sin(\phi) \sin(\theta) \right] \Big|_{t_{ret}}, \quad (1.66b)$$

where the right-hand side is computed at retarded time $t_{ret} = t - \frac{r}{c}$, and where we recall that such amplitudes are defined with respect to the plane transverse to the propagation of the gravitational waves. In particular, aside from being a superposition of plane waves, they take a form analogous to (1.28) in the frame with axes parallel to $(\hat{\mathbf{u}}, \hat{\mathbf{v}}, \hat{\mathbf{n}})$ [103].

By recalling equation (1.43) it's also possible to evaluate the power emitted by the source via gravitational waves. In particular, as shown in reference [103], the only angular dependence is due

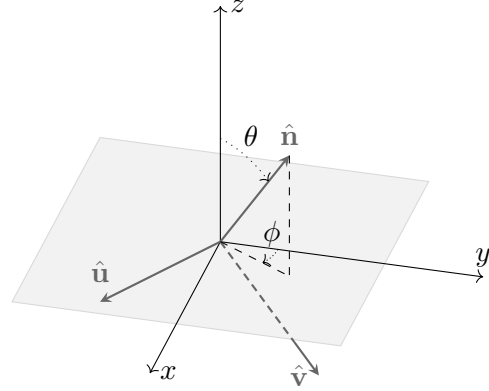


FIGURE 1.4 — A scheme of the coordinate systems employed for the evaluation of mass quadrupole radiation. Notice that the $\hat{\mathbf{u}}$ vector lies in the xy plane, which has been outlined, while the $\hat{\mathbf{v}}$ vector points downwards. Also, to be consistent with [103], we defined the angle ϕ as starting from the y axis and not the x . To obtain the opposite, customary definition, one should substitute $\phi \rightarrow \frac{\pi}{2} - \phi$. Figure based on [103].

to $\Lambda_{ij,kl}(\hat{\mathbf{n}})$, and it holds

$$\Lambda_{ij,kl} \Lambda_{kl,mn} = \Lambda_{ij,mn} , \quad \int d\Omega \Lambda_{ij,kl}(\hat{\mathbf{n}}) = \frac{2\pi}{15} (11\delta_{ik}\delta_{jl} - 4\delta_{ij}\delta_{kl} + \delta_{il}\delta_{jk}) ; \quad (1.67)$$

therefore the total power radiated, also known as total gravitational luminosity of the source, in the quadrupole radiation approximation, is given by [103]

$$P_{quad} = \frac{G}{5c^5} \langle \ddot{Q}^{ij} \ddot{Q}^{ij} \rangle |_{t_{ret}} , \quad (1.68)$$

where the right hand side is evaluated at retarded time $t_{ret} = t - \frac{r}{c}$ as usual.

We can see that, even though the linearized theory predicts the total energy and the total momentum of the source to be conserved, due to (1.60a) and (1.60b), this cannot be true, as the emission of gravitational waves will produce a radiation reaction force on the source itself, as explained in [103], and in particular the energy of the source will decrease per unit time as given by (1.68). Still the previous statement presents a couple of subtleties which makes it valid only for low velocities $\frac{v}{c} \ll 1$ inside the source: equation (1.68) refers only to the quadrupole radiation, which is dominant only in the low-velocity limit; and more importantly, as will be outlined in section 1.6, due to the non linearities of general relativity, at higher orders in perturbation theory it won't be possible anymore to equate the energy carried away by gravitational waves, as measured at infinity at time t , with the energy lost by the source at time t_{ret} .

1.4 | Compact binaries evolution and radiation in linearized theory

In this section, based mostly on [103], we'll apply the concepts developed so far to study the amplitude of gravitational waves emitted by binary systems; finally we discuss also the effects that such an emission has on the evolution of the binary itself.

1.4.1 — Gravitational radiation from non-relativistic point particles

The energy-momentum tensor of a system of n free point particles, labelled by the index $A = 1, \dots, n$, moving in flat spacetime along trajectories $x^{\mu A}(t)$, is given by [103]

$$T^{\mu\nu} = \sum_{A=1}^n \frac{p_A^\mu p_A^\nu}{\gamma_A m_A} \delta^{(3)}(\mathbf{x} - \mathbf{x}_A(t)) , \quad (1.69)$$

where m_A is the mass of particle A , $\gamma_A = \left(1 - \frac{v_A^2}{c^2}\right)^{-\frac{1}{2}}$ its Lorentz factor, and $p_A^\mu = \gamma_A m_A \frac{dx_A^\mu}{dt} = \left(\frac{E}{c}, \mathbf{p}\right)$ its four momentum.

Notice that the requirements of free particles moving along flat space geodesics, that is, $\dot{p}_A^\mu = 0$, is mandatory for the tensor (1.69) to be exactly conserved. Nonetheless we may use the energy-momentum tensor (1.69) to evaluate the gravitational waves at leading order, in the mass quadrupole radiation approximation (1.66), along generic trajectories $\mathbf{x}_A(t)$ for non relativistic point particles, as for a self-gravitating system the gravitational potential energy which should be considered in $T_{\mu\nu}$ is of higher order, because $-\frac{Gm_A m_B}{r_{AB}} \sim O\left(\frac{v}{c}\right)^2$, due to the virial theorem [103].

■ Non-relativistic self-gravitating binary point particle system

For definiteness we'll consider, from now on, the case of a system of two particles, $A = 1, 2$. In the non-relativistic limit $v_A \ll c$ equation (1.69) reads

$$T^{\mu\nu} = \sum_{A=1,2} m_A \frac{dx_A^\mu}{dt} \frac{dx_A^\nu}{dt} \delta^{(3)}(\mathbf{x} - \mathbf{x}_A(t)) + O\left(\frac{v^2}{c^2}\right) . \quad (1.70)$$

We can notice that the hierarchy $T^{00} = O(v^0)$, $T^{0i} = O\left(\frac{v}{c}\right)$ and $T^{ij} = O\left(\frac{v^2}{c^2}\right)$ holds; therefore, as already pointed out in the multipole expansion section 1.3.4, if we trade the stress momenta S for the mass M and momentum P ones, we can work at leading order (and actually also next-to-leading order [103]) without considering interaction terms. Furthermore it holds $\partial_\mu T^{0\mu} = 0$ at lowest order even along trajectories which do not satisfy the equation of motions [103], which at this order would read $\dot{p}_A^\mu = 0$, and therefore the derivation done in the multipole expansion section still goes through, at lowest order, even along generic trajectories.

Working in the non-relativistic case, specifically up to $O\left(\frac{v^2}{c^2}\right)$ order, we can use the classical definition of center-of-mass frame [103]. Therefore we define the relative coordinate as $\mathbf{x}_0 = \mathbf{x}_1 - \mathbf{x}_2$, the center-of-mass coordinate as

$$\mathbf{x}_{CM} = \frac{m_1 \mathbf{x}_1 + m_2 \mathbf{x}_2}{m}, \quad (1.71)$$

with $m = m_1 + m_2$ the total mass, and $\mu = \frac{m_1 m_2}{m}$ the reduced mass. For an isolated system \mathbf{x}_{CM} is not accelerated, therefore such a term won't produce gravitational waves, and hence we can choose the frame where $\mathbf{x}_{CM} = \mathbf{0}$. Such a choice lets us single out, as usual in classical mechanics, only a single degree of freedom, therefore in the center-of-mass frame we can work with just a single effective particle of mass μ and coordinates $\mathbf{x}_0(t)$ [103].

We can now easily evaluate equation (1.63), with $\rho(t, \mathbf{x}) = \mu \delta^{(3)}(\mathbf{x} - \mathbf{x}_0(t))$, which results in a second mass moment and its second time derivative

$$M^{ij}(t) = \mu x_0^i(t) x_0^j(t), \quad \ddot{M}^{ij}(t) = \mu \left(\ddot{x}_0^i(t) x_0^j(t) + 2 \dot{x}_0^i(t) \dot{x}_0^j(t) + x_0^i(t) \ddot{x}_0^j(t) \right). \quad (1.72)$$

where we assumed $\dot{\mu} = 0$. Substituting these results in equations (1.66) we can finally evaluate the gravitational waves produced by such a system in the mass quadrupole radiation approximation. Furthermore, recalling definition (1.64) and defining $r_0^2(t) \equiv \mathbf{x}_0^2(t) = \delta_{ij} x_0^i(t) x_0^j(t)$, the quadrupole moment reads

$$Q^{ij}(t) = \mu \left(x_0^i(t) x_0^j(t) - \frac{1}{3} \delta^{ij} r_0^2(t) \right), \quad (1.73)$$

from which we may obtain the power emitted in the quadrupole radiation approximation employing expression (1.68).

1.4.2 — Quadrupole radiation from a circular binary system

To specify the formulae shown in the previous section to a prototypical scenario of physical interest, even if an idealized one, we will consider a binary system composed of two massive bodies, orbiting each other at non-relativistic speeds, along circular orbits.

Adopting definitions from section 1.4.1, and constructing the center-of-mass frame as described therein, we rotate such a frame so that the orbit lies in the xy plane. Denoting with R the distance between the two bodies, which we still treat as point particles, the relative separation $\mathbf{x}_0(t)$ reads

$$\begin{aligned} x_0(t) &\equiv x_0^1(t) = R \cos\left(\omega_s t + \frac{\pi}{2}\right), \\ y_0(t) &\equiv x_0^2(t) = R \sin\left(\omega_s t + \frac{\pi}{2}\right), \\ z_0(t) &\equiv x_0^3(t) = 0; \end{aligned} \quad (1.74)$$

where we translated the origin of time to be consistent with [103], and we defined the orbital angular frequency as $\omega_s \equiv 2\pi f_s$, with f_s the orbital frequency.

Specializing formula (1.72) to this case we obtain that the only non vanishing second time derivatives of the second mass moment are:

$$\ddot{M}^{11} = -\ddot{M}^{22} = 2\mu R^2 \omega_s^2 \cos(2\omega_s t) , \quad (1.75a)$$

$$\ddot{M}^{12} = \ddot{M}^{21} = 2\mu R^2 \omega_s^2 \sin(2\omega_s t) . \quad (1.75b)$$

We may now substitute such expressions into formulae (1.66), using the same coordinate frame shown in figure 1.4. In particular we may consider a distant observer who is in position $\mathbf{r} = r\hat{\mathbf{n}}$ with respect to the source, and who therefore observes plane waves propagating along direction $\hat{\mathbf{n}}$. In the quadrupole radiation approximation, the amplitudes of the gravitational waves observed at time t , which were therefore produced by the binary system at retarded time t_{ret} , read:

$$\begin{aligned} h_+(t, \theta, \phi) &= \frac{1}{r} \frac{G}{c^4} \left[\ddot{M}_{11} \cos(2\phi) (1 + \cos^2(\theta)) - \ddot{M}_{12} \sin(2\phi) (1 + \cos^2(\theta)) \right] \Big|_{t_{ret}} \\ &= \frac{4}{r} \frac{G}{c^4} \mu R^2 \omega_s^2 \left(\frac{1 + \cos^2(\theta)}{2} \right) \cos(2\omega_s t_{ret} + 2\phi) , \end{aligned} \quad (1.76a)$$

$$\begin{aligned} h_\times(t, \theta, \phi) &= \frac{1}{r} \frac{G}{c^4} \left[2\ddot{M}_{11} \sin(2\phi) \cos(\theta) + 2\ddot{M}_{12} \cos(2\phi) \cos(\theta) \right] \Big|_{t_{ret}} \\ &= \frac{4}{r} \frac{G}{c^4} \mu R^2 \omega_s^2 \cos(\theta) \sin(2\omega_s t_{ret} + 2\phi) . \end{aligned} \quad (1.76b)$$

We can see that for such a system, the frequency of gravitational waves, in the quadrupole radiation approximation, is twice the orbital frequency ω_s ; actually in such an approximation we may define the gravitational wave frequency ω as $\omega \equiv 2\omega_s$. This also means that such an harmonic will dominate the spectrum of gravitational radiation of most binary system; at least until the orbital velocity remains low and the orbital eccentricity negligible; in fact in real, non idealized cases, gravitational waves of different harmonics are also produced [103].

Moreover, as pointed out in reference [103], in the application of formulae (1.76), the angle θ is equivalently denoted as ι , which is the angle between the normal to the orbit and the line of sight of the distant observer. Furthermore, as can be seen from the first equality in each equation of (1.76), the angular dependence $h_+ \sim (1 + \cos^2(\iota))$ and $h_\times \sim \cos(\iota)$ is due to the general structure expression (1.66), hence it's present for all systems with $\ddot{M}_{i3} = 0$ and $\ddot{M}_{22} = -\ddot{M}_{11}$. Also, care should be taken if the observation time is long (of the order of months), as the distance from the observer to the source r may vary due to the Earth motion with respect to the Solar System Baricenter; and also if the source undergoes proper motion, as that could make the angle ϕ vary. Otherwise we may take r and ϕ to be constant; in such cases the angle ϕ cannot be observed and therefore is usually dropped by a redefinition of the origin of time.

Similarly from equation (1.73), noticing that $r_0^2(t) = R^2$, we have

$$\ddot{\ddot{Q}}^{11} = -\ddot{\ddot{Q}}^{22} = -4\mu R^2 \omega_s^3 \sin(2\omega_s t) , \quad (1.77a)$$

$$\ddot{\ddot{Q}}^{12} = \ddot{\ddot{Q}}^{21} = 4\mu R^2 \omega_s^3 \cos(2\omega_s t) ; \quad (1.77b)$$

therefore, recalling formula (1.68), the power emitted via gravitational waves by the binary system, in the quadrupole radiation limit, is given by:

$$P_{circ,quad} = \frac{G\mu^2}{10c^5} R^4 \omega^6 \Big|_{t_{ret}} , \quad (1.78)$$

where we the right hand side is to be evaluated at retarded time t_{ret} .

1.4.3 — Evolution of self-gravitating binary systems

We can now discuss how the back-reaction due to the emission of gravitational waves modifies the dynamics of a binary system. In particular, this discussion is valid only at leading order, in the linearized theory, but the key concepts we'll find are actually there in the full theory.

■ Quasi-circular orbit approximation

As we found previously in equation (1.78), the non relativistic binary system will lose energy (and angular momentum too, as pointed out in section 1.3.3) via emission of gravitational waves. Such energy must necessarily come from within the isolated binary system itself; furthermore, because we're assuming it to be composed of point particles, there are no additional internal degrees of freedom which could release energy. Remarkably, also in a realistic system the internal structure of astrophysical bodies has normal frequencies much higher than the orbital one, at least in the non relativistic regime: hence such internal degrees of freedom effectively do not contribute to the power balance [103].

Taking into account these considerations, we have that we can estimate the total energy of the system, at leading order, by

$$E_{tot} = \frac{1}{2}m_1v_1^2 + \frac{1}{2}m_2v_2^2 - G\frac{m_1m_2}{r_0} = \frac{1}{2}\mu v_0^2 - G\frac{\mu m}{r_0}, \quad (1.79)$$

where $\mathbf{v}_0 \equiv \mathbf{v}_1 - \mathbf{v}_2$. By the virial theorem it follows, as an average over time, that $v_0^2 = \frac{Gm}{r_0}$; this relation is actually exact in the case of circular orbits. Assuming a circular orbit, and accordingly adopting the same notation $R = r_0$ used previously, we take the time derivative of the total energy of the system, obtaining:

$$\dot{E}_{tot,circ} = \frac{1}{2}G\frac{\mu m}{R^2}\dot{R}, \quad (1.80)$$

where we assumed $\dot{m}_1 = \dot{m}_2 = 0$. Hence we see that, to satisfy the leading order energy balance $\dot{E}_{tot,circ} = -P_{circ,quad} < 0$, we must allow the relative distance between the two bodies to decrease $\dot{R} < 0$.

We should now perform calculations akin to the ones presented previously for a system in a decaying orbit. Nonetheless, to simplify the matter, we can recognize that if in the derivation of section 1.4.2 we let the relative distance R between the two bodies vary as a function of time, aside from the $R \rightarrow R(t)$ substitution, the key differences arise is in formulae (1.75) and (1.77), where the time derivative now acts also on $R(t)$, therefore giving $\dot{R}(t)$ and $\ddot{R}(t)$ terms. Actually if the system is self-gravitating, in our limit where Newtonian dynamics can be applied, a time dependent $R(t)$ will induce a time dependent orbital angular frequency $\omega_s \rightarrow \omega_s(t)$, as can be seen by Kepler's third law $\omega_s^2 = \frac{Gm}{R^3}$. Therefore we should also perform the $\omega_s t \rightarrow \phi_s(t)$ substitution in (1.75a), with $\phi_s(t)$ the orbital phase, and hence we'd expect also $\dot{\omega}_s$ and $\ddot{\omega}_s$ terms to appear in the subsequent derivation.

Nevertheless, if the variation of the orbital radius is much slower than the other velocity into play, which is the relative orbital velocity $v_0 = \omega_s R$, these new terms are subleading and may therefore be neglected as a first approximation. This is the so called *quasi-circular motion* approximation: the formulae (1.76) and (1.78) can be applied as a first approximation, even though the relative distance R is not constant anymore, as long as it varies slowly, in the sense that $\dot{R} \ll \omega_s R = v$ and $\ddot{R} \ll \omega_s v$ must hold.

■ Inspiral of a binary system in the linearized theory

From the analysis just presented, we may employ the quasi-circular orbit approximation to evaluate how a binary system, with bodies moving along circular orbits, evolves over time.

First, as we're working in a non-relativistic regime, we have to demand the initial relative distance R to be large enough, so that $v = \omega_s R = \sqrt{\frac{Gm}{R}} \ll c$ can be satisfied. We may then proceed to evaluate the orbital decay rate \dot{R} by resorting to the energy balance, therefore by equating formula (1.80) to the opposite of formula (1.78), obtaining:

$$\dot{R} = -\frac{64 G^3 \mu m^2}{5 c^5 R^3} . \quad (1.81)$$

Nonetheless, because we can measure only the time-varying amplitude and frequency of a gravitational signal, it's better to express all quantities as a function of the gravitational wave angular frequency $\omega = 2\omega_s$, or of its frequency $f_{gw} \equiv \frac{\omega}{2\pi} = \frac{\omega_s}{\pi}$. In such a way equation (1.81) becomes

$$\dot{f}_{gw} = \frac{96}{5} \pi^{\frac{8}{3}} \frac{G^{\frac{5}{3}}}{c^5} M_c^{\frac{5}{3}} f_{gw}^{\frac{11}{3}} ; \quad (1.82)$$

where we defined the *chirp mass* as [103]

$$M_c \equiv \mu^{\frac{3}{5}} m^{\frac{2}{5}} = \frac{(m_1 m_2)^{\frac{3}{5}}}{(m_1 + m_2)^{\frac{1}{5}}} . \quad (1.83)$$

Such quantity has the dimension of a mass and it is usually present in most formula regarding the emission of gravitational waves from binary systems: this is due to the fact that, at least at leading order, the total mass m and the reduced mass μ enter in the observables a distant observer may measure only through the combination (1.83). Therefore such a degeneracy prevents us from estimating the former parameters separately; hence it's better to work only with M_c as it can be measured more precisely.

The solution to these differential equations can be found by employing the method of the separation of variables; e.g. equation (1.81) can be integrated to obtain

$$R(t) = R_{in} \left(1 - \frac{256 G^3 \mu m^2}{5 c^5 R_{in}^4} (t - t_{in}) \right)^{\frac{1}{4}} . \quad (1.84)$$

It's actually useful to change the time variable, analogously to reference [103], adopting the *time to coalescence*:

$$\tau \equiv t_{coal} - t ; \quad (1.85)$$

where t_{coal} is the moment of coalescence. In our leading order approximation we may estimate the latter as the instant when the relative separation becomes zero, that is $R(t = t_{coal}) = 0$; its value is then given by

$$t_{coal} = t_{in} + \frac{5 c^5 R_{in}^4}{256 G^3 \mu m^2} . \quad (1.86)$$

Let us also remember that in general the formulae concerning the source as seen by the distant observer must be evaluated at retarded time t_{ret} ; however, using this time variable we can also overlook the usage of the retarded time, as it holds $\tau = t_{coal} - t = t_{coal} - \frac{r}{c} - t + \frac{r}{c} = t_{coal,ret} - t_{ret}$.

Expressing the radial separation as a function of the time of coalescence we obtain

$$R(\tau) = \left(\frac{256 G^3 \mu m^2}{5 c^5} \right)^{\frac{1}{4}} \tau^{\frac{1}{4}} \approx 83.8 \text{ km} \left(\frac{\mu m^2}{M_{\odot}^3} \right)^{\frac{1}{4}} \left(\frac{\tau}{1 \text{ s}} \right)^{\frac{1}{4}} ; \quad (1.87)$$

it also holds $R(\tau) = R(\tau_{in}) \left(\frac{\tau}{\tau_{in}} \right)^{\frac{1}{4}}$. In equation (1.87), as we'll do again in the following, we explicitly computed the numerical value of such an expression normalizing the parameters to some

typical values, to get a sense of the quantities we're working with. Still let us notice, as pointed out in section 1.2.2, that the compact bodies of astrophysical origin we're most interested in, such as black holes or neutron stars, have masses of at least $M \gtrsim 1.2 M_\odot$: actually for most black holes detected so far we have $M \approx 10 \sim 100 M_\odot$, and for supermassive black holes the mass could get as high as $M \approx O(10^9 M_\odot)$.

Even more useful is the expression for the gravitational wave frequency as a function of time to coalesce $f_{gw}(\tau)$, in the non-relativistic quadrupole radiation approximation, which, integrating (1.82) or equivalently employing Kepler's third law in (1.87), reads:

$$f_{gw}(\tau) = \left(\frac{256 G^{\frac{5}{3}}}{5 c^5} \pi^{\frac{8}{3}} M_c^{\frac{5}{3}} \right)^{-\frac{3}{8}} \tau^{-\frac{3}{8}} \approx 151 \text{ Hz} \left(\frac{M_\odot}{M_c} \right)^{\frac{5}{8}} \left(\frac{1 \text{ s}}{\tau} \right)^{\frac{3}{8}}. \quad (1.88)$$

Finally we can also evaluate the amplitude of the gravitational waves as seen by an observer at a distance r . To do so we can employ equations (1.76), with the substitution $2\omega_s t = \omega_{gw} t \rightarrow \Phi(t)$, where $\Phi(t)$ is the phase of the emitted gravitational waves, or twice the orbital phase, and is given by integrating the time-dependent frequency as [103]:

$$\Phi(t) = \Phi(t_{in}) + \int_{t_{in}}^t dt' \omega_{gw}(t'). \quad (1.89)$$

In our case we can directly integrate (1.88) to obtain

$$\Phi(\tau) = \Phi_0 - \frac{8}{5} 2\pi f_{gw}(\tau) \tau, \quad (1.90)$$

with Φ_0 an integration constant, equal to the phase of the gravitational wave signal at the time of coalescence.

Performing this substitution in equations (1.76), in the non relativistic quadrupole radiation approximation, for the amplitudes of the gravitational waves we obtain:

$$h_+(t) = \frac{4\pi^{\frac{2}{3}} G^{\frac{5}{3}}}{r c^4} M_c^{\frac{5}{3}} f_{gw}^{\frac{2}{3}}(t_{ret}) \left(\frac{1 + \cos^2(\iota)}{2} \right) \cos(\Phi(t_{ret})), \quad (1.91a)$$

$$h_\times(t) = \frac{4\pi^{\frac{2}{3}} G^{\frac{5}{3}}}{r c^4} M_c^{\frac{5}{3}} f_{gw}^{\frac{2}{3}}(t_{ret}) \cos(\iota) \sin(\Phi(t_{ret})), \quad (1.91b)$$

where we dropped the 2ϕ term with respect to the generic formula, as it amounts to a shift of the origin of time, or equivalently to a shift of $\Phi(t_{in})$; and where ι is the angle between the normal to the orbital plane and the observer direction, and is equal to what was denoted as θ in figure 1.4. A numerical estimate of the expected amplitude for gravitational waves, e.g. such that $h_\times(t) = \mathcal{A}(t) \cos(\iota) \cos(\Phi(t_{ret}))$, for a prototypical astrophysical source is given by:

$$\mathcal{A}(t) \equiv \frac{4\pi^{\frac{2}{3}} G^{\frac{5}{3}}}{r c^4} M_c^{\frac{5}{3}} f_{gw}^{\frac{2}{3}}(t) = 3.4 \cdot 10^{-23} \left(\frac{100 \text{ Mpc}}{r} \right) \left(\frac{M_c}{M_\odot} \right)^{\frac{5}{4}} \left(\frac{1 \text{ s}}{\tau} \right)^{\frac{1}{4}}. \quad (1.92)$$

From such an estimate we can notice that the more massive a systems is, the more likely it is to be detected, because the amplitude of the signal it produces is higher. Nonetheless as we'll see in section 1.5, interferometric detectors are most sensitive only in a certain range of frequency, therefore the systems we may detect are limited by both constraints, as a too heavy binary will emit frequencies lower than the ones to which present day interferometers are sensitive.

Fortunately, thanks to the *matched filtering* technique used in the data analysis of the time series recorded by gravitational wave interferometers, as long as we know the shape, or *template*, of the

signal we're looking for, it's not strictly necessary for the signal to have an amplitude higher than the noise at any given moment for it to be detected: it suffices that the integrated signal-to-noise ratio, or some similar statistic, is high enough; therefore also the number of cycles spent in the detector bandwidth plays an important role.

From the previous analysis we can then estimate the number of cycles of the waveform in the time interval $[t_{in}, t_{fin}]$ as

$$N_{cyc} = \frac{1}{2\pi} (\Phi(t_{fin}) - \Phi(t_{in})) = \int_{t_{in}}^{t_{fin}} dt' f_{gw}(t') = \int_{f_{gw,min}}^{f_{gw,max}} df_{gw} \frac{f_{gw}}{f_{gw}}. \quad (1.93)$$

We can evaluate the last integral recalling (1.82), to obtain

$$N_{cyc} = \frac{\pi^{-\frac{8}{3}}}{32} \left(\frac{c^3}{G}\right)^{\frac{5}{3}} M_c^{-\frac{5}{3}} \left(f_{gw,min}^{-\frac{5}{3}} - f_{gw,max}^{-\frac{5}{3}}\right) \approx 2.2 \cdot 10^4 \left(\frac{1 M_\odot}{M_c}\right)^{\frac{5}{3}} \left(\frac{10 \text{ Hz}}{f_{gw,min}}\right)^{\frac{5}{3}}, \quad (1.94)$$

where we assumed $f_{gw,min} \ll f_{gw,max}$, as this is usually the case [103].

For example in the analysis of the signal from the first observed binary neutron star system, up to 4200 waveform cycles were used, thereby greatly increasing the accuracy of the estimated parameters [146]. For next generations detectors, such as LISA, it's actually expected that in particular cases, e.g. for an *extreme mass ratio inspiral* (EMRI), as could be the inspiral of a black hole of mass $m_2 = O(10 M_\odot)$ into a supermassive black hole of mass $m_1 = O(10^6 M_\odot)$, up to $N_{cyc} = O(10^4 \sim 10^5)$ of waveforms cycles could lie in the detector's sensitive frequency range [147].

To exemplify what we've seen so far, in figure 1.5 we plotted the most relevant quantities derived in this section for a prototypical system which may be detected by present date gravitational wave observatories. From the plots we can explicitly see that initially the radius decreases slowly, as the power lost via gravitational waves is relatively small; as times goes on the system inspirals ever so fast, as the rate of orbital decay increases, until we approach the plunge phase: now the orbital separation is really small and decreases very rapidly due to strong gravitational wave emission. Simultaneously the frequency of the gravitational waves progressively increases, as does the amplitude, resulting in the so called *chirp* signal. Still, as we'll see in section 1.4.4, the accuracy of our approximations degrades as we get closer to the merger: in the last seconds we may trust the plots in figure 1.5 only to understand the trend of the evolution of the binary system, as the evaluation of those quantities would by then require different approximation schemes, as will be outlined in section 1.6.

■ Corrections due to cosmological redshift and orbital eccentricity

The analysis we have presented so far assumed a static flat spacetime, in addition to the fact that the source frame and the observer frame where not moving relative to each other. Such assumptions apply only if the source is close enough and its center of mass is moving relatively slowly with respect to the observer, so that the cosmological and the doppler redshifts can be neglected: hence the time as measured in both the source and the observer frame is equivalent; and so is also the time to coalescence as measured in the source frame, τ_{source} , with respect to the one measured by the observer, τ_{obs} . Quite the opposite, most of the binary systems which have been currently detected are quite far away, at *cosmological redshift* of $z = O(0.1 \sim 1)$ [5], which therefore cannot be neglected if we aim for accurate estimates.

Nonetheless, if we assume a spatially flat Friedmann-Robertson-Walker universe, the formulae reported in this section still hold once we perform the following replacements: $\tau \rightarrow \tau_{obs}$, as we work with the observer time; $r \rightarrow d_L(z)$, where d_L is the luminosity distance of the source; and

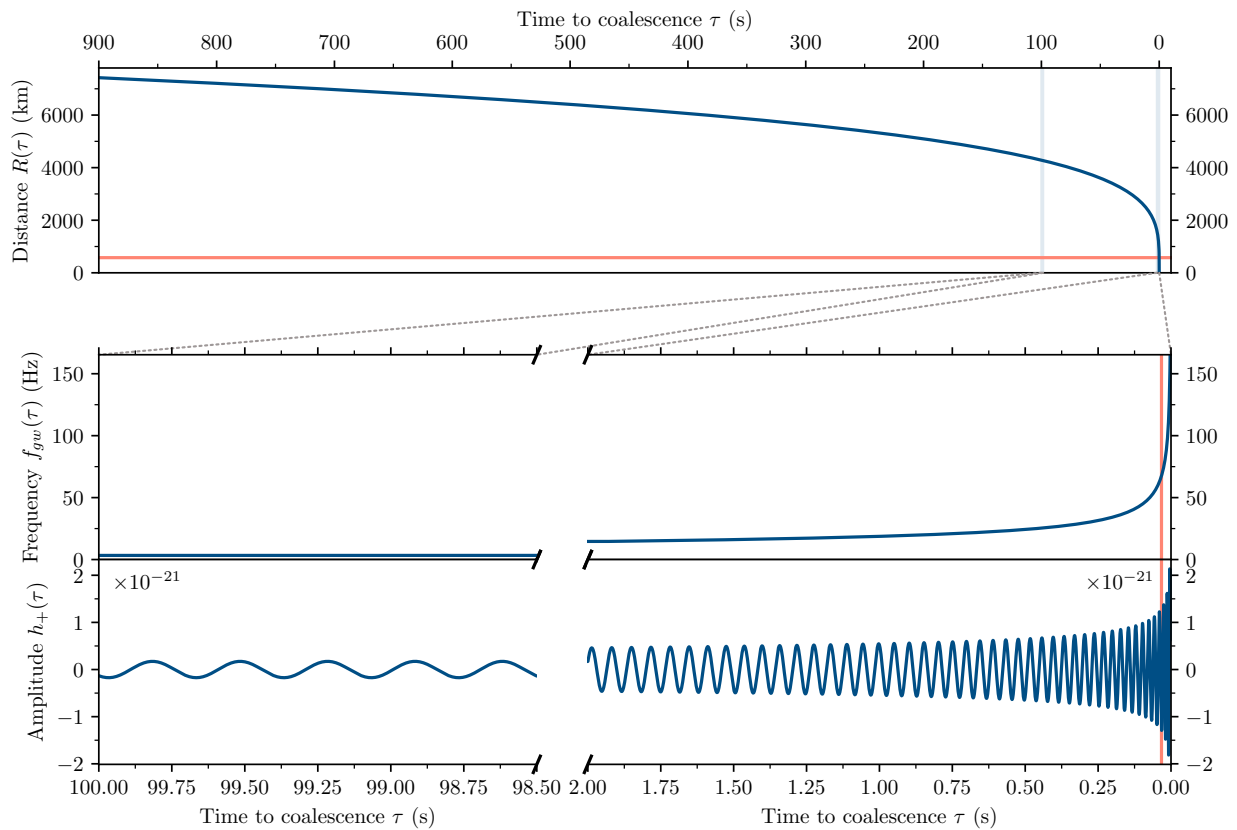


FIGURE 1.5 — Plots of several quantities regarding the evolution of a prototypical binary system and the gravitational waves it emits during the last stage of the inspiral phase. They were evaluated using the formulae presented in this section, in the context of the quadrupole approximation in the linearized theory, for quasi-circular orbits.

In the top panel we show the relative separation between the two bodies $R(\tau)$, in the middle panel the frequency of the emitted gravitational waves $f_{gw}(\tau)$, while in the bottom panel we show the amplitude $h_+(\tau)$ of the gravitational wave signal as it would have been measured by the distant observer; all of these as a function of the time to coalescence τ . In particular for the top we consider the last 900 s before coalescence; whereas in the middle panel and in the bottom panel we zoom into two short time intervals: on the left we consider $\tau \in [100, 98.5]$ s, while on the right we consider $\tau \in [2, 0]$ s, just before coalescence.

For the binary system we assumed as parameters $m_1 = 35M_\odot$, $m_2 = 30M_\odot$, $r = 400$ Mpc, $\Phi_0 = 0$ rad and $\iota = 0$ rad; therefore we assume to be observing the system along the normal to the orbital plane. The parameters were thus chosen so as to allow a comparison with a system similar to the one discovered with the first gravitational wave signal detection [1, 2], for example shown also in figure 1.1.

To be precise at such a distance the cosmological redshift is $z \sim 0.1$, therefore we would have needed to apply the corrections which will be discussed in the following; nonetheless for clarity of exposition we simply plotted the non-redshifted formulae with the aforementioned parameters.

Let us notice that the closer we are to coalescence, the less accurate our approximations and therefore our estimates will be: in particular we cut off the frequency and amplitude plot in the right panels at $\tau = 3$ ms, as otherwise they would have diverged. Physically this is not the case, hence this signal the breakdown of our formulae: this actually happens even before, for example when the system reaches the Innermost Stable Circular Orbit (ISCO), as discussed in section 1.4.4. For reference we plotted the moment when such point is reached: in the top panel the horizontal red line shows the value of $R_{ISCO} = 576$ km, while in the middle and bottom panels the vertical red lines indicate the time $\tau_{ISCO} = 33$ ms.

Still, although our formulae aren't so accurate, the plot can be useful to understand the trend of the evolution of the binary system: in particular we can see that, due to the ever increasing power lost via gravitational waves, the relative distance decays increasingly fast, while the frequency and the amplitude of the gravitational waves become increasingly higher and louder, in what's called a chirp signal. This is the behaviour to be expected for the inspiral phase of the system, while for the evolution in its last moments we may refer to figure 1.1, which reports results from an accurate numerical relativity simulation. Finally it will be interesting to compare these plots with figure 6.1, which shows the effect of the 2PN corrections on this systems.

$M_c \rightarrow \mathcal{M}_c \equiv (1+z)M_c$, with \mathcal{M}_c the redshifted chirp mass. In fact from the detection of a gravitational wave signal one can extract the redshifted masses, hence with chirp mass one refers to \mathcal{M}_c ; also the masses of each compact object m_1 , m_2 , the total mass m and the reduced mass μ have to be redshifted, i.e. multiplied by a $(1+z)$ factor. Still, once one assumes a cosmological model, it's possible to evaluate the quantities as they would have been measured in a frame near the source; for example the masses so corrected are denoted as *source masses* [5].

We may also expect most binary system to start in an *eccentric orbit*, and therefore we would like to gather to what extent the analysis of the quasi-circular motion carries over: it's in fact possible to derive quantitative results, as shown in [103], by following a procedure analogous to the circular orbits case. Doing so we would find that an eccentric orbit increases the power emitted via gravitational waves, as near the periastron the accelerations that come into play are now larger, and that the frequency spectrum of the emitted gravitational radiation now comprises all harmonics of the orbital frequency.

Still the most interesting fact is that, because gravitational waves carry away energy and angular momentum, as we've seen in section 1.3.3, the eccentricity of the orbit decreases substantially over time. Hence the effect of gravitational waves is to *circularize* the orbit, up to the point that, if not other mechanism counteract such an effect, the eccentricity of the orbit at the end of the inspiral phase will be almost vanishing to an high accuracy [103]: therefore in the last inspiral stage, where the amplitude is higher and so is our chance to detect such systems, the circular orbit approximation may be well satisfied by many astrophysical systems. At last, given two systems which initially have the same orbital periods, one in a circular and one in an elliptic orbit, the time to coalescence for the elliptic system is lower compared to the former one.

1.4.4 — Regime of validity of the approximations employed

We'd like finally to discuss the extent to which we may trust the formulae presented up until now, in the last sections, to make explicit the need of higher order corrections or different approximations schemes altogether, which will be outlined in section 1.6.

To summarize, the assumptions we made are the ones of be working in a weak-field and low-velocity regime, with quasi-circular orbits; hence to hope for our estimates to be accurate we must check when we satisfy such conditions.

The weak-field and low velocity assumptions require, for a self-gravitating system, $\frac{v}{c} = \omega_s \frac{R}{c} = 0.025 \left(\frac{f_{gw}}{1 \text{ Hz}} \frac{m}{M_\odot} \right)^{\frac{1}{3}} \ll 1$, which therefore reads $f_{gw} \ll 65 \text{ kHz} \left(\frac{M_\odot}{m} \right)$, or $\tau \gg 0.1 \mu\text{s} \left(\frac{m}{\mu} \frac{m}{M_\odot} \right)$. This can be cast equivalently into $\frac{v}{c} = \frac{1}{\sqrt{2}} \sqrt{\frac{R_s}{R}} \ll 1$, so $R \gg \frac{R_s}{2}$, where R_s is the Schwarzschild radius associated to the total mass m of the system as in equation (1.5); hence we can see that the farther apart are the bodies, the more accurate our estimates will be, as we were expecting.

The quasi-circular motion approximation holds instead as long as $\dot{R} \ll R\omega_s$, or equivalently $\dot{\omega}_s \ll \omega_s^2$, which numerically reads $\tau \gg 0.01 \text{ ms} \left(\frac{M_c}{M_\odot} \right)$ or $f_{gw} \ll 10 \text{ kHz} \left(\frac{M_\odot}{M_c} \right)$. These conditions are hence satisfied until the last stages of the binary evolution for most astrophysical system of interest, and formally the breakdown happens when $R \sim O(R_s)$, as found before. Nonetheless we must point out that, especially for events that will stay in the detector bandwidth for many cycles, the really high accuracy needed for the waveforms requires higher order corrections even well before the end of the inspiral phase.

We can further study the regime of validity of our expansion by comparing the results we found with similar ones obtained in the full theory, in which we can exactly probe also the strong field regime. For example, consider the Schwarzschild solution for non rotating and non charged spherically

symmetric compact objects: it exhibits a value of the radial coordinate r below which no massive test body can continue to orbit the bigger compact object. Such last possible orbit is called *Innermost Stable Circular Orbit*, or ISCO, and the value for the radial coordinate is given by

$$R_{ISCO} = \frac{6Gm}{c^2} \approx 8.86 \text{ km} \left(\frac{m}{M_\odot} \right). \quad (1.95)$$

with m the total mass of the binary; it is three times the associated Schwarzschild radius, $R_{ISCO} = 3R_s$. Actually expression (1.95) is exact only in the test mass limit, e.g. $m_2 \rightarrow 0$ [103], and for bodies with vanishing spin, otherwise corrections are due. Let us also notice that the radial coordinate r of the Schwarzschild metric does not correspond per se to the radial coordinate we adopted in the linearized theory; nonetheless if we equate their numerical values and compute observables, the results we may obtain are of the same order of magnitude of the results one can obtain evaluating the same observables in the exact Schwarzschild metric [103].

By employing Kepler's third law we obtain that, when the system relative distance is $R = R_{ISCO}$, the frequency of the emitted gravitational waves is

$$f_{gw,ISCO} = \frac{6^{-\frac{3}{2}} c^3}{\pi G m} \approx 4.4 \text{ kHz} \left(\frac{M_\odot}{m} \right); \quad (1.96)$$

while correspondingly the time left to coalescence, in our approximation, reads

$$\tau_{ISCO} = \frac{405 G m^2}{16 c^3 \mu} \approx 0.125 \text{ ms} \left(\frac{m}{\mu} \frac{m}{M_\odot} \right); \quad (1.97)$$

for reference we also reported such quantities in figure 1.5, for the system under consideration therein.

Therefore after this limit we can consider our approximations to no longer be accurate, as for sure no circular orbit can be sustained any longer, contrary to what Newtonian dynamics would predict. In fact when the compact objects are so close to each other the flat space approximation cannot hold anymore, as the respective gravitational field is too strong, and general relativistic effect become dominant, marking the transition to the plunge phase. Moreover in section 1.6 we'll see that the physics which characterize the following phases is so drastically different from the one we described so far that it's necessary to adopt different approximation schemes altogether.

1.5 | Gravitational waves detectors

As outlined in section 1.2.1, historically there have been several attempts to create instruments capable of detecting gravitational waves: nonetheless their amplitude is so faint that only interferometric detectors, which offer an exquisite sensitivity over a quite large frequency band (about two-three frequency decades), are capable of detecting them. Actually there are exceptions to the above statement: the pulsar timing arrays work in a similar way to the interferometers, looking for the perturbation which gravitational waves add on the arrival time of signal emitted with a known, constant frequency, in this case by millisecond pulsars (neutron stars rotating with an incredible steadiness) [134]; and also by observing CMB data we may be able to directly infer the energy density and power spectrum of primordial tensor perturbations (for example gravitational waves created during inflation) [129].

Focusing on the interferometer detectors, their working principle is that a gravitational wave passing in the instrument will modify the relative phase between two laser beams, which had been traveling along the two perpendicular arms [103, 113]. Therefore, when the two laser beam recombine at the beam splitter, the relative phase acquired will create an interference pattern, modulating the

power which is seen at the antisymmetric port of the interferometer, which otherwise is adjusted to be (almost) dark [103]. By analyzing this output therefore it's possible to reconstruct the temporal evolution of the amplitude and the phase of gravitational wave signals with frequency from a few tens to few hundreds of Hz (in ground based interferometers). We can notice that the bandwidth of interferometers is quite large, and that they can be built to be sensitive to frequencies relevant in the inspiral and merger of astrophysical compact object binaries.

■ Noise sources

The limits to the sensitivity of these detectors are due to several noise sources [103]: at low frequency the limiting factors are the *radiation pressure noise*, due to the fluctuating radiation pressure exerted by the photons of the laser beam (as their number fluctuates according to the Poisson distribution); several sources of *thermal noise*, which induce vibrations in key components of the detector; the *seismic noise*, due to the motion of the Earth's ground, which can be attenuated by a suitable suspension system; the *Newtonian noise*, which is due to the time-varying gravitational force exerted on the instrument by moving masses which are surrounding the detectors (as could be also the atmospheric turbulence) and physically cannot be screened, as it couples to the detector just like a gravitational wave would. At high frequency instead the limiting factor is the laser *shot noise*: to measure the signal at high frequency we need to count the number of photons impinging on the photodetector in a short time frame; then also in this case we're limited by the Poissonian error due to the finite number of photons. Let us notice that if we were to increase the power of the circulating laser to attenuate the *shot noise*, we would increase the *radiation pressure noise* (and actually also the mirror thermal noise): then both noise sources are collectively denoted as *quantum noise*, and this trade-off implies the standard quantum limit on the sensitivity of the instrument (which however may be circumvented using frequency dependent quantum squeezing).

Mathematically the total amount of noise in a gravitational wave detector is quantified, in frequency space, by the noise power spectral density $S_n(f)$, or by its square root, the amplitude spectral density $\sqrt{S_n(f)}$ [103, 148]. In particular, if $n(t)$ is the irreducible noise recorded as output of the detector, assuming it to be *stationary*, we define the single sided noise power spectral density as

$$\langle \tilde{n}^*(f) \tilde{n}(f') \rangle \equiv \frac{1}{2} \delta(f - f') S_n(f) ; \quad (1.98)$$

where $\tilde{n}(f)$ is the Fourier transform of $n(t)$, and $\langle \cdot \rangle$ denotes the ensemble average. Then lower is the value of this quantity at a given frequency f , the more sensitive the instrument will be to signals of that frequency.

To suitably deal with the aforementioned noise sources, in order to actually reach the exquisite sensitivity required for detecting gravitational waves, present-day detectors use a much more complex design than what we've previously sketched, and which is called the Dual-recycled Fabry-Perot Michelson interferometer [103, 149]. In particular Fabry-Perot arm cavities are employed to increase the laser power circulating in the arms, while other cavities and laser mode filters are employed to enhance the signal even more, which is actually encoded in sidebands of the carrier laser signal [103]. Most recently frequency-dependent quantum squeezing is being implemented in the advanced stage [149, 150] of current (second generation) interferometers to reduce shot noise and quantum radiation pressure [151]. Newtonian noise mitigation is in the study as well for third generation detectors, such as Einstein Telescope in Europe [152]: to reduce this source of noise, some next generation detectors will probably be built underground. Detectors of gravitational waves at even lower frequencies, below the Hz, are planned, but due to seismic noise they're feasible only in space: this is the concept of the Laser Interferometer Space Antenna (LISA) [91]. Such a mission has also the potential to study quantities and phenomena of interest in cosmology [126], such as the presence of a cosmological stochastic gravitational wave background: among other things it could

probe gravitational waves produced in some inflationary scenarios [127, 128] in a complementary way with respect to the usual study of the B modes of the CMB [129].

■ Matched filtering technique

A quite remarkable point is that, at any given moment in time, the amount of noise in a detector is in practice always higher than the signal which we expect from typical binary sources. What allows us to actually spot a real signal in the noise is the *matched filtering* technique.

This technique is based on the fact that time series which is output of the detector $o(t)$ (which we take to be the dimensionless strain), at any moment in time, will be given by the sum of the noise in the detector $n(t)$, and eventually by the signal $h(t)$ due to an impinging gravitational wave (this latter signal is actually modulated by the transfer function of the detector); so $o(t) = n(t) + h(t)$. Then if we have a *template* $\bar{h}(t)$ for the waveform of the signal we're looking for and that we expect to find in the detector, we can multiply together the output of the detector by the template and average over time, to obtain [103]:

$$\frac{1}{T} \int_0^T dt o(t) \bar{h}(t) = \underbrace{\frac{1}{T} \int_0^T dt n(t) \bar{h}(t)}_{\propto T^{-\frac{1}{2}} \rightarrow 0} + \underbrace{\frac{1}{T} \int_0^T dt h(t) \bar{h}(t)}_{\propto \text{const}} ; \quad (1.99)$$

where the first integral in the right hand side oscillates asymptotically to zero, since the noise and the waveform are uncorrelated (i.e. $\int dt n(t) \bar{h}(t) \propto T^{\frac{1}{2}}$ due to its random walk behavior), while the second term will average to a constant value (the average value of $h^2(t)$).

It can be shown that the matched filtering is an optimal technique for extracting a known signal from a noisy output when we adopt as Wiener filter $K(f) \propto \frac{\bar{h}(f)}{S_n(f)}$, i.e. the signal h itself weighted by the power spectral density (1.98). As a consequence of this, one introduces the corresponding whitened quantities, such as the *whitened strain*: this is defined as the output of the detector weighted by the amplitude spectral density $\frac{\tilde{o}(f)}{\sqrt{S_n(f)}}$; and so gives more relevance to the frequencies of the signal which we can better observe. In fact this is the quantity that it's routinely employed during the analysis (to which other filters are also applied) [153], and the template that's used in the research is the whitened template.

Let us now better formalize these concepts, extending them also to the case of signals collected by N detectors (as seeing the same signal in coincidence between different detector greatly increase our confidence about its astrophysical origin) [154, 155]. Then let us denote with $\mathbf{g} = \{g_\alpha(t)\}_{\alpha=1, \dots, N}$ the vector containing the N signals, one for each of the detectors. Then we can introduce the scalar product between two such vectors \mathbf{g} and \mathbf{k} as:

$$(\mathbf{g} | \mathbf{k}) \equiv 2 \int_0^{+\infty} df [S_n(f)^{-1}]^{\alpha\beta} \left(\tilde{g}_\alpha^*(f) \tilde{k}_\beta(f) + \tilde{g}_\alpha(f) \tilde{k}_\beta^*(f) \right) ; \quad (1.100)$$

where for example $\tilde{g}_\alpha(f)$ represents the Fourier transform of the corresponding $g_\alpha(t)$ signal, and $[S_n(f)^{-1}]^{\alpha\beta}$ is the matrix of the power spectral noise density for the noise (auto)correlation between several detectors, which generalizes equation (1.98):

$$\langle \tilde{n}_\alpha^*(f) \tilde{n}_\beta(f') \rangle \equiv \frac{1}{2} \delta(f - f') S_n(f)_{\alpha\beta} . \quad (1.101)$$

With these definitions we can evaluate the ideal signal-to-noise ratio for a given gravitational waveform \mathbf{h} as [103, 155]:

$$\frac{S}{N}[\mathbf{h}] \equiv \sqrt{(\mathbf{h} | \mathbf{h})} . \quad (1.102)$$

In this case the signal-to-noise ratio (SNR) quantifies the strength of the signal with respect to the background noise; roughly speaking, during gravitational wave searches, candidate events are recognized as such when their signal-to-noise ratio is above $\text{SNR} > 8$.

Finally let us point out that in practice, in order to achieve this optimal signal-to-noise ratio, and so a high probability of detecting a candidate signal, the template must closely match the actual signal due to the real gravitational wave (i.e. $\bar{\mathbf{h}} = \mathbf{h}$). This is one of the several reasons why more accurate waveform models are needed for next generation gravitational wave observatories (and hence why post-Newtonian corrections are important). Furthermore, regarding the online search analysis of gravitational events, to perform the aforementioned matched filtering analysis, a large template bank has been created: in this way the signal recorded by gravitational wave observatories is almost instantaneously compared with millions of precomputed waveform templates, which sample densely enough the parameter space.

1.5.1 — Interaction of gravitational waves in linearized theory

Here we will briefly outline which is the response of an idealized interferometric detector to a gravitational wave passing by.

To do so it useful to move in TT gauge: in this frame any test-mass with constant spatial coordinates ($x^i = \text{const}$) will actually be moving along its geodesic (so it may describe a test mass which is not under the influence of any external force) [103]. Then the perturbations due to the gravitational wave is actually encoded in the varying spacetime interval Δs^2 between two spacetime events: we see that in order to detect this perturbation of the spacetime we actually need to compare the invariant distance of at least two objects (as dictated by the Einstein's equivalence principle and the geodesic deviation equation); whereas the value of the coordinates x^μ by themselves are not physically meaningful in general relativity.

Let us point out that for ground-based interferometers the approximation of considering the suspended mirrors as test masses is quite good: in fact these mirrors do not move along the geodesics as the suspension system, which keeps them from falling into the ground, exert on them an external force; yet when working in Fourier space, for the frequencies of interest, they behave as if they were freely falling test masses. On the other hand space-based observatories, such as LISA, will actually provide an almost exact realization of freely falling test masses, as the spacecraft will actually follow the geodesic of an almost unperturbed cubic test mass inside of it; used as the reference point to perform interferometric measurement.

We may then consider a coordinate frame in which one of the two ends (e.g. the mirror or the beam splitter) of one of the arms of the interferometer is placed at the origin, $x_1^\mu = (t, \mathbf{0})$ (in fact up to higher order corrections the proper time of a still test mass in TT gauge is equivalent to the coordinate time t [103]), while the other one is placed in position \mathbf{l} , so $x_2^\mu = (t, \mathbf{l})$. Then we have to consider the electromagnetic wave (i.e. the laser light) travelling between these two end points, along a null geodesic $ds^2 = 0$. In TT-gauge, i.e. under the constraints (1.26), the definition (1.6) becomes:

$$ds^2 = g_{\mu\nu} dx^\mu dx^\nu = -c^2 dt^2 + (\delta_{ij} + h_{ij}^{TT}(t, \mathbf{x})) dx^i dx^j ; \quad (1.103)$$

and therefore along the null geodesic it holds $c^2 dt^2 = (\delta_{ij} + h_{ij}^{TT}(t, \mathbf{x})) dx^i dx^j$. We define with $L = |\mathbf{l}| = \sqrt{\delta_{ij} \hat{l}^i \hat{l}^j}$ the spatial distance between the two end points x_1 and x_2 , and expand at linear order in $h_{\mu\nu} \ll 1$ the previous relation along $dx^i = \hat{l}^i L du$, with $\hat{\mathbf{l}} \equiv \frac{\mathbf{l}}{|\mathbf{l}|}$ and $0 \leq u \leq 1$, obtaining:

$$dt = du \frac{L}{c} \left(1 + \frac{1}{2} h_{ij}^{(TT)}(t, \mathbf{x}) \hat{l}^i \hat{l}^j + \mathcal{O}(h^2) \right) . \quad (1.104)$$

We now define as $T \equiv \frac{L}{c}$ the propagation time from x_1 to x_2 for a light signal in the unperturbed spacetime (so in absence of gravitational waves), denoting instead with ΔT the delay or speed up due to the presence of a gravitational wave perturbation. Then, assuming the electromagnetic wave to start in x_1 at time t , we can integrate (1.104) to find:

$$\begin{aligned} T + \Delta T(t) &= \int_0^{T+\Delta T(t)} d\tilde{t} = \frac{L}{c} \int_0^1 du \left(1 + \frac{1}{2} h_{ij}^{(TT)}(t(u), \mathbf{x}(u)) \hat{l}^i \hat{l}^j \right) + \mathcal{O}(h^2) \\ &= \underbrace{\frac{L}{c}}_{=T} + \frac{L}{2c} \int_0^1 du h_{ij}^{(TT)}(t(u), \mathbf{x}(u)) \hat{l}^i \hat{l}^j + \mathcal{O}(h^2), \end{aligned} \quad (1.105)$$

where we evaluate $h_{ij}^{(TT)}$ at position $(t(u), \mathbf{x}(u))$ assuming the propagation of the light beam in the absence of gravitational waves, up to higher order corrections; i.e. $t(u) = t + Tu$ and $\mathbf{x}(u) = \hat{\mathbf{I}} Lu$.

We may now restrict ourselves to useful case of a far away localized source of gravitational waves, which then propagate in direction $\hat{\mathbf{n}}$ towards us (hence the system is located in direction $-\hat{\mathbf{n}}$ for the observer). Then we may recall equation (1.30) and the $(\hat{\mathbf{u}}, \hat{\mathbf{v}}, \hat{\mathbf{n}})$ orthonormal frame defined in that section; from relation (1.105) we find:

$$\begin{aligned} \Delta T(t, \hat{\mathbf{l}}) &= \frac{L}{2c} \hat{l}^i \hat{l}^j \int_{-\infty}^{+\infty} df \int_0^1 du \left(\tilde{h}_+(f) e_{ij}^+(\hat{\mathbf{n}}) + \tilde{h}_\times(f) e_{ij}^\times(\hat{\mathbf{n}}) \right) e^{-i2\pi ft} e^{-i2\pi fu(T - \frac{L}{c} \hat{\mathbf{n}} \cdot \mathbf{l})} + \mathcal{O}(h^2) \\ &= \frac{L}{2c} \hat{l}^i \hat{l}^j \int_{-\infty}^{+\infty} df \left(\tilde{h}_+(f) e_{ij}^+(\hat{\mathbf{n}}) + \tilde{h}_\times(f) e_{ij}^\times(\hat{\mathbf{n}}) \right) e^{-i2\pi f(t + \frac{T}{2}(1 - \hat{\mathbf{n}} \cdot \mathbf{l}))} \text{sinc} \left(\pi f \frac{L}{c} (1 - \hat{\mathbf{n}} \cdot \mathbf{l}) \right), \end{aligned} \quad (1.106)$$

where we used the identity $\int_0^1 du e^{iCu} = \frac{1}{iC} (e^{iC} - 1) = \frac{e^{\frac{i}{2}C}}{iC} (e^{\frac{i}{2}C} - e^{-\frac{i}{2}C}) = e^{\frac{i}{2}C} \text{sinc}(\frac{C}{2})$, with $\text{sinc}(x) \equiv \frac{\sin(x)}{x}$ and $\text{sinc}(0) = 1$.

Then in a simplified setup of an idealized Michelson interferometer, to observe gravitational waves we compare the round trip time for the laser light along two perpendicular arms of (almost) equal length L , which we may denote as a and b . For definiteness we may assume arm a to lie on the $\hat{\mathbf{x}}$ axis, such that $\hat{\mathbf{l}}_a = \hat{\mathbf{x}}$, and arm b to lie on the $\hat{\mathbf{y}}$ axis, such that $\hat{\mathbf{l}}_a = \hat{\mathbf{y}}$. Then, using equation (1.106) we find the round trip for the light in the first arm to be given by $\Delta T_a(t) = \Delta T(t - \frac{2L}{c}, \hat{\mathbf{x}}) + \Delta T(t - \frac{L}{c}, -\hat{\mathbf{x}})$, and similarly for other arm $\Delta T_b(t)$. Finally, taking the difference between these round trip times $\Delta T_a(t) - \Delta T_b(t)$ we can evaluate (multiplying by the laser frequency) the observable shift in the phase of the two laser beams as they join at the beam splitter. In particular, dividing instead this time difference $\Delta T_a(t) - \Delta T_b(t)$ by the total round trip time $2T$, we can recast this observable as the dimensionless strain $h(t)$ measured in the detector, that is:

$$h(t) = \frac{c}{2L} \left(\Delta T \left(t - \frac{2L}{c}, \hat{\mathbf{x}} \right) + \Delta T \left(t - \frac{L}{c}, -\hat{\mathbf{x}} \right) - T \left(t - \frac{2L}{c}, \hat{\mathbf{y}} \right) - \Delta T \left(t - \frac{L}{c}, -\hat{\mathbf{y}} \right) \right). \quad (1.107)$$

In the regime of low frequency gravitational waves, so $f \ll \frac{c}{L}$, which is the case for the sensitivity band of the ground based detectors ($\frac{c}{3\text{km}} \sim 10^5$ Hz) we can approximate the $\text{sinc}(x)$ function as $\text{sinc}(f \frac{L}{c}) \approx 1$, therefore (1.106) and (1.107) yield:

$$\begin{aligned} h(t) &= \frac{1}{2} \underbrace{(\hat{x}^i \hat{x}^j - \hat{y}^i \hat{y}^j)}_{\equiv D^{ij}} \underbrace{\int_{-\infty}^{+\infty} df \left(\tilde{h}_+(f) e_{ij}^+(\hat{\mathbf{n}}) + \tilde{h}_\times(f) e_{ij}^\times(\hat{\mathbf{n}}) \right) e^{-i2\pi ft}}_{=h_{ij}^{TT}(t)} \\ &= D^{ij} h_{ij}^{TT}(t); \end{aligned} \quad (1.108)$$

with the gravitational waves $h_{ij}^{TT}(t)$ evaluated at the position of the beam splitter, and with D^{ij} being called the *detector tensor* [103]. We can further simplify the above equation by parametrizing the direction of propagation of the gravitational wave with $\hat{\mathbf{n}} = (\cos(\phi) \sin(\theta), \sin(\phi) \sin(\theta), \cos(\theta))$ in the detector frame, to obtain:

$$h(t) = F_+(\phi, \theta) h_+(t) + F_\times(\phi, \theta) h_\times(t) , \quad (1.109)$$

with h_+ and h_\times the polarizations as in (1.28) (which numerically for example could be given by results (1.91)), and where F_+ and F_\times are the *pattern functions* of the interferometer. To obtain the explicit expression for the pattern functions of this Michelson interferometer we can apply the relevant rotation matrix, to obtain [103]:

$$F_+(\phi, \theta) = \frac{1}{2}(1 + \cos^2(\theta)) \cos(2\phi) , \quad (1.110a)$$

$$F_\times(\phi, \theta) = \cos(\theta) \sin(2\phi) . \quad (1.110b)$$

From these expressions we understand that interferometers are all-sky instruments, capable of detecting gravitational waves coming from almost any direction; yet the angular dependence implies that some directions are still observed better than others.

1.6 | Beyond the linearized theory

The results we've obtained up to this point have been worked out in the linearized general relativity theory. Nonetheless, if we wanted to insist on trying to describe the dynamics of a self-gravitating system assuming a flat background spacetime, we'd be using Newtonian gravity instead of general relativity [103]; in fact the dynamics we've obtained in section 1.4 for a non-relativistic binary system are essentially ascribable to the Newtonian gravity theory, with only the addition of the quadrupole power loss formula (1.68) due to gravitational waves emission.

Nevertheless these results were only the leading order ones, whereas the non-linear Einstein's equations in general predict much more complex behaviors and dynamics, which must be taken into account once the gravitational field becomes strong if we aim for accurate estimates. But this isn't an easy endeavour: as already pointed out, aside from few idealized settings in which exact analytical solutions can be found, some of which have been presented in section 1.1, to obtain generic solutions in general relativity one has to resort to some kind of approximation scheme. Furthermore it's usually necessary to tailor the approximation scheme to the problem at hand: to be as effective as possible, and to make the calculations manageable, each formalism relies on different assumptions or expands in a different parameter, being then valid only in a specific regime. Hereafter, and in figure 1.6, we outline some of the most widely used approximation schemes in the study of binary coalescence [37, 103, 132]:

- *Linearized general relativity*, which is the first order expansion about flat spacetime we've studied in the previous sections: it's a quite useful approximation because the equations become easier to deal with, and because the intrinsic weak field assumption is actually well satisfied in many physical settings, as outlined in section 1.3.1. Therein we've also seen that the linearized theory can describe the Newtonian limit; but, at the same time, it can deal as well with systems moving and being accelerated at relativistic speeds: in fact, for a system not too massive, such that the curvature it produces on the background spacetime is little to none, and which is also not governed by gravitational forces, one may use formula (1.50) to compute the gravitational waves emitted in such scenario [103]. Furthermore, as long as we're studying non-relativistic stationary sources, the linearized theory can also be cast in the *gravitoelectromagnetism* formulation, which presents equations analogous to the Maxwell ones

in the absence of time-varying fields [101]; in such a representation some general relativistic effects, such as the Lense-Thirring precession, become evident.

- The *post-Minkowskian* expansion (PM), which is a perturbative expansion in the Newton constant G , understood as the strength of the gravitational field $\frac{Gm}{rc^2} \ll 1$. This expansion imposes no constraints on the velocities v at play, which hence could be relativistic. Therefore such a formalism is particularly useful when dealing with unbound motion of bodies with a large relative separation, e.g. two body gravitational scatterings; but also bound binary systems in highly elliptic orbits. However, thanks to suitable procedures, it's actually possible to extract information about the dynamics of bound systems even by studying their unbound motion in the post-Minkowskian framework [71–73]. Currently results up to the fourth post-Minkowskian order (4PM, so G^4) are known [158–161].
- The *post-Newtonian* (PN) systematic expansion, which is applied to bound systems and therefore expands in the parameter $\frac{v^2}{c^2} \sim \frac{Gm}{rc^2} \ll 1$: it is meant to describe the general relativistic corrections to the Newton gravitational potential for bound systems, as well as

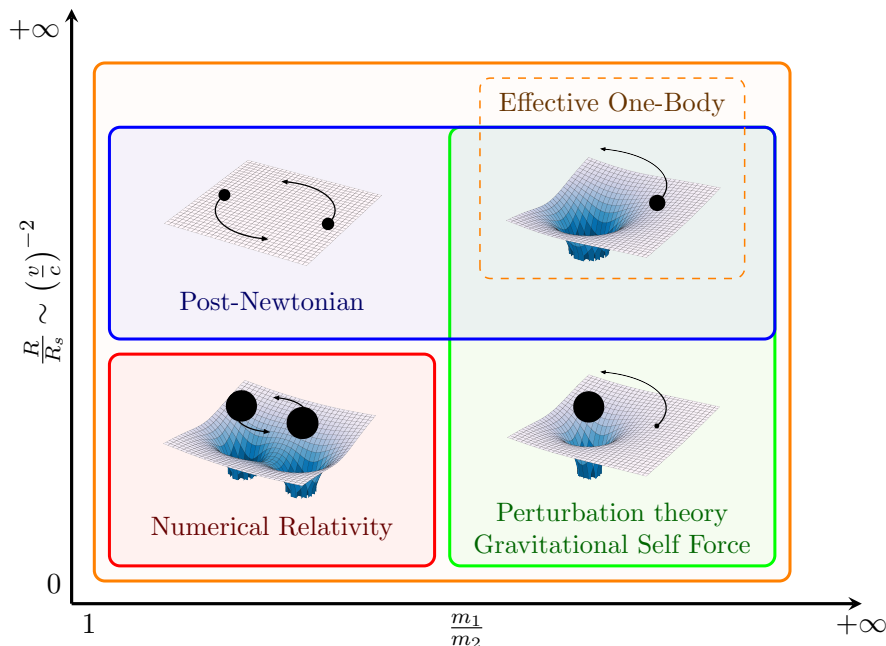


FIGURE 1.6 — Domain of the two body problem in general relativity, during the inspiral phase, for self-gravitating binary systems, for which hence holds $\frac{R}{R_s} \sim \left(\frac{v}{c}\right)^{-2}$, represented in a plane with the mass ratio $\frac{m_1}{m_2}$ on the horizontal axis and the relative distance, in Schwarzschild radii units, $\frac{R}{R_s}$ on the vertical axis. In reality the domains are not sharply separated as shown in figure, also because the accuracy of the several approximations degrades smoothly over the plane. The purpose of such an illustration is instead to depict the qualitative behavior and the strengths of each formalism. As such the Post-Newtonian expansion perturbs the metric and other quantities around a flat spacetime, and it's accurate when velocities are small, or equivalently the relative separation is large. The gravitational self-force formalism instead starts from the exact curved metric solution for a massive body, and evaluates the perturbation and the dynamics of the system in presence of a much lighter body. Numerical Relativity allows to compute numerical solutions of the full non-linear Einstein's equations; nonetheless it's extremely resource and time demanding, therefore it's applied where it's most useful: to compute dynamics in the strong field regime which is not covered by the other schemes. Finally the effective one-body formalism, to which the top right sub-picture refers, encompasses elements from all the other ones, translating the two body problem into the one of a single effective body moving in a suitably deformed effective curved spacetime; its validity region spans over the whole parameter space, and it's goal is to describe the full waveform. Figure based on [37, 156, 157].

the power lost by the system due gravitational wave emission. Such a formalism therefore is accurate only in the low-velocity and weak field regime, which is the case for example when the relative separation between the two compact objects is large: therefore this framework is suitable to describe the inspiral phase of compact binary systems [37]. We'll explore more thoroughly this formalism in section 1.6.1.

- *Numerical relativity* (NR), which solves the full non linear Einstein's equations resorting to numerical methods. The biggest advantage of this method is that it is the only one which can accurately deal with the non-linear, strong gravity, regime of general relativity, which is reached during the merger phase; and further it can take into account many widely different physical processes which are actually expected to be important during a binary coalescence. Then numerical relativity both allows to better study or constraint these several phenomena and also let us produce the possibly most accurate waveforms: in fact numerical relativity waveforms are usually taken as a benchmark to compare the ones obtained via other methods, and some formalisms and waveform models are actually calibrated against the numerical relativity results, in a synergistic approach. Yet the solution obtained with numerical relativity will still be an approximation because spacetime, and all other relevant quantities, have to be discretized; moreover the treatment of the singularities and the gauge redundancy intrinsic to general relativity must appropriately be dealt with; and numerical errors will be a limiting factor to the accuracy of any simulation. All of these issues were the reason why the first accurate direct numerical simulations of the merger of black holes have been obtained only recently, since 2005 [26–29]; and still today one of the main drawbacks of numerical relativity is the fact that it is quite resource demanding: the computation of hundreds of gravitational wave cycles, which may cover only the last stages of a binary evolution, take on the order of $O(10^5 \sim 10^6)$ CPU-hours, which means the results may require months of computations even on a large computer cluster [162]. On top of this, neutron star mergers present an even more complicated environment to study: it's necessary to take into account also nuclear reactions and neutrino transport phenomena, to model the still unknown equation of state of neutron stars, and to perform magnetohydrodynamic studies to reckon with the strong magnetic fields [132, 163]. These complications are the reason why presently there are still only a few thousands numerical relativity waveforms, despite the great effort behind it [29]: this implies that by themselves they cannot cover densely enough the binary system parameter space, so numerical relativity is complemented by semi-analytical models; yet also surrogate numerical relativity models have been built, which for example use reduced order modeling techniques to extract and interpolate the relevant information from the full simulation, providing fast and almost as accurate new waveforms [164–166].
- The *Gravitational self-force* (GSF) approach, which uses perturbation theory to describe the motion of a small body in the stationary spacetime of a larger body, but taking into account also the back reaction due to the smaller body, from early to late inspiral [37, 132, 156, 167]. The natural expansion parameter hence is the mass ratio $\frac{m_1}{m_2}$ (more precisely the symmetric mass ratio $\nu \equiv \frac{m_1 m_2}{(m_1 + m_2)^2}$), and there are no formal requirements on the velocity or the separation between the two bodies; in particular the stationary spacetime could for example be the Kerr one if the larger body is a spinning black hole. This expansion then is suitable to describe the dynamics of the *extreme mass ratio inspiral* (EMRI) events, where a lighter object orbits for up to tens of thousand of times a much larger objects (as could be a supermassive black hole) before merging. The expansion has been evaluated to first order in ν , even though recently there has been progress toward the evaluation of the second order ν^2 [168].
- *Black-hole perturbation theory*, which can be used to study the behavior of black holes slightly displaced from their relaxed state [32–35]. This happens for example when the external

environment presents perturbations instead of the perfect vacuum assumed by the few known exact black hole solutions in general relativity; or when the black holes starts in an excited states and relaxes back to its equilibrium configuration. In particular the latter case is of interest for the study of the ringdown phase: after the merger of two compact objects, the new compact object (generically a black hole) will be in an excited state; then it will quickly radiate away this excess energy via gravitational waves. In particular to describe this system one perturbs the exact general relativistic solution, usually taking advantage of the symmetries of the system (so employing the spherical harmonics when spherical symmetry is present), obtaining for example the Regge–Wheeler–Zerilli equations in the case of a Schwarzschild black hole. From these equations, formally similar to the Schrödinger equation, one can evaluate the *quasi-Normal modes* (QNM) of the system, which describe the oscillations of space time produced by the excited black hole: to each of these modes is associated a specific frequency and a different decay rate; asymptotically the decay rate is given a power-law tail [37, 132, 169, 170].

- The *Effective-One-Body* (EOB) formalism, which is an analytic approach that combines elements from many of the ones presented above. Introduced in 1998 [30, 31] with the goal of describing the whole waveform from inspiral to ringdown, it is based on the assumption that a system composed of comparable mass compact objects is a smooth deformation of known, exact, single body solutions of general relativity [37, 169]. In practice the two body problem is mapped into the one with an effective one body, that is, the problem of a test particle moving through a properly deformed effective external metric. The effective metric may be constructed for example by starting from the Schwarzschild metric associated to the total mass m , or better the Kerr metric, and deforming it using as a deformation parameter the symmetric mass ratio $\nu \equiv \frac{\mu}{m}$ [30]; therefore in the test mass limit $\nu \rightarrow 0$ one recovers the exact result, which for example would not be the case when using the post-Newtonian expansion. Then when the test particle reaches the light ring (at $\frac{3}{2}R_s$) of the effective metric, there is the transition to the plunge phase: the system is now mapped to an excited black hole with its associated quasi-normal modes; in fact from black hole perturbation theory one finds that the effective potential for the quasi normal modes potential has a maximum at the light ring, which then acts as a high-pass filter for the gravitational waves emitted by any infalling body. This formalism therefore leverages also information from the previously presented methods, as the post-Newtonian, post-Minkowskian and black hole perturbation theory, and actually resums them appropriately, in such a way to capture also non-perturbative and strong-field effects [30, 37, 169]. Furthermore, since the first numerical relativity simulations, free coefficients in the effective metric were further calibrated by comparing and fitting the EOB waveforms against the numerical relativity ones, obtaining a really good accuracy throughout the evolution of the system. In fact the effective one body formalism was used to generate most of the waveforms in the template bank used by LIGO-Virgo for its compact binary searches [171]; yet being still a semi-analytical model, the evaluation time of each of its waveform isn't the fastest, therefore when performing the Bayesian analysis of candidate events faster phenomenological waveform models may still be employed [172].

1.6.1 — The post-Newtonian formalism

The *post-Newtonian* formalism is an approximation scheme of general relativity, which can be applied to the study of systems in which the gravitational field is weak, $\frac{Gm}{c^2 r} \ll 1$, and the velocities are low, $\frac{v^2}{c^2} \ll 1$ [36, 103]. In this formalism in fact the complicated non-linear structure of general relativity is simplified by expanding the relevant quantities in the expansion parameter $\epsilon \ll 1$,

where the previous assumption are quantified as:

$$\epsilon \sim \frac{v^2}{c^2} \sim \frac{Gm}{c^2 r} \ll 1 ; \quad (1.111)$$

that is, we also demand the square of the velocity to be of the same order of magnitude of the value of the gravitational field.

We can then see that this formalism is particularly well suited to describe the dynamics of gravitationally bound compact binary systems during their inspiral phase, when the relative velocity is low enough. In fact systems which are tightly bound together by the gravitational force are denoted as self-gravitating systems, and for them it holds the virial theorem, according to which the relation $\frac{v^2}{c^2} \sim \frac{R_s}{d}$ is satisfied as an average over time, where v is the typical velocity of the system, d its typical size, R_s the Schwarzschild radius (1.5) associated to its total mass m [103]. Applying such a relation to the case of a binary system made of compact objects, which is self-gravitating, we obtain more precisely

$$\frac{v^2}{c^2} \sim \frac{Gm}{c^2 r} = \frac{R_s}{2r} ; \quad (1.112)$$

hence we see that for such systems relation (1.111) is actually fulfilled, and so the post-Newtonian expansion applies to them.

Furthermore the customary notation in the post-Newtonian formalism is to denote with v^2 (or with c^{-2}), instead of ϵ , the expansion parameter. Then the expansion is organized as an infinite series of corrections in v^2 to the leading order quantities: the terms of order v^{2n} are denoted as n PN corrections. Still, due to the relation (1.111), the corrections at order n PN are actually given by a series of terms of the kind $\left(\frac{v^2}{c^2}\right)^{n-m} \left(\frac{Gm}{c^2 r}\right)^{1+m}$, with $m = 0, \dots, n$, as depicted also in figure 1.7. The underlying physical idea is that we're evaluating both corrections due to the non-vanishing velocity, but also due to deviations of the background from flat spacetime; this also justifies the statement we made in section 1.3.4: to perform a consistent expansion in v^2 we must also consider terms with varying powers of G , which is related to the strength of the gravitational field and so to the curvature of the spacetime.

In fact the name *post-Newtonian* of this scheme is due to the fact that the leading order (0PN) term in the expansion is the Newtonian potential: therefore this formalism correctly reproduces the classical Newtonian theory of gravitation when the expansion parameter $\epsilon \sim v^2$ vanishes; whereas all the higher order corrections take into account the contributions due to general relativity.

Additionally, to include the emission of gravitational waves in the dynamics of the system we have to break the time-reversal symmetry, as we need to impose no-incoming radiation boundary conditions [36, 103]. Then this causes the appearance of terms with odd powers in the velocity v as well: for example the leading radiation-reaction effects are of order $\mathcal{O}(v^5)$ with respect to the leading order Newtonian equations of motions, therefore they represent a 2.5PN correction. In fact radiation effects first enter at the 2.5PN order, and from there on they may contribute to both integer and half-integer PN orders.

On top of this, as already mentioned, the non linear structure of general relativity will affect also the propagation of gravitational waves, such that they will back-scatter on the curved background spacetime or will scatter with themselves. Therefore, for example, at higher orders in the post-Newtonian expansion part of the gravitational radiation is delayed, in such a way that a distant observer will measure a wavefront, travelling at the speed of light, followed by a *tail*, which arrives later [103]. At these higher orders then the behavior of the theory also becomes more complicated: the aforementioned tail effect is one of the many *hereditary effects* which arise, and physically they imply that the dynamics of the system depend not only on its current configuration, but also on its whole past history [175].

From an historical point of view, the post-Newtonian formalism has been one of the most studied, because it is suitable to evaluate many observables in the theory of general relativity in physically relevant scenarios. In fact the post-Newtonian (and also the similar post-Minkowskian) expansion has been introduced by Einstein himself [171], as it posed to be well suited for solar system calculations: the assumption of non-relativistic velocities makes the time derivative of higher order with respect to the spatial derivatives, $\frac{1}{c} \frac{\partial}{\partial t} \ll \frac{\partial}{\partial x^i}$, thereby simplifying considerably the calculations, and eventually allowing to obtain also the Newtonian limit while working in general relativity [171]. The next-to-leading order (1PN) corrections are given in the Einstein-Infeld-Hoffmann Lagrangian, after who derived it in 1938 [171]; nonetheless the 1PN dynamics of a two-body system had been computed already in 1917, by Droste and Lorentz [13, 36]. The computation of higher order PN corrections instead required much more time, because it presented several subtleties [103, 171]; actually this is still an active area of research.

In fact these complications and inconsistencies led to the creation of several different methods with which one could evaluate the same post-Newtonian corrections to the binary dynamics: for example the *Blanchet–Damour approach*, which performs a post-Newtonian expansion in the near region and a post-Minkowskian one outside the source, matching them in the intermediate region [37, 103, 176]; the *direct integration of the relaxed einstein equations* which regularizes integrals by restricting their integration domain [37, 103]; the *ADM Hamiltonian* formalism, particularly efficient for computing conservative corrections to the binary dynamics [37, 177]; the *effective field theory approach* (NRGR, non relativistic general relativity), which has been formalized by [43], and which is the main focus of this thesis, see chapter 3. Furthermore there are also other approaches, such as the *Tutti Frutti* method [20, 23], which employ analytical information obtained from a variety of formalism to evaluate post-Newtonian corrections.

Currently it has been possible to evaluate the post-Newtonian corrections up to 4PN order in several of these approaches [36–39]. Nonetheless several partial results are known at higher order, or have been computed in only one formalism: presently the conservative potential for non spinning

	0PN	1PN	2PN	3PN	4PN	5PN	6PN	...
1PM	G	$+ G v^2$	$+ G v^4$	$+ G v^6$	$+ G v^8$	$+ G v^{10}$	$+ G v^{12}$	$+ \dots$
2PM		G^2	$+ G^2 v^2$	$+ G^2 v^4$	$+ G^2 v^6$	$+ G^2 v^8$	$+ G^2 v^{10}$	$+ \dots$
3PM			G^3	$+ G^3 v^2$	$+ G^3 v^4$	$+ G^3 v^6$	$+ G^3 v^8$	$+ \dots$
4PM				G^4	$+ G^4 v^2$	$+ G^4 v^4$	$+ G^4 v^6$	$+ \dots$
5PM					G^5	$+ G^5 v^2$	$+ G^5 v^4$	$+ \dots$
6PM						G^6	$+ G^6 v^2$	$+ \dots$
7PM							G^7	$+ \dots$
⋮								⋮

FIGURE 1.7 — Scheme depicting how the post-Newtonian (PN) expansion is organized as a series of corrections in powers of v^2 and G (see text). In particular all the terms in a given column enter in the corresponding PN order. Furthermore let us recall that the post-Minkowskian (PM) formalism is an expansion in G only, where the expressions are exact in the velocities: then all the terms along the same row belong to the same PM order; in fact expanding the corrections of a given PM order we obtain corrections which contribute to infinite PN orders. In particular the contributions up to the 4PN order, which have been evaluated in several formalisms [36–38], are shaded in dark blue; the contributions up to 6PN, which are partially known [20–23, 59, 64, 65, 77, 78, 173, 174] and necessary for next generation gravitational wave observatories, are shaded in light blue; whereas the contributions up to the 4PM order, which have been recently evaluated [158–161], are contained in the red box. Figure based on [39, 167].

binaries is known up to the 5PN order [20, 22, 173, 174], also in the EFT framework [59, 64, 65]; and progress is being made toward evaluating the 6PN conservative contributions, see references [21, 23] and [77, 78], and toward resolving discrepancies involving radiative contributions [178–181]. On top of this, as we’ll explain below, at higher order it’s also necessary to evaluate others corrections due to spin and finite size effects: then the conservative contributions due to spin corrections, which are organized in several sub-sectors depending on the power of the spin, have been evaluated up to 5PN order [182], with some contributions evaluated only via the effective field theory approach [79–82]; furthermore much work is being carried out in the evaluation of higher-order finite size corrections [83, 84].

Some of the most important applications of the post-Newtonian formalism have been to evaluate the orbital dynamics in the solar system to the required accuracy (1PN, also for N -bodies), to compute the orbital decay rate of the Hulse-Taylor binary pulsar due to gravitational wave emission (2.5PN), and to evaluate the dynamics of compact binary system prior to their coalescence (requiring possibly up to order 6PN-7PN for next generation gravitational wave observatories) [36]. Only the latter system can produce gravitational waves with an amplitude high enough to be detected by gravitational wave observatories, and this is the biggest reason why our investigation will focus on them.

The reason why we need to compute corrections to such an high accuracy is that interferometric observatories employ the matched filtering technique to find gravitational waves signal in the output of the detectors, as explained in section 1.5. As a rough estimate, e.g. following [103], to apply this procedure it’s then necessary to be able to evaluate the absolute phase ϕ of the gravitational waveform within $\mathcal{O}(1)$; that is, the number of cycles N , which we computed in equation (1.94), within order unity (as $\phi = 2\pi N$). Then we see that $N \propto f^{-\frac{5}{3}}$, and approximating $f \sim \frac{v}{r} \sim \frac{v^3}{c^2 R_s}$ using also relation (1.112), we find the scaling $N \sim \mathcal{O}(v^{-5})$ with respect to the expansion parameter. Then we have to consider all the post-Newtonian corrections up to $\mathcal{O}(v^5)$ (so 2.5PN) to be able to obtain a precision of order $\delta N \sim \mathcal{O}(1)$; actually also many higher PN corrections are needed to accurately reconstruct the gravitational wave signal.

Regarding the theoretical setup, the post-Newtonian expansion is usually carried out in *harmonic coordinates*, where the *harmonic gauge*, or De Donder gauge, is imposed by means of the harmonic gauge condition [103, 183]:

$$\partial_\mu (\sqrt{-g}g^{\mu\nu}) = 0 . \quad (1.113)$$

One also requires the matter energy-momentum tensor to have a spatially compact support, so for example that it can be enclosed in a time-like world tube with $r \leq D$ for some finite D [103]. Additionally the condition of low velocity is understood to be valid for all velocities inside the binary system, also inside each individual body: therefore we require also the sources themselves to be weakly stressed [103].

A general point of the Newtonian expansion is that it exploits the hierarchies and separation of scales that arise in the limit of non relativistic velocities $v \ll 1$: for example in the region near the compact bodies we can approximate the retardation effects in the interactions as a series of correction. It is also customary the treat separately the far away region where gravitational waves propagate; then any corresponding quantities in the near and far regions are connected by matching them in an intermediate buffer region, and this is possible only as long as $v \ll 1$ holds [36]. We will take advantage of these hierarchies also in the effective field theory approach to the post-Newtonian formalism, which will be discussed in chapter 3.

Nonetheless mathematically the post-Newtonian expansion is not a convergent series, but actually an *asymptotic expansion* [103, 184]: this means that even if we were to evaluate all the PN corrections, the series would not converge for finite values of v^2 ; instead in practice above a certain PN

order the corrections will start to make the evaluated quantities oscillate and diverge in a non-physical manner. This is what happens when the compact objects reach relativistic speed $v \sim \mathcal{O}(1)$ just before the coalescence, and so there the post-Newtonian expansion breaks down; yet prior to that point the higher order corrections are accurate and necessary.

Let us notice as well that, despite the fact that formally the post-Newtonian expansion does not require the masses of the two compact objects to be comparable, in practice systems with a large mass ratio $\frac{m_1}{m_2}$ will perform many orbits at highly relativistic speed before merging; this is the reason why the post-Newtonian expansion is not best suited to describe the last stages of these systems, as opposed to the gravitational self-force formalism.

■ Finite size effects and spin

An interesting feature of the post-Newtonian expansion is that the specific details of the internal structure of the compact bodies become relevant only starting from the quite high 5PN order: this is known as the *effacement principle* [103]. The corrections that arise from that order onward are due to the fact that the first body creates a non homogeneous gravitational field, which exerts tidal forces on the second body, making it bulge (more precisely inducing in it a quadrupole moment); then it's this deviation from the spherical symmetry of the second body that exerts a force on the first body, modifying its trajectory [103]. In practice this means that we can treat the compact objects just as point particles, regardless if they are black holes or neutron stars: as we just said the difference can be probed only starting from the 5PN order, where it is encoded by the Λ *tidal deformability* parameter. Nonetheless these corrections are extremely interesting from a phenomenological point of view, since they allow us to assess if the compact objects are black holes (as non-rotating black holes have vanishing Love numbers [185], i.e. tidal deformability) or neutron stars. In the latter case measuring the tidal deformability also reveals information about their equation of state [186], providing clues about the behavior of QCD in extreme, high density, environments, which could not be probed otherwise [187].

The post-Newtonian expansion allows to take into account as well the spin of the compact objects, that is, the intrinsic rotation of each object. In particular the spin first contributes at 1.5PN order with the spin-orbit coupling, and at 2PN with the spin-spin coupling, contributing from there at any half-integer post-Newtonian order [182]. From the phenomenological point of view, these corrections induce a modulation of the observed waveform. Furthermore also the spin may induce a deformation of the compact object, which can be described by a series of multipoles; then, similarly to what we've discussed above, these multipoles induce post-Newtonian corrections [188].

Both spin and finite size effect corrections have to be included in order to obtain accurate results for the waveform. In fact for next generation gravitational wave observatories the corrections up to 6PN order will be needed in order to keep the systematic error at an acceptable level, and we may expect to observe compact binary systems also with a high spin [39, 189].

EFFECTIVE THEORIES AND MULTI-LOOP TECHNIQUES IN QUANTUM FIELD THEORY

In this chapter we present some concepts and techniques that are used in the rest of this thesis work. In particular in section 2.1 we will recall some concepts from quantum field theory and effective field theories that will prove to be useful in the following, such as the path integral formalism, the procedure to integrate out fields, and the in-in formalism. In section 2.2 instead we will present the modern computational techniques that are currently employed to evaluate multi-loop integrals arising in quantum field theory, and that will be extensively used in this thesis: this is due to the fact that the diagrams that we will have to evaluate will result in integrals that can equivalently be mapped to multi-loop diagrams appearing in massless quantum field theories.

From this chapter onward we will often adopt $\hbar = c = 1$ units, see [Notation](#) for further details.

2.1 | Quantum field theory and effective theories

2.1.1 — Partition function and generating functionals in quantum field theory

In the path integral formulation of quantum field theory, given the fields $\{\phi_r\}$ and the corresponding fictitious source currents $\{J_r(x)\}$ in \tilde{d} dimensions (e.g. $\tilde{d} = 4$), the *partition function* of the theory is defined as [190, 191]:

$$Z[\{J_r\}] = \int D\phi_r e^{iS[\{\phi_r\}] + i\sum_r \int d^{\tilde{d}}x J_r(x)\Phi_r(x)}, \quad (2.1)$$

which is a functional integration, with a measure of integration given by $D\phi_r$. It is particularly useful because it is the generating functional for correlation functions of fields, and hence is also denoted as *functional generator of disconnected n-points functions*; in fact the n-point function can be obtained by taking functional derivatives of the partition function as [190, 191]:

$$G_{n,\{r_1,\dots,r_n\}}(x_1,\dots,x_n) = \langle T(\phi_{r_1}(x_1)\dots\phi_{r_n}(x_n)) \rangle = (-i)^n \frac{1}{Z[0]} \frac{\delta^n Z[J]}{\delta J_{r_1}(x_1)\dots\delta J_{r_n}(x_n)} \Big|_{J=0}, \quad (2.2)$$

where $T(O)$ is the time ordered product of operator O .

Usually the partition function cannot be computed exactly, therefore perturbative methods are employed. In particular the partition function is the vacuum-to-vacuum transition amplitude in quantum field theory [191], so we can evaluate it by summing over all vacuum Feynman diagrams, both connected and disconnected; instead the n-point correlation function, given in (2.2), may be

evaluated as the sum of all Feynman diagram with corresponding n external legs without vacuum bubble diagrams, i.e. excluding diagrams that contain a part not connected to any external line [191].

It is also useful to define another related generating functional, the *functional generator of connected n -points functions* $W[J]$, which is related to the logarithm of the partition function by

$$W[J] = -i \ln(Z[J]) . \quad (2.3)$$

While the partition function generates both the connected and disconnected amplitudes, $W[J]$ can be used to obtain only the connected n -point functions as [191]:

$$G_{n,\{r_1,\dots,r_n\}}^c(x_1,\dots,x_n) = \langle T(\phi_{r_1}(x_1)\dots\phi_{r_n}(x_n)) \rangle_c = (-i)^{n-1} \frac{\delta^n W[J]}{\delta J_{r_1}(x_1)\dots\delta J_{r_n}(x_n)} \Big|_{J=0} . \quad (2.4)$$

In particular by summing only over connected diagrams, one obtains the logarithm of the partition function, that is, $\ln(Z[J]) = iW[J]$.

2.1.2 — Integrating out fields and effective action

In the following chapter 3 we'll be interested in finding equivalent descriptions of a system while not taking into account all of its degrees of freedom. In quantum field theory this is possible by *integrating out* a field, to find an effective action which describes the exact dynamics of all other fields, without ever referencing the now removed degree of freedom.

Assuming for definiteness to have two field ϕ and χ , we can integrate out the field χ by noticing that we can formally rewrite the partition function as:

$$Z = \int D\phi D\chi e^{iS[\phi,\chi]} = \int D\phi e^{iS_{eff}[\phi]} , \quad (2.5)$$

where we have defined the *effective action*

$$S_{eff}[\phi] \equiv -i \ln \left(\int D\chi e^{iS[\phi,\chi]} \right) . \quad (2.6)$$

We can see that the operation of integrating out a degree of freedom, which may be a field or also just its high energy modes, is formally exact as it has been presented in formulae (2.5) and (2.6); nonetheless, analogously to the previous cases, their actual computation may not be feasible. We can notice however that the expression for effective action (2.6) is formally equivalent to the one for the connected functional $W[J]$ as in (2.3); therefore we can obtain the expression for iS_{eff} by summing over all connected vacuum diagrams which have only the χ field propagating, i.e. where the other field are taken as constant.

To be more precise about this last claim, let us consider the general case where $\{\phi\}$ and $\{\chi\}$ each possibly represent a set of fields, with the $\{\chi\}$ fields to be integrated out, and let us express the total initial action in (2.5) as $S[\{\phi\},\{\chi\}] = S_\phi[\{\phi\}] + S_\chi[\{\chi\}] + S_{mixed}[\{\phi\},\{\chi\}]$, where S_ϕ , S_χ , S_{mixed} refer to the terms of the action which respectively include only $\{\phi\}$, $\{\chi\}$ or both type of fields. In this case the effective action for the fields $\{\phi\}$ is given by $S_{eff}[\phi] = S_\phi[\{\phi\}] + S_{eff}^{int}[\{\phi\}]$, with:

$$i S_{eff}^{int}[\{\phi\}] = \ln \left(\int D\chi e^{i(S_\chi[\{\chi\}] + S_{mixed}[\{\phi\},\{\chi\}])} \right) . \quad (2.7)$$

Then the analytic expression for iS_{eff}^{int} can be obtained by summing the connected diagrams obtained in a theory with action $S_\chi[\chi] + S_{mixed}[\phi,\chi]$, and in which we consider only the fields $\{\chi\}$

that we want to integrate out: that is, the other fields $\{\phi\}$ are to be understood as constants which will enter only in the coefficients of the Feynman rules of the vertices of this theory; in particular the only propagators will be those of the $\{\chi\}$ fields, and in the diagrams there can be only lines of the fields $\{\chi\}$ we're integrating out.

After this procedure we expect the new effective action $S_{eff}[\{\phi\}]$ to contain all possible operators allowed by the symmetries of the system, and actually possibly also non-local terms, in which case a suitable expansion has to be performed in order to find an equivalent local Lagrangian. Hence in general we have [192]:

$$S_{eff}[\{\phi\}] = \int d^{\tilde{d}}x \sum_i c_i O_i(\{\phi\}(x)) , \quad (2.8)$$

where c_i are the *Wilson coefficients* of the corresponding local operators $O_i(\{\phi\}(x))$. The net result of integrating out fields is therefore to either modify the Wilson coefficients of the operators of the $\{\phi\}$ fields already present in the original theory, or to generate new operators of these fields altogether.

Let us notice that the Wilson coefficients c_i encode the information about the degrees of freedom we integrated out, and in particular, due to the renormalization group flow, this implies that their value will depend on the physical scale we're probing. In the Wilsonian view of the renormalization group, if we take a theory with a cutoff at an energy scale Λ and lower it down to the energy scale Λ' , the Wilsonian coefficient associated to an operator with mass dimension $[O_i] = \Delta_i$ scales as:

$$c_i(\lambda) = \lambda^{\Delta_i - \tilde{d}} c_i(1) \quad (2.9)$$

where we have defined $\lambda = \frac{\Lambda'}{\Lambda} < 1$. In particular operators which have a mass dimension $\Delta_i < \tilde{d}$ are denoted as relevant operators, and we expect them to dominate the dynamics of the system at lower energy [38, 190]. This will be a key point for the next section 2.1.3, as we'll see that at low energy, to reach a finite accuracy for the physical observables, it should suffice to consider only the relevant and at most a few additional operators, selecting them in order of increasing mass dimension, as all the other ones become increasingly suppressed.

Finally let us also point out that truncating the sum only at tree level diagrams, so integrating the functional integral at the classical level, corresponds to solving the equation of motions for the fields we're integrating out, eventually neglecting the kinetic term, and substituting the solution in the original action, as may be shown by performing a saddle point approximation of path integral [193].

We'll exemplify some of the concepts presented so far in section 3.1.

2.1.3 — Effective field theories

An *effective field theory* may be regarded as an approximate theory, which captures only the relevant degrees of freedom needed to describe, to the desired accuracy, the dynamics of the system in a selected and limited range of validity.

The effective field theory approach is a paradigm which is used a lot in physics and related fields, sometimes more or less consciously: to describe the dynamics of a macroscopic object here on Earth one employs classical mechanics, without performing complicated quantum mechanical or general relativistic calculations, and such an approach suffices for most applications.

In fact, even if we have at our disposal a more complete and therefore more accurate theory, in some regimes one may find simpler theories which provide an equivalent description of the dynamics of the system: the range of validity and the accuracy of such predictions may be limited, but under the right circumstances these effective theories may be preferable, because, given the same finite

computational effort, one may evaluate more higher order corrections thanks to the simplified setup, possibly obtaining more precise theoretical predictions.

The idea underlying effective field theories is that dynamics at low energy, or equivalently large distances, does not depend on the details of the dynamics at high energy, or short distances. This allows us to employ a simplified theory, for example a Lagrangian with fewer degrees of freedom, to describe the same phenomena [194]; under suitable conditions this is for example proven by the decoupling theorem [195–197]. In particular, the viewpoint according to which the Standard Model of particle physics and general relativity are just the leading terms of some effective field theory, and not complete theories per se, is becoming increasingly widespread [198].

Actually EFTs are well suited also when widely different scales appear in the problem being tackled, as they can connect those different scales via renormalization group flow, resumming large logarithms which otherwise could have spoiled the perturbative expansion [193, 199].

As will be explained in the following, in the context of quantum field theories, an effective field theory may be constructed either by following the *top-down* or the *bottom-up* approach, or also a mix of the two.

■ Top-down approach

The top-down approach is a procedure that can be employed to construct an effective field theory, but requires the knowledge of a more complete theory, also called UV (ultraviolet, in the sense of high energy) theory.

This approach is based on the assumption that the high energy degrees of freedom will be off-shell, and therefore cannot be excited or directly produced by the phenomena we’re studying. Nonetheless they exist and play a role in the dynamics of the complete theory, so we expect their presence to still be in the effective theory: this happens via modification of the values of the Wilson coefficients for the effective theory, and via scale-dependent renormalization group flow of those same coefficients, akin to what we’ve seen in section 2.1.2.

In particular the procedure can be so summarized:

- Identify the scale Λ , which for definiteness could be an energy scale, below which the effective field theory is meant to be applied;
- Identify the high energy degrees of freedom, which for example have an energy $E > \Lambda$, and the low energy degrees of freedom of the theory, with $E < \Lambda$, eventually by splitting the fields into two components if needed;
- Find a *power counting* scheme that allows to organize the calculations; for example expand the Lagrangian and the relevant quantities as a function of the scale Λ , in such way to be able to easily recognize the finite subset of terms that must be evaluated in order to achieve the required accuracy in a given calculation;
- *Integrate out* the high energy (or heavy) degrees of freedom; that is, obtain an equivalent effective field theory with only the low energy (or light) degrees of freedom, but which describes the same dynamics of the UV theory in its regime of validity, e.g. for $E < \Lambda$;
- If the theory presents several physical scales, one should perform this steps at the boundary of each scale, while in between evaluating the running of the coefficients of the operators via renormalization group techniques.

The physical scales we’re mentioning could be the masses of the high energy degrees of freedom. For definiteness, considering the UV theory, we may start our procedure from a really high renormaliza-

tion scale μ , e.g. such that μ is larger than all the other masses or such that all nonrenormalizable operators may be neglected, and we may lower the scale using renormalization group techniques, which imply a running of the couplings. When the renormalization scale reaches a physical scale, for example $\mu = M$, with M the mass of a heavy degree of freedom, we should integrate out such field by matching the initial theory to a new effective theory, which now doesn't include that heavy degree of freedom anymore. One then applies again the renormalization group techniques to lower the renormalization scale, and this procedure is to be repeated until we arrive at the scale Λ we're interested in [192, 200]; this also allows the resummation of large logarithmic factors which otherwise may spoil the perturbative expansion [193, 199]. In practice, this *matching* of the theories is performed by imposing that observables, or also S-matrix elements, as evaluated in both theories are the same [192, 194, 200], e.g. by comparing both quantities after having expanded them in the same parameter.

One may also integrate out the heavy degrees of freedom as explained in section 2.1.2 [193]. Furthermore, as we pointed out there, due to the operation of integrating out fields, and due to the renormalization group flow, we expect the action of the effective field theory to contain all operators permitted by the symmetries of the system.

■ Bottom-up approach

This is the alternative approach to the construction of an effective field theory. The key steps here are [193, 194]:

- Identify the relevant degrees of freedom of the theory, at the energy scale of interest;
- Identify the symmetries of the system;
- Identify the correct expansion parameters, which will let us organize systematically the perturbative expansion;
- Write down all the possible operators which are consistent with the aforementioned symmetries;
- Perform a *matching* procedure to find the values of the Wilson coefficients of the operators, either by computing observables and comparing them with physical measurements, or by matching them with the ones computed from a known UV theory.

As the number of operators may be infinite, one usually performs the last matching operation up to some finite accuracy, considering only the subset of operators which are the most relevant for the calculation, as suggested by the expansion parameter [197]; also to compare different physical scales the couplings of the theory should be evolved via renormalization group equations [196, 199].

This bottom-up approach is justified on the basis that, at least at low energy, we expect physics to be described by quantum field theory, therefore writing down the most general possible Lagrangian will yield the most general possible theory [201]. Furthermore this approach is necessary when we don't have a more complete (UV) theory to start with, as in this case we may only perform the matching with the experiments; still the resulting EFT may actually give insights useful for finding such an UV theory [193].

2.1.4 — In-in formalism

The action principle, and the framework of quantum and effective theories, have proven to be really successful in describing physical phenomena, yet their usual formulation, where we evaluate transition amplitudes between an in-state and an out-state, is not suited when dissipative phenomena are involved. In fact, in order to correctly account for dissipative effects that arise when dealing

with systems whose evolution is non-time symmetric, it is necessary to employ the *in-in formalism*, also known as Schwinger-Keldysh formalism, or CTP (closed time path) formalism [202–204] (see also [197, 205, 206] for further details and applications).

In fact the in-in formalism has been applied in many context that are concerned with non-equilibrium processes [202–204], and also for example in Cosmology [207, 208]. Regarding the two-body problem in General Relativity, the in-out formalism actually suffices for evaluating conservative contributions to the dynamics of the system; instead when evaluating dissipative contribution, where radiation gravitons are involved, the symmetric nature of the Feynman propagator may lead to wrong and non-causal results, therefore the in-in formalism becomes necessary [202]. Furthermore at higher perturbative orders it may not even be possible to clearly distinguish all conservative and dissipative contributions: one solution may be to directly evaluate the equation of motions for the system to automatically incorporate both effects [180].

The in-in framework, first introduced by Schwinger [209], allows, once defined the initial in-state, to compute the expectation value of an operator with respect to these fields at a later time [210]. To do so one doubles the degrees of freedom: one consider the evolution of two generic in-states toward the same, arbitrary, out-state; integrates over all possible future states, and finally sets both initial in-states to be the same, actual, in-state that one is concerned with.

For example, if the initial theory contains a field ϕ , coupled to a source current J , with an action $S[\phi, J]$, then to implement the in-in formalism we have to double the degrees of freedom: first we introduce the fields ϕ_1 and ϕ_2 , which are involved respectively in the forward evolution and the backward evolution to and from the same arbitrary out-state (this condition is enforced imposing $\phi_1(t = \infty) = \phi_2(t = \infty)$), and then we introduce the sources currents J_1 and J_2 , which couple respectively to ϕ_1 and ϕ_2 [202, 206]. It can be shown that, given the path integral [202]

$$e^{iW[J_1, J_2]} = \int D\phi_1 D\phi_2 e^{iS[\phi_1] - iS[\phi_2] + i \int d^{d+1}x J_1(x)\phi_1(x) - i \int d^{d+1}x J_2(x)\phi_2(x)} \quad (2.10)$$

where we enforce $\phi_1 = \phi_2$ at $t = \infty$, by evaluating the one-point functions for the ϕ_1 and ϕ_2 fields in the in-in formalism

$$\langle \phi_1(t, \mathbf{x}) \rangle_{in-in} \equiv \frac{\delta W}{\delta J_1(t, \mathbf{x})}_{J_1=J_2=0}, \quad \langle \phi_2(t, \mathbf{x}) \rangle_{in-in} \equiv -\frac{\delta W}{\delta J_2(t, \mathbf{x})}_{J_1=J_2=0}, \quad (2.11)$$

we obtain the correct and causal expressions for the expectation value of the original field ϕ evaluated in the vacuum state, $\langle \phi_1(t, \mathbf{x}) \rangle_{in-in} = \langle \phi_2(t, \mathbf{x}) \rangle_{in-in} = \langle 0 | \phi(t, \mathbf{x}) | 0 \rangle$ [202].

Usually it is more convenient to work in the so called *Keldysh representation*, in which every quantity F_1 and F_2 is redefined into the quantities F_+ and F_- according to:

$$F_+ \equiv \frac{1}{2} (F_1 + F_2), \quad (2.12a)$$

$$F_- \equiv F_1 - F_2; \quad (2.12b)$$

in particular this transformation has to be applied to both the fields $\phi_1, \phi_2 \rightarrow \phi_+, \phi_-$ and the sources $J_1, J_2 \rightarrow J_+, J_-$.

If the action $S[\phi, J]$ for a massive (or also massless) scalar field ϕ has only a linear interaction term, so $S[\phi, J] = \frac{1}{2} \partial_\mu \phi \partial^\mu \phi - \frac{1}{2} m^2 \phi^2 + J(x)\phi(x)$, then, after doubling the degrees of freedom and employing the Keldysh representation (2.12), one finds that the path integral (2.10) can be exactly solved to yield [202]:

$$W[J_+, J_-] = \frac{i}{2} \int d^{d+1}x \int d^{d+1}y J_A(x) D^{AB}(x-y) J_B(y), \quad (2.13)$$

with $A, B = \pm$ indices related to the Keldysh representation and D^{AB} the matrix of two-point functions given by [202]

$$D^{AB}(x-y) = \begin{pmatrix} 0 & -iD_{adv}(x-y) \\ -iD_{ret}(x-y) & \frac{1}{2}D_H(x-y) \end{pmatrix}, \quad (2.14)$$

where, defined the Wightman functions [202, 205]

$$\Delta_{\pm}(t, \mathbf{x}) = \int \frac{d^{d+1}k}{(2\pi)^{d+1}} \frac{e^{\mp ik^0 t + i\mathbf{k}\cdot\mathbf{x}}}{2k^0} = \int \frac{d^{d+1}k}{(2\pi)^{d+1}} \theta(\pm k^0) \delta((k^0)^2 - \mathbf{k}^2) e^{-ik^0 t + i\mathbf{k}\cdot\mathbf{x}}, \quad (2.15)$$

we have that [202, 205, 206]

$$D_{adv}(t, \mathbf{x}) = -i\theta(-t) (\Delta_+(t, \mathbf{x}) - \Delta_-(t, \mathbf{x})) \quad (2.16a)$$

$$D_{ret}(t, \mathbf{x}) = i\theta(t) (\Delta_+(t, \mathbf{x}) - \Delta_-(t, \mathbf{x})) \quad (2.16b)$$

$$D_H(t, \mathbf{x}) = \Delta_+(t, \mathbf{x}) + \Delta_-(t, \mathbf{x}) \quad (2.16c)$$

are respectively the *advanced propagator*, the *retarded propagator*, and the *Hadamard propagator*.

Finally in the Keldysh basis the vacuum expectation value for the scalar field ϕ can be evaluated via [202]:

$$\langle 0|\phi(t, \mathbf{x})|0\rangle = \langle \phi_+(t, \mathbf{x}) \rangle_{in,in} \Big|_{J_{\pm}=0} = \frac{\delta W}{\delta J_-(t, \mathbf{x})} \Big|_{J_{\pm}=0}. \quad (2.17)$$

For a practical application, we'll employ this formalism in section 5.2.

2.2 | Multi-loop techniques in quantum field theory

2.2.1 — Dimensional regularization

When working in perturbative quantum field theory, often one encounters divergences. The divergent integrals can be regularized by appropriate regularization schemes, one of the most used being *dimensional regularization*. The basic idea is that in loop integrals one formally replaces the dimension of space-time ($3+1 = 4$) with a real, or possibly complex, parameter d [211]. In this way ultraviolet or infrared divergences show up as poles in the complex d -plane; the final result can then be Laurent expanded around $d = 4 + 2\epsilon$ with $\epsilon \rightarrow 0$, and the result so obtained properly renormalized. In general one requires the d -dimensional integral to satisfy all the usual properties of integrals, like linearity, translation invariance and scaling behaviour [211].

Furthermore, when we encounter some integrals that are divergent in $d = 4$, we may work around this by instead keeping the dimension d of space-time arbitrary in order to obtain convergent results for some values of d . If this is the case one can then *define* the initial integral as the convergent result just obtained, and analytically continue this new definition to the other values of d , eventually also $d = 4$ [194]. As we'll see later, this is the case for scaleless integrals; similarly, keeping d arbitrary allows for integration-by-parts identities to vanish on the boundary, as wanted.

■ Direct evaluation of spherically symmetric integrals in dimensional regularization

While working in dimensional regularization, the loop integrals that one may be able to directly evaluate usually present a spherical symmetry; in such cases then it's useful to perform a change of variables, from the cartesian \mathbf{k} system to the hyperspherical d -dimensional coordinates. This allows for a clear treatment of a continuous number $d \in \mathbb{R}$ of variables of integration: the aforementioned change of variables is a reparametrization of the d components $\{k^1, \dots, k^d\}$ as a function of a single

radial variable, i.e. $K \equiv |\mathbf{k}|$ with $K \in [0, +\infty)$, and of $d-1 \in \mathbb{R}$ angular variables, which for $d \in \mathbb{N}$ ($d \geq 2$) can be interpreted as the usual $d-2$ angles $\phi_1, \dots, \phi_{d-2}$ with domain $[0, \pi]$ radians and the last angle ϕ_{d-1} with domain $[0, 2\pi)$ radians. Under this change of variables the integration measure factorizes as

$$d^d \mathbf{k} = K^{d-1} dK d\Omega_{d-1} \quad (2.18)$$

where $d\Omega_{d-1}$ is the area element of a unit $(d-1)$ -sphere.

If the integrand then enjoys spherical symmetry, i.e. is a function of the radial component K only, we may directly factor out the angular integration, obtaining the total area $\Omega_{d-1} \equiv \int d\Omega_{d-1}$ of the unit $(d-1)$ -sphere. Such a factor can be evaluated in arbitrary d -dimension via the gaussian integral trick:

$$(\sqrt{\pi})^d = \left(\int_{-\infty}^{+\infty} dx e^{-x^2} \right)^d = \int d^d \mathbf{x} e^{-((x^1)^2 + \dots + (x^n)^2)} = \underbrace{\int d\Omega_{d-1}}_{=\Omega_{d-1}} \underbrace{\int_0^{+\infty} dr r^{d-1} e^{-r^2}}_{=\frac{1}{2}\Gamma(\frac{d}{2})}, \quad (2.19)$$

where we recalled the definition of gamma function (B.2), to obtain

$$\Omega_{d-1} = \frac{2\pi^{\frac{d}{2}}}{\Gamma(\frac{d}{2})}. \quad (2.20)$$

■ Scaleless integrals

A property of dimensional regularization is that integrals which do not depend on external quantities may vanish identically. In fact, by dimensional arguments, if the integrand has mass dimension $[f(k)] = a$, then given a mass scale μ the integral must scale like

$$\int \frac{d^d k}{(2\pi)^d} f(k) \sim \mu^{d+a}. \quad (2.21)$$

Nonetheless, if $a \neq -d$ and the integrand $f(k)$ is a function of the integral variable k only, i.e. the integrand does not depend on any other external dimensional quantity, then there is no scale μ to which the integral may be proportional to; therefore it must be equal to zero [211]. More formally each integral in dimensional regularization is defined by analytical continuation from the set of values of the parameters where such integral is convergent [212]. This means for example that in dimensional regularization we can define [212]

$$\int \frac{d^d k}{(2\pi)^d} \frac{1}{(k^2)^\alpha} = 0 \quad (2.22)$$

where we employed also the result (C.4). Let us point out that according to reference [211] for the specific value $\alpha = \frac{d}{2}$ the above integral actually is proportional (up to normalization of the measure) to $\Gamma(1-d)$; in fact if we evaluate (C.4) in $d = 4 + 2\epsilon$ dimensions, and with $\alpha = \frac{d}{2}$, the above integral is still divergent even if we regulate it with a mass, the final results having a pole of the kind $\frac{1}{\epsilon} + \ln(m) + O(\epsilon)$. In practice, when both UV and IR divergences are present, it may not be possible to set scaleless integral to zero, see references [213, 214].

2.2.2 — Tensor decomposition

When evaluating a diagram it is customary to break it apart into its tensorial (and Dirac) structure and its scalar part: this allows to simplify the problem, since these structures can be solved for separately.

To be more specific, restricting ourselves to the case with no Dirac structures, let us assume to have a term $I^{\mu\dots\rho}(p_1, \dots, p_E)$, which carries tensor indices $\mu\dots\rho$ and depends on E external momenta p_1, \dots, p_E , and that can be cast into (a sum over terms of) the form

$$I^{\mu\dots\rho}(p_1, \dots, p_E) = \int \prod_{i=1}^L \left(\frac{d^d k_i}{(2\pi)^d} \right) \frac{\mathcal{N}^{\mu\dots\rho}(\{k_j\}, \{p_j\})}{\mathcal{D}(\{k_j\}, \{p_j\})}, \quad (2.23)$$

so these terms for example may be some complicated integration over L loop momenta k_1, \dots, k_L , with $\mathcal{D}(\{k_j\}, \{p_j\})$ the scalar denominator and $\mathcal{N}^{\mu\dots\rho}(\{k_j\}, \{p_j\})$ the numerator which carries the tensor indices. In particular let us notice that such a numerator, i.e. its tensor quantities, may depend on both the loop momenta $\{k_j\}$ and on the external momenta $\{p_j\}$, nonetheless once we perform the integration, the result $I^{\mu\dots\rho}(\{p_j\})$ cannot depend anymore on the loop momenta, but still must carry a tensorial structure compatible with the one which was present in the numerator. This means that the most general form of the result $I^{\mu\dots\rho}(\{p_j\})$ is given by a sum over all such possible tensorial structures, each multiplied by a scalar coefficient which is called *form factor*.

Therefore the *tensor decomposition* procedure, aimed at solving integral (2.23), involves writing $I^{\mu\dots\rho}(p_1, \dots, p_E)$ as a sum over all the possible tensors $\{t_q^{\mu\dots\rho}\}$ with the correct tensor structure, each multiplied by their scalar form factor $\{F_q\}$, i.e.

$$I^{\mu\dots\rho}(p_1, \dots, p_E) = \sum_q F_q(p_1, \dots, p_E) t_q^{\mu\dots\rho}(p_1, \dots, p_E). \quad (2.24)$$

In particular the set $\{t_q^{\mu\dots\rho}\}$ of all possible tensors is obtained by multiplying all the tensorial quantities on which $I^{\mu\dots\rho}$ may depend upon, in all the possible ways, until the number of indices is saturated, and then by considering all the possible permutations of the indices. Such tensorial quantities are for example given by the metric $g^{\mu\nu}$ (which is the Kronecker delta δ^{ij} in Euclidean flat space) and by all the external momenta p_1^μ, \dots, p_E^μ , while no loop momenta may appear. Let us also notice that in principle one should consider also the Levi-Civita symbol, e.g. ϵ^{ijk} in three dimensions and $\epsilon^{\mu\nu\rho\sigma}$ in four dimensions, but while working in dimensional regularization this tensor isn't well defined and instead must be treated appropriately, just like Dirac structures; this may be accomplished by treating differently the 3 (or 4) space-time dimensions with respect to the remaining $d-3$ (or $d-4$) dimensional space [211, 215].

The problems now has been reduced to the one of finding the explicit expression of the form factors. To do so we can project the tensor expression (2.24) by applying an appropriate set of projectors $\{P_{r,\mu\dots\rho}\}$, to obtain a set of scalar expressions, one for each projector we applied. If we can obtain as many independent scalar expressions as the number of the form factors (i.e. of different tensors $\{t_q^{\mu\dots\rho}(p_1, \dots, p_E)\}$), which we assume to be Q , then we can solve the system of linear equations we just found, to obtain the explicit expression of the form factors. In particular, keeping only the set of projectors which give independent scalar conditions for the system, so $\{P_{r,\mu\dots\rho}\}$ with $r = 1, \dots, Q$, then:

$$\begin{aligned} \underbrace{P_{r,\mu\dots\rho} I^{\mu\dots\rho}(p_1, \dots, p_E)}_{\equiv (\vec{I})_r} &= \sum_q \underbrace{P_{r,\mu\dots\rho} t_q^{\mu\dots\rho}(p_1, \dots, p_E)}_{(T)_{rq}} \underbrace{F_q(p_1, \dots, p_E)}_{(\vec{F})_q} \iff \vec{I} = T \vec{F} \\ \implies \vec{F} = T^{-1} \vec{I} &\iff F_q(p_1, \dots, p_E) = \sum_{s=1}^Q (T^{-1})_{qs} P_{s,\mu\dots\rho} I^{\mu\dots\rho}(p_1, \dots, p_E). \end{aligned} \quad (2.25)$$

To find the set of projectors needed to accomplish this feat, one usually just makes the *ansatz* of simply choosing as the set of projectors $\{P_{r,\mu\dots\rho}\}$ the set of the tensors $\{t_r^{\mu\dots\rho}\}$ themselves, raising or lowering the indices as needed in order to be able to correctly contract these quantities.

At last let us also notice that in general, starting from an expression (2.23) which foresees an integration over the loop momenta $\{k_j\}$, then the tensor decomposition procedure will yield a set of scalar form factors whose expression will still present the integration over loop momenta, but now with a modified integrand, still dependent on both the loop $\{k_j\}$ and the external $\{p_j\}$ momenta, but which in particular will be now be scalar quantity, so without any tensor index. Therefore the tensor decomposition procedure lets us reduce the complicated problem of integrating an expression of the kind (2.23) to the more common problem of solving a *scalar integral*.

An explicit application of this procedure will be shown in section 4.3.2.

2.2.3 — Scalar integrals algebraic manipulation

Once one has applied the tensor decomposition procedure just outlined to the relevant diagram expression, one will be left with a scalar integral. Such integrals can then be further manipulated to cast them into Feynman integrals. In particular, let us consider again a generic Feynman diagram with k_1, \dots, k_L internal loop momenta and p_1, \dots, p_E external momenta. Now the general structure of the scalar integrals associated to such a diagram will be given by:

$$\mathcal{M}(p_1, \dots, p_E) = \int \prod_{i=1}^L \left(\frac{d^d k_i}{(2\pi)^d} \right) \frac{\mathcal{N}(\{k\}, \{p\})}{D_1^{\alpha_1}(\{k\}, \{p\}) \cdots D_m^{\alpha_m}(\{k\}, \{p\})} ; \quad (2.26)$$

where D_1, \dots, D_m are the m denominators, in general associated to the propagators and each raised to the respective power $\alpha_1, \dots, \alpha_m$, while \mathcal{N} is the numerator; all of these terms are scalars, and therefore depend on the scalar product between the momenta, possibly both internal $\{k_i\}$ and external $\{p_i\}$. Let us also notice that in a diagram with $n > 0$ external legs, due to momentum conservation there are only $n - 1$ independent external momenta; therefore in the following we assume all the E external momenta to be independent.

■ Reduction to scalar Feynman integrals

To proceed further, we'd like to rewrite the integrand in equation (2.26) as a sum of terms, each of which is a product of denominators only. To do so we can notice that, because both the denominators are functions of scalar products, we may invert these relations to express a generic scalar product as a function of the denominators $\{D_i\}$; we may then employ such relation to re-express the scalar products appearing in the numerator as a function of the denominators only.

This operation requires the inversion of a system of equations; therefore is possible as long as the number m of denominators is greater or equal than the number of k -dependent scalar products appearing in the numerator; in fact scalar products between external momenta only are constants for what concerns the loop integration. Recalling that the scalar product is symmetric, the maximum number of scalar products with at least one loop momenta which may appear in the numerator is

$$N = \underbrace{\frac{L(L+1)}{2}}_{k_i \cdot k_j} + \underbrace{LE}_{k_i \cdot p_j} = \frac{L}{2} (L + 2E + 1) . \quad (2.27)$$

While for 1-loop calculations ($L = 1$) there are no issues, as it holds $m = n = E + 1 = N$, in general for $L > 1$ it may be needed to artificially enlarge the set of denominators in order to be able to invert the system of equations. The scalar products which can be written as a function of the original denominators are called *reducible scalar products* (RSPs), while the ones which cannot are called *irreducible scalar products* (IRSPs); the new denominators which we choose in order to satisfy $m' = N$ are called *auxiliary denominators*: we may choose some irreducible scalar products as auxiliary denominators in order to obtain a complete *basis* of denominators, i.e. the constraint

on our arbitrary choice is the one of obtaining an invertible system of equations with an unique solution [216, 217].

At the end of this whole procedure, the integrand will be a function of the denominators only, up to k -independent factors; we also assume that such a function can be expressed as a sum over products of powers of denominators only; for example this is possible if the initial numerator $\mathcal{N}(\{k\}, \{p\})$ is a polynomial in the scalar products. This procedure let us cast equation (2.26) into the form

$$\mathcal{M}(p_1, \dots, p_E) = \sum_j c_j I_j \quad (2.28a)$$

$$I_j(p_1, \dots, p_E) \equiv \int \prod_{i=1}^L \left(\frac{d^d k_i}{(2\pi)^d} \right) \frac{1}{D_1^{\alpha_{1,j}}(\{k\}, \{p\}) \cdots D_m^{\alpha_{m,j}}(\{k\}, \{p\})}, \quad (2.28b)$$

with c_j constants in the loop momenta; in particular we may denote the integrals $I_j(p_1, \dots, p_E)$ as *scalar Feynman integrals* [218]. It is customary to denote as *integral family* the set of integrals, written in form (2.28b), which have the same set of independent denominators $\{D_i\}$ and powers $\alpha_i \in \mathbb{Z}$ (with $i = 1, \dots, N$). Furthermore, given an integral family, one defines a *topology* (or *sector*) as the set of integrals in which all the non-auxiliary denominators are raised to some positive power, therefore to a topology we may directly associate a diagram where momentum conservation holds at each vertex. Additionally a *subtopology* of given a topology is defined as the set of integrals in which some non-auxiliary denominators are raised to zero power, hence the diagram associated to such a subtopology can be obtained by taking the one of the parent topology and pinching, i.e. removing, the propagators corresponding to the missing denominators; in such a diagram momentum conservation still holds at each vertex [55, 219, 220].

An application of this procedure of reduction to scalar Feynman integrals will be shown in section 4.3.2.

2.2.4 — Reduction to Master Integrals

Our goal is now to further simplify the problem of evaluating the $\{I\}$ scalar Feynman integrals given by expression (2.28b); in particular we want to rewrite each of them in terms of a smaller set of independent integrals, known as *master integrals* $\{I^{MI}\}$, which form a basis of integrals in dimensional regularization [205, 211]: this means that the amplitude can be fully decomposed as a linear combinations of master integrals [211], i.e.

$$\mathcal{M}(p_1, \dots, p_E) = \sum_i \beta_i(p_1, \dots, p_E) I_i^{MI}(p_1, \dots, p_E); \quad (2.29)$$

in practice, if we express each of the Feynman scalar integrals $\{I\}$ in equation (2.28) as a function of the master integrals as $I_j = \sum_i d_i^{(j)} I_i^{MI}$, then the coefficient explicitly read $\beta_i = \sum_j c_j d_i^{(j)}$.

The reduction of the amplitude as a linear combination of master integrals therefore is equivalent to the reduction of each scalar integral $I_j = \sum_i d_i^{(j)} I_i^{MI}$, that is, to finding the coefficients $d_i^{(j)}$. This can be accomplished by employing relations between scalar integrals, in order to reduce the number of integrals down to the minimal set given by the master integrals; such relations for example are given by *symmetry relations*, *integration-by-parts identities* (IBPs), *Lorentz invariance identities* and *dimensional recurrence relations* [221].

On a side note let us point out that since any Feynman integral can be expressed as a linear combination of master integrals, then one may look for an inner product to equip the vector space of integrals with: in such a way the coefficients in front of the master integrals can be directly

computed via the inner product, instead of having to solve the large system of linear equations produced by IBPs and similar relations. This approach is studied by *intersection theory* [211, 222, 223].

An explicit application of this procedure of reduction to master integrals is shown in appendix C.5.1.

■ Symmetry relations

The first set of identities which relate integrals in the same integral family can be obtained by changing the integration variables, i.e. performing a redefinition of the the loop momenta, in a way that doesn't modify the result of the integration [205, 224].

This may be accomplished by looking for a transformation of the loop momenta which has a trivial Jacobian, but which modifies the integrand in such a way to relate two different integrals belonging to the same family; for example such a transformation may be given by the shift of some loop momenta by some external momenta.

The identities so obtained may either map two different topologies into each other, decreasing the number of independent topologies; or else may map a topology into itself, thereby yielding relations between integrals in that topology [205, 224].

■ Integration-by-parts identities

The integration-by-parts identities, first introduced in [45, 46], relate scalar Feynman integrals of the same family, as defined in formula (2.28b), which differ by values of the powers of the denominators $(\alpha_{1,j}, \dots, \alpha_{m,j})$ [211].

They are based on the fact that, while working in dimensional regularization, the integral of a total derivative vanishes [211]:

$$\int \prod_{r=1}^L \left(\frac{d^d k_r}{(2\pi)^d} \right) \frac{\partial}{\partial k_s^\mu} \left(w^\mu(\{k\}) \frac{1}{D_1^{\alpha_1(\{k\})} \dots D_m^{\alpha_m(\{k\})}} \right) = 0 \quad (s = 1, \dots, L), \quad (2.30)$$

which is a consequence of the generalized Stokes' theorem if we assume the quantity inside brackets to vanish sufficiently fast on the boundary of the integration domain, otherwise it follows from the assumption of translation invariance of integrals in dimensional regularization [211]. We may then take this generic vector to be any linear combination of loop and external momenta, so

$$w^\mu = \sum_{j=1}^L a_j k_j^\mu + \sum_{j=1}^E b_j p_j^\mu, \quad (2.31)$$

and by employing Leibniz rule on equation (2.30), noticing that $\frac{\partial k_j^\mu}{\partial k_s^\mu} = \delta_\mu^\mu \delta_{js} = d \delta_{js}$, we obtain for $s = 1, \dots, L$:

$$\begin{aligned} d a_s \int \prod_{r=1}^L \left(\frac{d^d k_r}{(2\pi)^d} \right) \frac{1}{D_1^{\alpha_1(\{k\})} \dots D_m^{\alpha_m(\{k\})}} \\ = - \int \prod_{r=1}^L \left(\frac{d^d k_r}{(2\pi)^d} \right) w^\mu(\{k\}) \frac{\partial}{\partial k_s^\mu} \left(\frac{1}{D_1^{\alpha_1(\{k\})} \dots D_m^{\alpha_m(\{k\})}} \right). \end{aligned} \quad (2.32)$$

We can see these equations provide a set of relations between scalar Feynman integrals belonging to the same family, i.e. of the same form of (2.28b), up to different powers of the denominators:

in fact the action of the derivative on the right hand side of formula (2.32) is to create a series of terms, each with different powers of the denominators and possibly with scalar products at the numerator. Nonetheless the numerator can be rewritten as a sum over scalar Feynman integrand of the kind (2.28b) using the same method outlined in section 2.2.3. This means that if we start with a complete basis of denominators, the integration-by-parts identities provide a set of relations between scalar Feynman integrals belonging to the same integral family: even though this means that they cannot lower the number of loop integration [224, 225], these identities let us reduce the initial set of scalar integrals into a smaller one, the set of the master integrals. This procedure may be implemented through Laporta algorithm [47], and it's been widely used in multi-loop calculations, for example in works like [226, 227].

■ Lorentz invariance identities

Similarly to integration-by-parts identities, one can obtain relations between scalar Feynman integrals by noticing that such integrals are Lorentz scalars (or invariant under d -dimensional rotations if we're in an Euclidean metric) which are invariant under Lorentz transformations (or d -dimensional rotations) of the external momenta $\{p_i\}$ [54].

To derive the Lorentz invariance identities, one may consider an infinitesimal Lorentz transformation acting on the external momenta

$$p_i^\mu \rightarrow (p')^\mu_i = p_i^\mu + \omega^{\mu\nu} p_{i,\nu} \quad (2.33)$$

with $\omega^{\mu\nu} = -\omega^{\nu\mu}$, under which, as pointed out, the scalar integrals (2.28b) must be invariant: expanding at linear order one then obtains

$$\begin{aligned} I(p_1, \dots, p_E) &\rightarrow I(p'_1, \dots, p'_E) = I(p_1, \dots, p_E) \\ &= \left(1 + \sum_{q=1}^E \omega^{\mu\nu} p_{q,\nu} \frac{\partial}{\partial p_q^\mu} \right) I(p_1, \dots, p_E) . \end{aligned} \quad (2.34)$$

Since the last equality must hold for any generic infinitesimal Lorentz transformation $\omega^{\mu\nu}$ we obtain the relation $\left(\sum_{q=1}^E p_{q,\nu} \frac{\partial}{\partial p_q^\mu} \right) I = 0$, which, once contracted with all the possible antisymmetric combinations of $p_i^\mu p_j^\nu$, yields the *Lorentz invariance identities* (LI):

$$(p_i^\mu p_j^\nu) \sum_{q=1}^E \left(p_{q,\nu} \frac{\partial}{\partial p_q^\mu} - p_{q,\mu} \frac{\partial}{\partial p_q^\nu} \right) I(p_1, \dots, p_E) = 0 . \quad (2.35)$$

Once again the presence of the derivative will generate relations between elements of the same integral family, with different powers of the denominators [205]. Let us also notice that in principle any Lorentz invariance identity can be expressed as a linear combination of integration-by-parts identities [228].

2.2.5 — Master integrals evaluation

The last step in the evaluation of a diagram, once we have reduced it to a linear combination of master integrals, is given by the explicit evaluation of such master integrals.

This can be accomplished either by the direct evaluation of the associated integrals, in which case some useful parametrization, which will be presented in section 2.2.5, may be useful; or otherwise by employing the methods of *differential equations* or *difference equations* [48, 49, 205].

The master integrals needed for the work carried out in this thesis have been explicitly derived in appendix C; furthermore an application of the method of differential equations is shown in appendix C.5.2.

■ Method of differential equations

The method of differential equations, first presented in [50–54], allows us to evaluate master integrals without requiring their direct integration: such a method rests on the fact that a given master integrals depends on external momenta $\{p_1, \dots, p_E\}$ and possibly on other external quantities, such as masses of the particles running in the loop; we may then differentiate the master integral with respect such external quantities, obtaining in general a sum over a series of terms in which some denominator gets raised to a higher power, and a new numerator is created.

We can then build upon the method previously presented: we can apply the methods presented in section 2.2.4 to reduce such an expression to a linear combination of scalar integrals, and employ the identities therein introduced to reduce the scalar integrals to the minimal set of master integral. In the end, considering eventually all the master integrals belonging to a given topology, and differentiating with respect to all the kinematic quantities at our disposal, we'll obtain a coupled system of differential equations, whose solution will give the explicit expression of the master integrals we were looking for [55].

Let us notice that to uniquely solve such a system of differential equations one must impose the right boundary conditions: this for example may be done by imposing that the resulting master integrals have the correct analytical behavior at some known kinematic point [55]. In general it may not be possible to exactly solve the system of differential equations; but in most cases one can work around this issue by expanding around the needed space(-time) dimension d , e.g. $d = 3 + \epsilon$ with $\epsilon \ll 1$, and solving the differential equations in a perturbative manner [56, 211].

■ Useful parametrizations for direct integration

To solve some integrals appearing in multi-loop calculations sometimes it may be useful to rewrite some terms in a different (integral) representations; below we outline two such tricks that will be used.

Feynman parameters

One may rewrite the product of two denominators by introducing auxiliary variables, known as *Feynman parameters*, using the identity [190]:

$$\frac{1}{AB} = \int_0^1 dx \frac{1}{(xA + (1-x)B)^2} = \int_0^1 dx \int_0^1 dy \delta(x+y-1) \frac{1}{(xA + yB)^2}; \quad (2.36)$$

which can be generalized by taking derivatives of the previous formula with respect to A or B ; obtaining:

$$\frac{1}{A^m B^n} = \frac{\Gamma(m+n)}{\Gamma(m)\Gamma(n)} \int_0^1 dx \frac{x^{m-1} (1-x)^{n-1}}{(xA + (1-x)B)^{m+n}}; \quad (2.37)$$

where we introduced the gamma function (B.1), see also appendix B.

The Feynman parameters are particularly useful when we're dealing with a denominator which is a function of the integration variable, but shifted by another vector, as they let us transform the denominator in a more manageable form; for example, working with spatial components:

$$\begin{aligned} \int \frac{d^d \mathbf{k}}{(2\pi)^d} \frac{1}{|\mathbf{k}|^2 |\mathbf{k} - \mathbf{p}|^2} &= \int_0^1 dx \int \frac{d^d \mathbf{k}}{(2\pi)^d} \frac{1}{(|\mathbf{k} - x\mathbf{p}|^2 + x(1-x)|\mathbf{p}|^2)^2}, \\ &= \int_0^1 dx \int \frac{d^d \mathbf{k}'}{(2\pi)^d} \frac{1}{(|\mathbf{k}'|^2 + \Delta)^2}, \end{aligned} \quad (2.38)$$

where we recognized $A = |\mathbf{k} - \mathbf{p}|^2 = |\mathbf{k}|^2 + |\mathbf{p}|^2 - 2\mathbf{k} \cdot \mathbf{p}$ and $B = |\mathbf{k}|^2$, so $x(A - B) + B = x(|\mathbf{p}|^2 - 2\mathbf{k} \cdot \mathbf{p}) + |\mathbf{k}|^2 = |\mathbf{k} - x\mathbf{p}|^2 + x|\mathbf{p}|^2 - x^2|\mathbf{p}|^2$, and where we performed the change of variables $\mathbf{k}' = \mathbf{k} - x\mathbf{p}$, which is just a shift and therefore doesn't modify the integration measure, and where finally we denoted $\Delta = x(1 - x)|\mathbf{p}|^2$.

Schwinger parameters

The *Schwinger parametrization* is similar to the previous one, but it is instead used to convert a multiplication of denominators into a sum inside an exponential. In fact, let us consider the following integral, with $A \in \mathbb{R}^+$:

$$\int_0^{+\infty} dt t^{m-1} e^{-At} = \frac{1}{A^m} \underbrace{\int_0^{+\infty} du u^{m-1} e^{-u}}_{=\Gamma(m)} = \frac{\Gamma(m)}{A^m}, \quad (2.39)$$

where we performed the change of variables $u = At$, and we recalled the definition of the gamma function (B.1). From the formula just obtained follow also the needed relations, for example:

$$\frac{1}{A} = \int_0^{+\infty} dx e^{-Ax} \quad (2.40a)$$

$$\frac{1}{A^m} = \frac{1}{\Gamma(m)} \int_0^{+\infty} dx x^{m-1} e^{-Ax} \quad (2.40b)$$

$$\frac{1}{A^m B^n} = \frac{1}{\Gamma(m)\Gamma(n)} \int_0^{+\infty} dx x^{m-1} \int_0^{+\infty} dy y^{n-1} e^{-(Ax+By)}. \quad (2.40c)$$

EFFECTIVE FIELD THEORY FOR THE INSPIRAL OF A COMPACT BINARY SYSTEM

In this chapter we'll present how the effective and quantum field theory frameworks we summarized in chapter 2 can be used to build an effective theory which describes the inspiral of a compact binary system, more specifically the post-Newtonian corrections to the binary dynamics.

This approach, first employed in [42], was clearly framed in the seminal paper [43] (see [38, 192, 213, 229] for reviews), which built upon effective field theories built to tackle non relativistic bound states in QED and QCD [230, 231], such as heavy quark effective theory, HQET [232–234]. Since then this method has proven to be really efficient when combined with multi-loop quantum field

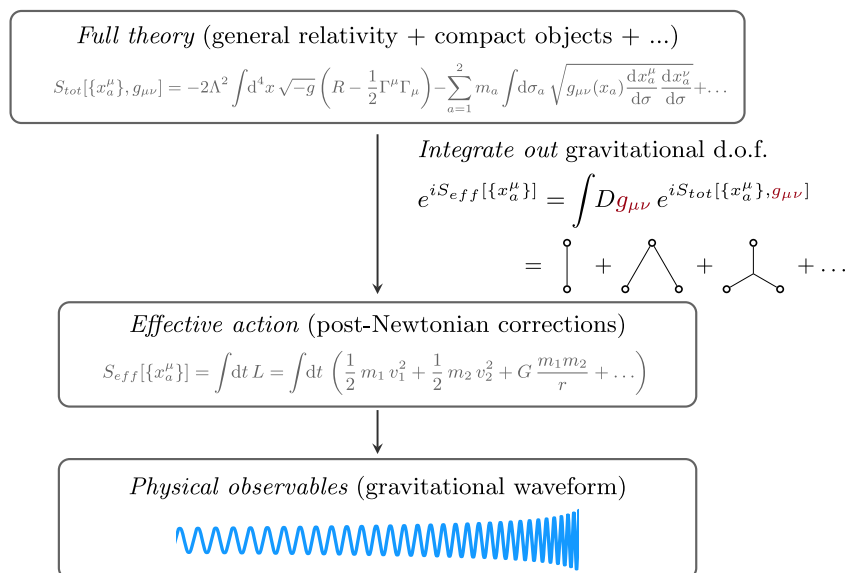


FIGURE 3.1 — Schematic idea behind the construction of an effective theory for the inspiral of a compact binary system: while the binary dynamics are prescribed by the full theory, given by general relativity coupled to the compact objects, we would like to work in a simpler effective theory in which we only have to deal with the positions of the two compact objects. Then it's possible, under certain assumptions, to integrate out the *nuisance* gravitational degrees of freedom in order to obtain the post-Newtonian corrections to the dynamics of the compact binary system. Then in this effective theory, which still formally encodes all the details of the full starting theory (restricting to the inspiral phase, and up to non-perturbative effects), we can evaluate more easily the observables for the system, such as the gravitational waveform: this will be the focus of chapter 6.

theory techniques, allowing for a steady advancement in the post-Newtonian calculations, especially in the conservative sector: the 1PN was computed already in reference [43], the 2PN in [235], the 3PN in [57], the 4PN in [44, 58], the 5PN in [59, 64, 65], and partial results have been obtained at 6PN [77, 78]. Furthermore this formalism is well suited to incorporate also corrections due to spin [79–82] and finite size effects [83, 84].

The basic idea at the basis of this approach is outlined in figure 3.1: in particular the post-Newtonian assumptions of weak field and slow velocities $\frac{Gm}{r} \sim v^2 \ll 1$ imply that the size of each compact object is much smaller than the orbital separation between the two bodies, which in turn is much smaller than the wavelength of the emitted gravitational waves. This allows to clearly single out three spatial regions, and to build a different effective theory for each of them: this let us deal with fewer degrees of freedom at a time, greatly simplifying the treatment of the two-body problem, both from a conceptual and a computational point of view. Furthermore the fact that we're working in a quantum field theory framework let us exploit the modern multi-loop evaluation techniques, which we introduced in section 2.2; yet remarkably the results that we will obtain will be fully classical. On top of this, other advantages of the effective field theory approach is that it allows for a systematic treatment of the spins and the finite size effects of the compact objects; and it may also be possible to obtain predictions in modified gravity theories, as any modification at the level of the original action will be connected to the change in physical observables.

In this chapter we'll adopt $\hbar = c = 1$ units and we'll often work in d spatial dimension to employ dimensional regularization, sending $d \rightarrow 3$ only at the end of the calculations; see [Notation](#) for further details. In section 3.1 we'll introduce a toy model to present some key concepts; in section 3.2 we'll introduce the actual effective theory for compact binary systems; finally in section 3.3 we'll use these framework to compute the Newtonian potential.

3.1 | Scalar gravity toy model

To better understand some key points presented in chapter 2, which will be used to construct the effective theory for a binary system, we'll first start working with a simpler toy model, following reference [192] (see also [205, 225, 236] for further discussions). In particular we'll explicitly present the procedure of integrating out fields, showing how it yields an effective action, and then how this result may be accomplished in a perturbative way using a diagrammatic approach.

The building blocks of this toy model, which may be called *scalar gravity*, are:

- the 3+1 space-time, which is assumed to be exactly Minkowski flat, $g_{\mu\nu} = \eta_{\mu\nu}$;
- a non self-interacting massless real scalar field $\phi(x)$;
- n point particles, with worldlines $x_a^\mu(\lambda)$, $a = 1, \dots, n$;
- a linear interaction term between the scalar field ϕ and the point particles.

The action of this toy model, as in [192], therefore is:

$$S[\phi, x_a^\mu] = \int d^4x \left(\frac{1}{2} \partial_\mu \phi \partial^\mu \phi \right) - \sum_{a=1}^n m_a \int d\tau_a \left(1 + \frac{\phi(x_a(\tau_a))}{2\sqrt{2}m_{Pl}} \right), \quad (3.1)$$

with $d\tau_a = \sqrt{\eta_{\mu\nu} dx^\mu dx^\nu}$ the proper time along the a -th particle worldline [236].

In the following we'll take $n = 2$ point particles to obtain the case of a binary system.

To obtain the dynamics of the system one needs to integrate out the scalar field ϕ , which represents the gravitational degree of freedom, to obtain an effective action $S_{eff}[x_a]$ which is a functional of the

worldlines $\{x_a\}$ only. As we have seen in the previous section 2.1, in the path integral formulation of quantum field theory this is given by:

$$e^{iS_{eff}[x_a]} = \int D\phi e^{iS[\phi, x_a]} . \quad (3.2)$$

Actually in this simplified model the path integral evaluation (3.2) can be carried out analytically [192], by noticing that the action (3.1) can be rewritten as

$$\begin{aligned} S[\phi, x_a^\mu] &= \int d^4x \left(\frac{1}{2} \partial_\mu \phi \partial^\mu \phi - \underbrace{\sum_{a=1}^n \int d\tau_a \frac{m_a}{2\sqrt{2}m_{Pl}} \delta^{(4)}(x - x_a(\tau_a)) \phi(x)}_{\equiv -J(x)} \right) - \sum_{a=1}^n \int d\tau_a m_a , \\ &= \int d^4x \left(\frac{1}{2} \partial_\mu \phi \partial^\mu \phi + J(x) \phi(x) \right) - \sum_{a=1}^n \int d\tau_a m_a \end{aligned} \quad (3.3)$$

where we defined

$$J(x) \equiv - \sum_{a=1}^n \frac{m_a}{2\sqrt{2}m_{Pl}} \int d\tau_a \delta^{(4)}(x - x_a(\tau_a)) \quad (3.4)$$

as an appropriate source function. Therefore equation (3.2) reduces to:

$$S_{eff}[x_a] = -i \ln \left(\int D\phi e^{iS[\phi, x_a]} \right) = - \sum_{a=1}^n \int d\tau_a m_a - i \ln (Z[J(x)]) , \quad (3.5)$$

with

$$Z[J] = \int D\phi \exp \left(i \int d^4x \left(\frac{1}{2} \partial_\mu \phi \partial^\mu \phi + J(x) \phi(x) \right) \right) \quad (3.6)$$

the partition function of a massless scalar field linearly coupled to an external source $J(x)$.

The analytic expression of the partition function is exactly known, as it is a gaussian integral in quantum field theory [190, 191]:

$$\begin{aligned} Z[J] &= \int D\phi \exp \left(i \int d^4x \left(\frac{1}{2} \partial_\mu \phi \partial^\mu \phi + J(x) \phi(x) \right) \right) \\ &= \exp \left(-\frac{1}{2} \int d^4x d^4y J(x) G_2(x-y) J(y) \right) \end{aligned} \quad (3.7)$$

which is normalized such that $Z[0] = 1$, and with

$$G_2(x-y) = \int \frac{d^4k}{(2\pi)^4} \frac{i}{k^2 + i\epsilon} e^{-ik(x-y)} \quad (3.8)$$

the *two-point correlation function* of the free theory, where $k^2 \equiv \eta_{\mu\nu} k^\mu k^\nu$. Notice that this is related to the Feynman propagator $\Delta_F(x-y)$ by $G_2(x-y) = i\Delta_F(x-y)$.

3.1.1 — Evaluation via the diagrammatic approach

As opposed to what we've just obtained, in the more complex NRGR case, it won't be possible to evaluate the result of path integral in a closed-form; instead it will be necessary to resort to

a perturbative expansion. Therefore, to get a grasp of the whole procedure, we'll compute the effective action (3.5) via the diagrammatic approach, as described in section 2.1.

We may apply these concepts to evaluate the (second term) of the effective action (3.5). The Feynman rules in momentum space for the field ϕ to be integrated out can be obtained from the action as re-written in equation (3.3):

$$\begin{array}{c} \xrightarrow{k} \\ \text{-----} \end{array} = \frac{i}{k^2 + i\epsilon} \quad (3.9)$$

$$\begin{array}{c} \text{-----} \\ | \\ \uparrow k \end{array} = i \int d^4x J(x) e^{ikx} = -i \sum_{a=1}^n \frac{m_a}{2\sqrt{2}m_{Pl}} \int d\tau_a e^{ikx_a(\tau_a)}. \quad (3.10)$$

To draw all the relevant Feynman diagrams, we can notice that the linear coupling $J\phi$, in equation (3.10), gives a free point for one end of the scalar propagator (3.9) to attach to. Therefore, to obtain the expression of the partition function, we have to draw an even number $2m$ of couplings to the source, and connect them with m scalar propagators in all possible ways, taking care of symmetry factors.

Still it's important to notice that, due to the fact that the source are static, they do not propagate in the Feynman diagrams [213]; therefore we could strip away the thick lines altogether. So we have that, fixed the order of Feynman diagram with m scalar propagators, all the possible ways ($\frac{(2m)!}{2^m m!}$ combinatorial factor) to connect the $2m$ identical sources, lead to the same result: this is represented by a diagram in which all scalar propagator are parallel, and the worldlines of the sources are joined one by another (even though we stress that there is no source propagator). The symmetry factor of a diagram with m scalar propagators is given by the inverse of the number of permutations of the sources, so $\frac{1}{(2m)!}$.

So for example, the diagram with a single scalar propagator ($m = 1$) is given by, noticing that we have to flip the sign of the momenta in the $J(y)$ source Feynman rule:

$$\begin{aligned} M_1(k) &\equiv \begin{array}{c} \text{-----} \\ | \\ k \downarrow \\ | \\ \text{-----} \end{array} \\ &= \left(\frac{2!}{2}\right) \left(\frac{1}{2!}\right) \left(i \int d^4x J(x) e^{-ikx}\right) \left(\frac{i}{k^2 + i\epsilon}\right) \left(i \int d^4y J(y) e^{+iky}\right) \\ &= -\frac{i}{2} \int d^4x \int d^4y J(x) \frac{1}{k^2 + i\epsilon} e^{-ik(x-y)} J(y). \end{aligned} \quad (3.11)$$

Summing instead all diagrams with m scalar propagators, we get:

$$\begin{aligned} M_m(\{k_j\}) &\equiv \begin{array}{c} \text{-----} \\ | \quad \quad \quad | \\ k_1 \downarrow \quad \dots \quad (m-2) \quad \dots \quad \downarrow k_m \\ | \quad \quad \quad | \\ \text{-----} \end{array} \\ &= \left(\frac{(2m)!}{2^m m!}\right) \left(\frac{1}{(2m)!}\right) \prod_j^m \left(i \int d^4x_j J(x_j) e^{-ik_j x_j}\right) \left(\frac{i}{k_j^2 + i\epsilon}\right) \left(i \int d^4y_j J(y_j) e^{+ik_j y_j}\right) \\ &= \frac{1}{m!} \prod_j^m \left(-\frac{i}{2} \int d^4x d^4y J(x) \frac{1}{k_j^2 + i\epsilon} e^{-ik_j(x-y)} J(y)\right). \end{aligned} \quad (3.12)$$

After integrating over all the free momenta k_j via $\prod_j^m \int \frac{d^4 k_j}{(2\pi)^4}$, we can notice that the sum of all diagrams obtained with these procedure gives the exact result (3.7) for the partition function. To see this, notice that at a given order m

$$\int \left(\prod_j^m \frac{d^4 k_j}{(2\pi)^4} \right) M_m(\{k_j\}) = \frac{1}{m!} \left(\int \frac{d^4 k}{(2\pi)^4} M_1(k) \right)^m \quad (3.13)$$

holds, and therefore we have that the sum of all diagrams, with free momenta integrated over:

$$\begin{aligned} M_{tot} &\equiv \text{---} \text{---} \text{---} + \text{---} \text{---} \text{---} + \text{---} \text{---} \text{---} + \dots \\ &= \sum_{m=0}^{+\infty} \left(\int \prod_j^m \left(\frac{d^4 k_j}{(2\pi)^4} \right) M_m(k_l) \right) \\ &= \sum_{m=0}^{+\infty} \frac{1}{m!} \left(\int \frac{d^4 k}{(2\pi)^4} M_1(k) \right)^m \\ &= \exp \left(\int \frac{d^4 k}{(2\pi)^4} M_1(k) \right) = \exp \left(\text{---} \text{---} \text{---} \right) \\ &= \exp \left(-\frac{1}{2} \int d^4 x d^4 y J(x) G_2(x-y) J(y) \right) = Z[J] \end{aligned} \quad (3.14)$$

where in the last lines we recalled the relations (3.11), (3.8) and (3.7).

From these relations we can also check that the logarithm of the partition function is actually given by the sum over connected diagrams only: in our case the only connected diagram is the one with two sources, $J(x)$ and $J(y)$, connected by a single ($m = 1$) propagator $\Delta_F(x-y)$; this single diagram is M_1 (3.11). This is what we were expecting from (3.14), as it holds

$$\ln(Z[J]) = \int \frac{d^4 k}{(2\pi)^4} M_1(k) = \text{---} \text{---} \text{---} . \quad (3.15)$$

The logarithm of the partition function is related to the effective action of the theory, and the notion that the diagrams contributing to the effective action are only the ones which remain connected after we strip away the thick worldlines, holds true also in the more complex NRGR case [192].

We can finally obtain the expression we were interested in for the effective gravitational action after having integrated the ϕ field out. From (3.5) we obtain:

$$\begin{aligned} S_{eff}[x_a] &= - \sum_{a=1}^n \int d\tau_a m_a - i \ln(Z[J(x)]) \\ &= - \sum_{a=1}^n \int d\tau_a m_a - i \int \frac{d^4 k}{(2\pi)^4} M_1(k) \\ &= - \sum_{a=1}^n \int d\tau_a m_a - \frac{1}{2} \int d^4 x d^4 y \frac{d^4 k}{(2\pi)^4} J(x) \frac{1}{k^2 + i\epsilon} e^{-ik(x-y)} J(y) . \end{aligned} \quad (3.16)$$

Recalling the definition of the source $J(x)$ from (3.4), we obtain:

$$\begin{aligned} S_{eff}[x_a] &= - \sum_{a=1}^n \int d\tau_a m_a - \frac{1}{2} \sum_{a,b}^{a \neq b} \frac{m_a m_b}{8 m_{Pl}^2} \int d\tau_a d\tau_b \frac{d^4 k}{(2\pi)^4} \frac{1}{k^2 + i\epsilon} e^{-ik(x_a(\tau_a) - x_b(\tau_b))} \\ &= - \sum_{a=1}^n \int d\tau_a m_a + \frac{i}{2} \sum_{a,b}^{a \neq b} \frac{m_a m_b}{8 m_{Pl}^2} \int d\tau_a d\tau_b G_2(x_a(\tau_a) - x_b(\tau_b)) , \end{aligned} \quad (3.17)$$

where we have neglected the $a = b$ unphysical case [192]. This unphysical case eventually will not be of concern in the real theory, as it will generally result in vanishing scaleless integrals.

This analysis could have been performed also including higher order operators, as in [236], such as $\lambda_n \phi^n$ higher order interactions, which would have made unavoidable the need of perturbation theory, and so of the diagrammatic approach hitherto shown.

3.2 | Effective theory for a compact binary system

We'll now apply what we've seen so far to construct the effective theory for a compact binary system. In particular let us point out that we'll employ a somewhat different notation for the conservative diagrams with respect to what is usually used in the literature; furthermore also the approach we adopt to the radiation effective theory is slightly different.

3.2.1 — Key ideas and outline of the construction procedure of the effective theory

■ Worldlines as non-dynamical degrees of freedom

The first point that must be addressed in order to correctly construct the effective field theory for a compact binary system which correctly yields the post-Newtonian corrections, is to notice that the evolution of the system is dictated by the interaction of each compact object with the gravitational field, which, simplifying the setup, mediates the gravitational force and dissipate energy and angular momentum via the emission of gravitational waves.

In particular, adopting a quantum field theory approach, we can think of all of this as taking place via the constant interaction of each compact objects with a huge number of gravitons, which are the quantized particles associated to the gravitational field. Nonetheless, as pointed out by reference [43], these gravitons have a momentum of order the inverse orbital separation or less, $|\mathbf{k}| \lesssim \frac{\hbar}{r}$; whereas the compact objects, even if assumed to be non relativistic, have a momentum $|\mathbf{p}| \sim mv$. This means that when each graviton interacts with a compact object, it induces a fractional recoil of order $\frac{|\mathbf{k}|}{|\mathbf{p}|} \sim \frac{\hbar}{r} \frac{1}{mv} = \frac{\hbar}{L} \ll 1$, where $L = mvr$ is the modulus of the classical orbital angular momentum associated to the compact object. In particular, using the virial theorem $v^2 \sim \frac{Gm}{r} \sim \frac{R_s}{2r}$, so $L \sim \frac{mR_s}{2v}$ already for a neutron star of $m \sim M_\odot$, we can estimate $\frac{L}{\hbar} \sim 1.7 \cdot 10^{77} \left(\frac{m}{M_\odot}\right)^2 \left(\frac{v}{0.1c}\right)^{-1}$. We may then assume that each compact objects is practically undisturbed by the interaction with each graviton, and therefore, for what concerns the latter, we can treat the positions of the compact objects (denoted as *worldlines* $\{x_a^\mu\}$) as non-dynamical, background, degrees of freedom; with which the dynamical gravitational degrees of freedom interact.

This means that there will be no propagator associated to the worldlines, similarly to the static sources $J(x)$ we encountered in the toy model of section 3.1, and instead the degrees of freedom that we'll have to integrate out will be the ones associated to the gravitational field. This remark, pointed out by reference [43], is the one which allows to correctly construct the EFT; it builds upon the similar treatment employed in the heavy quark effective theory [232–234].

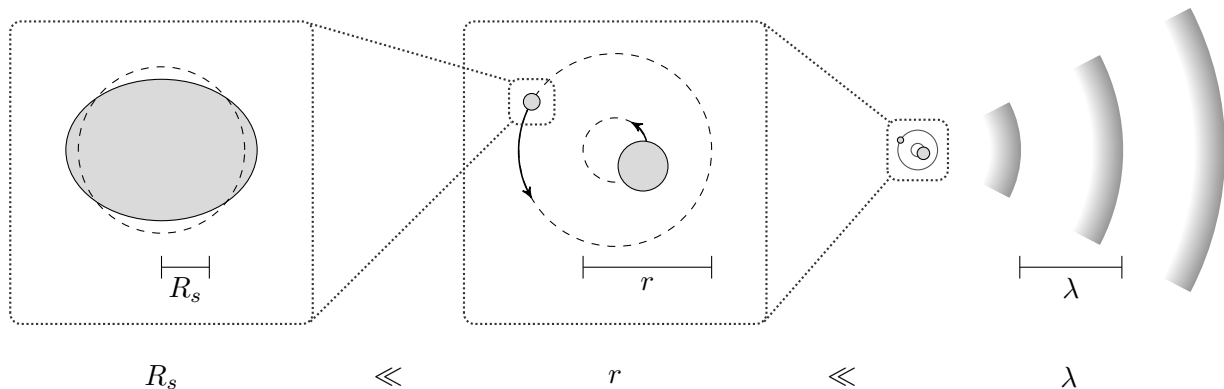


FIGURE 3.2 — Figure depicting the separation of scales which is present in the non-relativistic two body problem. From the left to the right we first have the internal zone, with characteristic length the Schwarzschild radius R_s , then the near zone, with characteristic length the orbital separation r , and finally the far zone, in which the typical length is given by the wavelength λ of the gravitational waves produced by the compact binary. Let us point out that this figure is meant only to illustrate this feature of the problem at hand, for example in reality we require the separation of these scales to be larger than what it has been depicted above.

Furthermore the huge number of gravitons involved assures us that this quantum-mechanical viewpoint in practice will be equivalent to the classical description, since quantum corrections will be subleading.

■ Separation of scales

Another key point which is exploited to construct the effective theory for a binary system is the *separation of scales* which is present in the *non-relativistic* two body problem, for gravitationally bound systems. In fact the dynamics of a binary system can be divided into [213, 237]:

- The *internal zone*, which has a length scale comparable to the size of each body; for the compact bodies we're considering therefore it can be estimated by their Schwarzschild radius $R_s = 2Gm$, see section 1.2.2. This is the scale which finite size effects extend over, as could be the spin of each body, or their deviations from spherical symmetry due to tidal deformations.
- The *near zone*, or *potential zone*, where the orbital dynamics play out; the length scale for example is given by the relative separation r between the bodies.
- The *far zone*, or *radiation zone*, which is the characteristic scale associated to gravitational waves propagation, and is given by their wavelength λ .

In particular under our assumptions of small velocities, $v^2 \ll 1$, and assuming comparable masses $m_1 \sim m_2 \sim m$, recalling section 1.6.1 we find that $r \sim \frac{Gm}{v^2} \sim \frac{R_s}{v^2} \gg R_s$, while as seen in section 1.4.2 we also expect $\lambda \sim \frac{r}{v} \gg r$. Then we see that under the condition of small velocities $v^2 \ll 1$ a *hierarchy of scales* becomes evident:

$$R_s \ll r \ll \lambda, \quad (3.18)$$

as depicted also in figure 3.2.

Let us point out that this separation of scales is used more or less implicitly also in other different approaches to the post-Newtonian theory, e.g. when matching post-Newtonian and multipolar-post-Minkowskian solutions in an intermediate buffer zone between the near and the far zone [36].

■ Tower of effective field theories

The separation of scales just presented above suggests the introduction of a *tower of effective field theories*, so one effective theory for each region, each specifically tailored to capture the dynamics of the relevant degrees of freedom therein [43, 192, 213, 238]. We can then match the several effective theories so introduced at the boundaries of their regions: in this way the details of the innermost regions, such as the internal dynamics of each compact object and their orbital evolution, will affect also the observables which are evaluated in the outermost region, such as the gravitational waveform seen by a far away observer.

In practice this procedure is (ideally) implemented by starting from the fundamental theory, such as general relativity coupled to the compact objects, and progressively integrating out the high-energy (so short distance) degrees of freedom as discussed in section 2.1.2, until we obtain an effective action which depends only on the positions of the compact objects; this is also sketched in figure 3.3. The procedure that we'll have to follow then is, denoting with $k^{-1} = \frac{1}{|\mathbf{k}|}$ the length scale at which we're progressively probing the system:

1. Introduce the fundamental theory; in particular the one which describes also the dynamics in the internal zone, so for the degrees of freedom with wavelength $k^{-1} < R_s$. In practice considering all the details of each compact objects is both too complicated and not even necessary for the precision we're aiming for. Therefore in section 3.2.2 we'll actually introduce an effective theory, known as *Worldline Effective Theory*, in a bottom-up approach, resorting to symmetry arguments: this theory will actually provide a coarse grained description of the internal dynamics at the level $k^{-1} \sim R_s$, so in practice will be useful to describe how the internal zone interacts with the near and the far zone [213, 238].
2. Integrate out the internal zone degrees of freedom, so the modes with wavelength $k^{-1} < R_s$, to obtain an effective theory which describes the dynamics in the internal zone, so of the degrees of freedom with $k^{-1} \sim r$. In practice this will be accomplished by considering one distinct worldline effective theory for each compact object.
3. Integrate out the near zone degrees of freedom, so the modes with wavelength $k^{-1} < r$, to obtain an effective theory which describes the dynamics in the far zone, so of the degrees of freedom with $k^{-1} \sim \lambda$. This will be accomplished by integrating out the potential modes of the gravitational field, and the needed setup will be developed in section 3.2.3.
4. Integrate out all of the remaining degrees of freedom, to obtain an effective theory, i.e. an

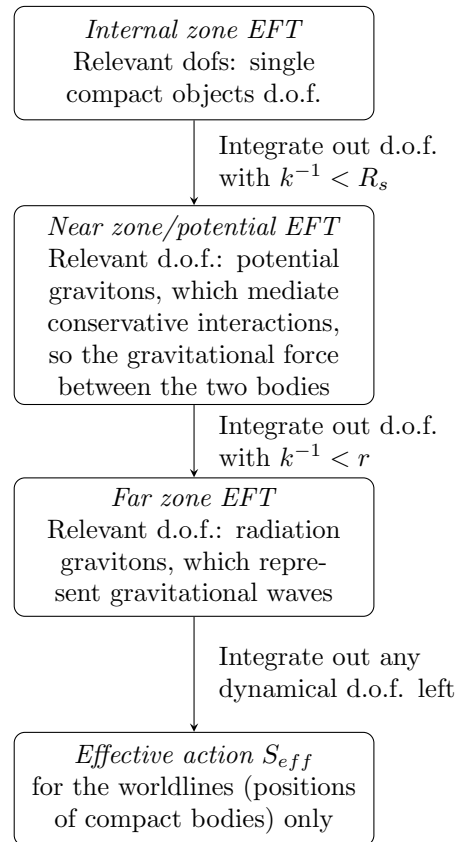


FIGURE 3.3 — A diagram outlining the key steps in the construction of the effective theory for a binary system. In particular we have to start from the shortest distances, and integrate out the relevant degrees of freedom (d.o.f.) in each intermediate effective theory until we obtain an effective action S_{eff} , which is a function of the position of the compact objects $\{x_a^\mu\}$ only. Let us point out that at higher PN order the distinction between conservative (potential gravitons) and dissipative (radiation gravitons) contributions isn't as simple as presented due to hereditary effects.

effective action $S_{eff}[\{x_a^\mu\}]$, which depends only on the positions $\{x_a^\mu\}$ of the compact objects (their worldlines): the coefficients of the post-Newtonian corrections therein will implicitly encode the corrections due to the full gravitational interactions, so due to general relativity, that we integrated out. In practice this step will be accomplished by integrating out also the remaining radiation modes of the gravitational field, as will be explained in section 3.2.4; nonetheless, before integrating out these d.o.f., we can evaluate also observables in the far zone, such as the gravitational waveform, as will be presented in section 3.2.5.

In particular, at higher PN order, we expect to also have renormalization group flow for certain observables as we probe them at different length (so energy) scales; which we have to evolve between the several matching procedures [43, 84, 192, 213].

3.2.2 — Worldline effective theory

In this initial stage we consider the dynamics of a single compact body coupled to general relativity. Therefore the complete dynamics are governed by the Einstein-Hilbert action S_{EH} and possibly also by the action S_M for the matter fields, which may be the matter that make up a neutron star; these actions are respectively given by formulae (1.1) and (1.2).

We're now interested in finding the effective field theory which describes the dynamics of the gravitational field $g_{\mu\nu}$ on scales larger than the Schwarzschild radius R_s ; therefore the degrees of freedom to integrate out are the ones which reside inside the internal zone, so with $k^{-1} \lesssim R_s$. To single them out we may separate the metric $g_{\mu\nu}$ as

$$g_{\mu\nu} = g_{\mu\nu}^{(S)} + g_{\mu\nu}^{(L)} \quad (3.19)$$

where $g_{\mu\nu}^{(S)}$ are the short distance modes, i.e. with $k^{-1} < R_s$, and $g_{\mu\nu}^{(L)}$ the complementary long distance modes. In this way the degrees of freedom to integrate out in this first step are the short modes of the gravitational field $g_{\mu\nu}^{(S)}$ and the matter fields [213].

This step ideally would be accomplished by integrating out the relevant degrees of freedom from the detailed UV description of the dynamics of each body, e.g. of the black holes or the neutron stars, in a top-down approach: nonetheless this description of any realistic compact body is in general extremely complicated and still not exactly known; for example the action for the matter fields may be interpreted as the one which describes all the particles which constitutes the compact body and their interactions. In practice therefore we have to resort to a bottom-up approach to build this effective field theory, denoted as *worldline effective theory* [43, 213]: we parametrize our ignorance about the internal dynamics of the compact objects by approximating them as point particles plus a series of higher order operators [213].

To do this methodically we have to proceed as presented in section 2.1.3: we start by noticing that after integrating out the modes with $k^{-1} < R_s$, the remaining low energy degrees of freedom, which are explicit in this effective theory, are given by [38, 192, 197, 213]:

1. the long wavelength modes of the gravitational field, so by $g_{\mu\nu}^{(L)}$;
2. by the particle worldline coordinate $x^\mu(\sigma)$, which is a function of the arbitrary affine parameter σ , and may be interpreted as parametrizing the position of the center of mass of the compact object;
3. by an orthonormal frame $e^\mu(\sigma)$ localized on the particle worldline, which described the orientation of the compact bodies and also its possibly non vanishing spin.

Actually neutron stars may contain additional low frequency modes which should be kept in the construction of this effective field theory, see [192]. Furthermore in this work we'll neglect the

spin of the compact objects (whose corrections first contribute at 1.5PN order) even though it is phenomenologically relevant and hence should be considered, see references [38, 80, 81, 182, 213, 229, 239–241] for more details about its treatment.

As already discussed, now we have to recognize the symmetries of the systems, which constraint the ways the previous degrees of freedom may couple, thereby reducing the number of operators we have to consider in the effective Lagrangian. The symmetries of the system we're considering are given by [192]:

1. diffeomorphism invariance for $x^\mu \rightarrow x'^\mu(x)$;
2. worldline reparametrization invariance, $\sigma \rightarrow \sigma'(\sigma)$.

To simplify calculations we'll make the additional assumption that the compact object is perfectly spherical, i.e. that it doesn't have any permanent moments relative to its own rest frame when in isolation [192, 213]. Therefore we have an additional symmetry given by [192]:

3. $SO(3)$ invariance.

The assumptions we've made so far therefore imply that the worldline effective theory we're constructing we'll be adequate to describe non-spinning, spherically symmetric black holes, that is, Schwarzschild black holes interacting with the external gravitational field [192].

To construct an effective Lagrangian that is compatible with the aforementioned symmetry, we can notice that diffeomorphism invariance can be satisfied by simply constructing scalars from $g_{\mu\nu}$ and $\frac{dx^\mu}{d\sigma}$, while to ensure invariance under worldline reparametrization we may simply use the proper time variable

$$d\tau^2 = g_{\mu\nu}^{(L)}(x(\sigma))dx^\mu dx^\nu, \quad (3.20)$$

which is an observable, physical, quantity, and hence must be invariant [192, 242].

Then the effective action will finally be given by [192, 213]:

$$S_{eff,worldline}[x^\mu, g_{\mu\nu}^{(L)}] = S_{EH}[g_{\mu\nu}^{(L)}] + S_{pp}[x^\mu, g_{\mu\nu}^{(L)}] \quad (3.21)$$

where $S_{EH}[g_{\mu\nu}^{(L)}]$ is the usual Einstein-Hilbert action (1.1), but restricted to long wavelengths only, while

$$S_{pp}[x^\mu, g_{\mu\nu}^{(L)}] = S_{pp}^{(PP)}[x^\mu, g_{\mu\nu}^{(L)}] + S_{pp}^{(FS)}[x^\mu, g_{\mu\nu}^{(L)}] \quad (3.22)$$

is the so called point particle action, which contains both the usual, leading order, point particle term $S_{pp}^{(PP)}$; but also all other higher order local operators allowed by symmetries in the expression $S_{pp}^{(FS)}$, which encodes finite size effects, such as the tidal deformability of the compact body due to the interaction with the non-homogeneous external gravitational field (eventually produced by the other compact object). Below we'll briefly outline both of these terms.

Furthermore, leveraging the separation of scales and the effective field theory approach, it's possible to take into account also additional phenomena, like the absorption of gravitational waves by the horizons of the black holes, which affects their masses and spins. In particular it's possible to more easily evaluate the cross section of such processes for isolated black holes, evaluating so the relevant Wilson coefficients of the effective theory, which can then be translated to the two body problem [43, 243].

■ Point particle term

The simplest coupling between the worldline $x^\mu(\sigma)$ and the long modes of the gravitational field $g_{\mu\nu}^{(L)}$ is given by the point particle action:

$$\begin{aligned} S_{pp}^{(PP)}[x^\mu, g_{\mu\nu}^{(L)}] &= -m \int d\tau \\ &= -m \int d\sigma d^{d+1}x \sqrt{g_{\mu\nu}^{(L)}(x) \frac{dx^\mu}{d\sigma} \frac{dx^\nu}{d\sigma}} \delta^{(d+1)}(x^\mu - x^\mu(\sigma)) \end{aligned} \quad (3.23)$$

In particular this action describes the motion of a test point particle of mass m , with coordinates $x^\mu(\sigma)$, along the geodesics given by the background metric $g_{\mu\nu}^{(L)}$, and therefore this action neglects the back reaction which the point particle exert on the spacetime itself [192, 197, 213].

■ Finite size effects and higher order operators

This expression contains all the others operators allowed by symmetries: in particular the first higher orders operators which encode finite size effects are given by [43, 206, 213]:

$$\begin{aligned} S_{pp}^{FS} &= c_R \int d\tau R^{(L)}(x(\tau)) + c_V \int d\tau R_{\mu\nu}^{(L)}(x(\tau)) \frac{dx^\mu}{d\tau}(\tau) \frac{dx^\nu}{d\tau}(\tau) \\ &+ \int d\tau (Q_E^{\mu\nu}(x(\tau)) E_{\mu\nu}(x(\tau)) + Q_B^{\mu\nu}(x(\tau)) B_{\mu\nu}(x(\tau))) \dots, \end{aligned} \quad (3.24)$$

where it is understood for example $\int d\tau R(x(\tau)) = \int d\sigma d^4x R(x) \sqrt{g_{\mu\nu}(x) \frac{dx^\mu}{d\sigma} \frac{dx^\nu}{d\sigma}} \delta^{(d+1)}(x^\mu - x^\mu(\sigma))$, and the $R^{(L)}(x)$, $R_{\mu\nu}^{(L)}(x)$ are respectively the Ricci scalar and tensor, which have been defined in the **Notation**, but built using $g_{\mu\nu}^{(L)}$. Similarly $Q_{E(B)}^{\mu\nu}$ are the symmetric trace-free quadrupole moments of the compact object, and, introduced the Weyl tensor $C_{\mu\nu\rho\sigma}$, we have that $E_{\mu\nu} \equiv C_{\mu\rho\nu\sigma} \frac{dx^\rho}{d\tau}(\tau) \frac{dx^\sigma}{d\tau}(\tau)$ is the electric part of the Weyl tensor, while $B_{\mu\nu} \equiv \frac{1}{2} \epsilon_{\mu\rho\sigma\lambda} C^{\rho\sigma}{}_{\nu\omega} \frac{dx^\lambda}{d\tau}(\tau) \frac{dx^\omega}{d\tau}(\tau)$ is the magnetic part of the Weyl tensor [206, 213].

Actually the operators linear in the curvature, presented in the first line of formula (3.24), are redundant and do not contribute to the dynamics of the system: the c_R and c_V coefficients can be set to zero as a consequence of Birkhoff's theorem, and also because they vanish by lower-order equation of motion, and so they may be redefined to be vanishing [43, 213].

Instead higher order operators encode information about finite size effects and absorption phenomena [43, 197, 206, 213, 242], for example they encode information about the Love number of the compact objects, which is vanishing for black holes but not for neutron stars: this implies also that from the observation of gravitational waves we can study the equation of state and the tidal deformability of the compact objects. About this point we can also recall the discussion outlined in section 1.6.1: due to the *effacement principle*, neglecting spin-induced tidal deformability, we actually expect such higher order operators, encoding finite size effects, to first contribute only from the 5PN order onward.

Then we find once again that, up to this really high perturbative order, the internal structure of each compact object isn't observable: therefore in the following it will suffice to model them using just the point particle term (3.23) [43, 206, 213].

3.2.3 — Near zone potential effective theory

The next step is the construction of the effective field theory which describes the dynamics of the near zone, i.e. at scale of the binary orbital separation r , hence the goal is to integrate out all

degrees of freedom with modes shorter than $k^{-1} < r$. At the orbital scale then these high energy degrees of freedom are:

1. what we denoted as long wavelengths mode of the gravitational field $g_{\mu\nu}^{(L)}$ in the previous section 3.2.2, so the modes of the gravitational fields with characteristic length $k^{-1} > R_s$;
2. two worldlines degrees of freedom x_a^μ with $a = 1, 2$, which encode the coarse-grained behavior of the two compact objects which compose the binary system; let us stress again nonetheless that this degrees of freedom are not dynamical.

The action which governs the dynamics of these degrees of freedom follows from (3.21), in particular we'll have the Einstein-Hilbert action S_{EH} for the gravitational field, and one point particle action S_{pp} , given by equation (3.22), for each worldline degree of freedom which appears in our effective field theory.

As previously pointed out, in this high-energy action we keep only the leading term in the point-particle action, given by (3.23), so $S_{pp} = S_{pp}^{(PP)}$. Furthermore we recall from section 2.2 that we'll be employing dimensional regularization to make sense of divergent quantities, so we're working in $d + 1$ dimensions, with $d \rightarrow 3$ spatial dimension. This implies a change of the mass dimension of the coupling constants, which we factor out as usual by introducing the renormalization scale μ , which can also be interpreted as the inverse of an arbitrary length scale l_0 , so $\mu \sim l_0^{-1}$. In particular, for what concerns the gravitational action, the coupling constant $m_{Pl} = (32\pi G)^{-\frac{1}{2}}$ in the Einstein-Hilbert 1.1 action becomes [36, 62, 80, 183]

$$\Lambda \equiv m_{Pl} \mu^{\frac{d-3}{2}}, \quad (3.25)$$

in such a way to obtain mass dimensions of $[m_{Pl}] = 1$ and $[\Lambda] = \frac{d-1}{2}$; let us point out that different normalization are also used in the literature [80, 81, 83, 84]. Hence the Einstein-Hilbert action, in dimensional regularization, now reads

$$S_{EH} = -2\Lambda^2 \int d^{d+1}x \sqrt{-g} R. \quad (3.26)$$

Additionally we have to take care of the gauge redundancy which general relativity enjoys due to its diffeomorphism invariance: hence, to remove the associated spurious degrees of freedom, we'll fix the harmonic gauge, whose condition is given by (1.113). In particular this can be accomplished by adding the harmonic gauge fixing term [38, 80, 205, 206, 225, 229, 235]

$$S_{GF} = \Lambda^2 \int d^{d+1}x \sqrt{-g} g_{\mu\nu} \Gamma^\mu \Gamma^\nu \quad (3.27)$$

to the Einstein-Hilbert action, where [206, 229, 244]

$$\Gamma^\mu \equiv \Gamma_{\alpha\beta}^\mu g^{\alpha\beta} = -\frac{1}{\sqrt{-g}} \partial_\nu (\sqrt{-g} g^{\mu\nu}) \quad (3.28)$$

and $\Gamma_{\alpha\beta}^\mu$ is the Christoffel symbol, defined in **Notation**; in such a way the harmonic gauge condition (1.113) reads $\Gamma^\mu = 0$ [205]. The choice of the harmonic gauge is especially useful since it introduces into the definition of our coordinate system a preferred Minkowskian structure, hence being well suited the post-Newtonian approximation [183].

Finally we can read off the full form of the action which governs the dynamics of the high energy degrees of freedom of the near zone, so at binary scale:

$$S_{near,UV}[\{x_a^\mu\}, g_{\mu\nu}^{(L)}] = S_{EH}[g_{\mu\nu}^{(L)}] + S_{GF}[g_{\mu\nu}^{(L)}] + \sum_{a=1}^2 S_{pp,a}^{(PP)}[x^\mu, g_{\mu\nu}^{(L)}]. \quad (3.29)$$

Our goal now is to obtain the effective action $S_{near,IR}$ which governs the dynamics of the lower energy degrees of freedom, i.e. those which have modes with wavelength $k^{-1} > r$ larger than the orbital scale; hence to do so we'll have to integrate out the high energy modes of the gravitational field $g_{\mu\nu}^{(L)}$ with $R_s < k^{-1} < r$.

■ Kaluza-Klein decomposition of the metric via Kol-Smolkin variables

The operation of integrating out these modes of the gravitational field $g_{\mu\nu}^{(L)}$ actually entails working with the specific components of the metric tensor: in fact the physical setup of a non relativistic binary naturally singles out the preferred coordinate frame in which the velocities of the system are small, and actually we're implicitly choosing such a frame for our computations. One of the consequences is that for example, in the point-particle action $S_{pp}^{(PP)}$, the gravitational field couples to the worldline in a non-homogeneous way, and in particular the spatial components of the metric are suppressed in powers of $v \ll 1$ with respect to the leading time component g_{00} of the metric.

We may actually exploit this fact at our advantage by performing a temporal *Kaluza-Klein* decomposition of the metric, by employing the *Kol-Smolkin* variables [245–248]; that is, we'll parametrize the metric in such a way that each of these variables will scale homogeneously in the expansion parameter of our theory, kind of singling out the g_{00} , g_{0i} and g_{ij} metric components; let us also notice that this parametrization resembles the Arnowitt-Deser-Misner (ADM) formalism [177]. These Kol-Smolkin variables, also known as *Non-Relativistic Gravity* (NRG) fields, are $\hat{\phi}(x)$, $\hat{A}_i(x)$ and $\hat{\sigma}_{ij}(x)$; using them we can parametrize the components of the long wavelengths modes of the metric $g_{\mu\nu}^{(L)}(x)$ in d -dimension as [57]:

$$g_{\mu\nu}^{(L)} = e^{2\frac{\hat{\phi}}{\Lambda}} \begin{pmatrix} 1 & & -\frac{\hat{A}_j}{\Lambda} \\ -\frac{\hat{A}_i}{\Lambda} & \frac{\hat{A}_i \hat{A}_j}{\Lambda} & -e^{-c_d \frac{\hat{\phi}}{\Lambda}} \gamma_{ij} \end{pmatrix}, \quad \gamma_{ij} \equiv \delta_{ij} + \frac{\hat{\sigma}_{ij}}{\Lambda}, \quad (3.30)$$

with

$$c_d \equiv 2 \frac{(d-1)}{(d-2)} \xrightarrow{d \rightarrow 3} 4. \quad (3.31)$$

Let us notice that we already normalized the Kol-Smolkin fields to the renormalized Planck mass Λ defined in equation (3.25), in order to recover the canonical mass dimension for the fields. Furthermore if the Kol-Smolkin fields are vanishing, i.e. $\hat{\phi} = \hat{A}_i = \hat{\sigma}_{ij} = 0$, we get back the flat metric $g_{\mu\nu} \rightarrow \eta_{\mu\nu} = \text{diag}(+, -, -, -)$, as one would have desired. This also means that in our weak field regime assumption, so $g_{\mu\nu} = \eta_{\mu\nu} + h_{\mu\nu}$ with $|h_{\mu\nu}| \ll 1$, also the Kol-Smolkin field will assume small values.

From now on then we'll trade the long wavelength modes of the gravitational field $g_{\mu\nu}^{(L)}(x)$ for the Kol-Smolkin fields $\hat{\phi}(x)$, $\hat{A}_i(x)$ and $\hat{\sigma}_{ij}(x)$, which will therefore be the degrees of freedom related to the gravitational fields which we'll have to integrate out. In particular we may identify the field $\hat{\phi}(x)$ as the Newtonian scalar, $\hat{A}_i(x)$ as the gravito-magnetic vector, and $\hat{\sigma}_{ij}(x)$ as the symmetric spatial tensor [38].

This decomposition procedure proves to significantly simplify the evaluation of the conservative sector (actually of the diagrams that will arise in this near zone EFT) at higher PN orders [206, 213, 235]. In fact, when working in harmonic gauge with $g_{\mu\nu} = \eta_{\mu\nu} + h_{\mu\nu}$, the two-point function of the metric perturbation $h_{\mu\nu}$ implies a mixing of the different components, $\langle T(h_{\mu\nu} h_{\rho\tau}) \rangle \neq 0$ also for $\mu\nu \neq \rho\tau$; instead the $\hat{\phi}$, \hat{A}_i , $\hat{\sigma}_{ij}$ fields do not mix, as the two-point functions $\langle T(\hat{\phi} \hat{A}_i) \rangle = \langle T(\hat{\phi} \hat{\sigma}_{ij}) \rangle = \langle T(\hat{A}_i \hat{\sigma}_{jk}) \rangle = 0$ are vanishing, in turn simplifying the diagram evaluation [235].

■ Explicit power counting in the point-particle action

Up until this point we have actually still made no assumptions about the relative typical velocity v between the two bodies, which could also be relativistic $v \sim 1$; in fact the Kaluza-Klein decomposition (3.30) is only a parametrization of the metric per se. The assumptions we implicitly used instead is the requirement of the gravitational field to be weak, for example in the scale separation requirement $R_s \ll r$ of having the typical scale of the bodies be much smaller than their relative distance. Hence the current description would be appropriate also for the post-Minkowskian approximation, for example to describe gravitational scattering events, once we'd perform an expansion of the full action in powers of Λ , see references [192, 205, 242].

Instead, as already explained in section 2.1.3, in order to more easily tackle the problem of integrating out the high energy modes we need to find a power counting scheme that allows us to evaluate the wanted results at the desired accuracy evaluating only a finite number of terms. Then, recognizing as the expansion parameter of the post-Newtonian approximation the typical velocity v of the system, we may explicitly enforce such a power counting already at the level of the action, such that we'll be able to determine which diagrams are needed to be taken into account to evaluate quantities at any finite PN order [43].

To do so we're required to explicitly choose the preferred coordinate frame in which the typical velocity v of the system is small $v \ll 1$, explicitly breaking diffeomorphism invariance also due to the gauge fixing, in a similar manner to what was done in the derivation of section 1.3. We can then exploit the reparametrization invariance of the particle worldlines (section 3.2.2) to use the time $t = x^0$ of a static, far away observer, as the affine parameter of the two point particle worldlines, so $\sigma_a = t$ for $a = 1, 2$. In such a way we obtain:

$$\frac{dx_a^\mu}{dt} = (1, \mathbf{v}_a) , \quad \text{with } (\mathbf{v}_a)^i = v_a^i \equiv \frac{dx_a^i}{dt} , \quad (3.32)$$

where v_a^i therefore is the three-velocity of the particle a as measured by such far away observer, and furthermore we define the modulus of the velocity of particle a as $v_a \equiv \sqrt{\mathbf{v}_a \cdot \mathbf{v}_a} = \sqrt{\delta_{ij} v_a^i v_a^j}$.

With such a choice of affine parameter, employing the Kol-Smolkin parametrization of the metric as defined in (3.30), the point particle action (3.23) associated to the worldline a with mass m_a reads:

$$\begin{aligned} S_{pp,a}^{(PP)}[x_a^\mu, \hat{\phi}, \hat{A}_i, \hat{\sigma}_{ij}] &= -m_a \int dt d^{d+1}x \sqrt{g_{\mu\nu}^{(L)}(x)} \frac{dx^\mu}{dt} \frac{dx^\nu}{dt} \delta^{(4)}(x^\mu - x_a^\mu(t)) \Big|_{g_{\mu\nu}=g_{\mu\nu}(\hat{W}_a)} \\ &= -m_a \int dt e^{\frac{\hat{\phi}}{\Lambda}} \left[1 - e^{-c_d \frac{\hat{\phi}}{\Lambda}} v_a^2 - 2 \frac{\hat{A}_i}{\Lambda} v_a^i + \left(\frac{\hat{A}_i \hat{A}_j}{\Lambda} - e^{-c_d \frac{\hat{\phi}}{\Lambda}} \frac{\hat{\sigma}_{ij}}{\Lambda} \right) v_a^i v_a^j \right]^{\frac{1}{2}} \Big|_{x=x(t)} . \end{aligned} \quad (3.33)$$

In particular, as it's explicitly derived in appendix A.2.1, the above expression of the point particle action for each worldline a factorizes into:

$$S_{pp,a}^{(PP)}[x_a^\mu, \hat{\phi}, \hat{A}_i, \hat{\sigma}_{ij}] = S_{pp,a}^{(kin)}[x_a^\mu] + S_{pp,a}^{(coupl)}[x_a^\mu, \hat{\phi}, \hat{A}_i, \hat{\sigma}_{ij}] ; \quad (3.34a)$$

$$S_{pp,a}^{(kin)}[x_a^\mu] = -m_a \int dt \sqrt{1 - v_a^2(t)} ; \quad (3.34b)$$

$$S_{pp,a}^{(coupl)}[x_a^\mu, \hat{\phi}, \hat{A}_i, \hat{\sigma}_{ij}] = -m_a \int dt \left(\frac{(2 + (c_d - 2)v_a^2)}{2\sqrt{1-v_a^2}} \hat{\phi} - \frac{1}{\sqrt{1-v_a^2}} \hat{A}_i v_a^i - \frac{1}{2\sqrt{1-v_a^2}} \hat{\sigma}_{ij} v^i v^j + \frac{((2 + c_d)v_a^2 - 2)}{2(1-v_a^2)^{3/2}} \hat{\phi} \hat{A}_i v^i + \dots \right) \Big|_{x=x(t)} ; \quad (3.34c)$$

so into a kinetic term only for the worldline, given by equation (3.34b), which is actually the special relativistic point particle action, i.e. in absence of gravitational field perturbations, specialized to the chosen reference frame; and the action (3.34c), which contains infinitely many operators that couple the worldline x_a^μ to the gravitational fields $\hat{\phi}$, \hat{A} , $\hat{\sigma}$. From expression (3.34c) we can already check the claim according to which the Kol-Smolkin field scale homogeneously in the v expansion parameter, in fact the $\hat{\phi}$ field is not contracted with any velocity vector, the \hat{A} field is contracted with one v^i vector, whereas the $\hat{\sigma}_{ij}$ with two $v^i v^j$ vectors.

In particular from the action (3.34c) follow also the Feynman rules for the interaction between the a -th particle and the gravitational degrees of freedom, $\hat{\phi}$, \hat{A}_i , $\hat{\sigma}_{ij}$; as we will see in appendix A.

■ Gauge fixed Einstein-Hilbert action in terms of Kol-Smolkin variables

We have also to rewrite the pure gravitational action, given by the sum of the Einstein-Hilbert action (3.26) and the gauge fixing term (3.27), as a function of the parametrization (3.30). Such action is also denoted as *bulk* action, $S_{bulk} = S_{EH} + S_{GF}$.

In order to derive the relevant term up to 2PN, we employed the `FeynRu1.m` module of the `EFTofPNG` package [249], which yields:

$$\begin{aligned} S_{bulk}[\hat{\phi}, \hat{A}_i, \hat{\sigma}_{ij}] &= S_{EH}[\hat{\phi}, \hat{A}_i, \hat{\sigma}_{ij}] + S_{GF}[\hat{\phi}, \hat{A}_i, \hat{\sigma}_{ij}] \\ &\supset \int d^{d+1}x \left[\left(c_d \dot{\hat{\phi}}^2 - c_d \partial^i \hat{\phi} \partial_i \hat{\phi} \right) + \left(\partial_j \hat{A}_i \partial^j \hat{A}^i - \partial_i \hat{A}_j \partial^j \hat{A}^i + (\partial_i \hat{A}^i)^2 - \dot{\hat{A}}_i \dot{\hat{A}}^i \right) \right. \\ &\quad + \frac{1}{4} \left(\partial^j \hat{\sigma}_i^i \partial_j \hat{\sigma}_k^k + 4(\partial_i \hat{\sigma}^{ij} \partial_k \hat{\sigma}_j^k - \partial_j \hat{\sigma}_{ik} \partial^k \hat{\sigma}^{ij}) - 2 \partial_k \hat{\sigma}_{ij} \partial^k \hat{\sigma}^{ij} + (\dot{\hat{\sigma}}_i^i)^2 - 2 \dot{\hat{\sigma}}_{ij} \dot{\hat{\sigma}}^{ij} \right) \\ &\quad + 4 \left(\dot{\hat{\phi}} \partial_i \hat{A}^i - \partial_i \hat{\phi} \dot{\hat{A}}^i \right) + \left(2(\dot{\hat{A}}^i \partial_j \hat{\sigma}_i^j - \partial^j \hat{A}^i \dot{\hat{\sigma}}_{ij}) + (\partial_i \hat{A}^i \dot{\hat{\sigma}}_j^j - \dot{\hat{A}}^i \partial_i \hat{\sigma}_j^j) \right) \\ &\quad + \frac{1}{2\Lambda} \left(c_d (2 \hat{\sigma}_{ij} \partial^i \hat{\phi} \partial^j \hat{\phi} - \hat{\sigma}_j^j \partial^i \hat{\phi} \partial_i \hat{\phi}) + 2 c_d (\hat{\phi} \partial_j \hat{A}_i \partial^j \hat{A}^i - \hat{\phi} \partial_i \hat{A}_j \partial^j \hat{A}^i) \right. \\ &\quad \left. + 2 c_d (\hat{\phi} (\partial_i \hat{A}^i)^2 - 2 \dot{\hat{\phi}} \dot{\hat{A}}^i \partial^i \hat{\phi}) - 2 c_d^2 \hat{\phi} (\dot{\hat{\phi}})^2 \right] , \end{aligned} \quad (3.35)$$

where the spatial indices are now raised, lowered and contracted with the d -dimensional kronecker delta δ^{ij} and δ_{ij} .

■ Potential and radiative fields modes separation in the non-relativistic regime

In the position where we're at, the Kol-Smolkin fields, which we may generically denote as $\hat{W}_a(x)$, with $\hat{W}_a = \hat{\phi}, \hat{A}_i, \hat{\sigma}_{ij}$, encode the long wavelengths modes of the gravitational field with $k^{-1} > R_s$: this means that they include also modes with a wavelength larger than the orbital scale $k^{-1} > r$, and so we'll need to separate these field further in order to single out the modes with $R_s < k^{-1} < r$. As will see, this step is actually necessary in order to obtain an explicit power counting in the typical velocity v for our effective theory, and it's possible thanks to the remarkable separation of scales between near and far zone which happens once we impose the constraint for the typical velocities to be non-relativistic, $v \ll 1$, as discussed in section 3.2.1.

Requiring $v \ll 1$, we can then split of the degrees of freedom associated with the gravitational field \hat{W}_a into potential modes W_a and radiative modes \bar{W}_a , as [192, 213, 242]

$$\hat{W}_a(k) = W_a(k) + \bar{W}_a(k) \quad (3.36)$$

where the distinction, which should more precisely be cast as (3.39), is based on to which momentum region the wavevector k^μ of the modes belongs to:

- the *potential* modes $W_a = \phi, A, \sigma$ have a wavevector which scales as $k^\mu = (k^0, \mathbf{k}) \approx (\frac{v}{r}, \frac{1}{r})$, where v is the modulus of the typical three velocity of the system; they represent off-shell space-like ($k^2 \neq 0$) potential gravitons, thus they can be thought of as the mediators of the gravitational force between the two compact bodies;
- the *radiative* modes $\bar{W} = \bar{\phi}, \bar{A}, \bar{\sigma}$ which have a wavevector that scales as $k^\mu = (k^0, \mathbf{k}) \approx (\frac{v}{r}, \frac{v}{r})$; they may be either on-shell modes ($k^2 = 0$), and hence they can be interpreted as the observable radiation gravitons, or they can be off-shell, in which case they generate both dissipative and conservative radiation reaction forces on the system [242].

Thanks to this separation we can now clearly single out the degrees of freedom to integrate out, i.e. the potential ones with $k^{-1} \lesssim r$. In fact the radiative modes satisfy

$$\partial_\alpha \bar{W}_a \sim \frac{v}{r} \bar{W}_a, \quad (3.37)$$

so they can be regarded as a slowly varying field with characteristic length $\frac{r}{v} \sim \lambda$, which is the wavelength of the emitted gravitational radiation, as we could have expected [192]. Instead the potential modes satisfy

$$\partial_0 W_a \sim \frac{v}{r} W_a, \quad \partial_i W_a \sim \frac{1}{r} W_a, \quad (3.38)$$

and they can be thought of as potential gravitons. In particular this non-homogeneous scaling of the time and spatial components of the potential modes will require us to expand their propagator $\propto \frac{1}{k^2 + i\epsilon} = \frac{1}{(k^0)^2 - |\mathbf{k}|^2}$ as $-\frac{1}{|\mathbf{k}|^2} \sum_{n=0}^{+\infty} \left(\frac{(k^0)^2}{|\mathbf{k}|^2} \right)^n$, in order to obtain a series of term, each one with a definite scaling $\left(\frac{(k^0)^2}{|\mathbf{k}|^2} \right)^n \sim v^{2n}$, more and more suppressed in $v \ll 1$: this will restore a definite scaling v for each diagram, and physically will be equivalent to considering the leading order interaction between the two bodies as instantaneous, plus an infinite series of retardation correction suppressed by powers of v^{2n} ; we'll return on this point later in this section.

Let us point out that references which do not employ the Kol-Smolkin parametrization expand instead the long wavelength modes as $g_{\mu\nu}^{(L)} = \eta_{\mu\nu} + \hat{h}_{\mu\nu} = \eta_{\mu\nu} + (h_{\mu\nu} + \bar{h}_{\mu\nu})$, with $h_{\mu\nu}$ the potential modes of the gravitational fields and $\bar{h}_{\mu\nu}$ its radiative modes. Then, because the Kol-Smolkin parametrization of the metric, defined by formula (3.30), is non linear, we expect it to not be equivalent to employ such parametrization in position with respect to momentum space. In practice in order to obtain the Feynman rules, as will be done in appendix A, we will substitute the Kol-Smolkin parametrization in position space, $g_{\mu\nu}(x) \rightarrow \hat{W}_a(x) \sim \hat{\phi}(x), \hat{A}(x), \hat{\sigma}(x)$, subsequently expanding the action terms in order to obtain a polynomial expression in the fields $\hat{W}_a(x)$; then we will perform the Fourier transform $\hat{W}_a(x) \rightarrow \int \frac{d^{d+1}k}{(2\pi)^{d+1}} \hat{W}_a(k) e^{-ikx}$, and finally split the modes into potential and radiative ones, $\hat{W}_a \rightarrow W_a + \bar{W}_a$. This will also assures us that potential W_a and radiation \bar{W}_a modes will not mix during propagation: we will see in appendix A.1 that, thanks to the overlapping support of their Fourier modes by definition, $W_a(k)\bar{W}_b(k) = 0$, mixed quadratic terms will vanish.

Discussion about the splitting of the gravitational modes

Nevertheless let us also point out that to be more precise equation (3.36) should be cast as:

$$\hat{W}_a(k) = f(k) W_a(k) + (1 - f(k)) \bar{W}_a(k) \quad (3.39)$$

where $f(k)$ is a *window function*, which eventually could allow for a smooth transition between the potential and the radiation modes. In practice nonetheless we'll choose such window function to be a step function, as could be $f(k) \sim \theta(K^2 - k^2)$, where $k^2 = \eta_{\mu\nu} k^\mu k^\nu$ while K is a specific threshold for the cutoff: the step function then forces the potential and radiation modes to have non-overlapping domain, and this assures us that the mixed quadratic term $W_a \bar{W}_a$ will vanish when we'll evaluate the expressions for the propagators of these fields, as we will explicitly see in appendix A.1, and hence potential and radiation modes will not mix during the free propagation.

Nonetheless, apart from this last point, the exact definition of the cutoff is never employed in the calculations: this is because, when evaluating integrals over the momentum d^4k , we'll promote them to live in $(d + 1)$ dimension, $d^4k \rightarrow d^{d+1}k$, as we're using dimensional regularization; and we'll extend the domain of integration over the whole \mathbb{R}^{d+1} space, indifferently if the k momenta were associated to a potential or a radiation modes; and this is the reason why we're not sensitive to the aforementioned cutoff.

Such a procedure however introduces some subtleties: while it allows us to easily employ all the multi-loop quantum field theory techniques which we introduced in section 2.2; formally with each integral we're evaluating some contributions which we demanded to be discarded. In particular whenever we perform a momentum integral concerning potential or radiation modes, we should restrict the integration domain over either the corresponding hard or soft set of momenta. However the procedure of extending the integration over the whole momentum space, disregarding the cutoff, is somehow justified within the so called *method of regions* [60, 213, 214, 250, 251]. Furthermore the splitting into potential and radiation modes is somewhat arbitrary, even though it allows to greatly simplify calculations: on the other hand this splitting sometimes actually introduces spurious divergences, both in the near zone (IR divergences) and in the far zone EFT (UV divergences), which nonetheless may be shown to cancel each other out once one employs suitable techniques, such as the zero-bin subtraction [60].

■ Integrating out the near zone scale

We can finally integrate out the scales of the near zone, that is, the degrees of freedom with modes which satisfy $R_s < k^{-1} < r$, hence whose characteristic length is of order of the orbital scale: such degrees of freedom are then given by the potential gravitational fields ϕ, A, σ .

The total action of the high energy theory was given by (3.29) as a function of the $g_{\mu\nu}(L)$ field, which we rewrote in terms of Kol-Smolkin variables \hat{W}_a in equations (3.33) and (3.35): performing the further aforementioned steps, in order to exchange the \hat{W}_a fields for the potential W_a and radiation \bar{W}_a modes, we obtain:

$$S_{near,UV}[\{x_a^\mu\}, \phi, A_i, \sigma_{ij}, \bar{\phi}, \bar{A}_i, \bar{\sigma}_{ij}] = S_{bulk}[\phi, A_i, \sigma_{ij}, \bar{\phi}, \bar{A}_i, \bar{\sigma}_{ij}] + \sum_{a=1}^2 S_{pp,a}^{(PP)}[x_a^\mu, \phi, A_i, \sigma_{ij}, \bar{\phi}, \bar{A}_i, \bar{\sigma}_{ij}]. \quad (3.40)$$

To obtain the effective action $S_{near,IR}$ which describes the dynamics of the system, as seen from the far zone, we have to integrate out the potential modes ϕ, A, σ from the complete high energy action (3.40), as explained in section 2.1.2:

$$e^{iS_{near,IR}[\{x_a^\mu\}, \bar{\phi}, \bar{A}_i, \bar{\sigma}_{ij}]} = \int D\phi DA_i D\sigma_{ij} e^{iS_{near,UV}[\{x_a^\mu\}, \phi, A_i, \sigma_{ij}, \bar{\phi}, \bar{A}_i, \bar{\sigma}_{ij}]} . \quad (3.41)$$

From what has been discussed so far, we can already recognize that some terms of the $S_{near,UV}$ do not depend on the potential fields, therefore those term can be directly extracted out of the path integration. In particular from equation (3.34a) we found that the $S_{pp,a}^{(kin)}[x_a^\mu]$ term doesn't depend on the gravitational fields at all; whereas in the bulk action (3.35) and in the worldline-gravity action (3.34c) some terms depend only on the radiation fields and possibly the worldlines, hence they need not to undergo the path integration.

The other terms which instead depend on the potential fields ϕ, A_i, σ_{ij} will instead be integrated out using a diagrammatic perturbative approach: such operation will yield a series of new terms, which may either depend only on the worldlines, and we will denote their sum as the *conservative action* $S_{cons}[\{x_a^\mu\}]$ for the binary, or they may depend also on the radiation fields (and possibly the worldlines too); this latter series of terms will yield operators which describe the effective self-interactions of the radiation fields (and respectively corrections to their couplings to the worldlines). All in all, the part of the low energy effective action $S_{near,IR}$ which depends on the radiation fields $\bar{\phi}, \bar{A}_i, \bar{\sigma}_{ij}$, and hence describe their effective dynamics and how they couple to the worldlines $\{x_a^\mu\}$, is called the effective action for the radiation theory and is denoted as $S_{eff}^{rad}[\{x_a^\mu\}, \bar{\phi}, \bar{A}_i, \bar{\sigma}_{ij}]$; such action will be key for the final far zone effective theory [213]. To summarize all of this in a schematic way, equation (3.41) can be recast as:

$$S_{near,IR}[\{x_a^\mu\}, \bar{\phi}, \bar{A}_i, \bar{\sigma}_{ij}] = \sum_{a=1}^2 S_{pp,a}^{(kin)}[x_a^\mu] \underbrace{-i \log \left(\int D\phi DA_i D\sigma_{ij} e^{i\tilde{S}_{near,UV}[\{x_a^\mu\}, \phi, A_i, \sigma_{ij}, \bar{\phi}, \bar{A}_i, \bar{\sigma}_{ij}]} \right)}_{\equiv S_{cons}[\{x_a^\mu\}] + S_{eff}^{rad}[\{x_a^\mu\}, \bar{\phi}, \bar{A}_i, \bar{\sigma}_{ij}]}, \quad (3.42)$$

where $\tilde{S}_{near,UV}$ is $S_{near,UV}$ with the terms that depend on the worldlines $\{x_a^\mu\}$ only removed. Let us point out that this effective action $S_{near,IR}[\{x_a^\mu\}, \bar{\phi}, \bar{A}_i, \bar{\sigma}_{ij}]$ it's also denoted as NRGR action $S_{NRGR}[\{x_a^\mu\}, \bar{\phi}, \bar{A}_i, \bar{\sigma}_{ij}]$, which stands for *non-relativistic general relativity* [43].

■ Conservative sector and radiation dissipative contributions

The division we performed in formula (3.42) reflects the way that the dynamics of the binary are usually treated: it is in fact customary to consider separately the *conservative sector* and the *dissipative* or *radiation* contributions. The former in practice gives the post-Newtonian corrections to the binding potential of the binary, while the latter mostly describes the dissipative effects due to the gravitational waves radiated by the system. It must however be noted that also the radiation effective theory does contribute to the conservative dynamics of the binary, for example due to the time non-local tail effects, in which gravitational waves back-scatter on the static curvature produced by the binary system, and are later reabsorbed by the system [213, 252].

To evaluate the conservative action $S_{cons}[\{x_a^\mu\}]$ one usually sets the radiation fields $\bar{\phi} = \bar{A} = \bar{\sigma}$ to zero and integrates out the potential modes; whereas the contribution from the radiation action $S_{eff}^{rad}[\{x_a^\mu\}, \bar{\phi}, \bar{A}_i, \bar{\sigma}_{ij}]$ is considered separately. Furthermore, whereas the leading order conservative contribution is the Newtonian potential (so 0PN order), the first dissipative contributions enters only at 2.5PN order [36]. Yet this latter contribution is sometimes denoted also as 0PN *relative* order, since it is the leading order contribution to the dissipative sector, and hence it must be accounted to obtain the leading order expression for the gravitational waveform.

■ Notation employed in the thesis for Feynman diagrams and fields

As already discussed, we'll perform the needed functional integrations by summing over the relevant Feynman diagrams. In particular the derivation and the expressions of the relevant Feynman rules are presented in appendix A.

To this end, in the Feynman diagrams we'll represent the potential and radiative modes of these Kol-Smolkin fields using the notation shown in figure 3.4.

Furthermore the action (3.34c) prescribes the coupling between the gravitational fields $\hat{\phi}, \hat{A}, \hat{\sigma}$ with the worldlines $\{x_a^\mu\}$, i.e. the (positions, velocity and higher derivatives, of the) compact objects. To represent this coupling we'll employ a notation different with respect to what is usually utilized in the literature: we do not draw any line for the worldlines degrees of freedom, since they're not propagating, as they're non dynamical d.o.f. in our effective theory. Instead we represent the coupling of gravitational fields ($\hat{\phi}, \hat{A}, \hat{\sigma}$) to the worldline x_a^μ , with generic worldline index a (eventually $a = 1, 2$), with a circle (left of equation (3.43a)) if we're working in the near zone effective theory, and with a square (left of equation (3.43)) if we're working in the far zone effective theory (which we'll present in section 3.2.4). The distinction between near (circle) and far zone (square) worldline-gravity vertices is that in the far zone the vertex is an *effective vertex*, obtained after integrating out all the potential fields.

To be more clear, we represent with a circle what in the literature, e.g. [43, 213], is usually represented with a single thick line, and with a square what in the literature is usually represented with a double thick line; hence for example (on the left the notation employed in our thesis, on the right the one customary in the literature):

$$\text{Diagram (3.43a): } \begin{array}{c} \text{Circle} \\ \downarrow \\ \phi \end{array} \sim \begin{array}{c} \text{Thick line} \\ \downarrow \\ \phi \end{array}, \quad (3.43a)$$

$$\text{Diagram (3.43b): } \begin{array}{c} \text{Square} \\ \downarrow \\ \bar{\phi} \end{array} \sim \begin{array}{c} \text{Double thick line} \\ \downarrow \\ \bar{\phi} \end{array}. \quad (3.43b)$$

Another difference, presented visually in equation (3.44), is that in the literature for the conservative diagrams it is customary to draw two thick lines, one running horizontally in the top and one in the bottom, which represent either one of the two compact object; and then to consider as different diagrams the ones in which the gravitational fields couple differently to this worldlines (the thick lines). In our notation instead, on the left of that same equation, we make clear the fact that we're summing over vacuum diagrams (as in fact the worldlines can always be stripped away in these post-Newtonian effective theories, as they don't propagate), and we keep generic the index of each worldline vertex (i.e. the letter inside the circle): then with our notation we understand the fact that when we write down the expression corresponding to the diagram, we have to keep generic the *worldline index* in the expression of the corresponding worldline-gravity Feynman rule; summing over them in the end (e.g $a = 1, 2, b = 1, 2, \dots$). To be more precise actually the vacuum diagram already understand this last summation, and therefore these indices are in reality muted, nonetheless we find it useful to still show them sometimes for comprehensibility, so that when we write down the corresponding expression for the Feynman rules it will be easier to distinguish which expression is associated to which vertex.

Potential fields	Radiation fields
ϕ	$\bar{\phi}$
A	\bar{A}
σ	$\bar{\sigma}$

FIGURE 3.4 — The diagrammatic representation of the propagators of the potential and radiative Kol-Smolkin gravitational fields.

So for example, a conservative diagram with 4 worldline vertices, which first contributes at 2PN and that we'll evaluate in equation (4.55c), actually understand three different diagrams in the notation that is customary in the literature (which may also have varying symmetry factors) [57, 235]:

Somewhat similarly happens also for the radiation diagrams: there in the literature it is customary to draw just one horizontal double line to represent the binary system as seen from far away, instead in our notation we will still use a vacuum diagram representation (albeit with the square, far zone, worldline-gravity vertices; and without worldline labels, as there is just a single multipole source in the radiation effective theory). Only to obtain the Feynman rules for the far zone, a procedure that will be carried out in appendix A.3, we'll have an arbitrary number of radiation fields represented as external legs in the diagram, yet the evaluation procedure will be similar to the one of a vacuum conservative diagram.

■ Power counting rules for the near zone effective field theory

As already pointed out in section 2.1.3, one of the important feature of effective field theories is the fact that calculations should be organized in a series of terms about some expansion parameter, in order to be able to evaluate only a finite number of terms, up to the desired accuracy.

In practice the construction of our effective field theory requires integrating out some fields by summing over an infinite series of diagrams, either vacuum ones or with external radiation lines, and our approximation scheme is the post-Newtonian expansion, hence it is natural to organize the diagrams in the infinite series by their respective scaling with regard to the post-Newtonian expansion parameters, and afterwards to truncate the sum at the PN desired order.

The goal of this section is then to find how each diagram scales with respect to the PN expansion parameters, which are the Newton gravitational constant G and the typical velocity v of the system. To do so we'll have to evaluate the scaling behavior of each propagator and each Feynman rule which compose a full diagram in the limit $d \rightarrow 3$.

Before proceeding, we point out explicitly the scaling behavior of the physical quantities which may appear in any diagram: let us recall from section 1.6.1 that in the post-Newtonian expansion it holds:

$$v^2 \sim \frac{Gm}{r} \quad (3.45)$$

and that, by construction, for the momenta of our potential modes it holds

$$k^0 \approx \frac{v}{r}, \quad |\mathbf{k}| \approx \frac{1}{r}. \quad (3.46)$$

Quantity	Scaling
k^0	$G^{-\frac{1}{2}} L^{-\frac{1}{2}} v^{\frac{5}{2}}$
$ \mathbf{k} $	$G^{-\frac{1}{2}} L^{-\frac{1}{2}} v^{\frac{3}{2}}$
∂_0	$G^{-\frac{1}{2}} L^{-\frac{1}{2}} v^{\frac{5}{2}}$
∂_i	$G^{-\frac{1}{2}} L^{-\frac{1}{2}} v^{\frac{3}{2}}$
t	$G^{\frac{1}{2}} L^{\frac{1}{2}} v^{-\frac{5}{2}}$
r	$G^{\frac{1}{2}} L^{\frac{1}{2}} v^{-\frac{3}{2}}$
m	$G^{-\frac{1}{2}} L^{\frac{1}{2}} v^{\frac{1}{2}}$
Λ	$G^{-\frac{1}{2}}$

TABLE 3.1 — Scaling of the quantities which are encountered during calculations.

It is customary to introduce also the orbital angular momentum $L = mvr$ as an explicit scaling parameter [192, 197]: in such a way we can express both m and r as a function of G , v and L only:

$$r \propto \sqrt{\frac{GL}{v^3}}, \quad m \propto \sqrt{\frac{Lv}{G}}. \quad (3.47)$$

Finally let us notice that the former expansion parameter is implicit in the gravitational coupling $\Lambda \stackrel{d=3}{\sim} G^{-\frac{1}{2}}$. We summarized all of this in table 3.1.

Propagator expansion in order to recover definite scaling

To find the PN order at which each diagram contribute, first we need the power counting rules for the propagators and the vertices which compose it. We can obtain the scaling of each Kol-Smolkin field by looking at their two point functions [192, 253], for definiteness let us consider the one for the potential ϕ field, as it has been derived in appendix A.1:

$$\langle T(\phi(x)\phi(y)) \rangle = \frac{1}{2c_d} \int \frac{d^{d+1}k}{(2\pi)^{(d+1)}} \frac{i}{k^2 + i\epsilon} e^{-ik(x-y)}. \quad (3.48)$$

From this expression at first glance we may not easily recognize any definite scaling behavior: this is because, as already pointed out, the time component k^0 of the momentum scales differently with respect to its spatial part \mathbf{k} , hence it is necessary to single out each of them. We can do so noticing that because ϕ is a potential mode, it is always off-shell, which means that $k^2 \neq 0$ and so that the $i\epsilon$ prescription can be neglected; hence we can employ the expansion

$$\frac{1}{k^2} = \frac{1}{(k_0)^2 - |\mathbf{k}|^2} = -\frac{1}{|\mathbf{k}|^2} \frac{1}{1 - \frac{(k_0)^2}{|\mathbf{k}|^2}} = -\frac{1}{|\mathbf{k}|^2} \sum_{n=0}^{+\infty} \left(\frac{(k_0)^2}{|\mathbf{k}|^2} \right)^n, \quad (3.49)$$

which holds for $k^0 \ll |\mathbf{k}|$, as in this case.

Inserting this expansion in the (3.48) two point function we obtain:

$$\langle T(\phi(x)\phi(y)) \rangle = -\frac{i}{2c_d} \int \frac{d^{d+1}k}{(2\pi)^{(d+1)}} e^{-ik(x-y)} \frac{1}{|\mathbf{k}|^2} \sum_{n=0}^{+\infty} \left(\frac{(k_0)^2}{|\mathbf{k}|^2} \right)^n. \quad (3.50)$$

Physically this actually amounts to expanding the non-instantaneous exact propagator (3.48) of the ϕ potential field about its instantaneous action, given by the leading $n = 0$ term

$$\langle T(\phi(x)\phi(y)) \rangle = -\frac{i}{2c_d} \underbrace{\int \frac{dk^0}{2\pi} e^{-ik^0(x^0-y^0)}}_{\delta(x^0-y^0)} \int \frac{d^d\mathbf{k}}{(2\pi)^d} e^{i\mathbf{k}\cdot(\mathbf{x}-\mathbf{y})} \frac{1}{|\mathbf{k}|^2} + \dots \quad (3.51)$$

and by then considering in a perturbative manner the higher order corrections, as the one at order n is subleading due to an additional scaling factor given by

$$\left((k_0)^2 \frac{1}{|\mathbf{k}|^2} \right)^n \approx \left(\frac{v^2}{r^2} r^2 \right)^n = (v^2)^n, \quad (3.52)$$

which means that it enters n PN orders higher than the leading one [206].

The Feynman rule in momentum space associated to the propagator of the potential ϕ field, which has been derived in appendix A.1, equation (A.18), is:

$$\begin{array}{c} \xrightarrow{k} \\ \text{---} \\ \phi \end{array} = \frac{1}{2c_d} \frac{i}{k^2 + i\epsilon}, \quad (3.53)$$

but, performing the aforementioned expansion needed to obtain definite power counting rules, we actually find that the Feynman rule associated to the leading order instantaneous contribution (3.51) is given by

$$\begin{array}{c} \xrightarrow{k} \\ \text{---} \phi \text{---} \end{array} = -\frac{1}{2c_d} \frac{i}{|\mathbf{k}|^2}, \quad (3.54)$$

while the higher order corrections are denoted as insertions of a cross in the propagator

$$\begin{array}{c} \xrightarrow{k} \\ \text{---} \otimes \text{---} \\ n \end{array} = -\frac{1}{2c_d} \frac{i}{|\mathbf{k}|^2} \left(\frac{(k^0)^2}{|\mathbf{k}|^2} \right)^n. \quad (3.55)$$

Finally we can estimate the scaling of the ϕ field from its leading order instantaneous contribution (3.51), to obtain:

$$\phi^2 \propto \left(\frac{v}{r} \right) \left(\frac{1}{r} \right)^3 r^2 \sim \frac{v}{r^2} \sim \frac{v^4}{GL}; \quad (3.56)$$

where we assumed $d = 3$ as we're interested in the PN scaling of the final result.

Scaling of the Feynman rules involving potential gravitons

Comparing the expression (3.53) for the momentum-space representation of the propagator for the ϕ potential field, with the explicit expressions of the propagators for the A potential field, given by equation (A.22), and for the σ potential field, given by equation (A.29), we can notice they differ by constants and tensorial structures which are dimensionless and not proportional to G , L or v ; therefore we can conclude that any potential field $W = \phi, A, \sigma$ scales as:

$$W \propto G^{-\frac{1}{2}} L^{-\frac{1}{2}} v^2. \quad (3.57)$$

The next step is to obtain the scaling behavior of the interaction vertices which involve potential gravitons: they can either be interaction vertices between the worldline and the fields, or bulk interaction vertices which involve gravitational fields only; we'll explicitly derive their expression in appendix A.

Restricting now our focus on conservative diagrams, i.e. connected vacuum diagrams involving only potential gravitons, hence with no external legs, we have that each of the two end point of any potential field propagator must necessarily connect to a leg of an interaction vertex. Therefore we'll adopt the convention according to which one incorporates the scaling due to the propagators and the corresponding integrations over the free momenta inside the interaction vertices: in practice this means that, once we multiply each interaction vertex by a factor (3.57) for each one of the potential field legs that it has, then we can simply neglect the propagators when we evaluate the scaling behavior, and so consider only the interaction vertices which appear in the diagram. One still must be careful that any propagator insertion instead still increases the PN order of the diagram.

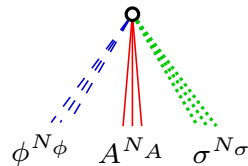
We can then derive the scaling behavior of a generic interaction vertex starting from the corresponding term the action; in particular, as explained in appendix A, to obtain the Feynman rules one considers the Fourier transformed fields and applies the needed functional derivatives. The net result of these actions on a potential field W , for what concerns the power scaling, is the substitution $\partial_0^p \partial_i^q W_A(x) \rightarrow C_A \int d^{d+1}k (k^0)^p (k^i)^q \delta^{(d+1)}(k - \dots) e^{ikx} \propto (k^0)^p |\mathbf{k}|^q$, up to some constant and tensorial structures. Furthermore, recognizing that any potential field appearing in the action will

be a potential field leg in the final Feynman rule, we directly add the scaling (3.57), according to the aforementioned convention. At last, considering that any potential field $W = \phi, A, \sigma$ is always divided by a Λ factor, due to the field normalization we employed; recalling the scaling rules from table 3.1, we can draw the conclusion that a term of the following kind, in the position space action, will scale like:

$$\frac{1}{\Lambda} \partial_0^p \partial_i^q W(x) \propto G^{-\frac{(p+q)}{2}} L^{-\frac{(p+q+1)}{2}} v^{\frac{(5p+3q+4)}{2}}. \quad (3.58)$$

To proceed further we have also to evaluate the contribution to the final scaling of a diagram due to the integrations which appear in the position-space action by considering that, for what concerns the near zone EFT we're considering, the typical scales which come into play are r and $t \sim O(\frac{r}{v})$; therefore to any factor $\int d^{d+1}x$ or $\int dt$ we'll associate the scaling $\int d^{d+1}x \propto t r^3$ and $\int dt \propto t$. One must also consider the power scaling of the Wilson coefficient c_i which multiplies the field operator in the Lagrangian: as explicitly worked out in appendix A.2.1, in the case of the point-particle action they're functions of v_a^2 , hence they may further suppress the corresponding Feynman rule by increasing its $v \ll 1$ scaling. We'll denote then with r the leading order scaling, in v^2 units, of the Wilson coefficient c_i associated to a Feynman rule. For example, looking at equation (A.35), we see that the Wilson coefficient of the operator which couples A^2 to the worldline reads $c_{A^2} = -\frac{v_a^2}{2(1-v_a^2)^{3/2}} \sim O(v^2)$, so $r = 1$; nonetheless most of the time the operators are not suppressed and therefore $c \sim O(1)$, from which follows $r = 0$.

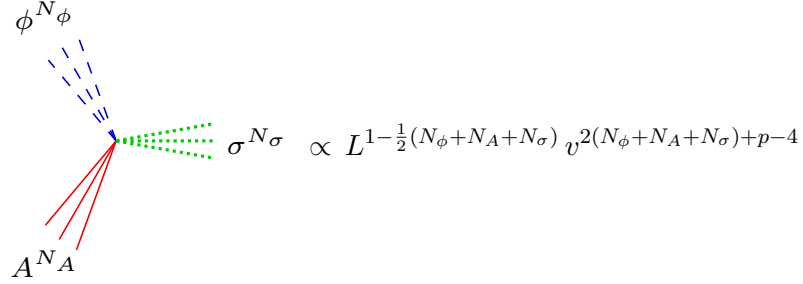
Now that we have all the necessary ingredients, we can evaluate the power scaling of a generic worldline-interaction vertex. Looking at the point particle action (3.23), and in particular its expanded form for the conservative sector that we report in appendix, see formulae (A.32) and (A.35), we see that there are no derivatives acting on the fields, so $p = q = 0$; that there is always a prefactor $m \int dt \propto m t = L v^{-2}$; and that any A_i field is contracted with a velocity spatial vector $v_a^i \propto v$, whereas any σ_{ij} is contracted with two velocities $v_a^i v_a^j \propto v^2$. We may also obtain r directly from the scaling of the factor which multiplies the W fields in formula (A.35). Therefore the power scaling a worldline-gravity interaction vertex with N_ϕ ϕ fields, N_A A_i fields and N_σ σ_{ij} fields is given by:



$$\propto L^{1-\frac{1}{2}(N_\phi+N_A+N_\sigma)} v^{2N_\phi+3N_A+4N_\sigma+2r-2}. \quad (3.59)$$

We can then proceed to evaluate also the scaling behavior of the bulk gravity self-interaction vertices, which involve only graviton fields, whose action is given by the sum of the regularized Einstein-Hilbert action (3.26) and the gauge fixing term (3.27), which up to 2PN reads (3.35) in the Kol-Smolkin parametrization. We can notice that such an action has a $\Lambda^2 \propto G^{-1}$ prefactor and an integration over $\int d^{d+1}x \propto G^2 L^2 v^{-7}$. Therefore the power scaling a bulk interaction vertex with N_ϕ ϕ fields, N_A A_i fields, N_σ σ_{ij} fields, p temporal derivatives ∂_0 and q spatial derivatives ∂_i in total acting on the fields, is given by $G^{1-\frac{1}{2}(p+q)} L^{2-\frac{1}{2}(N_\phi+N_A+N_\sigma+p+q)} v^{2(N_\phi+N_A+N_\sigma)+\frac{1}{2}(5p+3q)-7}$. However, since any bulk vertex is derived from the regularized Einstein-Hilbert action (3.26) with the addition of the gauge fixing term (3.27), which recalling Notation, schematically read $S_{EH} \sim R \sim g \partial^2 g^2$ and $S_{GH} \sim g \Gamma^2 \sim g \partial^2 g^2$; then all the terms in the bulk action will have exactly 2 derivatives, i.e. it holds $p + q = 2$ for any bulk vertex. We can use this constraint to simplify the

expression of the former power scaling of a generic bulk vertex down to:



$$\sigma^{N_\sigma} \propto L^{1-\frac{1}{2}(N_\phi+N_A+N_\sigma)} v^{2(N_\phi+N_A+N_\sigma)+p-4} ; \quad (3.60)$$

let us notice that the scaling with respect to G dropped out; and that in this case $r = 0$ because the Wilson coefficients of the operators in the bulk action cannot be proportional to the velocity of the compact objects (as it's the purely gravitational action).

3.2.4 — Far zone radiation effective theory

The last effective theory we have to consider is the one related to the far zone, so the radiation zone, which has as characteristic scale the wavelength λ of the gravitational waves produced by the binary. The high-energy degrees of freedom which are now present at this scale are

1. the gravitational radiation fields $\bar{\phi}, \bar{A}_i, \bar{\sigma}_{ij}$;
2. the two worldlines degrees of freedom $\{x_a^\mu\}$, which still are non dynamical.

The high-energy action which governs their dynamics in this region, $S_{far,UV}[\{x_a^\mu\}, \bar{\phi}, \bar{A}_i, \bar{\sigma}_{ij}]$, is given by the near zone low-energy effective theory $S_{near,IR}[\{x_a^\mu\}, \bar{\phi}, \bar{A}_i, \bar{\sigma}_{ij}]$, that we derived in equation (3.42) in the previous section 3.2.3.

Then the final effective theory will be obtained by integrating out the high energy degrees of freedom, i.e. the the gravitational radiation fields, which in general have a wavelength $k^{-1} > r$ by construction; so:

$$e^{iS_{far,IR}[\{x_a^\mu\}]} = \int D\bar{\phi} D\bar{A}_i D\bar{\sigma}_{ij} e^{iS_{far,UV}[\{x_a^\mu\}, \bar{\phi}, \bar{A}_i, \bar{\sigma}_{ij}]} ; \quad (3.61)$$

in particular the terms that will undergo functional integration are the ones comprising what we denoted as $S_{eff}^{rad}[\{x_a^\mu\}, \bar{\phi}, \bar{A}_i, \bar{\sigma}_{ij}]$ in the equation (3.42). Once we will have done so we'll obtain the effective action

$$S_{eff}[\{x_a^\mu\}] = S_{far,IR}[\{x_a^\mu\}] , \quad (3.62)$$

which describes the full dynamics for the two worldlines $\{x_a^\mu\}$ evolving under the influence of the gravitational fields, while making no reference to the dynamics of the latter.

To recap, recalling the expansion (3.42), factoring out the terms taht won't undergo the functional integration, we find that the final effective action reads:

$$S_{eff}[\{x_a^\mu\}] = \sum_{a=1}^2 S_{pp,a}^{(kin)}[x_a^\mu] + S_{cons}[\{x_a^\mu\}] - i \log \left(\int D\bar{\phi} D\bar{A}_i D\bar{\sigma}_{ij} e^{iS_{eff}^{rad}[\{x_a^\mu\}, \bar{\phi}, \bar{A}_i, \bar{\sigma}_{ij}]} \right) . \quad (3.63)$$

Let us notice however that to correctly compute the above action we would need to employ the in-in formalism [202, 203, 205, 206], which we introduced in section 2.1. In fact the far zone effective theory introduces dissipative phenomena, which then must be dealt with the in-in approach, since the classical Lagrangian formalism can account only for conservative dynamics.

■ Matching procedure and multipole expansion

In the literature it is now customary to build the far zone effective theory in more of a bottom-up approach, by introducing the action starting from symmetry arguments [213, 254, 255]; in practice at this scale the binary system is effectively treated as composite particle, i.e. a single point-like object equipped with a series of multipole moments, the latter giving a coarse-grained description of the dynamics taking place in the near and internal zone. Let us notice that this treatment is similar to the multipole expansion of a generic source that we performed in section 1.3.

As previously stated, for the construction of the far zone effective theory we'll proceed instead somewhat differently with respect to what is customary in the literature; more akin to a top-down approach, and along the lines of the original paper [43] and reference [206]. In practice we'll simply integrate out the radiation fields as in (3.61) via a diagrammatic approach, similarly to what we did for the near zone effective theory.

This procedure will nonetheless require a kind-of intermediate *matching procedure*, that we'll explicitly carry out in appendix A.3, which will yield the Feynman rules for the far zone. In fact these Feynman rules follow from the radiation effective action $S_{eff}^{rad}[\{x_a^\mu\}, \bar{\phi}, \bar{A}_i, \bar{\sigma}_{ij}]$ that we defined in equation (3.42); but such an action is the result of a path integral operation: then, as we discussed in section 2.1, to obtain each Feynman rule (each associated to a term of S_{eff}^{rad}) of the far zone theory (so with a given number of radiation gravitons lines) we'll have to evaluate an infinite series of diagrams involving also potential gravitons. Here the radiation gravitons will be treated as external particles with given momentum, whereas we'll have to integrate out the potential gravitons in a similar way to what we'll do for the conservative diagrams.

Nonetheless also at this step we need to have power counting rules, in order to be able to obtain a finite precision considering only a finite number of diagrams. It then become necessary to perform a *multipole expansion* of the radiation fields inside the Feynman rules. As an example, the Fourier transformed Feynman rule for the worldline-radiation vertex will have a Fourier exponential as $e^{-ikx} = e^{-ik^0 t} e^{i\mathbf{k}\cdot\mathbf{x}}$, nonetheless recalling the discussion previously presented in section 3.2.3, the momentum of radiation scales like $|\mathbf{k}| \propto \frac{v}{r}$, whereas $|\mathbf{x}| \sim \frac{1}{r}$ considering the characteristic length scale of the binary system. Therefore to obtain a well defined scaling in v it becomes necessary to Taylor expand the exponential in $\mathbf{k}\cdot\mathbf{x} \propto v$. The physical meaning of this Fourier expansion is that we're performing a multipole expansion of the radiation fields $\bar{\phi}, \bar{A}_i, \bar{\sigma}_{ij}$.

Then we recall that the multipole expansion of a generic function $f(t, \mathbf{x}_a)$ around around an arbitrary point \mathbf{X} , introducing $\delta\mathbf{x}_a \equiv \mathbf{x}_a - \mathbf{X}$, is given by:

$$f(t, \mathbf{x}_a) = f(t, \mathbf{X}) + \delta x_a^i (\partial_i f(t, \mathbf{x}))|_{\mathbf{x}=\mathbf{X}} + \frac{1}{2} \delta x_a^i \delta x_a^j (\partial_i \partial_j f(t, \mathbf{x}))|_{\mathbf{x}=\mathbf{X}} + \dots ; \quad (3.64)$$

we also recall that in order to not spoil the convergence of the series it is advisable to chose the origin of the multipole expansion near the center of the binary system, for example we may choose \mathbf{X} to be the center of mass of the binary, and usually one also chooses the coordinate system such that it holds $\mathbf{X} = \mathbf{0}$. When we actually apply such an expansion to the Fourier transformed expression, the derivatives act on the Fourier exponential, yielding:

$$\begin{aligned} e^{i\mathbf{k}\cdot\mathbf{x}_a(t_1)} &= e^{i\mathbf{k}\cdot\mathbf{X}} + i \delta x_a^i k_i e^{i\mathbf{k}\cdot\mathbf{X}} - \frac{1}{2} \delta x_a^i \delta x_a^j k_i k_j e^{i\mathbf{k}\cdot\mathbf{X}} + \dots \\ &= e^{i\mathbf{k}\cdot\mathbf{X}} \left(1 + i(\delta\mathbf{x}_a \cdot \mathbf{k}) + \frac{i^2}{2} (\delta\mathbf{x}_a \cdot \mathbf{k})^2 + \dots \right) ; \end{aligned} \quad (3.65)$$

here we can see that each additional term is further suppressed by a power of $(\delta\mathbf{x} \cdot \mathbf{k}) \propto v$.

In practice then, integrating by parts, we'll exchange the multipole expansion of the radiation fields (which we'll integrate out in the end), with a multipole expansion of the binary system, which will

come follow from combinations and sums over the δx_a^i terms: in fact if we chose $\mathbf{X} = \mathbf{0}$, we find exactly $\delta \mathbf{x}_a = \mathbf{x}_a$, and for example the combination $\sum_{a=1,2} m_a x_a^i x_a^j = M^{ij}$ will be equal to the mass multipole that we already encountered in equations (1.63) and (1.72).

In some diagrams it may also be necessary to perform the aforementioned expansion in the spatial propagators, when e.g. due to the spatial momentum Dirac delta present in bulk vertices, potential \mathbf{k}_1 and radiation \mathbf{k} momenta may mix, for example as $\frac{1}{|\mathbf{k}_1 - \mathbf{k}|^2}$; we'll see an example of this in diagram (A.104), and expression (A.106). We can then notice that $|\mathbf{k}_1 - \mathbf{k}|$ does not scale in a definite post-Newtonian manner, because as usual the spatial momenta of the potential mode \mathbf{k}_1 scales like $|\mathbf{k}_1| \propto \frac{1}{r}$, while the spatial momenta of the radiation mode \mathbf{k} scales like $|\mathbf{k}| \propto \frac{v}{r}$. Nonetheless we can restore a definite power counting by noticing that then it holds $\frac{|\mathbf{k}|}{|\mathbf{k}_1|} \propto v \ll 1$, and hence, using the fact that $|\mathbf{k}_1 - \mathbf{k}|^2 = |\mathbf{k}_1|^2 - 2(\mathbf{k}_1 \cdot \mathbf{k}) + |\mathbf{k}|^2$, we can perform the expansion of the propagator as

$$\frac{1}{|\mathbf{k}_1 - \mathbf{k}|^2} = \frac{1}{|\mathbf{k}_1|^2} \left(1 + 2 \underbrace{\left(\frac{\mathbf{k}_1 \cdot \mathbf{k}}{|\mathbf{k}_1| |\mathbf{k}_1|} \right)}_{\mathcal{O}(v)} + \underbrace{\left(4 \left(\frac{\mathbf{k}_1 \cdot \mathbf{k}}{|\mathbf{k}_1| |\mathbf{k}_1|} \right)^2 - \frac{|\mathbf{k}|^2}{|\mathbf{k}_1|^2} \right)}_{\mathcal{O}(v^2)} + \mathcal{O}(v^3) \right); \quad (3.66)$$

where we single out the leading order contribution, and an infinite series of ever more suppressed corrections.

■ Multipole moments and coupling to conserved quantities

We'll evaluate the corrections due to the far zone effective theory in chapter 5; nonetheless for the present work we'll restrict to the evaluation of the leading order corrections only.

In particular we'll derive the relevant Feynman rules in appendix A.3, where we'll employ the following definitions for the multipole moments [103, 206]:

$$m \equiv \sum_{a=1,2} m_a, \quad (3.67a)$$

$$E_N \equiv \frac{1}{2} \sum_{a=1}^2 m_a v_a^2 - \frac{Gm_1 m_2}{r}, \quad (3.67b)$$

$$\mathbf{x}_{CM} \equiv \frac{1}{m} \sum_{a=1,2} m_a \mathbf{x}_a, \quad (3.67c)$$

$$\mathbf{p}_{CM} \equiv \sum_{a=1,2} m_a \mathbf{v}_a, \quad (3.67d)$$

$$M^{ij} \equiv \sum_{a=1,2} m_a x_a^i x_a^j, \quad (3.67e)$$

$$M \equiv \delta_{ij} M^{ij}, \quad (3.67f)$$

$$\mathbf{L} \equiv \sum_{a=1,2} m_a (\mathbf{x}_a \times \mathbf{v}_a). \quad (3.67g)$$

which are respectively the total mass of the system, the Newtonian energy of the system, the position of the center of mass for the system, the total linear momentum of the system, the mass quadrupole moment of the system, the trace of the mass quadrupole moment of the system, and the total orbital angular momentum of the system. The angular momentum is assumed to be

computed in the center of mass frame, about its origin; furthermore the k -th spatial component of the total orbital angular momentum can also be expressed as $L_k \equiv \sum_{a=1,2} m_a \epsilon_{kij} x_a^i v_a^j$, where ϵ_{kij} is the three dimensional Levi-Civita symbol which we defined in [Notation](#).

Let us notice that the above definitions only hold at leading order: at higher post-Newtonian order they may receive corrections. For example the $\mathcal{O}(v^2)$ correction to the expression for the center of mass \mathbf{x}_{CM} of the binary system will actually be the inclusion of the leading order interaction potential and kinetic energy: this makes clear the fact we actually should be considering the center of energy of the binary instead of its center of mass [103, 254]. This must be the case since in general relativity not only mass but any form of energy gravitates, hence also the gravitational binding energy contained in the gravitational field must be taken into account. This is further corroborated by the fact that, as discussed also in [43], in order to assure gauge invariance, and to obtain the correct Feynman rules and final results, we have to consider also diagrams which involve bulk vertices, for example (A.104) in appendix A.3.2. The bulk vertices encode the non-linear interactions between gravitons, both potential and radiation, due to the non-linear (non-Abelian) structure of general relativity; in practice they're equivalent to the contributions coming from the stress-energy *pseudotensor* $\tau^{\mu\nu}$, which is otherwise introduced in order to take into account these contributions due to the gravitational field. Then we see that not only the compact objects, but also the gravitational field itself, contribute to the dynamics of the composite point particle and to the emitted gravitational waves.

We're also interested in simplifying the expression that we'll obtain: in order to do so, restricting to the leading order precision which we're aiming for, we will choose the arbitrary point \mathbf{X} around which we'll perform the multipole expansion to be the position of the center of mass \mathbf{x}_{CM} of the binary system, furthermore demanding also the origin of the frame of reference to coincide with the position of the the center of mass, hence obtaining $\mathbf{X} = \mathbf{x}_{CM} = \mathbf{0}$. Still let us notice that at higher PN order one may have to generalize this condition in order to account for PN corrections, for example to impose the condition for the origin to coincide with the center of mass it may be needed to impose the dipole moment of the binary to be vanishing [36, 256, 257].

The fact that we're restricting to the leading order only also leads to additional simplifications in the evaluation: in fact, as pointed out also by references [43, 206], at the leading order the several multipole moments defined above in equations (3.67) are conserved, that is, their derivative with respect to time is vanishing. In fact for example the mass of the compact objects comprising the binary system may vary over time, for example due to gravitational waves absorption, but this effect enters at higher order [43, 243]. As we'll find, radiation diagrams will be proportional to the integral (C.50) (which we will evaluate in appendix C.4); from this will follow that in the final results there will be time derivatives acting the multipole moments, and therefore we can already neglect diagrams which at leading order only provide coupling to the (approximately) conserved quantities, which are the total mass m , the Newtonian energy of the system E_N , the position of the center of mass \mathbf{x}_{CM} and the orbital angular momentum \mathbf{L} .

■ Employing the equations of motion

Finally, when deriving the Feynman rules in appendix A.3, sometimes we will have to use the equations of motion of the system in order to recast the expressions into the usual multipole expansion; an example of this is given in appendix in expressions (A.89) and (A.90). This step is also performed in references [206]; and it is somewhat akin to what we have done in linearized general relativity (in section 1.3.4), where we employed the conservation of the stress-energy momentum tensor of the source (1.24) in order to recast the expressions in a well defined multipole expansion.

■ Power counting rules for the radiation effective theory

As we already said, also in this effective field theory we have to enforce a definite power counting, which allows us to obtain the wanted precision considering only a finite number of diagrams: to do so we need to know the scaling behavior of each radiation legs and radiation fields.

In particular we'll be able to evaluate the scaling of diagrams comprising radiation gravitons, in the near zone effective theory: this is needed in order to recognize which diagrams must be evaluated in order to obtain the Feynman rules for the far zone effective theory. Then the real (leading order) scaling of the specific Feynman rules in this far zone effective theory will instead depend on the expression resulting from this matching procedure, as for example conserved quantities may increase the order at which a given Feynman rule first contributes, see also appendix A.3.2.

Then the power counting procedure is similar to the one presented in section 3.2.3 for the near zone effective theory, but in this case we have to consider that the temporal and the spatial components of the momenta of a radiation field $\bar{W}_a(k)$, by virtue of the separation into potential and radiation gravitational modes we performed in the previous subsection, scale both like $k \sim \frac{v}{r}$, see equation (3.37). Then we can employ table 3.1 to evaluate the power scaling behavior of a Feynman rule in the PN expansion parameters, taking care only of the fact that for a radiation mode it holds

$$k^0 \propto \frac{v}{r} \implies k^0 \propto G^{-\frac{1}{2}} L^{-\frac{1}{2}} v^{\frac{5}{2}}, \quad (3.68a)$$

$$|\mathbf{k}| \propto \frac{v}{r} \implies |\mathbf{k}| \propto G^{-\frac{1}{2}} L^{-\frac{1}{2}} v^{\frac{5}{2}}. \quad (3.68b)$$

Let us recall again for clarity that we're adopting the convention according to which we include in our scaling rules half of the scaling of the propagator and of the associated integral over the momentum, for each leg which is present in a Feynman rule. Because the radiation modes can be on-shell, we cannot perform the expansion of the propagators we performed for the potential modes (see 3.2.3); and therefore the propagator associated to the radiation modes scales differently, like

$$\int \frac{d^{d+1}k}{(2\pi)^{d+1}} \frac{1}{k^2 + i\epsilon} \stackrel{d=3}{\propto} k^2 \propto \left(\frac{v}{r}\right)^2 \propto G^{-1} L^{-1} v^5; \quad (3.69)$$

therefore for each radiation leg in a Feynman rule we'll add a factor equal to

$$\bar{W} \propto G^{-\frac{1}{2}} L^{-\frac{1}{2}} v^{\frac{5}{2}}. \quad (3.70)$$

In practice this means that we can evaluate the leading order scaling of a Feynman rule of the near zone effective theory simply by recalling formulae (3.59) and (3.60), and multiplying it for a factor $v^{\frac{1}{2}}$ for each leg which is a radiation field \bar{W}_a instead of a potential field W_a , in order to compensate the different scaling for the two field, which are given respectively by equations (3.70) and (3.57).

3.2.5 — Physical observables in the EFT for a binary system

Performing the whole procedure which we just outlined in sections 3.2.2, 3.2.3 and 3.2.4, so by summing over the relevant vacuum diagrams, we will be left with equation (3.63).

In the following we will describe how to obtain observables from this result: this will be useful for chapter 6, where we will apply in practice these methods to obtain the analytical expression for the gravitational waveform. In particular to do so we will need the energy associated to the binary system, the power loss of the system and the gravitational field $h_{ij}^{(TT)}$ as evaluated by a far away observer in TT gauge. Then we may derive the energy of the binary system from the Hamiltonian associated to its conservative action (which is the result of the near zone EFT), the power loss from the dissipative part of the far zone action, and we'll see that we'll be able to directly evaluate the gravitational field $h_{ij}^{(TT)}$ as well in the far zone effective theory.

■ Selecting only the classical contributions to the compact binary dynamics

At this point however one may be concerned that, with the construction outlined above, we may be including also quantum corrections to the binary dynamics: in fact, as we've seen in chapter 2, we're employing exactly the same techniques used in quantum field theory.

To be more precise the whole procedure outlined above does actually yield also the quantum corrections to the binary dynamics: in fact it requires us to sum over *all* the vacuum connected diagrams, including also diagrams which yield genuine quantum loop contributions. Moreover, to be fair, if we had a fully consistent theory of quantum gravity, these corrections should be accounted, since they would be related to real physical effects due to quantum mechanics.

Nevertheless, as already pointed out in section 3.2.1, from a physical point of view we can expect the quantum contributions that we're disregarding to be subleading: in fact the scales (e.g. masses, distances, and so on) involved in a compact binary system are huge with respect to the quantum ones. As an example we have already seen that the ratio of the orbital angular momentum to the reduced Planck constant is $\frac{\hbar}{L} \sim 10^{-77} \left(\frac{m}{M_\odot}\right)^{-2} \left(\frac{v}{0.1c}\right)$, hence we may expect any quantum correction, expressed as a series in \hbar powers, to be extremely suppressed.

Furthermore in this case we're not interested in computing the perturbative quantum corrections to general relativity, being instead interested in obtaining solely the classical contributions to the binary dynamics. To do so then we can straightforwardly restrict our summation over the *tree level* connected vacuum diagrams when integrating out the relevant fields. Then in practice we have to sum only over diagrams akin to the one represented in figure 3.5; whereas we have to discard loop diagrams, as is the case with the one in figure 3.6: the latter diagram in fact yields a genuine 1-loop quantum contribution due to the massless scalar field running in the loop. Additionally, since we're purposefully discarding diagrams involving quantum loops, there is no need to consider ghosts fields for the gravitational fields [43].

Finally, on a side note, let us show that in this setup the orbital angular momentum L actually is a loop counting parameter for the conservative diagrams. To do so let us consider a generic Feynman diagram \mathcal{M} , where for simplicity we don't keep track of the specific potential field ϕ , A or σ , but consider any of them just as a generic potential gravity field W . We denote then with V_w worldline-gravity vertices and N_w^W gravity legs connected in total to such worldline vertices, with V_b bulk vertices and N_b^W gravity legs connected in total to such bulk vertices. From the power counting rules (3.59) and (3.60) we find that the power scaling of such a diagram, up to v factors, is given by:

$$\mathcal{M} \propto L^{V_w+V_b-\frac{1}{2}(N_w^W+N_b^W)} v^{(\dots)} . \quad (3.71)$$

We can then recall the Euler-Poincaré characteristic formula, according to which the number of loops l in a connected diagrams is given by $l = p - v + 1$, where p is the number of propagators in the diagram and v the number of vertices. Recognizing that any propagators connects two gravity legs, so $p = \frac{1}{2} (N_w^W + N_b^W)$, and that $v = V_w + V_b$, it follows:

$$\mathcal{M} \propto L^{1-l} v^{(\dots)} . \quad (3.72)$$

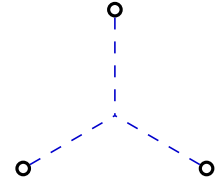


FIGURE 3.5 — tree level connected vacuum diagram, which therefore yields classical contributions and must be considered. In fact this diagram first contributes at 2PN and will be evaluated in chapter 4.

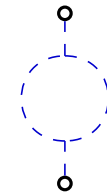


FIGURE 3.6 — 1-loop connected vacuum diagram, which therefore yields quantum contributions and must be discarded.

Therefore we found the result pointed out by references [43, 192], according to which the loop counting parameter for any diagram in the conservative sector is given by one minus the power of L .

■ Obtaining the classical dynamics of the compact bodies

Once we've constructed the effective theory for the compact binary and we've completed the procedure of integrating out all the gravitational degrees of freedom, we'll be left with the effective action S_{eff} , formally given in equation (3.63), in which the only degrees of freedom are the positions of the worldlines $\{x_a^\mu\}$, i.e. of the two compact bodies in the binary system. Generally the conservative contributions will explicitly depend on the positions of the two bodies in harmonic coordinates, whereas the dissipative contributions will depend on such position via the definition of the multipoles of the binary as in (3.67), usually evaluated in the center of mass (or energy) of the binary.

At this point the S_{eff} effective action can be interpreted as classical Lagrangian for a system of two point particles, evolving under the influence of the gravitational interaction; with the addition of an infinite series of post-Newtonian corrections: we can then employ the Lagrangian formulation of classical mechanics to study the dynamics of these two bodies. We only have to be careful about correctly studying the dissipative contributions (since the usual Lagrangian formulation isn't suited for dissipative systems): we'll discuss this point in the following.

Lagrangian formulation of classical mechanics

Given the generalized coordinates $q = \{q_i\}$ and the generalized velocities $\dot{q} = \{\dot{q}_i\}$ of a system of N particles, then action S is given by the integral of the *Lagrangian* $L(q, \dot{q}, t)$ [258]:

$$S = \int_{t_1}^{t_2} dt L(q, \dot{q}, t) ; \quad (3.73)$$

and in particular we can interpret the Lagrangian as the sum of a kinetic term $T(q, \dot{q}, t)$ for the particles, minus the potential $V(q, \dot{q}, t)$ which governs the interaction between the particles:

$$L(q, \dot{q}, t) = T(q, \dot{q}, t) - V(q, \dot{q}, t) . \quad (3.74)$$

Once we have the Lagrangian, the dynamics of the system can be obtained by employing the *principle of least action*: the motion of the system, parametrized by the coordinates $\{q, \dot{q}\}$, is such that to extremize the action, i.e. to make the variation of the action vanishing $\delta S = 0$. This condition can be recast into the form [258]

$$\frac{d}{dt} \left(\frac{\partial L}{\partial \dot{q}_i} \right) - \frac{\partial L}{\partial q_i} = 0 \quad (i = 1, \dots, N) \quad (3.75)$$

which are called the *Euler-Lagrange equations* and represent the equations of motion of the system.

Let us anticipate the fact that, as we will see in chapter 4 and 6, higher order post-Newtonian corrections introduce in the Lagrangian terms which are higher time derivatives of the positions q , such as the acceleration \ddot{q} , so $L = L(q, \dot{q}, \ddot{q}, \dots)$. Then it is useful to generalize the Euler-Lagrange equations (3.75) as [256, 259]:

$$\dots - \frac{d^2}{dt^2} \left(\frac{\partial L}{\partial \ddot{q}_i} \right) + \frac{d}{dt} \left(\frac{\partial L}{\partial \dot{q}_i} \right) - \frac{\partial L}{\partial q_i} = 0 \quad (i = 1, \dots, N) . \quad (3.76)$$

Furthermore the Lagrangian, and the action, are not physical observables per se: in fact two Lagrangians which differ by terms that do not modify the equations of motions are *equivalent*,

because they describe the same dynamics. This implies that we can add constants and total time derivatives to the Lagrangian, and so to the potential, without modifying the physical observables [258]:

$$L'(q, \dot{q}, t) \sim L(q, \dot{q}, t) + \frac{d}{dt} (f(q, \dot{q}, t)) + C ; \quad (3.77)$$

we'll exploit this fact to manipulate these quantities in the rest of this work.

Dynamics of the compact bodies of the binary system

The connection of the effective action S_{eff} with the Lagrangian formulation of classical mechanics comes by considering S_{eff} , the effective theory we find after integrating out all the gravitational degrees of freedom, to the definition (3.73).

To be more specific let us recall once again from section 2.1.2 that the sum over all the relevant connected diagrams $\{\mathcal{A}_{(i)}\}$, up to the desired PN order, gives exactly $i S_{eff}$, i.e. the logarithm of equation (3.61); hence

$$\sum_i \mathcal{A}_{(i)} = i S_{eff}[\{x_a^\mu\}] , \quad (3.78)$$

and therefore, separating the several terms in the action as in equation (3.63), such a sum over the relevant vacuum diagrams will yield, up to the desired PN order:

$$\begin{aligned} S_{eff}[\{x_a^\mu\}] &= -i \left(\sum_i \mathcal{A}_{(i)} \right) \\ &= \sum_{a=1}^2 S_{pp,a}^{(kin)}[x_a^\mu] + S_{cons}[\{x_a^\mu\}] - i \log \left(\int D\bar{\phi} D\bar{A}_i D\bar{\sigma}_{ij} e^{iS_{eff}^{rad}[\{x_a^\mu\}, \bar{\phi}, \bar{A}_i, \bar{\sigma}_{ij}]} \right) . \end{aligned} \quad (3.79)$$

From this result we can see that the final effective theory will correctly contain the full relativistic kinetic terms $T(q, \dot{q})$ for the two bodies, thanks to the $\sum_{a=1}^2 S_{pp,a}^{(kin)}[x_a^\mu]$ term whose expression is (3.34b). The $S_{cons}[\{x_a^\mu\}]$ instead will give the conservative contributions to the Lagrangian, so to the potential $V(q, \dot{q}, \dots)$; whereas the contributions due to integrating out the radiation modes, $-i \log \left(\int D\bar{\phi} D\bar{A}_i D\bar{\sigma}_{ij} e^{iS_{eff}^{rad}[\{x_a^\mu\}, \bar{\phi}, \bar{A}_i, \bar{\sigma}_{ij}]} \right)$, will generally produce both real and imaginary contributions to the Lagrangian: the real contribution could be included in the potential $V(q, \dot{q}, \dots)$, whereas the imaginary contributions represent the power loss of the system, i.e. the dissipative contributions, and may then be evaluated resorting to the *optical theorem*, presented in equation (3.82).

Let us also point out that, since we'll be working in dimensional regularization, it will be necessary to expand the results around $d = 3$ spatial dimensions in order to recover the classical quantities. Doing so nonetheless poles, for example of the kind $\frac{1}{\epsilon}$ may arise, and will have to be subtracted via a redefinition of the worldline parameters.

Energy of the system

Regarding the conservative sector, we'll be interested in obtaining the binding energy of the system, as this will be a key observable in the evolution of the binary system.

Generically, given a Lagrangian, we can obtain the energy of the system by performing a *Legendre transformation* on such Lagrangian, in order to obtain the Hamiltonian: since when restricting only to the conservative sector there is no explicit time dependence and no power loss, then the Hamiltonian is a first integral and represent the total mechanical energy associated to the system, as it's the conserved Noether charge associated to invariance under time translations.

Introducing the conjugate momenta $p = \frac{\partial L}{\partial \dot{q}}$, we define the *Hamiltonian* as:

$$H(q, p, t) \equiv \left(\sum_i p_i \dot{q}_i - L(q, \dot{q}, t) \right) \Big|_{\dot{q}=\dot{q}(p)} ; \quad (3.80)$$

from which we could also derive the Hamilton's equation of motion as:

$$\dot{q}_i = \frac{\partial H}{\partial p_i}(q, p, t) , \quad \dot{p}_i = -\frac{\partial H}{\partial q_i}(q, p, t) . \quad (3.81)$$

■ Optical theorem and power loss of the system

Regarding instead the dissipative sector, the other key quantity for the evolution of the binary system is the power loss due to gravitational waves emission, which we'll evaluate in section 5.1.

A formally correct evaluation of dissipative phenomena requires the introduction of the in-in formalism, nonetheless for the precision we're aiming for, we can evaluate also the power loss of the system from the imaginary part of the Lagrangian via the *optical theorem*: this is reminiscent of how in particle physics the imaginary part of the two point function is related to the decay width of an unstable particle.

In practice, denoting as in [213] with $d\Gamma$ the differential rate of radiation, which is similar to a decay width, and with T an arbitrary long time, it holds [213]:

$$\frac{1}{T} \text{Im}(S_{eff}[\{x_a^\mu\}]) = \frac{1}{2} \int dE d\Omega \frac{d^2\Gamma}{d\Omega dE} ; \quad (3.82)$$

and this is related to the radiated power via [213]:

$$P \equiv dP = \int d\Gamma E = \int dE d\Omega E \frac{d^2\Gamma}{d\Omega dE} . \quad (3.83)$$

In practice the in-in formalism amounts to imposing the correct retarded boundaries condition for the propagators; yet applying the optical theorem to the result obtained using the Feynman propagator still may give the correct result, since such result comprise half contributions from the advanced and half from the retarded propagators [205, 213].

■ Far away gravitational field and gravitational waveform

The final observable we're interested in is the value of the gravitational field $h_{\mu\nu}$ far away from the binary the gravitational waveform: this tensor encodes the exact expression of the gravitational waves produces by the system, i.e. the tensor perturbation that we can detect using gravitational wave detectors.

In the customary treatment of the radiation effective theory present in the literature, it's possible to obtain a closed form expression which gives the value of the h_{ij} tensor at infinity, as a function of the source multipoles, see for example references [197, 255, 260].

Nonetheless also in the formalism we constructed up until now it's possible to directly obtain the expression for the gravitational field as seen from a distant observer: in order to do so we have to notice that such a field must be of the radiative kind, as it has to be able to propagate indefinitely, and so, recalling also the discussion about gravitational waves in linearized general relativity which we presented in section 1.3, the gravitational waveform can be obtained by studying

the on-shell radiation gravitons that propagate towards infinity in the previous effective field theory construction.

We also have to recall the discussion we carried out in section 1.3.2: to extract the physical information from the waveform we have to remove any residual gauge freedom, and this is usually accomplished by choosing the TT gauge, defined by the conditions (1.26). In practice this is done by projecting each Fourier mode of the spatial components of the $h_{\mu\nu}(\mathbf{k})$ field via the $\Lambda_{ij,kl}(\hat{\mathbf{k}})$ tensor, defined in equation (1.32).

Then, working in $d = 3$ dimensions, and assuming the observer to be far away from the source, for a gravitational wave propagating in direction $\hat{\mathbf{n}} = \frac{\mathbf{k}}{|\mathbf{k}|}$, we can write:

$$h_{ij}^{TT}(t, \mathbf{x}) = \Lambda_{ij,kl}(\hat{\mathbf{n}}) \langle h^{kl}(t, \mathbf{x}) \rangle . \quad (3.84)$$

where $\langle h^{kl}(t, \mathbf{x}) \rangle$ is the expectation value for the metric perturbation, far away from the source.

From the construction of our effective field theory, and the above discussion, we conclude that in this zone the relevant gravitational degrees of freedom are the radiation modes $\langle h^{kl}(t, \mathbf{x}) \rangle \sim \langle \bar{h}^{kl}(t, \mathbf{x}) \rangle$; and we can draw the connection with the $\bar{\phi}$, \bar{A} and $\bar{\sigma}$ fields we used in the radiative effective field theory by recalling the Kol-Smolkin parametrization (3.30) and expanding it at linear order in the fields (under the weak field approximation $|h_{\mu\nu}| \ll 1$) reads:

$$g_{\mu\nu} = \eta_{\mu\nu} + h_{\mu\nu} = \begin{pmatrix} 1 + 2\frac{\hat{\phi}}{\Lambda} & & -\frac{\hat{A}_j}{\Lambda} \\ -\frac{\hat{A}_i}{\Lambda} & -\delta_{ij} + (c_d - 2)\frac{\hat{\phi}}{\Lambda}\delta_{ij} - \frac{\hat{\sigma}_{ij}}{\Lambda} & \end{pmatrix} + \mathcal{O}(h^2) ; \quad (3.85)$$

Then, recalling that in TT gauge only the spatial components of the $h_{\mu\nu}$ tensor are non vanishing we obtain $h_{ij} = (c_d - 2)\frac{\hat{\phi}}{\Lambda}\delta_{ij} - \frac{\hat{\sigma}_{ij}}{\Lambda}$, and further recalling that the $\Lambda_{ij,kl}$ selects only the traceless components of the h_{ij} field, from equation (3.84) we finally obtain the expression we were looking for:

$$h_{ij}^{TT}(t, \mathbf{x}) = -\Lambda_{ij,kl}(\hat{\mathbf{n}}) \langle \frac{\bar{\sigma}^{kl}}{\Lambda}(t, \mathbf{x}) \rangle . \quad (3.86)$$

To avoid confusion, $\Lambda_{ij,kl}$ is the Lambda tensor projector defined in (1.32), whereas $\frac{1}{\Lambda}$ is the inverse of the renormalized Planck mass defined in (3.25).

This means that we can evaluate the gravitational field, produced by the binary system, at a large distance from it, by evaluating the vacuum expectation value of the $\bar{\sigma}_{ij}$ radiation field in the same spacetime point. To evaluate this expectation value we have to work in the far zone effective field, considering the connected vacuum diagrams with one $\bar{\sigma}_{ij}$ leg. We'll explicitly do this at leading order in section 5.2, where it will prove to be necessary to employ the in-in formalism in order to obtain causal results, see also references [202, 206, 242].

3.3 | Newtonian potential in the effective theory for binary systems

We'll now exemplify the concept described so far by explicitly obtaining the leading order (0PN) conservative contribution to the binary dynamics: that is, the classical Newtonian potential.

Summarizing the previous points, after integrating out the internal zone, we're left worldline effective theory we're with the near zone effective action (3.29). We recall from 3.2.2 that we consider only the point particle term for the worldline, since finite size effects are higher order contributions. Therefore in practice we have to perform the path integral (3.42) in a perturbative way: in particular, as already discussed, the Newtonian potential is a purely conservative contributions, therefore will be included in $S_{cons}[\{x_a^\mu\}]$. Then this contribution won't be affected by the last path integral

which concerns the far zone effective theory, (3.63), since when deriving the Newtonian potential no radiation gravitons are involved. Instead the leading order contributions will be formally of order 2.5PN, and we'll derive them in section 5.1.

■ Diagram contributing to the Newtonian potential

This means that to obtain the Newtonian potential we can focus only on performing the path integral (3.42): as discussed in section 2.1 and in this whole chapter, to do it we have to sum over all the connected vacuum diagrams involving only potential fields. We then have to select only the leading order contribution, since all others diagrams will yield post-Newtonian corrections to the Newtonian potential, and will be the topic of interest of chapter 4. In particular in section 4.1 we'll study how to methodically draw all the required diagrams and evaluate the corresponding symmetry factors. Nonetheless employing the power counting rules (3.59) and (3.60) we can already see that there is only a single connected diagram that we can construct and which contributes at order $L v^0$ (which is the expected scaling of the Newtonian potential, since $S = \int dt \frac{Gm_1 m_2}{r} \propto L v^0$ using table 3.1): this diagram is the one involving only two worldline- ϕ vertices, connected by a ϕ propagator, which is represented in figure 3.7. In section 4.1.2 we will explain of to evaluate the symmetry factor of this diagram; nonetheless we can conclude that it is $\frac{1}{2}$ already by drawing an analogy with the diagram (3.11) of the toy model, see section 3.1.1.

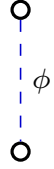


FIGURE 3.7 — the only diagram contributing at leading order in the conservative sector.

■ Diagram evaluation

In order to write down the expression corresponding to the diagram in figure 3.7 we need the expression for the ϕ propagator and for the worldline- ϕ interaction vertex. The explicit derivation of the relevant Feynman rules is presented in appendix A; in particular the aforementioned Feynman rules are respectively given by equation (A.18) and equation (A.39); and therefore, integrating also over the k free momenta, we obtain:

$$\begin{aligned}
 \mathcal{A}_{(Newton)} \equiv & \quad \begin{array}{c} \textcircled{a} \\ \uparrow k \\ \text{---} \phi \text{---} \\ \downarrow \\ \textcircled{b} \end{array} \\
 = & \frac{1}{2} \int \frac{d^{d+1}k}{(2\pi)^{d+1}} \left(-i \sum_{a=1}^2 \frac{m_a}{\Lambda} \int dt \left(\frac{2 + (-2 + c_d) v_a^2}{2\sqrt{1 - v_a^2}} \right) e^{-ikx_a(t)} \right) \left(\frac{1}{2c_d k^2 + i\epsilon} \right) \\
 & \times \left(-i \sum_{b=1}^2 \frac{m_b}{\Lambda} \int dt' \left(\frac{2 + (-2 + c_d) v_b^2}{2\sqrt{1 - v_b^2}} \right) e^{ikx_b(t')} \right). \quad (3.87)
 \end{aligned}$$

The above expression nonetheless still doesn't have a well defined scaling in the post-Newtonian parameters: both because the expression worldline- ϕ vertex is a function of v^2 , and therefore entails an infinite series of corrections in v^2 ; and also because we need to expand the potential propagator as described in section 3.2.3. In particular we can expand the off-shell potential propagator employing formula (3.49), which results in (3.54). Then we can also expand in Taylor series each of the two expand worldline- ϕ vertices around $v^2 \sim 0$, keeping the leading order term only: the leading order

contribution due to the vertex is given by (A.41a). Doing all of this, diagram (3.87) results in:

$$\begin{aligned} \mathcal{A}_{(Newton)} &= \frac{1}{2} \int \frac{d^{d+1}k}{(2\pi)^{d+1}} \left(-i \sum_{a=1}^2 \frac{m_a}{\Lambda} \int dt e^{-ikx_a(t)} \right) \left(-\frac{1}{2c_d} \frac{i}{|\mathbf{k}|^2} \right) \left(-i \sum_{b=1}^2 \frac{m_b}{\Lambda} \int dt' e^{ikx_b(t')} \right) + \mathcal{O}(Lv^2) \\ &= \frac{i}{4c_d \Lambda^2} \sum_{a=1}^2 \sum_{b=1}^2 m_a m_b \int dt dt' \int \frac{d^{d+1}k}{(2\pi)^{d+1}} e^{-ik(x_a(t) - x_b(t'))} \frac{1}{|\mathbf{k}|^2} + \mathcal{O}(Lv^2) \end{aligned} \quad (3.88)$$

where the $\mathcal{O}(Lv^2)$ understand that in the above expression we're neglecting higher order terms due to the aforementioned expansion we truncated. This fact, according to which any post-Newtonian diagram contributes also at higher post-Newtonian order beyond its leading order, is quite general; we'll return on this point in chapter 4.

To proceed with the evaluation of (3.88) we can perform the dk^0 integral, recalling the **Notation** for the conventions about the Dirac deltas. Therefore, noticing also that $x(t) = (t, \mathbf{x}(t))$ and that we're working in mostly minus metric, so $kx(t) = k^0 t - \mathbf{k} \cdot \mathbf{x}(t)$:

$$\begin{aligned} \mathcal{A}_{(Newton)} &= \frac{i}{4c_d \Lambda^2} \sum_{a=1}^2 \sum_{b=1}^2 m_a m_b \int dt dt' \underbrace{\int \frac{dk^0}{2\pi} e^{-ik^0(t-t')}}_{=\delta(t-t')} \int \frac{d^d \mathbf{k}}{(2\pi)^d} e^{i\mathbf{k}(\mathbf{x}_a(t) - \mathbf{x}_b(t'))} \frac{1}{|\mathbf{k}|^2} + \mathcal{O}(Lv^2) \\ &= \frac{i}{4c_d \Lambda^2} \sum_{a=1}^2 \sum_{b=1}^2 m_a m_b \int dt \int \frac{d^d \mathbf{k}}{(2\pi)^d} e^{i\mathbf{k}(\mathbf{x}_a(t) - \mathbf{x}_b(t))} \frac{1}{|\mathbf{k}|^2} + \mathcal{O}(Lv^2) . \end{aligned} \quad (3.89)$$

Now we need to evaluate the integral in the spatial components \mathbf{k} of the momenta: we explicitly evaluated all the integrals needed in this thesis in appendix C. For the case at hand we evaluated this class of Fourier integrals, which we denoted as $I_F(d, a)[\mathbf{x}]$, in appendix C.3, in particular the result is given by (C.31). We can then recognize the function $I_F(d, 1)$ in expression (3.89), to obtain the final result for the diagram:

$$\begin{aligned} \mathcal{A}_{(Newton)} &= \frac{i}{4c_d \Lambda^2} \sum_{a=1}^2 \sum_{b=1}^2 m_a m_b \int dt \underbrace{\int \frac{d^d \mathbf{k}}{(2\pi)^d} e^{i\mathbf{k}(\mathbf{x}_a(t) - \mathbf{x}_b(t))}}_{=I_F(d, 1)[\mathbf{x}_a(t) - \mathbf{x}_b(t)]} \frac{1}{|\mathbf{k}|^2} + \mathcal{O}(Lv^2) \\ &= \frac{i}{4c_d \Lambda^2} \sum_{a=1}^2 \sum_{b=1}^2 m_a m_b \int dt \left(2^{-2} \pi^{-\frac{d}{2}} \frac{\Gamma\left(\frac{d}{2} - 1\right)}{\Gamma(1)} |\mathbf{x}_a(t) - \mathbf{x}_b(t)|^{2-d} \right) + \mathcal{O}(Lv^2) \quad (3.90) \\ &= \frac{i \pi^{-\frac{d}{2}}}{16c_d \Lambda^2} \Gamma\left(\frac{d}{2} - 1\right) \sum_{a=1}^2 \sum_{b=1}^2 m_a m_b \int dt |\mathbf{x}_a(t) - \mathbf{x}_b(t)|^{2-d} + \mathcal{O}(Lv^2) ; \end{aligned}$$

where $\Gamma(z)$ is the gamma function which we present in appendix B.1; in particular we see from table B.1 that $\Gamma(1) = 1$.

■ Obtaining the potential from the diagram expression

In order to extract the classical potential from the above expression (3.90), we'll recall the concepts we introduced in section 3.2.5. In particular equation (3.78) gives the exact relation between the

sum of connected vacuum diagrams and the effective action S_{eff} ;

$$\begin{aligned} S_{eff}[\{x_a^\mu\}] &= -i \sum_j \mathcal{A}_{(j)} = -i \mathcal{A}_{(Newton)} + \mathcal{O}(L v^2) \\ &= \frac{\pi^{-\frac{d}{2}}}{16 c_d \Lambda^2} \Gamma\left(\frac{d}{2} - 1\right) \sum_{a=1}^2 \sum_{b=1}^2 m_a m_b \int dt |\mathbf{x}_a(t) - \mathbf{x}_b(t)|^{2-d} + \mathcal{O}(L v^2) . \end{aligned} \quad (3.91)$$

We can then expand around $d = 3$, recalling also the definitions (3.25) of Λ and (3.31) of c_d , to obtain the expression of a classical action:

$$S_{eff}[\{x_a^\mu\}] = \frac{G}{2} \sum_{a=1}^2 \sum_{b=1}^2 m_a m_b \int dt \frac{1}{|\mathbf{x}_a(t) - \mathbf{x}_b(t)|} + \mathcal{O}(d - 3) + \mathcal{O}(L v^2) . \quad (3.92)$$

At this point the above expression would seem to imply a divergence when the summation runs over $a = b$: nonetheless, as we'll see in section 4.3, this is not the case when performing a more thoughtful derivation, because the $a = b$ contributions will in general be proportional to a scaleless integral, and therefore be vanishing, as already discussed in section 2.2.1. For the moment we can nonetheless simply restrict the summation $\sum_{a=1}^2 \sum_{b=1}^2$ to run over $\sum_{a=1}^2 \sum_{b \neq a}$; doing so expression (3.92) finally reduces to:

$$S_{eff}[\{x_a^\mu\}] = \int dt \frac{G m_1 m_2}{|\mathbf{x}_1(t) - \mathbf{x}_2(t)|} + \mathcal{O}(d - 3) + \mathcal{O}(L v^2) . \quad (3.93)$$

Recalling the definitions (3.73) and (3.74), that is, $S_{eff} = \int dt L(t) = \int dt (T(t) - V(t))$, and comparing this with expression (3.93), we can then directly recognize the classical *Newtonian potential*:

$$V(t) = - \frac{G m_1 m_2}{|\mathbf{x}_1(t) - \mathbf{x}_2(t)|} ; \quad (3.94)$$

this is in fact the classical Newtonian gravitational interaction potential between two point particles, of mass m_1 and m_2 , at a distance $|\mathbf{x}_1(t) - \mathbf{x}_2(t)|$.

We can also see that this potential (3.94) prescribes an instantaneous interaction between the two far away bodies, as both the two different positions \mathbf{x}_1 and \mathbf{x}_2 are evaluated at the same time t : this would seem to imply a violation of the speed of light, when framed in the theories of special relativity and general relativity. Nonetheless this is not the case: in fact this potential is the result of considering only the leading order expansion of the propagator (3.49); but at higher post-Newtonian order we have to consider an infinite series of corrections, given by the same diagrams with propagator insertions (3.55). These corrections take into account perturbatively the retardation effects due to the finite speed of propagation of any interaction, as prescribed by special and general relativity, where there can be no causal connection between two events separated by a space-like interval.

■ Leading order classical conservative Lagrangian

Furthermore, let us also recall, as shown in equation (3.79), that the effective action S_{eff} also contains the kinetic term for the two point particles, given by expression (3.34b). We can then expand it up to order $\mathcal{O}(L v^0)$

$$S_{pp}^{(kin)}[x_a^\mu] = \sum_{a=1}^2 \left(-m_a \int dt \sqrt{1 - v_a^2(t)} \right) = -m_a + \frac{m_a}{2} v_a^2 + \mathcal{O}(L v^2) ; \quad (3.95)$$

in particular, if we were to take the Legendre transform (3.80) to obtain the Hamiltonian, then we would recognize the $-m_a$ term to be the rest energy of the two compact objects, i.e. $E = mc^2$.

Finally, neglecting this rest energy term, we can obtain the full leading order ($\mathcal{O}(L v^0)$) conservative Lagrangian for compact binary system:

$$L(t) = \sum_{a=1}^2 \frac{1}{2} m_a v_a^2(t) + \frac{G m_1 m_2}{r(t)} ; \quad (3.96)$$

where we introduced the spatial relative separation \mathbf{r} between the two compact objects (in harmonic gauge)

$$\mathbf{r}(t) \equiv \mathbf{x}_1(t) - \mathbf{x}_2(t) \quad (3.97)$$

and its modulus $r = |\mathbf{r}|$, so:

$$r(t) \equiv |\mathbf{x}_1(t) - \mathbf{x}_2(t)| . \quad (3.98)$$

■ Leading order equations of motion

As a last result, that will be useful in the following, we can apply the Euler-Lagrange equations (3.75) on the Lagrangian (3.96), recognizing the coordinates $\mathbf{q}_a = \mathbf{x}_a$ and generalized velocities $\dot{\mathbf{q}}_a = \mathbf{v}_a$, $a = 1, 2$, to obtain:

$$\ddot{\mathbf{x}}_1 = - \frac{G m_2}{|\mathbf{x}_1 - \mathbf{x}_2|^3} (\mathbf{x}_1 - \mathbf{x}_2) , \quad (3.99)$$

which is the acceleration due to the classical Newtonian gravitational force. The corresponding equation of motion for the worldline \mathbf{x}_2 is obtained by considering the ($1 \leftrightarrow 2$) version of (3.99), so

$$\ddot{\mathbf{x}}_2 = \frac{G m_1}{|\mathbf{x}_1 - \mathbf{x}_2|^3} (\mathbf{x}_1 - \mathbf{x}_2) . \quad (3.100)$$

POST-NEWTONIAN CONSERVATIVE CORRECTIONS

In this chapter we proceed to evaluate the conservative diagrams related to the procedure of integrating out the potential gravitational modes in the near zone effective theory, which we presented in section 3.2.3. Doing so we will obtain the post-Newtonian correction to the binary dynamics up to 2PN order, so up to the next-to-next-to-leading order corrections to the Newtonian potential that we obtained in section 3.3.

In particular in section 4.1 we outline the procedure needed to evaluate these diagrams; proceeding then in section 4.2 with the explicit evaluation of all the diagrams contributing at 1PN order. In section 4.3 we discuss how to generalize this evaluation procedure to higher post-Newtonian order, also relying on the multi-loop quantum field theory techniques which we introduced in section 2.2. In section 4.4 we outline the `Mathematica` code which we developed, based on the previous procedure, in order to evaluate higher order post-Newtonian correction; in appendix D we also show some extract from the code. In section 4.5 then we present the results so obtained for the conservative corrections at 2PN order. Finally in section 4.6 we present the results obtained regarding the evaluation of a few selected diagrams which first contribute at 7PN order.

4.1 | Evaluation procedure for the conservative sector

4.1.1 — Relevant diagrams generation

The first step in the evaluation of the post-Newtonian corrections up to n -PN order is the generation of all the diagrams which scale like v^{2n} or less. To evaluate the scaling of these diagrams we can employ the power scaling rules for the conservative sector which we obtained in section 3.2.3, in particular formula (3.59) for a generic worldline-gravity interaction vertex and (3.60) for a generic bulk interaction vertex.

In particular let us recall that in the conservative sector the corrections at order n PN are considered with respect to the Newtonian potential result: we already evaluated it with the diagram (3.87) obtaining (3.94); schematically:

$$S_{eff} \propto \begin{array}{c} \circ \\ | \\ \phi \\ | \\ \circ \end{array} \propto \int dt \frac{G m_1 m_2}{r} \propto G^0 L^1 v^0 ; \quad (4.1)$$

as could be expected since the action S_{eff} has the same physical dimensions of the angular momentum L ; this also agrees with what we were expecting from the power counting rule (3.59) for the

worldline-gravity vertex. Then with these power counting rules, we expect any diagram entering at n PN order to scale like $G^0 L^1 v^{2n}$.

The customary procedure to generate all the relevant diagrams up to the wanted PN order is to first organize them according to the post-Minkowskian (PM) expansion: this means that we first perform the power counting in the gravitational constant G only [205, 225, 229, 235], defining as G^m topology the equivalence relation of all connected diagrams that scale like G^m [224, 225]. This proves to be useful since this power counting is easier to perform; and so only later one specializes to the post-Newtonian approximation, keeping at order n -PN only those diagrams which actually scale with the wanted powers of the velocity v^{2n} .

To gauge up to which PM order one has to first build diagrams we can use the PN relation (1.111), so $G \sim v^2$, and notice that, whereas the order 0PN is given by the Newtonian potential, which scales like $G v^0$, at order n -PN we'll have contributions from terms like G^{n+1} , $G^m v^2$, $G^{n-1} v^4 \dots$, $G v^{2n}$, i.e. $G^a v^b$ with $a + \frac{b}{2} = n + 1$ and $a \geq 1, b \geq 0$, see also figure 1.7. Therefore all the relevant diagrams at order n -PN are just a subset of the diagrams which scale like G^{n+1} or less, so the ones entering the $(n + 1)$ -PM expansion.

To evaluate explicitly the G -scaling of a diagram we can notice that any Kol-Smolkin field is normalized to $\Lambda \sim G^{-\frac{1}{2}}$, while the only other place where a G factor may come out from is from the bulk action, i.e. the regularized Einstein-Hilbert action (3.26) plus the gauge fixing term (3.27), which both carry a $\Lambda^2 \sim G^{-1}$ prefactor; on the other hand we can see from the explicit expression of the propagators, given in appendix A.1, that they carry no explicit G factors. Hence we can notice that any of the ϕ, A, σ potential fields scales in the same way with respect to G , so we may consider the generic potential gravity field W in place of its three specific realizations; additionally we'll denote this W field with a black dotted line in the Feynman diagrams.

From this premises, adopting the same notation which we used in equation (3.71), we come to the conclusion that any worldline-gravity vertex scales like $G^{\frac{1}{2}n_w}$, while any bulk interaction vertex scales like $G^{\frac{1}{2}n_b - 1}$, with n_W the number of legs attached to the vertex. Therefore a diagram with N_w^W legs attached to worldline-gravity vertices, with V_b bulk vertices and N_b^W legs attached to bulk vertices will scale like $G^{\frac{1}{2}(N_w^W + N_b^W) - V_b} = G^{p - V_b}$, where used again the fact that the number of propagators in a diagram is given by $p = \frac{1}{2}(N_w^W + N_b^W)$, because each propagator must connect two legs.

We can then draw all the diagrams that belong to the G^m topology, i.e. that scale with G^m and so contribute to the m post-Minkowskian order, by considering all the possible diagrams with $m = p - V_b$ which we can build from the Feynman rules of the theory. As we want to consider only diagrams without loops, $l = 0$, the Euler-Poincaré characteristic formula reduces to $p = v - 1 = V_w + V_b - 1$, therefore any loop-less diagram belonging to the G^m topology will have exactly and only $V_w = m + 1$ worldline-gravity vertices and $p = m + V_b$ propagators. Additionally, since any bulk vertex has at least three legs, whereas any worldline-gravity vertex has at least one, it holds $p = \frac{1}{2}(N_w^W + N_b^W) \geq \frac{1}{2}(3V_b + V_w)$ from which follows the inequality $V_b \leq m - 1$. This implies that to build all the diagrams at order G^m we can first draw the $m + 1$ worldline-gravity vertices, and then iterate over the number of bulk vertices $V_b = 0, 1, \dots, m - 1$: for any of these values of V_b we keep all the connected diagrams we can build using exactly $p = m + V_b$ propagators.

Then in figures 4.1, 4.2 and 4.3 we draw all the diagrams belonging respectively to the G^1, G^2 and G^3 topologies; these results will be useful to obtain the diagrams contributing up to 2PN order. In particular in these figures we denote a generic gravitational field W_a with a gluon-like propagator.

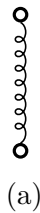


FIGURE 4.1 — Diagram belonging to the G^1 topology ($m = 1, V_w = 2, V_b \leq 0$).

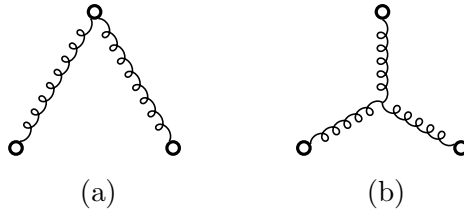


FIGURE 4.2 — Diagrams belonging to the G^2 topology ($m = 2, V_w = 3, V_b \leq 1$).

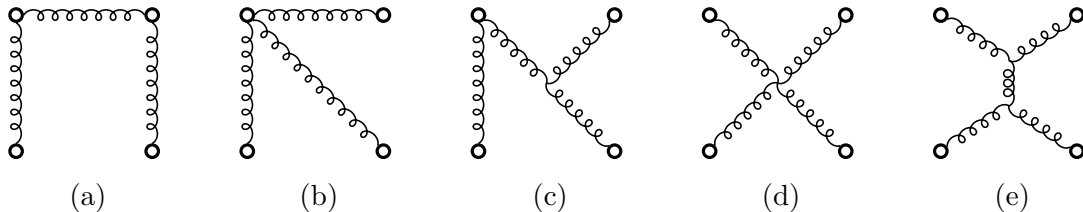


FIGURE 4.3 — Diagrams belonging to the G^3 topology ($m = 3, V_w = 4, V_b \leq 2$).

■ Diagrams contributing up to 2PN order

We can now find all the diagrams which contribute up to 2PN order, using the method just outlined. We therefore specialize the generic potential field W to any of the three ϕ , A or σ potential fields in all of the diagrams belonging to the G^m topologies with $m < 3$ which we just found, and then evaluate their leading order PN scaling using the power scaling rules (3.59) and (3.60), keeping only the diagrams which scale like v^4 or less. We still have to keep track of propagator insertions as explained in section 3.2.3, each of which adds a v^2 factor to the diagram; furthermore any diagrams first appearing at a given PN order will contribute also at higher PN orders because, in order to evaluate fewer diagrams, instead of considering vertex-velocity insertions as we present in appendix A.2 (in particular relations (A.41b) and (A.41c)), we simply chose to keep the worldline-gravity couplings exact, expanding in series their generic dependence on the velocity v only at the end of calculations.

Performing the aforementioned steps we found that at 0PN contributes a single diagram, depicted in figure 4.4, which as expected is exactly the Newtonian diagram which we evaluated in section 3.3. We find then that the three diagrams represented in figure 4.5 first contribute at 1PN order, whereas the twelve diagrams shown in figure 4.6 first contribute at 2PN order. Then we find that not all the G^m topologies which we found previously, e.g. in figure 4.3, contribute at a given PN order: this is due to the velocity suppression of the related vertices. Let us stress again however that at any given PN order we have to consider also the higher-order contributions due to all the diagrams of lower PN order.

All the relevant Feynman rules, for the propagators and the interaction vertices, which are needed to evaluate these diagrams, up to 2PN order, have been explicitly derived in appendix A.

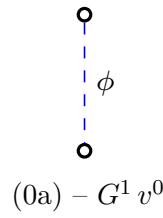


FIGURE 4.4 — Diagram contributing at 0PN at leading order. We stress again that this diagram, like any other, will contribute also at higher PN orders, as in the end we'll have to expand the Wilson coefficient of the worldline-gravity vertex in powers of v .

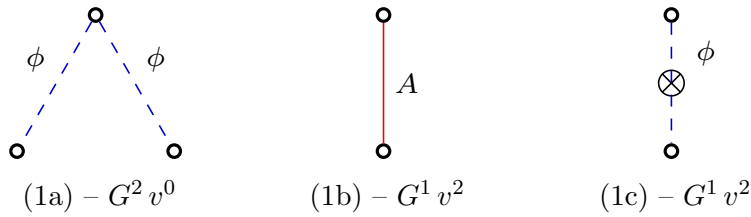


FIGURE 4.5 — Diagrams contributing at 1PN at leading order.

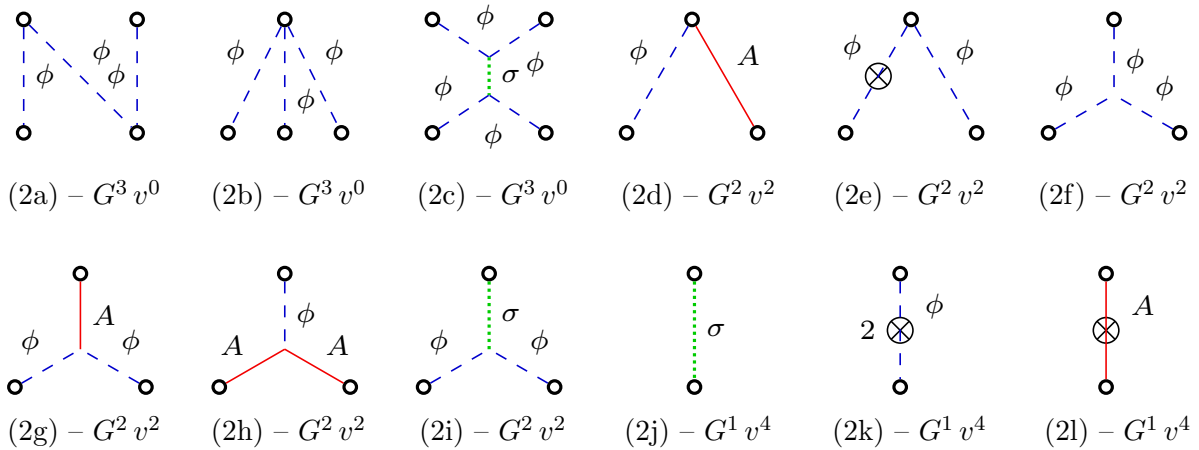


FIGURE 4.6 — Diagrams contributing at 2PN at leading order.

4.1.2 — Symmetry factor of a diagram

Before proceeding with the explicit evaluation of the diagrams, first we have to recognize that to each diagram is associated a *symmetry factor*, by which the expression of the diagram must be multiplied in order to recover the correct result. In particular the symmetry factor of a diagram is given by the ratio between the positive multiplicity and the inverse multiplicity of the diagram itself.

The *positive multiplicity* of a diagram is given by the number of different ways in which we can connect the several field legs entering the vertices with the given propagators. In practice to evaluate the positive multiplicity of a diagram we have to first assign a different label to each vertex which belongs to the diagram, and then we have to uniquely label also each leg entering any of these vertices; this is needed in order to make them distinguishable for the counting. With this construction we can directly evaluate the positive multiplicity of the diagram by counting the number of different connected labelled diagrams that we can correctly construct by joining the labelled legs with the given propagators. To be more precise, given a diagram we can regard it as

Diagram	(0a)	(1a)	(1b)	(1c)	(2a)	(2b)	(2c)	(2d)
Symmetry factor	$\frac{1}{2!}$	$\frac{2}{2! 2!}$	$\frac{1}{2!}$	$\frac{1}{2!}$	$\frac{4 \cdot 2}{(2!)^2 2! 2!}$	$\frac{3 \cdot 2}{3! 3!}$	$\frac{4 \cdot 3 \cdot 2}{(2!)^2 4! 2!}$	$\frac{1}{1}$
Diagram	(2e)	(2f)	(2g)	(2h)	(2i)	(2j)	(2k)	(2l)
Symmetry factor	$\frac{2 \cdot 2}{2! 2!}$	$\frac{3 \cdot 2}{3! 3!}$	$\frac{2}{2! 2!}$	$\frac{2}{2! 2!}$	$\frac{2}{2! 2!}$	$\frac{1}{2!}$	$\frac{1}{2!}$	$\frac{1}{2!}$

TABLE 4.1 — Symmetry factors associated to the diagrams listed in figures 4.4, figure 4.5 and figure 4.6, i.e. the ones contributing to the conservative sector up to 2PN order. The numerator of each symmetry factor represents its positive multiplicity, while the denominator its inverse multiplicity.

the non-ordered set of non-ordered pairs of leg-labels to which any propagator is attached to. Then, given two diagrams, we consider them as equivalent if their associated sets of pairs of leg-labels are the same, with no concern about the order of the pairs. Then the positive multiplicity is given by the number of nonequivalent connected diagrams we can construct with the given propagators.

Furthermore one has to be careful about evaluating the positive multiplicity symmetry factor of any diagram in which propagators with insertions are present: one could evaluate it by considering the corresponding diagram with only exact relativistic propagators, expanding then their expressions in the non-relativistic regime via the geometric sum over propagator insertions, and finally selecting the terms of the expansion with the wanted number of insertions; from these one can recover the symmetry factor of the wanted diagram. Equivalently this procedure can be streamlined by instead evaluating the positive multiplicity of the given diagram with propagators with insertions as explained generically before, but taking care of considering a propagator with n insertions not equivalent to any other: more precisely we do not consider two diagrams as equivalent if the same two labelled legs are connected by propagators which carry a different number of insertions.

Generically we may have to discard also the diagrams which give rise to quantum loops, as discussed in section 3.2.5, but in this case the diagram construction procedure outlined above, and the Euler–Poincaré formula, assure us that any connected diagrams will have no quantum loops.

The *inverse multiplicity* of a diagram instead is related to its symmetry group, and is given by the product of the inverse multiplicities of each of its vertices, multiplied by the inverse multiplicity of the diagram itself. The inverse multiplicity of a given vertex can be evaluated by counting how many identical field legs enter in the vertex, separately for each field, afterwards by taking the factorial of each of these number, and then by multiplying these factorials together; similarly the inverse multiplicity of the diagram can be obtained by counting how many identical vertices are there in the diagram, separately for each type of vertex, then by taking the factorial of each of these numbers, and finally by multiplying these factorials together.

In table 4.1 we report the symmetry factors associated to the diagrams which will be evaluated in the following.

4.2 | Einstein–Infeld–Hoffmann Lagrangian - 1 PN order

In this section we’ll compute the next-to-leading corrections to the Newtonian potential, which we evaluated in section 3.3. In particular these contributions of order $\mathcal{O}(Lv^2)$, so the 1PN Lagrangian, is denoted as the *Einstein–Infeld–Hoffmann* Lagrangian [12], as in 1938 they jointly derived these new predictions for the theory of General Relativity, with respect to the classical Newtonian gravity.

In this derivation we’ll present the application of some of the ideas we introduced in chapter 3; this will also be useful in order to streamline the derivation of the conservative diagrams: in particular

in section 4.3 we'll outline the generic procedure to evaluate conservative diagrams, which will then be implemented in the `Mathematica` code discussed in section 4.4.

In the following then we will proceed with the explicit evaluation of the diagrams relevant up to 1PN, so the ones depicted in figure 4.5, and the 1PN correction coming from the 0PN diagram in figure 4.4. All the relevant Feynman rules have been derived and are presented in appendix A.

In particular in this section, for simplicity and compactness, we will evaluate only the leading order contribution associated to the relevant diagram: in fact by expanding the intermediate expressions in v^2 and keeping only the leading order term, the evaluation simplifies significantly. However this also means that at higher PN order we will have to compute these corrections which we are momentarily neglecting; we'll do so in section 4.5.

■ Diagram with two worldline- ϕ vertices and one worldline- ϕ^2 vertex

The relevant Feynman rules needed to evaluate this diagram are presented in table A.1 in appendix A.2; in particular we recall the rules (A.49a) and (A.49d), in addition to the ϕ potential propagator (A.18).

To exemplify the evaluation of symmetry factors, we can compute the symmetry factor of this diagram by considering that we have one worldline- ϕ^2 vertex, and two worldline- ϕ vertices, and we fix them by labeling each vertex differently. Then, to obtain the positive multiplicity, we have to consider in how many different ways we can connect the labelled legs of the vertices with propagators, with the constraint of obtaining a connected diagram. Then we have $2 \cdot 1 = 2$ different ways in which we may connect these vertices. The inverse multiplicity is instead given by the symmetry group of the diagram: we have that we could swap the two identical worldline- ϕ vertices, so the number of ways we could permute them is $(2!)$; furthermore we could also swap the two identical ϕ legs in the worldline- ϕ^2 vertex, therefore obtaining another additional $(2!)$ permutation factor; in total the inverse multiplicity factor is $(2!)(2!) = 4$. Finally the total symmetry factor is obtained by multiplying the positive multiplicity of the diagram by the inverse of its inverse multiplicity, therefore obtaining $\frac{(2 \cdot 1)}{(2!)(2!)} = \frac{2}{4} = \frac{1}{2}$.

Then we can construct the expression associated to this diagram by multiplying together the relevant Feynman rules, taking care of relabeling differently the variables which are repeated, and integrating over the free momenta:

$$\begin{aligned}
 \mathcal{A}_{(1a)} = & \text{Diagram} = \frac{1}{2} \int_{k_1, k_2} \left(-i \sum_{a=1}^2 \frac{m_a}{\Lambda} \int dt_1 \left(\frac{2 + (-2 + c_d) v_a^2}{2\sqrt{1 - v_a^2}} \right) e^{ik_1 x_a(t_1)} \right) \\
 & \left(\frac{1}{2c_d} \frac{i}{k_1^2 + i\epsilon} \right) \left(-i \sum_{b=1}^2 \frac{m_b}{\Lambda^2} \int dt_2 e^{-i(k_1 + k_2) x_b(t_2)} \right. \\
 & \quad \times \left[\frac{(4 + v_b^2)(-8 - 2(-2 + c_d)c_d + (-2 + c_d)^2 v_b^2)}{4(1 - v_b^2)^{3/2}} \right] \left. \right) \\
 & \left(\frac{1}{2c_d} \frac{i}{k_2^2 + i\epsilon} \right) \left(-i \sum_{c=1}^2 \frac{m_c}{\Lambda} \int dt_3 \left(\frac{2 + (-2 + c_d) v_c^2}{2\sqrt{1 - v_c^2}} \right) e^{ik_2 x_c(t_3)} \right).
 \end{aligned} \tag{4.2}$$

Defining then, for compactness, the function of the velocities only

$$\begin{aligned}
f(v_a, v_b, v_c) &\equiv \left(\frac{2 + (-2 + c_d) v_a^2}{2\sqrt{1 - v_a^2}} \right) \left[\frac{(4 + v_b^2 (-8 - 2(-2 + c_d) c_d + (-2 + c_d)^2 v_b^2))}{4(1 - v_b^2)^{3/2}} \right] \\
&\quad \times \left(\frac{2 + (-2 + c_d) v_c^2}{2\sqrt{1 - v_c^2}} \right) \\
&= 1 + \frac{1}{2} (-1 + c_d) (v_a^2 + v_b^2 - c_d v_b^2 + v_c^2) + \mathcal{O}(v^4) \\
&\stackrel{d=3}{=} 1 + \mathcal{O}(v^2) + \mathcal{O}(d - 3) .
\end{aligned} \tag{4.3}$$

we obtain:

$$\begin{aligned}
\mathcal{A}_{(1a)} &= -\frac{1}{2} \frac{i}{4c_d^2} \sum_{a,b,c=1}^2 \frac{m_a m_b m_c}{\Lambda^4} \int dt_1 dt_2 dt_3 f(v_a, v_b, v_c) \int_{k_1, k_2} \left[\frac{1}{k_1^2 + i\epsilon} \frac{1}{k_2^2 + i\epsilon} \right. \\
&\quad \left. e^{-i[k_1(x_b(t_2) - x_a(t_1)) + k_2(x_b(t_2) - x_c(t_3))]} \right] .
\end{aligned} \tag{4.4}$$

We can now perform the expansion of both the propagators at leading order

$$\begin{aligned}
\frac{1}{k_1^2 + i\epsilon} \frac{1}{k_2^2 + i\epsilon} &= \left(-\frac{1}{|\mathbf{k}_1|^2} \sum_{m=0}^{+\infty} \left(\frac{(k_1^0)^2}{|\mathbf{k}_1|^2} \right)^m \right) \left(-\frac{1}{|\mathbf{k}_2|^2} \sum_{n=0}^{+\infty} \left(\frac{(k_2^0)^2}{|\mathbf{k}_2|^2} \right)^n \right) \\
&= \frac{1}{|\mathbf{k}_1|^2 |\mathbf{k}_2|^2} \left(1 + \mathcal{O} \left(\frac{(k^0)^2}{|\mathbf{k}|^2} \right) \right) ,
\end{aligned} \tag{4.5}$$

to obtain, neglecting terms at order $\mathcal{O} \left(\frac{(k^0)^2}{|\mathbf{k}|^2} \right)$:

$$\begin{aligned}
\mathcal{A}_{(1a)} &= -\frac{1}{2} \frac{i}{4c_d^2} \sum_{a,b,c=1}^2 \frac{m_a m_b m_c}{\Lambda^4} \int dt_1 dt_2 dt_3 f(v_a, v_b, v_c) \left[\underbrace{\int \frac{dk_1^0}{2\pi} e^{-ik_1^0(t_2 - t_1)}}_{=\delta(t_2 - t_1)} \underbrace{\int \frac{dk_2^0}{2\pi} e^{-ik_2^0(t_2 - t_3)}}_{=\delta(t_2 - t_3)} \right. \\
&\quad \left. \underbrace{\int \frac{d^d \mathbf{k}_1}{(2\pi)^d} \frac{1}{|\mathbf{k}_1|^2} e^{i\mathbf{k}_1 \cdot (\mathbf{x}_b(t_2) - \mathbf{x}_a(t_1))}}_{=I_F(d,1)[\mathbf{x}_b(t_2) - \mathbf{x}_a(t_1)]} \underbrace{\int \frac{d^d \mathbf{k}_2}{(2\pi)^d} \frac{1}{|\mathbf{k}_2|^2} e^{i\mathbf{k}_2 \cdot (\mathbf{x}_b(t_2) - \mathbf{x}_c(t_3))}}_{=I_F(d,1)[\mathbf{x}_b(t_2) - \mathbf{x}_c(t_3)]} \right] \\
&= -\frac{1}{2} \frac{i}{4c_d^2} \sum_{a,b,c=1}^2 \frac{m_a m_b m_c}{\Lambda^4} \int dt [f(v_a, v_b, v_c) \\
&\quad \frac{\Gamma(\frac{d}{2} - 1)}{(4\pi)^{\frac{d}{2}} \Gamma(1)} \left(\frac{|\mathbf{x}_b(t) - \mathbf{x}_a(t)|}{2} \right)^{2-d} \frac{\Gamma(\frac{d}{2} - 1)}{(4\pi)^{\frac{d}{2}} \Gamma(1)} \left(\frac{|\mathbf{x}_b(t) - \mathbf{x}_c(t)|}{2} \right)^{2-d}] \\
&\stackrel{d \rightarrow 3}{=} -\frac{1}{2 \cdot 4 \cdot 16} \frac{i}{(32\pi G)^{-2}} \sum_{a,b,c=1}^2 \frac{m_a m_b m_c}{\Lambda^4} \int dt \left[f(v_a, v_b, v_c) \frac{\Gamma(\frac{1}{2})^2}{(4\pi)^3} \left(\frac{2}{|\mathbf{x}_b(t) - \mathbf{x}_a(t)|} \frac{2}{|\mathbf{x}_b(t) - \mathbf{x}_c(t)|} \right) \right] \\
&\stackrel{d=3}{=} -\frac{1}{2} i G^2 \sum_{a,b,c=1}^2 m_a m_b m_c \int dt \left[f(v_a, v_b, v_c) \left(\frac{1}{|\mathbf{x}_b(t) - \mathbf{x}_a(t)|} \frac{1}{|\mathbf{x}_b(t) - \mathbf{x}_c(t)|} \right) \right] \\
&\stackrel{d=3}{=} -\frac{1}{2} i G^2 \sum_{b=1}^2 \sum_{a \neq b} \sum_{c \neq b} m_a m_b m_c \int dt \left(\frac{1}{|\mathbf{x}_b(t) - \mathbf{x}_a(t)|} \frac{1}{|\mathbf{x}_b(t) - \mathbf{x}_c(t)|} \right) + \mathcal{O}(L v^4) ,
\end{aligned} \tag{4.6}$$

where in the last line we recalled the expansion of $f(v_a, v_b, v_c)$ as shown in formula (4.3), and we kept only the leading order term $f(v_a, v_b, v_c) = 1 + O(v^2)$. In this case we also neglected the terms $b = a$ or $b = c$ in the sum: in fact, as already pointed out in section 3.3, when generalizing this procedure in section 4.3, we'll find the corresponding contributions to vanish in dimensional regularization, as they will be proportional to scaleless integrals. Finally, specializing the previous expression to $N = 2$ bodies in $d = 3$, and recalling the relations $\int dt V(t) = -S_{eff} = +i\mathcal{A}_{(1a)}$, we obtain:

$$\begin{aligned} \mathcal{A}_{(1a)} &= -i \int dt \left[\frac{G^2}{2} (m_1 m_2^2 + m_2 m_1^2) \frac{1}{|\mathbf{x}_1(t) - \mathbf{x}_2(t)|^2} + \mathcal{O}(L v^4) \right] \\ \implies V_{(1a)}(t) &= \frac{G^2}{2} \frac{m m_1 m_2}{|\mathbf{x}_1(t) - \mathbf{x}_2(t)|^2} + \mathcal{O}(L v^4) ; \end{aligned} \quad (4.7)$$

where we have already singled out the contribution to the potential V of the Lagrangian.

■ Diagram with two worldline- A vertices

In this case we need the A_i propagator, given in equation (A.22), and the worldline- A interaction vertex, given by formula (A.49b). The symmetry factor is $\frac{1}{2}$, as we have only one way to connect the labelled vertices with the propagator, while the symmetry group of the diagram entails the permutation of the two identical vertices, so a $(2!)$ inverse multiplicity.

$$\begin{aligned} \mathcal{A}_{(1b)} = & \begin{array}{c} \textcircled{a} \ i \\ \downarrow k \\ \textcircled{b} \ j \end{array} = \frac{1}{2} \int_k \left(-i \sum_{a=1}^2 \frac{m_a}{\Lambda} \int dt_1 e^{ikx_a(t_1)} \left(-\frac{1}{\sqrt{1-v_a^2}} \right) v_a^i \right) \left(-\frac{\delta_{ij}}{2} \frac{i}{k^2 + i\epsilon} \right) \\ & \left(-i \sum_{b=1}^2 \frac{m_b}{\Lambda} \int dt_2 e^{-ikx_b(t_2)} \left(-\frac{1}{\sqrt{1-v_b^2}} \right) v_b^j \right) . \end{aligned} \quad (4.8)$$

In this diagram we define, analogously as before, the scalar function $f(v_a, v_b)$ given by the product of the vertex coefficients; but in this case we also include the contraction of the tensorial structure $v_a^i \delta_{ij} v_b^j$, as it doesn't contain any dependence on the momentum k and hence can be taken out of the corresponding momentum integral:

$$f(\mathbf{v}_a, \mathbf{v}_b) \equiv \left(-\frac{1}{\sqrt{1-v_a^2}} \right) \left(-\frac{1}{\sqrt{1-v_b^2}} \right) \underbrace{\left(v_a^i \delta_{ij} v_b^j \right)}_{=\mathbf{v}_a \cdot \mathbf{v}_b} = \mathbf{v}_a \cdot \mathbf{v}_b + O(v^4) , \quad (4.9)$$

$$\begin{aligned}
\mathcal{A}_{(1b)} &= \frac{1}{2} \left(+\frac{i}{2} \right) \sum_{a,b=1}^2 \frac{m_a m_b}{\Lambda^2} \int dt_1 dt_2 f(v_a, v_b) \int_k e^{-ik(x_b(t_2) - x_a(t_1))} \left(\frac{1}{k^2 + i\epsilon} \right) \\
&= \frac{1}{2} \left(+\frac{i}{2} \right) \sum_{a,b=1}^2 \frac{m_a m_b}{\Lambda^2} \int dt_1 dt_2 f(v_a, v_b) \int_k e^{-ik(x_b(t_2) - x_a(t_1))} \left(-\frac{1}{|\mathbf{k}|^2} \right) + O(Lv^4) \\
&= \frac{1}{2} \left(-\frac{i}{2} \right) \sum_{a,b=1}^2 \frac{m_a m_b}{\Lambda^2} \int dt_1 dt_2 f(v_a, v_b) \underbrace{\int \frac{dk^0}{2\pi} e^{-ik^0(t_2 - t_1)}}_{=\delta(t_2 - t_1)} \\
&\quad \times \underbrace{\int \frac{d^d \mathbf{k}}{(2\pi)^d} e^{i\mathbf{k} \cdot (\mathbf{x}_b(t_2) - \mathbf{x}_a(t_1))} \frac{1}{|\mathbf{k}|^2}}_{=I_F(d,1)[\mathbf{x}_b(t_2) - \mathbf{x}_a(t_1)]} + O(Lv^4) \tag{4.10} \\
&= \frac{1}{2} \left(-\frac{i}{2} \right) \sum_{a,b=1}^2 \frac{m_a m_b}{\Lambda^2} \int dt f(v_a, v_b) \frac{\Gamma(\frac{d}{2} - 1)}{(4\pi)^{\frac{d}{2}} \Gamma(1)} \left(\frac{2}{|\mathbf{x}_b(t) - \mathbf{x}_a(t)|} \right)^{d-2} + O(Lv^4) \\
&\stackrel{d \rightarrow 3}{=} \frac{1}{2} \left(-\frac{i}{2} \right) \sum_{a,b=1}^2 \frac{m_a m_b}{(32\pi G)^{-1}} \int dt f(v_a, v_b) \frac{\sqrt{\pi}}{8\pi^{\frac{3}{2}}} \frac{2}{|\mathbf{x}_b(t) - \mathbf{x}_a(t)|} + O(Lv^4) \\
&\stackrel{d=3}{=} \frac{1}{2} (-4iG) \sum_{a \neq b}^2 m_a m_b \int dt \frac{(\mathbf{v}_a \cdot \mathbf{v}_b)}{|\mathbf{x}_b(t) - \mathbf{x}_a(t)|} + O(Lv^4) \\
&\stackrel{d=3}{=} -i \int dt \left[4G \frac{m_1 m_2 (\mathbf{v}_1 \cdot \mathbf{v}_2)}{|\mathbf{x}_1(t) - \mathbf{x}_2(t)|} \right] + O(Lv^4).
\end{aligned}$$

■ Diagram with two worldline- ϕ vertices, with one ϕ propagator insertion

We recognize that this diagram, first contributing at 1PN, is a next-to-leading order correction to the Newtonian potential, which arises from the expansion of the potential ϕ propagator. We recall then the expression (3.55) for the ϕ propagator insertion; whereas the Feynman rule for the vertex is still given by (A.49a). Then we find the associated expression to be:

$$\begin{aligned}
\mathcal{A}_{(1c)} &= \begin{array}{c} \textcircled{a} \\ | \\ \phi \otimes \downarrow k \\ | \\ \textcircled{b} \end{array} = \frac{1}{2} \int_k \left(-i \sum_{a=1}^2 \frac{m_a}{\Lambda} \int dt_1 e^{ikx_a(t_1)} \left(\frac{2 + (-2 + c_d) v_a^2}{2\sqrt{1 - v_a^2}} \right) \right) \\
&\quad \times \left(-\frac{1}{2c_d} \frac{i}{|\mathbf{k}|^2} \left(\frac{(k^0)^2}{|\mathbf{k}|^2} \right) \right) \left(-i \sum_{b=1}^2 \frac{m_b}{\Lambda} \int dt_2 e^{-ikx_b(t_2)} \left(\frac{2 + (-2 + c_d) v_b^2}{2\sqrt{1 - v_b^2}} \right) \right). \tag{4.11}
\end{aligned}$$

We define then the function

$$\begin{aligned}
f(\mathbf{v}_a, \mathbf{v}_b) &= \left(\frac{2 + (-2 + c_d) v_a^2}{2\sqrt{1 - v_a^2}} \right) \left(\frac{2 + (-2 + c_d) v_b^2}{2\sqrt{1 - v_b^2}} \right) \\
&\stackrel{d \rightarrow 3}{=} 1 + O(v^2) + \mathcal{O}(d - 3)
\end{aligned} \tag{4.12}$$

recalling that we understand the time dependence of velocities, so for example explicitly $\mathbf{v}_a = \mathbf{v}_a(t)$;

and therefore we obtain:

$$\begin{aligned}
\mathcal{A}_{(1c)} &= \frac{1}{2} \left(\frac{i}{2c_d} \right) \sum_{a,b}^2 \frac{m_a m_b}{\Lambda^2} \int dt_1 dt_2 f(\mathbf{v}_a(t_1), \mathbf{v}_b(t_2)) \int_k \left(\frac{(k^0)^2}{|\mathbf{k}|^4} e^{-ik(x_b(t_2) - x_a(t_1))} \right) \\
&= \frac{1}{2} \left(\frac{i}{2c_d} \right) \sum_{a,b}^2 \frac{m_a m_b}{\Lambda^2} \int dt_1 dt_2 \frac{dk^0}{2\pi} (k^0)^2 e^{-ik^0(t_2 - t_1)} f(\mathbf{v}_a(t_1), \mathbf{v}_b(t_2)) \underbrace{\int \frac{d^d \mathbf{k}}{(2\pi)^d} \frac{e^{i\mathbf{k} \cdot (\mathbf{x}_b(t_2) - \mathbf{x}_a(t_1))}}{|\mathbf{k}|^4}}_{=I_F(d,2)[\mathbf{x}_b(t_2) - \mathbf{x}_a(t_1)]}.
\end{aligned} \tag{4.13}$$

We can now recognize an expression with a structure analogous to the following one, with $g(t_1, t_2)$ a generic well-behaved function of the two time variables, and D_1, D_2 their respective integration domains which we display explicitly:

$$\begin{aligned}
&\int_{D_1, D_2} \frac{dk^0}{2\pi} dt_1 dt_2 (k^0)^2 e^{-ik^0(t_2 - t_1)} g(t_1, t_2) \\
&= \int_{D_1, D_2} \frac{dk^0}{2\pi} dt_1 dt_2 \frac{1}{(-i)i} \frac{\partial^2 e^{-ik^0(t_2 - t_1)}}{\partial t_2 \partial t_1} g(t_1, t_2) \\
&= \int_{D_1, D_2} \frac{dk^0}{2\pi} dt_1 dt_2 \left[\frac{\partial}{\partial t_2} \left(\frac{\partial e^{-ik^0(t_2 - t_1)}}{\partial t_1} g(t_1, t_2) \right) - \frac{\partial e^{-ik^0(t_2 - t_1)}}{\partial t_1} \frac{\partial g(t_1, t_2)}{\partial t_2} \right] \\
&= \int_{D_1} \frac{dk^0}{2\pi} dt_1 \underbrace{\left[\frac{\partial e^{-ik^0(t_2 - t_1)}}{\partial t_1} g(t_1, t_2) \right]}_{=0} \Big|_{\partial D_2} - \int_{D_1, D_2} \frac{dk^0}{2\pi} dt_1 dt_2 \left[\frac{\partial e^{-ik^0(t_2 - t_1)}}{\partial t_1} \frac{\partial g(t_1, t_2)}{\partial t_2} \right] \\
&= - \int_{D_1, D_2} \frac{dk^0}{2\pi} dt_2 dt_1 \left[\frac{\partial}{\partial t_1} \left(e^{-ik^0(t_2 - t_1)} \frac{\partial g(t_1, t_2)}{\partial t_2} \right) - e^{-ik^0(t_2 - t_1)} \frac{\partial^2 g(t_1, t_2)}{\partial t_1 \partial t_2} \right] \\
&= - \int_{D_2} \frac{dk^0}{2\pi} dt_2 \underbrace{\left[e^{-ik^0(t_2 - t_1)} \frac{\partial g(t_1, t_2)}{\partial t_2} \right]}_{=0} \Big|_{\partial D_1} + \int_{D_1, D_2} \frac{dk^0}{2\pi} dt_2 dt_1 \left[e^{-ik^0(t_2 - t_1)} \frac{\partial^2 g(t_1, t_2)}{\partial t_1 \partial t_2} \right] \\
&= \int_{D_1, D_2} dt_1 dt_2 \underbrace{\frac{dk^0}{2\pi} e^{-ik^0(t_2 - t_1)}}_{=\delta(t_2 - t_1)} \frac{\partial^2 g(t_1, t_2)}{\partial t_1 \partial t_2} \\
&= \int_{D_1, D_2} dt_1 dt_2 \delta(t_2 - t_1) \frac{\partial^2 g(t_1, t_2)}{\partial t_1 \partial t_2}
\end{aligned} \tag{4.14}$$

where we choose to take one derivative for each temporal variable in order to obtain a symmetric expression and with no second derivative for the same time variable in $g(t_1, t_2)$; and where we assumed the function $g(t_1, t_2)$ and its time derivatives to vanish on the boundary of the integration domain.

Therefore the diagram expression (4.13) can be recast as:

$$\begin{aligned}
\mathcal{A}_{(1c)} &= \frac{1}{2} \left(\frac{i}{2c_d} \right) \sum_{a,b}^2 \frac{m_a m_b}{\Lambda^2} \int dt_1 dt_2 \delta(t_2 - t_1) \\
&\quad \times \frac{\partial^2}{\partial t_1 \partial t_2} \left(f(\mathbf{v}_a(t_1), \mathbf{v}_b(t_2)) \frac{\Gamma(\frac{d}{2} - 2)}{(4\pi)^{\frac{d}{2}} \Gamma(2)} \left(\frac{|\mathbf{x}_b(t_2) - \mathbf{x}_a(t_1)|}{2} \right)^{4-d} \right).
\end{aligned} \tag{4.15}$$

In practice such an expression, when the time derivatives are applied to the $f(\mathbf{v}_a(t_1), \mathbf{v}_b(t_2))$ function, imply the appearance of the accelerations: nonetheless this is not the case at this order, since

the leading order contribution is given by truncating $f = 1 + \mathcal{O}(v^2)$; the acceleration will instead appear when we'll evaluate the 2PN contributions due to this diagram, see equation (4.55p).

Therefore we find:

$$\begin{aligned} \frac{\partial}{\partial t} (|\mathbf{x}_a(t) - \mathbf{x}_b(t')|^p) &= \frac{\partial}{\partial t} \left[\left((\mathbf{x}_a(t) - \mathbf{x}_b(t')) \cdot (\mathbf{x}_a(t) - \mathbf{x}_b(t')) \right)^{\frac{p}{2}} \right] \\ &= \frac{p}{2} |\mathbf{x}_a(t) - \mathbf{x}_b(t')|^{p-2} \frac{\partial}{\partial t} \left[(\mathbf{x}_a(t) - \mathbf{x}_b(t')) \cdot (\mathbf{x}_a(t) - \mathbf{x}_b(t')) \right] \\ &= p |\mathbf{x}_a(t) - \mathbf{x}_b(t')|^{p-2} (\mathbf{v}_a(t) \cdot (\mathbf{x}_a(t) - \mathbf{x}_b(t'))) , \end{aligned} \quad (4.16)$$

and so the expression for the Feynman diagram becomes:

$$\begin{aligned} \mathcal{A}_{(1c)} &= \frac{1}{2} \left(\frac{i}{2c_d} \right) \frac{\Gamma(\frac{d}{2} - 2) 2^{d-4}}{(4\pi)^{\frac{d}{2}} \Gamma(2)} \sum_{a,b}^2 \frac{m_a m_b}{\Lambda^2} \int dt_1 dt_2 \delta(t_2 - t_1) \frac{\partial^2}{\partial t_1 \partial t_2} \left(|\mathbf{x}_b(t_2) - \mathbf{x}_a(t_1)|^{4-d} \right) \\ &= \frac{1}{2} \left(\frac{i}{2c_d} \right) \frac{\Gamma(\frac{d}{2} - 2) 2^{d-4}}{(4\pi)^{\frac{d}{2}} \Gamma(2)} \sum_{a,b}^2 \frac{m_a m_b}{\Lambda^2} \int dt_1 dt_2 \delta(t_2 - t_1) \\ &\quad \frac{\partial}{\partial t_1} \left((4-d) |\mathbf{x}_b(t_2) - \mathbf{x}_a(t_1)|^{2-d} (\mathbf{v}_b(t_2) \cdot (\mathbf{x}_b(t_2) - \mathbf{x}_a(t_1))) \right) \\ &= \frac{1}{2} \left(-\frac{i}{2c_d} \right) \frac{\Gamma(\frac{d}{2} - 2) 2^{d-4}}{(4\pi)^{\frac{d}{2}} \Gamma(2)} (4-d) \sum_{a,b}^2 \frac{m_a m_b}{\Lambda^2} \int dt_1 dt_2 \delta(t_2 - t_1) \\ &\quad \left[(2-d) |\mathbf{x}_b(t_2) - \mathbf{x}_a(t_1)|^{-d} (\mathbf{v}_a(t_1) \cdot (\mathbf{x}_b(t_2) - \mathbf{x}_a(t_1))) (\mathbf{v}_b(t_2) \cdot (\mathbf{x}_b(t_2) - \mathbf{x}_a(t_1))) \right. \\ &\quad \left. + |\mathbf{x}_b(t_2) - \mathbf{x}_a(t_1)|^{2-d} (\mathbf{v}_b(t_2) \cdot \mathbf{v}_a(t_1)) \right] \\ &= \frac{1}{2} \left(-\frac{i}{2c_d} \right) \frac{\Gamma(\frac{d}{2} - 2) 2^{d-4}}{(4\pi)^{\frac{d}{2}} \Gamma(2)} (4-d) \sum_{a,b}^2 \frac{m_a m_b}{\Lambda^2} \int dt |\mathbf{x}_b(t) - \mathbf{x}_a(t)|^{2-d} [(\mathbf{v}_b(t) \cdot \mathbf{v}_a(t)) \\ &\quad + (2-d) |\mathbf{x}_b(t) - \mathbf{x}_a(t)|^{-2} (\mathbf{v}_a(t) \cdot (\mathbf{x}_b(t) - \mathbf{x}_a(t))) (\mathbf{v}_b(t) \cdot (\mathbf{x}_b(t) - \mathbf{x}_a(t)))] \\ &\stackrel{d \rightarrow 3}{=} \frac{1}{2} \left(-\frac{i}{8} \right) \frac{\Gamma(-\frac{1}{2}) 2^{-1}}{(4\pi)^{\frac{3}{2}} \Gamma(2)} \sum_{a \neq b}^2 \frac{m_a m_b}{(32\pi G)^{-1}} \int dt \frac{1}{|\mathbf{x}_b(t) - \mathbf{x}_a(t)|} [(\mathbf{v}_b(t) \cdot \mathbf{v}_a(t)) \\ &\quad - \left(\mathbf{v}_a(t) \cdot \left(\frac{\mathbf{x}_b(t) - \mathbf{x}_a(t)}{|\mathbf{x}_b(t) - \mathbf{x}_a(t)|} \right) \right) \left(\mathbf{v}_b(t) \cdot \left(\frac{\mathbf{x}_b(t) - \mathbf{x}_a(t)}{|\mathbf{x}_b(t) - \mathbf{x}_a(t)|} \right) \right)] \\ &\stackrel{d=3}{=} \frac{1}{2} \left(-\frac{i}{8} \right) \frac{(-2\sqrt{\pi})}{8\pi^{\frac{3}{2}}} \frac{1}{2} (32\pi G) 2m_1 m_2 \int dt \frac{1}{|\mathbf{x}_1 - \mathbf{x}_2|} [(\mathbf{v}_1 \cdot \mathbf{v}_2) \\ &\quad - \left(\mathbf{v}_2 \cdot \left(\frac{\mathbf{x}_1 - \mathbf{x}_2}{|\mathbf{x}_1 - \mathbf{x}_2|} \right) \right) \left(\mathbf{v}_1 \cdot \left(\frac{\mathbf{x}_1 - \mathbf{x}_2}{|\mathbf{x}_1 - \mathbf{x}_2|} \right) \right)] \\ &\stackrel{d=3}{=} -i \int dt \left[-\frac{G}{2} \frac{m_1 m_2}{|\mathbf{x}_1 - \mathbf{x}_2|} \left((\mathbf{v}_1 \cdot \mathbf{v}_2) - \left(\mathbf{v}_2 \cdot \left(\frac{\mathbf{x}_1 - \mathbf{x}_2}{|\mathbf{x}_1 - \mathbf{x}_2|} \right) \right) \left(\mathbf{v}_1 \cdot \left(\frac{\mathbf{x}_1 - \mathbf{x}_2}{|\mathbf{x}_1 - \mathbf{x}_2|} \right) \right) \right) \right] \end{aligned} \quad (4.17)$$

■ Diagram with two worldline- ϕ vertices, with one worldline- ϕ vertex insertion

We also need to consider the $O(v^2)$ correction to the Newtonian diagram, which we computed in section 3.3. Usually one would simply compute the diagram once, with vertex coefficients exact to all orders in v , and then expand the resulting expression up to the needed PN order. Nonetheless in this case we'll show explicitly how to derive the same result by the diagrammatic representation of such an expansion via vertex velocity insertion, so by considering the $O(v^2)$ correction to the worldline- ϕ vertex, whose expression is reported in the appendix, see formula (A.41b).

Even in this case we could proceed in two ways: we may either consider the original diagram expression, as reported in formula (3.87), and perform two insertion separately, one in the upper vertex and one in the lower one, and then sum the result; otherwise equivalently we may consider this diagram as a new one altogether, independent of the original $O(v^0)$ Newtonian one, therefore we'd be working with one leading-order worldline- ϕ vertex and with one $O(v^2)$ worldline- ϕ vertex, so with a single velocity insertion. The former procedure can be seen as expanding each vertex coefficient separately in the original diagram, while the latter one implies to be working with a different diagram altogether: in fact the latter procedure requires re-evaluating the symmetry factor, and in fact, differently with respect to the Newtonian diagram, the vertices are not identical anymore, therefore the symmetry factor of the diagram would be 1 instead of the original $\frac{1}{2}$. Because the first procedure could create misunderstandings, as it requires the modification of the expression of a diagram, and does not correspond to the usual evaluation of the corresponding pictorial representations, we'll proceed with the second procedure.

Therefore the diagram to evaluate in this case is:

$$\mathcal{A}_{(0a)}^{(1PN)} = \phi \begin{array}{c} \textcircled{a} \\ \vdots \\ \downarrow k \\ \textcircled{b} \end{array} = 1 \cdot \int_k \left(-i \sum_{a=1}^2 \frac{m_a}{\Lambda} \int dt_1 e^{ikx_a(t_1)} \left(\frac{c_d - 1}{2} \right) v_a^2 \right) \left(\frac{1}{2c_d} \frac{i}{k^2 + i\epsilon} \right) \left(-i \sum_{a=1}^2 \frac{m_b}{\Lambda} \int dt_2 e^{-ikx_b(t_2)} \right), \quad (4.18)$$

where we used the already expanded expression (A.41a) for the leading order vertex and (A.41b) for the one with a single velocity insertion. Considering now only the leading order expansion of the propagator, as we're already working at $O(Lv^2)$, we obtain:

$$\begin{aligned} \mathcal{A}_{(0a)}^{(1PN)} &= i \left(\frac{c_d - 1}{4c_d} \right) \sum_{a,b} \frac{m_a m_b}{\Lambda^2} \int dt_1 dt_2 v_a^2 \underbrace{\int \frac{dk^0}{2\pi} e^{-ik^0(t_2-t_1)}}_{=\delta(t_2-t_1)} \underbrace{\int \frac{d^d \mathbf{k}}{(2\pi)^d} \frac{1}{|\mathbf{k}|^2} e^{i\mathbf{k} \cdot (\mathbf{x}_b(t_2) - \mathbf{x}_a(t_1))}}_{=I_F(d,1)[\mathbf{x}_b(t_2) - \mathbf{x}_a(t_1)]} \\ &= i \left(\frac{c_d - 1}{4c_d} \right) \frac{\Gamma(\frac{d}{2} - 1)}{(4\pi)^{\frac{d}{2}} \Gamma(1)} \sum_{a \neq b} \frac{m_a m_b}{\Lambda^2} \int dt v_a^2 \left(\frac{2}{|\mathbf{x}_b(t) - \mathbf{x}_a(t)|} \right)^{d-2} \\ &\stackrel{d \rightarrow 3}{=} -i \int dt \left[-\frac{3}{2} G \frac{m_1 m_2}{|\mathbf{x}_1 - \mathbf{x}_2|} (v_1^2 + v_2^2) \right] \end{aligned} \quad (4.19)$$

4.2.1 — Corrections to the two-body potential at 1PN order

Finally, recalling what we have presented in chapter 3 and in particular equation (3.79), and proceeding analogously to what we have seen in section 3.3, we can recognize that the sum of all the diagrams we computed above gives the 1PN conservative corrections (i.e. of order $O(Lv^2)$) to the Lagrangian of the two body system. To be more precise, by factoring out the $-i \int dt$ factors previously we have already singled out the corrections to the potential V , which enters in the Lagrangian as $L = T - V$.

Therefore, summing the results (4.7), (4.10), (4.17) and (4.19), the next-to-leading order (1PN)

contribution to the potential explicitly reads:

$$\begin{aligned} \Delta V_{1PN} &= \frac{G^2}{2} \frac{m m_1 m_2}{|\mathbf{x}_1(t) - \mathbf{x}_2(t)|^2} + 4G \frac{m_1 m_2 (\mathbf{v}_1 \cdot \mathbf{v}_2)}{|\mathbf{x}_1(t) - \mathbf{x}_2(t)|} - \frac{3}{2} G \frac{m_1 m_2}{|\mathbf{x}_1 - \mathbf{x}_2|} (v_1^2 + v_2^2) \\ &\quad - \frac{G}{2} \frac{m_1 m_2}{|\mathbf{x}_1 - \mathbf{x}_2|} \left((\mathbf{v}_1 \cdot \mathbf{v}_2) - \left(\mathbf{v}_2 \cdot \left(\frac{\mathbf{x}_1 - \mathbf{x}_2}{|\mathbf{x}_1 - \mathbf{x}_2|} \right) \right) \left(\mathbf{v}_1 \cdot \left(\frac{\mathbf{x}_1 - \mathbf{x}_2}{|\mathbf{x}_1 - \mathbf{x}_2|} \right) \right) \right) \quad (4.20) \\ &= -\frac{G m_1 m_2}{2r} \left(-G \frac{(m_1 + m_2)}{r} - 7(\mathbf{v}_1 \cdot \mathbf{v}_2) + 3(v_1^2 + v_2^2) - (\mathbf{v}_1 \cdot \hat{\mathbf{r}})(\mathbf{v}_2 \cdot \hat{\mathbf{r}}) \right) \end{aligned}$$

where we understand the dependence of the quantities on the time t ; recalling as well the definition of the relative separation \mathbf{r} from equation (3.97) to introduce its corresponding versor:

$$\hat{\mathbf{r}} \equiv \frac{\mathbf{x}_1 - \mathbf{x}_2}{|\mathbf{x}_1 - \mathbf{x}_2|}. \quad (4.21)$$

Let us notice that above expression (4.20) is the first correction to the Newtonian potential, which we had found in equation (3.94).

Furthermore we have also to consider the corrections to the kinetic term K , which arise from the point particle relativistic action (3.34b), and at 1PN read:

$$\Delta T_{1PN} = \frac{1}{8} m_1 v_1^4 + \frac{1}{8} m_2 v_2^4. \quad (4.22)$$

Finally the algebraic sum of (4.22) and (4.20) gives the full 1PN Lagrangian:

$$L_{1PN} = \Delta T_{1PN} - \Delta V_{1PN}; \quad (4.23)$$

which is also called the *Einstein–Infeld–Hoffmann* Lagrangian [12]. Such a Lagrangian actually describes the dynamics also of N bodies; yet, up to this order, also the results we derived above could have been extended to $N > 2$ compact objects simply by extending the summations to $a, b, c = 1, \dots, N$.

4.3 | General procedure to evaluate a conservative diagram

Building upon the explicit evaluation which we have just seen, we can now generalize and systematize the procedure for the evaluation of any given conservative diagram. Actually in the following we will slightly deviate from what we have done before, employing instead the multi-loop quantum field theory techniques which we have presented in section 2.2: they are actually needed in order to address the evaluation of higher order post-Newtonian corrections. In fact in the following procedure we will find that the expressions corresponding to post-Newtonian corrections can be interpreted as Feynman integral arising in a massless quantum field theory. This realization, and the application of the aforementioned techniques, has allowed for the steady progress in the computations of post-Newtonian corrections [44, 57–65].

In particular the evaluation procedure can be made algorithmic:

1. Write down the specific expression related to the diagram by multiplying together the corresponding Feynman rules and its symmetry factor. Let us point out that one has to take care of assigning a unique worldline index and a unique dummy integration variable to each worldline-gravity vertex, and to flip the sign of the momenta which are outgoing from the vertices. Additionally, for each propagator one has to add one $d^{d+1}k_i$ momenta integration over the momenta k_i running inside the propagator; also if the diagram presents propagators with insertions one should use the corresponding corrected expressions for the propagators.

2. In order to simplify the following calculations, one may single out the momenta $\{k_j\}$ running in the diagram by extracting the scalar and vector quantities which do not depend on them, i.e. by defining a time-dependent coefficient $C_{i_1, \dots, i_n}(\{\mathbf{v}_a, \dots, \mathbf{v}_l\})$ which may carry spatial indices i_1, \dots, i_n .
3. Enforce momentum conservation at each bulk vertex, if any, by integrating the corresponding $d + 1$ dimensional momenta Dirac delta.
4. Split the integration over the remaining momenta $\{k_1, \dots, k_m\}$ into an integration over the temporal components $\{k_1^0, \dots, k_m^0\}$ and one over the d -dimensional spatial ones $\{\mathbf{k}_1, \dots, \mathbf{k}_m\}$; in the exponential this decomposition will read $e^{-ikx} = e^{-ik^0 x^0} e^{+i\mathbf{k}\cdot\mathbf{x}}$, see [Notation](#).
5. Trade all of the momenta temporal components $\{k_1^0, \dots, k_m^0\}$ for time derivatives: if the diagram expression presents a temporal momenta component at the numerator k_j^0 , rewrite it as a time derivative acting on the related exponential $k_j^0 e^{-ik_j^0 t} = i \frac{d}{dt} (e^{-ik_j^0 t})$, and then integrate by parts to move the derivative on the rest of the expression. The integration by parts, which acts also on the time-dependent coefficient $C_{i_1, \dots, i_n}(\{\mathbf{v}_a, \dots, \mathbf{v}_l\})$, may yield higher derivatives of the positions; furthermore it will act also on the exponential term $e^{+i\mathbf{k}_j \cdot \mathbf{x}(t)}$ resulting in terms like $k_j^i v_i$ at the numerator of the expression.
6. Perform the integration over the momenta temporal components $\{k_1^0, \dots, k_m^0\}$, which will yield a series of Dirac deltas in the time components $\{t_1, \dots, t_l\}$ via $\int \frac{dk^0}{2\pi} e^{-ik^0(t_1 - t_2)} = \delta(t_1 - t_2)$.
7. Enforce the temporal Dirac deltas in the time variables just obtained by integrating over all but one of the time variables $\{t_1, \dots, t_l\}$. After this operation all the time-dependent quantities should depend on a single time variable which we may denote as t , and there should be only a single $\int dt$ time integration in front of the expression.
8. Perform the summation over the worldline indices $a, b, \dots = 1, 2$: in full generality, to streamline the diagram evaluation, one can fix $a = 1$ and perform the summation over all the other worldline indices, adding the symmetric ($1 \leftrightarrow 2$) term at the end of calculations.
9. Considering the argument of the exponential, for the terms in which it's not vanishing, denote the difference of the worldline positions as $\mathbf{r}(t) = \mathbf{x}_1(t) - \mathbf{x}_2(t)$, and then the linear combination of spatial momenta which are in the dot product with the \mathbf{r} vector as the Fourier momenta \mathbf{p} . In particular perform a change of variable in the integration over the spatial momenta, in order to single out this single inverse Fourier transform integral, as opposed to all the other integrals which we'll denote as loop integrals.
10. Evaluate what we denoted in the previous point as loop integrals: in fact we can recognize these integrals to be equivalent to massless loop integrals, and to evaluate them we may resort to the techniques presented in [section 2.2](#). In particular if at the numerator of the integrand the loop momenta are contracted with some other quantities, we have to write these scalar products as contraction of two vectors, and then include in the numerator of the integrand the tensorial structure which depends on the loop momenta only. Afterwards, if the integrand presents a tensorial structure, we'll have to perform the tensor decomposition procedure, as already explained in [section 2.2.2](#), recognizing that the Fourier momentum vector, if present in some scalar product of the integrand, will be the external vector to which the tensor decomposition may be proportional to. Furthermore we may find some loop integrals to be scaleless integrals, which hence will be vanishing in dimensional regularization, see [section 2.2.1](#); in particular this happens for sure when the whole loop integrand doesn't depend on any external quantity, like \mathbf{p} .
11. Evaluate the remaining Fourier integral. Analogously to the previous point, if the numerator

of the integrand presents some scalar products between the Fourier momenta and any external vector, then we should break apart such contractions and include only the Fourier momenta vector in the integrand. Then, if the integrand presents a tensorial structure at the numerator, we'll need to perform once again the tensor decomposition, recognizing that the \mathbf{r} vector is the external vector to which the tensor decomposition may be proportional to, as it appears in the integrand, inside the argument of the exponential. Finally, in full generality, we can use formula (C.39), which we derived in section C.3, to evaluate the resulting integral.

12. Add the $(1 \leftrightarrow 2)$ symmetric term, noticing that $\mathbf{r} \xrightarrow{(1 \leftrightarrow 2)} -\mathbf{r}$, to obtain the final, exact expression of the diagram.

Finally, in order to obtain the contribution of the diagram to the conservative potential at a given n PN order, one has to expand in Taylor series the expression just obtained above, both around the dimension of space $d = 3$ (at higher orders this may also lead to poles of the kind $\frac{1}{d-3}$), and then in the PN expansion parameter. To perform the latter expansion one can use the scaling rules outlined in table 3.1, multiplying any quantity in the expression of the diagram by its corresponding scaling: doing so one should find that the common scaling $G^0 L^1$ factorizes in front of the expression, while the dependence on the velocity parameter v is instead non-polynomial in general; then one has to Taylor expand this function in the parameter v , up to order v^{2n} included, in order to obtain the contribution at n PN order.

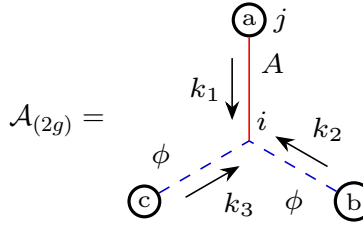
Let us also point out that it is advisable to first evaluate all the loop integrals in the whole diagram expression, then to collect common terms that may arise in order to simplify the expression, and only then to evaluate the so resulting Fourier integrals: in this way the number of terms to evaluate will be lower, and furthermore some terms may simplify altogether already after the loop integral evaluation.

4.3.1 — Example of the evaluation procedure

We will now apply the general procedure presented above to the specific case of diagram (2g), as denoted in figure 4.6. The leading order scaling of this diagram is $G^2 v^2$, so it first contributes at order 2PN.

■ Expression associated to the diagram

The Feynman rules associated to this diagram have been derived in appendix A; in particular the Feynman rule for the $\phi^2 A$ bulk vertex is given by formula (A.70), the Feynman rules for the worldline- A and worldline- ϕ vertices are given respectively by formulae (A.49b) and (A.49a), whereas the Feynman rules associated to the propagators are given by equations (A.31a) and (A.31b), both with $n = 0$ insertions. Finally we can read the symmetry factor from table 4.1.



$$\begin{aligned}
\mathcal{A}_{(2g)} = &= \frac{2}{2!2!} \int_{k_1, k_2, k_3} \left(-i (2\pi)^{d+1} \delta^{(d+1)}(k_1 + k_2 + k_3) \frac{2c_d}{\Lambda} (k_2^0 k_3^i + k_3^0 k_2^i) \right) \\
&\times \left(-i \sum_{a=1}^2 \frac{m_a}{\Lambda} \int dt_1 e^{ik_1 x_a(t_1)} \left(-\frac{1}{\sqrt{1-v_a^2}} \right) v_a^j \right) \left(\frac{\delta_{ij}}{2} \frac{i}{|\mathbf{k}_1|^2} \right) \\
&\times \left(-i \sum_{b=1}^2 \frac{m_b}{\Lambda} \int dt_2 e^{ik_2 x_b(t_2)} \left(\frac{2 + (-2 + c_d) v_b^2}{2\sqrt{1-v_b^2}} \right) \right) \left(-\frac{1}{2c_d} \frac{i}{|\mathbf{k}_2|^2} \right) \\
&\times \left(-i \sum_{c=1}^2 \frac{m_c}{\Lambda} \int dt_3 e^{ik_3 x_c(t_3)} \left(\frac{2 + (-2 + c_d) v_c^2}{2\sqrt{1-v_c^2}} \right) \right) \left(-\frac{1}{2c_d} \frac{i}{|\mathbf{k}_3|^2} \right). \tag{4.24}
\end{aligned}$$

Once we enforce the bulk momentum conservation by integrating over the k_1 momenta, such an expression simplifies to:

$$\begin{aligned}
\mathcal{A}_{(2g)} = &= -\frac{i}{8c_d} \sum_{a,b,c=1}^2 \frac{m_a m_b m_c}{\Lambda^4} \int dt_1 dt_2 dt_3 \left(-\frac{v_{a,i}}{\sqrt{1-v_a^2}} \right) \left(\frac{2 + (-2 + c_d) v_b^2}{2\sqrt{1-v_b^2}} \right) \left(\frac{2 + (-2 + c_d) v_c^2}{2\sqrt{1-v_c^2}} \right) \\
&\times \int_{k_2, k_3} (k_2^0 k_3^i + k_3^0 k_2^i) \left(e^{-ik_2(x_a(t_1) - x_b(t_2)) - ik_3(x_a(t_1) - x_c(t_3))} \right) \left(\frac{1}{|\mathbf{k}_2 + \mathbf{k}_3|^2} \frac{1}{|\mathbf{k}_2|^2} \frac{1}{|\mathbf{k}_3|^2} \right). \tag{4.25}
\end{aligned}$$

■ Evaluation of the integrals of the temporal components of the momenta

As already explained, to evaluate the integrals of the temporal components k_2^0 and k_3^0 of the momenta we may rewrite any factors of them at the numerator of the expression as a time derivative acting on the exponential, and then integrate by parts. After this all of the integrals will act only on the exponential, hence yielding Dirac deltas in time variables. These steps in general can be performed using a formula similar to equation (4.14): assuming the $g(t, \dots)$ function to be well behaved and to vanish on the boundary of the integration domain D , it holds

$$\begin{aligned}
&\int_D \frac{dk^0}{2\pi} dt k^0 e^{-ik^0(t'-t)} g(t, \dots) = \int_D \frac{dk^0}{2\pi} dt \frac{1}{i} \frac{\partial}{\partial t} \left(e^{-ik^0(t'-t)} \right) g(t, \dots) \\
&= -i \int_D \frac{dk^0}{2\pi} dt \left[\frac{\partial}{\partial t} \left(e^{-ik^0(t'-t)} g(t, \dots) \right) - e^{-ik^0(t'-t)} \frac{\partial g(t, \dots)}{\partial t} \right] \\
&= -i \left(\underbrace{\int_D \frac{dk^0}{2\pi} \left[e^{-ik^0(t'-t)} g(t, \dots) \right]}_{=0} \Big|_{\partial D} - \int_D \frac{dk^0}{2\pi} dt \left[e^{-ik^0(t'-t)} \frac{\partial g(t, \dots)}{\partial t} \right] \right) \\
&= i \int_D \frac{dk^0}{2\pi} dt e^{-ik^0(t'-t)} \frac{\partial g(t, \dots)}{\partial t} = i \int dt \delta(t' - t) \frac{\partial g(t, \dots)}{\partial t}. \tag{4.26}
\end{aligned}$$

Then we can summarize these results as:

$$\int \frac{dk^0}{(2\pi)} e^{-ik^0(t-t')} g(t, \dots) = \delta(t-t') g(t, \dots), \tag{4.27a}$$

$$\int \frac{dk^0}{2\pi} dt k^0 e^{-ik^0(t'-t)} g(t, \dots) = i \int dt \delta(t' - t) \frac{\partial g(t, \dots)}{\partial t} . \quad (4.27b)$$

which we may apply to our expression (4.25) to obtain:

$$\begin{aligned} \mathcal{A}_{(2g)} &= \frac{1}{8c_d} \sum_{a,b,c=1}^2 \frac{m_a m_b m_c}{\Lambda^4} \int dt_1 dt_2 dt_3 \left(-\frac{v_{a,i}}{\sqrt{1-v_a^2}} \right) \delta(t_1 - t_2) \delta(t_1 - t_3) \\ &\quad \times \int \frac{d^d \mathbf{k}_2}{(2\pi)^d} \frac{d^d \mathbf{k}_3}{(2\pi)^d} \left(\frac{1}{|\mathbf{k}_2 + \mathbf{k}_3|^2} \frac{1}{|\mathbf{k}_2|^2} \frac{1}{|\mathbf{k}_3|^2} \right) \\ &\quad \times \left[k_3^i \left(\frac{2 + (-2 + c_d) v_c^2}{2\sqrt{1-v_c^2}} \right) e^{i\mathbf{k}_3 \cdot (\mathbf{x}_a(t_1) - \mathbf{x}_c(t_3))} \frac{\partial}{\partial t_2} \left(\frac{2 + (-2 + c_d) v_b^2(t_2)}{2\sqrt{1-v_b^2(t_2)}} e^{i\mathbf{k}_2 \cdot (\mathbf{x}_a(t_1) - \mathbf{x}_b(t_2))} \right) \right. \\ &\quad \left. + k_2^i \left(\frac{2 + (-2 + c_d) v_b^2}{2\sqrt{1-v_b^2}} \right) e^{i\mathbf{k}_2 \cdot (\mathbf{x}_a(t_1) - \mathbf{x}_b(t_2))} \frac{\partial}{\partial t_3} \left(\frac{2 + (-2 + c_d) v_c^2(t_3)}{2\sqrt{1-v_c^2(t_3)}} e^{i\mathbf{k}_3 \cdot (\mathbf{x}_a(t_1) - \mathbf{x}_c(t_3))} \right) \right] \\ &= \frac{1}{8c_d} \sum_{a,b,c=1}^2 \frac{m_a m_b m_c}{\Lambda^4} \int dt_1 dt_2 dt_3 \left(-\frac{v_{a,i}}{\sqrt{1-v_a^2}} \right) \delta(t_1 - t_2) \delta(t_1 - t_3) \\ &\quad \times \int \frac{d^d \mathbf{k}_2}{(2\pi)^d} \frac{d^d \mathbf{k}_3}{(2\pi)^d} \left(\frac{1}{|\mathbf{k}_2 + \mathbf{k}_3|^2} \frac{1}{|\mathbf{k}_2|^2} \frac{1}{|\mathbf{k}_3|^2} \right) e^{i\mathbf{k}_2 \cdot (\mathbf{x}_a(t_1) - \mathbf{x}_b(t_2)) + i\mathbf{k}_3 \cdot (\mathbf{x}_a(t_1) - \mathbf{x}_c(t_3))} \\ &\quad \times \left[k_3^i \left(\frac{2 + (-2 + c_d) v_c^2}{2\sqrt{1-v_c^2}} \right) \left(\frac{2 + (-2 + c_d) v_b^2}{2\sqrt{1-v_b^2}} (-i\mathbf{k}_2 \cdot \mathbf{v}_b) + \frac{\mathbf{v}_b \cdot \mathbf{a}_b}{2(1-v_b^2)^{\frac{3}{2}}} (2c_d - 2 + v_b^2(2 - c_d)) \right) \right. \\ &\quad \left. + k_2^i \left(\frac{2 + (-2 + c_d) v_b^2}{2\sqrt{1-v_b^2}} \right) \left(\frac{2 + (-2 + c_d) v_c^2}{2\sqrt{1-v_c^2}} (-i\mathbf{k}_3 \cdot \mathbf{v}_c) + \frac{\mathbf{v}_c \cdot \mathbf{a}_c}{2(1-v_c^2)^{\frac{3}{2}}} (2c_d - 2 + v_c^2(2 - c_d)) \right) \right] \end{aligned} \quad (4.28)$$

We can now perform explicitly the integration over the time integrals $\int dt_2 dt_3$, and rename $t_1 \rightarrow t$, to obtain:

$$\begin{aligned} \mathcal{A}_{(2g)} &= \frac{1}{8c_d} \sum_{a,b,c=1}^2 \frac{m_a m_b m_c}{\Lambda^4} \int dt \left(-\frac{v_{a,i}}{\sqrt{1-v_a^2}} \right) \\ &\quad \times \int \frac{d^d \mathbf{k}_2}{(2\pi)^d} \frac{d^d \mathbf{k}_3}{(2\pi)^d} \left(\frac{1}{|\mathbf{k}_2 + \mathbf{k}_3|^2} \frac{1}{|\mathbf{k}_2|^2} \frac{1}{|\mathbf{k}_3|^2} \right) e^{i\mathbf{k}_2 \cdot (\mathbf{x}_a(t) - \mathbf{x}_b(t)) + i\mathbf{k}_3 \cdot (\mathbf{x}_a(t) - \mathbf{x}_c(t))} \\ &\quad \times \left[k_3^i \left(\frac{2 + (-2 + c_d) v_c^2}{2\sqrt{1-v_c^2}} \right) \left(\frac{2 + (-2 + c_d) v_b^2}{2\sqrt{1-v_b^2}} (-i\mathbf{k}_2 \cdot \mathbf{v}_b) + \frac{\mathbf{v}_b \cdot \mathbf{a}_b}{2(1-v_b^2)^{\frac{3}{2}}} (2c_d - 2 + v_b^2(2 - c_d)) \right) \right. \\ &\quad \left. + k_2^i \left(\frac{2 + (-2 + c_d) v_b^2}{2\sqrt{1-v_b^2}} \right) \left(\frac{2 + (-2 + c_d) v_c^2}{2\sqrt{1-v_c^2}} (-i\mathbf{k}_3 \cdot \mathbf{v}_c) + \frac{\mathbf{v}_c \cdot \mathbf{a}_c}{2(1-v_c^2)^{\frac{3}{2}}} (2c_d - 2 + v_c^2(2 - c_d)) \right) \right] \\ &= \frac{1}{8c_d} \sum_{a,b,c=1}^2 \frac{m_a m_b m_c}{\Lambda^4} \int dt \left(-\frac{v_{a,i}}{\sqrt{1-v_a^2}} \right) \int \frac{d^d \mathbf{k}_2}{(2\pi)^d} \frac{d^d \mathbf{k}_3}{(2\pi)^d} e^{i\mathbf{k}_2 \cdot (\mathbf{x}_a(t) - \mathbf{x}_b(t)) + i\mathbf{k}_3 \cdot (\mathbf{x}_a(t) - \mathbf{x}_c(t))} \\ &\quad \times \left(\frac{1}{|\mathbf{k}_2 + \mathbf{k}_3|^2} \frac{1}{|\mathbf{k}_2|^2} \frac{1}{|\mathbf{k}_3|^2} \right) \left(C_{1,j}^{(b,c)}(t) k_3^i k_2^j + C_2^{(b,c)}(t) k_3^i + C_{1,j}^{(c,b)}(t) k_2^i k_3^j + C_2^{(c,b)}(t) k_2^i \right) , \end{aligned} \quad (4.29)$$

where we defined the coefficients

$$C_{1,j}^{(\alpha,\beta)}(t) = -i \left(\frac{2 + (-2 + c_d) v_\beta^2}{2\sqrt{1 - v_\beta^2}} \right) \left(\frac{2 + (-2 + c_d) v_\alpha^2}{2\sqrt{1 - v_\alpha^2}} v_{\alpha,j} \right) ; \quad (4.30a)$$

$$C_2^{(\alpha,\beta)}(t) = \left(\frac{2 + (-2 + c_d) v_\beta^2}{2\sqrt{1 - v_\beta^2}} \right) \left(\frac{\mathbf{v}_\alpha \cdot \mathbf{a}_\alpha}{2(1 - v_\alpha^2)^{\frac{3}{2}}} (2c_d - 2 + v_\alpha^2(2 - c_d)) \right) ; \quad (4.30b)$$

in which all the quantities are now evaluated at the time t . In particular we also introduced the acceleration of body a as:

$$\mathbf{a}_a(t) \equiv \frac{d\mathbf{v}_a(t)}{dt} , \quad (4.31)$$

and its scaling in the PN parameters is $|\mathbf{a}| \propto k^0 v \propto v^{\frac{7}{2}} G^{-\frac{1}{2}} L^{-\frac{1}{2}}$.

■ Summation over the worldline indices

We can now perform the summation over the worldline indices $a, b, c = 1, 2$. In particular, as already pointed out, in full generality we'll fix $a = 1$, and perform the summation over b and c only, taking care of adding the $(1 \leftrightarrow 2)$ terms at the end of the calculations. Therefore, understanding the time dependence of the worldline positions \mathbf{x} and of the C_1 and C_2 coefficients, we obtain:

$$\begin{aligned} \mathcal{A}_{(2g)} = & \frac{1}{8c_d \Lambda^4} \int dt \left(-\frac{v_{1,i}}{\sqrt{1 - v_1^2}} \right) \int \frac{d^d \mathbf{k}_2}{(2\pi)^d} \frac{d^d \mathbf{k}_3}{(2\pi)^d} \left(\frac{1}{|\mathbf{k}_2 + \mathbf{k}_3|^2} \frac{1}{|\mathbf{k}_2|^2} \frac{1}{|\mathbf{k}_3|^2} \right) \\ & \times \left[m_1 m_1 \left(C_{1,j}^{(1,1)} k_3^i k_2^j + C_2^{(1,1)} k_3^i + C_{1,j}^{(1,1)} k_2^i k_3^j + C_2^{(1,1)} k_2^i \right) \right. \\ & + m_1 m_2 e^{i\mathbf{k}_3 \cdot (\mathbf{x}_1 - \mathbf{x}_2)} \left(C_{1,j}^{(1,2)} k_3^i k_2^j + C_2^{(1,2)} k_3^i + C_{1,j}^{(2,1)} k_2^i k_3^j + C_2^{(2,1)} k_2^i \right) \\ & + m_2 m_1 e^{i\mathbf{k}_2 \cdot (\mathbf{x}_1 - \mathbf{x}_2)} \left(C_{1,j}^{(2,1)} k_3^i k_2^j + C_2^{(2,1)} k_3^i + C_{1,j}^{(1,2)} k_2^i k_3^j + C_2^{(1,2)} k_2^i \right) \\ & \left. + m_2 m_2 e^{i(\mathbf{k}_2 + \mathbf{k}_3) \cdot (\mathbf{x}_1 - \mathbf{x}_2)} \left(C_{1,j}^{(2,2)} k_3^i k_2^j + C_2^{(2,2)} k_3^i + C_{1,j}^{(2,2)} k_2^i k_3^j + C_2^{(2,2)} k_2^i \right) \right] \\ & + (1 \leftrightarrow 2) . \end{aligned} \quad (4.32)$$

■ Recognizing loop and Fourier integrals

We can notice that the summation over the worldline indices, which we just performed above in equation (4.32), produces a series of terms with different exponential: for example the argument of the exponential of the first term is vanishing, as it comes from $e^{i\mathbf{k}_2 \cdot (\mathbf{x}_a - \mathbf{x}_b) + i\mathbf{k}_3 \cdot (\mathbf{x}_a - \mathbf{x}_c)} \xrightarrow{a=1, b=1, c=1} e^0$, while the other terms have different combination of momenta \mathbf{k}_2 or \mathbf{k}_3 which multiplies the difference of the worldline positions $(\mathbf{x}_1 - \mathbf{x}_2)$.

It is then useful to denote such a difference between the positions of the worldlines with the spatial vector \mathbf{r} , as:

$$\mathbf{r}(t) \equiv \mathbf{x}_1(t) - \mathbf{x}_2(t) ; \quad (4.33)$$

and to recognize the spatial momenta \mathbf{k} which multiplies the vector \mathbf{r} in the argument of the exponential, or the linear combination of spatial momenta, as the Fourier momenta \mathbf{p} . In practice this amounts to performing a change of variables, but as long as we trade just one \mathbf{k} integration momenta which appears in the exponential for the \mathbf{p} vector, the Jacobian of the transformation will be equal to one.

Performing explicitly the aforementioned steps to formula (4.32) we obtain:

$$\begin{aligned}
\mathcal{A}_{(2g)} = & \frac{1}{8c_d} \frac{m_1}{\Lambda^4} \int dt \left(-\frac{v_{1,i}}{\sqrt{1-v_1^2}} \right) \\
& \times \left[m_1 m_1 \int \frac{d^d \mathbf{k}_2}{(2\pi)^d} \frac{d^d \mathbf{k}_3}{(2\pi)^d} \left(\frac{\left(C_{1,j}^{(1,1)} (k_3^i k_2^j + k_2^i k_3^j) + C_2^{(1,1)} (k_2^i + k_3^i) \right)}{|\mathbf{k}_2 + \mathbf{k}_3|^2 |\mathbf{k}_2|^2 |\mathbf{k}_3|^2} \right) \right. \\
& + m_1 m_2 \int \frac{d^d \mathbf{k}_2}{(2\pi)^d} \frac{d^d \mathbf{p}}{(2\pi)^d} e^{i\mathbf{p}\cdot\mathbf{r}} \frac{\left(C_{1,j}^{(1,2)} p^i k_2^j + C_2^{(1,2)} p^i + C_{1,j}^{(2,1)} k_2^i p^j + C_2^{(2,1)} k_2^i \right)}{|\mathbf{k}_2 + \mathbf{p}|^2 |\mathbf{k}_2|^2 |\mathbf{p}|^2} \\
& + m_2 m_1 \int \frac{d^d \mathbf{p}}{(2\pi)^d} \frac{d^d \mathbf{k}_3}{(2\pi)^d} e^{i\mathbf{p}\cdot\mathbf{r}} \frac{\left(C_{1,j}^{(2,1)} k_3^i p^j + C_2^{(2,1)} k_3^i + C_{1,j}^{(1,2)} p^i k_3^j + C_2^{(1,2)} p^i \right)}{|\mathbf{p} + \mathbf{k}_3|^2 |\mathbf{p}|^2 |\mathbf{k}_3|^2} \\
& \left. + m_2 m_2 \int \frac{d^d \mathbf{k}_2}{(2\pi)^d} \frac{d^d \mathbf{p}}{(2\pi)^d} e^{i\mathbf{p}\cdot\mathbf{r}} \frac{1}{|\mathbf{p}|^2 |\mathbf{k}_2|^2 |\mathbf{p} - \mathbf{k}_2|^2} \left(C_{1,j}^{(2,2)} (p^i - k_2^i) k_2^j \right. \right. \\
& \left. \left. + C_2^{(2,2)} (p^i - k_2^i) + C_{1,j}^{(2,2)} k_2^i (p^j - k_2^j) + C_2^{(2,2)} k_2^i \right) \right] + (1 \leftrightarrow 2). \tag{4.34}
\end{aligned}$$

4.3.2 — Evaluation of the integrals in the spatial components of the momenta

To continue we have to evaluate the integrals in the spatial components of the momenta. Let us recall from section 4.3 that at this point it would be better to first evaluate all the loop integrals in expression (4.34), then to collect common terms, and only after to independently evaluate all the Fourier integrals; this is actually the procedure we implemented in the `Mathematica` code which will be presented in the next section 4.4. However, in order to not clutter this pages too much, we find it useful to single out the several integrals in the spatial momenta which appear in expression (4.34): let us then define

$$I_1^{ij}(\mathbf{r}) \equiv \int \frac{d^d \mathbf{p}}{(2\pi)^d} \frac{d^d \mathbf{k}}{(2\pi)^d} e^{i\mathbf{p}\cdot\mathbf{r}} \frac{k^i k^j}{|\mathbf{k}|^2 |\mathbf{p}|^2 |\mathbf{k} - \mathbf{p}|^2}; \tag{4.35a}$$

$$I_2^{ij}(\mathbf{r}) \equiv \int \frac{d^d \mathbf{p}}{(2\pi)^d} \frac{d^d \mathbf{k}}{(2\pi)^d} e^{i\mathbf{p}\cdot\mathbf{r}} \frac{k^i p^j}{|\mathbf{k}|^2 |\mathbf{p}|^2 |\mathbf{k} - \mathbf{p}|^2}; \tag{4.35b}$$

$$I_3^i(\mathbf{r}) \equiv \int \frac{d^d \mathbf{p}}{(2\pi)^d} \frac{d^d \mathbf{k}}{(2\pi)^d} e^{i\mathbf{p}\cdot\mathbf{r}} \frac{k^i}{|\mathbf{k}|^2 |\mathbf{p}|^2 |\mathbf{k} - \mathbf{p}|^2}; \tag{4.35c}$$

$$I_4^i(\mathbf{r}) \equiv \int \frac{d^d \mathbf{p}}{(2\pi)^d} \frac{d^d \mathbf{k}}{(2\pi)^d} e^{i\mathbf{p}\cdot\mathbf{r}} \frac{p^i}{|\mathbf{k}|^2 |\mathbf{p}|^2 |\mathbf{k} - \mathbf{p}|^2}; \tag{4.35d}$$

$$I_5^{ij} \equiv \int \frac{d^d \mathbf{k}_1}{(2\pi)^d} \frac{d^d \mathbf{k}_2}{(2\pi)^d} \frac{k_1^i k_2^j}{|\mathbf{k}_1|^2 |\mathbf{k}_2|^2 |\mathbf{k}_1 + \mathbf{k}_2|^2}; \tag{4.35e}$$

$$I_6^i \equiv \int \frac{d^d \mathbf{k}_1}{(2\pi)^d} \frac{d^d \mathbf{k}_2}{(2\pi)^d} \frac{k_1^i}{|\mathbf{k}_1|^2 |\mathbf{k}_2|^2 |\mathbf{k}_1 + \mathbf{k}_2|^2}. \tag{4.35f}$$

With these definitions, up to some spatial momenta redefinition and $\mathbf{k} \rightarrow -\mathbf{k}$ change of variable,

which are transformations with unit Jacobian, equation (4.34) can be cast into:

$$\begin{aligned}
\mathcal{A}_{(2g)} &= \frac{1}{8c_d} \frac{m_1}{\Lambda^4} \int dt \left(-\frac{v_{1,i}}{\sqrt{1-v_1^2}} \right) \left[m_1 m_1 \left(C_{1,j}^{(1,1)} (I_5^{ji} + I_5^{ij}) + C_2^{(1,1)} (2I_6^i) \right) \right. \\
&\quad + m_1 m_2 \left(C_{1,j}^{(1,2)} (-I_2^{ji}(\mathbf{r})) + C_2^{(1,2)} I_4^i(\mathbf{r}) + C_{1,j}^{(2,1)} (-I_2^{ij}(\mathbf{r})) + C_2^{(2,1)} (-I_3^i(\mathbf{r})) \right) \\
&\quad + m_2 m_1 \left(C_{1,j}^{(2,1)} (-I_2^{ij}(\mathbf{r})) + C_2^{(2,1)} (-I_3^i(\mathbf{r})) + C_{1,j}^{(1,2)} (-I_2^{ji}(\mathbf{r})) + C_2^{(1,2)} (I_4^i(\mathbf{r})) \right) \\
&\quad \left. + m_2 m_2 \left(C_{1,j}^{(2,2)} (I_2^{ji}(\mathbf{r}) + I_2^{ij}(\mathbf{r})) + C_2^{(2,2)} I_4^i(\mathbf{r}) - 2 C_{1,j}^{(2,2)} I_1^{ij}(\mathbf{r}) \right) \right] + (1 \leftrightarrow 2) \quad (4.36) \\
&= \frac{1}{8c_d} \frac{m_1}{\Lambda^4} \int dt \left(-\frac{v_{1,i}}{\sqrt{1-v_1^2}} \right) \left[m_1 m_1 \left(C_{1,j}^{(1,1)} (I_5^{ji} + I_5^{ij}) + C_2^{(1,1)} (2I_6^i) \right) \right. \\
&\quad + 2 m_1 m_2 \left(C_{1,j}^{(1,2)} (-I_2^{ji}(\mathbf{r})) + C_2^{(1,2)} I_4^i(\mathbf{r}) + C_{1,j}^{(2,1)} (-I_2^{ij}(\mathbf{r})) + C_2^{(2,1)} (-I_3^i(\mathbf{r})) \right) \\
&\quad \left. + m_2 m_2 \left(C_{1,j}^{(2,2)} (I_2^{ji}(\mathbf{r}) + I_2^{ij}(\mathbf{r}) - 2 I_1^{ij}(\mathbf{r})) + C_2^{(2,2)} I_4^i(\mathbf{r}) \right) \right] + (1 \leftrightarrow 2).
\end{aligned}$$

We'll now show explicitly the full evaluation of the integral $I_1^{ij}(\mathbf{r})$, given by formula (4.35a); the evaluation of the other integrals, defined in formulae (4.35), proceeds in a similar way, hence we'll directly present the related results at the end of the section.

In order to evaluate the integral $I_1^{ij}(\mathbf{r})$, we'll first have to evaluate the innermost loop integral, in the \mathbf{k} spatial momenta, and only at the end the Fourier integral in \mathbf{p} . Hence we'll recast formula (4.35a) as:

$$I_1^{ij}(\mathbf{r}) \equiv \int \frac{d^d \mathbf{p}}{(2\pi)^d} e^{i\mathbf{p}\cdot\mathbf{r}} \frac{1}{|\mathbf{p}|^2} \underbrace{\int \frac{d^d \mathbf{k}}{(2\pi)^d} \frac{k^i k^j}{|\mathbf{k}|^2 |\mathbf{k} - \mathbf{p}|^2}}_{\equiv I^{ij}(\mathbf{p})}. \quad (4.37)$$

We'll now proceed with the evaluation, starting from the integral $I^{ij}(\mathbf{p})$, and to do so we'll resort to the multi-loop techniques which have been presented in section 2.2.

■ Tensor decomposition

Because the integral $I^{ij}(\mathbf{r})$ carries tensorial quantities at the numerator, the first step in its evaluation involves the tensor decomposition of the integral, a procedure which has already been explained in section 2.2.2. To recall it briefly, such a procedure has the goal of disentangling the tensorial structure from the integral calculation, in order to simplify the evaluation of the latter: the integral in the end will yield scalar form factors, which will be multiplied by tensorial quantities.

In this particular case, as the integrand depend on the external vector \mathbf{p} , the tensor decomposition yields:

$$I^{ij}(\mathbf{p}) = F_1(\mathbf{p}) \delta^{ij} + F_2(\mathbf{p}) p^i p^j \quad (4.38)$$

with form factors

$$F_1(\mathbf{p}) = \frac{1}{(d-1)} \frac{1}{|\mathbf{p}|^2} \int \frac{d^d \mathbf{k}}{(2\pi)^d} \frac{(|\mathbf{k}|^2 |\mathbf{p}|^2 - (\mathbf{k} \cdot \mathbf{p})^2)}{|\mathbf{k}|^2 |\mathbf{k} - \mathbf{p}|^2}, \quad (4.39a)$$

$$F_2(\mathbf{p}) = \frac{1}{(d-1)} \frac{1}{|\mathbf{p}|^4} \int \frac{d^d \mathbf{k}}{(2\pi)^d} \frac{(d(\mathbf{k} \cdot \mathbf{p})^2 - |\mathbf{k}|^2 |\mathbf{p}|^2)}{|\mathbf{k}|^2 |\mathbf{k} - \mathbf{p}|^2}. \quad (4.39b)$$

■ Integrand manipulation

The next step in the evaluation procedure of the loop integral $I^{ij}(\mathbf{p})$ requires the expression of the integrands which are present in the previous form factors (4.39) as a function of the denominators only: this step has been presented in section 2.2.3, and can be accomplished by employing relations between the scalar products of the several vector quantities.

In both form factors the denominator of the integrated in this particular case is the product of D_1 and D_2 , both to the power of 1, where we defined

$$D_1 \equiv |\mathbf{k}|^2, \quad (4.40a)$$

$$D_2 \equiv |\mathbf{k} - \mathbf{p}|^2; \quad (4.40b)$$

with this convention we can then rewrite the only other \mathbf{k} -dependent quantity which appears in the numerator, which is $(\mathbf{k} \cdot \mathbf{p})$, as a function of D_1 and D_2 ; in fact $|\mathbf{k} - \mathbf{p}|^2 = |\mathbf{k}|^2 - 2(\mathbf{k} \cdot \mathbf{p}) + |\mathbf{p}|^2$, hence:

$$(\mathbf{k} \cdot \mathbf{p}) = \frac{1}{2} (D_1 - D_2 + |\mathbf{p}|^2). \quad (4.41)$$

In this way we may rewrite also the numerator of the integrand as a sum over a series of terms involving only powers of D_1 and D_2 , and possibly constants in \mathbf{k} like the term $|\mathbf{p}|^2$; doing so we may rewrite formulae (4.39a) and (4.39b) as:

$$\begin{aligned} F_1(\mathbf{p}) &= \frac{1}{(d-1)} \frac{1}{|\mathbf{p}|^2} \int \frac{d^d \mathbf{k}}{(2\pi)^d} \left[\frac{1}{4} \frac{4D_1 |\mathbf{p}|^2 - (D_1 - D_2 + |\mathbf{p}|^2)^2}{D_1 D_2} \right] \\ &= \frac{1}{4(d-1)} \frac{1}{|\mathbf{p}|^2} \int \frac{d^d \mathbf{k}}{(2\pi)^d} \left[4 \frac{|\mathbf{p}|^2}{D_2} - \frac{D_1}{D_2} - \frac{D_2}{D_1} - \frac{|\mathbf{p}|^4}{D_1 D_2} + 2 - 2 \frac{|\mathbf{p}|^2}{D_2} + 2 \frac{|\mathbf{p}|^2}{D_1} \right], \end{aligned} \quad (4.42a)$$

$$\begin{aligned} F_2(\mathbf{p}) &= \frac{1}{(d-1)} \frac{1}{|\mathbf{p}|^4} \int \frac{d^d \mathbf{k}}{(2\pi)^d} \left[\frac{1}{4} \frac{d(D_1 - D_2 + |\mathbf{p}|^2)^2 - 4D_1 |\mathbf{p}|^2}{D_1 D_2} \right] \\ &= \frac{d}{4(d-1)} \frac{1}{|\mathbf{p}|^4} \int \frac{d^d \mathbf{k}}{(2\pi)^d} \left[\frac{D_1}{D_2} + \frac{D_2}{D_1} + \frac{|\mathbf{p}|^4}{D_1 D_2} - 2 + 2 \frac{|\mathbf{p}|^2}{D_2} - 2 \frac{|\mathbf{p}|^2}{D_1} - \frac{4}{d} \frac{|\mathbf{p}|^2}{D_2} \right]. \end{aligned} \quad (4.42b)$$

■ Scalar integral evaluation

The last step in the solution of the loop integral $I^{ij}(\mathbf{p})$ is the explicit evaluation of the integrals which appear in the form factors cast in the form (4.42), which are denoted as *scalar integrals*. In full generality this procedure is usually accomplished by first reducing the scalar integrals to a smaller set of *master integrals*, as explained in section 2.2.4, and then by explicitly evaluating only these master integrals, for example as explained in section 2.2.5: we perform explicitly these computation in appendix C.5.

Nonetheless, for the case at hand, the solution of the integrals which appear in formulae (4.42) can be obtained in full generality for arbitrary values of the exponents of the denominators, as it's been explicitly derived in appendix C. Therefore we may directly evaluate formulae (4.42a) and (4.42b) by recognizing that in this particular case it holds

$$\int \frac{d^d \mathbf{k}}{(2\pi)^d} \frac{1}{D_1^a D_2^b(\mathbf{p})} = I_{S,1L}(d, a, b)[\mathbf{p}], \quad (4.43)$$

where $I_{S,1L}$ is the scalar integral (C.7) which has been explicitly evaluated in section C.2.1. Performing the computations, one finds that in formulae (4.42) only the scalar integral $I_{S,1L}(d, 1, 1)[\mathbf{p}]$

is non vanishing and instead yields $I_{S,1L}(d, 1, 1)[\mathbf{p}] = 2^{-d}\pi^{-\frac{d}{2}} \frac{\Gamma(2-\frac{d}{2})(\Gamma(\frac{d}{2}-1))^2}{\Gamma(d-2)} |\mathbf{p}|^{d-4}$; hence the form factors read:

$$F_1(\mathbf{p}) = -\frac{2^{-d-2}\pi^{-\frac{d}{2}} \Gamma(2-\frac{d}{2}) (\Gamma(\frac{d}{2}-1))^2}{(d-1) \Gamma(d-2)} |\mathbf{p}|^{d-2} = \frac{2^{-2d} \pi^{\frac{(3-d)}{2}}}{\sin(d\frac{\pi}{2}) \Gamma(\frac{d+1}{2})} |\mathbf{p}|^{d-2}, \quad (4.44a)$$

$$F_2(\mathbf{p}) = 2^{-d-2}\pi^{-\frac{d}{2}} \frac{d}{(d-1)} \frac{\Gamma(2-\frac{d}{2}) (\Gamma(\frac{d}{2}-1))^2}{\Gamma(d-2)} |\mathbf{p}|^{d-4} = -d \frac{2^{-2d} \pi^{\frac{(3-d)}{2}}}{\sin(d\frac{\pi}{2}) \Gamma(\frac{d+1}{2})} |\mathbf{p}|^{d-4}; \quad (4.44b)$$

where we used the properties of the Γ function presented in appendix B.1. Therefore, recalling the decomposition (4.38) for the loop integral $I^{ij}(\mathbf{p})$, the full initial integral $I_1^{ij}(\mathbf{r})$, given by expression (4.37), now reads

$$I_1^{ij}(\mathbf{r}) = \int \frac{d^d \mathbf{p}}{(2\pi)^d} e^{i\mathbf{p}\cdot\mathbf{r}} \frac{1}{|\mathbf{p}|^2} \left(\left(\frac{2^{-2d} \pi^{\frac{(3-d)}{2}}}{\sin(d\frac{\pi}{2}) \Gamma(\frac{d+1}{2})} \right) \left(|\mathbf{p}|^{d-2} \delta^{ij} - d |\mathbf{p}|^{d-4} p^i p^j \right) \right). \quad (4.45)$$

■ Fourier integral evaluation

The last step now requires us to perform the inverse Fourier transform integral which are left in equation (4.45). In general, as pointed out in appendix C.5.3, we would proceed in a similar way to what's has just been done, so by first performing a further tensor decomposition on the integrand in order to obtain scalar integrals only, with \mathbf{r} the external vector quantity which may enter in the tensor decomposition, and then evaluate the scalar Fourier transformations: this procedure is what has been implemented in the `Mathematica` code.

Nonetheless for simplicity in this section we'll directly use the results for the Fourier transform which have been obtained in appendix C.3, and in particular formulae (C.31) and its tensorial generalization (C.33). Doing so equation (4.45) reads:

$$\begin{aligned} I_1^{ij}(\mathbf{r}) &= \left(\frac{2^{-2d} \pi^{\frac{(3-d)}{2}}}{\sin(d\frac{\pi}{2}) \Gamma(\frac{d+1}{2})} \right) \left(\left(2^{d-4} \pi^{-\frac{d}{2}} \frac{\Gamma(d-2)}{\Gamma(2-\frac{d}{2})} |\mathbf{r}|^{4-2d} \delta^{ij} \right) \right. \\ &\quad \left. - d \left(2^{d-5} \pi^{-\frac{d}{2}} \frac{\Gamma(d-2)}{\Gamma(3-\frac{d}{2})} |\mathbf{r}|^{4-2d} \left(\delta^{ij} + (4-2d) \frac{r^i r^j}{|\mathbf{r}|^2} \right) \right) \right) \quad (4.46) \\ &= \left(-\frac{2^{-4-d} \pi^{\frac{3-d}{2}} \Gamma(d-1)}{\sin(d\frac{\pi}{2}) \Gamma(\frac{d+1}{2}) \Gamma(3-\frac{d}{2})} |\mathbf{r}|^{4-2d} \right) \left(\delta^{ij} - d \frac{r^i r^j}{|\mathbf{r}|^2} \right); \end{aligned}$$

which is the result of the integral (4.35a) we were looking for.

■ Evaluation of the other integrals

The evaluation of the other integrals defined in equation (4.35) goes along in a similar way; therefore in equations (4.47) below we present directly the final results, by using the formulae derived in appendix C, for example also equation (C.32).

$$I_1^{ij}(\mathbf{r}) \equiv \int \frac{d^d \mathbf{p}}{(2\pi)^d} \frac{d^d \mathbf{k}}{(2\pi)^d} e^{i\mathbf{p}\cdot\mathbf{r}} \frac{k^i k^j}{|\mathbf{k}|^2 |\mathbf{p}|^2 |\mathbf{k}-\mathbf{p}|^2} = -\frac{2^{-4-d} \pi^{\frac{3-d}{2}} \Gamma(d-1)}{\sin(d\frac{\pi}{2}) \Gamma(\frac{d+1}{2}) \Gamma(3-\frac{d}{2})} |\mathbf{r}|^{4-2d} \left(\delta^{ij} - d \frac{r^i r^j}{|\mathbf{r}|^2} \right); \quad (4.47a)$$

$$I_2^{ij}(\mathbf{r}) \equiv \int \frac{d^d \mathbf{p}}{(2\pi)^d} \frac{d^d \mathbf{k}}{(2\pi)^d} e^{i\mathbf{p}\cdot\mathbf{r}} \frac{k^i p^j}{|\mathbf{k}|^2 |\mathbf{p}|^2 |\mathbf{k}-\mathbf{p}|^2} = -\frac{2^{-6} \pi^{1-d} \Gamma(\frac{d}{2}-1)}{\sin(d\frac{\pi}{2}) \Gamma(3-\frac{d}{2})} |\mathbf{r}|^{4-2d} \left(\delta^{ij} - 2(d-2) \frac{r^i r^j}{|\mathbf{r}|^2} \right); \quad (4.47b)$$

$$I_3^i(\mathbf{r}) \equiv \int \frac{d^d \mathbf{p}}{(2\pi)^d} \frac{d^d \mathbf{k}}{(2\pi)^d} e^{i\mathbf{p}\cdot\mathbf{r}} \frac{k^i}{|\mathbf{k}|^2 |\mathbf{p}|^2 |\mathbf{k} - \mathbf{p}|^2} = -i \frac{2^{-6} \pi^{1-d} \Gamma\left(\frac{d}{2} - 1\right)}{\sin\left(\frac{d\pi}{2}\right) \Gamma\left(3 - \frac{d}{2}\right)} |\mathbf{r}|^{4-2d} r^i ; \quad (4.47c)$$

$$I_4^i(\mathbf{r}) \equiv \int \frac{d^d \mathbf{p}}{(2\pi)^d} \frac{d^d \mathbf{k}}{(2\pi)^d} e^{i\mathbf{p}\cdot\mathbf{r}} \frac{p^i}{|\mathbf{k}|^2 |\mathbf{p}|^2 |\mathbf{k} - \mathbf{p}|^2} = -i \frac{2^{-5} \pi^{1-d} \Gamma\left(\frac{d}{2} - 1\right)}{\sin\left(\frac{d\pi}{2}\right) \Gamma\left(3 - \frac{d}{2}\right)} |\mathbf{r}|^{4-2d} r^i ; \quad (4.47d)$$

$$I_5^{ij} \equiv \int \frac{d^d \mathbf{k}_1}{(2\pi)^d} \frac{d^d \mathbf{k}_2}{(2\pi)^d} \frac{k_1^i k_2^j}{|\mathbf{k}_1|^2 |\mathbf{k}_2|^2 |\mathbf{k}_1 + \mathbf{k}_2|^2} = 0 ; \quad (4.47e)$$

$$I_6^i \equiv \int \frac{d^d \mathbf{k}_1}{(2\pi)^d} \frac{d^d \mathbf{k}_2}{(2\pi)^d} \frac{k_1^i}{|\mathbf{k}_1|^2 |\mathbf{k}_2|^2 |\mathbf{k}_1 + \mathbf{k}_2|^2} = 0 . \quad (4.47f)$$

In particular we can notice that it holds $I_4^i(\mathbf{r}) = 2 I_3^i(\mathbf{r})$, where the factor of two is due to the tensor decomposition and relation (4.41). Furthermore we find that integrals I_5^{ij} and I_6^i , given by equations (4.47e) and (4.47f), are identically vanishing: the integral I_6^i is vanishing already at the level of the tensor decomposition, because the integrand doesn't depend on any external vector quantity which has only one free spatial index (like \mathbf{r}), and therefore must be vanishing. The integral I_5^{ij} instead could be proportional to the Kronecker delta, $I_5^{ij} \propto \delta^{ij}$, but the resulting scalar integral is scaleless (as it was also in the case of the I_6^i integral), i.e. it depends on no external quantities: as explained in section 2.2.1 these scalar integrals are actually vanishing.

■ Final result of the diagram

Having evaluated the integrals, we can now use these results in equation (4.36). In particular, from (4.47b), we can notice that $I_2^{ij}(\mathbf{r})$ is symmetric, $I_2^{ij}(\mathbf{r}) = I_2^{ji}(\mathbf{r})$. Therefore we obtain:

$$\begin{aligned} \mathcal{A}_{(2g)} = & \frac{2^{-8} \pi^{1-d} \Gamma\left(\frac{d}{2} - 1\right)}{c_d \sin\left(\frac{d\pi}{2}\right) \Gamma\left(3 - \frac{d}{2}\right)} \frac{m_1 m_2}{\Lambda^4} \int dt \frac{|\mathbf{r}|^{4-2d}}{\sqrt{1 - v_1^2}} \\ & \times \left[\left((m_2 C_{1,j}^{(2,2)}) \left(\frac{1}{(d-1)} \left(v_1^j - (d-2)^2 \frac{(\mathbf{r} \cdot \mathbf{v}_1)}{|\mathbf{r}|^2} r^j \right) \right) \right) \right. \\ & + \left((-m_1 C_{1,j}^{(1,2)} - m_1 C_{1,j}^{(2,1)}) \left(\left(v_1^j - 2(d-2) \frac{(\mathbf{r} \cdot \mathbf{v}_1)}{|\mathbf{r}|^2} r^j \right) \right) \right) \\ & \left. + \left((2m_1 C_2^{(1,2)} - m_1 C_2^{(2,1)} + m_2 C_2^{(2,2)}) (i(\mathbf{r} \cdot \mathbf{v}_1)) \right) \right] + (1 \leftrightarrow 2) , \end{aligned} \quad (4.48)$$

and we can then substitute the explicit expression of the C coefficients, defined in equation (4.30), to obtain the final, full expression for the diagram (2g):

$$\begin{aligned}
\mathcal{A}_{(2g)} = & i \frac{2^{-8} \pi^{1-d} \Gamma\left(\frac{d}{2} - 1\right)}{c_d \sin\left(\frac{d\pi}{2}\right) \Gamma\left(3 - \frac{d}{2}\right)} \frac{m_1 m_2}{\Lambda^4} \int dt \frac{|\mathbf{r}|^{4-2d}}{\sqrt{1-v_1^2}} \left(\frac{2 + (c_d - 2)v_2^2}{2\sqrt{1-v_2^2}} \right) \\
& \times \left[\left(-m_2 \left(\frac{2 + (-2 + c_d)v_2^2}{2\sqrt{1-v_2^2}} \right) \left(\frac{1}{(d-1)}(\mathbf{v}_1 \cdot \mathbf{v}_2) - \frac{(d-2)^2}{(d-1)}(\hat{\mathbf{r}} \cdot \mathbf{v}_1)(\hat{\mathbf{r}} \cdot \mathbf{v}_2) \right) \right) \right. \\
& + \left(m_1 \left(\frac{2 + (-2 + c_d)v_1^2}{2\sqrt{1-v_1^2}} \right) (v_1^2 + (\mathbf{v}_1 \cdot \mathbf{v}_2) - 2(d-2)(\hat{\mathbf{r}} \cdot \mathbf{v}_1)((\hat{\mathbf{r}} \cdot \mathbf{v}_1) + (\hat{\mathbf{r}} \cdot \mathbf{v}_2))) \right) \\
& + \left(2m_1 \left(\frac{(\mathbf{r} \cdot \mathbf{v}_1)(\mathbf{v}_1 \cdot \mathbf{a}_1)}{2(1-v_1^2)^{\frac{3}{2}}} (2c_d - 2 + v_1^2(2 - c_d)) \right) \right) \\
& - m_1 \left(\frac{2 + (-2 + c_d)v_1^2}{2\sqrt{1-v_1^2}} \right) \left(\frac{(\mathbf{r} \cdot \mathbf{v}_1)(\mathbf{v}_2 \cdot \mathbf{a}_2)}{(1-v_2^2)} \frac{(2c_d - 2 + v_2^2(2 - c_d))}{2 + (-2 + c_d)v_2^2} \right) \\
& \left. + m_2 \left(\frac{(\mathbf{r} \cdot \mathbf{v}_1)(\mathbf{v}_2 \cdot \mathbf{a}_2)}{2(1-v_2^2)^{\frac{3}{2}}} (2c_d - 2 + v_2^2(2 - c_d)) \right) \right] + (1 \leftrightarrow 2) .
\end{aligned} \tag{4.49}$$

To evaluate the potential, we can then expand the above result around $d = 3$, obtaining:

$$\begin{aligned}
\mathcal{A}_{(2g)} \stackrel{d \rightarrow 3}{=} & -i 2 G^2 m_1 m_2 \int dt \frac{1}{|\mathbf{r}|^2} \frac{1}{\sqrt{1-v_1^2}} \left(\frac{1 + v_2^2}{\sqrt{1-v_2^2}} \right) \\
& \times \left[\left(-m_2 \left(\frac{1 + v_2^2}{\sqrt{1-v_2^2}} \right) \left(\frac{1}{2}(\mathbf{v}_1 \cdot \mathbf{v}_2) - \frac{1}{2}(\hat{\mathbf{r}} \cdot \mathbf{v}_1)(\hat{\mathbf{r}} \cdot \mathbf{v}_2) \right) \right) \right. \\
& + \left(m_1 \left(\frac{1 + v_1^2}{\sqrt{1-v_1^2}} \right) (v_1^2 + (\mathbf{v}_1 \cdot \mathbf{v}_2) - 2(\hat{\mathbf{r}} \cdot \mathbf{v}_1)((\hat{\mathbf{r}} \cdot \mathbf{v}_1) + (\hat{\mathbf{r}} \cdot \mathbf{v}_2))) \right) \\
& + \left(2m_1 \left(\frac{(\mathbf{r} \cdot \mathbf{v}_1)(\mathbf{v}_1 \cdot \mathbf{a}_1)}{(1-v_1^2)^{\frac{3}{2}}} (3 - v_1^2) \right) \right) \\
& - m_1 \left(\frac{1 + v_1^2}{\sqrt{1-v_1^2}} \right) \left(\frac{(\mathbf{r} \cdot \mathbf{v}_1)(\mathbf{v}_2 \cdot \mathbf{a}_2)}{(1-v_2^2)} \frac{(3 - v_2^2)}{1 + v_2^2} \right) \\
& \left. + m_2 \left(\frac{(\mathbf{r} \cdot \mathbf{v}_1)(\mathbf{v}_2 \cdot \mathbf{a}_2)}{(1-v_2^2)^{\frac{3}{2}}} (3 - v_2^2) \right) \right] + (1 \leftrightarrow 2) + \mathcal{O}(d-3) ;
\end{aligned} \tag{4.50}$$

and finally expanding up to 2PN order we obtain:

$$\begin{aligned}
\mathcal{A}_{(2g)} = & -i \int dt \left[\frac{G^2 m_1 m_2}{|\mathbf{r}|^2} (2m_1 v_1^2 + (2m_1 - m_2)(\mathbf{v}_1 \cdot \mathbf{v}_2) - 4m_1(\hat{\mathbf{r}} \cdot \mathbf{v}_1)^2 \right. \\
& \left. + (-4m_1 + m_2)(\hat{\mathbf{r}} \cdot \mathbf{v}_1)(\hat{\mathbf{r}} \cdot \mathbf{v}_2)) \right] + (1 \leftrightarrow 2) + \mathcal{O}(d-3) + \mathcal{O}(L v^6) .
\end{aligned} \tag{4.51}$$

From equation (4.51) we can then read the contribution of diagram (2g) to the 2PN potential, i.e. by explicitly adding the $(1 \leftrightarrow 2)$ term, recalling also that in general $\mathbf{r} \xrightarrow{(1 \leftrightarrow 2)} -\mathbf{r}$, we obtain:

$$\begin{aligned}
V_{(2g)}(t) = & \frac{G^2 m_1 m_2}{r^2} (2m_1 v_1^2 + 2m_2 v_2^2 - (m_1 + m_2)(3(\hat{\mathbf{r}} \cdot \mathbf{v}_1)(\hat{\mathbf{r}} \cdot \mathbf{v}_2) - \mathbf{v}_1 \cdot \mathbf{v}_2) \\
& - 4m_1(\hat{\mathbf{r}} \cdot \mathbf{v}_1)^2 - 4m_2(\hat{\mathbf{r}} \cdot \mathbf{v}_2)^2) + \mathcal{O}(L v^6) ;
\end{aligned} \tag{4.52}$$

which exactly agrees with the result reported in reference [235], in which the corresponding contribution is the sum of diagrams (m) and (n).

4.4 | Mathematica code for the automatic evaluation of conservative diagrams

We implemented the general procedure for the evaluation of generic conservative diagrams, which we discussed in the above section 4.3, in a `Mathematica` code.

In particular this code is able to evaluate the generic expression of a conservative diagram, exact in the velocity v (up to propagator insertions) and in the space dimension d , once one specifies the action terms for the bulk actions, which for example we reported in equation (3.35), and the results for the master integrals that are left after the integration-by-parts procedure. In particular we obtained the expression for the bulk action, up to 2PN, by using the `FeynRu1.m` module of the `EFTofPNG` package [249]; instead we explicitly evaluated the master integrals needed up to 2PN (which where up to 2-loop Feynman integrals) in appendix C.2.

Therefore, once initialized the code (loading quantities precomputed by the code itself to speed up the subsequent evaluation), and created the diagram (by specifying the relevant Feynman rules, the propagators and the symmetry factor), the code automatically evaluates its expression, exactly in v and in d . Eventually such expression can also be expanded around $d = 3$ and in the PN expansion parameters to obtain the expression for the corresponding conservative potential.

In fact we employed this code to evaluate the diagrams contributing to the 2PN order, as we report in section 4.5, finding exact agreement with the results of reference [235]. Then in section 4.6 we also employed this same code to evaluate a few selected conservative diagrams contributing at 7PN order.

The actual `Mathematica` package, written as a separate `.wl` package with 2000+ lines of code, implements the functions needed for the actual evaluation of the diagrams. In particular each diagrams is represented via a structure, which contains the several mathematical expressions associated to such diagram: these expression are actually are kept split in homogeneous sub-expression, which are processed separately in order to simplify their evaluation. The package then implements routines to perform the necessary manipulations and simplifications of these expressions, the tensor decomposition procedure, to solve the temporal sector (for example by exchanging the temporal components of the momenta for time derivatives, performing the relevant integrations and enforcing the temporal Dirac deltas), to evaluate the multi-loop Feynman integrals and the Fourier transform. In particular the needed tensor algebra is performed using the `xTensor` package [261], whereas the evaluation of the loop integrals is performed by interfacing with the `LiteRed` package [216, 217, 262] for integral reduction via integration-by-parts identities; the resulting expression, which is a function of only a few master integrals, is then separately evaluated using the results reported in appendix C. Finally we also implemented a routine to expand the exact diagram expression so obtained around $d = 3$ and in the PN expansion parameters, to obtain the corresponding contributions to the potential. Furthermore the worldline Feynman rules can be computed to any arbitrary order directly in the library.

The procedure which we implemented in the code is also schematically represented in the flowchart in figure 4.7.

Furthermore in appendix D we report some extracts of the code, also showing as an example how it can be used to compute diagram $\mathcal{A}_{(2g)}$, which is the one we just evaluated explicitly in section 4.3. Even though the library isn't particularly optimized (if not for the precomputation of the tensor decompositions and the integration-by-parts basis), the evaluation of the diagram $\mathcal{A}_{(2g)}$ reported in

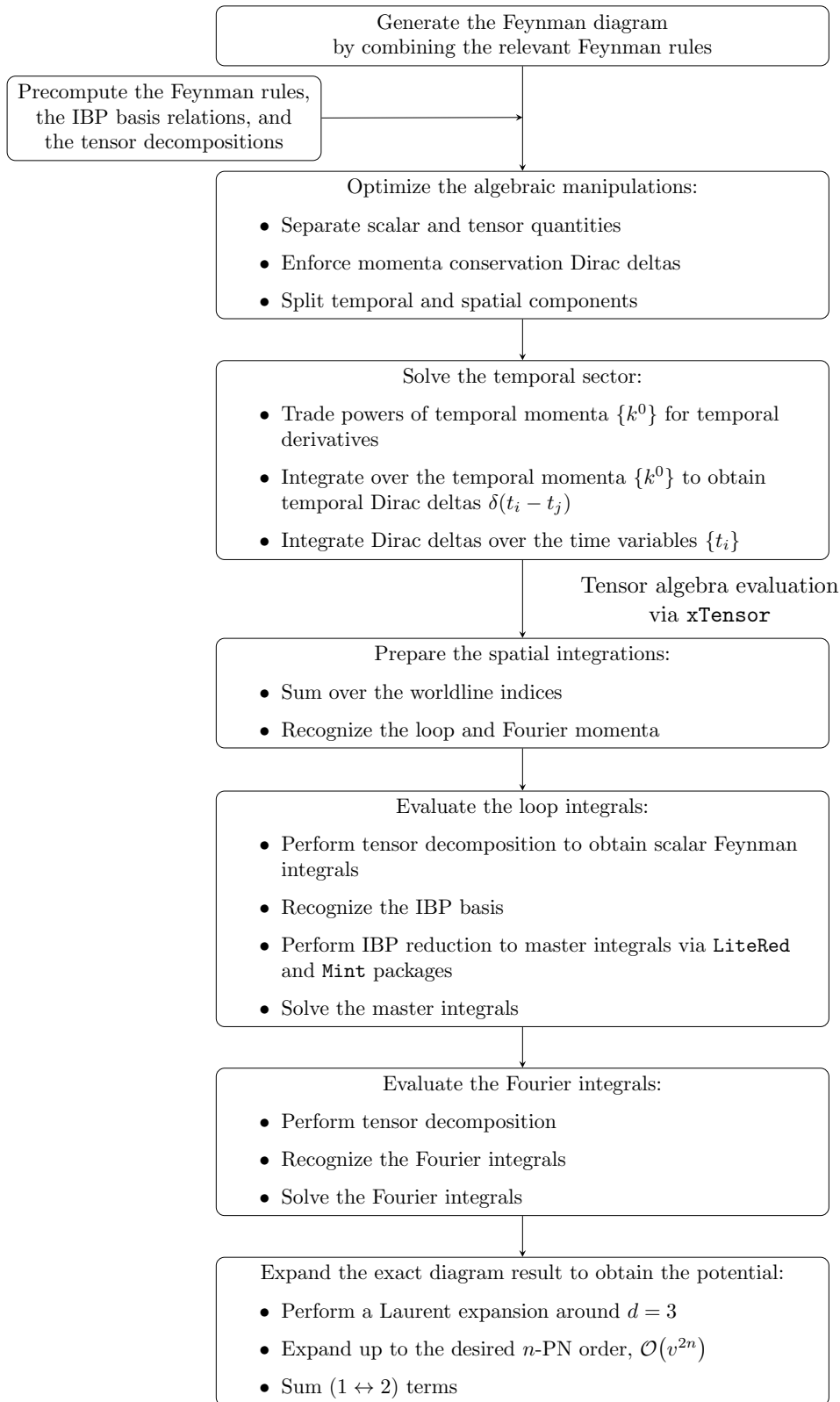


FIGURE 4.7 — Flowchart of the `Mathematica` code developed for the evaluation of a generic conservative diagram.

appendix D (which is performed by the `automaticEvaluateDiagram` function) runs in about half a minute on a standard laptop computer, and the potential is obtained in a few more seconds from that exact relation. In particular a great portion of the time is being spent on the simplifications of the intermediate and final results of the evaluation, via the standard `Simplify` command of `Mathematica`.

4.5 | Conservative contributions to the potential at 2PN order

In this section then we report the results for the conservative sector up to 2PN, which represent a next-to-next-to-leading order correction to the Newtonian potential. In particular we computed these results using the `Mathematica` code just outlined above in section 4.4.

These results we found are in exact agreement with the results of reference [235]; yet to explicitly show this we have to perform some integration by parts, using in particular the following relations:

$$\frac{d\mathbf{r}}{dt} = \mathbf{v} \equiv \mathbf{v}_1 - \mathbf{v}_2 \quad (4.53a)$$

$$\frac{dr}{dt} = \mathbf{v} \cdot \hat{\mathbf{r}} = (\mathbf{v}_1 \cdot \hat{\mathbf{r}}) - (\mathbf{v}_2 \cdot \hat{\mathbf{r}}) \quad (4.53b)$$

$$\frac{d\hat{\mathbf{r}}}{dt} = \frac{1}{r} (\mathbf{v} - \hat{\mathbf{r}} (\mathbf{v} \cdot \hat{\mathbf{r}})) = \frac{1}{r} (\mathbf{v}_1 - \mathbf{v}_2 - \hat{\mathbf{r}} (\mathbf{v}_1 \cdot \hat{\mathbf{r}}) + \hat{\mathbf{r}} (\mathbf{v}_2 \cdot \hat{\mathbf{r}})) \quad (4.53c)$$

$$\int dt \frac{(\mathbf{a}_1 \cdot \hat{\mathbf{r}})}{r} = \underbrace{\int dt \frac{d}{dt} \left(\frac{(\mathbf{v}_1 \cdot \hat{\mathbf{r}})}{r} \right)}_{\simeq 0} + \int dt \frac{1}{r^2} (2 (\mathbf{v}_1 \cdot \hat{\mathbf{r}}) ((\mathbf{v}_1 \cdot \hat{\mathbf{r}}) - (\mathbf{v}_2 \cdot \hat{\mathbf{r}})) - v_1^2 + (\mathbf{v}_1 \cdot \mathbf{v}_2)) \quad (4.54a)$$

$$\int dt \frac{(\mathbf{a}_2 \cdot \hat{\mathbf{r}})}{r} = \underbrace{\int dt \frac{d}{dt} \left(\frac{(\mathbf{v}_2 \cdot \hat{\mathbf{r}})}{r} \right)}_{\simeq 0} + \int dt \frac{1}{r^2} (2 (\mathbf{v}_2 \cdot \hat{\mathbf{r}}) ((\mathbf{v}_1 \cdot \hat{\mathbf{r}}) - (\mathbf{v}_2 \cdot \hat{\mathbf{r}})) + v_2^2 - (\mathbf{v}_1 \cdot \mathbf{v}_2)) \quad (4.54b)$$

Additionally the computation of this diagrams resulted in new master integrals, up to 2-loop level, which we explicitly evaluated in appendix C.2.

Then below we report the expression for the relevant diagrams, already expanded to the 2PN order and around $d = 3$; in particular we already singled out the contribution to the potential inside the square bracket; and already summed the $(1 \leftrightarrow 2)$ terms.

■ Diagram (2a)

$$\begin{aligned} \mathcal{A}_{(2a)} &= \begin{array}{c} \circ \quad \circ \\ \phi \quad \phi \\ \phi \quad \phi \\ \circ \quad \circ \end{array} = \int dt \left[\frac{im_1^2 m_2^2 \pi^{-3d/2} r^{6-3d}}{65536 c_d^3 (-1+v_1^2)^2 (-1+v_2^2)^2 \Lambda^6} (2 + (-2 + c_d) v_1^2) \right. \\ &\quad \times (4 - 2(4 - 2c_d + c_d^2) v_1^2 + (-2 + c_d)^2 v_1^4) (2 + (-2 + c_d) v_2^2) \\ &\quad \left. \times (4 - 2(4 - 2c_d + c_d^2) v_2^2 + (-2 + c_d)^2 v_2^4) \Gamma \left(-1 + \frac{d}{2} \right)^3 \right] + (1 \leftrightarrow 2) \\ &= -i \int dt \left[-\frac{G^3 m_1^2 m_2^2}{r^3} \right] + \mathcal{O}(L v^6) \end{aligned} \quad (4.55a)$$

This result agrees with the corresponding (s) diagram of reference [235].

■ **Diagram (2b)**

$$\mathcal{A}_{(2b)} = \begin{array}{c} \phi \\ \circ \quad \circ \quad \circ \\ \phi \quad \phi \end{array} = -i \int dt \left[-\frac{G^3 m_1 m_2 (m_1^2 + m_2^2)}{6r^3} \right] + \mathcal{O}(L v^6) \quad (4.55b)$$

This result agrees with the corresponding (q) diagram of reference [235].

■ **Diagram (2c)**

$$\mathcal{A}_{(2c)} = \begin{array}{c} \phi \quad \phi \\ \circ \quad \circ \\ \phi \quad \phi \\ \phi \quad \phi \end{array} = -i \int dt \left[-\frac{G^3 m_1 m_2 (m_1^2 + 6m_1 m_2 + m_2^2)}{3r^3} \right] + \mathcal{O}(L v^6) \quad (4.55c)$$

This result agrees with the corresponding (r) + (t) + (u) diagrams of reference [235].

■ **Diagram (2d)**

$$\mathcal{A}_{(2d)} = \begin{array}{c} \phi \\ \circ \quad \circ \\ A \end{array} = -i \int dt \left[-\frac{4G^2 m_1 m_2}{r^2} (m_1 + m_2) (\mathbf{v}_1 \cdot \mathbf{v}_2) \right] + \mathcal{O}(L v^6) \quad (4.55d)$$

This result agrees with the corresponding (h) diagram of reference [235].

■ **Diagram (2e)**

$$\begin{aligned} \mathcal{A}_{(2e)} = \begin{array}{c} \phi \\ \circ \quad \circ \\ \phi \end{array} &= -i \int dt \left[\frac{G^2 m_1 m_2}{2r^2} (m_1 v_1^2 + m_2 v_2^2 + m_1 r (\mathbf{a}_1 \cdot \hat{\mathbf{r}}) - m_1 (\mathbf{v}_1 \cdot \hat{\mathbf{r}})^2 \right. \\ &\quad \left. - m_2 (r (\mathbf{a}_2 \cdot \hat{\mathbf{r}}) + (\mathbf{v}_2 \cdot \hat{\mathbf{r}})^2) \right] + \mathcal{O}(L v^6) \\ &= -i \int dt \left[\frac{G^2 m_1 m_2}{2r^2} ((m_1 + m_2) (\mathbf{v}_1 \cdot \mathbf{v}_2) + m_1 (\mathbf{v}_1 \cdot \hat{\mathbf{r}})^2 + m_2 (\mathbf{v}_2 \cdot \hat{\mathbf{r}})^2 \right. \\ &\quad \left. - 2(m_1 + m_2) (\mathbf{v}_1 \cdot \hat{\mathbf{r}}) (\mathbf{v}_2 \cdot \hat{\mathbf{r}}) \right] + \mathcal{O}(L v^6) \end{aligned} \quad (4.55e)$$

In the last equality we employed formulae (4.54a) and (4.54b) to recast the result in the form of reference [235] (diagram (i)), by adding total time derivatives to the Lagrangian.

■ **Diagram (2f)**

$$\begin{aligned}
 \mathcal{A}_{(2f)} = \begin{array}{c} \circ \\ | \phi \\ \phi \quad \phi \\ \circ \quad \circ \end{array} &= -i \int dt \left[\frac{G^2 m_1 m_2}{6r^2} \left(-((5m_1 + 8m_2)v_1^2) - (8m_1 + 5m_2)v_2^2 \right. \right. \\
 &\quad - 8(m_1 + m_2)r(\mathbf{a}_1 \cdot \hat{\mathbf{r}}) + 8(m_1 + m_2)r(\mathbf{a}_2 \cdot \hat{\mathbf{r}}) + 4m_1(\mathbf{v}_1 \cdot \mathbf{v}_2) \\
 &\quad + 4m_2(\mathbf{v}_1 \cdot \mathbf{v}_2) + 13m_1(\mathbf{v}_1 \cdot \hat{\mathbf{r}})^2 + 16m_2(\mathbf{v}_1 \cdot \hat{\mathbf{r}})^2 \\
 &\quad \left. \left. - 8(m_1 + m_2)(\mathbf{v}_1 \cdot \hat{\mathbf{r}})(\mathbf{v}_2 \cdot \hat{\mathbf{r}}) + (16m_1 + 13m_2)(\mathbf{v}_2 \cdot \hat{\mathbf{r}})^2 \right) \right] + \mathcal{O}(L v^6) \\
 &= -i \int dt \left[\frac{G^2 m_1 m_2}{2r^2} \left(-4(m_1 + m_2)(\mathbf{v}_1 \cdot \mathbf{v}_2) - m_1(\mathbf{v}_1 \cdot \hat{\mathbf{r}})^2 - m_2(\mathbf{v}_2 \cdot \hat{\mathbf{r}})^2 \right. \right. \\
 &\quad \left. \left. + 8(m_1 + m_2)(\mathbf{v}_1 \cdot \hat{\mathbf{r}})(\mathbf{v}_2 \cdot \hat{\mathbf{r}}) + m_1 v_1^2 + m_2 v_2^2 \right) \right] + \mathcal{O}(L v^6) \tag{4.55f}
 \end{aligned}$$

In the last equality we employed formulae (4.54a) and (4.54b) to recast the result in the form of reference [235] (diagram (j)), by adding total time derivatives to the Lagrangian.

■ **Diagram (2g)**

$$\begin{aligned}
 \mathcal{A}_{(2g)} = \begin{array}{c} \circ \\ | A \\ \phi \quad \phi \\ \circ \quad \circ \end{array} &= -i \int dt \left[\frac{G^2 m_1 m_2}{r^2} (2m_1 v_1^2 + 2m_2 v_2^2 - 3(m_1 + m_2)(\mathbf{v}_1 \cdot \hat{\mathbf{r}})(\mathbf{v}_2 \cdot \hat{\mathbf{r}}) \right. \\
 &\quad \left. + (m_1 + m_2)(\mathbf{v}_1 \cdot \mathbf{v}_2) - 4m_1(\mathbf{v}_1 \cdot \hat{\mathbf{r}})^2 - 4m_2(\mathbf{v}_2 \cdot \hat{\mathbf{r}})^2 \right] + \mathcal{O}(L v^6) \tag{4.55g}
 \end{aligned}$$

This result, which we also evaluated thoroughly in section 4.3.1, agrees with the corresponding (q) diagram of reference [235].

■ **Diagram (2h)**

$$\begin{aligned}
 \mathcal{A}_{(2h)} = \begin{array}{c} \circ \\ | \phi \\ A \quad A \\ \circ \quad \circ \end{array} &= -i \int dt \left[-\frac{4G^2 m_1 m_2}{r^2} (m_1 v_1^2 + m_2 v_2^2 - 2(m_1 + m_2)(\mathbf{v}_1 \cdot \mathbf{v}_2)) \right] + \mathcal{O}(L v^6) \tag{4.55h}
 \end{aligned}$$

This result agrees with the corresponding (k) + (l) diagrams of reference [235].

■ **Diagram (2i)**

$$\begin{aligned}
 \mathcal{A}_{(2i)} = \begin{array}{c} \circ \\ | \sigma \\ \phi \quad \phi \\ \circ \quad \circ \end{array} &= -i \int dt \left[-\frac{G^2 m_1 m_2}{2r^2} \left((4m_1 - m_2)v_1^2 - (m_1 - 4m_2)v_2^2 \right. \right. \\
 &\quad \left. \left. + (-8m_1 + m_2)(\mathbf{v}_1 \cdot \hat{\mathbf{r}})^2 + (m_1 - 8m_2)(\mathbf{v}_2 \cdot \hat{\mathbf{r}})^2 \right) \right] + \mathcal{O}(L v^6) \tag{4.55i}
 \end{aligned}$$

This result agrees with the corresponding (o) + (p) diagram of reference [235].

■ **Diagram (2j)**

$$\mathcal{A}_{(2j)} = \begin{array}{c} \circ \\ \vdots \\ \sigma \\ \circ \end{array} = -i \int dt \left[\frac{2Gm_1m_2}{r} (v_1^2v_2^2 - (\mathbf{v}_1 \cdot \mathbf{v}_2)^2) \right] + \mathcal{O}(Lv^6) \quad (4.55j)$$

This result agrees with the corresponding (f) diagram of reference [235].

■ **Diagram (2k)**

$$\mathcal{A}_{(2k)} = 2 \begin{array}{c} \circ \\ \otimes \\ \phi \\ \circ \end{array} = -i \int dt \left[\frac{Gm_1m_2}{8r} (r^2(\mathbf{a}_1 \cdot \mathbf{a}_2) + r^2(\mathbf{a}_1 \cdot \hat{\mathbf{r}})(\mathbf{a}_2 \cdot \hat{\mathbf{r}}) \right. \\ \left. + rv_1^2(\mathbf{a}_2 \cdot \hat{\mathbf{r}}) - rv_2^2(\mathbf{a}_1 \cdot \hat{\mathbf{r}}) - 2r(\mathbf{a}_1 \cdot \mathbf{v}_2)(\mathbf{v}_2 \cdot \hat{\mathbf{r}}) + 2r(\mathbf{a}_2 \cdot \mathbf{v}_1)(\mathbf{v}_1 \cdot \hat{\mathbf{r}}) \right. \\ \left. + r(\mathbf{a}_1 \cdot \hat{\mathbf{r}})(\mathbf{v}_2 \cdot \hat{\mathbf{r}})^2 - r(\mathbf{a}_2 \cdot \hat{\mathbf{r}})(\mathbf{v}_1 \cdot \hat{\mathbf{r}})^2 \right. \\ \left. - v_1^2v_2^2 - 2(\mathbf{v}_1 \cdot \mathbf{v}_2)^2 + v_1^2(\mathbf{v}_2 \cdot \hat{\mathbf{r}})^2 + v_2^2(\mathbf{v}_1 \cdot \hat{\mathbf{r}})^2 \right. \\ \left. + 4(\mathbf{v}_1 \cdot \mathbf{v}_2)(\mathbf{v}_1 \cdot \hat{\mathbf{r}})(\mathbf{v}_2 \cdot \hat{\mathbf{r}}) - 3(\mathbf{v}_1 \cdot \hat{\mathbf{r}})^2(\mathbf{v}_2 \cdot \hat{\mathbf{r}})^2 \right] + \mathcal{O}(Lv^6) \quad (4.55k)$$

This result agrees with the corresponding (c) diagram of reference [235].

■ **Diagram (2l)**

$$\mathcal{A}_{(2l)} = \begin{array}{c} \circ \\ \otimes \\ A \\ \circ \end{array} = -i \int dt \left[-\frac{2Gm_1m_2}{r} (r^2(\mathbf{a}_1 \cdot \mathbf{a}_2) + r(\mathbf{a}_2 \cdot \mathbf{v}_1)(\mathbf{v}_1 \cdot \hat{\mathbf{r}}) - r(\mathbf{a}_1 \cdot \mathbf{v}_2)(\mathbf{v}_2 \cdot \hat{\mathbf{r}}) \right. \\ \left. + (\mathbf{v}_1 \cdot \mathbf{v}_2)(\mathbf{v}_1 \cdot \hat{\mathbf{r}})(\mathbf{v}_2 \cdot \hat{\mathbf{r}}) - (\mathbf{v}_1 \cdot \mathbf{v}_2)^2) \right] + \mathcal{O}(Lv^6) \quad (4.55l)$$

This result agrees with the corresponding (e) diagram of reference [235].

■ **Diagram (0a) at 2PN**

$$\mathcal{A}_{(0a)}|_{2PN} = \begin{array}{c} \circ \\ \vdots \\ \phi \\ \circ \end{array} \Big|_{2PN} = -i \int dt \left[-\frac{Gm_1m_2}{8r} (7v_1^4 + 18v_1^2v_2^2 + 7v_2^4) \right] + \mathcal{O}(Lv^6) \quad (4.55m)$$

This result agrees with the corresponding (a) diagram of reference [235].

■ Diagram (1a) at 2PN

$$\mathcal{A}_{(1a)}|_{2PN} = \begin{array}{c} \circ \\ \phi \quad \phi \\ \diagdown \quad \diagup \\ \circ \quad \circ \end{array} \quad \Big|_{2PN} = -i \int dt \left[\frac{3G^2 m_1 m_2}{4r^2} (2m_1 v_1^2 - 3m_2 v_1^2 - 3m_1 v_2^2 + 2m_2 v_2^2) \right] + \mathcal{O}(L v^6) \quad (4.55n)$$

This result agrees with the corresponding (g) diagram of reference [235].

■ Diagram (1b) at 2PN

$$\mathcal{A}_{(1b)}|_{2PN} = \begin{array}{c} \circ \\ | \\ \circ \end{array} A \quad \Big|_{2PN} = -i \int dt \left[\frac{2Gm_1 m_2}{r} (v_1^2 + v_2^2) (\mathbf{v}_1 \cdot \mathbf{v}_2) \right] + \mathcal{O}(L v^6) \quad (4.55o)$$

This result agrees with the corresponding (d) diagram of reference [235].

■ Diagram (1c) at 2PN

$$\mathcal{A}_{(1c)}|_{2PN} = \begin{array}{c} \circ \\ | \\ \otimes \\ | \\ \circ \end{array} \phi \quad \Big|_{2PN} = -i \int dt \left[\frac{3Gm_1 m_2}{4r} (2r ((\mathbf{a}_2 \cdot \mathbf{v}_2)(\mathbf{v}_1 \cdot \hat{\mathbf{r}}) - (\mathbf{a}_1 \cdot \mathbf{v}_1)(\mathbf{v}_2 \cdot \hat{\mathbf{r}})) - (v_1^2 + v_2^2) ((\mathbf{v}_1 \cdot \mathbf{v}_2) - (\mathbf{v}_1 \cdot \hat{\mathbf{r}})(\mathbf{v}_2 \cdot \hat{\mathbf{r}}))) \right] + \mathcal{O}(L v^6) \quad (4.55p)$$

This result agrees with the corresponding (b) diagram of reference [235].

4.5.1 — Contribution of order 2PN to the conservative two-body Lagrangian

The full 2PN potential, in harmonic gauge, is given by the sum of the contributions (4.55a) through (4.55p), which reads:

$$\begin{aligned} \Delta V_{2PN} = & -\frac{G^3 m_1 m_2}{2r^3} (m_1^2 + 6m_1 m_2 + m_2^2) \\ & -\frac{G^2 m_1 m_2}{4r^2} (8m_1 v_1^2 + 7m_2 v_1^2 + 7m_1 v_2^2 + 8m_2 v_2^2 - 14(m_1 + m_2)(\mathbf{v}_1 \cdot \mathbf{v}_2) \\ & \quad + 2m_2(\mathbf{v}_1 \cdot \hat{\mathbf{r}})^2 + 2m_1(\mathbf{v}_2 \cdot \hat{\mathbf{r}})^2) \\ & -\frac{Gm_1 m_2}{8r} (7v_1^4 + 3v_1^2 v_2^2 + 7v_2^4 + 15r^2(\mathbf{a}_1 \cdot \mathbf{a}_2) - r v_1^2(\mathbf{a}_2 \cdot \hat{\mathbf{r}}) - 10v_1^2(\mathbf{v}_1 \cdot \mathbf{v}_2) \\ & \quad - 10v_2^2(\mathbf{v}_1 \cdot \mathbf{v}_2) + 2(\mathbf{v}_1 \cdot \mathbf{v}_2)^2 + 14r(\mathbf{a}_2 \cdot \mathbf{v}_1)(\mathbf{v}_1 \cdot \hat{\mathbf{r}}) - 12r(\mathbf{a}_2 \cdot \mathbf{v}_2)(\mathbf{v}_1 \cdot \hat{\mathbf{r}}) \\ & \quad - v_2^2(\mathbf{v}_1 \cdot \hat{\mathbf{r}})^2 + r(\mathbf{a}_2 \cdot \hat{\mathbf{r}})(\mathbf{v}_1 \cdot \hat{\mathbf{r}})^2 + 12r(\mathbf{a}_1 \cdot \mathbf{v}_1)(\mathbf{v}_2 \cdot \hat{\mathbf{r}}) - 14r(\mathbf{a}_1 \cdot \mathbf{v}_2)(\mathbf{v}_2 \cdot \hat{\mathbf{r}}) \\ & \quad - 6v_1^2(\mathbf{v}_1 \cdot \hat{\mathbf{r}})(\mathbf{v}_2 \cdot \hat{\mathbf{r}}) - 6v_2^2(\mathbf{v}_1 \cdot \hat{\mathbf{r}})(\mathbf{v}_2 \cdot \hat{\mathbf{r}}) + 12(\mathbf{v}_1 \cdot \mathbf{v}_2)(\mathbf{v}_1 \cdot \hat{\mathbf{r}})(\mathbf{v}_2 \cdot \hat{\mathbf{r}}) \\ & \quad - v_1^2(\mathbf{v}_2 \cdot \hat{\mathbf{r}})^2 + 3(\mathbf{v}_1 \cdot \hat{\mathbf{r}})^2(\mathbf{v}_2 \cdot \hat{\mathbf{r}})^2 - r(\mathbf{a}_1 \cdot \hat{\mathbf{r}}) (-v_2^2 + r(\mathbf{a}_2 \cdot \hat{\mathbf{r}}) + (\mathbf{v}_2 \cdot \hat{\mathbf{r}})^2)) \\ & + \mathcal{O}(L v^6) . \end{aligned} \quad (4.56)$$

Let us recall that the dynamics of the system are prescribed by the full Lagrangian $L = T - V$, and so we have also to consider the corrections from the expansion of the relativistic kinetic term (3.34b), which at 2PN gives the contributions:

$$\Delta T_{2PN} = \frac{1}{16}m_1v_1^6 + \frac{1}{16}m_1v_1^6 ; \quad (4.57)$$

and therefore the 2PN contributions to the Lagrangian are given by (4.57) minus (4.56):

$$L_{2PN} = \Delta T_{2PN} - \Delta V_{2PN} . \quad (4.58)$$

4.6 | Subset of conservative contributions at 7PN

In order to show the flexibility of the `Mathematica` code that we wrote in order to evaluate conservative diagrams, which we outlined in section 4.4, we'll present the results regarding a small subset of diagrams which contribute at 7PN (v^{14}) in the conservative sector.

These results are some of the N^7 LO corrections to the Newtonian potential: to the best of our knowledge they are not present in the literature, which explicitly discuss post-Newtonian corrections up to the 6PN order; with some results eventually obtained also by complementing information from other approximation schemes, such as post-Minkowskian and self-force, as in the *Tutti-Frutti* method [20–23, 63–65, 77, 78, 173, 263]. However, since below we're considering only diagrams with at most 4 worldline vertices, it means that we're evaluating conservative contributions that are contained in up to the third conservative post-Minkowskian (3PM) order, which has been derived recently [69, 74, 158, 264–270]; in fact the diagrams that we're considering are also somewhat trivial, since they don't require the evaluation of any new master integral. Nonetheless the post-Minkowskian results are related to the results obtained by summing over all the corresponding post-Newtonian diagrams, while here instead we're explicitly and independently evaluating each diagram in the post-Newtonian framework.

Therefore, as an example, let us consider the contribution coming from all the diagrams we've computed so far: having evaluated diagrams $\mathcal{A}_{(0a)}$ to $\mathcal{A}_{(2l)}$ exactly in v (whose contributions at 2PN are given in equations (4.55a) to (4.55p)), we can directly evaluate their contribution at the 7PN level (so their contributions of order $\mathcal{O}(L v^{14})$).

In particular, we will define $\tilde{r} \equiv \sqrt{4\pi} \mu r$, with the μ parameter coming from the renormalization of the Planck mass via the definition (3.25) of the d -dimensional Λ coupling constant; γ is the Euler-Mascheroni constant (B.9). Then in this result we will also find logarithmic terms $\log(\tilde{r})$, which depend on the arbitrary scale μ : they arise starting from the 3PN order, nonetheless they're expected to cancel out once we evaluate any physical observable [57].

We have also to point out that this result won't be complete: in fact for some bulk vertices, which we derived in appendix A.2, we're considering only the lowest order contribution for their expression. Yet in the Einstein-Hilbert Lagrangian there could be terms with more temporal derivatives, instead of spatial derivatives: these terms contribute at higher PN order, as we evaluated in the power-counting formula (3.60). Then in the following formulae ((4.59) and (4.60)) we will omit these terms, which nonetheless must be considered in order to obtain the full 7PN result corresponding to the aforementioned subset of diagrams, also regarding the divergent $\frac{1}{\epsilon}$ part.

Given this premises, the evaluated expression reads (here the ellipses understand the fact that we actually dropped most of the terms of order G^1 and G^2 since the full expression was too long, yet we show the full result for the G^3 terms):

$$\begin{aligned}
\Delta V_{7PN,subset} = & \\
& - \frac{G^3 m_1 m_2}{512 r^3} (m_1^2 (4743 v_1^{10} + 22737 v_2^8 v_1^8 + 50694 v_2^4 v_1^6 + 67650 v_2^6 v_1^4 + 51075 v_2^8 v_1^2 + 16093 v_2^{10}) \\
& \quad - 2048 m_2 m_1 (7 v_1^{10} - 27 v_2^2 v_1^8 - 68 v_2^4 v_1^6 - 68 v_2^6 v_1^4 - 27 v_2^8 v_1^2 + 7 v_2^{10}) \\
& \quad + m_2^2 (16093 v_1^{10} + 51075 v_2^2 v_1^8 + 67650 v_2^4 v_1^6 + 50694 v_2^6 v_1^4 + 22737 v_2^8 v_1^2 + 4743 v_2^{10})) \\
& - \frac{G^2 m_1 m_2}{6144 r^2} (20480 m_1 v_1^{12} + 36827 m_2 v_1^{12} + 198656 m_1 v_2^2 v_1^{10} + 148604 m_2 v_2^2 v_1^{10} - 40960 m_1 (\mathbf{v}_1 \cdot \hat{\mathbf{r}})^2 v_1^{10} - 7756 m_2 (\mathbf{v}_1 \cdot \hat{\mathbf{r}})^2 v_1^{10} \\
& \quad - 53248 m_1 (\mathbf{v}_2 \cdot \hat{\mathbf{r}})^2 v_1^{10} - 37240 m_2 (\mathbf{v}_2 \cdot \hat{\mathbf{r}})^2 v_1^{10} - 32768 m_1 r (\mathbf{a}_2 \cdot \hat{\mathbf{r}}) v_1^{10} - 34580 m_2 r (\mathbf{a}_2 \cdot \hat{\mathbf{r}}) v_1^{10} \\
& \quad - 65536 m_1 (\mathbf{v}_1 \cdot \mathbf{v}_2) v_1^{10} - 134008 m_2 (\mathbf{v}_1 \cdot \mathbf{v}_2) v_1^{10} + 57344 m_1 (\mathbf{v}_1 \cdot \hat{\mathbf{r}}) (\mathbf{v}_2 \cdot \hat{\mathbf{r}}) v_1^{10} + 15512 m_2 (\mathbf{v}_1 \cdot \hat{\mathbf{r}}) (\mathbf{v}_2 \cdot \hat{\mathbf{r}}) v_1^{10} \\
& \quad + 232960 m_1 v_2^4 v_1^8 + 231088 m_2 v_2^4 v_1^8 - 143360 a_1^2 m_1 r^2 v_1^8 + 8192 a_2^2 m_1 r^2 v_1^8 + 163840 a_1^2 \gamma m_1 r^2 v_1^8 + 49152 a_2^2 \gamma m_1 r^2 v_1^8 \\
& \quad - 20720 a_1^2 m_2 r^2 v_1^8 + 76680 a_2^2 m_2 r^2 v_1^8 + 21280 a_1^2 \gamma m_2 r^2 v_1^8 + 14400 a_2^2 \gamma m_2 r^2 v_1^8 - 135168 m_1 v_2^2 (\mathbf{v}_1 \cdot \hat{\mathbf{r}})^2 v_1^8 \\
& \quad - 26280 m_2 v_2^2 (\mathbf{v}_1 \cdot \hat{\mathbf{r}})^2 v_1^8 - 92160 m_1 v_2^2 (\mathbf{v}_2 \cdot \hat{\mathbf{r}})^2 v_1^8 - 104400 m_2 v_2^2 (\mathbf{v}_2 \cdot \hat{\mathbf{r}})^2 v_1^8 + 327680 a_1^2 m_1 r^2 \log(\tilde{r}) v_1^8 \\
& \quad + 98304 a_2^2 m_1 r^2 \log(\tilde{r}) v_1^8 + 42560 a_1^2 m_2 r^2 \log(\tilde{r}) v_1^8 + 28800 a_2^2 m_2 r^2 \log(\tilde{r}) v_1^8 - 49152 m_1 r v_2^2 (\mathbf{a}_2 \cdot \hat{\mathbf{r}}) v_1^8 \\
& \quad - 95400 m_2 r v_2^2 (\mathbf{a}_2 \cdot \hat{\mathbf{r}}) v_1^8 + 163840 \gamma m_1 r^2 (\mathbf{j}_1 \cdot \mathbf{v}_1) v_1^8 - 143360 m_1 r^2 (\mathbf{j}_1 \cdot \mathbf{v}_1) v_1^8 + 21280 \gamma m_2 r^2 (\mathbf{j}_1 \cdot \mathbf{v}_1) v_1^8 \\
& \quad - 20720 m_2 r^2 (\mathbf{j}_1 \cdot \mathbf{v}_1) v_1^8 + 327680 m_1 r^2 \log(\tilde{r}) (\mathbf{j}_1 \cdot \mathbf{v}_1) v_1^8 + 42560 m_2 r^2 \log(\tilde{r}) (\mathbf{j}_1 \cdot \mathbf{v}_1) v_1^8 + 49152 \gamma m_1 r^2 (\mathbf{j}_2 \cdot \mathbf{v}_2) v_1^8 \\
& \quad + 8192 m_1 r^2 (\mathbf{j}_2 \cdot \mathbf{v}_2) v_1^8 + 14400 \gamma m_2 r^2 (\mathbf{j}_2 \cdot \mathbf{v}_2) v_1^8 + 76680 m_2 r^2 (\mathbf{j}_2 \cdot \mathbf{v}_2) v_1^8 + 98304 m_1 r^2 \log(\tilde{r}) (\mathbf{j}_2 \cdot \mathbf{v}_2) v_1^8 \\
& \quad + 28800 m_2 r^2 \log(\tilde{r}) (\mathbf{j}_2 \cdot \mathbf{v}_2) v_1^8 - 172032 m_1 v_2^2 (\mathbf{v}_1 \cdot \mathbf{v}_2) v_1^8 - 245040 m_2 v_2^2 (\mathbf{v}_1 \cdot \mathbf{v}_2) v_1^8 + 122880 m_1 r (\mathbf{a}_2 \cdot \mathbf{v}_2) (\mathbf{v}_1 \cdot \hat{\mathbf{r}}) v_1^8 \\
& \quad + 4320 m_2 r (\mathbf{a}_2 \cdot \mathbf{v}_2) (\mathbf{v}_1 \cdot \hat{\mathbf{r}}) v_1^8 - 196608 m_1 r (\mathbf{a}_2 \cdot \mathbf{v}_2) (\mathbf{v}_2 \cdot \hat{\mathbf{r}}) v_1^8 - 154800 m_2 r (\mathbf{a}_2 \cdot \mathbf{v}_2) (\mathbf{v}_2 \cdot \hat{\mathbf{r}}) v_1^8 \\
& \quad + 110592 m_1 v_2^2 (\mathbf{v}_1 \cdot \hat{\mathbf{r}}) (\mathbf{v}_2 \cdot \hat{\mathbf{r}}) v_1^8 + 38160 m_2 v_2^2 (\mathbf{v}_1 \cdot \hat{\mathbf{r}}) (\mathbf{v}_2 \cdot \hat{\mathbf{r}}) v_1^8 + 240896 m_1 v_2^6 v_1^6 + 240896 m_2 v_2^6 v_1^6 \\
& \quad + 253952 a_1^2 m_1 r^2 v_2^2 v_1^6 + 4096 a_2^2 m_1 r^2 v_2^2 v_1^6 + 196608 a_1^2 \gamma m_1 r^2 v_2^2 v_1^6 + 57344 a_2^2 \gamma m_1 r^2 v_2^2 v_1^6 - 17280 a_1^2 m_2 r^2 v_2^2 v_1^6 \\
& \quad + 187904 a_2^2 m_2 r^2 v_2^2 v_1^6 + 57600 a_1^2 \gamma m_2 r^2 v_2^2 v_1^6 + 45056 a_2^2 \gamma m_2 r^2 v_2^2 v_1^6 + 114688 \gamma m_1 r^2 (\mathbf{a}_2 \cdot \mathbf{v}_2)^2 v_1^6 \\
& \quad + 8192 m_1 r^2 (\mathbf{a}_2 \cdot \mathbf{v}_2)^2 v_1^6 + 52096 \gamma m_2 r^2 (\mathbf{a}_2 \cdot \mathbf{v}_2)^2 v_1^6 + 152320 m_2 r^2 (\mathbf{a}_2 \cdot \mathbf{v}_2)^2 v_1^6 + 229376 m_1 r^2 \log(\tilde{r}) (\mathbf{a}_2 \cdot \mathbf{v}_2)^2 v_1^6 \\
& \quad + 104192 m_2 r^2 \log(\tilde{r}) (\mathbf{a}_2 \cdot \mathbf{v}_2)^2 v_1^6 - 121856 m_1 v_2^4 (\mathbf{v}_1 \cdot \hat{\mathbf{r}})^2 v_1^6 - 41216 m_2 v_2^4 (\mathbf{v}_1 \cdot \hat{\mathbf{r}})^2 v_1^6 - 52736 m_1 v_2^4 (\mathbf{v}_2 \cdot \hat{\mathbf{r}})^2 v_1^6 \\
& \quad - 129536 m_2 v_2^4 (\mathbf{v}_2 \cdot \hat{\mathbf{r}})^2 v_1^6 + 393216 a_1^2 m_1 r^2 v_2^2 \log(\tilde{r}) v_1^6 + 114688 a_2^2 m_1 r^2 v_2^2 \log(\tilde{r}) v_1^6 + 115200 a_1^2 m_2 r^2 v_2^2 \log(\tilde{r}) v_1^6 \\
& \quad + 90112 a_2^2 m_2 r^2 v_2^2 \log(\tilde{r}) v_1^6 - 28672 m_1 r v_2^4 (\mathbf{a}_2 \cdot \hat{\mathbf{r}}) v_1^6 - 115456 m_2 r v_2^4 (\mathbf{a}_2 \cdot \hat{\mathbf{r}}) v_1^6 + 196608 \gamma m_1 r^2 v_2^2 (\mathbf{j}_1 \cdot \mathbf{v}_1) v_1^6 \\
& \quad + \dots) \\
& - \frac{G m_1 m_2}{2048 r} (891 v_1^{14} + 574 v_2^2 v_1^{12} - 133 (\mathbf{v}_2 \cdot \hat{\mathbf{r}})^2 v_1^{12} - 133 r (\mathbf{a}_2 \cdot \hat{\mathbf{r}}) v_1^{12} - 1365 (\mathbf{v}_1 \cdot \mathbf{v}_2) v_1^{12} - 483 (\mathbf{v}_1 \cdot \hat{\mathbf{r}}) (\mathbf{v}_2 \cdot \hat{\mathbf{r}}) v_1^{12} + 596 v_2^4 v_1^{10} \\
& \quad + 450 a_2^2 r^2 v_1^{10} + 266 (\mathbf{v}_1 \cdot \mathbf{v}_2)^2 v_1^{10} - 133 v_2^2 (\mathbf{v}_1 \cdot \hat{\mathbf{r}})^2 v_1^{10} + 133 r (\mathbf{a}_2 \cdot \hat{\mathbf{r}}) (\mathbf{v}_1 \cdot \hat{\mathbf{r}})^2 v_1^{10} - 225 v_2^2 (\mathbf{v}_2 \cdot \hat{\mathbf{r}})^2 v_1^{10} \\
& \quad + 399 (\mathbf{v}_1 \cdot \hat{\mathbf{r}})^2 (\mathbf{v}_2 \cdot \hat{\mathbf{r}})^2 v_1^{10} - 133 r (\mathbf{a}_1 \cdot \hat{\mathbf{r}}) (\mathbf{v}_2 \cdot \hat{\mathbf{r}})^2 v_1^{10} + 133 r v_2^2 (\mathbf{a}_1 \cdot \hat{\mathbf{r}}) v_1^{10} - 225 r v_2^2 (\mathbf{a}_2 \cdot \hat{\mathbf{r}}) v_1^{10} \\
& \quad - 133 r^2 (\mathbf{a}_1 \cdot \hat{\mathbf{r}}) (\mathbf{a}_2 \cdot \hat{\mathbf{r}}) v_1^{10} + 450 r^2 (\mathbf{j}_2 \cdot \mathbf{v}_2) v_1^{10} - 210 v_2^2 (\mathbf{v}_1 \cdot \mathbf{v}_2) v_1^{10} + 742 r (\mathbf{a}_2 \cdot \mathbf{v}_1) (\mathbf{v}_1 \cdot \hat{\mathbf{r}}) v_1^{10} \\
& \quad - 1596 r (\mathbf{a}_2 \cdot \mathbf{v}_2) (\mathbf{v}_1 \cdot \hat{\mathbf{r}}) v_1^{10} - 742 r (\mathbf{a}_1 \cdot \mathbf{v}_2) (\mathbf{v}_2 \cdot \hat{\mathbf{r}}) v_1^{10} - 900 r (\mathbf{a}_2 \cdot \mathbf{v}_2) (\mathbf{v}_2 \cdot \hat{\mathbf{r}}) v_1^{10} - 798 v_2^2 (\mathbf{v}_1 \cdot \hat{\mathbf{r}}) (\mathbf{v}_2 \cdot \hat{\mathbf{r}}) v_1^{10} \\
& \quad + 476 (\mathbf{v}_1 \cdot \mathbf{v}_2) (\mathbf{v}_1 \cdot \hat{\mathbf{r}}) (\mathbf{v}_2 \cdot \hat{\mathbf{r}}) v_1^{10} + 499 v_2^6 v_1^8 + 1330 a_1^2 r^2 v_2^2 v_1^8 + 616 a_2^2 r^2 v_2^2 v_1^8 + 1232 r^2 (\mathbf{a}_2 \cdot \mathbf{v}_2)^2 v_1^8 \\
& \quad + \dots) \\
& + \mathcal{O}(L v^{16}) ;
\end{aligned} \tag{4.59}$$

Furthermore the 7PN contributions also comprise the $\frac{1}{\epsilon}$ ($d = 3 + \epsilon$) divergent piece:

$$\begin{aligned}
\Delta V_{7PN,subset,div} = & \\
& \frac{G^2 m_1 m_2}{192} \frac{1}{\epsilon} (24 (\mathbf{a}_1 \cdot \mathbf{v}_1) (\mathbf{a}_2 \cdot \mathbf{v}_2) (m_1 (256 v_1^6 + 224 v_1^4 v_2^2 + 176 v_1^2 v_2^4 + 75 v_2^6) + m_2 (75 v_1^6 + 176 v_1^4 v_2^2 + 224 v_1^2 v_2^4 + 256 v_2^6)) \\
& \quad + 4 (\mathbf{a}_1 \cdot \mathbf{v}_1)^2 (m_1 (7504 v_1^6 + 6552 v_1^4 v_2^2 + 1806 v_1^2 v_2^4 + 407 v_2^6) + 2 m_2 (665 v_1^6 + 1350 v_1^4 v_2^2 + 1056 v_1^2 v_2^4 + 448 v_2^6)) \\
& \quad + 4 (\mathbf{a}_2 \cdot \mathbf{v}_2)^2 (2 m_1 (448 v_1^6 + 1056 v_1^4 v_2^2 + 1350 v_1^2 v_2^4 + 665 v_2^6) + m_2 (407 v_1^6 + 1806 v_1^4 v_2^2 + 6552 v_1^2 v_2^4 + 7504 v_2^6)) \\
& \quad + 5120 m_1 v_1^8 (\mathbf{j}_1 \cdot \mathbf{v}_1) + 6144 m_1 v_1^6 v_2^2 (\mathbf{j}_1 \cdot \mathbf{v}_1) + 2688 m_1 v_1^4 v_2^4 (\mathbf{j}_1 \cdot \mathbf{v}_1) + 1408 m_1 v_1^2 v_2^6 (\mathbf{j}_1 \cdot \mathbf{v}_1) + 450 m_1 v_2^8 (\mathbf{j}_1 \cdot \mathbf{v}_1) \\
& \quad + 665 m_2 v_1^8 (\mathbf{j}_1 \cdot \mathbf{v}_1) + 1800 m_2 v_1^6 v_2^2 (\mathbf{j}_1 \cdot \mathbf{v}_1) + 2112 m_2 v_1^4 v_2^4 (\mathbf{j}_1 \cdot \mathbf{v}_1) + 1792 m_2 v_1^2 v_2^6 (\mathbf{j}_1 \cdot \mathbf{v}_1) + 1536 m_2 v_2^8 (\mathbf{j}_1 \cdot \mathbf{v}_1) \\
& \quad + 1536 m_1 v_1^8 (\mathbf{j}_2 \cdot \mathbf{v}_2) + 1792 m_1 v_1^6 v_2^2 (\mathbf{j}_2 \cdot \mathbf{v}_2) + 2112 m_1 v_1^4 v_2^4 (\mathbf{j}_2 \cdot \mathbf{v}_2) + 1800 m_1 v_1^2 v_2^6 (\mathbf{j}_2 \cdot \mathbf{v}_2) + 665 m_1 v_2^8 (\mathbf{j}_2 \cdot \mathbf{v}_2) \\
& \quad + 450 m_2 v_1^8 (\mathbf{j}_2 \cdot \mathbf{v}_2) + 1408 m_2 v_1^6 v_2^2 (\mathbf{j}_2 \cdot \mathbf{v}_2) + 2688 m_2 v_1^4 v_2^4 (\mathbf{j}_2 \cdot \mathbf{v}_2) + 6144 m_2 v_1^2 v_2^6 (\mathbf{j}_2 \cdot \mathbf{v}_2) + 5120 m_2 v_2^8 (\mathbf{j}_2 \cdot \mathbf{v}_2) \\
& \quad + 5120 a_1^2 m_1 v_1^8 + 6144 a_1^2 m_1 v_1^6 v_2^2 + 2688 a_1^2 m_1 v_1^4 v_2^4 + 1408 a_1^2 m_1 v_1^2 v_2^6 + 450 a_1^2 m_1 v_2^8 + 665 a_1^2 m_2 v_1^8 + 1800 a_1^2 m_2 v_1^6 v_2^2 \\
& \quad + 2112 a_1^2 m_2 v_1^4 v_2^4 + 1792 a_1^2 m_2 v_1^2 v_2^6 + 1536 a_1^2 m_2 v_2^8 + 1536 a_2^2 m_1 v_1^8 + 1792 a_2^2 m_1 v_1^6 v_2^2 + 2112 a_2^2 m_1 v_1^4 v_2^4 \\
& \quad + 1800 a_2^2 m_1 v_1^2 v_2^6 + 665 a_2^2 m_1 v_2^8 + 450 a_2^2 m_2 v_1^8 + 1408 a_2^2 m_2 v_1^6 v_2^2 + 2688 a_2^2 m_2 v_1^4 v_2^4 + 6144 a_2^2 m_2 v_1^2 v_2^6 + 5120 a_2^2 m_2 v_2^8) + \mathcal{O}(L v^{16}) \\
& \tag{4.60}
\end{aligned}$$

which must be properly renormalized via a redefinition or shift of the worldline parameters [43, 57, 213, 271].

Furthermore below, as an example, we present the contributions of three diagrams which actually first contribute at 7PN. In these results appear also higher derivatives of the position, hence we introduced: the jerk \mathbf{j} , which is the time derivative of the acceleration, so the third time derivative of the position $\mathbf{j}_a(t) \equiv \frac{d^3 \mathbf{x}_a}{dt^3}(t)$; the snap \mathbf{s} , which is the time derivative of the jerk, so the fourth time derivative of the position $\mathbf{s}_a(t) \equiv \frac{d^4 \mathbf{x}_a}{dt^4}(t)$; and finally the crackle \mathbf{c} , which is the time derivative of the snap, so the fifth time derivative of the position $\mathbf{c}_a(t) \equiv \frac{d^5 \mathbf{x}_a}{dt^5}(t)$. Additionally, recalling section 4.1.2, we evaluated the symmetry factor of diagram (4.61a) to be $\frac{2 \cdot 2}{2! 2!}$, of diagram (4.61b) to be $\frac{2}{2! 2!}$, of diagram (4.61c) to be $\frac{2}{2! 2!}$. Then the explicit expressions of these diagrams are:

$\mathcal{A}_{(7a)} =$

$$\begin{aligned}
&= -i \int dt \left[-\frac{G^2 m_1 m_2}{6r^2} (v_1^2 v_2^2 - (\mathbf{v}_1 \cdot \mathbf{v}_2)^2) (9m_1 v_2^2 v_1^6 - 9m_1 (\mathbf{v}_1 \cdot \mathbf{v}_2)^2 v_1^4 - 18m_1 v_2^2 (\mathbf{v}_1 \cdot \hat{\mathbf{r}})^2 v_1^4 + 18m_1 r v_2^2 (\mathbf{a}_1 \cdot \hat{\mathbf{r}}) v_1^4 \right. \\
&\quad + 9m_2 v_2^6 v_1^2 + 6j_2^2 m_2 r^4 v_1^2 + 9m_1 v_2^2 (\mathbf{v}_1 \cdot \hat{\mathbf{r}})^4 v_1^2 + 9m_2 v_2^2 (\mathbf{v}_2 \cdot \hat{\mathbf{r}})^4 v_1^2 + 24m_2 r (\mathbf{a}_2 \cdot \mathbf{v}_2) (\mathbf{v}_2 \cdot \hat{\mathbf{r}})^3 v_1^2 + 45a_1^2 m_1 r^2 v_2^2 v_1^2 \\
&\quad + 45a_2^2 m_2 r^2 v_2^2 v_1^2 - 36m_1 r^2 (\mathbf{a}_1 \cdot \mathbf{v}_2)^2 v_1^2 + 9m_1 r^2 v_2^2 (\mathbf{a}_1 \cdot \hat{\mathbf{r}})^2 v_1^2 + 72m_2 r^2 (\mathbf{a}_2 \cdot \mathbf{v}_2)^2 v_1^2 + 9m_2 r^2 v_2^2 (\mathbf{a}_2 \cdot \hat{\mathbf{r}})^2 v_1^2 \\
&\quad - 18m_1 r (\mathbf{a}_1 \cdot \hat{\mathbf{r}}) (\mathbf{v}_1 \cdot \mathbf{v}_2)^2 v_1^2 + 18m_1 (\mathbf{v}_1 \cdot \mathbf{v}_2)^2 (\mathbf{v}_1 \cdot \hat{\mathbf{r}})^2 v_1^2 - 18m_1 r v_2^2 (\mathbf{a}_1 \cdot \hat{\mathbf{r}}) (\mathbf{v}_1 \cdot \hat{\mathbf{r}})^2 v_1^2 - 18m_2 v_2^4 (\mathbf{v}_2 \cdot \hat{\mathbf{r}})^2 v_1^2 \\
&\quad + 36a_2^2 m_2 r^2 (\mathbf{v}_2 \cdot \hat{\mathbf{r}})^2 v_1^2 + 18m_2 r v_2^2 (\mathbf{a}_2 \cdot \hat{\mathbf{r}}) (\mathbf{v}_2 \cdot \hat{\mathbf{r}})^2 v_1^2 + 36m_2 r^2 (\mathbf{j}_2 \cdot \mathbf{v}_2) (\mathbf{v}_2 \cdot \hat{\mathbf{r}})^2 v_1^2 + 8m_2 r^4 (\mathbf{a}_2 \cdot \mathbf{s}_2) v_1^2 \\
&\quad - 18m_2 r v_2^4 (\mathbf{a}_2 \cdot \hat{\mathbf{r}}) v_1^2 - 36a_2^2 m_2 r^3 (\mathbf{a}_2 \cdot \hat{\mathbf{r}}) v_1^2 + 2m_2 r^4 (\mathbf{c}_2 \cdot \mathbf{v}_2) v_1^2 + 48m_1 r^2 v_2^2 (\mathbf{j}_1 \cdot \mathbf{v}_1) v_1^2 + 48m_2 r^2 v_2^2 (\mathbf{j}_2 \cdot \mathbf{v}_2) v_1^2 \\
&\quad - 36m_2 r^3 (\mathbf{a}_2 \cdot \hat{\mathbf{r}}) (\mathbf{j}_2 \cdot \mathbf{v}_2) v_1^2 - 24m_2 r^3 (\mathbf{a}_2 \cdot \mathbf{v}_2) (\mathbf{j}_2 \cdot \hat{\mathbf{r}}) v_1^2 + 3m_1 r^3 v_2^2 (\mathbf{s}_1 \cdot \hat{\mathbf{r}}) v_1^2 - 3m_2 r^3 v_2^2 (\mathbf{s}_2 \cdot \hat{\mathbf{r}}) v_1^2 \\
&\quad - 36m_1 r^2 (\mathbf{j}_1 \cdot \mathbf{v}_2) (\mathbf{v}_1 \cdot \mathbf{v}_2) v_1^2 + 12m_1 r^2 v_2^2 (\mathbf{j}_1 \cdot \hat{\mathbf{r}}) (\mathbf{v}_1 \cdot \hat{\mathbf{r}}) v_1^2 - 72m_1 r (\mathbf{a}_1 \cdot \mathbf{v}_2) (\mathbf{v}_1 \cdot \mathbf{v}_2) (\mathbf{v}_1 \cdot \hat{\mathbf{r}}) v_1^2 \\
&\quad - 72m_2 r^3 (\mathbf{a}_2 \cdot \mathbf{j}_2) (\mathbf{v}_2 \cdot \hat{\mathbf{r}}) v_1^2 - 108m_2 r v_2^2 (\mathbf{a}_2 \cdot \mathbf{v}_2) (\mathbf{v}_2 \cdot \hat{\mathbf{r}}) v_1^2 + 72m_2 r^2 (\mathbf{a}_2 \cdot \mathbf{v}_2) (\mathbf{a}_2 \cdot \hat{\mathbf{r}}) (\mathbf{v}_2 \cdot \hat{\mathbf{r}}) v_1^2 \\
&\quad + 12m_2 r^2 v_2^2 (\mathbf{j}_2 \cdot \hat{\mathbf{r}}) (\mathbf{v}_2 \cdot \hat{\mathbf{r}}) v_1^2 - 24m_2 r^3 (\mathbf{s}_2 \cdot \mathbf{v}_2) (\mathbf{v}_2 \cdot \hat{\mathbf{r}}) v_1^2 - 9m_1 (\mathbf{v}_1 \cdot \mathbf{v}_2)^2 (\mathbf{v}_1 \cdot \hat{\mathbf{r}})^4 - 9m_2 (\mathbf{v}_1 \cdot \mathbf{v}_2)^2 (\mathbf{v}_2 \cdot \hat{\mathbf{r}})^4 \\
&\quad + 24m_1 r (\mathbf{a}_1 \cdot \mathbf{v}_2) (\mathbf{v}_1 \cdot \mathbf{v}_2) (\mathbf{v}_1 \cdot \hat{\mathbf{r}})^3 - 24m_2 r (\mathbf{a}_2 \cdot \mathbf{v}_1) (\mathbf{v}_1 \cdot \mathbf{v}_2) (\mathbf{v}_2 \cdot \hat{\mathbf{r}})^3 + 6j_1^2 m_1 r^4 v_2^2 + 72m_1 r^2 v_2^2 (\mathbf{a}_1 \cdot \mathbf{v}_1)^2 \\
&\quad - 36m_2 r^2 v_2^2 (\mathbf{a}_2 \cdot \mathbf{v}_1)^2 - 6m_1 r^4 (\mathbf{j}_1 \cdot \mathbf{v}_2)^2 - 6m_2 r^4 (\mathbf{j}_2 \cdot \mathbf{v}_1)^2 - 9m_2 v_2^4 (\mathbf{v}_1 \cdot \mathbf{v}_2)^2 - 9a_1^2 m_1 r^2 (\mathbf{v}_1 \cdot \mathbf{v}_2)^2 \\
&\quad - 9a_2^2 m_2 r^2 (\mathbf{v}_1 \cdot \mathbf{v}_2)^2 - 9m_1 r^2 (\mathbf{a}_1 \cdot \hat{\mathbf{r}})^2 (\mathbf{v}_1 \cdot \mathbf{v}_2)^2 - 9m_2 r^2 (\mathbf{a}_2 \cdot \hat{\mathbf{r}})^2 (\mathbf{v}_1 \cdot \mathbf{v}_2)^2 + 18m_2 r v_2^2 (\mathbf{a}_2 \cdot \hat{\mathbf{r}}) (\mathbf{v}_1 \cdot \mathbf{v}_2)^2 \\
&\quad - 12m_1 r^2 (\mathbf{j}_1 \cdot \mathbf{v}_1) (\mathbf{v}_1 \cdot \mathbf{v}_2)^2 - 12m_2 r^2 (\mathbf{j}_2 \cdot \mathbf{v}_2) (\mathbf{v}_1 \cdot \mathbf{v}_2)^2 - 3m_1 r^3 (\mathbf{s}_1 \cdot \hat{\mathbf{r}}) (\mathbf{v}_1 \cdot \mathbf{v}_2)^2 + 3m_2 r^3 (\mathbf{s}_2 \cdot \hat{\mathbf{r}}) (\mathbf{v}_1 \cdot \mathbf{v}_2)^2 \\
&\quad + 36a_1^2 m_1 r^2 v_2^2 (\mathbf{v}_1 \cdot \hat{\mathbf{r}})^2 - 36m_1 r^2 (\mathbf{a}_1 \cdot \mathbf{v}_2)^2 (\mathbf{v}_1 \cdot \hat{\mathbf{r}})^2 + 18m_1 r (\mathbf{a}_1 \cdot \hat{\mathbf{r}}) (\mathbf{v}_1 \cdot \mathbf{v}_2)^2 (\mathbf{v}_1 \cdot \hat{\mathbf{r}})^2 \\
&\quad + 36m_1 r^2 v_2^2 (\mathbf{j}_1 \cdot \mathbf{v}_1) (\mathbf{v}_1 \cdot \hat{\mathbf{r}})^2 - 36m_1 r^2 (\mathbf{j}_1 \cdot \mathbf{v}_2) (\mathbf{v}_1 \cdot \mathbf{v}_2) (\mathbf{v}_1 \cdot \hat{\mathbf{r}})^2 - 36m_2 r^2 (\mathbf{a}_2 \cdot \mathbf{v}_1)^2 (\mathbf{v}_2 \cdot \hat{\mathbf{r}})^2 \\
&\quad + 18m_2 v_2^2 (\mathbf{v}_1 \cdot \mathbf{v}_2)^2 (\mathbf{v}_2 \cdot \hat{\mathbf{r}})^2 - 18m_2 r (\mathbf{a}_2 \cdot \hat{\mathbf{r}}) (\mathbf{v}_1 \cdot \mathbf{v}_2)^2 (\mathbf{v}_2 \cdot \hat{\mathbf{r}})^2 - 36m_2 r^2 (\mathbf{j}_2 \cdot \mathbf{v}_1) (\mathbf{v}_1 \cdot \mathbf{v}_2) (\mathbf{v}_2 \cdot \hat{\mathbf{r}})^2 \\
&\quad + 8m_1 r^4 v_2^2 (\mathbf{a}_1 \cdot \mathbf{s}_1) + 36a_1^2 m_1 r^3 v_2^2 (\mathbf{a}_1 \cdot \hat{\mathbf{r}}) - 36m_1 r^3 (\mathbf{a}_1 \cdot \mathbf{v}_2)^2 (\mathbf{a}_1 \cdot \hat{\mathbf{r}}) + 36m_2 r^3 (\mathbf{a}_2 \cdot \mathbf{v}_1)^2 (\mathbf{a}_2 \cdot \hat{\mathbf{r}}) \\
&\quad + 2m_1 r^4 v_2^2 (\mathbf{c}_1 \cdot \mathbf{v}_1) + 36m_1 r^3 v_2^2 (\mathbf{a}_1 \cdot \hat{\mathbf{r}}) (\mathbf{j}_1 \cdot \mathbf{v}_1) - 8m_1 r^4 (\mathbf{a}_1 \cdot \mathbf{v}_2) (\mathbf{s}_1 \cdot \mathbf{v}_2) - 8m_2 r^4 (\mathbf{a}_2 \cdot \mathbf{v}_1) (\mathbf{s}_2 \cdot \mathbf{v}_1) \\
&\quad - 72m_2 r^2 (\mathbf{a}_2 \cdot \mathbf{v}_1) (\mathbf{a}_2 \cdot \mathbf{v}_2) (\mathbf{v}_1 \cdot \mathbf{v}_2) - 2m_1 r^4 (\mathbf{c}_1 \cdot \mathbf{v}_2) (\mathbf{v}_1 \cdot \mathbf{v}_2) - 2m_2 r^4 (\mathbf{c}_2 \cdot \mathbf{v}_1) (\mathbf{v}_1 \cdot \mathbf{v}_2) \\
&\quad - 36m_1 r^3 (\mathbf{a}_1 \cdot \hat{\mathbf{r}}) (\mathbf{j}_1 \cdot \mathbf{v}_2) (\mathbf{v}_1 \cdot \mathbf{v}_2) - 24m_1 r^3 (\mathbf{a}_1 \cdot \mathbf{v}_2) (\mathbf{j}_1 \cdot \hat{\mathbf{r}}) (\mathbf{v}_1 \cdot \mathbf{v}_2) - 36m_2 r^2 v_2^2 (\mathbf{j}_2 \cdot \mathbf{v}_1) (\mathbf{v}_1 \cdot \mathbf{v}_2) \\
&\quad + 36m_2 r^3 (\mathbf{a}_2 \cdot \hat{\mathbf{r}}) (\mathbf{j}_2 \cdot \mathbf{v}_1) (\mathbf{v}_1 \cdot \mathbf{v}_2) + 24m_2 r^3 (\mathbf{a}_2 \cdot \mathbf{v}_1) (\mathbf{j}_2 \cdot \hat{\mathbf{r}}) (\mathbf{v}_1 \cdot \mathbf{v}_2) - 12m_1 r^2 (\mathbf{j}_1 \cdot \hat{\mathbf{r}}) (\mathbf{v}_1 \cdot \mathbf{v}_2)^2 (\mathbf{v}_1 \cdot \hat{\mathbf{r}}) \\
&\quad + 72m_1 r^3 v_2^2 (\mathbf{a}_1 \cdot \mathbf{j}_1) (\mathbf{v}_1 \cdot \hat{\mathbf{r}}) - 72m_1 r^3 (\mathbf{a}_1 \cdot \mathbf{v}_2) (\mathbf{j}_1 \cdot \mathbf{v}_2) (\mathbf{v}_1 \cdot \hat{\mathbf{r}}) + 24m_1 r^3 v_2^2 (\mathbf{s}_1 \cdot \mathbf{v}_1) (\mathbf{v}_1 \cdot \hat{\mathbf{r}}) \\
&\quad - 72m_1 r^2 (\mathbf{a}_1 \cdot \mathbf{v}_2) (\mathbf{a}_1 \cdot \hat{\mathbf{r}}) (\mathbf{v}_1 \cdot \mathbf{v}_2) (\mathbf{v}_1 \cdot \hat{\mathbf{r}}) - 24m_1 r^3 (\mathbf{s}_1 \cdot \mathbf{v}_2) (\mathbf{v}_1 \cdot \mathbf{v}_2) (\mathbf{v}_1 \cdot \hat{\mathbf{r}}) \\
&\quad + 12m_1 r (\mathbf{a}_1 \cdot \mathbf{v}_1) (2r^2 (\mathbf{j}_1 \cdot \hat{\mathbf{r}}) v_2^2 - 6r (\mathbf{a}_1 \cdot \mathbf{v}_2) (\mathbf{v}_1 \cdot \mathbf{v}_2) + (\mathbf{v}_1 \cdot \hat{\mathbf{r}}) (6r (\mathbf{a}_1 \cdot \hat{\mathbf{r}}) v_2^2 + (9v_1^2 - 2(\mathbf{v}_1 \cdot \hat{\mathbf{r}})^2) v_2^2 - 3(\mathbf{v}_1 \cdot \mathbf{v}_2)^2)) \\
&\quad + 36m_2 r (\mathbf{a}_2 \cdot \mathbf{v}_2) (\mathbf{v}_1 \cdot \mathbf{v}_2)^2 (\mathbf{v}_2 \cdot \hat{\mathbf{r}}) - 12m_2 r^2 (\mathbf{j}_2 \cdot \hat{\mathbf{r}}) (\mathbf{v}_1 \cdot \mathbf{v}_2)^2 (\mathbf{v}_2 \cdot \hat{\mathbf{r}}) + 72m_2 r^3 (\mathbf{a}_2 \cdot \mathbf{v}_1) (\mathbf{j}_2 \cdot \mathbf{v}_1) (\mathbf{v}_2 \cdot \hat{\mathbf{r}}) \\
&\quad + 72m_2 r v_2^2 (\mathbf{a}_2 \cdot \mathbf{v}_1) (\mathbf{v}_1 \cdot \mathbf{v}_2) (\mathbf{v}_2 \cdot \hat{\mathbf{r}}) - 72m_2 r^2 (\mathbf{a}_2 \cdot \mathbf{v}_1) (\mathbf{a}_2 \cdot \hat{\mathbf{r}}) (\mathbf{v}_1 \cdot \mathbf{v}_2) (\mathbf{v}_2 \cdot \hat{\mathbf{r}}) \\
&\quad \left. + 24m_2 r^3 (\mathbf{s}_2 \cdot \mathbf{v}_1) (\mathbf{v}_1 \cdot \mathbf{v}_2) (\mathbf{v}_2 \cdot \hat{\mathbf{r}}) \right] + \mathcal{O}(L v^{16})
\end{aligned} \tag{4.61a}$$

$$\mathcal{A}_{(7c)} = \begin{array}{c} \circ \\ \text{---} A \text{---} \\ \text{---} \sigma \text{---} \\ \text{---} \sigma \text{---} \\ \circ \quad \circ \end{array} = -i \int dt \left[\frac{24G^3 m_1 m_2}{r^3} (m_1^2 + m_2^2) (\mathbf{v}_1 \cdot \mathbf{v}_2) ((\mathbf{v}_1 \cdot \mathbf{v}_2)^2 - v_1^2 v_2^2)^2 \right] + \mathcal{O}(L v^{16}) \quad (4.61c)$$

These results, while being extremely partial (since for example reference [65] evaluated about 190000 diagrams already at 5PN order) corroborate the strength of this effective field theory and diagrammatic approach to the computation of the post-Newtonian corrections: the possibility to build upon many advanced multi-loop techniques (and computational packages) developed first in particle physics, and the way these computations can be made systematic, allow to obtain results at really high perturbative order.

DISSIPATIVE RADIATION CORRECTIONS

In this chapter we're interested in computing the leading order dissipative contributions to the binary dynamics, so in practice the leading order contributions due to the far zone effective theory, which we presented in section 3.2.4; see also references [43, 202, 203, 206].

Let us notice that this leading order dissipative contribution is actually of order 2.5PN with respect to the Newtonian potential in the equation of motion [36]: therefore sometimes the order of the dissipative contributions is evaluated with respect to this leading (2.5PN) order dissipative contribution; this is then their *relative* post-Newtonian order. With this notation then the radiation contributions that we'll evaluate in this chapter are a 0PN relative correction, and in fact they're needed to evaluate the *leading order* expression for observables. This is because, as we'll see in chapter 6, the evolution of the binary is effectively dictated by the ratio of conservative over dissipative contributions, i.e. the ratio of the binding energy over the power loss: we can then see that to evaluate the observables at v^{2n} precision we need both the n -PN conservative corrections and the n -PN relative (so $(2.5 + n)$ -PN) dissipative corrections.

In particular in section 5.1 we will evaluate the leading order expression for the power loss of the system; whereas in section 5.2 we will evaluate the gravitational field far away from the source employing the in-in formalism.

5.1 | Power loss in the far zone effective theory

In order to evaluate the power loss of the binary system via gravitational waves we recall section 3.2.5 where we presented the optical theorem: then using equation (3.83) it's possible to connect the power loss of the system to the imaginary part of the effective action $S_{eff}[\{x_a^\mu\}]$. The latter is then obtained by integrating out all the radiative degrees of freedom in the far zone action, as discussed in section 3.2.4.

Since, as we've just pointed out above, the leading order dissipative contribution is of order 2.5PN, i.e. $\mathcal{O}(Lv^5)$; recalling the scaling rules for the far zone theory from section 3.2.4 and proceeding almost analogously to the discussion of section 4.1, we find that to obtain the leading order expression for the power loss of the system via gravitational waves we have evaluate the vacuum diagrams shown in figure 5.1.

In appendix A.3 we have evaluated the Feynman rules for the far zone theory performing the matching procedure which we outlined in section 3.2.4, up to the accuracy needed to obtain all the contributions up to leading order ($\mathcal{O}(Lv^5)$) in the final diagram. In appendix A.1 we also obtained the expression for the propagators of the radiative modes.

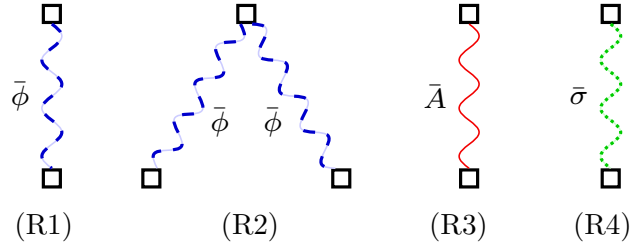


FIGURE 5.1 — Diagrams contributing to the power loss of the system at leading order.

In particular let us notice that in the far zone theory the radiation modes can be on-shell, $k^2 \sim 0$, therefore we cannot perform the perturbative expansion of the propagators which we employed in the conservative sector (chapter 4) to simplify their evaluation. Finally also the results regarding the power loss should be obtained using the in-in formalism, especially when computing higher order hereditary effects, yet for the precision which we're aiming for it will suffice to use the optical theorem [43, 213].

■ Diagram (R1)

To obtain the expression for the first diagram in figure 5.1 we recall the Feynman rule (A.91), which we obtained through a matching procedure, as explained in section 3.2.4. The propagator instead is given by (A.19). Furthermore the symmetry factor can be computed similarly to what we have presented in section 4.1. Then we find:

$$\begin{aligned}
 \mathcal{A}_{(R1)} = \bar{\phi} \uparrow^k &= \frac{1}{2} \int \frac{d^{d+1}k}{(2\pi)^{d+1}} \left(i \frac{1}{\Lambda} \int dt_1 e^{-ik^0 t_1} \left(-m + \frac{1}{2} k^i k^j M_{ij}(t_1) - E_N \right. \right. \\
 &\quad \left. \left. + \frac{1}{2} (k^0)^2 M(t_1) \right) + \mathcal{O}(G^{\frac{1}{2}} L v) \right) \left(\frac{1}{2 c_d k^2 + i\epsilon} \right) \left(i \frac{1}{\Lambda} \int dt_2 e^{ik^0 t_2} \left(-m \right. \right. \\
 &\quad \left. \left. + \frac{1}{2} k^k k^l M_{kl}(t_2) - E_N + \frac{1}{2} (k^0)^2 M(t_2) \right) + \mathcal{O}(G^{\frac{1}{2}} L v) \right) + \mathcal{O}(d-3),
 \end{aligned} \tag{5.1}$$

which also reads:

$$\begin{aligned}
 \mathcal{A}_{(R1)} = -i \frac{1}{2} \frac{1}{c_d \Lambda^2} \int dt_1 dt_2 \int \frac{dk^0}{(2\pi)} e^{-ik^0(t_1-t_2)} \int \frac{d^d \mathbf{k}}{(2\pi)^d} \left(-m + \frac{1}{2} k^i k^j M_{ij}(t_1) - E_N \right. \\
 \left. + \frac{1}{2} (k^0)^2 M(t_1) \right) \left(\frac{1}{k^2 + i\epsilon} \right) \\
 \times \left(-m + \frac{1}{2} k^k k^l M_{kl}(t_2) - E_N + \frac{1}{2} (k^0)^2 M(t_2) \right) + \mathcal{O}(L v^6) + \mathcal{O}(d-3).
 \end{aligned} \tag{5.2}$$

We can then perform the change of variables $t = t_1$ and $s = t_2 - t_1$, with unit Jacobian, to obtain:

$$\begin{aligned}
 \mathcal{A}_{(R1)} = -\frac{i}{4 c_d \Lambda^2} \int dt \int ds \int \frac{dk^0}{(2\pi)} e^{ik^0 s} \frac{1}{k^2 + i\epsilon} \int \frac{d^d \mathbf{k}}{(2\pi)^d} \left(-m + \frac{1}{2} k^i k^j M_{ij}(t) - E_N + \frac{1}{2} (k^0)^2 M(t) \right) \\
 \times \left(-m + \frac{1}{2} k^k k^l M_{kl}(t+s) - E_N + \frac{1}{2} (k^0)^2 M(t+s) \right) + \mathcal{O}(L v^6) + \mathcal{O}(d-3).
 \end{aligned} \tag{5.3}$$

In particular we can simplify this expression by noticing that it is proportional to the integrals (5.5) and (C.50): in particular this latter integral in practice exchanges the k^0 and k^i factors for

time derivatives acting on the source multipoles, which we defined in equations (3.67). Then, as discussed also therein in section 3.2.4, at the leading order in which we're working, some multipoles are conserved, i.e. their time derivative will be vanishing; in practice such multipoles (like the mass monopole) will not radiate and so will not contribute to the dynamics of the binary system. Then we can already drop such constant multipoles, such as the mass m and the Newtonian energy E_N of the system, to obtain:

$$\begin{aligned} \mathcal{A}_{(R1)} = & -\frac{i}{16 c_d \Lambda^2} \int dt \int ds \int \frac{dk^0}{(2\pi)} e^{ik^0 s} \frac{1}{k^2 + i\epsilon} \int \frac{d^d \mathbf{k}}{(2\pi)^d} (k^i k^j M_{ij}(t) + (k^0)^2 M(t)) \\ & \times \left(k^k k^l M_{kl}(t+s) + (k^0)^2 M(t+s) \right) + \mathcal{O}(L v^6) + \mathcal{O}(d-3). \end{aligned} \quad (5.4)$$

Let us then define the generic integral

$$I_R(d, a, b)^{i_1 \dots i_n} [f](t) = \int ds f(t+s) \int \frac{dk^0}{2\pi} e^{ik^0 s} \int \frac{d^d \mathbf{k}}{(2\pi)^d} \frac{k^{i_1} \dots k^{i_n} (k^0)^b}{k^2 + i\epsilon |\mathbf{k}|^{2a}}. \quad (5.5)$$

The first step in its evaluation requires the tensor decomposition of the integrand: nonetheless, because this integrand doesn't depend on any external vector, then the result of the integral can be proportional only to a (symmetrized) product of Kronecker delta δ^{ij} . From this fact it follows that if n is odd then the integral (5.5) vanishes identically, otherwise it's can be recast as:

$$\int \frac{d^d \mathbf{k}}{(2\pi)^d} \frac{1}{k^2 + i\epsilon} \frac{k^{i_1} \dots k^{i_n}}{|\mathbf{k}|^{2a}} = C(d, n) (\delta^{i_1 i_2} \dots \delta^{i_{n-1} i_n} + [\text{other pairings}]) \int \frac{d^d \mathbf{k}}{(2\pi)^d} \frac{1}{k^2 + i\epsilon} \frac{1}{|\mathbf{k}|^{2a-n}} \quad (5.6)$$

where with [other pairings] we mean the sum over the series of inequivalent terms given by product of $\frac{n}{2}$ Kronecker deltas; in practice this series can be obtained by considering as spatial indices of the Kronecker deltas all the possible unordered pairings one can construct from the set $\{i_1, \dots, i_n\}$ of spatial indices, i.e. for $n = 4$ it's given by $(\delta^{i_1 i_2} \delta^{i_3 i_4} + \delta^{i_1 i_3} \delta^{i_2 i_4} + \delta^{i_1 i_4} \delta^{i_2 i_3})$. The constant $C(d, n)$ instead follows from the tensor decomposition, and in particular by explicitly evaluating it we find that:

$$C(d, n) = \begin{cases} 0 & \text{if } n \text{ is odd} \\ 1 & \text{if } n = 0 \\ \frac{1}{d} & \text{if } n = 2 \\ \frac{1}{d(d+2)} & \text{if } n = 4 \\ \frac{1}{d(d+2)(d+4)} & \text{if } n = 6. \end{cases} \quad (5.7)$$

Recognizing integral (5.5) in equation (5.4), we can recast the latter as:

$$\begin{aligned} \mathcal{A}_{(R1)} = & -\frac{i}{16 c_d \Lambda^2} \int dt \int ds \int \frac{dk^0}{(2\pi)} e^{ik^0 s} \frac{1}{k^2 + i\epsilon} \int \frac{d^d \mathbf{k}}{(2\pi)^d} \left(M_{ij}(t) \frac{\delta^{ij} \delta^{kl} + \delta^{ik} \delta^{jl} + \delta^{il} \delta^{kj}}{15 |\mathbf{k}|^{-4}} M_{kl}(t+s) \right. \\ & \left. + \frac{2}{3} |\mathbf{k}|^2 (k^0)^2 M(t) M(t+s) + (k^0)^4 M(t) M(t+s) \right) + \mathcal{O}(L v^6) + \mathcal{O}(d-3). \end{aligned} \quad (5.8)$$

Let us now also introduce the traceless mass quadrupole moment $Q^{ij}(t)$, defined in $d = 3$ dimensions as:

$$Q^{ij}(t) \equiv M^{ij} - \frac{1}{3} M \delta^{ij} = M^{ij} - \frac{1}{3} (\delta_{kl} M^{kl}) \delta^{ij}, \quad (5.9)$$

for which indeed holds $\delta_{ij}Q^{ij} = 0$. Doing so we obtain the result:

$$\begin{aligned} \mathcal{A}_{(R1)} = & -\frac{i}{16 c_d \Lambda^2} \int dt \int ds \int \frac{d^d \mathbf{k}^0}{(2\pi)^d} e^{ik^0 s} \frac{1}{k^2 + i\epsilon} \int \frac{d^d \mathbf{k}}{(2\pi)^d} \left(\frac{2|\mathbf{k}|^4}{15} Q_{ij}(t) Q^{ij}(t+s) \right. \\ & \left. + \frac{|\mathbf{k}|^4}{9} M(t) M(t+s) + \frac{2}{3} |\mathbf{k}|^2 (k^0)^2 M(t) M(t+s) + (k^0)^4 M(t) M(t+s) \right) + \mathcal{O}(L v^6) + \mathcal{O}(d-3). \end{aligned} \quad (5.10)$$

■ Second $\bar{\phi}$ diagram

To evaluate the second diagram in figure 5.1 we have to recall the worldline- $\bar{\phi}$ radiation field Feynman rule (A.91) and the worldline- $\bar{\phi}^2$ Feynman rule (A.93). The expression reads:

$$\begin{aligned} \mathcal{A}_{(R2)} = & \begin{array}{c} \text{Diagram: A worldline with two vertices (squares) and two external legs (dashed lines) labeled } k_1 \text{ and } k_2. \text{ The worldline is labeled } \bar{\phi}. \end{array} \\ & = \frac{2}{2! 2!} \int_{k_1, k_2} \left(-i \frac{1}{\Lambda^2} \int dt_1 e^{-i(k_1^0 + k_2^0)t_1} m + \mathcal{O}(G L v^0) \right) \\ & \quad \times \left(i \frac{1}{\Lambda} \int dt_2 e^{ik_1^0 t_2} (-m) + \mathcal{O}(G^{\frac{1}{2}} L v^0) \right) \left(\frac{1}{2 c_d} \frac{i}{k_1^2 + i\epsilon} \right) \\ & \quad \times \left(i \frac{1}{\Lambda} \int dt_3 e^{ik_2^0 t_3} (-m) + \mathcal{O}(G^{\frac{1}{2}} L v^0) \right) \left(\frac{1}{2 c_d} \frac{i}{k_2^2 + i\epsilon} \right) \end{aligned} \quad (5.11)$$

If we perform the redefinition $t = t_1$, $s = t_2 - t_1$ and $u = t_3 - t_1$ we obtain:

$$\begin{aligned} \mathcal{A}_{(R2)} = & -i \frac{1}{8 c_d^2 \Lambda^4} \int dt m(t) \underbrace{\int ds m(t+s) \int \frac{d^d \mathbf{k}_1^0}{2\pi} e^{ik_1^0 s} \int \frac{d^d \mathbf{k}_1}{(2\pi)^d} \frac{1}{k_2^2 + i\epsilon}}_{=I_R(d,0,0)[m](t)} \\ & \quad \times \underbrace{\int du m(t+u) \int \frac{d^d \mathbf{k}_2^0}{2\pi} e^{ik_2^0 u} \int \frac{d^d \mathbf{k}_2}{(2\pi)^d} \frac{1}{k_1^2 + i\epsilon}}_{=I_R(d,0,0)[m](t)} + \mathcal{O}(L v^6) \quad (5.12) \\ & = 0 + \mathcal{O}(L v^6) ; \end{aligned}$$

where we recalled result (C.50), and we used again the fact that at leading order, in $d = 3$ dimension, the total mass of the binary system is constant in time, i.e. $\frac{dm}{dt} = 0$.

■ \bar{A} diagram

Using the worldline- \bar{A} Feynman rule, derived in equation (A.101), and the propagator given by (A.23), we obtain:

$$\begin{aligned} \mathcal{A}_{(R3)} = & \begin{array}{c} \text{Diagram: A worldline with two vertices (squares) labeled } i \text{ and } j. \text{ The worldline is labeled } \bar{A}. \text{ An external leg is labeled } k. \end{array} \\ & = \frac{1}{2} \int \frac{d^{d+1} k}{(2\pi)^{d+1}} \left(\frac{i}{\Lambda} \int dt_1 e^{-ik^0 t_1} \left(\frac{i}{2} \epsilon^{ikl} k_k L_l(t_1) + \frac{1}{2} k^0 M^{ik}(t_1) k_k \right) \right. \\ & \quad \left. + \mathcal{O}(G^{\frac{1}{2}} L v) \right) \left(-\frac{\delta_{ij}}{2} \frac{i}{k^2 + i\epsilon} \right) \\ & \quad \times \left(\frac{i}{\Lambda} \int dt_2 e^{ik^0 t_2} \left(-\frac{i}{2} \epsilon^{jmn} k_m L_n(t_2) + \frac{1}{2} k^0 M^{jm}(t_2) k_m \right) + \mathcal{O}(G^{\frac{1}{2}} L v) \right); \end{aligned} \quad (5.13)$$

where we point out that the Levi-Civita symbol ϵ^{ijk} defined, as in **Notation**, is taken to be in $d = 3$ spatial dimension; just like the source multipole we've using here.

We can perform the change of variables $t = t_1$ and $s = t_2 - t_1$, and as discussed before, drop the angular momentum L^m , since it is a conserved quantity as well at the leading order, to obtain:

$$\begin{aligned} \mathcal{A}_{(R3)} &= i \frac{\delta^{ij}}{16} \frac{1}{\Lambda^2} \int dt_1 dt_2 \int \frac{dk^0}{2\pi} e^{-ik^0(t_1-t_2)} \int \frac{d^d \mathbf{k}}{(2\pi)^d} \left(k^0 M_{ik}(t_1) k^k \right) \\ &\quad \times \left(k^0 M_{jm}(t_2) k^m \right) \left(\frac{1}{k^2 + i\epsilon} \right) + \mathcal{O}(L v^6) \\ &= i \frac{\delta^{ij}}{16} \frac{1}{\Lambda^2} \int dt \int ds \int \frac{dk^0}{2\pi} e^{ik^0 s} M_{ik}(t) M_{jm}(t+s) \int \frac{d^d \mathbf{k}}{(2\pi)^d} \frac{(k^0)^2 k^k k^m}{k^2 + i\epsilon} + \mathcal{O}(L v^6) \end{aligned} \quad (5.14)$$

Performing the tensor decomposition, and then substituting $Q_{ij} = M_{ij} - \frac{1}{3} \delta_{ij} M$:

$$\begin{aligned} \mathcal{A}_{(R3)} &= i \frac{\delta^{ij}}{16} \frac{1}{\Lambda^2} \int dt \int ds \int \frac{dk^0}{2\pi} e^{ik^0 s} M_{ik}(t) M_{jm}(t+s) \frac{\delta^{km}}{3} \int \frac{d^d \mathbf{k}}{(2\pi)^d} \frac{(k^0)^2 |\mathbf{k}|^2}{k^2 + i\epsilon} + \mathcal{O}(L v^6) \\ &= i \frac{1}{16} \frac{1}{\Lambda^2} \int dt \int ds \int \frac{dk^0}{2\pi} e^{ik^0 s} \int \frac{d^d \mathbf{k}}{(2\pi)^d} \\ &\quad \times \left(\frac{1}{3} Q^{ij}(t) Q_{ij}(t+s) + \frac{1}{9} M(t) M(t+s) \right) \frac{(k^0)^2 |\mathbf{k}|^2}{k^2 + i\epsilon} + \mathcal{O}(L v^6) \end{aligned} \quad (5.15)$$

■ $\bar{\sigma}$ diagram

In this case the Feynman rule for the worldline- $\bar{\sigma}$ interaction vertex that we need is given by (A.112), while the propagator is given by (A.30).

$$\begin{aligned} \mathcal{A}_{(R4)} &= \bar{\sigma} \begin{array}{c} \square \text{ } ij \\ \text{---} \uparrow k \\ \square \text{ } kl \end{array} = \frac{1}{2} \int \frac{d^{d+1} k}{(2\pi)^{d+1}} \left(-i \frac{1}{4\Lambda} \int dt_1 e^{-ik^0 t_1} (k^0)^2 M^{ij}(t_1) + \mathcal{O}\left(G^{\frac{1}{2}} L v\right) \right) \\ &\quad \times \left(\frac{1}{2} \frac{i}{k^2 + i\epsilon} \left(-\frac{2}{d-2} \delta_{ij} \delta_{kl} + \delta_{ik} \delta_{jl} + \delta_{il} \delta_{jk} \right) \right) \\ &\quad \times \left(-i \frac{1}{4\Lambda} \int dt_2 e^{ik^0 t_2} (-k^0)^2 M^{kl}(t_2) + \mathcal{O}\left(G^{\frac{1}{2}} L v\right) \right) + \mathcal{O}(d-3). \end{aligned} \quad (5.16)$$

which also reads

$$\begin{aligned} \mathcal{A}_{(R4)} &= -i \frac{1}{64\Lambda^2} \int dt_1 \int dt_2 \int \frac{dk^0}{2\pi} e^{-ik^0(t_1-t_2)} \int \frac{d^d \mathbf{k}}{(2\pi)^d} \left((k^0)^4 \frac{1}{k^2 + i\epsilon} \right. \\ &\quad \left. \times M^{ij}(t_1) (-2\delta_{ij} \delta_{kl} + \delta_{ik} \delta_{jl} + \delta_{il} \delta_{jk}) M^{kl}(t_2) \right) + \mathcal{O}(L v^6) \mathcal{O}(d-3). \end{aligned} \quad (5.17)$$

Performing again the substitution $M_{ij} = Q_{ij} + \frac{1}{3} \delta_{ij} M$, and the needed tensor algebra, we find:

$$\begin{aligned} \mathcal{A}_{(R4)} &= -i \frac{1}{16\Lambda^2} \int dt \int ds \int \frac{dk^0}{2\pi} e^{ik^0 s} \int \frac{d^d \mathbf{k}}{(2\pi)^d} \frac{(k^0)^4}{k^2 + i\epsilon} \\ &\quad \times \left(\frac{1}{2} Q^{ij}(t) Q_{ij}(t+s) - \frac{1}{3} M(t) M(t+s) \right) + \mathcal{O}(L v^6) \mathcal{O}(d-3). \end{aligned} \quad (5.18)$$

■ Sum of the leading order diagrams

We can now sum the result obtained in equations (5.10), (5.12), (5.15), (5.18) to obtain their contribution to the final effective action $S_{eff}(\{x_a^\mu\})$. At leading order then we find:

$$\begin{aligned}
\mathcal{A}_{(R,LO)} &= \mathcal{A}_{(R1)} + \mathcal{A}_{(R2)} + \mathcal{A}_{(R3)} + \mathcal{A}_{(R4)} \\
&= -i \frac{1}{16 \Lambda^2} \int dt \left[\left(\frac{1}{30} Q_{ij}(t) I_R(d, -2, 0) [Q^{ij}] + \frac{1}{36} M(t) I_R(d, -2, 0) [M] \right) \right. \\
&\quad + \left(-\frac{1}{3} Q^{ij}(t) I_R(d, -1, 2) [Q_{ij}] + \frac{1}{18} M(t) I_R(d, -1, 2) [M] \right) \\
&\quad \left. + \left(\frac{1}{2} Q^{ij}(t) I_R(d, 0, 4) [Q_{ij}] - \frac{1}{12} M(t) I_R(d, 0, 4) [M] \right) \right] + \mathcal{O}(L v^6) + \mathcal{O}(d-3) .
\end{aligned} \tag{5.19}$$

We can notice that all the terms proportional to the trace $M(t)$ of the mass quadrupole moment cancel each other, as we were expecting due to the results found in section 1.3.4.

We can then recall the $I_R(d, a, b)[f](t)$ scalar integral (C.50), which we evaluated in appendix C.4, to find:

$$\begin{aligned}
\mathcal{A}_{(R,LO)} &= \mathcal{A}_{(R1)} + \mathcal{A}_{(R2)} + \mathcal{A}_{(R3)} + \mathcal{A}_{(R4)} \\
&= -i \frac{1}{16 \Lambda^2} \int dt \left[\left(-\frac{1}{20 \pi} Q^{ij}(t) \frac{d^5}{dt^5} Q_{ij}(t) \right) - i \frac{1}{20} \int \frac{d^d \mathbf{k}}{(2\pi)^d} |\mathbf{k}|^3 \right. \\
&\quad \left. \times \left(e^{-i(|\mathbf{k}|+k^0)t} Q^{ij}(k^0) Q_{ij}(|\mathbf{k}|) + e^{i(|\mathbf{k}|-k^0)t} Q^{ij}(k^0) Q_{ij}^*(|\mathbf{k}|) \right) \right] + \mathcal{O}(L v^6) + \mathcal{O}(d-3) \\
&= -i \left(-\frac{G}{10} \int dt Q^{ij}(t) \frac{d^5}{dt^5} (Q_{ij}(t)) - i \frac{\pi G}{10} \int \frac{d^d \mathbf{k}}{(2\pi)^d} |\mathbf{k}|^3 \right. \\
&\quad \left. \times (Q^{ij}(-|\mathbf{k}|) Q_{ij}(|\mathbf{k}|) + Q^{ij}(|\mathbf{k}|) Q_{ij}^*(|\mathbf{k}|)) \right) + \mathcal{O}(L v^6) + \mathcal{O}(d-3) \\
&= -i \left(-\frac{G}{10} \int dt Q^{ij}(t) \frac{d^5}{dt^5} (Q_{ij}(t)) - i \frac{\pi G}{5} \int \frac{d^d \mathbf{k}}{(2\pi)^d} |\mathbf{k}|^3 |Q^{ij}(|\mathbf{k}|)|^2 \right) + \mathcal{O}(L v^6) + \mathcal{O}(d-3)
\end{aligned} \tag{5.20}$$

where we used the fact that $Q^{ij}(-k^0) = Q^{*ij}(k^0)$ thanks to the the fact that $Q^{ij}(t)$ is a real quantity, and we defined $|Q^{ij}(|\mathbf{k}|)|^2 \equiv Q^{ij}(|\mathbf{k}|) Q_{ij}^*(|\mathbf{k}|)$.

We can also notice that the real part of this expression is actually vanishing, since integrating by parts it holds $\int dt \frac{d^m f}{dt^m} \frac{d^n g}{dt^n} = (-1)^p \int dt \frac{d^{(m+p)} f}{dt^{(m+p)}} \frac{d^{(n-p)} g}{dt^{(n-p)}}$, and therefore $\int dt Q^{ij}(t) \frac{d^5}{dt^5} Q_{ij}(t) = -\int dt \frac{d^5}{dt^5} Q^{ij}(t) Q_{ij}(t) = 0$. Since to compute the power loss we're interested only in the imaginary part, this isn't a problem; yet at higher order one may have to employ the in-in formalism also in these computations.

■ Power loss of the system

We're now in the position to evaluate the power loss of the system, by recalling the optical theorem (3.82) from section 3.2.4. In particular we can recognize the expression for differential decay width Γ from the immaginary part of S_{eff} , which we just found at leading order in (5.20):

$$\begin{aligned}
\text{Im}(S_{eff}[\{x_a^\mu\}]) &= \text{Im}(-i \mathcal{A}_{(R,LO)}) = \frac{\pi G}{5} \int \frac{d^d \mathbf{k}}{(2\pi)^d} |\mathbf{k}|^3 |Q^{ij}(|\mathbf{k}|)|^2 \\
&= \frac{G}{40\pi^2} \int d\Omega_2 \int_0^{+\infty} dK K^5 |Q^{ij}(K)|^2 .
\end{aligned} \tag{5.21}$$

To do so we first notice that K is the Fourier variable of the Q quantities, which we can equivalently denote $K = k^0 = \omega = E$, where the last identity is due to the relation $E = \omega \hbar$ which relates the

angular frequency of the modes of the massless on-shell graviton to their energy, with $\hbar = 1$. Then comparing equation (3.82) and (5.21) we can recognize the differential decay width to be:

$$\frac{d^2\Gamma}{d\Omega d\omega} = \frac{1}{T} \frac{G}{20\pi^2} \omega^5 |Q^{ij}(\omega)|^2. \quad (5.22)$$

We can then use the above result (5.22) in the formula (3.83) for the power loss of the system, to finally find:

$$\begin{aligned} P &= \frac{1}{T} \frac{G}{20\pi^2} \underbrace{\int d\Omega_2}_{4\pi} \int_0^{+\infty} d\omega \omega^6 |Q^{ij}(\omega)|^2 = \frac{1}{T} \frac{G}{5\pi} \int_0^{+\infty} d\omega \omega^6 Q^{ij}(\omega) Q_{ij}^*(\omega) \\ &= \frac{1}{T} \frac{G}{5\pi} \int_0^{+\infty} d\omega \int dt \int dt' \omega^6 Q^{ij}(t) Q_{ij}(t') e^{i\omega(t-t')} \\ &= \frac{1}{T} \frac{G}{5\pi} \int dt \int dt' \ddot{Q}^{ij}(t) \ddot{Q}_{ij}(t') \underbrace{\frac{1}{2} \int_{-\infty}^{+\infty} d\omega e^{i\omega(t-t')}}_{2\pi \delta(t-t')} = \frac{G}{5} \frac{1}{T} \int dt \underbrace{\ddot{Q}^{ij}(t) \ddot{Q}_{ij}(t)}_{\langle \ddot{Q}^{ij}(t) \ddot{Q}_{ij}(t) \rangle} \\ &= \frac{G}{5} \langle \ddot{Q}^{ij}(t) \ddot{Q}_{ij}(t) \rangle ; \end{aligned} \quad (5.23)$$

where we recognized the temporal average. We can see that this result agrees with the expression (1.68) we found in linearized general relativity, as expected. The only exception is that here the quantities are not explicitly evaluated at retarded time, but we may include this information ad hoc since we would not expect otherwise. However in the computation of hereditary effects it may be necessary to employ the in-in formalism all along to obtain the correct results.

5.2 | Far away gravitational field and gravitational waveform

In order to evaluate the gravitational waveform, we can recall equation (3.86), which therefore requires us to evaluate the vacuum expectation value of $\bar{\sigma}_{ij}$.

However, as we already pointed out in section 2.1.4, because we're dealing with radiation gravitons, and hence dissipative phenomena, in order to obtain correct and causal results we need to employ the in-in formalism, similarly to references [202, 205, 206]. Yet in this section we'll try to proceed still in a kind of top-down approach, akin to [206], without resorting to symmetry argument to build the radiation effective action; yet, contrary to [206], we'll explicitly perform the evaluation in the Kol-Smolkin parametrization.

In particular we're interested in the vacuum-expectation value for the radiative $\bar{\sigma}_{ij}$ mode, and in the Keldysh representation of the in-in formalism it can be obtained via:

$$\langle \bar{\sigma}_{ij}(k^0, \mathbf{k}) \rangle = \frac{\delta W}{\delta J_-^{ij}(k^0, \mathbf{k})} \Big|_{\mathbf{x}_a = \mathbf{0}, \mathbf{x}_{a+} = \mathbf{x}, \mathbf{J}_{a\pm} = \mathbf{0}, J_{\pm}^{ij} = 0}. \quad (5.24)$$

Then we have to compute the expression for the functional generator of the connected n-point functions, W : to do so we can generalize equation (2.10). First of all we have to recognize that the action that governs the dynamics of the $\bar{\sigma}_{ij}$ field is given by (3.42), so $S = S_{cons}[\{x_a^\mu\}] + S_{eff}^{rad}[\{x_a^\mu\}, \bar{\phi}, \bar{A}_i, \bar{\sigma}_{ij}]$; in the following with S_{cons} we'll actually understand the piece of the action $S_{cons} = \sum_a S_{pp,a}^{kin}[x_a^\mu] + S_{cons}[\{x_a^\mu\}]$ which is independent of the radiation modes.

From such an expression for the action then we expect the generalization of the path integral (2.10) to be

$$e^{iW} = e^{i(S_{\text{cons}}[\{x_{a,1}^\mu\}] - S_{\text{cons}}[\{x_{a,2}^\mu\}])} \times \exp \left(i \left(S_{\text{int}} \left[\{x_{a,1}^\mu\}, -\frac{i\delta}{\delta J_1^{ij}} \right] - S_{\text{int}} \left[\{x_{a,2}^\mu\}, \frac{i\delta}{\delta J_2^{ij}} \right] \right) \right) Z_0[J_1^{ij}, J_2^{ij}]. \quad (5.25)$$

where $S_{\text{int}} = S_{\text{eff}}^{\text{rad}} - S_0$ is the effective radiation action without the quadratic terms, and furthermore we stress that there is a difference for the sign between $\bar{\sigma}_1 \sim -\frac{i\delta}{\delta J_1}$ and $\bar{\sigma}_2 \sim +\frac{i\delta}{\delta J_2}$, as prescribed by equation (2.11).

First of all we're interested in computing the value of the free partition function Z_0 in the in-in formalism, such an quantity will be related to the generalization of the W functional restricted to the free part of the action S_0 , which for a free scalar field was given by (2.13). To proceed we recognize that the free term S_0 , quadratic in the $\bar{\sigma}_{ij}$ field and which therefore prescribes its propagation, is contained in the action $S_{\text{eff}}^{\text{rad}}$: this follows directly from the separation of the potential and radiative modes $\hat{\sigma}_{ij} \rightarrow \sigma_{ij} + \bar{\sigma}_{ij}$ that we performed in the gauge fixed Einstein-Hilbert action (3.35) using the procedure explained in section 3.2.3.

Then, to find the free partition function Z_0 for the tensor field $\bar{\sigma}_{ij}$, we'll first evaluate it in the usual in-out formalism: the explicit expression of the quadratic terms in the $\bar{\sigma}_{ij}$ field, which give the free action S_0 , following the discussion in appendix A.1 are given by formula (A.25):

$$S_0[\bar{\sigma}_{ij}] = \frac{1}{2} \int \frac{d^{d+1}k}{(2\pi)^{(d+1)}} \bar{\sigma}_{kl}(k) \left(\underbrace{-\frac{1}{2}(\delta^{kl}\delta^{mn} - 2\delta^{km}\delta^{ln})}_{\equiv \mathcal{D}_\sigma^{klmn}(k)} k^2 \right) \bar{\sigma}_{mn}(-k); \quad (5.26)$$

from which follows that free generating functional Z_0 is given by, similarly to the procedure carried out in section 3.1:

$$\begin{aligned} Z_0[J^{ij}] &\equiv \int D\bar{\sigma}_{ij} \exp \left(iS_0[\bar{\sigma}] + i \int d^{d+1}x J^{ij}(x) \bar{\sigma}_{ij}(x) \right) \\ &= \exp \left(-\frac{1}{2} \int d^{d+1}x d^{d+1}y J^{ij}(x) D_{ijkl}(x-y) J^{kl}(y) \right) \end{aligned} \quad (5.27)$$

with, analogously to equation (A.29):

$$D_{ijkl}(x-y) \equiv \int \frac{d^{d+1}k}{(2\pi)^{d+1}} \frac{1}{2} \frac{i}{k^2 + i\epsilon} \left(-\frac{2}{d-2} \delta_{ij} \delta_{kl} + \delta_{ik} \delta_{jl} + \delta_{il} \delta_{jk} \right). \quad (5.28)$$

Then, in order to evaluate this same quantity in the in-in framework, we follow the procedure outlined in section 2.1.4: we double the degrees of freedom $\bar{\sigma}_{ij} \rightarrow \bar{\sigma}_{1,ij}, \bar{\sigma}_{2,ij}$ and write the corresponding path integral functional, analogously to (2.10), to obtain

$$\begin{aligned} Z_0[J_+^{ij}, J_-^{ij}] &\equiv \int D\bar{\sigma}_{ij} \exp \left(i(S_0[\bar{\sigma}_1] - S_0[\bar{\sigma}_2]) + i \int d^{d+1}x \left(J_1^{ij}(x) \bar{\sigma}_{1,ij}(x) - J_2^{ij}(x) \bar{\sigma}_{2,ij}(x) \right) \right) \\ &= \int D\bar{\sigma}_{ij} \exp \left(i(S_0[\bar{\sigma}_1] - S_0[\bar{\sigma}_2]) + i \int d^{d+1}x \left(J_+^{ij}(x) \bar{\sigma}_{-,ij}(x) + J_-^{ij}(x) \bar{\sigma}_{+,ij}(x) \right) \right) \end{aligned} \quad (5.29)$$

where in the second equality we switched to the Keldysh representation, according to equations (2.12). Here the explicit expression for the difference of the actions is given by

$$S_0[\bar{\sigma}_1] - S_0[\bar{\sigma}_2] = \frac{1}{2} \int \frac{d^{d+1}k}{(2\pi)^{(d+1)}} \left(\sigma_{-,kl}(k) \mathcal{D}_\sigma^{klmn}(k) \sigma_{+,mn}(-k) + \sigma_{+,kl}(k) \mathcal{D}_\sigma^{klmn}(k) \sigma_{-,mn}(-k) \right) \quad (5.30)$$

still with $\mathcal{D}_\sigma^{klmn}(k) \equiv -\frac{1}{2}(\delta^{kl}\delta^{mn} - 2\delta^{km}\delta^{ln}) k^2$.

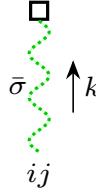
The free partition function (5.29) can then be evaluated proceeding by analogy with the result we found for the scalar field (2.13), so employing the Keldysh indices $A, B = \pm$ we find [202]:

$$Z_0[J_+^{ij}, J_-^{ij}] = \exp\left(-\frac{1}{2} \int d^{d+1}x d^{d+1}y J_a^{ij}(x) D_{ijkl}^{ab}(x-y) J_b^{kl}(y)\right) \quad (5.31)$$

where, comparing with equation (2.14), the matrix of two-point functions generalizes to [202]

$$D_{ijkl}^{AB}(x-y) = \begin{pmatrix} D^{++} & D^{+-} \\ D^{-+} & D^{--} \end{pmatrix} = \begin{pmatrix} 0 & -i D_{adv} \\ -i D_{ret} & \frac{1}{2} D_H \end{pmatrix} \left(\frac{1}{2} \left(-\frac{2}{d-2} \delta_{ij} \delta_{kl} + \delta_{ik} \delta_{jl} + \delta_{il} \delta_{jk} \right) \right). \quad (5.32)$$

Then, in order to proceed with the evaluation of the path integral (5.25), we need also the expression for the interaction terms $S_{int}[\{x_a^\mu\}, \bar{\phi}, \bar{A}_i, \bar{\sigma}_{ij}]$ which are contained in the $S_{eff}^{rad}[\{x_a^\mu\}, \bar{\phi}, \bar{A}_i, \bar{\sigma}_{ij}]$ action; actually we'll need only the term linear in $\bar{\sigma}_{ij}$. To find it we proceed in a top-down manner, turning at the matching procedure that we performed in appendix A.3: the far zone Feynman rule (A.112), which reads



$$\bar{\sigma}_{ij} \uparrow k = i \frac{1}{4\Lambda} \int dt e^{-ik^0 t} \frac{d^2 M^{ij}}{dt^2}(t) + \mathcal{O}(G^{\frac{1}{2}} L v) + \mathcal{O}(d-3), \quad (5.33)$$

implies that the action for the far zone effective action contains a term, which produces the above Feynman rule, of the kind:

$$S_{int} \supset \frac{1}{4} \int dt \frac{d^2 M^{ij}}{dt^2} \frac{\bar{\sigma}_{ij}(t, \mathbf{X})}{\Lambda} \quad (5.34)$$

where the radiation field doesn't depend on the position \mathbf{x} because we multipole expanded it about the \mathbf{X} point, which we actually took to be $\mathbf{X} = \mathbf{x}_{CM} = \mathbf{0}$. In the following we'll formally reinstate the dependence of the $\bar{\sigma}$ field on the position \mathbf{x} , nonetheless in the end we'll impose such position to be equal to the position of the center of mass, so $\mathbf{x} = \mathbf{0}$. Manipulating further the expression:

$$S_{int} = \frac{1}{4\Lambda} \int dt \frac{d^2 M^{ij}}{dt^2} \bar{\sigma}_{ij}(t, \mathbf{x}) = \frac{1}{4\Lambda} \int dt \frac{d^2}{dt^2} \left(Q^{ij} + \frac{1}{3} \delta^{ij} M \right) \bar{\sigma}_{ij}(t, \mathbf{x}) \quad (5.35)$$

where we exchanged the mass multipole M^{ij} for its traceless counterpart Q^{ij} , since the $\Lambda_{ii,kl}$ tensor will project away the trace.

Returning to the expression of the path integral (5.25), we can switch to the Keldysh basis using the fact that $\frac{\delta}{\delta J_1^{ij}} = \frac{1}{2} \frac{\delta}{\delta J_+^{ij}} + \frac{\delta}{\delta J_-^{ij}}$ and $\frac{\delta}{\delta J_2^{ij}} = \frac{1}{2} \frac{\delta}{\delta J_+^{ij}} - \frac{\delta}{\delta J_-^{ij}}$, to obtain:

$$\begin{aligned} & S_{int} \left[\{x_{a,1}^\mu\}, -\frac{i\delta}{\delta J_1^{ij}} \right] - S_{int} \left[\{x_{a,2}^\mu\}, \frac{i\delta}{\delta J_2^{ij}} \right] \\ &= -\frac{i}{4\Lambda} \int dt \left(\ddot{Q}_1^{ij}(t) \frac{\delta}{\delta J_1^{ij}} + \ddot{Q}_2^{ij}(t) \frac{\delta}{\delta J_2^{ij}} + \frac{\delta^{ij}}{3} \left(\ddot{M}_1(t) \frac{\delta}{\delta J_1^{ij}} + \ddot{M}_2(t) \frac{\delta}{\delta J_2^{ij}} \right) \right) \\ &= -\frac{i}{4\Lambda} \int dt \left(\ddot{Q}_+^{ij}(t) \frac{\delta}{\delta J_+^{ij}} + \ddot{Q}_-^{ij}(t) \frac{\delta}{\delta J_-^{ij}} + \frac{\delta^{ij}}{3} \left(\ddot{M}_+(t) \frac{\delta}{\delta J_+^{ij}} + \ddot{M}_-(t) \frac{\delta}{\delta J_-^{ij}} \right) \right), \end{aligned} \quad (5.36)$$

where we used the results

$$Q_+^{ij}(t) \equiv \frac{1}{2} \left(Q_1^{ij}(t) + Q_2^{ij}(t) \right) = \sum_a m_a \left(x_{a+}^i x_{a+}^j - \frac{1}{3} \delta^{ij} |\mathbf{x}_{a+}|^2 + \frac{1}{4} \underbrace{\left(x_{a-}^i x_{a-}^j - \frac{1}{3} \delta^{ij} |\mathbf{x}_{a-}|^2 \right)}_{\mathcal{O}(x_-^2)} \right) \quad (5.37a)$$

$$Q_-^{ij}(t) \equiv Q_1^{ij}(t) - Q_2^{ij}(t) = \sum_a m_a \left(x_{a-}^i x_{a+}^j + x_{a+}^i x_{a-}^j - \frac{2}{3} \delta^{ij} (\mathbf{x}_{a-} \cdot \mathbf{x}_{a+}) \right), \quad (5.37b)$$

which are consistent with the one reported in reference [202], and as they argue, we'll neglect the $\mathcal{O}(x_-^2)$ terms because they represent the perturbation of the trajectories of the compact objects due to quantum fluctuations of the radiation graviton field. Furthermore, even though we expect the trace M to not contribute to the gravitational waveform, for completeness we defined:

$$M_+(t) \equiv \frac{1}{2} (M_1(t) + M_2(t)) = \sum_a m_a \left(|\mathbf{x}_{a+}|^2 + \frac{1}{4} |\mathbf{x}_{a-}|^2 \right), \quad (5.38a)$$

$$M_-(t) \equiv M_1(t) - M_2(t) = 2 \sum_a m_a (\mathbf{x}_{a-} \cdot \mathbf{x}_{a+}). \quad (5.38b)$$

We're now in a position where we can evaluate the sought-after expectation value (5.24) for the $\bar{\sigma}_{ij}$ field. In particular, since $W = -i \log(e^{iW})$, the piece depending only on $S_{cons}[\{x_a^\mu\}]$ doesn't give any contribution once we perform the function derivative with respect to J_- , while it suffices to consider the linear $\mathcal{O}(\bar{\sigma})$ part for the exponential of expression (5.36). In fact, quadratic terms or higher in $\bar{\sigma}$, that originate from the $\exp\left(i \left(S_{int}[\{x_{a,1}^\mu\}, -\frac{i\delta}{\delta J_+^{ij}}] - S_{int}[\{x_{a,2}^\mu\}, \frac{i\delta}{\delta J_-^{ij}}] \right)\right)$ term of the path integral (5.25), we'll give a vanishing contribution once we take the needed functional derivatives with respect to the J_- source and set the sources to zero. Therefore from (5.36) follows:

$$e^{iW[\dots]} = e^{i(S_{cons}[\{x_{a,1}^\mu\}] - S_{cons}[\{x_{a,2}^\mu\}])} \\ \times \left(1 + \frac{1}{4\Lambda} \int dt \left(\left(\ddot{Q}_+^{ij}(t) + \frac{\delta^{ij}}{3} \ddot{M}_+(t) \right) \frac{\delta}{\delta J_+^{ij}} + \left(\ddot{Q}_-^{ij}(t) + \frac{\delta^{ij}}{3} \ddot{M}_-(t) \right) \frac{\delta}{\delta J_-^{ij}} \right) \right) Z_0[J_+^{ij}, J_-^{ij}]. \quad (5.39)$$

and finally

$$\langle \bar{\sigma}_{ij}(x) \rangle = \frac{\delta W}{\delta J_-^{ij}(x)} \Big|_{\mathbf{x}_{a-}=\mathbf{0}, \mathbf{x}_{a+}=\mathbf{x}, \mathbf{J}_{a\pm}=\mathbf{0}, J_\pm^{ij}=0} = \left(-i e^{-iW[\dots]} \frac{\delta e^{iW[\dots]}}{\delta J_-^{ij}(x)} \right) \Big|_{\mathbf{x}_{a-}=\mathbf{0}, \mathbf{x}_{a+}=\mathbf{x}, \mathbf{J}_{a\pm}=\mathbf{0}, J_\pm^{ij}=0} \\ = -\frac{i}{4\Lambda} \int dt' \left(\left(\ddot{Q}_+^{kl}(t') + \frac{\delta^{kl}}{3} \ddot{M}_+(t') \right) \frac{\delta}{\delta J_+^{kl}(w)} + \left(\ddot{Q}_-^{kl}(t') + \frac{\delta^{kl}}{3} \ddot{M}_-(t') \right) \frac{\delta}{\delta J_-^{kl}(w)} \right) \\ \times \frac{\delta}{\delta J_-^{ij}(x)} \exp \left(-\frac{1}{2} \int d^{d+1}y d^{d+1}z J_A^{mn}(y) D_{mnop}^{AB}(y-z) J_B^{op}(z) \right). \quad (5.40)$$

Recalling the two-point function matrix (5.32), we can see that in this computation the $\frac{\delta^2}{\delta^2 J_-^{ij}}$ term will yield a term D^{--} , which is proportional to the Hadamard two-point function (2.16c); nonetheless this term is coupled to $\ddot{Q}_-^{kl} + \frac{\delta^{kl}}{3} \ddot{M}_-$ (quantities defined in expressions (5.37b) and (5.38b)): we can see that in the end such term will vanish due to the $\mathbf{x}_{a-} = \mathbf{0}$ Schwinger-Keldysh

condition. Therefore we find:

$$\begin{aligned}
\langle \bar{\sigma}_{ij}(x) \rangle &= \frac{i}{8\Lambda} \int dt' \left(\left(\ddot{Q}_+^{kl}(t') + \frac{\delta^{kl}}{3} \ddot{M}_+(t') \right) \frac{\delta}{\delta J_+^{kl}(w)} \right) \\
&\quad \times \int d^{d+1}y \left(D_{ijmn}^{-+}(x-y) J_+^{mn}(y) + J_+^{mn}(y) D_{mnij}^{+-}(y-x) \right) + \mathcal{O}(x_-) \\
&= -\frac{1}{8\Lambda} \int dt' \left(\ddot{Q}_+^{kl}(t') + \frac{\delta^{kl}}{3} \ddot{M}_+(t') \right) \\
&\quad \times (D_{ret}(x-w) + D_{adv}(w-x)) \left(\frac{1}{2} \left(-\frac{2}{d-2} \delta_{ij} \delta_{kl} + \delta_{ik} \delta_{jl} + \delta_{il} \delta_{jk} \right) \right) + \mathcal{O}(x_-) \\
&= -\frac{1}{8\Lambda} \int dt' \left(2 \ddot{Q}_{+,ij}(t') - \frac{4 \delta_{ij}}{3(d-2)} \ddot{M}_+(t') \right) D_{ret}(x-w) + \mathcal{O}(x_-) ;
\end{aligned} \tag{5.41}$$

where we used the fact that $D_{adv}(x-y) = D_{ret}(y-x)$ and that $\frac{1}{2} \left(-\frac{2}{d-2} \delta_{ij} \delta_{kl} + \delta_{ik} \delta_{jl} + \delta_{il} \delta_{jk} \right)$ is symmetric under the $ij \leftrightarrow kl$ exchange.

Finally we impose the Schwinger-Keldysh conditions, setting to zero \mathbf{x}_- and all the sources. Then, we make explicit $x = (t, \mathbf{x})$ for the position of the observer, and $w = (t', \mathbf{0})$ for the position of the center of the multipole expansion we performed in the radiation effective theory; doing so, and recalling from reference [202] that for the retarded propagator it holds $D_{ret}(t-t', \mathbf{x}) = -\theta(t-t') \frac{\delta(t-t'-|\mathbf{x}|)}{4\pi|\mathbf{x}|}$, in $d=3$ we obtain:

$$\langle \frac{\bar{\sigma}_{ij}}{\Lambda}(t, \mathbf{x}) \rangle = \frac{2G}{|\mathbf{x}|} \left(\ddot{Q}_{ij}(t-|\mathbf{x}|) - \frac{2 \delta_{ij}}{3} \ddot{M}_+(t-|\mathbf{x}|) \right) \tag{5.42}$$

Finally, recalling formula (3.86), and from section section 1.3.2 the property according to which the $\Lambda_{ij,kl}$ tensor projects away the trace of any spatial symmetric tensor, we can find the waveform as seen from a far away observer in position \mathbf{x} (and so with $\hat{\mathbf{n}} = \frac{\mathbf{x}}{|\mathbf{x}|}$ the direction of propagation of the gravitational wave, approximated as a plane wave):

$$h_{ij}^{TT}(t, \mathbf{x}) = -2G \Lambda_{ij,kl}(\hat{\mathbf{n}}) \frac{\ddot{Q}^{kl}(t-|\mathbf{x}|)}{|\mathbf{x}|} . \tag{5.43}$$

We may notice that this result is consistent with formula (1.62) we found in linearized general relativity, once we reinstate the c factors, we recognize that $|\mathbf{x}| = r$ and take into account the opposite sign of the metric, which requires considering the opposite of $h_{\mu\nu}$ tensor, $h_{\mu\nu} \leftrightarrow -h_{\mu\nu}$.

POST-NEWTONIAN CORRECTIONS TO OBSERVABLES

The goal of this chapter is to evaluate the post-Newtonian corrections to the physical observables, such as the gravitational waveform potentially observable by gravitational wave detectors, starting from the results we obtained in chapter 4 and 5, and complementing them with known results from the literature; see also references [36, 103, 260, 272].

In particular in section 6.1 we evaluate several observables, such as the energy of the binary system and its power loss, and its orbital phase. This quantities will be useful to evaluate the full gravitational waveform: then in section 6.2 we will summarize the results, reporting the analytical expression for the gravitational waveform, both in time and frequency domain.

Let us recall from the **Notation** that in this chapter we'll switch back again to the mostly plus metric, as it is customary in the literature about gravitational waves observations; moreover in some expression we'll reinstate the factors of c to aid their numerical evaluation.

6.1 | Post-Newtonian corrections to the binary dynamics

We're now interested in understanding how we can employ the results we obtained in chapters 4 and 5 in order to evaluate the gravitational waveform, as seen by a far away observer. In particular we are interested in obtaining the explicit expression for the $h_{ij}^{(TT)}$ perturbation of the metric tensor, since this is what in the end is measured by gravitational wave observatories (opportunely projected onto the detector tensor, see section 1.5.1 and equation (1.108)).

We recall so that in section 3.2.5 we have already shown how we may directly evaluate the $h_{ij}^{(TT)}$ perturbation of the metric tensor in our EFT formalism; and in fact we obtained its leading order expression in section 5.2, i.e. equation (5.43). However that expression is still an explicit function of the multipole moments of the source, since Q^{ij} is the traceless part (5.9) of the mass quadrupole moment which we defined in (3.67e). Then to evaluate the waveform $h_{ij}^{(TT)}$ we need the explicit expressions for the positions $\mathbf{x}_a(t)$ of both compact objects $a = 1, 2$ as a function of the time variable t of the asymptotic observer.

In principle in section 3.2.5 we have already outlined how one would go on to evaluate the positions $\mathbf{x}_a(t)$, so equivalently the dynamics of the binary: once we integrate out all the gravitational degrees of freedom, performing the whole procedure outlined in chapter 3, we're left with the effective action $S_{eff}[\{x_a^\mu\}]$ (formally given in equation (3.63)) which is a function only of the worldline of the compact bodies, so of their positions $\mathbf{x}_a(t)$. Then we can employ the (generalized) Euler-Lagrange

equation of motions (3.76) to obtain the differential equations which prescribe the motion of the two compact objects; the solution of these differential equation will be exactly the positions $\mathbf{x}_a(t)$ that we needed, explicitly expressed as a function of time. With this result finally we can directly evaluate the mass quadrupole moment (3.67e) and any other higher multipole moments, obtaining the explicit sought-after expression for $h_{ij}^{(TT)}(t)$, as a function of time. Let us notice that to apply the previous construction we would have to employ the in-in formalism when evaluating diagrams in the radiation effective theory, otherwise we would obtain non-causal dynamics, as we've discussed in chapter 5.

6.1.1 — Quasi-circular orbit approximation and energy balance equation

The above construction, while being completely general, is however quite involved: in fact the resulting differential equations may be too complicated to be solved analytically, and so we would have to resort to numerical methods.

Nonetheless, recalling also the discussion of section 1.4.3, it is expected that compact binary systems will have circularized to a really high degree by the time their signal will be detectable in gravitational wave observatories [36, 103, 273]. We can then employ the *adiabatic, quasi-circular* orbits approximation. Doing so in fact the dynamics of the system will be completely determined by the energy balance equation:

$$\frac{dE}{dt} = -\mathcal{F}, \quad (6.1)$$

where E is the invariant energy of the compact binary, and \mathcal{F} the total energy flux, also denoted as gravitational wave luminosity [273]. In particular the former follows from the conservative dynamics of the system, while the latter is related to the dissipative effects; we'll evaluate these quantities below. The above relation is based on the assumption that any amount of energy lost by the system per unit time is simply radiated away as gravitational waves; in particular we will employ this first order differential equation to compute the evolution of the orbital frequency of the binary system, for example as a function of time.

Let us notice that at higher post-Newtonian orders the radiation effective theory will produce also conservative corrections, so will modify also the expression of the binding energy E of the binary system. Actually, as pointed by references [65, 180], at higher order it may not be possible to clearly distinguish conservative contributions from dissipative ones, for example when considering the non-linear memory terms which are due to self-interactions between gravitational waves [180]: then to obtain unambiguous results it may be necessary to evaluate the actual full equations of motion, accounting directly for radiation-reaction effects [180, 257].

Furthermore let us notice that gravitational waves carry away also angular momentum and linear momentum from the binary systems. In fact, after the coalescence, the newly formed compact object may get a quite strong kick due to the recoil induced by an asymmetrical emission of gravitational waves; despite this being an higher post-Newtonian correction [256, 274]. Therefore also the angular and linear momentum, which are first integrals of the conservative Lagrangian, evolve in time when one accounts for dissipative effects.

■ Definition of customary parameters

In order to obtain more compact expression, and also to improve the numerical stability when evaluating them, it's useful and customary to introduce some dimensionless variables [36, 103].

First of all we'll trade the masses m_1 and m_2 of the binary for the reduced mass $\mu \equiv \frac{m_1 m_2}{(m_1 + m_2)}$ and

for the dimensionless symmetric mass ratio

$$\nu \equiv \frac{\mu}{m} = \frac{m_1 m_2}{(m_1 + m_2)^2} \quad ; \quad (6.2)$$

with $m = m_1 + m_2$ the total mass of the system. The symmetric mass ratio ν is particularly useful as it assumes values only in the range $\nu \in (0, \frac{1}{4}]$, and in particular $\nu = \frac{1}{4}$ for equal mass systems ($m_1 = m_2$), and $\nu \rightarrow 0$ in the test particle limit.

Then we introduce the customary post-Newtonian dimensionless parameter [36, 103]

$$x \equiv \left(\frac{Gm\omega}{c^3} \right)^{\frac{2}{3}} = \left(\frac{G\mu\omega}{\nu c^3} \right)^{\frac{2}{3}} \quad , \quad (6.3)$$

where ω is the orbital frequency, and $x = \mathcal{O}(v^2)$ according to the post-Newtonian scaling; furthermore this frequency-dependent x parameter is invariant in the coordinate systems which are asymptotically flat at infinity [275]. Furthermore in the following, to avoid ambiguities, we'll define $\epsilon = \mathcal{O}(v^2) \ll 1$ as the PN expansion parameter, so $v = \mathcal{O}(\epsilon^{\frac{1}{2}})$ and $G = \mathcal{O}(\epsilon)$.

Adopting these definitions then the energy balance equation (6.1) can be recast as:

$$\frac{dx}{dt} \frac{dE(x)}{dx} = -\mathcal{F}(x) \quad \implies \quad \frac{dx}{dt} = -\frac{\mathcal{F}(x)}{\left(\frac{dE(x)}{dx} \right)} \quad . \quad (6.4)$$

Hence we see that in the approximation of quasi-circular orbits the knowledge of the expression $E(x)$ and $\mathcal{F}(x)$ are enough to determine the dynamics of the system (i.e. the evolution of the dimensionless orbital frequency x as a function of time).

Next we introduce as well the dimensionless time variable [36, 103]

$$\Theta \equiv \frac{\nu c^3}{5Gm} (t_c - t) = \frac{\nu^2 c^3}{5G\mu} (t_c - t) \quad , \quad (6.5)$$

where t_c denotes the time of coalescence, at which the frequency will tend toward infinity.

Sometimes then energy balance equation (6.4) is recast also as a function of this dimensionless time variable Θ , by noticing that from equation (6.5) follows $\frac{dt}{d\Theta} = -\frac{5G\mu}{\nu^2}$. Therefore:

$$\frac{dx}{d\Theta} = \frac{dt}{d\Theta} \frac{dx}{dt} = \left(-\frac{5G\mu}{\nu^2} \right) \left(-\frac{\mathcal{F}(\Theta)}{\left(\frac{dE}{dx} \right)(\Theta)} \right) \quad . \quad (6.6)$$

In the following then we'll be first concerned with obtaining the expression for the center-of-mass energy $E(x)$ and the flux $\mathcal{F}(x)$ of the binary system as a function of the dimensionless frequency x ; and only in the end we'll obtain also the time-domain evolution for the system.

6.1.2 — Binding energy of the binary system

We're now interested in evaluating the center-of-mass energy E of the binary system, which we take to include both the kinetic energy and potential energy of the system: this would then be equivalent to the total energy of the system once we add the rest energy of the two compact bodies, and the energy contained in their excited modes and spin degrees of freedom, if any.

To find E then we'll use the procedure outlined in section 3.2.5, and in particular we will evaluate the center-of-mass Hamiltonian for the system as given by relation (3.80). Actually strictly speaking

the Lagrangian and the Hamiltonian are not gauge invariant quantities per se: nonetheless the Hamiltonian is related to the total energy of the binary system, and this is a gauge invariant quantity when written as a function of the orbital frequency [259].

To perform the Legendre transform then we need the conservative Lagrangian of the binary system: this is exactly the quantity which we evaluated in section 3.3 and chapter 4, up to 2PN order. Its expression in harmonic gauge, given by the kinetic minus the potential contributions $L = T - V$, is therefore given by the algebraic sum of the 0PN contribution (3.96), the 1PN contributions (4.22) and (4.20), and the 2PN contributions (4.56) and (4.57). Explicitly we find:

$$\begin{aligned}
L = & \frac{1}{2}m_1v_1^2 + \frac{1}{2}m_2v_2^2 + \frac{1}{8}m_1v_1^4 + \frac{1}{8}m_2v_2^4 + \frac{1}{16}m_1v_1^6 + \frac{1}{16}m_2v_2^6 \\
& + \frac{G^3m_1m_2}{2r^3} (m_1^2 + 6m_1m_2 + m_2^2) \\
& + \frac{G^2m_1m_2}{4r^2} (-2m_1 - 2m_2 + 8m_1v_1^2 + 7m_2v_1^2 + 7m_1v_2^2 + 8m_2v_2^2 \\
& \quad - 14(m_1 + m_2)(\mathbf{v}_1 \cdot \mathbf{v}_2) + 2m_2(\mathbf{v}_1 \cdot \hat{\mathbf{r}})^2 + 2m_1(\mathbf{v}_2 \cdot \hat{\mathbf{r}})^2) \\
& + \frac{Gm_1m_2}{8r} (8 + 12v_1^2 + 7v_1^4 + 12v_2^2 + 3v_1^2v_2^2 + 7v_2^4 + 15r^2(\mathbf{a}_1 \cdot \mathbf{a}_2) - rv_1^2(\mathbf{a}_2 \cdot \hat{\mathbf{r}}) \\
& \quad - 28(\mathbf{v}_1 \cdot \mathbf{v}_2) - 10v_1^2(\mathbf{v}_1 \cdot \mathbf{v}_2) - 10v_2^2(\mathbf{v}_1 \cdot \mathbf{v}_2) + 2(\mathbf{v}_1 \cdot \mathbf{v}_2)^2 \\
& \quad + 14r(\mathbf{a}_2 \cdot \mathbf{v}_1)(\mathbf{v}_1 \cdot \hat{\mathbf{r}}) - 12r(\mathbf{a}_2 \cdot \mathbf{v}_2)(\mathbf{v}_1 \cdot \hat{\mathbf{r}}) - v_2^2(\mathbf{v}_1 \cdot \hat{\mathbf{r}})^2 + r(\mathbf{a}_2 \cdot \hat{\mathbf{r}})(\mathbf{v}_1 \cdot \hat{\mathbf{r}})^2 \\
& \quad + 12r(\mathbf{a}_1 \cdot \mathbf{v}_1)(\mathbf{v}_2 \cdot \hat{\mathbf{r}}) - 14r(\mathbf{a}_1 \cdot \mathbf{v}_2)(\mathbf{v}_2 \cdot \hat{\mathbf{r}}) - 4(\mathbf{v}_1 \cdot \hat{\mathbf{r}})(\mathbf{v}_2 \cdot \hat{\mathbf{r}}) \\
& \quad - 6v_1^2(\mathbf{v}_1 \cdot \hat{\mathbf{r}})(\mathbf{v}_2 \cdot \hat{\mathbf{r}}) - 6v_2^2(\mathbf{v}_1 \cdot \hat{\mathbf{r}})(\mathbf{v}_2 \cdot \hat{\mathbf{r}}) + 12(\mathbf{v}_1 \cdot \mathbf{v}_2)(\mathbf{v}_1 \cdot \hat{\mathbf{r}})(\mathbf{v}_2 \cdot \hat{\mathbf{r}}) \\
& \quad - v_1^2(\mathbf{v}_2 \cdot \hat{\mathbf{r}})^2 + 3(\mathbf{v}_1 \cdot \hat{\mathbf{r}})^2(\mathbf{v}_2 \cdot \hat{\mathbf{r}})^2 - r(\mathbf{a}_1 \cdot \hat{\mathbf{r}}) (-v_2^2 + r(\mathbf{a}_2 \cdot \hat{\mathbf{r}}) + (\mathbf{v}_2 \cdot \hat{\mathbf{r}})^2)) \\
& + \mathcal{O}(Lv^6) .
\end{aligned} \tag{6.7}$$

As already discussed in the above expression there should be also the term $\delta L = -m_1 - m_2$, coming from the expansion of the action (3.34b), however we neglected it since it represents the rest mass energy of the two compact objects, as can be seen by taking the Legendre transform to obtain the Hamiltonian.

■ Higher order time derivatives

As we can notice from result (4.56), starting from the 2PN order the Lagrangian presents time derivatives of the position of the compact objects higher than the velocities, as for example the accelerations \mathbf{a}_1 and \mathbf{a}_2 are explicitly present in the Lagrangian 6.7.

A workaround could be to reduce the order of these time derivatives by substituting them with their corresponding expression as prescribed by the equations of motion: for definiteness, by evaluating the Euler-Lagrange equations from the 0PN or 1PN Lagrangian, we would find a relation of the kind $\mathbf{a}_1 = f(\mathbf{v}, \mathbf{x})$, which we could then substitute in (6.7) to remove the accelerations. Nonetheless doing so would entail a redefinition of the variables, which means a change in gauge [235, 259, 276, 277]. In fact it has been shown that in harmonic coordinates (which we're employing), starting from 2PN, it's not possible anymore to have a Lagrangian L which doesn't contain accelerations [256]; therefore using the equation of motions or performing a coordinate shift to perform an order reduction will be equivalent to changing gauge, for example going into ADM-like coordinates [256, 276, 277].

What we can do instead is to employ the generalized Euler-Lagrange equations that we already introduced in equation (3.76), and a generalization of the Legendre transform. The only caveat is

that, in order to do so, the Lagrangian must be at most linear in the higher derivatives. When this is not the case, we can proceed by adding suitable terms to the Lagrangian: such terms must not contribute to the equations of motions (so to not modify the observable), yet they can remove the problematic dependence of the Lagrangian on the higher order time derivatives.

This is in fact the case with our expression (6.7): here we have to recast in a different form the term $+15r^2(\mathbf{a}_1 \cdot \mathbf{a}_2)$, which is quadratic in the acceleration, in order to recover a Lagrangian linear in the acceleration. This can be accomplished with the addition of *double-zero terms*, which are terms that vanish at the current PN order when using the lower PN equations of motions: adding them modifies the expression of the Lagrangian, but does not change the equation of motion nor the gauge [235]. In particular we can add

$$\delta L = -\frac{15}{8}Gm_1m_2r \left(\left(\mathbf{a}_1 + \frac{Gm_2}{r^3} \mathbf{r} \right) \cdot \left(\mathbf{a}_2 - \frac{Gm_1}{r^3} \mathbf{r} \right) \right) \quad (6.8)$$

to the Lagrangian (6.7) to remove the aforementioned term quadratic in the acceleration.

Before proceeding further with the evaluation of the Hamiltonian, it is however useful to simplify the problem by exploiting its symmetry, so by moving to the center of mass frame and using polar coordinates. Actually it should already be possible to obtain the binding energy of the system also by evaluating the Noether charge of the conservative Lagrangian associated to the time translations; for example this procedure is performed in reference [257].

■ Center of mass frame and polar coordinates

To simplify the problem it is useful to first move to the center of mass frame. Next, since we consider spinless compact objects, and so the normal to the orbital plane does not undergo precession, then it will be useful to parametrize the motion of the bodies in that plane by employing a polar coordinate system.

In the following then we will perform a change of the dynamical coordinates, going to the center of mass frame, so $(\mathbf{x}_1, \mathbf{x}_2) \rightarrow (\mathbf{x}_{CM}, \mathbf{r})$. In particular we employ the usual definition (3.97) for the orbital separation $\mathbf{r} = \mathbf{x}_1 - \mathbf{x}_2$ in harmonic gauge, and we define the position of the center of mass to be:

$$\mathbf{x}_{CM} = \frac{m_1\mathbf{x}_1 + m_2\mathbf{x}_2}{m}. \quad (6.9)$$

Additionally, to further simplify the problem, we will take the center of mass to coincide with the origin of the coordinate frame, so $\mathbf{x}_{CM} = \mathbf{0}$.

We have to point out however that we may expect the condition (6.9), which singles out the center of mass frame from all the generic harmonic coordinate frames, to be modified at higher PN orders [257]. In fact when dealing with generic motion one should define the position of the center-of-mass frame by evaluating the linear momentum of the system as a Noether charge, and then imposing such linear momentum to vanish. So for example the quantity G^i (actually \tilde{G}^i) of references [257, 275] is the expression for the position of the center-of-mass as evaluated in a generic frame in harmonic coordinates: then imposing $G^i = 0$ perturbatively produces a series of corrections to expression (6.9). In practice for example, only under the assumptions of quasi-circular orbits, the expressions for the position \mathbf{x}_1 of the first compact body, as evaluated in the center of mass frame, simplifies to [36, 256] $\mathbf{x}_1 = \frac{\mu}{m_1} \mathbf{r} (1 + \mathcal{O}(v^4))$. Observing the Lagrangian (6.7) we would expect this $\mathcal{O}(v^4)$ correction to enter via the leading order kinetic term from the Newtonian Lagrangian (3.93): yet to obtain the 2PN result for the binding energy, using the procedure outlined in the following, we found that imposing the constraint (6.9) was sufficient. Given this discrepancy we may cast a doubt on our intermediate steps, in particular when we're not imposing the quasi-circular orbit

approximation. Hence following the procedure presented in references [36, 256, 257, 275] would be advisable.

Nonetheless proceeding with the procedure we outlined in this chapter, since we're considering spinless compact objects, there will be no precession of the orbital plane [278]: therefore we can parametrize the relative separation \mathbf{r} between the two compact objects with a spherical coordinate system $\mathbf{r} = \mathbf{r}(r, \phi, \theta)$; as shown in figure 1.4, with $\mathbf{r} = r\hat{\mathbf{n}}$, but the with the ϕ angle redefined as $\phi \rightarrow \frac{\pi}{2} - \phi$, such that now ϕ is vanishing when \mathbf{r} points along the x axis. Doing so we find the angle θ to be a cyclical coordinate, to which is associated a Noether charge and which does not contribute to the dynamics of the system, so in practice we can neglect it.

We can therefore simply parametrize the two dimensional orbital plane in polar coordinates (r, ϕ) and using the orthonormal vectors $(\hat{\mathbf{r}}, \hat{\phi})$, whose three dimensional cartesian coordinates read $\hat{\mathbf{r}} = (\cos(\phi), \sin(\phi), 0)$ and $\hat{\phi} = (-\sin(\phi), \cos(\phi), 0)$. Then, taking \mathbf{r} to be the relative separation between the two compact objects, and defined

$$\omega \equiv \frac{d\phi}{dt}, \quad \alpha \equiv \frac{d\omega}{dt}, \quad (6.10)$$

it holds:

$$\mathbf{r} = r\hat{\mathbf{r}}, \quad \mathbf{v} = \dot{r}\hat{\mathbf{r}} + \omega r\hat{\phi}, \quad \mathbf{a} = (\ddot{r} - \omega^2 r)\hat{\mathbf{r}} + (2\omega\dot{r} + \alpha r)\hat{\phi}; \quad (6.11)$$

and also the following identities hold:

$$(\mathbf{v} \cdot \hat{\mathbf{r}}) = \dot{r}, \quad (\mathbf{a} \cdot \hat{\mathbf{r}}) = \ddot{r} - \omega^2 r, \quad (\mathbf{a} \cdot \mathbf{v}) = \dot{r}(\ddot{r} - \omega^2 r) + \omega r(2\omega\dot{r} + \alpha r). \quad (6.12)$$

Finally, applying all of the aforementioned procedure to Lagrangian (6.7) we find:

$$\begin{aligned} L = & \frac{\mu}{16\nu^3 r^3} (2G^3 \mu^3 (31\nu + 4) + 4G^2 \mu^2 \nu r (7(1 - 2\nu)r^2 \omega^2 + 15\nu r \ddot{r} + (9 - 5\nu)\dot{r}^2 - 2) \\ & + 2G\mu\nu^2 r^2 (-26\alpha\nu r^3 \dot{r}\omega + 2\dot{r}^2 (4\nu + (7 - 2\nu(\nu + 14))r^2 \omega^2 - 13\nu r \ddot{r} + 6) \\ & + r^2 ((\nu(\nu + 18) - 7)(-r^2)\omega^4 + \omega^2(4\nu + \nu(-r)\ddot{r} + 12) + \nu\dot{r}^2) + (7 - 12\nu)\dot{r}^4 + 8) \\ & + \nu^3 r^3 (r^2 \omega^2 + \dot{r}^2) ((5(\nu - 1)\nu + 1)r^4 \omega^4 + 2(1 - 3\nu)r^2 \omega^2 \\ & + 2\dot{r}^2 (-3\nu + (5(\nu - 1)\nu + 1)r^2 \omega^2 + 1) + (5(\nu - 1)\nu + 1)\dot{r}^4 + 8)) . \end{aligned} \quad (6.13)$$

■ Legendre transform and energy of the binary system

We may now obtain the expression for the energy of the binary system by evaluating the Hamiltonian corresponding to the Lagrangian (6.13).

To do so we have to generalize the definition of the Legendre transform (3.80). In particular, following reference [257], we may define the generalized conjugate momenta:

$$\mathbf{p} = \frac{\delta L}{\delta \mathbf{v}} \equiv \frac{\partial L}{\partial \mathbf{v}} - \frac{d}{dt} \left(\frac{\partial L}{\partial \mathbf{a}} \right), \quad (6.14a)$$

$$\mathbf{q} = \frac{\delta L}{\delta \mathbf{a}} \equiv \frac{\partial L}{\partial \mathbf{a}}. \quad (6.14b)$$

From them it is possible to derive the generalized Hamiltonian, i.e. the conserved energy E , via [257]:

$$E = (\mathbf{p} \cdot \mathbf{v}) + (\mathbf{q} \cdot \mathbf{a}) - L \quad (6.15)$$

In our case, recalling equation (6.11), since we're employing a polar coordinate frame, the generalized coordinates now are (r, ϕ) ; therefore the generalized velocity is $\mathbf{v} = (\dot{r}, \omega)$, and the generalized acceleration $\mathbf{a} = (\ddot{r}, \alpha)$. Hence specializing equation (6.14) to our case we have:

$$p_r = \frac{\partial L}{\partial \dot{r}} - \frac{d}{dt} \left(\frac{\partial L}{\partial \ddot{r}} \right) , \quad (6.16a)$$

$$q_r = \frac{\partial L}{\partial \ddot{r}} . \quad (6.16b)$$

$$p_\phi = \frac{\partial L}{\partial \omega} - \frac{d}{dt} \left(\frac{\partial L}{\partial \alpha} \right) , \quad (6.16c)$$

$$q_\phi = \frac{\partial L}{\partial \alpha} . \quad (6.16d)$$

where the explicit expression of L is given by (6.13). Then the Hamiltonian, so the energy of the system, is given by:

$$E = p_r \dot{r} + q_r \ddot{r} + p_\phi \omega + q_\phi \alpha - L . \quad (6.17)$$

Performing the evaluation, explicitly we find:

$$\begin{aligned} E = \frac{\mu}{16\nu^3 r^3} & \left(-2G^3 \mu^3 (31\nu + 4) + 4G^2 \mu^2 \nu r (7(1 - 2\nu)r^2 \omega^2 + (10\nu + 9)\dot{r}^2 + 2) \right. \\ & + 2G\mu\nu^2 r^2 (2\dot{r}^2 (4\nu - 3(\nu(2\nu + 19) - 7)r^2 \omega^2 - \nu r \ddot{r} + 6) - 2\nu r^2 \dot{r} (12\alpha r \omega + \ddot{r})) \\ & + r^2 (-3(\nu(\nu + 18) - 7)r^2 \omega^4 + 4\omega^2(\nu + 6\nu r \ddot{r} + 3) + \nu \dot{r}^2) + (21 - 36\nu)\dot{r}^4 - 8) \\ & + \nu^3 r^3 (r^2 \omega^2 + \dot{r}^2) (5(5(\nu - 1)\nu + 1)r^4 \omega^4 + 6(1 - 3\nu)r^2 \omega^2 \\ & \left. + 2\dot{r}^2 (-9\nu + 5(5(\nu - 1)\nu + 1)r^2 \omega^2 + 3) + 5(5(\nu - 1)\nu + 1)\dot{r}^4 + 8) \right) . \end{aligned} \quad (6.18)$$

Nevertheless, since we're assuming circular orbits, the orbital decay \dot{r} would be vanishing if not for the power loss due to gravitational wave emission, which however, as we've seen, first enters at 2.5PN contributions. This implies that $\dot{r} = \mathcal{O}(v^5)$, and from this follows as well that the velocity in (6.11) reduces to $v = \sqrt{\dot{r}^2 + \omega^2 r^2} = \omega r + \mathcal{O}(v^9)$ [275].

Then, for the precision we're aiming for, we can restrict the result (6.18) to the case of circular orbits only, hence imposing $\dot{r} = 0 + \mathcal{O}(v^5)$, and also any higher time derivative of r to vanish. Doing so we find the simplified expression for the energy:

$$\begin{aligned} E = \frac{\mu}{16\nu^3 r^3} & \left(4G^2 \mu^2 \nu r (7(1 - 2\nu)r^2 \omega^2 + 2) - 2G^3 \mu^3 (31\nu + 4) + 2G\mu\nu^2 r^2 (-3(\nu(\nu + 18) - 7)r^4 \omega^4 \right. \\ & \left. + 4(\nu + 3)r^2 \omega^2 - 8) + \nu^3 r^5 \omega^2 (5(5(\nu - 1)\nu + 1)r^4 \omega^4 + 6(1 - 3\nu)r^2 \omega^2 + 8) \right) . \end{aligned} \quad (6.19)$$

■ Energy as a function of the post-Newtonian parameters

Since as we've already said we're interested in the energy $E(x)$, so written as a function of x , the last step we have to perform is to rewrite both the modulus of the relative separation r and the orbital frequency ω as a function of the dimensionless post-Newtonian x parameter, which we defined in (6.3).

In particular to obtain the expression for $\omega(x)$ it suffices to invert that relation, so

$$\omega(x) = \frac{\nu c^3}{G\mu} x^{\frac{3}{2}} . \quad (6.20)$$

Then we could use such a relation to obtain $r(x)$, if we could find an expression which relates r and ω . This in fact can be done, for example by proceeding as in reference [260], so by evaluating the equation of motion for the r variable under the circular orbit condition.

To obtain this equation of motion for the r variable we can apply the generalized Euler-Lagrange equations, which we introduced in equation (3.76), on the Lagrangian (6.13) with $q = r$:

$$-\frac{d^2}{dt^2} \left(\frac{\partial L}{\partial \ddot{r}} \right) + \frac{d}{dt} \left(\frac{\partial L}{\partial \dot{r}} \right) - \frac{\partial L}{\partial r} = 0 . \quad (6.21)$$

Imposing then the conditions of circular orbit, so \dot{r} and higher derivative to be vanishing, and also $\alpha = 0$ and higher derivative of ω to be vanishing, we find:

$$0 = \mu \left(-\frac{3G^3\mu^3(31\nu+4)}{\nu r} + 8G^2\mu^2 + G\mu\nu r (3r^4 (-(\nu(\nu+18) - 7)\omega^4)) \right. \\ \left. + 4(\nu+3)r^2\omega^2 - 8) + \nu^2 r^4 \omega^2 (3(5(\nu-1)\nu+1)r^4\omega^4 + 4(1-3\nu)r^2\omega^2 + 8) \right) . \quad (6.22)$$

At this point we can substitute the $\omega(x)$ relation we found in (6.20) into expression (6.22), and solve the equality iteratively to obtain $r(x)$, order by order in x .

So to solve iteratively equation (6.22) (where we already replaced $\omega \rightarrow \omega(x)$), recalling the discussion written below equation (6.3), we introduce an auxiliary $\epsilon \sim \mathcal{O}(v^2)$ parameter to keep track of the PN order of each term. In particular it holds $x = \mathcal{O}(\epsilon)$, and due to the PN scaling rules, also $G = \mathcal{O}(\epsilon)$; therefore in the expression we'll send $x \rightarrow \epsilon x$ and $G \rightarrow \epsilon G$. We can then expand the expression so obtained in Taylor series around $\epsilon = 0$, finding at leading order $\epsilon(G^4\mu^4\nu r - c^6 G\mu\nu^4 r^4 x^3) = 0$; which we can solve keeping the only non vanishing real solution

$$r(x) = \frac{G\mu}{c^2\nu} \frac{1}{x} . \quad (6.23)$$

This result is consistent with what we were expecting: in fact from relation (6.20), from the virial theorem $v^2 = \frac{Gm}{r}$ and from the quasi-circular orbit relation $v = \omega r + \mathcal{O}(v^9)$ we could have concluded that at leading order it must hold $r \sim \left(\frac{G\mu}{\nu c^2} \right) \frac{1}{x}$.

We proceed then by looking for the 1PN correction (i.e. order $\mathcal{O}(\epsilon)$) to such an expression, by making the ansatz

$$r = \frac{G\mu}{c^2\nu} \frac{1}{x} (1 + a_1 \epsilon) \quad (6.24)$$

and substituting it into the previous expression. We can perform once again the Taylor expansion around $\epsilon = 0$, keeping the leading order term, and solving for the placeholder coefficient a_1 , to find $a_1 = \left(\frac{\nu}{3} - 1 \right) x$. Finally making the ansatz

$$r = \frac{G\mu}{c^2\nu} \frac{1}{x} \left(1 + \left(\frac{\nu}{3} - 1 \right) x \epsilon + a_2 \epsilon^2 \right) , \quad (6.25)$$

and proceeding analogously to before, we find $a_2 = \frac{1}{36}\nu(4\nu+171)x^2$, which scales like x^2 , as expected. Since the expression we're using is valid only at 2PN, we cannot proceed further. To finish instead we can just set the auxiliary parameter to $\epsilon = 1$ to obtain:

$$r(x) = \frac{G\mu}{c^2\nu} \frac{1}{x} \left(1 + \left(\frac{\nu}{3} - 1 \right) x + \frac{\nu}{36}(4\nu+171)x^2 + \mathcal{O}(x^3) \right) . \quad (6.26)$$

Om a side note, if instead of replacing $\omega \rightarrow \omega(x)$ at the start of the previous procedure we went on by expanding in ω^2 , then we would have found also the following relation:

$$\omega^2(r) = \frac{G\mu}{\nu r^3} \left(1 + \frac{G\mu}{\nu r c^2} (\nu - 3) + \frac{G^2\mu^2}{4\nu^2 r^2 c^4} (\nu(4\nu+41) + 24) + \mathcal{O}\left(\frac{G^3\mu^3}{r^3} \right) \right) . \quad (6.27)$$

Returning to the main topic, having found relation (6.26), and recalling equation (6.20) as well, we can now substitute them into the expression (6.19) for the energy, Taylor expanding then in the parameter x around $x = 0$, and keeping all the contributions up to 2PN, to find:

$$E(x) = -\frac{c^2 \mu x}{2} \left(1 - \frac{1}{12}(9 + \nu)x - \frac{1}{24}(81 - 57\nu + \nu^2)x^2 + \mathcal{O}(x^3) \right). \quad (6.28)$$

This is exactly the result for the energy of the binary system, written as a function of the dimensionless frequency x , which we were looking for. Moreover this result (6.28) is in complete agreement with the one reported in references [36, 103]; let us also notice that in the literature this result is currently known to a much higher PN order, as already discussed.

6.1.3 — Power loss of the binary system

Similarly to what we have just done for the energy of the binary system, we can express the energy flux \mathcal{F} as a function of the dimensionless frequency x .

As already discussed in chapter 3, we can directly evaluate the flux \mathcal{F} in our EFT construction. In fact we did so in section 5.1, finding the leading order result (5.23):

$$\mathcal{F} = \frac{G}{5c^5} \langle \ddot{Q}^{ij}(t) \ddot{Q}_{ij}(t) \rangle, \quad (6.29)$$

where the angled brackets denote a temporal average.

Let us also notice again that this is the same result (1.68) which we found also in linearized general relativity. Therefore, since in practice in section 1.4.2 we performed same procedure, albeit only at leading order, which we have just performed in section 6.1.2, then we can directly recall result (1.78), taking care of redefining $\omega \rightarrow 2\omega$, since there it was the quadrupole frequency of the gravitational wave instead of the source. Therefore, using also relations (6.20) and (6.26), at leading order we find:

$$\mathcal{F} = \frac{32}{5} \frac{c^5 \nu^2}{G} x^5 + \mathcal{O}(x^6). \quad (6.30)$$

Let us also notice that we chose the center of mass frame when we evaluated the multipoles entering in the computation of the power loss: then to be consistent this center of mass frame should coincide with the one we employed in the previous section 6.1.2. In practice then one may define the center of mass by actually imposing the dipole multipole to be vanishing. Nevertheless also in this case, at higher PN order, we expect the expressions for the multipoles to be corrected: as an example the mass should be substituted by the total energy, which takes into account also the binding energy of the system.

Another point is that in this work we have evaluated the Lagrangian for the binary system up to 2.5PN order: this means that we have evaluated the conservative sector (so the binding energy (6.28)) up to 2PN, but the dissipative sector only to 0PN *relative* order (so the power loss (6.30) only to leading order). Then, since the energy balance equation (6.6) requires a ratio of these two quantities, in order to be able to obtain the 2PN accurate expression for the phase of the binary system, and so for the phase of the waveform, then we'll need also the PN corrections to the power loss up to 2PN. In reality these results are known to even higher order in the literature; still we will report the expression up to 2PN order for the emitted flux, so the power lost from the binary system due to gravitational waves emission, as given in references [36, 103]:

$$\begin{aligned} \mathcal{F}(x) = & \left(\frac{32\nu^2}{5G} \right) x^5 + \left(\frac{32\nu^2}{5G} \left(-\frac{35\nu}{12} - \frac{1247}{336} \right) \right) x^6 + \left(\frac{128\pi\nu^2}{5G} \right) x^{\frac{13}{2}} \\ & + \left(\frac{32\nu^2}{5G} \left(\frac{65\nu^2}{18} + \frac{9271\nu}{504} - \frac{44711}{9072} \right) \right) x^7 + \mathcal{O}\left(x^{\frac{15}{2}}\right); \end{aligned} \quad (6.31)$$

the terms highlighted in red are exactly these higher order corrections which we didn't compute in this thesis work. Nevertheless let us notice that we could have obtained them also by working in the EFT framework, but to do so we would have had to evaluate additional diagrams in the radiation effective theory; furthermore at higher PN order hereditary effects complicate these calculations, as already discussed.

6.1.4 — Power balance equation and time evolution of the orbital phase

Having obtained the expressions for both the energy of the binary system and its power loss due to gravitational wave emission, we can then turn back to the energy balance equation (6.1), which we discussed in section 6.1.1.

Let us however point out that there are several ways to manipulate the analytical information we've found, in order to study the dynamics of the binary system. In particular in the following we will use the Taylor approximants (T-approximants) method for evaluating the corrections to phase of the binary; yet there exist more refined methods, such as Padé resummation (P-approximants), which may yield better result once the velocity v of the system becomes high, so toward the end of the inspiral phase [272, 279, 280]. Furthermore, even when using T-approximants, there are different ways in which one could express the post-Newtonian corrections to the observables: since we're interested in finding the orbital frequency as a function of time, we will obtain what is denoted as *TaylorT3 approximant*. Nonetheless let us notice that there are other T-approximants which do not make explicit the time dependence, and doing so actually they may be able provide a better accuracy; see also reference [272].

Given this premise, since we have obtained both the energy $E(x)$ (in equation (6.28)) and the flux $\mathcal{F}(x)$ (in equation (6.31)) as a function of the dimensionless PN parameter x , we can evaluate directly equation (6.6). In particular, expanding the ratio therein as a Taylor approximation in x around $x = 0$ up to 2PN order, we find:

$$\frac{dx}{d\Theta} = (-64)x^5 + \left(176\nu + \frac{2972}{21}\right)x^6 + (-256\pi)x^{\frac{13}{2}} + \left(-\frac{1888\nu^2}{9} - \frac{27322\nu}{63} - \frac{68206}{567}\right)x^7 + \mathcal{O}\left(x^{\frac{15}{2}}\right). \quad (6.32)$$

Solving the above differential equation then we will obtain the formula for the (dimensionless) orbital frequency x as a function of (dimensionless) time Θ .

To proceed then, we can first solve the above differential equation at leading order by employing the separation of variable methods, such that $\frac{dx}{x^5} = -64 d\Theta + \mathcal{O}(\epsilon^{-3})$, which implies $x(\Theta) = \frac{1}{4}(\Theta + c)^{-\frac{1}{4}}$. We set the integration constant $c = 0$ because we expect the frequency x to diverge at coalescence time $\Theta = 0$; doing so we find the leading Newtonian result:

$$x(\Theta) = \frac{1}{4}\Theta^{-\frac{1}{4}} + \mathcal{O}(x^2) ; \quad (6.33)$$

from this result we see that $\Theta = \mathcal{O}(\epsilon^{-4})$.

We can then compute the post-Newtonian corrections to this result by starting from the ansatz, where we make explicit all the ϵ the dependence:

$$x(\Theta) = \frac{\epsilon}{4}\Theta^{-\frac{1}{4}} \left(\sum_{n \in \mathbb{N}} \epsilon^{\frac{n}{2}} a_{\frac{n}{2}} \Theta^{-\frac{n}{8}} \right) ; \quad (6.34)$$

and deriving it with respect to Θ to obtain

$$\frac{dx}{d\Theta}(\Theta) = \frac{\epsilon^5}{4}\Theta^{-\frac{5}{4}} \left(\sum_{n \in \mathbb{N}} \left(-\frac{1}{4} - \frac{n}{8} \right) \epsilon^{\frac{n}{2}} a_{\frac{n}{2}} \Theta^{-\frac{n}{8}} \right) . \quad (6.35)$$

We can then equate this equation (6.35) with the result (6.32), substituting x with the ansatz (6.34) in the latter, expanding in $\epsilon^{\frac{1}{2}}$, and solving for the coefficients $a_{\frac{n}{2}}$ by working order by order in the expansion parameter. Doing so, and then setting $\epsilon = 1$, we find:

$$x(\Theta) = \frac{1}{4}\Theta^{-\frac{1}{4}} \left(1 + \left(\frac{11\nu}{48} + \frac{743}{4032} \right) \Theta^{-\frac{1}{4}} + \left(-\frac{\pi}{5} \right) \Theta^{-\frac{3}{8}} \right. \\ \left. + \left(\frac{31\nu^2}{288} + \frac{24401\nu}{193536} + \frac{19583}{254016} \right) \Theta^{-\frac{1}{2}} + \mathcal{O}\left(\Theta^{-\frac{5}{8}}\right) \right); \quad (6.36)$$

which exactly agrees with references [36, 103]. This is the analytic expression which relates the invariant orbital frequency x of the binary with the dimensionless time variable Θ , up to 2PN accuracy. Proceeding similarly to what has just been done we may also invert this relation, by substituting the ansatz $\Theta(x) = \frac{x^{-4}\epsilon^{-4}}{4} \left(\sum_{n \in \mathbb{N}} \epsilon^{\frac{n}{2}} b_{\frac{n}{2}} x^{\frac{n}{2}} \right)$ in equation (6.36), and imposing that $x(\Theta(x)) = x + \mathcal{O}\left(\epsilon^{\frac{7}{2}}\right)$. Doing so we find:

$$\Theta(x) = \frac{x^{-4}}{256} \left(1 + \left(\frac{11\nu}{3} + \frac{743}{252} \right) x + \left(-\frac{32\pi}{5} \right) x^{\frac{3}{2}} + \left(\frac{617\nu^2}{72} + \frac{5429\nu}{504} + \frac{3058673}{508032} \right) x^2 + \mathcal{O}\left(x^{\frac{5}{2}}\right) \right). \quad (6.37)$$

In particular equation (6.36) let us also evaluate the orbital phase of the binary as a function of the dimensionless time: in fact, inverting the definition (6.3) of x to obtain $\omega = x^{\frac{3}{2}} \frac{\nu}{G\mu}$, and recalling that $\omega \equiv \frac{d\phi}{dt} = \frac{d\Theta}{dt} \frac{d\phi}{d\Theta}$ is the orbital angular frequency of the binary, it follows that:

$$\phi(\Theta) = \int_{\Theta_0}^{\Theta} d\Theta' \left(\frac{dt}{d\Theta'} \omega(\Theta') \right) = \int_{\Theta_0}^{\Theta} d\Theta' \left(\left(-\frac{5G\mu}{\nu^2} \right) \left((x(\Theta'))^{\frac{3}{2}} \frac{\nu}{G\mu} \right) \right); \quad (6.38)$$

which we can evaluate by employing result (6.36) in $x^{\frac{3}{2}}$, expanding in $\epsilon^{\frac{1}{2}}$ up to 2PN accuracy with $\Theta = \mathcal{O}(\epsilon^{-4})$, and then integrating in the Θ' variable. Doing so we find that the orbital phase of the binary system is given by:

$$\phi(\Theta) = \phi_0 - \frac{\Theta^{\frac{5}{8}}}{\nu} \left(1 + \left(\frac{55\nu}{96} + \frac{3715}{8064} \right) \Theta^{-\frac{1}{4}} + \left(-\frac{3\pi}{4} \right) \Theta^{-\frac{3}{8}} \right. \\ \left. + \left(\frac{1855\nu^2}{2048} + \frac{284875\nu}{258048} + \frac{9275495}{14450688} \right) \Theta^{-\frac{1}{2}} + \mathcal{O}\left(\Theta^{-\frac{5}{8}}\right) \right), \quad (6.39)$$

where ϕ_0 is an integration constant, that at this PN order has the meaning of the phase of the binary at coalescence time $\Theta = 0$ [103]. This result once again exactly agrees with the one of references [36, 103].

From equations (6.26) and (6.36) we can also evaluate the orbital separation r (which is *not* a gauge invariant quantity) in the harmonic gauge that we adopted in the calculations of the conservative contributions, as a function of dimensionless time variable, finding

$$r(\Theta) = \frac{4G\mu}{\nu} \Theta^{\frac{1}{4}} \left(1 + \left(-\frac{7\nu}{48} - \frac{1751}{4032} \right) \Theta^{-\frac{1}{4}} + \left(\frac{\pi}{5} \right) \Theta^{-\frac{3}{8}} \right. \\ \left. + \left(-\frac{37\nu^2}{768} + \frac{5489\nu}{21504} - \frac{701263}{16257024} \right) \Theta^{-\frac{1}{2}} + \mathcal{O}\left(\Theta^{-\frac{5}{8}}\right) \right). \quad (6.40)$$

This last relation starts to diverge as we approach the merger for $\Theta \rightarrow 0$: despite being gauge-dependent and therefore unobservable, it is a manifestation of the breakdown of the PN expansion, since the latter is not a convergent series.

6.2 | Analytic expression of the gravitational waveform

6.2.1 — Gravitational waveform in the time domain

Recalling the discussion of sections 1.3.2, 1.3.4 and 1.4, in order to evaluate the waveform, as could be measured by a far away observer, we need to evaluate there the spatial perturbation of the metric in TT-gauge h_{ij}^{TT} . In particular this is the result that we obtained, at leading order, in formula (5.43), evaluating it directly from the effective field theory construction we presented in section 3.2.4.

Still this is the same (leading order) result that we obtained in linearized general relativity, as we would have expected, see equation (5.43) and (1.62), up to the different notation between the two chapters, as already pointed out in section 5.2. Then expression (1.91) gives us the expression for the gravitational waveform of the gravitational signal as seen by a far away observer, under the quasi-circular orbit approximations. Then, neglecting corrections to the amplitude, the post-Newtonian corrections to the phase (6.39) we evaluated above enter in the waveform just as a modification of the leading order expression (1.90) for the phase.

The approximation of keeping the leading order approximation for the amplitude of the gravitational wave signal (i.e. (1.92)) while considering only the corrections to the phase of the signal (i.e. (6.39)), which we suggested above, is denoted as *restricted* PN approximation and is quite common. In fact the corrections to the phase of the gravitational signal (the one we evaluated) are of uttermost importance for gravitational waves observations, since the matched filtering technique requires the analytical template to not go out of phase with the observed signal, otherwise the detection probability will become drastically lower. On the other hand instead the precise evolution in time of amplitude of the signal isn't so crucial for this technique; it is nevertheless considered in data analysis: it introduces several harmonics of the source frequency, inducing a modulation of the signal.

Nonetheless, for completeness, below we report from references [36, 103] also the next-to-leading order correction to the amplitude, which we'll employ when evaluating and plotting the 2PN-phase corrected waveform in figure 6.1: we do this in order to give corroborate the validity of the restricted post-Newtonian approximation. In particular, we point out again that in this chapter we're adapting our notations in order to be consistent with the literature about gravitational waves observations, where it is customary to employ the mostly plus $\eta_{\mu\nu} = \text{diag}(-, +, +, +)$ metric. Furthermore we'll use also the common choice for the orientation of the polarization tensors, which we defined in (1.29): using the definitions already introduced in chapter 1, referring in particular to figure 1.4, we choose the $\hat{\mathbf{u}}$ axis to lie along the projections on the sky of the major axis of the orbit, oriented toward the ascending node [103].

Then using these same convention of reference [103], complementing our results with those of [36, 103], the time-domain gravitational waveform is given by, with $A = +, \times$:

$$h_A(t) = \frac{2G\mu x}{c^2 r} \left(H_A^{(0)} + x^{\frac{1}{2}} H_A^{(\frac{1}{2})} + \mathcal{O}\left(\frac{v^2}{c^2}\right) \right) \quad (6.41)$$

with

$$H_+^{(0)}(t) = -(1 + \cos^2(\iota)) \cos(2\phi(t)) , \quad (6.42a)$$

$$H_\times^{(0)}(t) = -2 \cos(\iota) \sin(2\phi(t)) , \quad (6.42b)$$

$$H_+^{(\frac{1}{2})}(t) = -\frac{1}{8} \sin(\iota) \sqrt{1 - 4\nu} \left((5 + \cos^2(\iota)) \cos(\phi(t)) - 9(1 + \cos^2(\iota)) \cos(3\phi(t)) \right) , \quad (6.42c)$$

$$H_\times^{(\frac{1}{2})}(t) = -\frac{3}{8} \sin(2\iota) \sqrt{1 - 4\nu} \left(\sin(\phi(t)) - 3 \sin(3\phi(t)) \right) , \quad (6.42d)$$

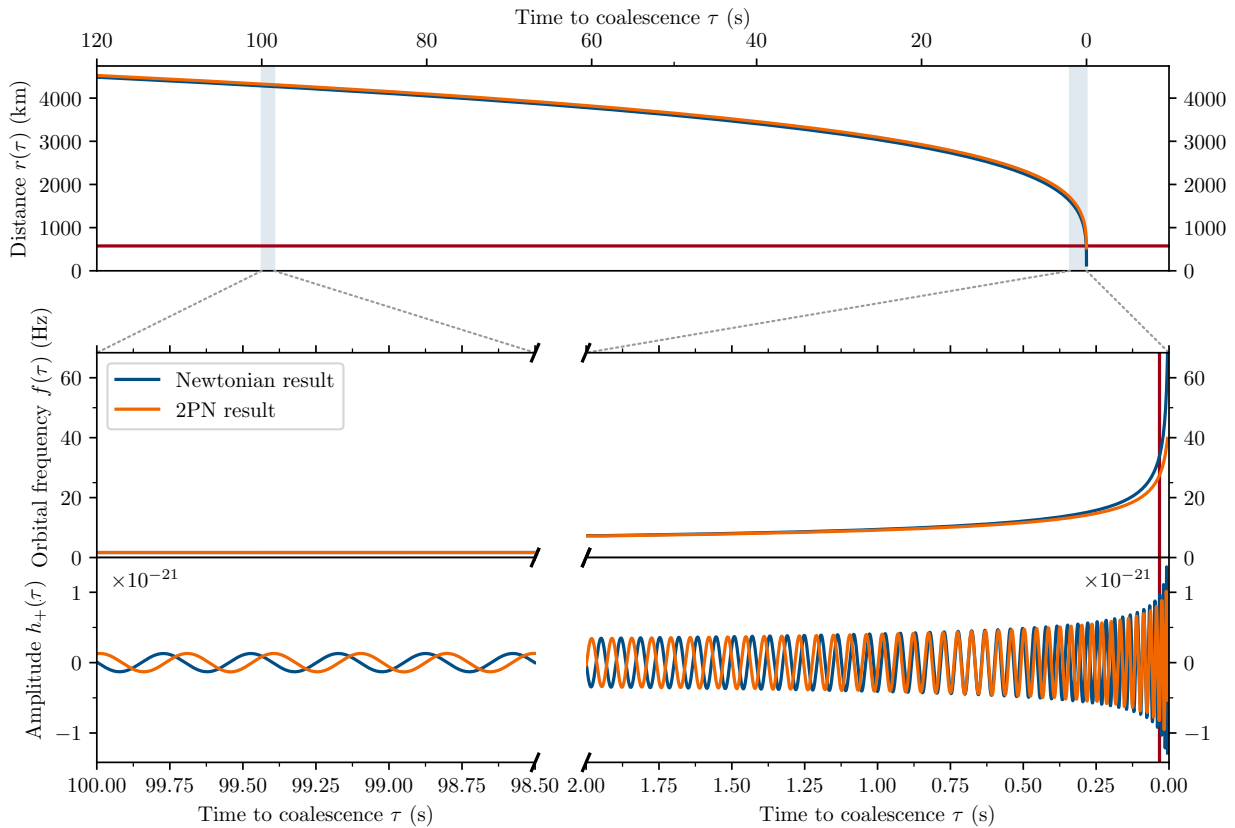


FIGURE 6.1 — Plots to be compared with figure 1.5: here we show in orange the 2PN corrections to the phase and next-to-leading order corrections to the amplitude (orange) with respect to the Newtonian quantities (blue), evaluated for that same system (non-redshifted source-frame $m_1 = 35M_\odot$, $m_2 = 30M_\odot$, $r = 400$ Mpc, $\phi_0 = 0$), as a function of the time to coalesce $\tau \equiv t_c - t$ as measured by a distant (non-redshifted, and in asymptotically flat spacetime) observer; with the only difference that $\iota = \frac{\pi}{4}$ rad in this plot, in order to show the (small) effect of higher harmonics on the waveform.

We can clearly see that while the PN corrections bring small adjustments to the distance $r(\tau)$ and to the amplitude of the waveform $h_+(\tau)$, they induce a significant change in the orbital frequency, especially toward the end of the inspiral $\tau \rightarrow 0$ (as expected, since the expansion parameter v becomes larger and so the PN correction more relevant), and even more so to the phase of the gravitational waveform $h_+(\tau)$. In practice this is what justifies the *restricted post-Newtonian* approximation that’s often employed: the amplitude of the waveform is evaluated at leading order, while only its phase is evaluated to the highest possible PN order. In fact the correction to the phase are the most important ones: the optimal method of *matched filtering* employed to find gravitational waves signal in the output recorded by gravitational detectors requires a precise knowledge of the waveform to look for, and any de-phasing of the waveform template with respect to the real signal (as for example happens between the Newtonian and the 2PN corrections in the bottom plot, where for most of the time the two waveform do not overlap) will significantly reduce the SNR of the faint signal, eventually making its detection outright impossible. Now we can also be more precise about our (gauge-dependent) definition of distance $r(\tau)$: it is the relative distance between the two bodies, as evaluated in harmonic gauge (1.113). Furthermore let us notice that in this plot we show the orbital frequency $f(\tau) \equiv \frac{\omega}{2\pi}$, which is related to the dominant quadrupole frequency of the gravitational waves $f_{gw}(\tau)$ by $f_{gw}(\tau) = 2f(\tau)$; yet the PN corrections to the amplitude introduce several harmonics of the orbital angular frequency ω , in this case also ω and 3ω , in addition to the leading order quadrupole 2ω .

Additionally the horizontal red line still represents the (Newtonian) value of the innermost stable circular orbit $R_{ISCO} = 576$ km, while in the middle and bottom panels the vertical red lines indicate the time $\tau_{ISCO} = 33$ ms, as discussed in figure 1.5 and section 1.4.4. Now we cut off the frequency and amplitude plot in the right panels at $\tau = 5$ ms as otherwise these quantities would diverge. Nonetheless let us notice that the 2PN corrections in this region (when we’ve almost approached the merger) are ill-behaved, as the expansion parameter v^2 becomes too large and the PN asymptotic series doesn’t converge anymore: in fact the radial distance $r(\tau)$ actually starts to diverge as $\Theta \sim \tau \rightarrow 0$, as expected from expression (6.40).

where $\phi(t) = \phi(\Theta(t))$ and is given by equation (6.39); in particular $\Theta(t)$ is the linear redefinition of the time which is defined as (6.5).

In the above expression we highlight in red the next-to-leading order term which we stress we didn't derive explicitly in this thesis: yet we could have obtained it by evaluating the next order multipoles in linearized general relativity in section 1.3.4 or by considering the next order corrections to the diagrams (and eventually higher PN radiation diagrams) in section 5.2. Furthermore at higher PN order logarithmic terms, e.g. due to hereditary effects, may appear [36, 103].

6.2.2 — Fourier transform of the gravitational waveform

In the analysis of gravitational wave signal, for example when employing the matched filtering technique, usually one actually employs the Fourier transform of the waveform. To obtain it, it is customary to resort to the *stationary phase approximation*, according to which the Fourier transform of the function $F(t) = A(t) \cos(\phi(t))$, for $f > 0$, may be approximated, under the conditions $\frac{1}{A} \frac{dA}{dt} \ll \frac{d\phi}{dt}(t)$, $\frac{d^2\phi}{dt^2} \ll \left(\frac{d\phi}{dt}\right)^2$ as [155, 281, 282]:

$$\tilde{F}(f) = \frac{1}{2} A(t(f)) \left(\frac{df}{dt}\right)^{-\frac{1}{2}} e^{i(2\pi f t(f) - \phi(t(f)) - \frac{\pi}{4})}; \quad (6.43)$$

where in particular $t(f)$ is defined as the time at which $\frac{d\phi}{dt}(t) = 2\pi f$ holds.

Such procedure can then be applied to the time domain, restricted (so with the amplitude truncated at the leading order $H_A^{(0)}(t)$ only), post-Newtonian waveform (6.41). We report the result of such procedure (which yields the *TaylorF2 approximant* [272]) from references [103, 281]: considering f as the quadrupolar frequency of the emitted gravitational wave, i.e. twice the source orbital frequency, then the expressions for the Fourier-transform of the plus and cross polarizations of the restricted waveforms up to 2PN are:

$$\tilde{h}_+(f) = \left(\frac{1 + \cos^2(\iota)}{2}\right) \mathcal{A}(f) e^{i\Psi(f)} \quad (6.44a)$$

$$\tilde{h}_\times(f) = \cos(\iota) \mathcal{A}(f) e^{i(\Psi(f) + \frac{\pi}{2})}; \quad (6.44b)$$

where amplitude is found to be

$$\mathcal{A}(f) = \left(\frac{5}{6}\right)^{\frac{1}{2}} \frac{\pi^{-\frac{2}{3}} c}{2 r} \left(\frac{G \mu^{\frac{3}{5}} m^{\frac{2}{5}}}{c^3}\right)^{\frac{5}{6}} f^{-\frac{7}{6}} \quad (6.45)$$

and the phase

$$\Psi(f) = 2\pi \left(t_c + \frac{r}{c}\right) f - \Phi_0 - \frac{\pi}{4} + 2\pi f_* \left(\frac{3}{5} \tau_0 \left(\frac{f}{f_*}\right)^{-\frac{5}{3}} + \tau_1 \left(\frac{f}{f_*}\right)^{-1} - \frac{3}{2} \tau_{1.5} \left(\frac{f}{f_*}\right)^{-\frac{2}{3}} + 3\tau_2 \left(\frac{f}{f_*}\right)^{-\frac{1}{3}}\right) \quad (6.46)$$

with t_c the moment of coalescence in retarded time, f_* a reference frequency (which could be the frequency when the quadrupolar gravitational signal enters in the detector bandwidth, or when the observation starts). The coefficients are given in [103]:

$$\tau_0 = \frac{5}{256\pi} f_*^{-1} \left(\frac{\pi G m}{c^3} f_*\right)^{-\frac{5}{3}} \nu^{-1}, \quad (6.47a)$$

$$\tau_1 = \frac{5}{192\pi} f_*^{-1} \left(\frac{\pi G m}{c^3} f_*\right)^{-1} \nu^{-1} \left(\frac{743}{336} + \frac{11}{4} \nu\right), \quad (6.47b)$$

$$\tau_{1.5} = \frac{1}{8} f_*^{-1} \left(\frac{\pi G m}{c^3} f_* \right)^{-\frac{2}{3}} \nu^{-1} , \quad (6.47c)$$

$$\tau_2 = \frac{5}{128\pi} f_*^{-1} \left(\frac{\pi G m}{c^3} f_* \right)^{-\frac{1}{3}} \nu^{-1} \left(\frac{3058673}{1016064} + \frac{5429}{1008} \nu + \frac{617}{144} \nu^2 \right) . \quad (6.47d)$$

OBSERVATIONAL CONSTRAINTS FROM FUTURE GW OBSERVATORIES

The goal of this chapter is to assess whether it will be possible to look for possible deviations from general relativity, performing a generic test of the post-Newtonian theory, in a regime complementary to the tests that are currently being carried out.

In section 7.1 we introduce the parametrized test that we will perform, and discuss how we may deal with systematic errors. In section 7.2 we introduce the LISA gravitational observatory, and how we may mathematically model it. In section 7.3 we introduce the Fisher matrix formalism, useful to perform analytical forecasts. Finally in section 7.4 we present and discuss the results of the forecast.

7.1 | Parametrizing deviations from the post-Newtonian predictions

The spirit of this test is to be as general and agnostic as possible about the underlying reasons for any possible deviation from general relativity.

First of all we assume general relativity and also its post-Newtonian expansion to provide a pretty accurate description of the dynamics of compact binary systems, and of the gravitational waves they emit, in the regimes we can currently probe. In fact many tests of general relativity have been performed [283, 284], also employing the quite general parametrized post-Newtonian formalism, and no significant deviations from general relativity have been found, to a really high precision. Such tests span over different length scales and different regimes, as could be solar system tests, binary pulsar tests, and strong gravity tests. In particular the recent direct observation of gravitational waves allowed to perform new tests of general relativity [92–96], also in the strong field regime during the merger and ringdown phases, all of which found no deviations from Einstein’s theory.

We will then perform a test similar to the one denoted as *parametrized tests of gravitational waves generation* in references [92–96]: in particular we’ll allow for generic deviations from general relativity which modify the phase of the gravitational wave signal, as this is the observable to which gravitational wave observatories are most sensitive.

In particular we’ll deform the 2PN expression (6.46) of the phase $\Psi(f)$ of the Fourier transformed waveforms (6.44), by introducing seven arbitrary parameters δ_{mn} :

$$\{\delta_{00}, \delta_{20}, \delta_{21}, \delta_{30}, \delta_{40}, \delta_{41}, \delta_{42}\} , \quad (7.1)$$

which will deform the expression of such a phase, so

$$\Psi(f) \longrightarrow \Psi(f, \delta_{00}, \delta_{20}, \delta_{21}, \delta_{30}, \delta_{40}, \delta_{41}, \delta_{42}) . \quad (7.2)$$

More quantitatively these δ_{mn} coefficients are applied as fractional corrections to the τ coefficients (schematically $\tau \rightarrow \tilde{\tau} = \tau(1 + \delta)$) defined in equations (6.47): in particular for each δ_{mn} the subscripts m and n specify that the correction affects the coefficient at $\frac{m}{2}$ PN order which is multiplied by the n -th power of ν . Explicitly this deformation amounts to redefining the coefficients (6.47) as:

$$\tilde{\tau}_0 = \frac{5}{256\pi} f_*^{-1} \left(\frac{\pi G m}{c^3} f_* \right)^{-\frac{5}{3}} \nu^{-1} (1 + \delta_{00}) , \quad (7.3a)$$

$$\tilde{\tau}_1 = \frac{5}{192\pi} f_*^{-1} \left(\frac{\pi G m}{c^3} f_* \right)^{-1} \nu^{-1} \left(\frac{743}{336} (1 + \delta_{20}) + \frac{11}{4} \nu (1 + \delta_{21}) \right) , \quad (7.3b)$$

$$\tilde{\tau}_{1.5} = \frac{1}{8} f_*^{-1} \left(\frac{\pi G m}{c^3} f_* \right)^{-\frac{2}{3}} \nu^{-1} (1 + \delta_{30}) , \quad (7.3c)$$

$$\tilde{\tau}_2 = \frac{5}{128\pi} f_*^{-1} \left(\frac{\pi G m}{c^3} f_* \right)^{-\frac{1}{3}} \nu^{-1} \left(\frac{3058673}{1016064} (1 + \delta_{40}) + \frac{5429}{1008} \nu (1 + \delta_{41}) + \frac{617}{144} \nu^2 (1 + \delta_{42}) \right) . \quad (7.3d)$$

In the limit in which all the $\delta_{mn} \rightarrow 0$, then we recover the standard post-Newtonian result, i.e. we recover general relativity. Actually, to be more precise actually, the τ coefficient may enter also in the function $t(f)$, which gives the time as a function of the frequency of the gravitational waves, see for example reference [103]: nevertheless we do not modify such expression of $t(f)$, so we do not modify the τ coefficients entering in it; instead we deform only the expression for the orbital phase as a function of the quadrupole frequency, $\Psi(f) \rightarrow \Psi(f, \{\delta_{00}, \delta_{20}, \delta_{21}, \delta_{30}, \delta_{40}, \delta_{41}, \delta_{42}\})$.

Let us notice that the parametrization we just introduced is not exactly the same as the one adopted for example in reference [96]: there they consider corrections up the 3.5PN order to the phase of the Fourier transformed waveform, and multiply the whole expression of each post-Newtonian order by a single deformation parameter (denoted as $\delta\phi_i$ instead of δ , eventually with an auxiliary $\delta\phi_{il}$ for terms logarithmic in the frequency); therefore they neglect the ν -structure of the post-Newtonian correction to the phase; on the other hand they also allow for -1PN dipolar and 0.5PN terms, which are not predicted by general relativity. The fact that they're neglecting the ν -dependence could somehow reduce the sensitivity of their test if the possible deviation from general relativity in the phase depends on the power of ν at a given PN order: this may be the case if the deviation affects differently the terms with different powers of G at the same PN order (looking at the 2PN conservative Lagrangian (6.7), for example if a 2PN term like $\frac{G^3 m_1 m_2}{2r^3} (m_1^2 + m_2^2)$ is modified differently with respect to another 2PN term like $\frac{G m_1 m_2}{8r} (7v_1^4 + 7v_2^4)$).

Furthermore reference [96] performs the test employing the observed waveform in its entirety, from the inspiral phase to the ringdown; nevertheless, since the parametrized modification affects only the post-Newtonian phase for the inspiral, in practice they taper off these corrections to zero once a certain threshold frequency is reached, falling back to standard hybrid waveform model (such as effective-one-body or phenomenological waveforms) to model the consequent merger and ringdown phases. However, actually as pointed out also in [96], we may expect any modification of general relativity to modify also the merger and the ringdown phases, possibly even more markedly than the inspiral phase; then to be fully consistent the test should somehow allow for a continuous deformation also in those regime; yet without assuming an underlying theoretical model for the expected modification of the theory of gravity, this doesn't seem feasible.

Therefore in this work we're instead concerned with the possibility of performing a similar test, looking for deviations from general relativity, but working solely in the post-Newtonian framework. In practice this means that this test looks for deviations from the post-Newtonian predictions for the dynamics of a binary system, yet deviations from the post-Newtonian theory would imply deviations from standard general relativity as well. However, in order to perform such a test using only the post-Newtonian predictions, we have to carefully assess which is the regime of validity of the such an approximation: in fact, in order to not spoil the validity of our results, the systematic error due to the fact that we're neglecting higher PN order corrections must be smaller than the statistical error due to the limited precision of any observation.

7.1.1 — Observation cut-off to limit the systematic error

To summarize, we're interested in assessing how well we may directly constraint the post-Newtonian coefficients with gravitational waves detectors. With directly we mean performing a test on the non-resummed post-Newtonian theory: this should allow us to disentangle this weak-field test of general relativity from other possible effects, either due to real phenomena possibly arising in the strong gravity regime near the merger, or due to systematical effects possibly introduced by the resummation procedures employed in some waveform models, which include informations also from other analytical and numerical methods.

Nevertheless to perform this test of the post-Newtonian theory, we must recognize that such theory is valid only in the weak field and slow velocities regime, therefore we have to restrict ourselves only the *early* inspiral phase of the compact binary systems, when they compact objects are still pretty far away from each others and their relative velocity v is small enough.

Then we need to quantify the magnitude of the systematic error which we inevitably introduce anytime we neglect the infinite series of higher order post-Newtonian corrections to the observables. Once we will have found such an estimate, then we may introduce a quantitative threshold after which we should stop using observational data, in order to limit such a systematic error from spoiling the validity of our test.

To do so we may turn to result (6.39) for the 2PN corrections to the orbital phase in time domain:

$$\begin{aligned} \phi(\Theta) = \phi_0 - \frac{\Theta^{\frac{5}{8}}}{\nu} \left(1 + \left(\frac{55\nu}{96} + \frac{3715}{8064} \right) \Theta^{-\frac{1}{4}} + \left(-\frac{3\pi}{4} \right) \Theta^{-\frac{3}{8}} \right. \\ \left. + \left(\frac{1855\nu^2}{2048} + \frac{284875\nu}{258048} + \frac{9275495}{14450688} \right) \Theta^{-\frac{1}{2}} + \mathcal{O}\left(\Theta^{-\frac{5}{8}}\right) \right). \end{aligned} \quad (7.4)$$

If we neglect logarithmic corrections that arise at higher PN order [36, 103], we may notice that these corrections to the phase are roughly of the form $\phi(\Theta) \sim \Theta^{\frac{5}{8}} \sum_n c_n \Theta^{-\frac{n}{8}}$, with c_n the coefficient related to the $\frac{n}{2}$ PN order, and we recognize that such coefficients are all of order $c_n \sim \mathcal{O}(1)$. Therefore, assuming such behavior to hold approximately true also at higher unknown orders, we may estimate the contribution from all the terms due to the post-Newtonian corrections beyond 2PN by using the geometric sum $\Delta\Theta_{>2PN} \equiv \sum_{n=5}^{+\infty} \Theta^{-\frac{n}{8}} = \frac{\Theta^{-\frac{5}{8}}}{1 - \Theta^{-\frac{1}{8}}}$, which is valid in the early inspiral phase with $\Theta \gg 1$. Therefore we'll consider our 2PN approximation to have reached the break down point when the contribution due to all the higher order terms becomes greater than the contribution of the smallest 2PN term in our expansion, so:

$$\Theta_{lim} \iff \Delta\Theta_{>2PN} \geq \Delta\Theta_{2PN} \iff \frac{\Theta^{-\frac{5}{8}}}{1 - \Theta^{-\frac{1}{8}}} \geq \Theta^{-\frac{1}{2}}; \quad (7.5)$$

whose solution is $\Theta_{lim} = 256$. Recalling the definition (6.5) of the variable Θ we then find that the

corresponding time to coalescence τ_{lim} is:

$$\tau_{lim} = \frac{5G\mu}{\nu^2 c^3} \Theta_{lim} = 100.9 \text{ ms} \left(\frac{\mu}{M_\odot} \right) \left(\frac{\nu}{0.25} \right)^{-2}; \quad (7.6)$$

and using the Newtonian estimate for the relative separation (1.87) we find:

$$R_{lim} = \frac{4mG}{c^2} \Theta_{lim}^{\frac{1}{4}} = 2R_s \Theta_{lim}^{\frac{1}{4}} = 8R_s. \quad (7.7)$$

where the Schwarzschild radius R_s is associated to the total mass m of the two compact objects. From this line of reasoning, as a rough estimate, we expect the 2.5PN (and higher order) post-Newtonian corrections to be for sure non negligible when the relative separation is $\frac{8}{3} \sim 2.6$ times the innermost stable circular orbit of a Schwarzschild black hole with mass $m = m_1 + m_2$.

On the other hand, if we want to measure deviations of the highest 2PN coefficients from the value predicted by general relativity with at least a relative precision ϵ , then correspondingly also the systematic error must be at least ϵ time smaller than the absolute value of the 2PN coefficients; hence in this case we have to stop the analysis of our data at:

$$\Theta_{lim,\epsilon} \iff \frac{\Delta\Theta_{>2PN}}{\Delta\Theta_{2PN}} \geq \epsilon \iff \frac{\Theta^{-\frac{1}{8}}}{1 - \Theta^{-\frac{1}{8}}} \geq \epsilon \implies \Theta_{lim,\epsilon} = \frac{(1 + \epsilon)^8}{\epsilon^8} \epsilon^{\ll 1} \approx \epsilon^{-8}, \quad (7.8)$$

which translates into

$$\tau_{lim,\epsilon} = \frac{5G\mu}{\nu^2 c^3} \epsilon^{-8} = 3.94 \cdot 10^4 \text{ s} \left(\frac{\mu}{M_\odot} \right) \left(\frac{\nu}{0.25} \right)^{-2} \left(\frac{\epsilon}{0.1} \right)^{-8}, \quad R_{lim,\epsilon} = 2 \epsilon^{-2} R_s; \quad (7.9)$$

where $3.94 \cdot 10^4$ seconds are almost 11 hours, and choosing $\epsilon = 0.1$ implies cutting off the observation when the relative separations is about 65 times the innermost stable circular orbit. Let us notice that for finite values of ϵ we should actually use the exact formula (7.8), so starting from formula (7.9) and below, we should substitute $\epsilon \rightarrow f(\epsilon) \equiv \frac{\epsilon}{1+\epsilon}$. Nonetheless for simplicity we'll neglect this point, treating ϵ as an effective parameter: in practice choosing $\epsilon = 0.1$ here below means imposing the cutoff threshold for $\frac{\Delta\Theta_{>2PN}}{\Delta\Theta_{2PN}} \geq 0.111$, instead of 0.1 (for higher values of ϵ the difference is larger, but then the PN approximation itself starts to breakdown; furthermore our estimate of the quantity $\Delta\Theta_{>2PN}$ may not even be accurate at $\mathcal{O}(1)$, let alone the order $\mathcal{O}(0.1)$ relative difference discussed above). Such an approximation proves to be useful also because, using equation (7.9) and the virial theorem (1.45), at the threshold we're considering we may expect the relative velocity of the two compact objects to be $\left(\frac{v_{lim,\epsilon}}{c} \right)^2 = \frac{R_s}{2} \frac{1}{R_{lim,\epsilon}} = \left(\frac{\epsilon}{2} \right)^2$, so in practice $\epsilon^2 \sim v^2$ is the PN expansion parameter, and we may expect any half-PN ($\propto v$) higher order contribution to be ϵ times lower than the preceding one.

One should be careful of assessing the impact that the choice of the ϵ parameter could have on the forecast: in fact the quantity $\tau_{lim,\epsilon}$ is highly sensitivity to the value of ϵ , since $\tau_{lim,\epsilon} \propto \epsilon^{-8}$. This may be explained by the fact that the relative distance $R_{lim,\epsilon}$ itself depends on ϵ via $R_{lim,\epsilon} \propto \epsilon^{-2}$, and the more distant the two compact object, the slower it's their orbital decay due to gravitational wave emission: this result could have been expected also from equation (1.84). Therefore the result which we will obtain may present a strong dependence on the ϵ parameter, and so we need to balance the tradeoff between the accuracy of the result (as increasing the ϵ value increases the systematic error due to the theoretical uncertainties, as we approach the merger phase) and the precision of the results (as lowering the ϵ parameter restricts our observation window to only the earliest part of the inspiral phase, where the amplitude of the signal is lower, and so the signal-to-noise ratio to be expected for the observation is lower, and so the precision of any measurement that can be performed on the collected signal).

In practice we will chose, even if somewhat arbitrarily, the threshold

$$\epsilon = 0.1 . \quad (7.10)$$

We argue that this should prove to be a good choice for the cutoff, possibly not too conservative, as it should still allow for signals to be observable in gravitational wave detectors. A justification instead for not choosing an higher value for it is that otherwise both the slow velocity $\frac{v}{c} \propto \epsilon \ll 1$ and the weak field $\frac{Gm}{r} \propto \epsilon^2 \ll 1$ assumptions would start to break down, as we expect strong gravity effects to be important when $r \rightarrow R_s$. Furthermore this choice for the threshold will be consistent if the forecast predicts an error bar on the 2PN parameters at least bigger than $|\delta_{4n}| > \epsilon = 0.1$, i.e. if the expected statistical error is larger than this estimated systematic error.

7.1.2 — Suitability of gravitational wave observatories to perform the test

It is now clear that, in order to directly constraint the post-Newtonian theory, we need a gravitational wave detector sensitive at low frequencies. This follows from the need to accurately measure many cycles of the gravitational signal, with an high enough signal-to-noise ratio (SNR), when the binary is still in its early inspiral phase: in this stage in fact the frequency of the gravitational signal is lower, as well as its amplitude. To be more quantitative about this point, the Newtonian estimate for the frequency of the gravitational wave at the time $\tau_{lim,\epsilon}$, using equation (1.88) is given by:

$$f_{gw,lim,\epsilon} = \frac{c^3}{8\pi G m} \epsilon^3 \approx 8.08 \text{ Hz} \left(\frac{m}{M_\odot} \right)^{-1} \left(\frac{\epsilon}{0.1} \right)^3 . \quad (7.11)$$

We can then see that to perform such a test ground-based gravitational wave detector are not optimal, be they present (LIGO-Virgo-KAGRA) or future (Einstein Telescope, Cosmic Explorer) ones: below about 10 Hz the seismic noise (and also the Newtonian noise) becomes dominant and therefore the detectors sensitivity curve rises quickly. So, apart from compact systems with a sub-solar total mass, or extremely loud (so near) events, we don't expect to be able to observe enough waveform cycles in the low frequency region of interest ($\lesssim 5$ Hz for solar mass systems, $\lesssim 0.1$ Hz for binary black holes systems with $m = 80M_\odot$ total mass) to allow for a powerful and accurate test. Loosening the requirement of $\epsilon \lesssim 0.1$ would increase the value of the cutoff frequency $f_{gw,lim,\epsilon}$, and so would allow to employ also data observed with ground-based gravitational waves detector to perform this test, nonetheless this would also increase the systematic error: first because higher order PN corrections become important, and also due to the breakdown of the post-Newtonian asymptotic series itself (adding higher order PN corrections may actually lead to a worsening of the convergence of the series when the relative velocity becomes high enough).

Therefore (future) space-based detectors (like LISA and DECIGO) seem to be better suited to explore this low-frequency region of the signal. In particular *in the following we will focus on the LISA detector*, performing the forecast on its ability to constraint the $\{\delta_{mn}\}$ parameters.

■ Initial frequency for the observation

To perform the forecast it will be necessary also to estimate the initial and the final frequencies of the observation: in practice we'll assume the observation to always reach the $f_{gw,lim,\epsilon}$ threshold frequency given by (7.11). Therefore we'll have the freedom to choose the observation time $\Delta\tau$, and this instead will fix the initial frequency of the binary, at the start of the observation.

To evaluate this initial frequency we recall once again equation (1.88), and once defined

$$\mathcal{B} = \frac{256 G^{\frac{5}{3}}}{5 c^5} \pi^{\frac{8}{3}} M_c^{\frac{5}{3}} = \frac{256 G^{\frac{5}{3}}}{5 c^5} \pi^{\frac{8}{3}} \mu^{\frac{5}{3}} \nu^{-\frac{2}{3}} = 122.82 \frac{\text{Hz}^{-\frac{8}{3}}}{\text{year}} \left(\frac{\mu}{M_\odot} \right)^{\frac{5}{3}} \left(\frac{\nu}{0.25} \right)^{-\frac{2}{3}} \quad (7.12)$$

it holds:

$$f_{gw}(\tau) = (\mathcal{B} \tau)^{-\frac{3}{8}}. \quad (7.13)$$

From this we can obtain:

$$f_{in}(\Delta\tau) = \left((f_{fin})^{-\frac{8}{3}} + \mathcal{B} \Delta\tau \right)^{-\frac{3}{8}}. \quad (7.14)$$

where $\Delta\tau \equiv \tau_{in} - \tau_{fin} = t_{fin} - t_{in}$ is the time elapsed between the moment in which the frequency of the gravitational wave was f_{in} and the moment in which it reached f_{fin} . Then, imposing the cutoff frequency to be (7.11), so $f_{fin} = f_{gw,lim,\epsilon}$, and the observation time to be $\Delta\tau$, the initial frequency f_{in} of the gravitational wave signal is given by:

$$\begin{aligned} f_{in}(\Delta\tau) &= \left(\left(\frac{256 G^{\frac{5}{3}}}{5 c^5} \pi^{\frac{8}{3}} \mu^{\frac{5}{3}} \nu^{-\frac{2}{3}} \right) \Delta\tau + \left(\frac{c^3}{8\pi G} \frac{1}{m} \epsilon^3 \right)^{-\frac{8}{3}} \right)^{-\frac{3}{8}} \\ &= 0.1646 \text{ Hz} \left(\frac{\mu}{M_{\odot}} \right)^{-\frac{5}{8}} \left(\frac{\nu}{0.25} \right)^{\frac{1}{4}} \left(\left(\frac{\Delta\tau}{1 \text{ year}} \right) + 1.2486 \cdot 10^{-3} \left(\frac{\mu}{M_{\odot}} \right) \left(\frac{\nu}{0.25} \right)^{-2} \left(\frac{\epsilon}{0.1} \right)^{-8} \right)^{-\frac{3}{8}}. \end{aligned} \quad (7.15)$$

This estimate actually is valid only at leading order, since it receives post-Newtonian corrections at higher order. Yet the precision of the estimates of the forecast probably won't be high enough to require the inclusion of such corrections, since there will be many other approximations involved.

In the following we will denote as *early inspiral* phase the period in which the binary system is inspiraling while emitting gravitational waves with a (quadrupole) frequency below the threshold given by (7.11); then in practice, given the observation time $\Delta\tau$ the observational window relevant for the test will go from frequency (7.15) to the cutoff frequency (7.11).

■ Synergy with future ground-based detectors

In order to perform the forecast we have also to recognize that, in order to perform the test, one has first to confidently detect the relevant binary system. Regarding this point, we'll base our considerations on the fact that in current observations the threshold needed to declare event detection confidently enough is for it to have an $\text{SNR} \gtrsim 8$ [5].

Nevertheless when multiple detectors observe the same event, the data can be combined in order to increase the SNR and obtain more precise estimates, as we have already seen in equation (1.102). Therefore in the following we'll consider also the possible scenario where a binary system may not accumulate enough SNR in the LISA detector alone (e.g. $\text{SNR} < 8$ for definiteness), but after some time, under suitable conditions, its chirping signal may sweep (possibly quite loudly) through the sensitivity band of ground-based detectors, such as the future Einstein Telescope and Cosmic Explorer, and be detected by them (since they should all come online in the same years). This should be the case of binary systems with total mass of about $1 M_{\odot} \lesssim m \lesssim 10^3 M_{\odot}$: after their detection by ET and CE it would be possible to search in the previous data recorded by LISA to possibly spot such a signal, which before was recorded only with an signal-to-noise ratio of $1 < \text{SNR} < 8$, and hence not promptly detected. At this point one could join these dataset a posteriori to greatly increase the precision of the estimates; and in particular, for what concerns the test we're describing in this chapter, once identified the signal it would be possible to perform the test we're describing here on the LISA stretch of data alone, as it contains all the information about the early inspiral phase.

On the other hand we do not expect systems with total mass $m < M_{\odot}$ or $m > 10^5 M_{\odot}$ to accumulate enough SNR in the LISA detector to perform meaningful a test. That is, barring the possibility of an extremely near event, these binary systems should accumulate less than $\text{SNR} < 1$ in the LISA detector: the binaries with sub-solar masses produce a signal too high in frequency; on the other

hand instead the binary systems with $m > 10^5 M_\odot$ may actually be detected with a quite high SNR by LISA; but then the SNR evaluated only on the *early* inspiral phase, as defined above, would be $\text{SNR} < 1$ (since we also expect these systems to be detected only at quite high redshifts); in fact in the early inspiral phase their frequency is below the frequencies to which LISA is most sensitive.

Let us also add that, recalling definition (7.11) for the cutoff frequency, sub-solar systems may actually be good candidates if we were to employ next-generation ground based interferometers to perform this test. However in that case we'd be most sensitive to the signal in proximity of its cutoff frequency, instead of its earliest inspiral phase; and furthermore probably we may not be able to observe the binary systems for as many cycles as LISA could.

7.2 | The LISA observatory

The *Laser Interferometer Space Antenna* (LISA) [91, 285] is a future space-based gravitational wave observatory. It was first proposed in the 1990s; in 2017 it was selected by the *European Space Agency* (ESA) as a large class mission in the *Cosmic Vision 2015-2025 Programme*, and recently the project has advanced into the refinement phase B1 [125]; currently its planned launch date is 2037 [286]. The nominal duration of the mission will be 4 years, but it could possibly be extended up to 10 years. Most of the technology necessary for this mission has already been tested by the *LISA Pathfinder* mission [287, 288].

LISA will be composed of three separate spacecrafts, each orbiting along heliocentric orbits, trailing Earth by about 50 million kilometers, as depicted in figure 7.1. The orbits are arranged in such a way that the combined motion of the three spacecraft will keep each of them at one vertex of an equilateral triangle shape, with side of length approximately 2.5 million kilometers. Each of the sides of this triangle will represent the arm of an interferometer.

In fact inside each of the three spacecrafts there will be two test masses, one for each of the two sides ending in that spacecraft. These test masses will be in almost perfect free fall, and a suitable interferometric apparatus will allow to measure the distances between these test masses [91]. Then by synthetically combining the data in a suitable way, employing for example also the technique of the time delay interferometry to limit the laser phase noise, it will be possible to measure the perturbations to the arms' length due to the passage of gravitational waves. This will allow LISA to measure gravitational waves with excellent sensitivity in the frequency band between 10^{-4} Hz and 0.1 Hz [91].

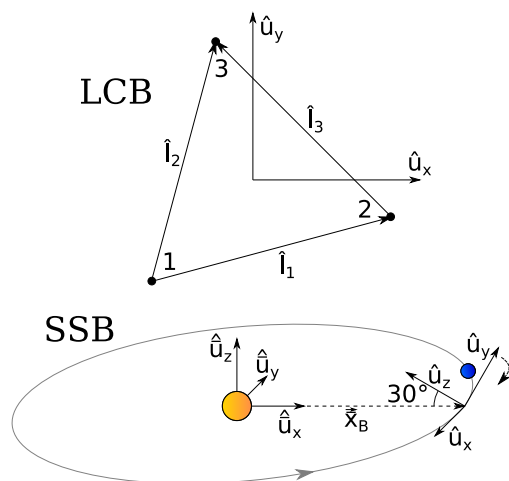


FIGURE 7.1 — Figure depicting the coordinate frames used in this work: the LISA Constellation Baricenter (LCB), which is the local coordinate frame of the instrument, and the Solar System Baricenter (SSB) global reference frame. Furthermore the orbital motion of LISA is also depicted, with the Sun in orange and the Earth in blue.

7.2.1 — Modeling of the LISA interferometer

In order to be able to estimate the precision with which LISA will be able to constraint the δ_{mn} deformation parameters, first of all we need to evaluate its response to the metric perturbation $h_{ij}^{(TT)}$: in fact, via relations (6.44), it reflects the modifications to the phase (7.2). In this section then we'll briefly outline how we modelize the LISA observatory in order to obtain the expression for its response function. Our treatment is based on the one of reference [154], updated with the

latest specifications [91, 285, 289], and while making several approximations, it captures most of the relevant effects which have to be taken into account to obtain accurate estimates.

Let us then recall the discussion in section 1.5 about gravitational detectors; and in particular the mathematical treatment presented in section 1.5.1. Space born gravitational detectors however require additional care: usually they composed of a constellation of several spacecraft orbiting in the solar system, and the signals they're expected to observe may sweep through the sensitivity band of the instrument over months or even years; the this means that we cannot assume the local coordinate frame of the detector to be approximately inertial, and instead we have to take into account the orbital motion. Furthermore the arms are extremely long, to the points that these detectors are able to observe signals also at frequencies $f \sim \frac{L}{c}$, hence the low frequency approximation employed in relation (1.108) strictly speaking doesn't hold anymore, and so the exact response function should be taken into account.

■ Relevant coordinate frames

The proceed it is useful to define two coordinate frame in which we will work: the LCB (LISA Constellation Barycenter) frame and the SSB (Solar System Barycenter) frame, which are represented in figure 7.1. In the following vector components evaluated in the LCB frame $\{\hat{\mathbf{u}}_x, \hat{\mathbf{u}}_y, \hat{\mathbf{u}}_z\}$ are denoted as \mathbf{x} ; whereas the ones evaluated in the SSB frame $\{\overline{\hat{\mathbf{u}}}_x, \overline{\hat{\mathbf{u}}}_y, \overline{\hat{\mathbf{u}}}_z\}$ are overlined, so $\overline{\mathbf{x}}$. In particular, up to higher order corrections, we can assume the SSB to be an inertial frame in the Newtonian sense. Therefore, up to a (almost) fixed relative velocity that would induce a Doppler shift correction, we can assume the relative distance between the compact binary system emitting gravitational wave and the barycenter of the solar system (which lies just outside the surface of the sun) to be constant.

Approximating then the orbit of the center of the constellation to be circular (i.e. the origin of the LCB frame, which is the center of the triangular constellation), up to a shift of the time variable and a rotation of the SSB frame, we can parametrize its position $\overline{\mathbf{x}}_B(t)$ in the SSB frame as

$$\overline{\mathbf{x}}_B(t) = R \left(\cos \left(\frac{2\pi}{T_o} t \right) \hat{\mathbf{u}}_x + \sin \left(\frac{2\pi}{T_o} t \right) \hat{\mathbf{u}}_y + 0 \hat{\mathbf{u}}_z \right), \quad (7.16)$$

where $T_o \approx 1$ year is the orbital period, and $R \approx 1\text{AU} \approx 1.5 \cdot 10^{11}$ m the radius of the orbit.

Switching to the LCB frame, here we parametrize the position \mathbf{x}_a of the spacecraft a , with $a = 1, 2, 3$, as depicted in figure 7.1, so with:

$$\mathbf{x}_a = \frac{L}{\sqrt{3}} (\cos(\phi_a) \hat{\mathbf{u}}_x + \sin(\phi_a) \hat{\mathbf{u}}_y + 0 \hat{\mathbf{u}}_z) \quad (7.17)$$

with $\phi_a = (a - 1) \frac{2\pi}{3} - \frac{3}{4}\pi$, where $L \approx 2.5 \cdot 10^9$ m is the length of the side of the triangle.

Now we have to take into account the orbital motion of the spacecraft, which can be done by finding a suitable, time dependent, rotation matrix $R_{ij}(t)$ which relates the vector components between the SSB frame and the (rotating) LCB frame, taking also into account the 60 degree offset between the $\hat{\mathbf{u}}_z$ and $\overline{\hat{\mathbf{u}}}_z$ versors (see figure 7.1). Performing this procedure we find the position of the a -th spacecraft in the SSB frame to be:

$$\begin{aligned} \overline{\mathbf{x}}_a(t) = \overline{\mathbf{x}}_B(t) + \frac{L}{\sqrt{3}} \left(\frac{1}{4} \left(3 \sin(\phi_a + \phi_0) - \sin \left(\phi_a + \phi_0 - 2 \frac{2\pi}{T_o} t \right) \right) \overline{\hat{\mathbf{u}}}_x \right. \\ \left. - \frac{1}{4} \left(3 \cos(\phi_a + \phi_0) + \cos \left(\phi_a + \phi_0 - 2 \frac{2\pi}{T_o} t \right) \right) \overline{\hat{\mathbf{u}}}_y + \frac{\sqrt{3}}{2} \sin \left(\phi_a + \phi_0 - \frac{2\pi}{T_o} t \right) \overline{\hat{\mathbf{u}}}_z \right); \end{aligned} \quad (7.18)$$

where ϕ_0 is a constant phase which encodes the orientation of the constellation at $t = 0$.

■ Pattern function of the interferometers

With all of the above definitions, we can now work in the (rotating) LCB frame to evaluate the pattern function of the LISA interferometer: we'll recall then what we've already seen in section 1.5.1. Moreover we assume the motion of the LCB frame to be negligible instant by instant: this approximation may break down for signals with a frequency comparable or below the (inverse of the) timescale of the orbital motion; nevertheless this shouldn't be the case for LISA, since it is sensitive to frequencies above $f > 10^5$ Hz whereas the timescale of the orbital motion is of the order of the year ($f \sim 10^{-8}$ Hz).

The other difference with respect to section 1.5.1 is that LISA triangular interferometric detector, hence composed of three arms which subtend a 60 degrees angle. Consistently with figure 7.1, in the LCB frame we denote the versors aligned with each of the three arms as $\hat{\mathbf{l}}_1 \equiv \frac{(\mathbf{x}_2 - \mathbf{x}_1)}{L}$, $\hat{\mathbf{l}}_2 \equiv \frac{(\mathbf{x}_3 - \mathbf{x}_1)}{L}$ and $\hat{\mathbf{l}}_3 \equiv \frac{(\mathbf{x}_3 - \mathbf{x}_2)}{L}$. Then we can similarly to section 1.5.1; yet in this case the three Michelson interferometer which we may build (one for each vertex of the triangle, using the two arms entering in the vertex) are not independent: that is, the strain which we may collect from this configuration would contain redundant information. Then what is customarily done, assuming the noise to be equal in all of these three Michelson interferometers, we can diagonalize such the noise matrix (i.e. the matrix of the power spectral density (1.101)). This procedure, while taking into account other technical details, leads to the A, E and T channels: two of them are sensitive to the gravitational wave signal, whereas the third is much less sensitive: yet it is useful as a null channel, to characterize the noise in the detector. Nonetheless we'll proceed with the simplified setup of reference [154], which considers only the two channels sensitive to gravitational waves, denoting them as I and II . The result is that, under the approximation of low frequency $f \lesssim \frac{c}{L} \approx 0.12$ Hz, the equivalent of equation (1.108) for the dimensionless strain is now given by

$$h_I(t) = \frac{1}{2} h_{ij}^{TT}(t) (l_1^i l_1^j - l_2^i l_2^j) , \quad (7.19a)$$

$$h_{II}(t) = \frac{1}{2\sqrt{3}} h_{ij}^{TT}(t) (l_1^i l_1^j + l_2^i l_2^j - 2l_3^i l_3^j) . \quad (7.19b)$$

From these expressions we can then obtain the corresponding pattern functions, similarly to equations (1.110), such that it holds (1.109).

To do so we have to specify precisely the frame for the polarization tensors e_{ij}^+ and e_{ij}^\times . In particular, working still in the LCB frame, for what will follow we choose $\hat{\mathbf{n}}$ to be the versor which points toward the source of gravitational waves starting for the detector (and so it's the opposite of the $\hat{\mathbf{n}}$ versor which we employed in chapter 1), which we parametrize by introducing the spherical angles θ_s and ϕ_s , via

$$\hat{\mathbf{n}} = (\sin(\theta_s) \cos(\phi_s), \sin(\theta_s) \sin(\phi_s), \cos(\theta_s)) . \quad (7.20)$$

Then we define the e_{ij}^+ and e_{ij}^\times polarization tensors in the orthonormal frame with $\{\hat{\mathbf{u}}, \hat{\mathbf{v}}, -\hat{\mathbf{n}}\}$, which is the same one depicted in figure 1.4 once we just relabel $\hat{\mathbf{n}} \rightarrow -\hat{\mathbf{n}}$ in that figure. Furthermore we also have to be consistent with the choice we performed in section 6.2.1, hence we chose again the $\hat{\mathbf{u}}$ axis to lie along the projections on the sky of the major axis of the orbit, oriented toward the ascending node.

In the LCB frame instead, using a spherical coordinate frame, we introduce the auxiliary versors $\hat{\mathbf{u}}' = (-\cos(\theta_s) \cos(\phi_s), -\cos(\theta_s) \sin(\phi_s), \sin(\theta_s))$, which points along the meridian in direction of increasing θ_s , and $\hat{\mathbf{v}}' = (-\sin(\phi_s), \cos(\phi_s), 0)$, which points along the parallel toward increasing ϕ_s . Then to superimpose the $\{\hat{\mathbf{u}}', \hat{\mathbf{v}}', -\hat{\mathbf{n}}\}$ orthonormal frame onto the $\{\hat{\mathbf{u}}, \hat{\mathbf{v}}, -\hat{\mathbf{n}}\}$ one we can perform a clockwise rotation of the $\hat{\mathbf{u}}'$ and $\hat{\mathbf{v}}'$ axes around the $-\hat{\mathbf{n}}$ axis, by an angle $\psi_s = \arctan(\frac{\hat{\mathbf{z}} \cdot \hat{\mathbf{v}}}{\hat{\mathbf{z}} \cdot \hat{\mathbf{u}}})$, which is called the *polarization angle*.

With all of these definitions we can finally evaluate the *pattern functions* for the $\alpha = I, II$ interferometric channels: since in practice both configurations are related by a rotation of an angle $\frac{\pi}{4}$ in the $\hat{\mathbf{u}}_x \hat{\mathbf{u}}_y$ plane, we can define the constant ϕ_α , such that $\phi_I = 0$ and $\phi_{II} = -\frac{\pi}{2}$. Then the expression for the pattern function is given by:

$$F_\alpha^+(\theta_s, \phi_s, \psi_s) = \frac{\sqrt{3}}{2} \left(\frac{(1 + \cos^2(\theta_s))}{2} \cos(2\phi_s + \phi_\alpha) \cos(2\psi_s) - \cos(\theta_s) \sin(2\phi_s + \phi_\alpha) \sin(2\psi_s) \right), \quad (7.21a)$$

$$F_\alpha^\times(\theta_s, \phi_s, \psi_s) = \frac{\sqrt{3}}{2} \left(\frac{(1 + \cos^2(\theta_s))}{2} \cos(2\phi_s + \phi_\alpha) \sin(2\psi_s) + \cos(\theta_s) \sin(2\phi_s + \phi_\alpha) \cos(2\psi_s) \right); \quad (7.21b)$$

in this way the dimensionless strain is given by

$$h_\alpha(t) = F_\alpha^+(\theta_s, \phi_s, \psi_s) h_+(t) + F_\alpha^\times(\theta_s, \phi_s, \psi_s) h_\times(t), \quad (7.22)$$

where $h_+(t)$ and $h_\times(t)$ are evaluated at the barycenter of the LISA constellation.

■ Modulation of the signal due to the orbital motion

We derived the above results, i.e. equations (7.21) and (7.22), in the LCB rotating frame: the last step that we have to perform is now to recast these results as evaluated in the SSB inertial frame. For example the components of the versor $\hat{\mathbf{n}}$, which are given by (7.20), are a function of time, $\theta_s = \theta_s(t)$ and $\phi_s = \phi_s(t)$: this is because the constellation is rotating on itself, and therefore in the LCB frame a far away fixed star will appear to be moving.

Switching to the inertial SSB frame we now parametrize the versor $\hat{\mathbf{n}}$, which points toward the distant binary system, in spherical coordinates as $\hat{\mathbf{n}} = (\sin(\bar{\theta}_s) \cos(\bar{\phi}_s), \sin(\bar{\theta}_s) \sin(\bar{\phi}_s), \cos(\bar{\theta}_s))$; let us recall that the overlined quantities $\bar{\theta}_s$ and $\bar{\phi}_s$ are in fact evaluated in the SSB frame. This means that these last angles are constant during the whole observational period, since the SSB frame is taken to be non-rotating with respect to the distant stars. Furthermore we assume the plane of the distant compact binary system to not be precessing, therefore also the polarization angle $\bar{\psi}_s$, evaluated in the SSB frame with a procedure analogous to before, is quantity constant in time.

The relations between the angles $\phi_s(t)$, $\theta_s(t)$ and $\psi_s(t)$ in the LCB frame and the corresponding (constant) quantities $\bar{\phi}_s$, $\bar{\theta}_s$ and $\bar{\psi}_s$ in the SSB frame can be found by applying the relevant rotation matrix $R_{ij}(t)$ which connects the two coordinate systems. In practice it's possible also to find these relations by evaluating suitable spatial scalar products (which are invariant under rotations) between the several versors we defined until now, to obtain:

$$\phi_s(t) = \arctan \left(\frac{\tan(\bar{\theta}_s)(\cos(\bar{\phi}_s + \phi_0 - 2\frac{2\pi}{T_o}t) - 3 \cos(\bar{\phi}_s - \phi_0)) - 2\sqrt{3} \cos(\frac{2\pi}{T_o}t - \phi_0)}{\tan(\bar{\theta}_s)(\sin(\bar{\phi}_s + \phi_0 - 2\frac{2\pi}{T_o}t) + 3 \sin(\bar{\phi}_s - \phi_0)) + 2\sqrt{3} \sin(\frac{2\pi}{T_o}t - \phi_0)} \right), \quad (7.23a)$$

$$\theta_s(t) = \arccos \left(\frac{\cos(\bar{\theta}_s)}{2} - \frac{\sqrt{3}}{2} \cos \left(\bar{\phi}_s - \frac{2\pi}{T_o}t \right) \sin(\bar{\theta}_s) \right), \quad (7.23b)$$

$$\psi_s(t) = \arctan \left(\frac{\sin(\bar{\psi}_s)(\sqrt{3} \cos(\bar{\theta}_s) \cos(\frac{2\pi}{T_o}t - \bar{\phi}_s) + \sin(\bar{\theta}_s)) - \sqrt{3} \cos(\bar{\psi}_s) \sin(\frac{2\pi}{T_o}t - \bar{\phi}_s)}{\cos(\bar{\psi}_s)(\sqrt{3} \cos(\bar{\theta}_s) \cos(\frac{2\pi}{T_o}t - \bar{\phi}_s) + \sin(\bar{\theta}_s)) + \sqrt{3} \sin(\bar{\psi}_s) \sin(\frac{2\pi}{T_o}t - \bar{\phi}_s)} \right). \quad (7.23c)$$

Since we'll be using the restricted PN waveform, we can recall the expression for the its amplitude from equation (6.41), and in particular (6.42a) and (6.42a). With those definitions, understanding

the replacement $\phi_s \rightarrow \phi_s(t, \bar{\phi}_s, \bar{\theta}_s, \bar{\psi}_s)$ via (7.23), and similarly for θ_s and ψ_s ; we can recast (7.22) as:

$$h_\alpha(t, \bar{\theta}_s, \bar{\phi}_s, \bar{\psi}_s) = A_\alpha(t, \bar{\theta}_s, \bar{\phi}_s, \bar{\psi}_s) \cos(\Phi(t) + \varphi_{p,\alpha}(t, \bar{\theta}_s, \bar{\phi}_s, \bar{\psi}_s)) \quad (7.24)$$

with

$$A_\alpha = \frac{2G\mu x}{c^2 r} \sqrt{((1 + \cos^2(\iota))F_\alpha^+)^2 + (2 \cos(\iota) F_\alpha^\times)^2}, \quad (7.25a)$$

$$\varphi_{p,\alpha} = \arctan\left(\frac{2 \cos(\iota) F_\alpha^\times}{(1 + \cos^2(\iota))F_\alpha^+}\right); \quad (7.25b)$$

and where we defined $\Phi(t) \equiv 2\phi(t)$, with $\phi(t)$ the orbital phase of the binary system, which we found at 2PN in equation (6.39).

Furthermore, as we've pointed out above, the $h_+(t)$ and $h_\times(t)$ quantities which enter in equation (7.22) are evaluated in the barycenter of the constellation; nevertheless this point is actually orbiting around the sun, as parametrized by (7.16). Then as a first approximation, we can evaluate the values of $h_+(t)$ and $h_\times(t)$ in the barycenter of the solar system, adding the phase $\varphi_D(t, \bar{\theta}_s, \bar{\phi}_s) = -2\pi f(t) \frac{-\hat{n} \cdot \vec{x}_B}{c} = 2\pi f(t) \frac{R}{c} \sin(\bar{\theta}_s) \cos(\frac{2\pi}{T_o} t - \bar{\phi}_s)$ to the phase $\Phi(t)$ in equation (7.24), with $f(t)$ the instantaneous frequency of the gravitational waves at time t ; this correction is needed to account for the difference in the phase of the gravitational signal between the barycenter of the LISA constellation and the barycenter of the solar system [154].

■ Fourier transform of the measured strain

As we will see, to perform the Fisher forecast we will need the Fourier transform of the above expression (7.24). To find it we can employ the stationary phase approximation, which we already introduced in equation (6.43). In this case we can use such an approximation since the frequency of the gravitational wave is much higher than the orbital motion, which then induce only a slow modulation of the carrier signal. In practice, following reference [154, 155], simplifying further given the slow evolution of the orbital modulation, we apply the stationary phase approximation only to the gravitational wave phase, adding afterwards the orbital modulation total phase ($\varphi_{p,\alpha} + \varphi_D$). Doing so we find:

$$\tilde{h}_\alpha(f) = \sqrt{\left(\frac{1 + \cos^2(\iota)}{2} F_\alpha^+(t(f))\right)^2 + (\cos(\iota) F_\alpha^\times(t(f)))^2} e^{-i(\varphi_{p,\alpha}(t(f)) + \varphi_D(t(f)))} \mathcal{A}(f) e^{i\Psi(f)}, \quad (7.26)$$

where $\mathcal{A}(f)$ is given in (6.45) $\Psi(f)$ is given in (6.46). Furthermore $t(f)$ gives the time as a function of the gravitational wave frequency, taking into account higher order PN corrections; the explicit expression for example is reported in [103].

Let us still recall that this modelization of the response function of LISA, while including all the essential features, is valid only as a first approximation; to perform a more detailed study one may have to consider a more accurate, potentially numerical, model.

7.2.2 — Noise power spectral density

As we will see in the next section 7.3, to perform the forecast we will also need to know how sensitive is each of the two I, II channels of LISA; i.e. we will need to know their joint noise power spectral density $S_n(f)$, which we defined in (1.101). In practice, since we already diagonalized such matrix with the previous construction, we assume such metric to be diagonal, with equal noise power spectral density $S_n(f)$ for both channels. For its analytical expression, which we also plot

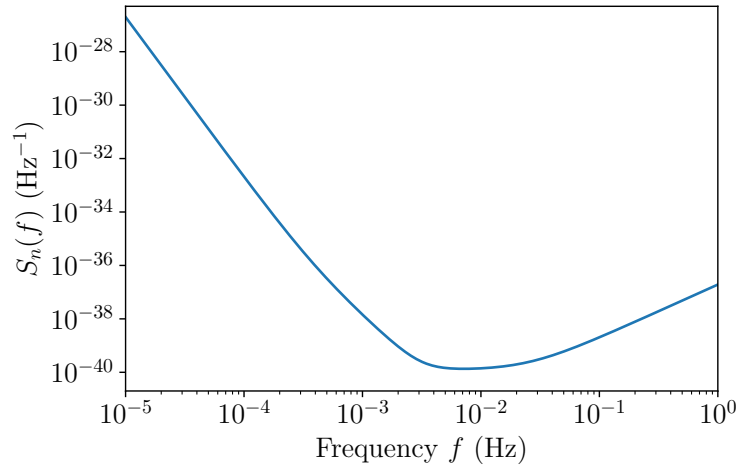


FIGURE 7.2 — The noise power spectral density $S_n(f)$ assumed for the *I* and *II* configurations of LISA.

in figure 7.2, we employ the sky and polarization averaged estimates of references [289, 290]:

$$S_n(f) = \frac{10}{3} \left(\frac{1}{(2\pi f)^4} \left(5.76 \cdot 10^{-48} \text{ Hz}^3 \left(1 + \left(\frac{0.4 \text{ mHz}}{f} \right)^2 \right) \right) + 3.6 \cdot 10^{-41} \frac{1}{\text{Hz}} \left(1 + \left(\frac{f}{25 \text{ mHz}} \right)^2 \right) \right). \quad (7.27)$$

However let us point out that here we're neglecting the *confusion noise* at low frequencies due to the superposition of the gravitational waves coming many non-resolvable binaries [154]; whereas at higher frequencies it may be needed to take into account the implementation of the virtual interferometry [291].

7.3 | Fisher matrix for observational forecasts

In order to assess the observational capabilities of future gravitational wave detectors it is customary to employ the *Fisher information matrix* technique. In practice, once the design and the sensitivity of a detector are specified, this analytical method allows one to evaluate the smallest error bars that such an experiment could ever achieve when observing the quantities of interest, once specified the fiducial value that one assumes for those quantities.

For the specific forecast that we are trying to perform, this means that once we specify how the $\{\delta_{mn}\}$ deformation parameters modify the waveform that could be observed by LISA, once we specify the sensitivity of the LISA instrument, and once we assume a fiducial value for the $\{\delta_{mn}\}$ parameters; then we can evaluate the minimum error bars associated to the measurement of the $\{\delta_{mn}\}$ parameters that we will possibly achieve. In particular, since general relativity still is our best model, we will chose as fiducial value $\delta_{mn} = 0$ for every m and n ; in fact in this case we recover the standard general relativity results.

Let us recall the notation we employed for the matched filtering technique in section 1.5, and the definition of the scalar product (1.100). Then the signal we measure in the several instruments is given by $\mathbf{o} = \mathbf{n} + \mathbf{h}$, with \mathbf{n} the noise contribution to the measured output, and \mathbf{h} the contribution due to the real gravitational wave. Then, assuming gaussian noise, the probability for a specific realization \mathbf{n}_0 of the noise is given by

$$p(\mathbf{n} = \mathbf{n}_0) \propto e^{-\frac{1}{2}(\mathbf{n}_0 | \mathbf{n}_0)} = e^{-\frac{1}{2}(\mathbf{o} - \mathbf{h} | \mathbf{o} - \mathbf{h})}, \quad (7.28)$$

which is the likelihood for observing such signal [103, 154]. Let us notice that in this notation (1.100) for the scalar product enters the power spectral density $S_n(f)$ of the detector, and hence

the information about the sensitivity of the detector. Let us then assume the gravitational waveform \mathbf{h} to depend on some parameter $\{\lambda\}$, so $\mathbf{h} = \mathbf{h}(\{\lambda\})$, which could be for example the masses of the compact objects, or specifically the $\{\delta_{mn}\}$ deformation parameters in our case. Next, given the prior $p(\{\lambda\})$ for these parameters, from the likelihood (7.28) we obtain the posterior

$$p(\{\lambda\}|\mathbf{o}) \propto p(\{\lambda\}) e^{(\mathbf{h}|\mathbf{o}) - \frac{1}{2}(\mathbf{h}|\mathbf{h})}, \quad (7.29)$$

which gives the probability for the true value of the $\{\lambda\}$ parameters given the observed detector output \mathbf{o} [103]. Then, in the limit of high SNR for the observation, we can assume the value $\{\bar{\lambda}\}$ that we will measure from the observation (e.g. the maximum a posteriori value obtained from a Bayesian analysis of the data) to be near the true value $\{\theta\}$ of these parameters; so we can define the error bar $\Delta\lambda_i$ on parameter i as $\theta^i \equiv \bar{\lambda}^i + \Delta\lambda^i$. Finally, assuming these errors to be small, the prior $p(\{\lambda\})$ to be (almost) uniform around the true value ($\{\lambda\}$) [281], and expanding the posterior (7.29), we obtain [103, 154]

$$p(\{\lambda\}|\mathbf{o}) \propto e^{-\frac{1}{2}\Gamma_{ij}\Delta\theta^i\Delta\theta^j}; \quad (7.30)$$

where, recalling that $\mathbf{h} = \mathbf{h}(\{\lambda\})$, and neglecting higher order terms,

$$\Gamma_{ij} = \left(\frac{\partial\mathbf{h}}{\partial\lambda^i} \middle| \frac{\partial\mathbf{h}}{\partial\lambda^j} \right) \quad (7.31)$$

is called the *Fisher information matrix*. We find that the inverse of this matrix gives an estimate for the expected covariance matrix of the estimates of the $\{\lambda\}$ parameters, as could be measured by the experiment. In fact the expectation value of the errors $\Delta\lambda^i$ is [103, 154]:

$$\langle \Delta\lambda^i \Delta\lambda^j \rangle = (\Gamma^{-1})^{ij} + \mathcal{O}\left(\left(\frac{S}{N}\right)^{-1}\right). \quad (7.32)$$

with these quantities evaluated in $\lambda^i = \bar{\lambda}^i$.

Let us point out that this method is still an approximation, even if quite good, and gives better results when the expected SNR for the observation is higher; in reality, especially when the SNR is low or the associated likelihood complicated, only a full numerical Markov Chain Monte Carlo (MCMC) analysis of the exact likelihood can give the most accurate results [292].

■ Expressions specialized to the case of the LISA detector

Recalling from section 7.2.1 that the observed signal is equivalent to two independent time series $h_I(t)$ and $h_{II}(t)$, we can employ the formalism which we developed in section 1.5 and here above, considering $N = 2$ detectors and assuming an optimal matched filtering.

In particular, given the parameters of a system, we can evaluate the SNR of a given observation employing formula (1.102). Furthermore, specializing the generic definition (7.31) of the Fisher matrix to this specific scenario we find:

$$\Gamma_{ij} = 4 \int_0^{+\infty} df \frac{1}{S_n(f)} \operatorname{Re} \left(\frac{\partial(\tilde{h}_I^*(f))}{\partial\lambda^i} \frac{\partial(\tilde{h}_I(f))}{\partial\lambda^j} + \frac{\partial(\tilde{h}_{II}^*(f))}{\partial\lambda^i} \frac{\partial(\tilde{h}_{II}(f))}{\partial\lambda^j} \right), \quad (7.33)$$

where $\operatorname{Re}(z) = \frac{z+z^*}{2}$ is the real part of the complex number, $\tilde{h}_\alpha(f)$ are given by equation (7.26) with $\alpha = I, II$, and $S_n(f)$ by expression (7.27).

In general relativity the waveform $\tilde{h}_\alpha(f)$ normally depends on 9 parameters, which for example are given by $(d_L, \nu, m, \bar{\mu}_s, \iota, \bar{\phi}_s, \bar{\psi}_s, \phi_0, t_c)$. They are associated to the spinless compact binary system (such as its masses, via m and ν), to its distance (d_L), and to the geometry of the observation

(through the inclination angle ι , the direction in the sky for the observer via $\bar{\mu}_s$ and $\bar{\phi}_s$, the polarization angle $\bar{\psi}_s$, and so on). Furthermore t_c is the time of coalescence for the observer, while ϕ_0 enters in equation (7.18) to encode the initial orientation of the constellation at time $t = 0$; we also defined $\bar{\mu}_s \equiv \cos(\bar{\theta}_s)$.

Generically then, to perform a Fisher forecast, we have to assume the $\{\lambda\}$ parameters to be (at least) all of the 9 aforementioned quantities. This has to be done since in a real analysis of the data, in order to detect a binary system, we have to estimate all of the above quantities. Then we must simulate the procedure of estimating all of these quantities simultaneously as well: in fact the covariance matrix (7.32) that we find with this method takes into account also the covariances between all the parameters. Trying instead to not estimate one of these parameters, so by not including it in the set of $\{\lambda\}$ parameters, amounts to conditioning over such a parameter: then we would find smaller error bars on all of the other parameters, since we've fixed the value of one of them, and so we're extracting less information from the data; nonetheless this would simply lead to an underestimation of the real error bars that the experiment could achieve.

Regarding the test that we want to perform instead, we're trying to estimate the δ_{mn} on top of all of the other 9 parameters: in fact to be able to perform the test we have also to correctly fit the real waveform with our analytical expression, so we still need to estimate all of the aforementioned parameters.

7.4 | Analysis and results

In this section we perform the analysis which we discussed above and report the results. To obtain the latter we wrote a `Mathematica` code, which we run on the CloudVeneto computing facilities [293] for a faster evaluation.

7.4.1 — Details of the analysis

To evaluate the forecast on the upper bound on a given δ_{mn} we proceeded similarly to the procedure of reference [96]: in particular therein it's pointed out that the parametrization (similar to) (7.2) presents correlations among different parameters; in light of this they vary only one parameter at a time, keeping fixed all the others, when performing the analysis. This allows to avoid having a multimodal or degenerate posterior probability density function for the values of the deformation parameters $\{\delta_{mn}\}$; yet the test so performed is still sensitive to generic deviations from general relativity which modify simultaneously more than one of such δ_{mn} parameters [294–296].

Therefore also in our code we proceeded analogously: to evaluate the upper bound on a chosen δ_{mn} parameters we fixed all others to be equally vanishing. More precisely then, recalling the discussion of section 7.3, the parameters $\{\lambda\}$ over which we performed the Fisher matrix evaluation are the 9 parameters associated to the spinless binary in general relativity ($d_L, \nu, m, \bar{\mu}_s, \iota, \bar{\phi}_s, \bar{\psi}_s, \phi_0, t_c$), plus the single additional δ_{mn} parameter.

With this procedure for each of the 7 deformation parameters $\{\delta_{mn}\}$ we evaluated a different 10×10 Fisher matrix Γ_{ij} as given in expression (7.33); next we took the inverse of each matrix; and from each of these inverse matrices then we obtained the expected 90% upper bound that data from LISA could provide in that scenario: we did so by properly rescaling the standard deviation which is given by the square root of the corresponding diagonal entry. Let us notice that trying to consider more than one δ_{mn} parameter at a time instead results in singular Fisher matrix due to the degenerancies present in that parameter space. Furthermore in the Fisher analysis we actually worked with $\log\left(\frac{d_L}{Mpc}\right)$ instead of d_L , with $\log\left(\frac{m_z}{M_\odot}\right)$ instead of m_z and with $\log\left(\frac{t_c}{s}\right)$ instead of

t_c : in fact these dimensional quantities usually span over several orders of magnitudes, and so by taking the logarithm then we were able to increase the numerical precision of the results.

To compute the relevant quantities in our analysis we chose the initial and final time of observation as we discussed in section 7.1.1, choosing $\epsilon = 0.1$. In particular, to simplify the analysis, we always stop the observation exactly at the cut-off frequency (7.11); then, when we modify the observation time $\Delta\tau$ of the system, in practice we only change the initial frequency of the system at the start of the observation using equation (7.15). For the analysis we'll chose $\Delta\tau = 4$ years, which is the nominal duration of the mission; nonetheless we do not expect any loud binary system to reach the cut-off frequency exactly at the end of the observation time: then this choice of $\Delta\tau$ actually reflects the typical observation time of a system we may expect during the extended 10 year LISA mission, accounting also for the 11% technical downtime.

Furthermore the systems relevant in this analysis are far away enough that cosmological corrections become important: then we implement them as outlined in section 1.4.3, assuming the customary flat Λ CDM Planck cosmology [297] to evaluate the luminosity distance d_L given the redshift z of the binary.

Regarding the limitations of this analysis, let us notice that the bounds obtained by Fisher information matrix are most optimistic estimates (since they're based on the Cramér-Rao bound for estimators), therefore this method may underestimate the actual error bars that an experiment may achieve [155, 292, 298]. Also to obtain accurate results we should make the setup as realistic as possible; in particular real gravitational wave data analyses include higher order PN corrections, and actually estimate the spin parameters $\{\chi\}$ (and possibly the tidal deformability $\tilde{\Lambda}$) from the observed signal: then we should do to same in our analysis, by forecasting the expected error bars on these additional parameters. This is in fact necessary to obtain accurate results, because as already discussed the addition of new parameters to be estimated decreases the precision with which we can measure the other ones; in fact now the parameter space is bigger, while the amount of information is the same. Finally, especially if we find the Fisher matrix to not be reliable, a full Monte Carlo analysis of the full non-linear likelihood may be needed to obtain accurate forecasts [292]. Yet, when the SNR is high enough, the underlying likelihood becomes more gaussian: in this case we may expect the Fisher matrix approximation to become more accurate, and so to do also for the experimental forecast [292].

7.4.2 — Results and discussion

In table 7.1 we report the main results of this analysis, showing the signal-to-noise ratio and the 90% upper bound on the deformation parameters $\{\delta_{mn}\}$ that are to be expected given the observation of the corresponding compact binary system with LISA, after an observation period of $\Delta\tau = 4$ years; see also the caption for further details. We focused on the binary system which may yield the best bounds on the deformation parameters, which we found to be the systems with a total mass between $10^2 M_\odot < m < 10^4 M_\odot$; and we also sampled the parameter space at typical redshifts $z = 0.1, 0.3, 1, 3$, fixing or averaging over the other relevant parameter, as explained in the caption.

Furthermore, to better asses which binary system could yield the best constraints on the $\{\delta_{mn}\}$ parameters, we chose a system similar to the first event GW150914 observed by the LIGO-Virgo collaboration [1, 2]: despite being one of the nearest binary black holes merger ever observed, it serves as a realistic benchmark for what we may expect to observe during the 4 planned years of the LISA mission. In particular for our similar system we chose the redshift $z = 0.087$ (corresponding to a luminosity distance $d_L \sim 410$ Mpc assuming a flat Λ CDM Planck cosmology [297]), source-frame masses $m_1 = 36M_\odot$ and $m_2 = 29M_\odot$, inclination angle between the normal to the orbital plane and our line of sight $\iota = 0.5$, and an observation time $\Delta\tau = 4$ years.

System parameters			Frequencies and SNR			Bounds on deformation parameters						
$m_1 (M_\odot)$	$m_2 (M_\odot)$	z	f_{in} (Hz)	f_{fin} (Hz)	SNR	δ_{00}	δ_{20}	δ_{21}	δ_{30}	δ_{40}	δ_{41}	δ_{42}
35	30	0.1	0.0161	0.113	3.1	0.0023	0.0029	0.0095	0.0081	0.56	1.27	6.5
35	30	0.3	0.0145	0.0956	1.2	0.0053	0.0071	0.022	0.019	1.3	3.0	15
35	30	1	<i>0.0111</i>	<i>0.0621</i>	<i>0.5</i>	<i>0.013</i>	<i>0.011</i>	<i>0.037</i>	<i>0.032</i>	<i>2.2</i>	<i>5.0</i>	<i>25</i>
35	30	3	<i>0.0072</i>	<i>0.0311</i>	<i>0.4</i>	<i>0.026</i>	<i>0.019</i>	<i>0.063</i>	<i>0.054</i>	<i>3.8</i>	<i>8.5</i>	<i>43</i>
80	20	0.1	0.0145	0.0734	4.0	0.0022	0.0063	0.031	0.013	0.74	2.5	20
80	20	0.3	0.0131	0.0621	1.5	0.0062	0.017	0.087	0.036	2.0	7.0	55
80	20	1	<i>0.0099</i>	<i>0.0404</i>	<i>0.7</i>	<i>0.016</i>	<i>0.043</i>	<i>0.21</i>	<i>0.09</i>	<i>5.0</i>	<i>17</i>	<i>130</i>
80	20	3	<i>0.0064</i>	<i>0.0202</i>	<i>0.4</i>	<i>0.046</i>	<i>0.082</i>	<i>0.41</i>	<i>0.17</i>	<i>9.3</i>	<i>32</i>	<i>250</i>
10 ²	10 ²	0.1	0.0079	0.0367	16	0.00054	0.00037	0.0012	0.0010	0.072	0.16	0.81
10 ²	10 ²	0.3	0.0072	0.0311	5.9	0.0017	0.0013	0.0041	0.0035	0.25	0.56	2.8
10 ²	10 ²	1	0.0054	0.0202	2.5	0.0072	0.0069	0.022	0.019	1.3	3.0	15
10 ²	10 ²	3	0.0035	0.0101	1.4	0.024	0.038	0.12	0.10	7.6	17	86
8·10 ²	2·10 ²	0.1	0.0033	0.0073	75	0.00052	0.00075	0.0038	0.0016	0.085	0.29	2.3
8·10 ²	2·10 ²	0.3	0.0029	0.0062	26	0.0017	0.0023	0.011	0.0048	0.25	0.89	7.0
8·10 ²	2·10 ²	1	0.0022	0.0040	7.8	0.0079	0.0087	0.044	0.018	0.98	3.4	26
8·10 ²	2·10 ²	3	0.0013	0.0020	1.8	0.044	0.033	0.16	0.070	3.7	13	100
10 ³	10 ³	0.1	0.0018	0.0037	150	0.00054	0.0020	0.0066	0.0057	0.43	0.96	4.8
10 ³	10 ³	0.3	0.0016	0.0031	44	0.0024	0.0090	0.029	0.025	1.9	4.2	21
10 ³	10 ³	1	0.0012	0.0020	9.0	0.015	0.097	0.31	0.27	21	47	240
10 ³	10 ³	3	0.00070	0.0010	1.4	0.10	2.2	7.1	6.1	500	1100	5500
8·10 ³	2·10 ³	0.1	0.00059	0.00073	42	0.0045	0.035	0.18	0.075	4.0	14	110
8·10 ³	2·10 ³	0.3	0.00051	0.00072	10	0.017	0.23	1.1	0.49	26	93	730
8·10 ³	2·10 ³	1	0.00035	0.00040	1.5	0.12	5.8	29	12	680	2300	10 ⁴
8·10 ³	2·10 ³	3	<i>0.00018</i>	<i>0.00020</i>	<i>0.1</i>	<i>1.4</i>	<i>230</i>	<i>1200</i>	<i>720</i>	<i>10⁴</i>	<i>10⁵</i>	<i>10⁶</i>
10 ⁴	10 ⁴	0.1	0.00031	0.00037	26	0.0065	0.88	2.8	2.7	230	520	2600
10 ⁴	10 ⁴	0.3	0.00026	0.00031	6	0.033	4.8	15	15	1300	2900	10 ⁴
10 ⁴	10 ⁴	1	<i>0.00016</i>	<i>0.00020</i>	<i>0.7</i>	<i>0.28</i>	<i>51</i>	<i>160</i>	<i>180</i>	<i>10⁴</i>	<i>10⁴</i>	<i>10⁵</i>
10 ⁴	10 ⁴	3	<i>0.000096</i>	<i>0.00010</i>	<i>0.1</i>	<i>3.3</i>	<i>620</i>	<i>2000</i>	<i>2200</i>	<i>10⁵</i>	<i>10⁵</i>	<i>10⁶</i>

TABLE 7.1 — Results of the Fisher forecast analysis for the LISA interferometer. We report here the 90% upper bounds on the (absolute value) of the deformation coefficients $|\delta_{mn}|$ that it may be possible to obtain, as a function of varying redshift z and source-frame masses m_1 and m_2 of the binary system. Since these results show a quite strong dependence also on the ι inclination of the binary system, and the duration of the observation $\Delta\tau$, in order to obtain consistent results we fix the inclination to be $\iota = 0.5$ rad and observation time to be $\Delta\tau = 4$ years. Furthermore we also show the initial f_{in} and final frequencies f_{fin} for the observation (evaluated as the frequency of the leading quadrupolar mode as measured in the detector frame): in particular the final frequency is given by the cutoff frequency (7.11) with $\epsilon = 0.1$, whereas the initial frequency is given by (7.15) with $\Delta\tau = 4$ years. Still each of the result above is actually the average over 40 realizations of the same system, as we vary other relevant parameter characterizing the system (we sampled $\bar{\phi}_s$ and ϕ_0 uniformly in $[0, 2\pi)$, $\bar{\psi}_s$ uniformly in $(-\frac{\pi}{2}, \frac{\pi}{2}]$ and $\bar{\mu}_s$ uniformly in $(-1, 1)$). The variability in these samples is about 5% for the SNR, and about 15% for the bounds on the δ parameters.

Finally, recalling the discussion from section 7.1.2, we report in boldface the signal-to-noise ratio above 8: for such system the data acquired by LISA alone should be enough to confidently detect such systems (yet extending the observation above the cutoff $f_{gw,lim,\epsilon}$ may increase the total SNR for the more massive systems). Conversely we italicize the rows which have an SNR < 1 , as for these systems the detection may not be confident even when complementing data with the observation of other detectors; furthermore also the results of the Fisher matrix analysis become less accurate for low values of the signal-to-noise ratio.

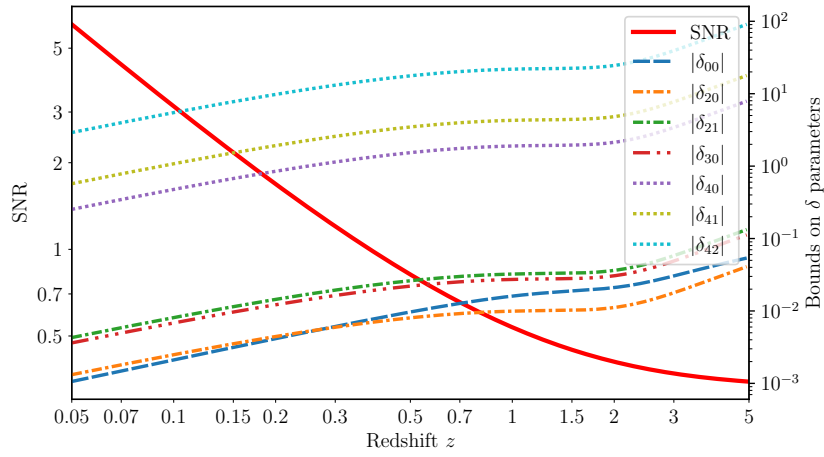


FIGURE 7.3 — Plot of the expected SNR and 90% upper bounds on the δ_{mn} deviation coefficients, as a function of the redshift z of the binary system. The system source-frame masses are taken to be $m_1 = 36M_\odot$ and $m_2 = 29M_\odot$, the inclination angle $\iota = 0.5$ rad, and the duration of the observation $\Delta\tau = 4$ years.

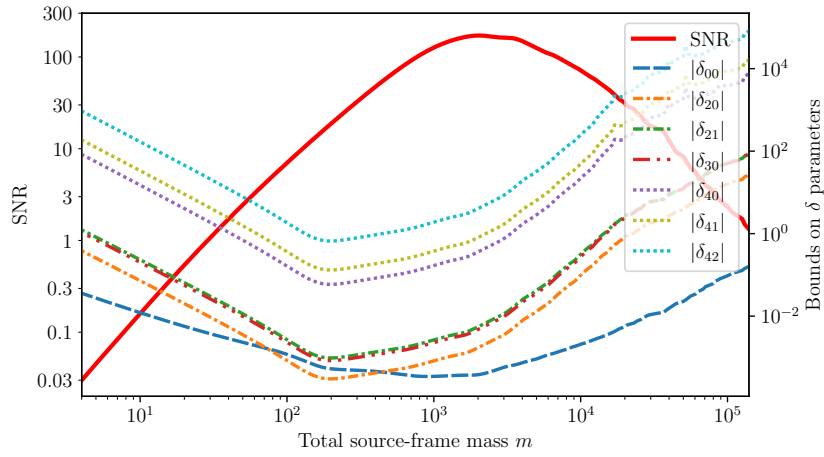


FIGURE 7.4 — Plot of the expected SNR and 90% upper bounds on the δ_{mn} deviation coefficients, as a function of the total mass m of the binary system, assuming equal mass components (so $m_1 = m_2 = \frac{m}{2}$, and $\nu = 0.25$). The system is assumed to be at a redshift $z = 0.087$ (corresponding to a luminosity distance $d_L \sim 410$ Mpc), its inclination angle to be $\iota = 0.5$ rad, and the duration of the observation $\Delta\tau = 4$ years. We applied a smoothing filter to the data in order to reduce oscillations due to limited numerical precision.

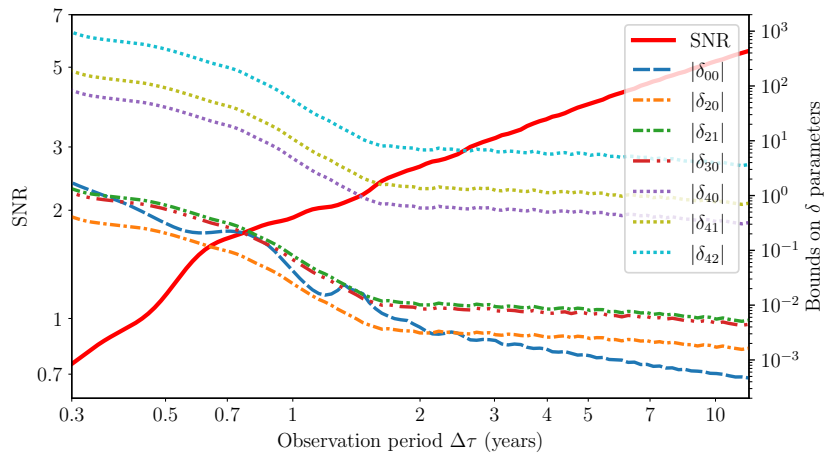


FIGURE 7.5 — Plot of the expected SNR and 90% upper bounds on the δ_{mn} deviation coefficients, as a function of the orbital inclination parameter ι . The system is assumed to be at a redshift $z = 0.087$, its source-frame masses to be $m_1 = 36M_\odot$ and $m_2 = 29M_\odot$ and the duration of the observation $\Delta\tau = 4$ years. We applied a smoothing filter to the data in order to reduce oscillations due to limited numerical precision.

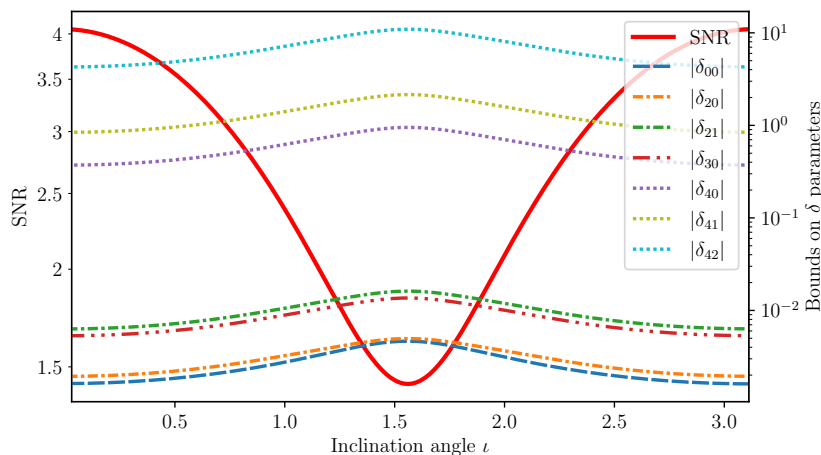


FIGURE 7.6 — Plot of the expected SNR and 90% upper bounds on the δ_{mn} deviation coefficients, as a function of the orbital inclination parameter ι . The system is assumed to be at a redshift $z = 0.087$, its source-frame masses to be $m_1 = 36M_\odot$ and $m_2 = 29M_\odot$ and the duration of the observation $\Delta\tau = 4$ years.

Then in figure 7.3 we look at how the SNR and the bounds on the $\{\delta_{mn}\}$ parameters behave as a function of the redshift z of the binary (so of its luminosity distance d_L), keeping fixed all other parameters; in figure 7.4 we vary instead the total mass of the system (assuming here an equal mass binary $m_1 = m_2 = \frac{m}{2}$); in figure 7.5 we vary the observation time; finally in figure 7.6 we vary the inclination angle ι .

■ Inclination angle ι

Let us first of all discuss the dependence on the angle ι : from figure 7.6 we can see that if we vary the inclination angle between the normal to orbital plane and our line of sight, then the signal-to-noise ratio is highest for $\iota = 0, \pi$ and lowest for $\iota = \frac{\pi}{2}$; and similarly the upper bounds which we may impose on the δ deformation parameters are better constrained (i.e. lower) when $\iota = 0, \pi$ and less constrained (i.e. highest) when $\iota = \frac{\pi}{2}$. In particular the relative difference between the best and the worst scenario is of about $\mathcal{O}(2.5)$ times: being lucky enough to observe a face-on system yields better results. This behavior can be directly linked to the dependence of the amplitude of the gravitational wave signal on the ι angle, see for example equations (6.44); furthermore let us recall that here we're employing only the restricted PN waveform; higher order corrections to the amplitude (see (6.42)) introduce a different functional relation on this angle, yet we don't expect much of a difference when taking them into account.

■ Observation time $\Delta\tau$

Referring to figure 7.5, increasing the observation time, the bounds we can impose on the deformation parameters δ become correspondingly better, as expected. In this case we expect the oscillations presents in the plot, for observational periods lower than a year, to be a consequence of the orbital modulation of the signal due to the orbital motion of LISA (which follows an orbit comparable to the Earth). An observational period of a few months (so e.g. a binary entering in LISA sensitivity band towards the really end of its mission) will provide only mild bounds $\delta \sim \mathcal{O}(0.1)$ on the lower PN coefficients (δ_{00} , δ_{20} , δ_{21} and δ_{30}), whereas extending the observation period to $\Delta\tau$ to about 1 to 2 years yields the greatest improvement to LISA constraining power, with $\delta \sim \mathcal{O}(0.005)$ for the lowest order coefficients and $\delta \sim \mathcal{O}(1)$ for the 2PN ones. Still let us notice that the timescale of this improvement depends on the total mass of the system: in fact we may expect that systems with $m = 100M_\odot$ or less (such as GW150914) that are more than 2 years away from the cutoff

frequency (7.11) may produce a signal almost too faint to be detected by LISA; hence increasing the observation time (into the earliest inspiral phase) doesn't improve much more the bounds that we may be able to impose. On the other hand more massive systems evolve more slowly, therefore for them the bounds may improve further by extending the observation time.

■ Redshift z

From both table 7.1 and figure 7.3 we can see that the higher the redshift z , the lower will be the SNR, and consequently the bounds we'll be able to impose will become worse. This is in line with what we were expecting, since a farther the system will produce a fainter signal, with the amplitude decreasing with $h \propto \frac{1}{d_L}$. In particular if we were to observe again a system like GW150914, so at a redshift of $z \sim 0.1$, we could obtain fair bounds on the lowest PN parameters ($\delta \sim \mathcal{O}(0.005)$) up to 1.5PN), and only mediocre bounds on the 2PN parameters ($\delta \sim \mathcal{O}(1)$).

Yet the most valuable information is to estimate which is the lowest value of the redshift at which we may expect to observe a system of a given mass: in fact by doubling the distance the probability of finding a coalescing system increases roughly by eight times, being proportional to the search volume; yet as we've seen the bounds consequently deteriorate. We'll elaborate on this point in the following.

■ Total mass m

Figure 7.4 shows a quite interesting dependence of the several quantities of interest as a function of the total mass m : in fact the SNR peaks for systems with about $m \sim 10^3 M_\odot$; yet the best bounds on the deformation parameters can be obtained by observing systems with $m \sim 10^2 M_\odot$, in particular for the higher order coefficients. The peak in the SNR is because systems with $m \sim 10^3 M_\odot$ are the ones which spend more time at the frequency at which LISA is most sensitive, as we can see comparing table 7.1 with figure 7.2 for the power spectral noise density $S_n(f)$. On the other hand, to explain the fact that the systems which yield the best bounds are lighter than the ones with the highest SNR, we can recognize that, fixed the observation time of 4 years, a more massive systems will perform less orbits: hence we will observe fewer waveform cycles in the detector, accumulating less phase ($\Delta\phi = 2\pi N_{cyc}$). Then, assuming a definite precision in the measurement of absolute variations of the phase, having accumulated a lower total phase means that we will be less sensitive to any relative modification of the phase, which is exactly what we're probing with our δ_{mn} parameters.

From table 7.1 we also realize that a system with total mass $m \sim 200 M_\odot$ could provide bounds 1 order of magnitude better than a GW150914-like could, if it were to coalesce at the same distance $z \sim 0.1$; and could instead provide comparable bounds if coalescing at a higher redshift, up to $z \sim 0.3$.

From the figure and the table we also understand that systems with total mass larger than $m \gtrsim 10^4 M_\odot$ do not yield competitive bounds, because the frequency of the gravitational waves emitted during their early inspiral is too low for LISA; furthermore we may not even expect to observe them as close as $z = 0.1$. Similarly also systems with less than a few solar masses, such as binary neutron stars, do not yet the best results: in this case actually we may expect a coalescence to take place at a redshift as low as $z \sim 0.01$, as for example was the case for GW170817 [121, 299]; yet also in this case the signal to noise ratio is below unity, as these lighter system emit gravitational waves with frequencies higher than the sensitivity band of LISA. Furthermore we don't report the results for systems with a mass ratio higher than $\frac{m_1}{m_2} = 4$, focusing instead on systems with similar mass in order to keep the systematic error as low as possible: in fact systems with higher mass ratios can reach higher velocities during the inspiral phase, as we pointed out in section 1.6.1.

■ Best bounds from realistic observations

As we have already pointed out, in order to assess which upper bounds we may realistically obtain from the LISA detector, we need to estimate the lowest redshift z at which any system of a given total mass m is expected to be observed during the 4 nominal years of observations. In this regard we would have to perform a throughout analysis of the expected merger rate density, also as a function of the redshift, taking into account the selection bias due to the fact that the detector is able to observe some system better than others, depending on their intrinsic parameters. Yet we expect LISA to observe only a handful of this kind of systems, therefore we'll proceed by considering estimates already present in the literature; in particular here we assume that the bounds will be mostly set by the single best observed *golden* event, i.e. by the closest system with the suitable total mass. Nonetheless in this case we may predict a considerable variability on the exact realization of this system, and so on the consequent $\{\delta_{mn}\}$ parameter estimation. On the other hand we also expect that the real analysis of LISA data will include a full Bayesian analysis taking into account all the suitable systems observed during the whole mission duration, similarly to what is already carried out in reference [96]: then the bounds on the $\{\delta_{mn}\}$ will be actually be better than the ones provided by the single best observed event (though of the same order of magnitude), yet providing more consistent results.

Let us then recall the discussion which we carried out in section 1.2.2 about the population of black hole binaries: while the merger rate of black holes with total mass $m < 100M_\odot$ is by now understood quite well [141], the merger rate of systems comprising intermediate mass black holes, with a total mass $10^2M_\odot < m < 10^5M_\odot$, is still quite elusive.

In particular it is expected that LISA will observe several binary systems with total mass $m < 100M_\odot$ and $\text{SNR} \gtrsim 8$ during its extended mission [300, 301]: actually only $\mathcal{O}(1)$ of such system will reach the end of the inspiral phase (so our cutoff frequency (7.11)) providing possibly the most constraining bounds on the 2PN coefficients. Despite this LISA will observe as well about $\mathcal{O}(10)$ systems which will remain in their earliest inspiral phase for the full duration of the mission. These latter systems will therefore be further away from coalescence, so the relative velocity of their components will be lower, and so correspondingly the bounds on the 2PN coefficients should be worse; nonetheless since we can observe many more systems in this earliest inspiral phase (since that's where they spend most of their final evolution), some of them may be near enough to have a quite high SNR, and therefore may provide good bounds on the lower PN coefficients.

Regarding the expected rates for observations of intermediate mass black holes, instead, there aren't solid estimates: they may vary between tens to hundreds observed events per year (but probably at high redshift), especially when LISA would be observing in synergy with Einstein Telescope [37, 86, 302, 303]; yet there are still many uncertainties in the underlying evolution models, and only actual observations will finally shed light on this topic.

As a benchmark for systems with about $\mathcal{O}(100 - 200) M_\odot$ we can nonetheless consider the case of the most massive system observed so far by LIGO-Virgo, which was event GW190521 [304, 305]. It's total mass was $m \sim 150 M_\odot$, and it took place at redshift $z \sim 0.8$; from this the collaboration estimated a merger rate for similar systems of about $R \sim 0.1 \text{ Gpc}^{-3} \text{ yr}^{-1}$. In this case then we may expect to observe $\mathcal{O}(1)$ events of this kind ($\sim 10^2$ total solar masses) at a redshift of $z \sim 0.3$ during the extended mission duration.

With this premises we may then expect that LISA, during its extended mission, will observe about $\mathcal{O}(1)$ events similar to GW150914, so with total mass $m \sim 60 M_\odot$ at a redshift $z \sim 1$; and approximately $\mathcal{O}(1)$ events similar to GW190521, so with a total mass $m \sim (100 - 200) M_\odot$ at a redshift $z \sim 0.3$. Referring then to table 7.1 we understand that this class of systems should be observed by LISA with an SNR between 2 and 6 already in their early inspiral phase (let us

recall that we cut off the observation frequency using the conservative threshold given by equation (7.11): then, as discussed in section 7.1.2, the SNR should further increase when including also the observation of the late inspiral phase; and could also be additionally augmented by the joint observation of this systems with Einstein Telescope and Cosmic Explorer (the coalescence happens about a week to a month later after they reach our cutoff frequency). Regarding the bounds on the $\{\delta_{mn}\}$ parameters, both classes of systems will yield comparable constraint, with the actual value depending on the specific realization of these system that will be observed. Nevertheless, restricting to order of magnitude estimates, in table 7.2 we report the forecast for the 90% upper bounds on the deformation coefficients that LISA will be able to achieve.

Deformation coefficient	$ \delta_{00} $	$ \delta_{20} $	$ \delta_{21} $	$ \delta_{30} $	$ \delta_{40} $	$ \delta_{41} $	$ \delta_{42} $
90% upper bounds	$\mathcal{O}(0.001)$	$\mathcal{O}(0.001)$	$\mathcal{O}(0.005)$	$\mathcal{O}(0.005)$	$\mathcal{O}(0.1)$	$\mathcal{O}(1)$	$\mathcal{O}(5)$

TABLE 7.2 — Forecast for the 90% upper bounds on the post-Newtonian deformation coefficients δ_{mn} that will be possible to obtain from the data of the LISA mission, in a realistic scenario. Here we report only the order of magnitude of these estimates, since their specific value depends on the particular realizations of the systems that will be observed, and therefore presents a considerable variability.

We can notice that the expected constraints on the lower PN parameters (for example δ_{00}) are much stronger with respect to the ones on the higher PN parameters (for example δ_{42}); this is expected since the higher order PN parameters are suppressed by increasing powers of $v^2 \ll 1$.

Additionally let us point out that if intermediate mass black holes, specifically with a total mass $m \sim (10^2 - 10^3) M_\odot$, will be found to have a much higher merger rate than anticipated, they may provide better bounds than what is reported above. Furthermore we can notice that the choice $\epsilon = 0.1$ for the threshold which we performed in section 7.1.1 is consistent, since the statistical errors that we expect on the 2PN parameters (e.g δ_{40}) are at least of the same order of magnitude of the ϵ systematic error.

■ Comparison with respect to current bounds

Finally we may try to compare our results with the ones of reference [96]: nonetheless first let us recall that in this work we have employed a somewhat different parametrization and a much more conservative cutoff for the observation, since we were aiming to perform a different test, as already discussed in the introduction of this chapter.

In fact, whereas we consider only the early inspiral phase by completely cutting off the observation at the threshold frequency $f_{gw,lim,\epsilon}$ given by (7.11), in order to limit systematic errors; reference [96] considers the deformation parameters up to a much higher threshold frequency (about $\mathcal{O}(10^2 \sim 10^3)$ times larger), after which they taper off these additional coefficients to analyse also the merger and ringdown phases in pure general relativity. Furthermore reference [96] implements deformations to the phase up to the 3.5PN order, but disregards their ν structure, differently with respect to this work.

Nonetheless we may extrapolate the results obtained above to conclude that in the quite likely case in which LISA were to observe even just a single event similar to GW150914 or to GW190521, it could improve the current upper bounds of reference [96] on the 0PN, 1PN and 1.5PN coefficients by about 1 to 2 orders of magnitude; obtaining instead at least a similar precision on the 2PN coefficients.

However let us stress again that we cannot directly compare these two tests. To make the comparison more fair we should be less conservative, increasing the value of our ϵ threshold in order

to have a cut off frequency (equation (7.11)) along the lines of reference [96]. Doing so we may expect great improvements on all the bounds, and in particular on the ones related to the 2PN coefficients (δ_{40} , δ_{41} and δ_{42}), especially when observing binary systems with a higher total mass. In fact increasing the ϵ threshold implies observing a system also at velocities higher than $\frac{v}{c} > 0.1$, and in this regime the contributions due to the 2PN coefficients become less suppressed: therefore also so any deviations from their predicted value will become more important, and hence could be better constrained.

CONCLUSIONS

In this thesis we have studied the dynamics of compact binary systems in general relativity, also in light of the recent developments in this well-established field. In particular we have discussed a broad range of topics, spanning from the theoretical computation of post-Newtonian corrections to a phenomenological analysis regarding future gravitational wave observatories, giving a unified overview of the whole procedure and of many of the techniques involved.

Specifically we focused on the post-Newtonian formalism, which is an approximation scheme useful to describe the inspiral phase of compact binary systems. In this analytical framework the general relativistic dynamics of binary systems, comprising black holes and neutron stars, are studied as a series of (post-Newtonian) corrections to the classical Newtonian result. This formalism historically has been one of the most studied, and its results are routinely employed (eventually in synergy with others techniques) by present-day gravitational wave observatories, such as LIGO and Virgo, to model the waveform of the gravitational waves emitted by a binary system in the stage prior to its coalescence.

Despite the immense amount of effort and the many developments which have been involved in the evaluation of these post-Newtonian corrections over the last century, this is still a current field of research: one of the main reasons is that the extremely sensitive next generation gravitational wave observatories (such as Einstein Telescope, Cosmic Explorer and LISA), which will come online in the next decade, will require a substantial improvement of the accuracy of the theoretical models for the gravitational waveform. Luckily, in the last years there has been a steady progress toward reaching this goal: a renewed momentum in this direction has been imparted by the application of modern effective field theory and quantum field theory techniques to the study of this problem.

In this approach to the post-Newtonian formalism, employed also in this thesis, the study of compact binary systems is framed and systematized in the effective field theory framework, and the evaluation of higher order corrections is addressed using advanced multi-loop quantum field theory techniques. This approach has proven to be really effective, allowing to advance the state of the art in the computation of post-Newtonian corrections. As a matter of fact these methods have allowed us to evaluate in this thesis also a few selected conservative diagrams, first contributing at the 7PN order, which are beyond the present state of the art: while being an extremely partial result, it highlights the strength of these techniques.

Among these strengths there is the fact that computations can be made systematic: by evaluating the post-Newtonian corrections as a sum over a series of diagrams, it's possible to take advantage of the many techniques developed for the evaluation of scattering amplitudes in particle physics, most of them being also implemented in software packages. In this way it is possible to streamline the evaluation of these contributions, eventually implementing the computation in a computer algebra software: this has been done in this thesis as well, and actually it becomes a necessity at higher post-Newtonian orders given the sheer number of diagrams. At the same time, these techniques also allow to actually evaluate these higher order corrections, whose complexity cannot be addressed by

many other approaches; and also to systematically account for spin and finite size effects, which are needed to obtain accurate predictions.

Regarding the phenomenological analysis, we have assessed the precision with which the future LISA gravitational wave detector will be able to constrain possible deviations from general relativity, and more precisely from the predictions of the post-Newtonian theory. In particular to parametrize these deviations we introduced seven deformation coefficients in the expression for the phase of the gravitational waveform which included post-Newtonian corrections up to 2PN, also leveraging the structure of the expression, differently with what is customary in the literature. Furthermore, since we were interested in performing a test restricted only to the post-Newtonian theory, we focused solely on the early inspiral phase of the binary system, in order to limit the expected systematic error due to the truncation of the post-Newtonian expansion.

The result of our forecast is that LISA will be able to constrain relative deviations of order $\mathcal{O}(0.1)$ from the values of the 2PN coefficients, and down to $\mathcal{O}(0.001)$ for the lower order 0PN and 1PN coefficients. Additionally, by extrapolating these results to the so called *parametrized tests of gravitational waves generation* of references [92–96], we may expect LISA to be able to improve the current bounds on that test by at least a factor $\mathcal{O}(10^2)$ for the lower order post-Newtonian deformation coefficients. These results suggest that LISA should be well suited to measure deviations from general relativity, using gravitational wave observations, during the early inspiral phase of compact binary systems: this will allow to perform these tests in a regime complementary to what is accessible to present day gravitational wave observatories.

Summary of the main results

In the following we summarize the most relevant results of this thesis work.

In chapter 1 and 2 we recalled several topics and techniques which proved useful for the thesis work.

In chapter 3 we thoroughly presented the construction of the effective theory for compact binary systems, developing the formalism somewhat differently with respect to what is customary in the literature: in particular our notation emphasizes the vacuum nature of the diagrams, incidentally grouping together several related contributions and so resulting in a lower number of diagrams.

In chapter 4 we evaluated all the diagrams which contribute up to next-to-next-to-leading order (2PN) in the conservative sector. In particular we derived explicitly all the Feynman rules and the master integrals needed to perform these calculations in appendices A and C, streamlining as well the derivation of a generic conservative Feynman rule given the action term, and the Fourier transform of tensorial expressions via tensor decomposition. This allowed us to develop in a systematic way the computation of the conservative diagrams, and to implement their full evaluation in a novel `Mathematica` code. Using it, in section 4.6 we also obtained the expressions of a few conservative diagrams first contributing at 7PN order, beyond the state of the art.

In chapter 5 we evaluated the leading order contribution to the dissipative sector, so the power loss, in the specific effective theory formalism which we presented; as well as the leading order gravitational field at infinity, employing the in-in formalism.

In chapter 6, complementing these results with others reported in the literature, we explicitly evaluated the observable gravitational waveform with up to 2PN corrections to the phase.

In chapter 7 we performed a forecast, employing the Fisher matrix formalism, to assess the precision with which the future LISA gravitational wave detector will be able to constrain possible generic deviations from the prediction of the post-Newtonian theory, so also deviations from general relativity. In particular we envisaged the test to be performed only on the early inspiral phase,

in order to limit systematic errors; additionally we introduced a different parametrization for the deformation coefficients with respect to what is customary in the literature, taking advantage of the structure of the post-Newtonian corrections; this may improve the sensitivity to specific deviations from general relativity. Specifically in section 7.4 we report the results of the forecast, summarized in table 7.2, and the corresponding discussion.

Possible future developments

Since this thesis work encompassed several topics, there are many possibilities to develop it further.

Among them, regarding the first part of the thesis, there would be the possibility of evaluating higher order post-Newtonian corrections, both concerning conservative and radiation diagrams. In particular it would be interesting to check if the specific variant of the formalism used in this work can be extended also to the evaluation of diagrams representing hereditary effects. For example tail effects are usually associated to diagrams involving simultaneously both potential and radiation modes; yet, when working in the far zone radiation theory as derived in a top-down approach, we expect only diagrams with no potential modes, and hence their effect should instead show up during the matching procedure. However working in this top-down approach, without introducing the source multipole expansion at the level of the action as customary in the literature, could make the computations too cumbersome. Another interesting extension could be the evaluation of higher order post-Newtonian corrections including the spin and finite size effects of the compact objects, which are relevant to obtain accurate predictions: in both case this can be done, in the formalism which we already developed, by systematically taking into account higher order operators in the point particle action for the internal zone, see also references [38, 80–84, 182, 213, 239, 241].

Regarding the derivation of physical observables from the post-Newtonian corrections, one could extend the work by considering higher order corrections; as well as the eccentricity of the binary system. Furthermore it would be interesting to explore the synergy with the Effective-One-Body formalism [30, 31], which builds upon the results obtained with the post-Newtonian and other formalism, augmenting them.

Regarding the phenomenological analysis, it would be interesting to increase the accuracy of the forecast, for example by relying on more advanced population studies for the binary systems or using mock catalogues of expected events, and performing a complete Markov Chain Monte Carlo analysis in lieu of the Fisher matrix one. It would be important as well to extend the forecast to take into account the whole network of several gravitational wave observatories. On a different note one could also perform a Bayesian analysis employing the data from already observed events.

Finally a really interesting development of this work would be its extension to specific models of modified gravity, and in principle the effective field theory approach which we employed should be well suited to this task. In fact in this work we obtained the expression for the observable gravitational waveform starting from the Einstein-Hilbert action associated to general relativity. Then to study the dynamics of a compact binary system, and the corresponding gravitational wave signal, in modified theories of gravity, it should suffice to introduce the suitable modification directly in the fundamental initial action; proceeding then more or less analogously to what has been presented. We expect modified (and possibly new) Feynman rules and diagrams to arise, yet these should not present novel issue per se: in fact similar modifications to the standard action are already routinely included when accounting for spin and finite size effects. This approach, actually, has already been employed to account for the presence of an electromagnetic field in addition to standard general relativity [197, 306] and has also been applied to some modified theories of gravity [206, 307–311]. From the results of such procedure then it should be possible to obtain observables in specific models of modified gravity; additionally the possibility of constraining the additional parameters would provide a much more specific and powerful test to look for possible deviations

from general relativity. However, let us notice that this field has already been extensively studied, also using several different formalism, and that the perturbative approach we outlined cannot take into account non-perturbative effects, which actually may be important for the dynamics derived from some specific classes of theories. On the other hand many observations have already constrained deviations from general relativity to be small, therefore in order to obtain accurate predictions it may be necessary to account also for higher order effects, such as spin and finite size effects of the compact objects, when evaluating observables in these theories: the systematic nature of the approach employed in this work could be suitable to include these phenomena.

ACKNOWLEDGMENTS

I would like to thank my supervisors, Prof. Pierpaolo Mastrolia, Prof. Nicola Bartolo and Dr. Angelo Ricciardone, for the advice and the support they gave me, not only during this thesis work, but also throughout my master's degree.

I would like to thank as well Prof. Marco Peloso, Prof. Sabino Matarrese, Dr. Manoj K. Mandal, Dr. Vsevolod Chestnov, Dr. Daniele Bertacca, Giacomo Brunello and Raj Patil for the help and the suggestions.

I would also like to thank Giovanna, my family, my friends, and everyone who has supported me during these years.

I acknowledge support by INFN for the attendance of the *workshop on EOB and Amplitudes for gravitational systems* at the university of Bologna (8 and 9 June 2023), where preliminary results of this thesis work have been presented. Furthermore I acknowledged support by INFN and CloudVeneto [293] for the computing and storage facilities used to perform the Fisher matrix analysis.

Software

In this thesis we employed the `Python` programming language and made extensive use of the `Mathematica 13.1` computation software. We also used the `xTensor` package [261] to deal with tensor algebra, adapted the `FeynRu1.m` module of the `EFTofPNG` package [249] to derive the expansion of the bulk action in the Kol-Smolkin parametrization, employed the `LiteRed 2` [216, 217] and `Mint` [262] packages to evaluate integration-by-parts identities.

DERIVATION OF THE FEYNMAN RULES

In this appendix we derive the Feynman rules which have been necessary for the evaluation of the diagrams presented in chapters 4 and 5.

In section A.1 we derive the expression for the propagators, both of the potential and the radiation fields. In section A.2 we derive the Feynman rules related to the near zone effective action which we presented in section 3.2.3, and which are needed to evaluate the conservative diagrams presented in chapter 4. In section A.3 we derive the Feynman rules related to the far zone effective action, which we presented in section 3.2.4: in particular we explicitly perform the matching procedure discussed therein, obtaining in the end the Feynman rules which are needed to evaluate the dissipative diagrams and the gravitational waveform in chapter 5.

Let us now discuss how to obtain these Feynman rules: to obtain the Feynman rules of a theory in momentum space, we start from the action S of the theory, and we substitute each field $W_A(x)$ with its $d + 1$ dimensional Fourier transform

$$W_A(x) = \int \frac{d^{d+1}k}{(2\pi)^{d+1}} W_A(k) e^{-ikx} , \quad (\text{A.1})$$

consistently with what we defined in the **Notation**, where A denotes a possible series of indices, e.g. $A = i$ or $A = jk$, or none for scalar fields.

Next we treat the resulting theory as a quantum field theory over a flat background, that is, with metric $\eta_{\mu\nu} = \text{diag}(+, -, -, -)$. Therefore we have that the free particle propagator of each field is the inverse of its quadratic term in the action, as written in momentum space; instead the Feynman rules for the interactions between fields can be obtained by taking the corresponding functional derivatives of the other terms in the action and by then setting the fields to zero: this singles out the sought-after interaction term. Finally in both cases we add the usual i factor to the so obtained expressions to get the corresponding Feynman rules.

Let us notice that in order to obtain a local Lagrangian it may be needed to expand the initial action about the point where the field are vanishing, in such a way to obtain a well defined series, where the operators of the Lagrangian are just powers of the fields evaluated at the same spacetime point. We may then consider, in our perturbative approach, only the lowest order terms, up to the required accuracy.

We also define the functional derivation as the operation fulfilling the following rules, for definiteness specialized to the momentum space and only to the case of bosonic fields (as we're not dealing with

any fermionic field or Grassmann variable) [191, 225]:

$$\frac{\delta W_A(k)}{\delta W_B(k')} = (2\pi)^{d+1} \delta^{(d+1)}(k - k') \delta_{AB} , \quad (\text{A.2a})$$

$$\frac{\delta(W_A(k)W_B(k'))}{\delta W_C(k'')} = (2\pi)^{d+1} \left(\delta^{(d+1)}(k - k'') \delta_{AC} W_B(k') + W_A(k) \delta^{(d+1)}(k' - k'') \delta_{BC} \right) , \quad (\text{A.2b})$$

where with δ_{AB} we understand the product of Kronecker deltas which enforce the two series of indices A and B to be equal. For example, for the case $W_A = A_i$:

$$\frac{\delta A_i(k)}{\delta A_j(k')} = (2\pi)^{d+1} \delta^{(d+1)}(k - k') \delta_{ij} . \quad (\text{A.3})$$

Furthermore let us point out that if the field has some particularly symmetry in its indices, it would be better to explicitly enforce it; hence, if instead we consider $W_A = \sigma_{ij}$, with the σ field symmetric in its two indices, i.e. $\sigma_{ij} = \sigma_{ji} = \sigma_{(ij)}$, then its functional derivatives should also preserve this symmetry:

$$\frac{\delta \sigma_{ij}(k)}{\delta \sigma_{kl}(k')} = (2\pi)^{d+1} \delta^{(d+1)}(k - k') \underbrace{\frac{1}{2} (\delta_{ik} \delta_{jl} + \delta_{jk} \delta_{il})}_{=\delta_{(i|k} \delta_{|j)l}} . \quad (\text{A.4})$$

Functional derivatives between different fields are vanishing, and let us notice that due to our normalization convention it holds:

$$\int \frac{d^{d+1}k}{(2\pi)^{d+1}} \frac{\delta W(k)}{\delta W(k')} = 1 . \quad (\text{A.5})$$

A.1 | Propagators of the gravitational fields

From the bulk action, written as a function of the Kol-Smolkin variables, as reported in expression (3.35), we can read off the propagators for the gravitational $\hat{\phi}$, \hat{A}_i and $\hat{\sigma}_{ij}$ fields; in particular we're interested in the quadratic parts in each field.

To introduce the procedure in a less cumbersome way, in the following we will restrict ourselves to the case of potential fields only, so by assuming the radiation fields $\bar{\phi} = \bar{A}_i = \bar{\sigma}_{ij} = 0$, in practice then we also drop the hat from the field variables. We will instead introduce back these radiation field in section A.3, when we will be concerned with the Feynman rules for the far zone effective theory.

On a side note, let us also introduce some useful identities, which for example would have been useful if we were to obtain the Feynman rule from the non-expanded expression of the bulk action, as in reference [229]. To do so let us recall that indices are raised and contracted using the d -dimensional metric tensor γ_{ij} or its inverse γ^{ij} , for which it holds (see also formula (3.30)):

$$\gamma_{ij} \equiv \delta_{ij} + \frac{\sigma_{ij}}{\Lambda} , \quad (\text{A.6})$$

thereby, using the Neumann series, we can approximate

$$\begin{aligned} \gamma^{ij} &= \delta^{ij} + \sum_{n=1}^{+\infty} \frac{(-1)^n}{\Lambda^n} \sum_{m_1, \dots, m_{(n+1)}} \delta^{im_1} \sigma_{m_1 m_2} \sigma_{m_2 m_3} \cdots \sigma_{m_n m_{(n+1)}} \delta^{m_{(n+1)} j} \\ &= \delta^{ij} - \frac{1}{\Lambda} \sum_{m_1, m_2} \delta^{im_1} \sigma_{m_1 m_2} \delta^{m_2 j} + \frac{1}{\Lambda^2} \sum_{m_1, m_2, m_3} \delta^{im_1} \sigma_{m_1 m_2} \sigma_{m_2 m_3} \delta^{m_3 j} + O(\sigma^3) . \end{aligned} \quad (\text{A.7})$$

Furthermore, assuming all the following operations to be well behaved, we can approximate the square root of the determinant of the spatial part of the metric, $\sqrt{\gamma}$, via the usual formal identity for a matrix M with eigenvalues $\{\lambda_i\}$:

$$\det(M) = \prod_i \lambda_i = e^{\log(\prod_i \lambda_i)} = e^{\sum_i \log(\lambda_i)} = e^{\text{tr}(\log(M))} , \quad (\text{A.8})$$

and assuming to be near the identity matrix $M = \mathbf{1} + A$ we can expand:

$$\log(M) = \sum_{n=1}^{+\infty} (-1)^{n+1} \frac{A^n}{n} . \quad (\text{A.9})$$

Therefore, recalling the linearity of the trace $\text{tr}(aA + bB) = a\text{tr}(A) + b\text{tr}(B)$, we have, for $\gamma = \mathbf{1} + \sigma$:

$$\sqrt{\gamma} = e^{\frac{1}{2}\text{tr}(\log(\mathbf{1}+\sigma))} = \exp\left(\frac{1}{2} \sum_{n=1}^{+\infty} \frac{(-1)^{n+1}}{n} \text{tr}(\sigma^n)\right) = \sum_{p=0}^{+\infty} \frac{1}{p!} \left(\sum_{n=1}^{+\infty} \frac{(-1)^{n+1}}{2n} \text{tr}(\sigma^n)\right)^p \quad (\text{A.10})$$

where explicitly the trace of the power n of σ is given by:

$$\text{tr}(\sigma^n) = \sum_{i, m_1, \dots, m_{n-1}} \sigma_{im_1} \sigma_{m_1 m_2} \cdots \sigma_{m_{n-1} i} . \quad (\text{A.11})$$

The first terms in the expansion hence read:

$$\sqrt{\gamma} = 1 + \frac{1}{2}\text{tr}(\sigma) + \frac{1}{8} \left((\text{tr}(\sigma))^2 - 2\text{tr}(\sigma^2) \right) + \frac{1}{48} \left((\text{tr}(\sigma))^3 - 6\text{tr}(\sigma)\text{tr}(\sigma^2) + 8\text{tr}(\sigma^3) \right) + O(\sigma^4) . \quad (\text{A.12})$$

In particular now we understand all indices to be contracted via Kronecker deltas, as instead we make explicit all $\gamma \sim \delta$ dependencies, so for example therefore $\text{tr}(\sigma) = \delta^{ij} \sigma_{ij}$.

Moreover we point out that for example, if we were to use the bulk action as reported in reference [229], some field interactions are implicit due to the simplified notation, for example:

$$(\nabla\phi)^2 = \gamma^{ij} \partial_i \phi \partial_j \phi = \delta^{ij} \partial_i \phi \partial_j \phi - \delta^{ik} \delta^{jl} \sigma_{kl} \partial_i \phi \partial_j \phi + O(\sigma^2 \phi^2) , \quad (\text{A.13})$$

while the expansion of the determinant (A.12) implies that for any term explicitly written inside curly brackets in the action (3.35), there are also higher order interaction terms with the σ_{ij} field due to the expansion in powers of $\text{tr}(\sigma)$. Hence it would be necessary to keep track of these terms when considering interaction vertices, as we will do later on; but as long as we're interested only in the free propagators for the potential field, we would need only the terms of the bulk action (3.35) quadratic in the fields: therefore, only in this case, we could truncate the series expansions at $\sqrt{\gamma} = 1 + O(\sigma)$ and $\gamma^{ij} = \delta^{ij} + O(\sigma)$.

■ Propagators for the potential ϕ and radiation $\bar{\phi}$ fields

Only in this section we'll actually show the full procedure to obtain the propagator for both the potential ϕ and radiation $\bar{\phi}$ modes, by reintroducing back the $\bar{\phi}$ radiation field.

In general we recall as well the discussion we presented in section 3.2.3, in particular below equation (3.36), on how to separate the potential and radiation modes, and also on the subtleties related to the extension of the Fourier integration domain over all the wavenumbers.

Returning to the computation of the ϕ and $\bar{\phi}$ propagators, first of all we have to find the propagator for the full $\hat{\phi}$ field in Fourier space. To do so we have to consider the relevant quadratic term in the bulk action (3.35), which are given by:

$$S_{bulk} \supset -c_d \int d^{d+1}x \left[\delta^{ij} \partial_i \hat{\phi} \partial_j \hat{\phi} - \dot{\hat{\phi}}^2 \right] + O(\hat{\phi}^3, \sigma \hat{\phi}^2) . \quad (\text{A.14})$$

We can then perform the Fourier transform and read off the propagator, see also [224, 225]:

$$\begin{aligned}
S_{bulk} \supset & -c_d \int d^{d+1}x \left(\delta^{ij} \partial_i \hat{\phi} \partial_j \hat{\phi} - \dot{\hat{\phi}}^2 \right) = (2c_d) \frac{1}{2} \int d^{d+1}x \eta^{\mu\nu} \partial_\mu \hat{\phi} \partial_\nu \hat{\phi} \\
& = -(2c_d) \frac{1}{2} \int d^{d+1}x \eta^{\mu\nu} \hat{\phi} \partial_\mu \partial_\nu \hat{\phi} \\
& = -(2c_d) \frac{1}{2} \int d^{d+1}x \frac{d^{d+1}k}{(2\pi)^{(d+1)}} \frac{d^{d+1}k'}{(2\pi)^{(d+1)}} \hat{\phi}(k) e^{-ikx} (-\eta^{\mu\nu} k'_\mu k'_\nu) \hat{\phi}(k') e^{-ik'x} \\
& = +(2c_d) \frac{1}{2} \int \frac{d^{d+1}k}{(2\pi)^{(d+1)}} \frac{d^{d+1}k'}{(2\pi)^{(d+1)}} \underbrace{d^{d+1}x e^{-i(k+k')x}}_{=(2\pi)^{d+1} \delta^{(d+1)}(-k-k')} (k')^2 \hat{\phi}(k) \hat{\phi}(k') \\
& = +\frac{1}{2} \int \frac{d^{d+1}k}{(2\pi)^{(d+1)}} \underbrace{(2c_d k^2)}_{=\mathcal{D}_{\hat{\phi}}(k)} \hat{\phi}(k) \hat{\phi}(-k)
\end{aligned} \tag{A.15}$$

with $k^2 \equiv \eta^\mu k_\mu k_\nu$, furthermore in second line we integrated by parts and assumed the field and its derivatives to vanish on the boundary of the integration domain. The propagator for the $\hat{\phi}$ field is now given by the inverse of the $\mathcal{D}_{\hat{\phi}}(k)$ function with the addition of the $+i\epsilon$ prescription, and the corresponding Feynman rule can then be obtained by adding an additional i factor, compare with section 3.1.

However, since we're interested in the propagators for the ϕ and $\bar{\phi}$ fields, we have to apply the separation between potential ϕ and radiation $\bar{\phi}$ modes, as in relation (3.36), so:

$$\hat{\phi}(k) = \phi(k) + \bar{\phi}(k) , \tag{A.16}$$

recalling as well that these modes have non overlapping support by construction (i.e. we assume a step function as the window function in equation (3.39), such that $\phi(k)\bar{\phi}(k) = 0$ for any Fourier mode k , which we take to hold also as $\phi(k)\bar{\phi}(-k) = 0$ since we perform the separation on the basis of the values of the modulus of k^0 and $|\mathbf{k}|$). This also assures us that there will be no mixing between the potential and the radiative modes during propagation.

Therefore, since in this case the mixed term $\phi\bar{\phi}$ vanish (this won't be the case in interaction terms, as they will be evaluated in different k_1 and k_2 momenta), the expression (A.15) becomes:

$$S_{bulk} \supset \frac{1}{2} \int \frac{d^{d+1}k}{(2\pi)^{(d+1)}} (2c_d k^2) (\phi(k)\phi(-k) + \bar{\phi}(k)\bar{\phi}(-k)) . \tag{A.17}$$

Then from the first term we can read off the propagator for the potential ϕ field. In particular, by taking the inverse of the $\mathcal{D}_{\hat{\phi}}(k)$ function, adding the $+i\epsilon$ prescription, and multiplying by the i factor (as discussed in section 3.1) we find:

$$\begin{array}{c} \xrightarrow{k} \\ \text{---} \phi \text{---} \end{array} = \frac{1}{2c_d} \frac{i}{k^2 + i\epsilon} \tag{A.18}$$

Applying this same procedure on the second term of expression (A.17) instead we obtain the propagator for the $\bar{\phi}$ radiation field:

$$\begin{array}{c} \xrightarrow{k} \\ \text{---} \bar{\phi} \text{---} \end{array} = \frac{1}{2c_d} \frac{i}{k^2 + i\epsilon} \tag{A.19}$$

Then we can see that both propagator formally have the same expression, and therefore in the following we will obtain simply the propagator for the potential modes; then the corresponding propagator for the radiation modes will present the same expression.

■ Propagator of the A_i potential field

To relevant quadratic term in the harmonic gauge fixed bulk action (3.35) is:

$$S_{bulk} \supset \int d^{d+1}x \left[\frac{1}{2} \delta^{ik} \delta^{jl} F_{ij} F_{kl} + (\delta^{ij} \partial_i A_j)^2 - \delta^{ij} \dot{A}_i \dot{A}_j \right] + O(\sigma A^2, \phi A^2); \quad (\text{A.20})$$

it can be rewritten as, by performing suitable integration by parts and Fourier transforms:

$$\begin{aligned} S_{bulk} &\supset \int d^{d+1}x \left[(\delta^{ik} \delta^{jl} - \delta^{il} \delta^{jk}) (\partial_i A_j \partial_k A_l) + (\delta^{ij} \partial_i A_j)^2 - \delta^{ij} \dot{A}_i \dot{A}_j \right] \\ &= \int d^{d+1}x \left[(\delta^{ik} \delta^{jl} - \delta^{il} \delta^{jk} + \delta^{ij} \delta^{kl}) (\partial_i A_j \partial_k A_l) - \delta^{ij} \partial_0 A_i \partial_0 A_j \right] \\ &= \int d^{d+1}x \left[- \left(\delta^{ik} \delta^{jl} - \underbrace{\delta^{il} \delta^{jk} + \delta^{kl} \delta^{ji}}_{=-2\delta^{[il} \delta^{j]k]}} \right) (A_j \partial_i \partial_k A_l) + \delta^{ij} A_i \partial_0 \partial_0 A_j \right] \\ &= \int d^{d+1}x \left[\delta^{ij} A_i \left(\underbrace{-\delta^{kl} \partial_k \partial_l + \partial_0 \partial_0}_{=\eta^{\mu\nu} \partial_\mu \partial_\nu} \right) A_j \right] \\ &= \int \frac{d^{d+1}k}{(2\pi)^{(d+1)}} \frac{d^{d+1}k'}{(2\pi)^{(d+1)}} \underbrace{d^{d+1}x e^{-i(k+k')x}}_{=(2\pi)^{d+1} \delta^{(d+1)}(-k-k')} [\delta^{ij} A_i(k) (-k')^2 A_j(k')] \\ &= \frac{1}{2} \int \frac{d^{d+1}k}{(2\pi)^{(d+1)}} A_i(k) \underbrace{(-2\delta^{ij} k^2)}_{\equiv \mathcal{D}_A^{ij}(k)} A_j(-k), \end{aligned} \quad (\text{A.21})$$

where in the third line we used the fact that $\partial_{[i} \partial_{k]} = \frac{1}{2}(\partial_i \partial_k - \partial_k \partial_i) = 0$, so $(-\delta^{il} \delta^{jk} + \delta^{kl} \delta^{ji}) \partial_i \partial_k = 0$. To obtain the propagator we need to invert $\mathcal{D}_A^{ij}(k)$: regarding the tensorial structure, the identity matrix δ^{ij} is its own inverse; therefore the propagator for the A_i potential field is given by:

$$i \xrightarrow{k} j \text{ --- } \frac{A}{A} = -\frac{\delta_{ij}}{2} \frac{i}{k^2 + i\epsilon}. \quad (\text{A.22})$$

From this expression, as discussed before, we can directly evaluate the propagator for the radiative field \bar{A} as well, which reads:

$$i \xrightarrow{k} j \text{ --- } \frac{\bar{A}}{A} = -\frac{\delta_{ij}}{2} \frac{i}{k^2 + i\epsilon}. \quad (\text{A.23})$$

■ Propagator of the σ_{ij} potential field

The relevant terms needed to extract the quadratic term in the σ_{ij} field are:

$$S_{bulk} \supset \frac{1}{4} \int d^{d+1}x \left(\delta^{ij} \partial_i \sigma \partial_j \sigma - 2\delta^{ij} \delta^{km} \delta^{ln} \partial_i \sigma_{kl} \partial_j \sigma_{mn} - \dot{\sigma}^2 + 2\delta^{km} \delta^{ln} \dot{\sigma}_{kl} \dot{\sigma}_{mn} \right) + O(\sigma^3, \sigma^2 \phi), \quad (\text{A.24})$$

Proceeding analogously as before we obtain:

$$\begin{aligned}
S_{bulk} &\supset \frac{1}{4} \int d^{d+1}x \left(\delta^{ij}(\delta^{kl}\delta^{mn} - 2\delta^{km}\delta^{ln})\partial_i\sigma_{kl}\partial_j\sigma_{mn} - (\delta^{kl}\delta^{mn} - 2\delta^{km}\delta^{ln})\dot{\sigma}_{kl}\dot{\sigma}_{mn} \right) \\
&= \frac{1}{4} \int d^{d+1}x \left((\delta^{kl}\delta^{mn} - 2\delta^{km}\delta^{ln}) \sigma_{kl} \left(\underbrace{-\delta^{ij}\partial_i\partial_j + \partial_0\partial_0}_{=\eta^{\mu\nu}\partial_\mu\partial_\nu} \right) \sigma_{mn} \right) \\
&= \frac{1}{4} \int \frac{d^{d+1}k}{(2\pi)^{(d+1)}} \frac{d^{d+1}k'}{(2\pi)^{(d+1)}} \underbrace{d^{d+1}x e^{-i(k+k')x}}_{=(2\pi)^{d+1}\delta^{(d+1)}(-k-k')} \left((\delta^{kl}\delta^{mn} - 2\delta^{km}\delta^{ln}) \sigma_{kl}(k) (-k')^2 \sigma_{mn}(k') \right) \\
&= \frac{1}{2} \int \frac{d^{d+1}k}{(2\pi)^{(d+1)}} \sigma_{kl}(k) \left(\underbrace{-\frac{1}{2}(\delta^{kl}\delta^{mn} - 2\delta^{km}\delta^{ln}) k^2}_{\equiv \mathcal{D}_\sigma^{klmn}(k)} \right) \sigma_{mn}(-k) .
\end{aligned} \tag{A.25}$$

To obtain the propagator we need to invert the tensorial structure of $\mathcal{D}_\sigma^{klmn}(k)$; in particular we need also to preserve the symmetry of the indices $\sigma_{kl} = \sigma_{lk}$ and $\sigma_{mn} = \sigma_{nm}$ of the fields; therefore we have to find a tensor $P^{klmn}(k)$ which satisfies [224]:

$$\mathcal{D}_\sigma^{klmn}(k)P_{mnpq}(k) = \frac{1}{2} \left(\delta_p^k \delta_q^l + \delta_q^k \delta_p^l \right) . \tag{A.26}$$

To do so we can start from the general ansatz

$$P_{mnpq}(k) = A(k)\delta_{mn}\delta_{pq} + B(k)\delta_{mp}\delta_{nq} + C(k)\delta_{mq}\delta_{np} , \tag{A.27}$$

and, recalling that in d spatial dimension the trace of the spatial identity is $\delta^{ij}\delta_{ij} = d$, we obtain:

$$\mathcal{D}_\sigma^{klmn}(k)P_{mnpq}(k) = -\frac{k^2}{2} \left(A(k)(d-2)\delta^{kl}\delta_{pq} + B(k)(\delta^{kl}\delta_{pq} - 2\delta_p^k\delta_q^l) + C(k)(\delta^{kl}\delta_{pq} - 2\delta_q^k\delta_p^l) \right) . \tag{A.28}$$

By comparing equations (A.26) and (A.28) we see that the coefficients are $B(k) = C(k) = \frac{1}{2k^2}$ and $A(k) = -\frac{1}{2k^2}\frac{2}{(d-2)}$. We conclude that equation (A.27) gives us the propagator, modulo the i factor; hence the Feynman rule for the propagator of the σ_{ij} field is given by:

$$ij \xrightarrow[\sigma]{k} kl = \frac{1}{2} \frac{i}{k^2 + i\epsilon} \left(-\frac{2}{d-2}\delta_{ij}\delta_{kl} + \delta_{ik}\delta_{jl} + \delta_{il}\delta_{jk} \right) . \tag{A.29}$$

Also in this case we can generalize the previous formula to obtain the expression for the propagator of the radiation $\bar{\sigma}$ field as well, which reads:

$$ij \xrightarrow[\bar{\sigma}]{k} kl = \frac{1}{2} \frac{i}{k^2 + i\epsilon} \left(-\frac{2}{d-2}\delta_{ij}\delta_{kl} + \delta_{ik}\delta_{jl} + \delta_{il}\delta_{jk} \right) . \tag{A.30}$$

A.1.1 — Non-relativistic expansion of the propagators

From the above expression for the potential propagators, we can directly apply the non-relativistic expansion (3.49) which we described in section 3.2.3: this expansion allows to recover the definite

PN scaling when evaluating the relevant diagrams. Then the explicit expression for a propagator with n insertions is given by:

$$-\text{---} \begin{array}{c} \xrightarrow{k} \\ \otimes \\ n \end{array} \text{---} = -\frac{1}{2c_d} \frac{i}{|\mathbf{k}|^2} \left(\frac{(k^0)^2}{|\mathbf{k}|^2} \right)^n, \quad (\text{A.31a})$$

$$i \text{---} \begin{array}{c} \xrightarrow{k} \\ \otimes \\ n \end{array} \text{---} j = \frac{\delta_{ij}}{2} \frac{i}{|\mathbf{k}|^2} \left(\frac{(k^0)^2}{|\mathbf{k}|^2} \right)^n, \quad (\text{A.31b})$$

$$ij \text{---} \begin{array}{c} \xrightarrow{k} \\ \otimes \\ n \end{array} \text{---} kl = -\frac{1}{2} \left(-\frac{2}{d-2} \delta_{ij} \delta_{kl} + \delta_{ik} \delta_{jl} + \delta_{il} \delta_{jk} \right) \frac{i}{|\mathbf{k}|^2} \left(\frac{(k^0)^2}{|\mathbf{k}|^2} \right)^n. \quad (\text{A.31c})$$

A.2 | Near zone Feynman rules for the conservative sector

A.2.1 — Worldline-gravitational fields interaction vertices

■ Expansion of the worldline point particle action

To evaluate the Feynman rules we need to expand the non linear action terms in order to obtain a polynomial expression in fields. Therefore, by considering the worldline point particle action written as a function of the Kol-Smolkin fields (3.33), and notice that it can be rewritten as

$$S_{pp}^{(PP)}[x_a^\mu, \hat{\phi}, \hat{A}_i, \hat{\sigma}_{ij}] = -\sum_{a=1}^2 m_a \int dt d^{d+1}x \delta^{(d+1)}(x - x_a(t)) f(\Phi, A, \Sigma) \quad (\text{A.32})$$

with

$$f(\Phi, A, \Sigma) = e^\Phi [(1 - A)^2 - e^{-c_d \Phi} v_a^2 - e^{-c_d \Phi} \Sigma]^{\frac{1}{2}} \quad (\text{A.33})$$

where we have defined $\Phi \equiv \frac{\hat{\phi}}{\Lambda}$, $A \equiv \frac{\hat{A}_i v_a^i}{\Lambda}$ and $\Sigma \equiv \frac{\hat{\sigma}_{ij} v_a^i v_a^j}{\Lambda}$.

Now we may obtain the coupling between the worldline, and $N_{\hat{\phi}}$ $\hat{\phi}$ fields, $N_{\hat{A}}$ \hat{A}_i fields and $N_{\hat{\sigma}}$ $\hat{\sigma}_{jk}$ fields by looking for the $\Phi^{N_{\hat{\phi}}} A^{N_{\hat{A}}} \Sigma^{N_{\hat{\sigma}}}$ term in the Taylor expansion of the $f(\Phi, A, \Sigma)$ function about $\Phi = \hat{A}_i = \hat{\sigma}_{jk} = 0$. In fact we obtain:

$$\begin{aligned} f(\Phi, A, \Sigma) &= \sum_{N_{\hat{\phi}}, N_{\hat{A}}, N_{\hat{\sigma}}=0}^{\infty} \frac{1}{N_{\hat{\phi}}! N_{\hat{A}}! N_{\hat{\sigma}}!} \frac{\partial^{(N_{\hat{\phi}}+N_{\hat{A}}+N_{\hat{\sigma}})} f(0, 0, 0)}{\partial^{N_{\hat{\phi}}} \Phi \partial^{N_{\hat{A}}} A \partial^{N_{\hat{\sigma}}} \Sigma} \Phi^{N_{\hat{\phi}}} A^{N_{\hat{A}}} \Sigma^{N_{\hat{\sigma}}} \\ &= f(\mathbf{0}) + \frac{\partial f(\mathbf{0})}{\partial \Phi} \Phi + \frac{\partial f(\mathbf{0})}{\partial A} A + \frac{\partial f(\mathbf{0})}{\partial \Sigma} \Sigma + \frac{\partial^2 f(\mathbf{0})}{\partial \Phi \partial A} \Phi A + \frac{\partial^2 f(\mathbf{0})}{\partial \Phi \partial \Sigma} \Phi \Sigma + \frac{\partial^2 f(\mathbf{0})}{\partial A \partial \Sigma} A \Sigma \\ &\quad + \frac{1}{2} \frac{\partial^2 f(\mathbf{0})}{\partial^2 \Phi} \Phi^2 + \frac{1}{2} \frac{\partial^2 f(\mathbf{0})}{\partial^2 A} A^2 + \frac{1}{2} \frac{\partial^2 f(\mathbf{0})}{\partial^2 \Sigma} \Sigma^2 + \frac{\partial^3 f(\mathbf{0})}{\partial \Phi \partial A \partial \Sigma} \Phi A \Sigma + \frac{1}{2} \frac{\partial^2 f(\mathbf{0})}{\partial^2 \Phi \partial A} \Phi^2 A + \dots \end{aligned} \quad (\text{A.34})$$

The explicit result can be promptly obtained in a software like `Mathematica`, and it reads:

$$\begin{aligned}
f(\Phi, A, \Sigma) = & \sqrt{1-v_a^2} + \left(\frac{2+(-2+c_d)v_a^2}{2\sqrt{1-v_a^2}} \right) \Phi + \left(-\frac{1}{\sqrt{1-v_a^2}} \right) A + \left(-\frac{1}{2\sqrt{1-v_a^2}} \right) \Sigma \\
& + \left(\frac{-2+(2+c_d)v_a^2}{2(1-v_a^2)^{3/2}} \right) \Phi A + \left(-\frac{2+c_d(-2+v_a^2)-2v_a^2}{4(1-v_a^2)^{3/2}} \right) \Phi \Sigma + \left(-\frac{1}{2(1-v_a^2)^{3/2}} \right) A \Sigma \\
& + \frac{1}{2} \left(\frac{4+v_a^2(-8-2(-2+c_d)c_d+(-2+c_d)^2v_a^2)}{4(1-v_a^2)^{3/2}} \right) \Phi^2 + \frac{1}{2} \left(-\frac{v_a^2}{(1-v_a^2)^{3/2}} \right) A^2 \\
& + \frac{1}{2} \left(-\frac{1}{4(1-v_a^2)^{3/2}} \right) \Sigma^2 + \left(\frac{2(-1+v_a^2)+c_d(2+v_a^2)}{4(1-v_a^2)^{5/2}} \right) \Phi A \Sigma \\
& + \frac{1}{2} \left(\frac{-4+v_a^2(8-2(-2+c_d)c_d-(2+c_d)^2v_a^2)}{4(1-v_a^2)^{5/2}} \right) \Phi^2 A + \dots
\end{aligned} \tag{A.35}$$

From this action we can derive the interaction vertices between a worldline and gravitational fields, both potential and radiative ones: this still follows from the expansion $\hat{W}_a = W_a + \bar{W}_a$ which we have already presented.

In the following we will present some explicit derivations of the Feynman rules corresponding to the interaction terms encoded in action (A.35); still for now we will restrict ourselves to the case of potential fields only.

■ Example: interaction vertex between worldline and potential ϕ field

As explained at the beginning of this appendix A, to obtain the momentum space Feynman rules for the interaction vertex between the worldline and a single potential ϕ field, we have to take a single functional derivative with respect to the $\phi(k)$ field in the (Fourier transformed) $S_{pp}[x_a^\mu, \phi, A^i, \sigma^{ij}]$ action, set all fields to zero, and finally add an i factor. We can directly start with the only relevant term in the expanded action (A.35) which will give a non vanishing contribution, which is given by:

$$S_{pp}^{(PP)}[x_a^\mu, \phi, A^i, \sigma^{ij}] \supset - \sum_{a=1}^2 m_a \int dt d^{d+1}x \delta^{(d+1)}(x-x_a(t)) \left(\frac{2+(-2+c_d)v_a^2}{2\sqrt{1-v_a^2}} \right) \frac{\phi(x)}{\Lambda}. \tag{A.36}$$

Inserting the Fourier transformed field $\phi(k)$ field we obtain:

$$\begin{aligned}
S_{pp}^{(PP)} & \supset - \sum_{a=1}^2 \frac{m_a}{\Lambda} \int dt d^{d+1}x \frac{d^{d+1}k}{(2\pi)^{d+1}} \delta^{(d+1)}(x-x_a(t)) \left(\frac{2+(-2+c_d)v_a^2}{2\sqrt{1-v_a^2}} \right) \phi(k) e^{-ikx} \\
& = - \sum_{a=1}^2 \frac{m_a}{\Lambda} \int dt \frac{d^{d+1}k}{(2\pi)^{d+1}} \left(\frac{2+(-2+c_d)v_a^2}{2\sqrt{1-v_a^2}} \right) \phi(k) e^{-ikx_a(t)}
\end{aligned} \tag{A.37}$$

Taking the functional derivatives, and setting all fields to zero, we obtain:

$$\begin{aligned}
\frac{\delta S_{pp}^{(PP)}}{\delta \phi(k')} & = - \sum_{a=1}^2 \frac{m_a}{\Lambda} \int dt \frac{d^{d+1}k}{(2\pi)^{d+1}} \left(\frac{2+(-2+c_d)v_a^2}{2\sqrt{1-v_a^2}} \right) (2\pi)^{d+1} \delta^{(d+1)}(k-k') e^{-ikx_a(t)} \\
& = - \sum_{a=1}^2 \frac{m_a}{\Lambda} \int dt \left(\frac{2+(-2+c_d)v_a^2}{2\sqrt{1-v_a^2}} \right) e^{-ik'x_a(t)}
\end{aligned}, \tag{A.38}$$

from which we can read the Feynman rules once we add the i factor, with the momentum incoming:

$$\begin{array}{c} \textcircled{a} \\ | \\ \phi \\ | \\ \uparrow k \end{array} = -i \sum_{a=1}^2 \frac{m_a}{\Lambda} \int dt \left(\frac{2 + (-2 + c_d) v_a^2}{2\sqrt{1 - v_a^2}} \right) e^{-ikx_a(t)}. \quad (\text{A.39})$$

Definite post-Newtonian scaling of the interaction vertex

Let us notice that the coefficient in front of ϕ depends on the velocities v_a^2 of the compact bodies, therefore to have a definite scaling in the post-Newtonian expansion, we have to expand it to the desired order:

$$\left(\frac{2 + (-2 + c_d) v_a^2}{2\sqrt{1 - v_a^2}} \right) = 1 + \frac{1}{2} (c_d - 1) v_a^2 + \frac{1}{8} (2c_d - 1) v_a^4 + \frac{1}{16} (3c_d - 1) v_a^6 + O(v_a^8). \quad (\text{A.40})$$

This can be done also diagrammatically, in which case the expression (A.39) is expanded as a leading term and a series of velocity insertion in the vertex, denoted with a crossed dot, so for example:

$$\begin{array}{c} \textcircled{a} \\ | \\ \phi \\ | \\ \uparrow k \end{array} = -i \sum_{a=1}^2 \frac{m_a}{\Lambda} \int dt e^{-ikx_a(t)}, \quad (\text{A.41a})$$

$$\begin{array}{c} \textcircled{a} \\ \otimes \\ | \\ \phi \\ | \\ \uparrow k \end{array} = -i \sum_{a=1}^2 \frac{m_a}{\Lambda} \int dt e^{-ikx_a(t)} \left(\frac{c_d - 1}{2} \right) v_a^2, \quad (\text{A.41b})$$

$$\begin{array}{c} \textcircled{a} \\ \otimes \\ \otimes \\ | \\ \phi \\ | \\ \uparrow k \end{array} = -i \sum_{a=1}^2 \frac{m_a}{\Lambda} \int dt e^{-ikx_a(t)} \left(\frac{2c_d - 1}{8} \right) v_a^4; \quad (\text{A.41c})$$

in particular if the diagram (A.41a) enters at order n -PN, (A.41b) and (A.41c) are corrections which enter respectively at order $(n + 1)$ -PN and $(n + 2)$ -PN. Nonetheless it is customary to use the vertex expression exact to all orders in v , i.e. the Feynman rule (A.39), and then expand the final result to the desired PN order only at the end of calculations; or at least after having joined all the Feynman rules [235].

■ Example: interaction vertex between worldline, one A_i and two σ_{jk} fields

To show how to generalize the previous result, let us consider the more general case of the interaction between a worldline, one A_i potential field and two σ_{jk} potential fields. The relevant term in the point particle action is given by:

$$S_{pp}^{(PP)} \supset - \sum_{a=1}^2 m_a \int dt d^{d+1} x \delta^{(d+1)}(x - x_a(t)) \left[\frac{1}{2\Lambda^3} \left(-\frac{3}{4(1 - v_a^2)^{5/2}} \right) (A_n v_a^n) (\sigma_{pq} v_a^p v_a^q) (\sigma_{rs} v_a^r v_a^s) \right]. \quad (\text{A.42})$$

We replace the usual Fourier transform of the fields to obtain, recalling our compact integral notation (see Notation), and we take the needed functional derivatives, recalling also the rule

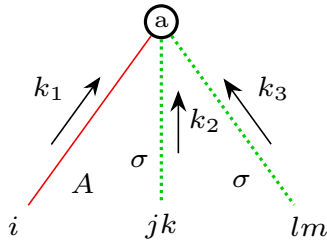
(A.2b) for the functional derivation of product of fields:

$$\begin{aligned}
S_{pp}^{(PP)} &\supset - \sum_{a=1}^2 m_a \int_{q_1, q_2, q_3} \int dt e^{-i(q_1+q_2+q_3)x_a(t)} \left[\frac{1}{2\Lambda^3} \left(-\frac{3}{4(1-v_a^2)^{5/2}} \right) \right. \\
&\quad \left. A_n(q_1) \sigma_{pq}(q_2) \sigma_{rs}(q_3) (v_a^n v_a^p v_a^q v_a^r v_a^s) \right] \\
\frac{\delta S_{pp}^{(PP)}}{\delta A_i(k_1)} &\supset - \sum_{a=1}^2 m_a \int_{q_2, q_3} \int dt e^{-i(k_1+q_2+q_3)x_a(t)} \left[\frac{1}{2\Lambda^3} \left(-\frac{3}{4(1-v_a^2)^{5/2}} \right) \right. \\
&\quad \left. \underbrace{\delta_{n}^i v_a^n}_{=v_a^i} \sigma_{pq}(q_2) \sigma_{rs}(q_3) (v_a^p v_a^q v_a^r v_a^s) \right] \\
\frac{\delta^2 S_{pp}^{(PP)}}{\delta \sigma_{jk}(k_2) \delta A_i(k_1)} &\supset - \sum_{a=1}^2 m_a \int_{q_2, q_3} \int dt e^{-i(k_1+q_2+q_3)x_a(t)} \left[\frac{1}{2\Lambda^3} \left(-\frac{3}{4(1-v_a^2)^{5/2}} \right) v_a^i (v_a^p v_a^q v_a^r v_a^s) \right. \\
&\quad \left. (2\pi)^{(d+1)} \left(\delta^{(2d+1)}(q_2 - k_2) \delta^j_p \delta^k_q \sigma_{rs}(q_3) + \sigma_{pq}(q_2) \delta^{(2d+1)}(q_3 - k_2) \delta^j_r \delta^k_s \right) \right].
\end{aligned} \tag{A.43}$$

Taking the final functional derivative and setting all fields to zero we obtain:

$$\begin{aligned}
\frac{\delta^3 S_{pp}^{(PP)}}{\delta \sigma_{lm}(k_3) \delta \sigma_{jk}(k_2) \delta A_i(k_1)} &= - \sum_{a=1}^2 m_a \int_{q_2, q_3} \int dt e^{-i(k_1+q_2+q_3)x_a(t)} \left[\frac{1}{2\Lambda^3} \left(-\frac{3}{4(1-v_a^2)^{5/2}} \right) v_a^i \right. \\
&\quad \left. (v_a^p v_a^q v_a^r v_a^s) (2\pi)^{2(d+1)} \left(\delta^{(2d+1)}(q_2 - k_2) \delta^j_p \delta^k_q \delta^{(2d+1)}(q_3 - k_3) \delta^l_r \delta^m_s \right. \right. \\
&\quad \left. \left. + \delta^{(2d+1)}(q_2 - k_3) \delta^l_p \delta^m_q \delta^{(2d+1)}(q_3 - k_2) \delta^j_r \delta^k_s \right) \right] \\
&= - \sum_{a=1}^2 \frac{m_a}{\Lambda^3} \int dt e^{-i(k_1+k_2+k_3)x_a(t)} \left[\left(-\frac{3}{4(1-v_a^2)^{5/2}} \right) v_a^i \right. \\
&\quad \left. (v_a^p v_a^q v_a^r v_a^s) \frac{1}{2} \left(\delta^j_p \delta^k_q \delta^l_r \delta^m_s + \delta^l_p \delta^m_q \delta^j_r \delta^k_s \right) \right] \\
&= - \sum_{a=1}^2 \frac{m_a}{\Lambda^3} \int dt e^{-i(k_1+k_2+k_3)x_a(t)} \left[-\frac{3}{4} (1-v_a^2)^{-\frac{5}{2}} v_a^i v_a^j v_a^k v_a^l v_a^m \right].
\end{aligned} \tag{A.44}$$

Therefore the Feynman rule for the worldline- $A\sigma^2$ interaction vertex, assuming all momenta to be incoming, is given by:



$$= -i \sum_{a=1}^2 \frac{m_a}{\Lambda^3} \int dt e^{-i(k_1+k_2+k_3)x_a(t)} \left(-\frac{3}{4} (1-v_a^2)^{-\frac{5}{2}} \right) (v_a^i v_a^j v_a^k v_a^l v_a^m).$$

$$\tag{A.45}$$

■ Generic interaction vertex between worldline and potential fields

We can generalize the derivation of the Feynman rules for the interaction between the worldline and potential fields by drawing on the examples we have seen so far.

Let us consider the interaction between N_ϕ ϕ fields, N_A A_i fields, N_σ σ_{jk} potential fields and a worldline. Recalling the expansion (A.34), the relevant term for the $\Phi^{N_\phi} A^{N_A} \Sigma^{N_\sigma}$ interaction in

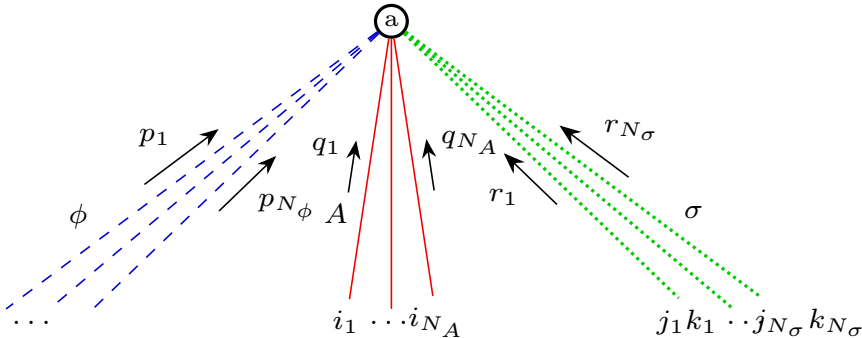
the point particle action is given by:

$$\begin{aligned}
S_{pp}^{(PP)}[x_a^\mu, \phi, A^i, \sigma^{ij}] &\supset - \sum_{a=1}^2 m_a \int dt d^{d+1}x \delta^{(d+1)}(x - x_a(t)) \\
&\quad \times \frac{1}{N_\phi! N_A! N_\sigma!} \frac{\partial^{(N_\phi+N_A+N_\sigma)} f(0,0,0)}{\partial^{N_\phi} \Phi \partial^{N_A} A \partial^{N_\sigma} \Sigma} \Phi^{N_\phi} A^{N_A} \Sigma^{N_\sigma} \\
&= - \frac{1}{N_\phi! N_A! N_\sigma!} \frac{1}{\Lambda^{N_\phi+N_A+N_\sigma}} \sum_{a=1}^2 m_a \int dt d^{d+1}x \delta^{(d+1)}(x - x_a(t)) \\
&\quad \left(\frac{\partial^{(N_\phi+N_A+N_\sigma)} f(0,0,0)}{\partial^{N_\phi} \Phi \partial^{N_A} A \partial^{N_\sigma} \Sigma} \phi^{N_\phi} (A_i v_a^i)^{N_A} (\sigma_{jk} v_a^j v_a^k)^{N_\sigma} \right). \tag{A.46}
\end{aligned}$$

We then Fourier transform all the fields:

$$\begin{aligned}
S_{pp}^{(PP)} &\supset - \frac{1}{N_\phi! N_A! N_\sigma!} \frac{1}{\Lambda^{N_\phi+N_A+N_\sigma}} \sum_{a=1}^2 m_a \int_{p_1, \dots, p_{N_\phi}, q_1, \dots, q_{N_A}, r_1, \dots, r_{N_\sigma}} dt d^{d+1}x \left[\delta^{(d+1)}(x - x_a(t)) \right. \\
&\quad \times e^{-i(p_1 + \dots + p_{N_\phi} + q_1 + \dots + q_{N_A} + r_1 + \dots + r_{N_\sigma})x} \frac{\partial^{(N_\phi+N_A+N_\sigma)} f(0,0,0)}{\partial^{N_\phi} \Phi \partial^{N_A} A \partial^{N_\sigma} \Sigma} \phi(p_1) \cdots \phi(p_{N_\phi}) \\
&\quad \left. \times (A_{s_1}(q_1) v_a^{s_1}) \cdots (A_{s_{N_A}}(q_{N_A}) v_a^{s_{N_A}}) (\sigma_{t_1 u_1}(r_1) v_a^{t_1} v_a^{u_1}) \cdots (\sigma_{t_{N_\sigma} u_{N_\sigma}}(r_{N_\sigma}) v_a^{t_{N_\sigma}} v_a^{u_{N_\sigma}}) \right]. \tag{A.47}
\end{aligned}$$

We then start performing the required functional derivatives. In particular, applying the generalization of the rule (A.2b) for the functional derivation of products of the same fields, we'll obtain the symmetrization of the Dirac delta over the momenta and of the Kronecker delta over the spatial indices. By performing the integrals and the sums over these delta functions, we'll obtain exactly the same factors $N_\phi!$ times for the ϕ fields, $N_A!$ for the A_i and $N_\sigma!$ for the σ_{jk} : in fact the momenta of each field appear only in the sum inside the exponential, therefore they can simply be reordered. Instead the Kronecker delta from the functional derivatives of the A_i and σ_{ij} fields are all contracted with the product of the same quantity, the three-velocity v_a^i of the body a ; hence also in this case we can reorder the terms to obtain exactly the same factor each time. This means that we can simply evaluate a single term and multiply it by $(N_\phi! N_A! N_\sigma!)$, which therefore will exactly cancel with the $\frac{1}{N_\phi! N_A! N_\sigma!}$ factor which came from the expansion of the action; and identify the external momenta directly with the momenta in the exponential, as long as they become to the same type of field. Finally, adding the i factor, we obtain the Feynman rule for the worldline- $\Phi^{N_\phi} A^{N_A} \Sigma^{N_\sigma}$ interaction vertex:



$$\begin{aligned}
&= -i \sum_{a=1}^2 m_a \int dt e^{-i(p_1 + \dots + p_{N_\phi} + q_1 + \dots + q_{N_A} + r_1 + \dots + r_{N_\sigma})x(t)} \left[\frac{1}{\Lambda^{N_\phi+N_A+N_\sigma}} \frac{\partial^{(N_\phi+N_A+N_\sigma)} f(0,0,0)}{\partial^{N_\phi} \Phi \partial^{N_A} A \partial^{N_\sigma} \Sigma} \right. \\
&\quad \left. \left((v_a^{i_1} \cdots v_a^{i_{N_A}}) (v_a^{j_1} v_a^{k_1} \cdots v_a^{j_{N_\sigma}} v_a^{k_{N_\sigma}}) \right) \right]. \tag{A.48}
\end{aligned}$$

Furthermore the symmetry factor associated to the above vertex (A.48) is given by $N_\phi! N_A! N_\sigma!$.

■ Explicit expression for the necessary worldline-potential field interaction vertices

We can obtain the sought-after Feynman rules for the necessary interaction vertices by specializing formula (A.48) to the corresponding case. In the following table A.1 we show the Feynman rules for the interaction vertices which have been used in this thesis work, and their leading order scaling.

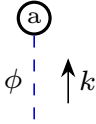
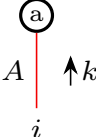
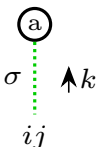
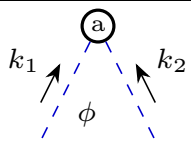
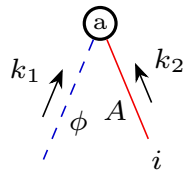
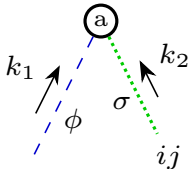
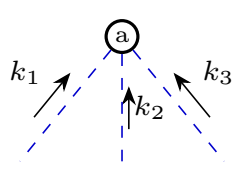
Vertex	Corresponding expression	LO scaling
	$= -i \sum_{a=1}^2 \frac{m_a}{\Lambda} \int dt e^{-ikx_a(t)} \left(\frac{2 + (-2 + c_d) v_a^2}{2\sqrt{1 - v_a^2}} \right)$ (A.49a)	$L^{\frac{1}{2}} v^0$
	$= -i \sum_{a=1}^2 \frac{m_a}{\Lambda} \int dt e^{-ikx_a(t)} \left(-\frac{1}{\sqrt{1 - v_a^2}} \right) v_a^i$ (A.49b)	$L^{\frac{1}{2}} v^1$
	$= -i \sum_{a=1}^2 \frac{m_a}{\Lambda} \int dt e^{-ikx_a(t)} \left(-\frac{1}{2\sqrt{1 - v_a^2}} \right) v_a^i v_a^j$ (A.49c)	$L^{\frac{1}{2}} v^2$
	$= -i \sum_{a=1}^2 \frac{m_a}{\Lambda^2} \int dt e^{-i(k_1+k_2)x_a(t)} \left[\frac{1}{4(1 - v_a^2)^{3/2}} \cdot (4 + v_a^2 (-8 - 2(-2 + c_d) c_d + (-2 + c_d)^2 v_a^2)) \right]$ (A.49d)	$L^0 v^2$
	$= -i \sum_{a=1}^2 \frac{m_a}{\Lambda^2} \int dt e^{-i(k_1+k_2)x_a(t)} \left(\frac{-2 + (2 + c_d) v_a^2}{2(1 - v_a^2)^{3/2}} \right) v_a^i$ (A.49e)	$L^0 v^3$
	$= -i \sum_{a=1}^2 \frac{m_a}{\Lambda^2} \int dt e^{-i(k_1+k_2)x_a(t)} \left[-\frac{1}{4(1 - v_a^2)^{3/2}} \cdot (2 + c_d (-2 + v_a^2) - 2v_a^2) v_a^i v_a^j \right]$ (A.49f)	$L^0 v^4$
	$= -i \sum_{a=1}^2 \frac{m_a}{\Lambda^3} \int dt e^{-i(k_1+k_2+k_3)x_a(t)} \left[\frac{1}{8(1 - v_a^2)^{5/2}} \cdot (8 + v_a^2 (-24 + 4c_d (3 + (-3 + c_d) c_d) + 24v_a^2 - 2c_d (12 + (-9 + c_d) c_d) v_a^2 + (-2 + c_d)^3 (v_a^2)^2)) \right]$ (A.49g)	$L^{-\frac{1}{2}} v^4$

TABLE A.1 — Feynman rules for the interaction vertices, between a worldline and potential fields, most of which have been used in this thesis. The last column reports the leading order scaling of the corresponding vertex, as evaluated by the power counting rules (3.59); in particular all of these vertices have $p = 0$, as for example the worldline- A^2 vertex has been neglected as it has $r = 2$, thereby scaling as $L^0 v^6$ instead of $L^0 v^4$.

A.2.2 — Gravitational potential fields self-interaction vertices

We now turn to the Feynman rules for the self-interaction vertices which are encoded in the bulk action (3.35). In this case we have already reported the expanded form of this non-linear action, therefore we can directly read the relevant terms from the expression of the action. If instead we had started with the action as reported in reference [229], then we would have needed to expand it as explained in section A.1. Let us also notice that in the bulk action (3.35) we report only the terms relevant up to 2PN: the same Feynman rules which we will derive in this section may actually receive corrections from terms in the bulk action with the exact same number of fields, but different number or time and spatial derivatives.

Let us recall once again that such action prescribes the interactions for the $\hat{W} = W + \bar{W}$ fields, so self-interaction vertices containing both potential and radiation fields; in the following instead for simplicity we will restrict ourselves to the case with only potential fields; we'll take into account also radiation fields in section A.3.

■ Example: ϕ^3 interaction vertex

To obtain the interaction vertex between three ϕ fields we can directly read the relevant term, proportional only to ϕ^3 , from the expanded bulk action (3.35), as this is the only one which is going to survive after the application of the relevant functional derivatives and setting the fields to zero. This term reads:

$$S_{bulk} \supset -\frac{c_d^2}{\Lambda} \int d^{d+1}x \dot{\phi}^2 \phi. \quad (\text{A.50})$$

We can then Fourier transform the ϕ fields and then take the functional derivatives, using the generalization of the rule (A.2b) for the functional derivative of the product of fields:

$$\begin{aligned} S_{bulk} &\supset -\frac{c_d^2}{\Lambda} \int_{q_1, q_2, q_3} d^{d+1}x e^{-i(q_1+q_2+q_3)x} \phi(q_1)(-iq_2^0)\phi(q_2)(-iq_3^0)\phi(q_3) \\ \frac{\delta S_{bulk}}{\delta \phi(k_1)} &\supset (2\pi)^{d+1} \frac{c_d^2}{\Lambda} \int_{q_1, q_2, q_3} d^{d+1}x e^{-i(q_1+q_2+q_3)x} q_2^0 q_3^0 \left(\delta^{(d+1)}(q_1 - k_1) \phi(q_2) \phi(q_3) \right. \\ &\quad \left. + \phi(q_1) \delta^{(d+1)}(q_2 - k_1) \phi(q_3) + \phi(q_1) \phi(q_2) \delta^{(d+1)}(q_3 - k_1) \right) \\ \frac{\delta^2 S_{bulk}}{\delta \phi(k_2) \delta \phi(k_1)} &\supset (2\pi)^{2(d+1)} \frac{c_d^2}{\Lambda} \int_{q_1, q_2, q_3} d^{d+1}x \left[e^{-i(q_1+q_2+q_3)x} q_2^0 q_3^0 \right. \\ &\quad \left(\delta^{(d+1)}(q_1 - k_1) \delta^{(d+1)}(q_2 - k_2) \phi(q_3) + \delta^{(d+1)}(q_1 - k_1) \phi(q_2) \delta^{(d+1)}(q_3 - k_2) \right. \\ &\quad \left. + \delta^{(d+1)}(q_1 - k_2) \delta^{(d+1)}(q_2 - k_1) \phi(q_3) + \phi(q_1) \delta^{(d+1)}(q_2 - k_1) \delta^{(d+1)}(q_3 - k_2) \right. \\ &\quad \left. + \delta^{(d+1)}(q_1 - k_2) \phi(q_2) \delta^{(d+1)}(q_3 - k_1) + \phi(q_1) \delta^{(d+1)}(q_2 - k_2) \delta^{(d+1)}(q_3 - k_1) \right) \left. \right] \\ \frac{\delta^3 S_{bulk}}{\delta \phi(k_3) \delta \phi(k_2) \delta \phi(k_1)} &\supset (2\pi)^{3(d+1)} \frac{c_d^2}{\Lambda} \int_{q_1, q_2, q_3} d^{d+1}x \left[e^{-i(q_1+q_2+q_3)x} q_2^0 q_3^0 \right. \\ &\quad \cdot \left(\delta^{(d+1)}(q_1 - k_1) \delta^{(d+1)}(q_2 - k_2) \delta^{(d+1)}(q_3 - k_3) + \delta^{(d+1)}(q_1 - k_1) \delta^{(d+1)}(q_2 - k_3) \delta^{(d+1)}(q_3 - k_2) \right. \\ &\quad \left. + \delta^{(d+1)}(q_1 - k_2) \delta^{(d+1)}(q_2 - k_1) \delta^{(d+1)}(q_3 - k_3) + \delta^{(d+1)}(q_1 - k_3) \delta^{(d+1)}(q_2 - k_1) \delta^{(d+1)}(q_3 - k_2) \right. \\ &\quad \left. + \delta^{(d+1)}(q_1 - k_2) \delta^{(d+1)}(q_2 - k_3) \delta^{(d+1)}(q_3 - k_1) + \delta^{(d+1)}(q_1 - k_3) \delta^{(d+1)}(q_2 - k_2) \delta^{(d+1)}(q_3 - k_1) \right) \left. \right]. \end{aligned} \quad (\text{A.51})$$

We can therefore see that the functional derivatives symmetrize the initial expression with respect to the momenta; in fact, performing the integration over the Fourier momenta q_1, q_2, q_3 , the Fourier

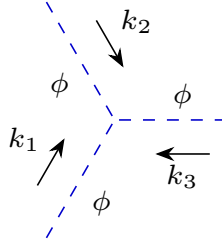
exponential evaluates always to the same expression $e^{-i(k_1+k_2+k_3)x}$, while the only difference between the $3!$ terms is due to the $q_2^0 q_3^0$ factor inside the integrand, thus this factor gets symmetrized. In fact, setting all fields to zero, the only term of the derived action that remains is the one we've been working on, and now it reads:

$$\frac{\delta^3 S_{bulk}}{\delta\phi(k_3)\delta\phi(k_2)\delta\phi(k_1)} = \frac{c_d^2}{\Lambda} \int d^{d+1}x e^{-i(k_1+k_2+k_3)x} (k_2^0 k_3^0 + k_3^0 k_2^0 + k_1^0 k_3^0 + k_1^0 k_2^0 + k_3^0 k_1^0 + k_2^0 k_1^0) . \quad (\text{A.52})$$

We can now perform the integration over the spatial variable:

$$\frac{\delta^3 S_{bulk}}{\delta\phi(k_3)\delta\phi(k_2)\delta\phi(k_1)} = \frac{2c_d^2}{\Lambda} (k_2^0 k_3^0 + k_1^0 k_3^0 + k_1^0 k_2^0) \underbrace{\int d^{d+1}x e^{-i(k_1+k_2+k_3)x}}_{=(2\pi)^{d+1}\delta^{(d+1)}(-k_1-k_2-k_3)} . \quad (\text{A.53})$$

Finally, adding the i factor, we have that the Feynman rule for the ϕ^3 self-interaction vertex, with all momenta incoming, reads:



$$= i(2\pi)^{d+1}\delta^{(d+1)}(k_1 + k_2 + k_3) \frac{2c_d^2}{\Lambda} (k_2^0 k_3^0 + k_1^0 k_3^0 + k_1^0 k_2^0) . \quad (\text{A.54})$$

We can notice the presence of the $d + 1$ dimensional Dirac delta in the k momenta, which enforces momentum conservation in this vertex.

■ Example: $\phi^2\sigma$ interaction vertex

To obtain the $\phi^2\sigma$ interaction vertex we read the relevant terms from the expanded bulk action (3.35) up to 2PN:

$$S_{bulk} \supset -\frac{c_d}{2\Lambda} \int d^{d+1}x [\sigma^i{}_i \partial_j \phi \partial^j \phi - 2(\sigma_{ij} \partial^i \phi \partial^j \phi)] \quad (\text{A.55})$$

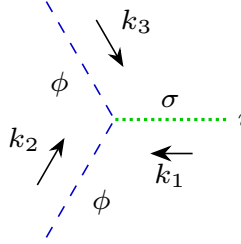
Let us now Fourier transform the expression and take the needed functional derivatives, enforcing the symmetry of the indices of the σ_{kl} field:

$$\begin{aligned} S_{bulk} &\supset -\frac{c_d}{2\Lambda} \int_{q_1, q_2, q_3} d^{d+1}x e^{-i(q_1+q_2+q_3)x} \left[\delta^{kl} \delta_{mn} (iq_2^m)(iq_3^n) - 2 \left((iq_2^k)(iq_3^l) \right) \right] \sigma_{kl}(q_1) \phi(q_2) \phi(q_3) \\ \frac{\delta S_{bulk}}{\delta\sigma_{ij}(k_1)} &\supset \frac{c_d}{2\Lambda} \int_{q_2, q_3} d^{d+1}x e^{-i(k_1+q_2+q_3)x} \left[\delta^{kl} (\mathbf{q}_2 \cdot \mathbf{q}_3) - 2 \left(q_2^k q_3^l \right) \right] \frac{1}{2} (\delta^i{}_k \delta^j{}_l + \delta^i{}_l \delta^j{}_k) \phi(q_2) \phi(q_3) \\ \frac{\delta^2 S_{bulk}}{\delta\phi(k_2)\delta\sigma_{ij}(k_1)} &\supset \frac{c_d}{2\Lambda} (2\pi)^{d+1} \int_{q_2, q_3} d^{d+1}x e^{-i(k_1+q_2+q_3)x} \left[\delta^{ij} (\mathbf{q}_2 \cdot \mathbf{q}_3) - \left(q_2^i q_3^j + q_2^j q_3^i \right) \right] \\ &\quad \times \left(\delta^{(d+1)}(q_2 - k_2) \phi(q_3) + \phi(q_2) \delta^{(d+1)}(q_3 - k_2) \right) \\ \frac{\delta^3 S_{bulk}}{\delta\phi(k_3)\delta\phi(k_2)\delta\sigma_{ij}(k_1)} &\supset \frac{c_d}{2\Lambda} (2\pi)^{2(d+1)} \int_{q_2, q_3} d^{d+1}x e^{-i(k_1+q_2+q_3)x} \left[\delta^{ij} (\mathbf{q}_2 \cdot \mathbf{q}_3) - \left(q_2^i q_3^j + q_2^j q_3^i \right) \right] \\ &\quad \times \left(\delta^{(d+1)}(q_2 - k_2) \delta^{(d+1)}(q_3 - k_3) + \delta^{(d+1)}(q_2 - k_3) \delta^{(d+1)}(q_3 - k_2) \right) . \end{aligned} \quad (\text{A.56})$$

Evaluating the integrals and setting the fields to zero we obtain:

$$\frac{\delta^3 S_{bulk}}{\delta\phi(k_3)\delta\phi(k_2)\delta\sigma_{ij}(k_1)} = \frac{c_d}{\Lambda} \left[\delta^{ij}(\mathbf{k}_2 \cdot \mathbf{k}_3) - \left(k_2^i k_3^j + k_2^j k_3^i \right) \right] \underbrace{\int d^{d+1}x e^{-i(k_1+k_2+k_3)x}}_{=(2\pi)^{d+1}\delta^{(d+1)}(-k_1-k_2-k_3)} \quad (\text{A.57})$$

Finally adding the i factor we obtain the corresponding Feynman rule:



$$= i (2\pi)^{d+1} \delta^{(d+1)}(k_1+k_2+k_3) \frac{c_d}{\Lambda} \left(\delta^{ij}(\mathbf{k}_2 \cdot \mathbf{k}_3) - \left(k_2^i k_3^j + k_2^j k_3^i \right) \right) . \quad (\text{A.58})$$

■ Feynman rules for generic potential bulk self-interaction vertices

The first step in the derivation of the Feynman rule is to substitute to each field its Fourier transform (A.1); after having done so, any temporal or spatial derivative is applied to the exponential, e.g. $\dot{W}_A(x) \rightarrow \int_q e^{-iqx} (-iq^0) W_A(q)$, and $\partial_j W_A(x) \rightarrow \int_q e^{-iqx} (+iq^j) W_A(q)$ and so forth for higher derivatives, for example $\partial_j \partial_k W_A(x) \rightarrow -\int_q e^{-iqx} q^j q^k W_A(q)$; let us remember that we take all the momenta as incoming.

The next step, as outlined at the start of this chapter, is to perform the functional derivatives with respect to the all the fields which appear in the action term. This step also tell us which is the diagrammatic representation that corresponds to the Feynman rule we're computing: considering for definiteness the Feynman rule (A.58), in its derivation (A.56) we obtain the Fourier transformed fields $\phi(q_1)\phi(q_2)\sigma_{kl}(q_3)$; then we'll have to take the functional derivative with respect to all of them. For this particular example we may do so by parametrizing these fields as $\sigma_{ij}(k_1)$, $\phi(k_2)$ and $\phi(k_3)$ and taking the functional derivative with respect to $\frac{\delta^3}{\delta\phi(k_3)\delta\phi(k_2)\delta\sigma_{ij}(k_1)}$: doing so we will obtain a diagram like the one depicted in (A.58), with the given k_1 , k_2 and k_3 momenta and ij indices.

Let us notice that if there is more than one field of the same type, e.g. ϕ^n with $n \geq 2$, then when applying the functional derivative we'll have to resort to the rule (A.2b) for the functional derivation of the product of fields: the net action of this procedure, once we integrate the Dirac delta in the momenta with the Fourier momenta integrals, is to kind-of symmetrize (as we're dealing with bosonic fields only) both the spatial indices and the momenta factor which appear in our expression. To make this point more clear, and point out the subtleties in the previous statement, let us assume to have a Lagrangian term of the following kind

$$\begin{aligned} \mathcal{L} &= c A_{j_1}(x) \partial_{j_4} A_{j_2}(x) \ddot{A}_{j_3}(x) \\ &= -i c \int_{q_1, q_2, q_3} (q_2^{j_4})(q_3^0)^2 A_{j_1}(q_1) A_{j_2}(q_2) A_{j_3}(q_3) e^{-i(q_1+q_2+q_3)x} \end{aligned} \quad (\text{A.59})$$

and, once defined for convenience $\delta_{rs}^{(q-k)} \equiv \delta^{(d+1)}(q-k) \delta_{rs}$ such that $\frac{\delta A_{j_1}(q_1)}{\delta A_{i_2}(k_2)} = (2\pi)^{d+1} \delta_{j_1 i_2}^{(q_1-k_2)}$, let us perform the aforementioned functional derivatives:

$$\begin{aligned} \frac{\delta \mathcal{L}}{\delta A_{i_1}(k_1)} &= -i (2\pi)^{d+1} c \int_{q_1, q_2, q_3} (q_2^{j_4})(q_3^0)^2 e^{-i(q_1+q_2+q_3)x} \left(\delta_{i_1 j_1}^{(q_1-k_1)} A_{j_2}(q_2) A_{j_3}(q_3) \right. \\ &\quad \left. + A_{j_1}(q_1) \delta_{i_1 j_2}^{(q_2-k_1)} A_{j_3}(q_3) + A_{j_1}(q_1) A_{j_2}(q_2) \delta_{i_1 j_3}^{(q_3-k_1)} \right) ; \end{aligned} \quad (\text{A.60a})$$

$$\begin{aligned}
\frac{\delta^2 \mathcal{L}}{\delta A_{i_2}(k_2) \delta A_{i_1}(k_1)} &= -i(2\pi)^{2(d+1)} c \int_{q_1, q_2, q_3} (q_2^{j_4})(q_3^0)^2 e^{-i(q_1+q_2+q_3)x} \\
&\times \left(\delta_{i_1 j_1}^{(q_1-k_1)} \delta_{i_2 j_2}^{(q_2-k_2)} A_{j_3}(q_3) + \delta_{i_1 j_1}^{(q_1-k_1)} A_{j_2}(q_2) \delta_{i_2 j_3}^{(q_3-k_2)} \right. \\
&+ \delta_{i_2 j_1}^{(q_1-k_2)} \delta_{i_1 j_2}^{(q_2-k_1)} A_{j_3}(q_3) + A_{j_1}(q_1) \delta_{i_1 j_2}^{(q_2-k_1)} \delta_{i_2 j_3}^{(q_3-k_2)} \\
&\left. + \delta_{i_2 j_1}^{(q_1-k_2)} A_{j_2}(q_2) \delta_{i_1 j_3}^{(q_3-k_1)} + A_{j_1}(q_1) \delta_{i_2 j_2}^{(q_2-k_2)} \delta_{i_1 j_3}^{(q_3-k_1)} \right) ; \tag{A.60b}
\end{aligned}$$

$$\begin{aligned}
\frac{\delta^3 \mathcal{L}}{\delta A_{i_3}(k_3) \delta A_{i_2}(k_2) \delta A_{i_1}(k_1)} &= -i(2\pi)^{3(d+1)} c \int_{q_1, q_2, q_3} (q_2^{j_4})(q_3^0)^2 e^{-i(q_1+q_2+q_3)x} \\
&\times \left(\delta_{i_1 j_1}^{(q_1-k_1)} \delta_{i_2 j_2}^{(q_2-k_2)} \delta_{i_3 j_3}^{(q_3-k_3)} + \delta_{i_1 j_1}^{(q_1-k_1)} \delta_{i_3 j_2}^{(q_2-k_3)} \delta_{i_2 j_3}^{(q_3-k_2)} \right. \\
&+ \delta_{i_2 j_1}^{(q_1-k_2)} \delta_{i_1 j_2}^{(q_2-k_1)} \delta_{i_3 j_3}^{(q_3-k_3)} + \delta_{i_3 j_1}^{(q_1-k_3)} \delta_{i_1 j_2}^{(q_2-k_1)} \delta_{i_2 j_3}^{(q_3-k_2)} \\
&\left. + \delta_{i_2 j_1}^{(q_1-k_2)} \delta_{i_3 j_2}^{(q_2-k_3)} \delta_{i_1 j_3}^{(q_3-k_1)} + \delta_{i_3 j_1}^{(q_1-k_3)} \delta_{i_2 j_2}^{(q_2-k_2)} \delta_{i_1 j_3}^{(q_3-k_1)} \right) \tag{A.60c} \\
&= -i(2\pi)^{3(d+1)} c \int_{q_1, q_2, q_3} (q_2^{j_4})(q_3^0)^2 e^{-i(q_1+q_2+q_3)x} \\
&\times \left(\sum_{\pi \in S_3} \delta_{i_{\pi(1)} j_1}^{(q_1-k_{\pi(1)})} \delta_{i_{\pi(2)} j_2}^{(q_2-k_{\pi(2)})} \delta_{i_{\pi(3)} j_3}^{(q_3-k_{\pi(3)})} \right) ;
\end{aligned}$$

where in formula (A.60c) we introduced S_n , which is the symmetric group formed out of n elements, and $\pi \in S_n$, which represents one out of the $n!$ permutations of n elements: therefore with the notation $\sum_{\pi \in S_3}$ we understand the sum over all the permutations of the numbers 1, 2, 3; e.g. $\sum_{\pi \in S_3} f(\pi(1), \pi(2), \pi(3)) = f(1, 2, 3) + f(1, 3, 2) + f(2, 1, 3) + f(2, 3, 1) + f(3, 1, 2) + f(3, 2, 1)$. Performing the integration over the Fourier momenta in equation (A.60c) we find

$$\begin{aligned}
\frac{\delta^3 \mathcal{L}}{\delta A_{i_3}(k_3) \delta A_{i_2}(k_2) \delta A_{i_1}(k_1)} &= -i c \sum_{\pi \in S_3} \left((k_{\pi(2)}^{j_4})(k_{\pi(3)}^0)^2 e^{-i(k_{\pi(1)}+k_{\pi(2)}+k_{\pi(3)})x} \delta_{i_{\pi(1)} j_1} \delta_{i_{\pi(2)} j_2} \delta_{i_{\pi(3)} j_3} \right) \\
&= -i c e^{-i(k_1+k_2+k_3)x} \sum_{\pi \in S_3} \left((k_{\pi(2)}^{j_4})(k_{\pi(3)}^0)^2 \delta_{i_{\pi(1)} j_1} \delta_{i_{\pi(2)} j_2} \delta_{i_{\pi(3)} j_3} \right) \\
&= -i c e^{-i(k_1+k_2+k_3)x} \left((k_2^{j_4})(k_3^0)^2 \delta_{i_1 j_1} \delta_{i_2 j_2} \delta_{i_3 j_3} + (k_3^{j_4})(k_2^0)^2 \delta_{i_1 j_1} \delta_{i_3 j_2} \delta_{i_2 j_3} \right. \\
&\quad + (k_1^{j_4})(k_3^0)^2 \delta_{i_2 j_1} \delta_{i_1 j_2} \delta_{i_3 j_3} + (k_3^{j_4})(k_1^0)^2 \delta_{i_2 j_1} \delta_{i_3 j_2} \delta_{i_1 j_3} \\
&\quad \left. + (k_1^{j_4})(k_2^0)^2 \delta_{i_3 j_1} \delta_{i_1 j_2} \delta_{i_2 j_3} + (k_2^{j_4})(k_1^0)^2 \delta_{i_3 j_1} \delta_{i_2 j_2} \delta_{i_1 j_3} \right) , \tag{A.61}
\end{aligned}$$

where in the second line we used the fact that the sum of momenta in the exponential takes the same form for each of the permutation π thanks to the commutative property of addition. We can notice that if there were no spatial or temporal derivatives acting on the fields in the original action term, then we would have achieved a complete symmetrization of the indices, hence obtaining $3! \delta_{i_1 j_1} \delta_{i_2 j_2} \delta_{i_3 j_3}$; instead the presence of derivatives create k terms, which then require us to sum appropriately over the permutations of the indices in order to get the correct result. Let us also recall that if we're dealing with the symmetric σ_{ij} field, then to preserve the symmetry of its indices we should use the symmetric formula (A.4) for its functional derivative.

Finally at the end of these steps, in the action the only integration left is the one over $d^{d+1}x$, which multiplies the Fourier exponential; in this exponential the position x is contracted with the sum of over all the field momenta, which we assumed to be incoming, therefore, recalling notation (N14) and that the Dirac delta is an even function, this terms yields:

$$\int d^{d+1}x e^{-i(\sum_i k_i)x} = (2\pi)^{d+1} \delta^{(d+1)}(\sum_i k_i) ; \tag{A.62}$$

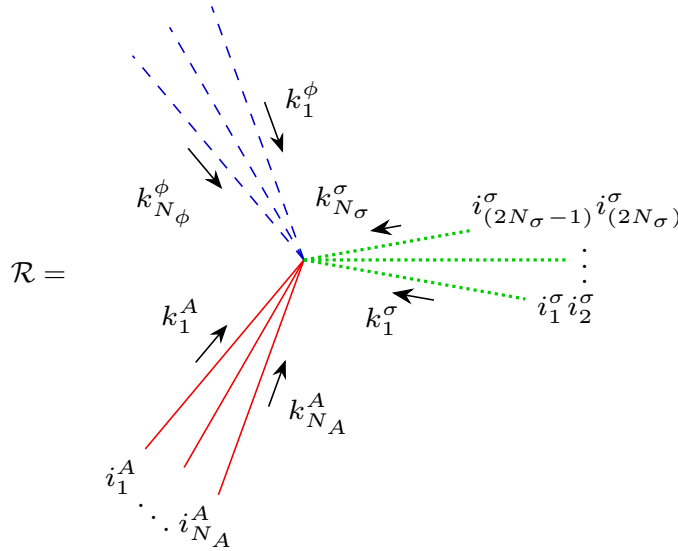
hence we can see that this Dirac delta enforces the momentum conservation for each bulk interaction vertex.

To parametrize the most general action term then we use the following compact notation

$$S \supset \mathcal{T}^{\mathcal{I}} \int d^{d+1}x \prod_{W=\phi,A,\sigma} \left[\prod_{b=1}^{N_W} \left(\left(\prod_{c=1}^{s_b^W} \partial_{j_c^{W,b}} \right) \left(\partial_0^{(t_b^W)} \right) W_{J_{\{b\}}^W} \right) \right]. \quad (\text{A.63})$$

In this expression W is the usual placeholder variable for the several potential fields, $W = \phi, A, \sigma$, and the outer product has the goal of considering each of these fields. We also introduced the general index J^W by which we understand the several indices that are carried by each W field, so $\phi_{J_{\{b\}}^\phi} = \phi$, $A_{J_{\{b\}}^A} = A_{j_b^A}$, $\sigma_{J_{\{b\}}^\sigma} = \sigma_{j_{(2b-1)j_{(2b)}}^\sigma}$; for example $\sigma_{J_{\{1\}}^\sigma} = \sigma_{j_1^\sigma j_2^\sigma}$. We then have to consider that each field can appear multiple times in each action term, and we denote with N_W the number of times the field W appears in the action term; hence the $\prod_{b=1}^{N_W}$ product iterates over them. Furthermore each of the fields, which this latter product is iterating over via the b variable, may possibly have several time derivatives and spatial derivatives acting on it; in fact, for the term identified by a given W and b variables, we denote with t_r^W the order of the temporal derivative acting on it, and with s_b^W the number of spatial derivatives acting on it; additionally we denote the index of the c -th spatial derivative as $j_c^{W,r}$. Finally $\mathcal{T}^{\mathcal{I}}$ is a position independent tensor which contracts all the free indices which appear inside the spacetime integral, so in particular \mathcal{I} is the ordered list of these indices, schematically $\mathcal{I} = (j_1^A j_2^A \dots j_1^\sigma \dots j_1^{\phi,1} j_2^{\phi,1} \dots j_1^{\phi,2} \dots j_1^{A,1} \dots j_1^{\sigma,1} \dots)$.

Let us now evaluate the Feynman rule corresponding to such an action term like (A.63): first we denote via k_b^W the incoming momentum of the b -th field of type W , and to it we also associate the generic spatial indices $I_{\{b\}}^W$, with the same convention presented above. Therefore the diagrammatic representation of this Feynman rule \mathcal{R} and its corresponding expression are:



$$\begin{aligned} \mathcal{R} = & \left(i (2\pi)^{d+1} \delta^{(d+1)}(\sum_i k_i) \right) \mathcal{T}^{\mathcal{I}} \\ & \times \prod_{W=\phi,A,\sigma} \left[\sum_{\pi \in S_{N_W}} \left(\prod_{b=1}^{N_W} \left(\left(\prod_{c=1}^{s_b^W} \left(+i \left(k_{\pi(b)}^W \right)^{j_c^{W,b}} \right) \right) \left((-i(k_{\pi(b)}^W)^0)^{(t_b^W)} \right) \delta_{I_{\{\pi(b)\}}^W J_{\{b\}}^W} \right) \right) \right]. \end{aligned} \quad (\text{A.64})$$

In the Feynman rule we added the usual i factor, we denoted with $\sum_i k_i = \sum_{W=\phi,A,\sigma} \sum_{b=1}^{N_W} k_b^W$ the sum over all the momenta of the fields, which we choose to be all incoming; furthermore we

denoted with $\pi(\cdot) \in S_{N_W}$ the permutations of the numbers $1, \dots, N_W$. Finally we introduced the tensor $\delta_{\{\pi(b)\} J_{\{b\}}^W}$, with the function of enforcing the corresponding spatial indices to be the same, that is

$$\delta_{\{b'\} J_{\{b\}}^W = \begin{cases} 1 & \text{if } W = \phi \\ \delta_{i_{b'} j_b} & \text{if } W = A \\ \frac{1}{2} \left(\delta_{i_{(2b'-1)j(2b-1)}} \delta_{i_{(2b')j(2b)}} + \delta_{i_{(2b')j(2b-1)}} \delta_{i_{(2b'-1)j(2b)}} \right) & \text{if } W = \sigma . \end{cases} \quad (\text{A.65})$$

The symmetry factor associated to the vertex (A.64) is given by

$$S_F = \prod_{W=\phi, A, \sigma} (N_W!) = N_\phi! N_A! N_\sigma! , \quad (\text{A.66})$$

as we're dealing with bosonic indistinguishable fields.

■ Potential $\phi^2 A$ interaction vertex

We can now employ the result (A.64) derived above to evaluate the Feynman rules which we will need. One of them is the $\phi^2 A$ self-interaction vertex. The relevant term in the bulk action (3.35) reads:

$$S_{bulk} \supset -\frac{2c_d}{\Lambda} \int d^{d+1}x \left[\dot{\phi} A_i \partial^i \phi \right] \quad (\text{A.67})$$

We can cast this expression into the form (A.63) by rewriting (A.67) as:

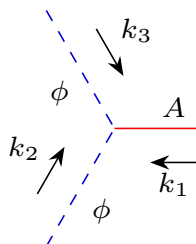
$$S_{bulk} \supset \underbrace{\left(-\frac{2c_d}{\Lambda} \delta^{j_1^{\phi,2} j_1^A} \right)}_{=\mathcal{T}^{j_1^{\phi,2} j_1^A}} \int d^{d+1}x \left[(\partial_0 \phi) \left(\partial_{j_1^{\phi,2}} \phi \right) \right] \left[A_{j_1^A} \right] , \quad (\text{A.68})$$

that is, we recognize that $N_\phi = 2$, $N_A = 1$, $N_\sigma = 0$, that the only temporal derivative results in $t_1^\phi = 1$, and that the only spatial derivative results in $s_2^\phi = 1$, while all other t_b^W and s_b^W coefficients are vanishing.

Then from formula (A.64) we can directly read off the corresponding Feynman rule, which reads

$$\begin{aligned} \mathcal{R} &= \left(i (2\pi)^{d+1} \delta^{(d+1)} (k_1^\phi + k_2^\phi + k_1^A) \right) \left(-\frac{2c_d}{\Lambda} \delta^{j_1^{\phi,2} j_1^A} \right) \\ &\times \left[\left(+i (k_2^\phi)^{j_1^{\phi,2}} \right) \left(-i (k_1^\phi)^0 \right) + \left(+i (k_1^\phi)^{j_1^{\phi,2}} \right) \left(-i (k_2^\phi)^0 \right) \right] \left[\delta_{i_1^A j_1^A} \right] , \end{aligned} \quad (\text{A.69})$$

and after a relabeling of the momenta and spatial indices:



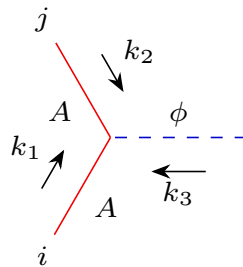
$$i = -i (2\pi)^{d+1} \delta^{(d+1)} (k_1 + k_2 + k_3) \frac{2c_d}{\Lambda} (k_2^0 k_3^i + k_3^0 k_2^i) . \quad (\text{A.70})$$

■ Potential ϕA^2 interaction vertex

We can proceed similarly to we have just done also to derive the Feynman rule also for the ϕA^2 self-interaction vertex. The relevant term in the bulk action is (3.35):

$$S_{bulk} \supset \frac{c_d}{\Lambda} \int d^{d+1}x \left[\left((\partial_i A^i)^2 - (\partial_i A_j \partial^j A^i) + (\partial_j A_i \partial^j A^i) \right) \phi \right]; \quad (\text{A.71})$$

and proceeding as presented above we find:



$$= -i (2\pi)^{d+1} \delta^{(d+1)}(k_1 + k_2 + k_3) \frac{2 c_d}{\Lambda} \left(\delta^{ij} (\mathbf{k}_1 \cdot \mathbf{k}_2) + k_1^i k_2^j - k_1^j k_2^i \right). \quad (\text{A.72})$$

Let us point out that in reference [65] the Feynman rule for the ϕA^2 vertex reports a prefactor of 2 in front of the Kronecker delta δ^{ij} with respect to the result we found (A.72). However in this thesis work we have employed the expression (A.72), for example in the evaluation (4.55h) of diagram $\mathcal{A}_{(2h)}$, obtaining the correct result according to the literature [235].

A.3 | Far zone Feynman rules for the dissipative sector

In this section we'll explicitly derive the Feynman rules relevant for the far zone effective theory, proceeding as discussed in section 3.2.4. In particular these results will be employed in chapter 5 to evaluate the leading order dissipative contributions.

A.3.1 — Feynman rules for bulk vertices involving radiation vertex

The derivation of the Feynman rules for the bulk vertices, so involving only gravitons, is similar to what has been presented so far: in practice up until now we've only considered potential gravitons W_a entering in the vertices, nonetheless the actual expression for the bulk action is written as a function of the generic \hat{W}_a fields, which are then separated into potential and radiation modes $\hat{W}_a = W_a + \bar{W}_a$, as already discussed in section 3.2.4.

Then we can directly derive the momentum space Feynman rules simply taking care of performing the aforementioned expansion, taking care of considering the potential and radiation modes as different when performing the functional derivations, and therefore selecting only the relevant contributions. Below we'll explicitly derive two mixed potential-radiation bulk vertices.

■ Example: $\phi^2 \bar{\phi}$ interaction vertex

To obtain this interaction vertex we have to consider the term in the bulk action (3.35) which contains exactly $\hat{\phi}$ fields, as it will be the only one which is going to remain after the application of the relevant functional derivatives and setting the fields to zero. This term reads:

$$S_{bulk} = -\frac{c_d^2}{\Lambda} \int d^{d+1}x \hat{\phi}^2 \hat{\phi} + O(\sigma \hat{\phi}^3). \quad (\text{A.73})$$

We can then Fourier transform the $\hat{\phi}$ fields and split them into potential and radiation modes, as $\hat{\phi} = \phi + \bar{\phi}$.

$$\begin{aligned} S_{bulk} &\supset -\frac{c_d^2}{\Lambda} \int_{q_1, q_2, q_3} \int d^{d+1}x e^{-i(q_1+q_2+q_3)x} \hat{\phi}(q_1) (-iq_2^0) \hat{\phi}(q_2) (-iq_3^0) \hat{\phi}(q_3) \\ &= +\frac{c_d^2}{\Lambda} \int_{q_1, q_2, q_3} q_2^0 q_3^0 \int d^{d+1}x e^{-i(q_1+q_2+q_3)x} (\phi(q_1) + \bar{\phi}(q_1)) (\phi(q_2) + \bar{\phi}(q_2)) (\phi(q_3) + \bar{\phi}(q_3)) \end{aligned} \quad (\text{A.74})$$

To proceed then we can take the functional derivatives, using the generalization of the rule (A.2b) for the functional derivative of the product of fields; in particular, as we're interested in finding the Feynman rule for the $\phi^2\bar{\phi}$ bulk vertex, in formula (A.74) we can keep only the terms containing two ϕ and only one $\bar{\phi}$.

$$\begin{aligned} \frac{\delta S_{bulk}}{\delta \bar{\phi}(k)} &\supset (2\pi)^{d+1} \frac{c_d^2}{\Lambda} \int_{q_1, q_2, q_3} \int d^{d+1}x e^{-i(q_1+q_2+q_3)x} q_2^0 q_3^0 \left(\delta^{(d+1)}(q_1 - k) \phi(q_2) \phi(q_3) \right. \\ &\quad \left. + \phi(q_1) \delta^{(d+1)}(q_2 - k) \phi(q_3) + \phi(q_1) \phi(q_2) \delta^{(d+1)}(q_3 - k) \right) \\ \frac{\delta^2 S_{bulk}}{\delta \phi(k_1) \delta \bar{\phi}(k)} &\supset (2\pi)^{2(d+1)} \frac{c_d^2}{\Lambda} \int_{q_1, q_2, q_3} \int d^{d+1}x \left[e^{-i(q_1+q_2+q_3)x} q_2^0 q_3^0 \right. \\ &\quad \left(\delta^{(d+1)}(q_1 - k) \delta^{(d+1)}(q_2 - k_1) \phi(q_3) + \delta^{(d+1)}(q_1 - k) \phi(q_2) \delta^{(d+1)}(q_3 - k_1) \right. \\ &\quad \left. + \delta^{(d+1)}(q_1 - k_1) \delta^{(d+1)}(q_2 - k) \phi(q_3) + \phi(q_1) \delta^{(d+1)}(q_2 - k) \delta^{(d+1)}(q_3 - k_1) \right. \\ &\quad \left. \left. + \delta^{(d+1)}(q_1 - k_1) \phi(q_2) \delta^{(d+1)}(q_3 - k) + \phi(q_1) \delta^{(d+1)}(q_2 - k_1) \delta^{(d+1)}(q_3 - k) \right) \right] \\ \frac{\delta^3 S_{bulk}}{\delta \phi(k_2) \delta \phi(k_1) \delta \bar{\phi}(k)} &\supset (2\pi)^{3(d+1)} \frac{c_d^2}{\Lambda} \int_{q_1, q_2, q_3} \int d^{d+1}x \left[e^{-i(q_1+q_2+q_3)x} q_2^0 q_3^0 \right. \\ &\quad \cdot \left(\delta^{(d+1)}(q_1 - k) \delta^{(d+1)}(q_2 - k_1) \delta^{(d+1)}(q_3 - k_2) + \delta^{(d+1)}(q_1 - k) \delta^{(d+1)}(q_2 - k_2) \delta^{(d+1)}(q_3 - k_1) \right. \\ &\quad \left. + \delta^{(d+1)}(q_1 - k_1) \delta^{(d+1)}(q_2 - k) \delta^{(d+1)}(q_3 - k_2) + \delta^{(d+1)}(q_1 - k_2) \delta^{(d+1)}(q_2 - k) \delta^{(d+1)}(q_3 - k_1) \right. \\ &\quad \left. \left. + \delta^{(d+1)}(q_1 - k_1) \delta^{(d+1)}(q_2 - k_2) \delta^{(d+1)}(q_3 - k) + \delta^{(d+1)}(q_1 - k_2) \delta^{(d+1)}(q_2 - k_1) \delta^{(d+1)}(q_3 - k) \right) \right]. \end{aligned} \quad (\text{A.75})$$

Performing the integration over the momenta we obtain:

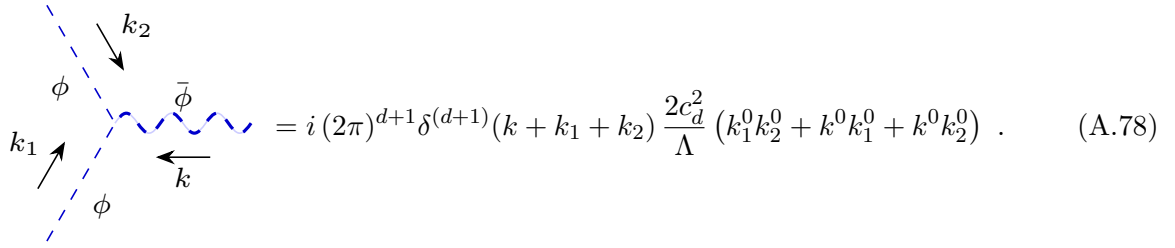
$$\frac{\delta^3 S_{bulk}}{\delta \phi(k_2) \delta \phi(k_1) \delta \bar{\phi}(k)} = \frac{c_d^2}{\Lambda} \int d^{d+1}x e^{-i(k+k_1+k_2)x} (k_1^0 k_2^0 + k_2^0 k_1^0 + k^0 k_2^0 + k^0 k_1^0 + k_2^0 k^0 + k_1^0 k^0) ; \quad (\text{A.76})$$

and performing then the integration over the spatial variable:

$$\frac{\delta^3 S_{bulk}}{\delta \phi(k_2) \delta \phi(k_1) \delta \bar{\phi}(k)} = \frac{2c_d^2}{\Lambda} (k_1^0 k_2^0 + k^0 k_1^0 + k^0 k_2^0) \underbrace{\int d^{d+1}x e^{-i(k+k_1+k_2)x}}_{=(2\pi)^{d+1} \delta^{(d+1)}(-k-k_1-k_2)}. \quad (\text{A.77})$$

Finally, adding the i factor, we have that the Feynman rule for the $\phi^2\bar{\phi}$ self-interaction vertex, with

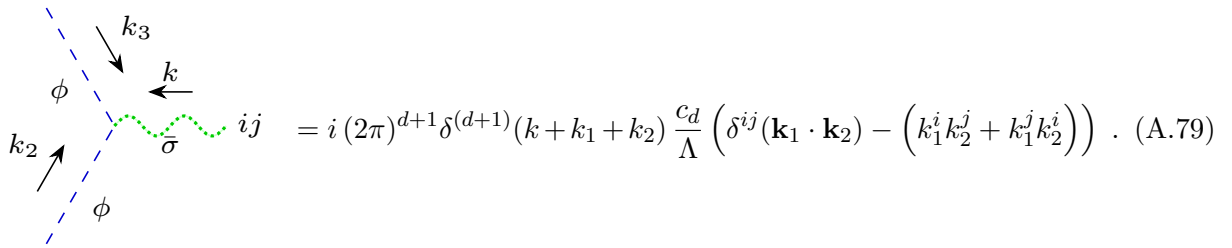
all momenta incoming, reads:



$$= i (2\pi)^{d+1} \delta^{(d+1)}(k + k_1 + k_2) \frac{2c_d^2}{\Lambda} (k_1^0 k_2^0 + k^0 k_1^0 + k^0 k_2^0) . \quad (\text{A.78})$$

■ $\phi^2 \bar{\sigma}$ interaction vertex

In the following we'll need the Feynman rule for the $\phi^2 \bar{\sigma}$ interaction. Its expression can be read off directly from equation (A.58), because the derivation goes through analogously once one considers $\bar{\sigma}$ instead of σ as the field with respect to which take the functional derivative: then the Feynman rule for the $\phi^2 \bar{\sigma}$ vertex reads



$$= i (2\pi)^{d+1} \delta^{(d+1)}(k + k_1 + k_2) \frac{c_d}{\Lambda} \left(\delta^{ij}(\mathbf{k}_1 \cdot \mathbf{k}_2) - (k_1^i k_2^j + k_1^j k_2^i) \right) . \quad (\text{A.79})$$

A.3.2 — Worldline-radiation vertex

We're now interested in computing the Feynman rules for the coupling between \bar{W}_a radiations field and a worldline vertex in the far zone effective theory: we recall from section 3.2 that in our notation the square in the diagrams represents the worldline in the far zone effective theory. From that section we also recall that in order to obtain these Feynman rules (or the associated terms in the action) we have to perform a kind of matching procedure: in fact we'll have to evaluate the corresponding diagrams in the near zone effective theory, by considering the relevant radiation fields \bar{W}_a as external particles with fixed momentum.

Doing so then the evaluation of the diagram still goes through similarly to the evaluation of conservative diagrams that we performed in chapter 4, yet we have to apply the methods presented in section 3.2.4 in order to correctly recover a definite post-Newtonian scaling behavior. On the other hand we recall the definition of the multipole moments from equation (3.67), but also that, for the precision we're aiming for, we may neglect the terms in the final far zone Feynman rule which are proportional to conserved quantities, as they will give a vanishing contribution to the final diagram: we'll exemplify this point below here.

■ Worldline- $\bar{\phi}$ vertex

In order to evaluate diagrams (R1) and (R2) in chapter 5, see figure 5.1, we need the Feynman rule for the Worldline- $\bar{\phi}$ in the far zone effective theory. The expression for such a vertex can then be obtained by performing a kind-of matching procedure with the near zone effective theory, which

amounts to evaluating in such theory the following diagrams:

$$\begin{aligned}
 \square \text{---} \bar{\phi}(k) &= \text{Diagram 1} + \text{Diagram 2} + \text{Diagram 3} \\
 &+ \text{Diagram 4} + \text{Diagram 5} + \text{Diagram 6} \\
 &+ \text{Diagram 7} + \text{Diagram 8} + \mathcal{O}\left(L^{\frac{1}{2}} v^{\frac{11}{2}}\right).
 \end{aligned} \tag{A.80}$$

In particular, recalling the discussion about the radiation scaling rules we carried out in section 3.2.4, we find that the first diagram after the equal sign contributes at leading order as $\mathcal{O}\left(L^{\frac{1}{2}} v^{\frac{1}{2}}\right)$, the second as $\mathcal{O}\left(L^{\frac{1}{2}} v^{\frac{5}{2}}\right)$, all the others as $\mathcal{O}\left(L^{\frac{1}{2}} v^{\frac{9}{2}}\right)$. In theory then we'd need all of the above diagrams in order to evaluate the radiation effective action, i.e. diagrams 5.1, up to order $\mathcal{O}\left(L v^{\frac{10}{2}}\right)$.

In practice, once we'll evaluate the first diagram below here in formula (A.82), we'll find that its first terms will be proportional to conserved quantities (in particular the mass m and position of the center of mass \mathbf{x}_{CM}), and the first non-conserved quantity will be the mass quadrupole moment M_{ij} : therefore, for the precision we're aiming for, the first diagrams effectively scales like $\mathcal{O}\left(L^{\frac{1}{2}} v^{\frac{5}{2}}\right)$. In fact, when in chapter 5 we'll construct the diagram expression starting from the Feynman rules (e.g. in the simplest case by taking the square of the same Feynman rule), we'll have that even if in the final results the temporal derivatives are applied to a non conserved quantity, which we'll denote with $g(t)$, then we can always integrate by parts at least once to move the time derivative to the other quantity, which we'll denote $f(t)$:

$$\int dt f(t) \frac{d^\alpha g(t)}{dt^\alpha} \sim - \int dt \frac{df(t)}{dt} \frac{d^{\alpha-1} g(t)}{dt^{\alpha-1}} ; \tag{A.81}$$

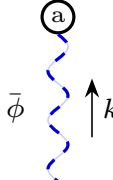
to obtain a vanishing result; it is then clear that if either $f(t)$ or $g(t)$ are conserved quantities, they won't contribute to the diagram we'll compute in chapter 5.

Therefore, once we choose the reference frame of the center of mass, we'll find that the first diagram actually first contributes at order $\mathcal{O}\left(L^{\frac{1}{2}} v^{\frac{5}{2}}\right)$, hence we'll need to consider only the first and the second diagram to obtain the needed Feynman rule at order $\mathcal{O}\left(L^{\frac{1}{2}} v^{\frac{5}{2}}\right)$; we evaluate them in the following, in a similar way to what is done in references [43, 206].

Worldline- $\bar{\phi}$ vertex – First diagram

We now explicitly evaluate the first diagram from expression (A.80): we need the expression for the worldline- $\bar{\phi}$ vertex, which nonetheless in practice is identical to the one for the worldline- ϕ

potential vertex. In fact in equation (A.37) we actually had found the expression for the generic worldline- $\hat{\phi}$ vertex, and there we could have considered the radiation $\bar{\phi}$ field instead of the potential ϕ field after performing the $\hat{\phi} = \phi + \bar{\phi}$ splitting, obtaining in practice the same expression (A.39). Using then that near zone Feynman rule, and considering the $\bar{\phi}$ field as an external particle with momentum k , we find:

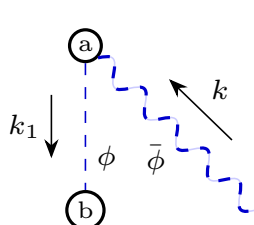


$$\begin{aligned}
\bar{\phi} \quad \uparrow k &= -i \sum_{a=1}^2 \frac{m_a}{\Lambda} \int dt e^{-ikx_a(t)} \left(\frac{2 + (-2 + c_d) v_a^2}{2\sqrt{1 - v_a^2}} \right) \\
&= -i \sum_{a=1}^2 \frac{m_a}{\Lambda} \int dt e^{-ik^0 t} e^{i(\mathbf{k} \cdot \mathbf{x}_a(t))} \left(1 + \frac{(c_d - 1)}{2} v_a^2 + \frac{2c_d - 1}{8} v_a^4 + \mathcal{O}(v^6) \right) \\
&= -i \sum_{a=1}^2 \frac{m_a}{\Lambda} \int dt e^{-ik^0 t} \left(1 + i(\mathbf{k} \cdot \mathbf{x}_a) - \frac{1}{2}(\mathbf{k} \cdot \mathbf{x}_a)^2 + \mathcal{O}(v^3) \right) \\
&\quad \times \left(1 + \frac{(c_d - 1)}{2} v_a^2 + \mathcal{O}(v^4) \right) \\
&= -i \frac{1}{\Lambda} \int dt e^{-ik^0 t} \left(\sum_{a=1}^2 m_a + i \left(\mathbf{k} \cdot \left(\sum_{a=1}^2 m_a \mathbf{x}_a \right) \right) - \frac{1}{2} \sum_{a=1}^2 m_a (\mathbf{k} \cdot \mathbf{x}_a(t))^2 \right. \\
&\quad \left. + \frac{(c_d - 1)}{2} \sum_{a=1}^2 m_a v_a^2 + \mathcal{O}(v^3) \right) \\
&= -i \frac{1}{\Lambda} \int dt e^{-ik^0 t} \left(m + i m k_i x_{CM}^i - \frac{1}{2} k^i k^j M_{ij} + \frac{(c_d - 1)}{2} \sum_{a=1}^2 m_a v_a^2 + \mathcal{O}(v^3) \right)
\end{aligned} \tag{A.82}$$

where we recall the definitions (3.67) for the multipole moments. As explained before, according to the choices we made in section 3.2.4, we can set $x_{CM}^i = 0$; on top of this also the first term can be neglected, as it is proportional to the total mass m , which at this order is a conserved quantity.

Worldline- $\phi\bar{\phi}$ vertex – Second diagram

To evaluate explicitly the second diagram from expression (A.80) we need the worldline- $\phi\bar{\phi}$ vertex; it can be derived as previously explained, by performing the splitting $\hat{\phi} = \phi + \bar{\phi}$ in the corresponding worldline- $\hat{\phi}^2$ expression from the action, and selecting the $\phi\bar{\phi}$ by performing the relevant functional derivatives. Then we find:



$$\begin{aligned}
&= \int_{k_1} \left(-i \sum_{a=1}^2 \frac{m_a}{\Lambda^2} \int dt_1 e^{-i(k-k_1)x_a(t_1)} \left[\frac{1}{4(1 - v_a^2)^{3/2}} \right. \right. \\
&\quad \left. \left. \times (4 + v_a^2 (-8 - 2(-2 + c_d) c_d + (-2 + c_d)^2 v_a^2)) \right] \right) \\
&\quad \times \left(-\frac{i}{2c_d} \frac{1}{|\mathbf{k}_1|^2} \right) \left(-i \sum_{b=1}^2 \frac{m_b}{\Lambda} \int dt_2 e^{-ik_1 x_b(t_2)} \left(\frac{2 + (-2 + c_d) v_b^2}{2\sqrt{1 - v_b^2}} \right) \right).
\end{aligned} \tag{A.83}$$

At leading order we can evaluate it as follows:

$$\begin{aligned}
&= i \frac{1}{2 c_d} \sum_{a,b=1}^2 \frac{m_a m_b}{\Lambda^3} \int dt_1 dt_2 e^{-ik^0 t_1} e^{i\mathbf{k} \cdot \mathbf{x}_a(t_1)} \underbrace{\int \frac{d^d k_1^0}{(2\pi)} e^{-ik_1^0(t_2-t_1)}}_{=\delta(t_1-t_2)} \\
&\quad \times \int \frac{d^d \mathbf{k}_1}{(2\pi)^d} \frac{e^{i\mathbf{k}_1 \cdot (\mathbf{x}_b(t_2) - \mathbf{x}_a(t_1))}}{|\mathbf{k}_1|^2} (1 + \mathcal{O}(v^2)) \\
&= i \frac{1}{2 c_d} \sum_{a,b=1}^2 \frac{m_a m_b}{\Lambda^3} \int dt e^{-ik^0 t} e^{i\mathbf{k} \cdot \mathbf{x}_a(t)} \int \frac{d^d \mathbf{k}_1}{(2\pi)^d} \frac{e^{i\mathbf{k}_1 \cdot (\mathbf{x}_b(t) - \mathbf{x}_a(t))}}{|\mathbf{k}_1|^2} (1 + \mathcal{O}(v^2)) \\
&= i \frac{1}{2 c_d} \frac{m_1}{\Lambda^3} \int dt e^{-ik^0 t} e^{i\mathbf{k} \cdot \mathbf{x}_1(t)} \left(m_1 \underbrace{\int \frac{d^d \mathbf{k}_1}{(2\pi)^d} \frac{1}{|\mathbf{k}_1|^2}}_{=0} + m_2 \underbrace{\int \frac{d^d \mathbf{k}_1}{(2\pi)^d} \frac{e^{i\mathbf{k}_1 \cdot (\mathbf{x}_2 - \mathbf{x}_1)}}{|\mathbf{k}_1|^2}}_{=I_F(d,1)[-r]} \right) (1 + \mathcal{O}(v^2)) + (1 \leftrightarrow 2) \\
&= i \frac{1}{2 c_d} \frac{m_1 m_2}{\Lambda^3} \int dt e^{-ik^0 t} e^{i\mathbf{k} \cdot \mathbf{x}_1(t)} \left(\frac{\pi^{-\frac{d}{2}}}{4} \Gamma\left(\frac{d}{2} - 1\right) |\mathbf{x}_1 - \mathbf{x}_2|^{2-d} \right) (1 + \mathcal{O}(v^2)) + (1 \leftrightarrow 2) \\
&= i \frac{\pi^{-\frac{d}{2}}}{8 c_d} \Gamma\left(\frac{d}{2} - 1\right) \frac{m_1 m_2}{\Lambda^3} \int dt e^{-ik^0 t} \left(e^{i\mathbf{k} \cdot \mathbf{x}_1(t)} + e^{i\mathbf{k} \cdot \mathbf{x}_2(t)} \right) |\mathbf{x}_1 - \mathbf{x}_2|^{2-d} (1 + \mathcal{O}(v^2)) .
\end{aligned} \tag{A.84}$$

Here the first integral in the third line vanishes because it's scaleless. Finally we can perform the multipole expansion by Taylor expanding both Fourier exponentials as explained in section 3.2.4; nonetheless we only need the leading order result which is equal to 1, hence:

$$= i \frac{\pi^{-\frac{d}{2}}}{8 c_d} \Gamma\left(\frac{d}{2} - 1\right) \frac{m_1 m_2}{\Lambda^3} \int dt e^{-ik^0 t} (1 + 1) |\mathbf{x}_1 - \mathbf{x}_2|^{2-d} (1 + \mathcal{O}(v^2)) . \tag{A.85}$$

Feynman rule for the worldline- $\bar{\phi}$ vertex

We can now obtain the expression corresponding to the diagram (A.80) for the worldline- $\bar{\phi}$ Feynman rule, at order $\mathcal{O}(L^{\frac{1}{2}} v^{\frac{5}{2}})$:

$$\text{Diagram (A.86)} = \text{Diagram 1} + \text{Diagram 2} + \mathcal{O}\left(L^{\frac{1}{2}} v^{\frac{5}{2}}\right) . \tag{A.86}$$

By summing the (A.82) and (A.85) results we obtain, enforcing the condition of $\mathbf{x}_{CM} = 0$ due to our frame choice:

$$\begin{aligned}
\bar{\phi} \uparrow k &= \left(-i \frac{1}{\Lambda} \int dt e^{-ik^0 t} \left(m + i m k_i x_{CM}^i - \frac{1}{2} k^i k^j M_{ij} + \frac{(c_d - 1)}{2} \sum_{a=1}^2 m_a v_a^2 + \mathcal{O}(v^3) \right) \right) \\
&\quad + \left(i \frac{\pi^{-\frac{d}{2}}}{4 c_d} \Gamma \left(\frac{d}{2} - 1 \right) \frac{m_1 m_2}{\Lambda^3} \int dt e^{-ik^0 t} |\mathbf{x}_1 - \mathbf{x}_2|^{2-d} (1 + \mathcal{O}(v^2)) \right) \\
&= i \frac{1}{\Lambda} \int dt e^{-ik^0 t} \left(-m + \frac{1}{2} k^i k^j M_{ij} - \frac{(c_d - 1)}{2} \sum_{a=1}^2 m_a v_a^2 \right. \\
&\quad \left. + \frac{\pi^{-\frac{d}{2}}}{4 c_d} \Gamma \left(\frac{d}{2} - 1 \right) \frac{m_1 m_2}{\Lambda^2} |\mathbf{r}|^{2-d} \right) + \mathcal{O}(G^{\frac{1}{2}} L v) .
\end{aligned} \tag{A.87}$$

Let us point out that $\mathcal{O}(G^{\frac{1}{2}} L v)$ scaling in the above (A.87) expression is different with respect to the $\mathcal{O}(L^{\frac{1}{2}} v^{\frac{7}{2}})$ we reported in the corresponding diagrammatic expression (A.86): this is because the $\mathcal{O}(G^{\frac{1}{2}} L v)$ scaling in the former is the real scaling of next order term in the expression, evaluated using the scaling rules of table 3.1; whereas the $\mathcal{O}(L^{\frac{1}{2}} v^{\frac{7}{2}})$ scaling in expression (A.86) includes the $G^{-\frac{1}{2}} L^{-\frac{1}{2}} v^{\frac{5}{2}}$ factor which we add for each radiation legs, as explained in section 3.2.4, see formula (3.70).

As explained in section 3.2.4, we can now employ the equation of motion in order to recast the last line of expression (A.87) into the usual multipole expansion. For the precision which we're aiming for it suffices to employ the leading order (so Newtonian) equation of motions, which we evaluated in equation (3.99); furthermore we can directly work in $d = 3$ dimension. These equations of motion explicitly read $G m_2 \frac{r^i}{|\mathbf{r}|^3} = -a_1^i + \mathcal{O}(G^{-\frac{1}{2}} L^{-\frac{1}{2}} v^{\frac{11}{2}})$ and $G m_1 \frac{r^i}{|\mathbf{r}|^3} = a_2^i + \mathcal{O}(G^{-\frac{1}{2}} L^{-\frac{1}{2}} v^{\frac{11}{2}})$, hence it holds:

$$\begin{aligned}
m_1 v_1^2 &= m_1 \delta_{ij} v_1^i v_1^j = \frac{\delta_{ij}}{2} m_1 \left(\frac{d}{dt} (x_1^i v_1^j + v_1^i x_1^j) - x_1^i a_1^j - a_1^i x_1^j \right) \\
&= \frac{\delta_{ij}}{2} m_1 \left(\frac{d^2}{dt^2} (x_1^i x_1^j) + x_1^i \left(G m_2 \frac{r^j}{|\mathbf{r}|^3} \right) + \left(G m_2 \frac{r^i}{|\mathbf{r}|^3} \right) x_1^j \right)
\end{aligned} \tag{A.88}$$

and therefore, adding the $(1 \leftrightarrow 2)$ term:

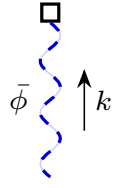
$$\begin{aligned}
\sum_{a=1}^2 m_a v_a^2 &= \delta_{ij} (m_1 v_1^i v_1^j + m_2 v_2^i v_2^j) = \frac{\delta_{ij}}{2} \left(\frac{d^2}{dt^2} \left(\sum_{a=1}^2 m_a x_a^i x_a^j \right) + 2 G m_1 m_2 \frac{r^i r^j}{|\mathbf{r}|^3} \right) \\
&= \frac{1}{2} \delta_{ij} \frac{d^2}{dt^2} (M^{ij}) + \frac{G m_1 m_2}{r} .
\end{aligned} \tag{A.89}$$

This result let us cast expression (A.87), expanded at leading order around $d = 3$, into:

$$\begin{aligned}
&= i \frac{1}{\Lambda} \int dt e^{-ik^0 t} \left(-m + \frac{1}{2} k^i k^j M_{ij} - \frac{3}{2} \sum_{a=1}^2 m_a v_a^2 + 2 \frac{Gm_1 m_2}{r} \right) + \mathcal{O}(G^{\frac{1}{2}} L v) + \mathcal{O}(d-3) \\
&= i \frac{1}{\Lambda} \int dt e^{-ik^0 t} \left(-m + \frac{1}{2} k^i k^j M_{ij} - \left(\frac{1}{2} \sum_{a=1}^2 m_a v_a^2 - \frac{Gm_1 m_2}{r} \right) \right. \\
&\quad \left. - \left(\frac{1}{2} \delta_{ij} \frac{d^2}{dt^2} (M^{ij}) + \frac{Gm_1 m_2}{r} \right) + \frac{Gm_1 m_2}{r} \right) + \mathcal{O}(G^{\frac{1}{2}} L v) + \mathcal{O}(d-3) \\
&= i \frac{1}{\Lambda} \int dt e^{-ik^0 t} \left(-m + \frac{1}{2} k^i k^j M_{ij} - E_N + \frac{1}{2} (k^0)^2 M \right) + \mathcal{O}(G^{\frac{1}{2}} L v) + \mathcal{O}(d-3)
\end{aligned} \tag{A.90}$$

where we integrated by parts the last term, recalling from definitions (3.67) both the Newtonian energy E_N of the system, which is a conserved quantity at this order, and the trace of the mass quadrupole moment M .

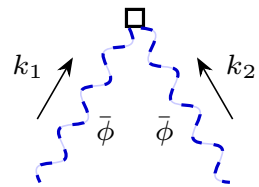
To summarize, the expression for the worldline- $\bar{\phi}$ Feynman rule, corresponding to the diagram (A.80), reads:



$$\bar{\phi} \uparrow k = i \frac{1}{\Lambda} \int dt e^{-ik^0 t} \left(-m + \frac{1}{2} k^i k^j M_{ij} - E_N + \frac{1}{2} (k^0)^2 M \right) + \mathcal{O}(G^{\frac{1}{2}} L v) + \mathcal{O}(d-3) . \tag{A.91}$$

■ Worldline- $\bar{\phi}^2$ vertex

To evaluate diagrams (R2) in chapter 5, see figure 5.1, we'll need the worldline- $\bar{\phi}^2$ vertex, given by:



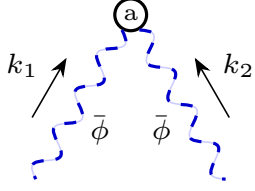
$$= \text{Diagram with a circle 'a' at the top} + \mathcal{O}(v^{\frac{10}{2}}) . \tag{A.92}$$

In fact we'll need to evaluate only its leading order expression, which amounts to evaluating the diagram (A.93).

Worldline- $\bar{\phi}^2$ vertex – First diagram

To evaluate such diagram we need the worldline- $\bar{\phi}^2$ Feynman rule in the near zone theory: it has the same expression as the one with two potential fields instead of two radiation fields, and is given

by (A.49d). Then we find:

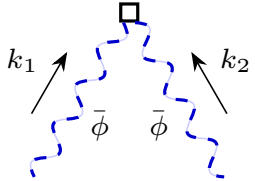


$$\begin{aligned}
 &= -i \sum_{a=1}^2 \frac{m_a}{\Lambda^2} \int dt e^{-i(k_1+k_2)x_a(t)} \left[\frac{1}{4(1-v_a^2)^{3/2}} \cdot \right. \\
 &\quad \left. \cdot (4 + v_a^2(-8 - 2(-2 + c_d)c_d + (-2 + c_d)^2 v_a^2)) \right] \\
 &= -i \sum_{a=1}^2 \frac{m_a}{\Lambda^2} \int dt e^{-i(k_1^0+k_2^0)t} (1 + i(\mathbf{k}_1 + \mathbf{k}_2) \cdot \mathbf{x}_a(t) + \mathcal{O}(v^2)) (1 + \mathcal{O}(v^2)) \\
 &= -i \frac{1}{\Lambda^2} \int dt e^{-i(k_1^0+k_2^0)t} (m + i(\mathbf{k}_1 + \mathbf{k}_2) \cdot (m \mathbf{x}_{CM})) + \mathcal{O}(GLv^0) \\
 &= -i \frac{1}{\Lambda^2} \int dt e^{-i(k_1^0+k_2^0)t} m + \mathcal{O}(GLv^0) ;
 \end{aligned} \tag{A.93}$$

where in the last line we used again the fact that, according to our choice of frame of reference, it holds $\mathbf{x}_{CM} = 0$.

Feynman rule for the worldline- $\bar{\phi}^2$ vertex

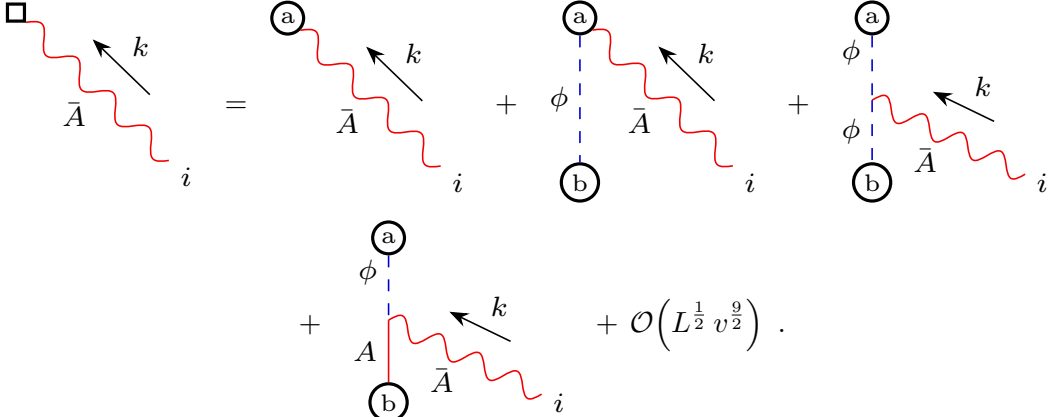
Summarizing, the expression for the worldline- $\bar{\phi}^2$ vertex in the far zone is given by:



$$= -i \frac{1}{\Lambda^2} \int dt e^{-i(k_1^0+k_2^0)t} m + \mathcal{O}(GLv^0) . \tag{A.94}$$

■ Worldline- \bar{A} vertex

To evaluate diagram (R3) in chapter 5, see figure 5.1, we'll need the Feynman rule for the worldline- \bar{A} vertex in the far zone; it can be obtained by evaluating:

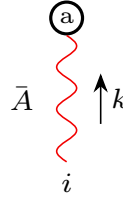


$$\tag{A.95}$$

According to the discussion about the radiation scaling rules which we carried out in section 3.2.4, the first diagram contributes at leading order at $\mathcal{O}(L^{\frac{1}{2}} v^{\frac{3}{2}})$, while all the others at order $\mathcal{O}(L^{\frac{1}{2}} v^{\frac{7}{2}})$. Nonetheless, similarly to what we found previously, once we put ourselves in the reference frame of the center of mass, we'll find that the first diagram gives a non vanishing contribution only since order $\mathcal{O}(L^{\frac{1}{2}} v^{\frac{5}{2}})$, hence it will be the only diagram we'll have to consider.

Worldline- \bar{A} vertex – First diagram

This is the only diagram we'll have to evaluate; evaluating the expression for the Feynman rule in the near zone EFT we find that it is analogous to expression (A.49b) for the potential modes. Therefore:



$$\begin{aligned}
 \bar{A} &= -i \sum_{a=1}^2 \frac{m_a}{\Lambda} \int dt e^{-ikx_a(t)} \left(-\frac{1}{\sqrt{1-v_a^2}} \right) v_a^i \\
 &= -i \sum_{a=1}^2 \frac{m_a}{\Lambda} \int dt e^{-ik^0 t} \left(1 + i(\mathbf{k} \cdot \mathbf{x}_a) - \frac{1}{2}(\mathbf{k} \cdot \mathbf{x}_a)^2 + \mathcal{O}(v^3) \right) (v_a^i + \mathcal{O}(v^3)) \\
 &= -i \frac{1}{\Lambda} \int dt e^{-ik^0 t} \left(\sum_{a=1}^2 m_a v_a^i + i k_j \sum_{a=1}^2 m_a x_a^j v_a^i + \mathcal{O}(v^3) \right).
 \end{aligned} \tag{A.96}$$

To proceed further we recall the identity involving the three dimensional Levi-Civita tensor $\epsilon^{ijk}\epsilon_{ilm} = \delta^j_l \delta^k_m - \delta^j_m \delta^k_l$, and that $\epsilon_{kij} = \epsilon_{ijk}$, and proceeding similarly to [206], we obtain:

$$\epsilon^{lmk} L_k = \sum_{a=1}^2 m_a \epsilon^{lmk} \epsilon_{ijk} x_a^i v_a^j = \sum_{a=1}^2 m_a (\delta^l_i \delta^m_j - \delta^l_j \delta^m_i) x_a^i v_a^j = \sum_{a=1}^2 m_a x_a^l v_a^m - \sum_{a=1}^2 m_a x_a^m v_a^l \tag{A.97}$$

and therefore

$$\int dt e^{-ik^0 t} x_a^j v_a^i = \int dt \left[\underbrace{\frac{d}{dt} (e^{-ik^0 t} x_a^j x_a^i)}_{\sim 0} + ik^0 e^{-ik^0 t} x_a^j x_a^i - e^{-ik^0 t} v_a^j x_a^i \right] \tag{A.98}$$

since the total derivative produces a surface term. Then, thanks to the time integral present in equation (A.96), we can recast the last term of that last line as:

$$\sum_{a=1}^2 m_a x_a^j v_a^i = \frac{1}{2} \sum_{a=1}^2 m_a x_a^j v_a^i + \frac{1}{2} \sum_{a=1}^2 m_a (ik^0 x_a^j x_a^i - v_a^j x_a^i) = -\frac{1}{2} \epsilon^{ijk} L_k + \frac{i}{2} k^0 M^{ij}; \tag{A.99}$$

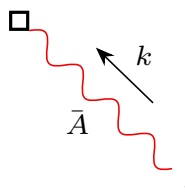
and therefore, recalling the quantities defined in equations (3.67), the diagram (A.96) is equivalent to:

$$\begin{aligned}
 &= -i \frac{1}{\Lambda} \int dt e^{-ik^0 t} \left(p_{CM}^i - \frac{i}{2} \epsilon^{ijk} k_j L_k - \frac{1}{2} k^0 M^{ij} k_j \right) + \mathcal{O}(G^{\frac{1}{2}} L v) \\
 &= -i \frac{1}{\Lambda} \int dt e^{-ik^0 t} \left(-\frac{i}{2} \epsilon^{ijk} k_j L_k - \frac{1}{2} k^0 M^{ij} k_j \right) + \mathcal{O}(G^{\frac{1}{2}} L v),
 \end{aligned} \tag{A.100}$$

where we explicitly made use of the fact that with our choice of coordinate frame $p_{CM}^i = 0$ since $\dot{\mathbf{x}}_{CM} = 0$.

Feynman rule for the worldline- \bar{A} vertex

To summarize the expression for the worldline- \bar{A} vertex in the far zone is given by:



$$\bar{A} = \frac{i}{\Lambda} \int dt e^{-ik^0 t} \left(\frac{i}{2} \epsilon^{ijk} k_j L_k + \frac{1}{2} k^0 M^{ij} k_j \right) + \mathcal{O}(G^{\frac{1}{2}} L v). \tag{A.101}$$

■ Worldline- $\bar{\sigma}$ vertex

In order to evaluate diagrams (R4) in section 5.1, see figure 5.1, and also the gravitational field far away from the source in section 5.2, we'll need the worldline- $\bar{\sigma}$ vertex evaluated in the far zone, which is given by:

$$\begin{array}{c} \square \\ \downarrow \\ \bar{\sigma} \\ \downarrow \\ ij \end{array} \xrightarrow{k} = \begin{array}{c} \textcircled{a} \\ \downarrow \\ \bar{\sigma} \\ \downarrow \\ ij \end{array} \xrightarrow{k} + \begin{array}{c} \textcircled{a} \\ \downarrow \phi \\ \downarrow \phi \\ \bar{\sigma} \\ \downarrow \\ ij \\ \textcircled{b} \end{array} \xrightarrow{k} + \mathcal{O}\left(L^{\frac{1}{2}} v^{\frac{7}{2}}\right). \quad (\text{A.102})$$

In this case we find that both diagrams contribute at leading order at $\mathcal{O}\left(L^{\frac{1}{2}} v^{\frac{5}{2}}\right)$, and therefore will be the only ones we'll have to consider.

Worldline- $\bar{\sigma}$ vertex – First diagram

We want to evaluate the first near zone diagram comprising expression (A.102). Then we need the worldline- $\bar{\sigma}$ vertex in the near zone EFT, nonetheless its expression is identical to the potential vertex (A.49c). Therefore:

$$\begin{array}{c} \textcircled{a} \\ \downarrow \\ \bar{\sigma} \\ \downarrow \\ ij \end{array} \xrightarrow{k} = -i \sum_{a=1}^2 \frac{m_a}{\Lambda} \int dt e^{-ikx_a(t)} \left(-\frac{1}{2\sqrt{1-v_a^2}} \right) v_a^i v_a^j \\
 = -i \sum_{a=1}^2 \frac{m_a}{\Lambda} \int dt e^{-ik^0 t} (1 + \mathcal{O}(v)) \left(-\frac{1}{2} v_a^i v_a^j + \mathcal{O}(v^4) \right) \\
 = i \frac{1}{2\Lambda} \int dt e^{-ik^0 t} \sum_{a=1}^2 m_a v_a^i v_a^j + \mathcal{O}\left(G^{\frac{1}{2}} L v\right). \quad (\text{A.103})$$

Worldline- $\bar{\sigma}$ vertex – Second diagram

To evaluate the second diagram instead we need the $\phi^2 \bar{\sigma}$ bulk vertex in the near zone; luckily we have already evaluated its expression before, and the result is given in equation (A.79). Let us recall that, as pointed out in section 3.2.4, this bulk vertex encodes the non-linear interactions due to the non-Abelian structure of general relativity.

$$\begin{array}{c} \textcircled{a} \\ \downarrow \phi \\ \downarrow \phi \\ \bar{\sigma} \\ \downarrow \\ ij \\ \textcircled{b} \end{array} \xrightarrow{k} \begin{array}{c} k_1 \downarrow \\ k_2 \downarrow \end{array} = \frac{2}{2!2!} \int_{k_1, k_2} \left(-i \sum_{a=1}^2 \frac{m_a}{\Lambda} \int dt_1 e^{ik_1 x_a(t_1)} \left(\frac{2 + (-2 + c_d) v_a^2}{2\sqrt{1-v_a^2}} \right) \right) \\
 \times \left(-i \sum_{b=1}^2 \frac{m_b}{\Lambda} \int dt_2 e^{-ik_2 x_b(t_2)} \left(\frac{2 + (-2 + c_d) v_b^2}{2\sqrt{1-v_b^2}} \right) \right) \\
 \times \left(i (2\pi)^{d+1} \delta^{(d+1)}(k + k_1 - k_2) \frac{c_d}{\Lambda} \left(-\delta^{ij}(\mathbf{k}_1 \cdot \mathbf{k}_2) + \left(k_1^i k_2^j + k_1^j k_2^i \right) \right) \right) \\
 \times \left(-\frac{i}{2c_d} \frac{1}{|\mathbf{k}_1|^2} \right) \left(-\frac{i}{2c_d} \frac{1}{|\mathbf{k}_2|^2} \right). \quad (\text{A.104})$$

Since we only need the leading order of this diagram, we can simplify the above expression to:

$$\begin{aligned}
&= \frac{i}{8c_d} \frac{1}{\Lambda^3} \sum_{a,b=1}^2 m_a m_b \int dt_1 \int dt_2 e^{-ikx_b(t_2)} \underbrace{\int \frac{d\mathbf{k}_1^0}{2\pi} e^{-ik_1^0(t_2-t_1)}}_{=\delta(t_1-t_2)} \\
&\quad \times \int \frac{d^d \mathbf{k}_1}{(2\pi)^d} \left(-\delta^{ij}(\mathbf{k}_1 \cdot \mathbf{k} + |\mathbf{k}_1|^2) + 2k_1^i k_1^j + k_1^i k^j + k^i k_1^j \right) \frac{e^{i\mathbf{k}_1 \cdot (\mathbf{x}_b(t_2) - \mathbf{x}_a(t_1))}}{|\mathbf{k}_1|^2 |\mathbf{k} + \mathbf{k}_1|^2} (1 + \mathcal{O}(v^2)) \\
&= \frac{i}{8c_d} \frac{1}{\Lambda^3} \sum_{a,b=1}^2 m_a m_b \int dt e^{-ik^0 t} \\
&\quad \times \int \frac{d^d \mathbf{k}_1}{(2\pi)^d} \left(-\delta^{ij}(\mathbf{k}_1 \cdot \mathbf{k} + |\mathbf{k}_1|^2) + 2k_1^i k_1^j + k_1^i k^j + k^i k_1^j \right) \frac{e^{i\mathbf{k}_1 \cdot (\mathbf{x}_b(t) - \mathbf{x}_a(t))}}{|\mathbf{k}_1|^2 |\mathbf{k} + \mathbf{k}_1|^2} (1 + \mathcal{O}(v)) \\
&= \frac{i}{8c_d} \frac{m_1}{\Lambda^3} \int dt e^{-ik^0 t} \int \frac{d^d \mathbf{k}_1}{(2\pi)^d} \left(m_1 \left(-\delta^{ij}(\mathbf{k}_1 \cdot \mathbf{k} + |\mathbf{k}_1|^2) + 2k_1^i k_1^j + k_1^i k^j + k^i k_1^j \right) \frac{1}{|\mathbf{k}_1|^2 |\mathbf{k} + \mathbf{k}_1|^2} \right. \\
&\quad \left. + m_2 \left(-\delta^{ij}(\mathbf{k}_1 \cdot \mathbf{k} + |\mathbf{k}_1|^2) + 2k_1^i k_1^j + k_1^i k^j + k^i k_1^j \right) \frac{e^{-i\mathbf{p} \cdot \mathbf{r}(t)}}{|\mathbf{k}_1|^2 |\mathbf{k} + \mathbf{k}_1|^2} \right) (1 + \mathcal{O}(v)) + (1 \leftrightarrow 2) .
\end{aligned} \tag{A.105}$$

When then recall the expansion (3.66) of the potential propagator which receives correction from the external radiation momentum \mathbf{k} , i.e. $\frac{1}{|\mathbf{k} + \mathbf{k}_1|^2}$, and so at leading order:

$$\begin{aligned}
&= \frac{i}{8c_d} \frac{m_1}{\Lambda^3} \int dt e^{-ik^0 t} \int \frac{d^d \mathbf{k}_1}{(2\pi)^d} \left(m_1 \left(-\delta^{ij}(\mathbf{k}_1 \cdot \mathbf{k} + |\mathbf{k}_1|^2) + 2k_1^i k_1^j + k_1^i k^j + k^i k_1^j \right) \frac{1}{|\mathbf{k}_1|^4} \right. \\
&\quad \left. + m_2 \left(-\delta^{ij}(\mathbf{k}_1 \cdot \mathbf{k} + |\mathbf{k}_1|^2) + 2k_1^i k_1^j + k_1^i k^j + k^i k_1^j \right) \frac{e^{-i\mathbf{k}_1 \cdot \mathbf{r}(t)}}{|\mathbf{k}_1|^4} \right) (1 + \mathcal{O}(v)) + (1 \leftrightarrow 2) \\
&= \frac{i}{8c_d} \frac{1}{\Lambda^3} m_1 m_2 \int dt e^{-ik^0 t} \left(-\delta^{ij} \left(k_l \int \frac{d^d \mathbf{p}}{(2\pi)^d} p^l \frac{e^{-i\mathbf{p} \cdot \mathbf{r}(t)}}{|\mathbf{p}|^4} + \int \frac{d^d \mathbf{p}}{(2\pi)^d} \frac{e^{-i\mathbf{p} \cdot \mathbf{r}(t)}}{|\mathbf{p}|^2} \right) \right. \\
&\quad \left. + 2 \int \frac{d^d \mathbf{p}}{(2\pi)^d} p^i p^j \frac{e^{-i\mathbf{p} \cdot \mathbf{r}(t)}}{|\mathbf{p}|^4} + k^j \int \frac{d^d \mathbf{p}}{(2\pi)^d} p^i \frac{e^{-i\mathbf{p} \cdot \mathbf{r}(t)}}{|\mathbf{p}|^4} + k^i \int \frac{d^d \mathbf{p}}{(2\pi)^d} p^j \frac{e^{-i\mathbf{p} \cdot \mathbf{r}(t)}}{|\mathbf{p}|^4} \right) (1 + \mathcal{O}(v)) + (1 \leftrightarrow 2)
\end{aligned} \tag{A.106}$$

where we dropped scaleless integrals and we recognized the integrals given in formulae (C.31), (C.32) and (C.33). Nonetheless, since $\frac{\mathbf{k}}{p} \propto v$, the leading order contribution is given only by:

$$\begin{aligned}
&= \frac{i}{8c_d} \frac{m_1 m_2}{\Lambda^3} \int dt e^{-ik^0 t} \left(\underbrace{-\delta^{ij} \int \frac{d^d \mathbf{p}}{(2\pi)^d} \frac{e^{-i\mathbf{p} \cdot \mathbf{r}(t)}}{|\mathbf{p}|^2}}_{=I_F(d,1)[-r]} + 2 \underbrace{\int \frac{d^d \mathbf{p}}{(2\pi)^d} p^i p^j \frac{e^{-i\mathbf{p} \cdot \mathbf{r}(t)}}{|\mathbf{p}|^4}}_{=I_F(d,2)^{ij}[-r]} \right) (1 + \mathcal{O}(v)) + (1 \leftrightarrow 2) \\
&= \frac{i}{8c_d} \frac{m_1 m_2}{\Lambda^3} \left(2^{-2} \pi^{-\frac{d}{2}} \Gamma\left(\frac{d}{2} - 1\right) \right) \int dt e^{-ik^0 t} |\mathbf{r}|^{2-d} \left((2-d) \frac{r^i r^j}{|\mathbf{r}|^2} \right) (1 + \mathcal{O}(v)) + (1 \leftrightarrow 2) \\
&= -i \frac{\pi^{-\frac{d}{2}} \Gamma\left(\frac{d}{2}\right)}{16c_d} \frac{m_1 m_2}{\Lambda^3} \int dt e^{-ik^0 t} \frac{r^i r^j}{|\mathbf{r}|^d} (1 + \mathcal{O}(v)) + (1 \leftrightarrow 2) \\
&= -i \frac{\pi^{-\frac{d}{2}} \Gamma\left(\frac{d}{2}\right)}{8c_d} \frac{m_1 m_2}{\Lambda^3} \int dt e^{-ik^0 t} \frac{r^i r^j}{|\mathbf{r}|^d} + \mathcal{O}\left(G^{\frac{1}{2}} L v\right) ;
\end{aligned} \tag{A.107}$$

which is the final result corresponding to diagram (A.104).

Feynman rule for the worldline- \bar{A} vertex

To summarize, the expression for the worldline- $\bar{\sigma}$ vertex in the far zone, represented in (A.102), is given by the sum of results (A.103) and (A.107).

$$= i \frac{1}{2\Lambda} \int dt e^{-ik^0 t} \sum_{a=1}^2 m_a v_a^i v_a^j - i \frac{\pi^{-\frac{d}{2}} \Gamma(\frac{d}{2})}{8 c_d} \frac{m_1 m_2}{\Lambda^3} \int dt e^{-ik^0 t} \frac{r^i r^j}{|\mathbf{r}|^d} + \mathcal{O}(G^{\frac{1}{2}} L v). \quad (\text{A.108})$$

To further simplify the above expression, and to recognize the relevant multipole moments of the source, we can proceed as explained in section 3.2.4 and as done previously: we first expand around $d = 3$, obtaining

$$= i \frac{1}{2\Lambda} \int dt e^{-ik^0 t} \left(\sum_{a=1}^2 m_a v_a^i v_a^j - G m_1 m_2 \frac{r^i r^j}{r^3} \right) + \mathcal{O}(G^{\frac{1}{2}} L v) + \mathcal{O}(d-3). \quad (\text{A.109})$$

We then use the leading order (Newtonian) equations of motion (3.99), so $G m_2 \frac{r^i}{r^3} = -a_1^i + \mathcal{O}(G^{-\frac{1}{2}} L^{-\frac{1}{2}} v^{\frac{11}{2}})$ and $G m_1 \frac{r^i}{r^3} = a_2^i + \mathcal{O}(G^{-\frac{1}{2}} L^{-\frac{1}{2}} v^{\frac{11}{2}})$, to manipulate the second term in the above expression:

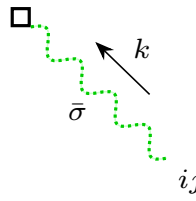
$$\begin{aligned} G m_1 m_2 \frac{r^i r^j}{r^3} &= \left(m_1 x_1^j \left(G m_2 \frac{r^i}{r^3} \right) - m_2 x_2^j \left(G m_1 \frac{r^i}{r^3} \right) \right) \\ &= - \left(m_1 x_1^j a_1^i + m_2 x_2^j a_2^i \right) + \mathcal{O}(G^{-\frac{1}{2}} L^{\frac{1}{2}} v^{\frac{9}{2}}) \\ &= - \sum_{a=1}^2 m_a \ddot{x}_a^i x_a^j + \mathcal{O}(G^{-\frac{1}{2}} L^{\frac{1}{2}} v^{\frac{9}{2}}). \end{aligned} \quad (\text{A.110})$$

Upon symmetrization of this identity with respect to i and j , and recalling the quantities defined in equations (3.67), we can recast (A.109) as:

$$\begin{aligned} &= i \frac{1}{4\Lambda} \int dt e^{-ik^0 t} \sum_{a=1}^2 m_a \underbrace{(2\dot{x}_a^i \dot{x}_a^j + \ddot{x}_a^i x_a^j + x_a^i \ddot{x}_a^j)}_{=\frac{d(\dot{x}_a^i x_a^j + x_a^i \dot{x}_a^j)}{dt}} + \mathcal{O}(G^{\frac{1}{2}} L v) + \mathcal{O}(d-3) \\ &= i \frac{1}{4\Lambda} \int dt e^{-ik^0 t} (i k^0) \sum_{a=1}^2 m_a \underbrace{(\dot{x}_a^i x_a^j + x_a^i \dot{x}_a^j)}_{=\frac{d(x_a^i x_a^j)}{dt}} + \mathcal{O}(G^{\frac{1}{2}} L v) + \mathcal{O}(d-3) \\ &= i \frac{1}{4\Lambda} \int dt e^{-ik^0 t} (i k^0)^2 \underbrace{\sum_{a=1}^2 m_a x_a^i x_a^j}_{=M^{ij}(t)} + \mathcal{O}(G^{\frac{1}{2}} L v) + \mathcal{O}(d-3) \\ &= i \frac{1}{4\Lambda} \int dt e^{-ik^0 t} \frac{d^2 M^{ij}}{dt^2}(t) + \mathcal{O}(G^{\frac{1}{2}} L v) + \mathcal{O}(d-3) \end{aligned} \quad (\text{A.111})$$

where we integrated by parts and neglected boundary terms, while considering the mass m_a of each compact object as time-independent, which is the case for the precision we're aiming for.

The final expression for the worldline- $\bar{\sigma}$ vertex in the far zone is then given by:



$$= i \frac{1}{4\Lambda} \int dt e^{-ik^0 t} \frac{d^2 M^{ij}}{dt^2}(t) + \mathcal{O}(G^{\frac{1}{2}} L v) + \mathcal{O}(d-3). \quad (\text{A.112})$$

COMMON MATHEMATICAL
FUNCTIONS**B.1 | Gamma function $\Gamma(z)$**

The *gamma function* can be defined, for a real and positive z argument, as:

$$\Gamma(z) \equiv \int_0^{+\infty} dt t^{z-1} e^{-t} \quad (\text{B.1})$$

which, defining $x = \sqrt{t}$, can be recast as:

$$\Gamma(z) = 2 \int_0^{+\infty} dx x^{2z-1} e^{-x^2} . \quad (\text{B.2})$$

The gamma function can be seen as a generalization of the factorial to real (and also complex) numbers, in fact integrating by parts it holds:

$$\Gamma(z) = [-t^{z-1} e^{-t}]_0^{+\infty} + (z-1) \int_0^{+\infty} dt t^{z-2} e^{-t} = (z-1)\Gamma(z-1) , \quad (\text{B.3})$$

therefore for integer n values it holds:

$$\Gamma(n) = (n-1)! . \quad (\text{B.4})$$

The value of the gamma function for integer z arguments can be obtained by employing repeatedly property (B.3) starting from $\Gamma(1)$, which can be evaluated recalling definition (B.1):

$$\Gamma(1) = \int_0^{+\infty} dt e^{-t} = [-e^{-t}]_0^{+\infty} = 1 ; \quad (\text{B.5})$$

while the value of $\Gamma(z)$ for half-integer z arguments can be evaluated analogously starting from the value of $\Gamma(\frac{1}{2})$, which can be computed using the alternative definition (B.2):

$$\Gamma\left(\frac{1}{2}\right) = 2 \int_0^{+\infty} dx e^{-x^2} = \int_{-\infty}^{+\infty} dx e^{-x^2} = \sqrt{\pi} , \quad (\text{B.6})$$

where we employed the known result for the Gaussian integral.

$\Gamma(1) = 1$	$\Gamma(2) = 1$	$\Gamma(3) = 2$	$\Gamma(4) = 6$
$\Gamma\left(\frac{1}{2}\right) = \sqrt{\pi}$	$\Gamma\left(\frac{3}{2}\right) = \frac{\sqrt{\pi}}{2}$	$\Gamma\left(\frac{5}{2}\right) = \frac{3\sqrt{\pi}}{4}$	$\Gamma\left(\frac{7}{2}\right) = \frac{15\sqrt{\pi}}{8}$

TABLE B.1 — Values of the gamma function $\Gamma(z)$ for some common arguments z .

■ Properties of the gamma function

Some useful identities involving the gamma functions, with $x \in \mathbb{R}$ and $z \in \mathbb{C}$, are:

$$\Gamma(-z) = -\frac{\pi}{z \sin(\pi z) \Gamma(z)} ; \quad (\text{B.7a})$$

$$\Gamma(2z) = 2^{2z-1} \pi^{-\frac{1}{2}} \Gamma(z) \Gamma\left(z + \frac{1}{2}\right) ; \quad (\text{B.7b})$$

$$\Gamma(x) = \sqrt{2\pi} x^{x-\frac{1}{2}} e^{-x} + O\left(\frac{1}{x}\right) = \sqrt{\frac{2\pi}{x}} e^{x(\log(x)-1)} + O\left(\frac{1}{x}\right) \quad (x \rightarrow +\infty) ; \quad (\text{B.7c})$$

where relation (B.7b) is the *Legendre duplication formula*, whereas the asymptotic expansion (B.7c) for $x \rightarrow +\infty$ is the *Stirling's approximation* of the gamma function.

■ Series expansion of the gamma function

The expansion of the gamma function around $z = 0 + \epsilon$ and $z = \frac{1}{2} + \epsilon$, for $\epsilon \rightarrow 0$, is given by:

$$\Gamma(\epsilon) = \frac{1}{\epsilon} - \gamma + \frac{1}{12} (6\gamma^2 + \pi^2) \epsilon + O(\epsilon^2) ; \quad (\text{B.8a})$$

$$\Gamma\left(\frac{1}{2} + \epsilon\right) = \sqrt{\pi} - \sqrt{\pi}(\gamma + \log(4)) \epsilon + O(\epsilon^2) ; \quad (\text{B.8b})$$

where

$$\gamma = 0.5772156649\dots \quad (\text{B.9})$$

is the *Euler-Mascheroni constant*; let us notice that the expansion of the gamma function around others integer or half integer arguments can be obtained by applying repeatedly the property (B.3).

B.2 | Beta function $B(a, b)$

The *beta function* is defined as

$$B(a, b) \equiv \frac{\Gamma(a) \Gamma(b)}{\Gamma(a+b)} . \quad (\text{B.10})$$

It can also be expressed in an integral representation, by recalling the definition (B.1) of the gamma function and manipulating the integrals; in particular it can be proved that:

$$B(a, b) = \int_0^1 du u^{a-1} (1-u)^{b-1} , \quad (\text{B.11})$$

and by letting $v = \frac{u}{1-u}$, with $du = (1+v)^{-2} dv$, it also holds

$$B(a, b) = \int_0^{+\infty} dv \frac{v^{a-1}}{(1+v)^{a+b}} . \quad (\text{B.12})$$

EVALUATION OF RECURRING SCALAR INTEGRALS

In this appendix we explicitly evaluate the integrals which have been needed to perform the computation reported in this thesis. In particular we recall the multi-loop quantum field theory techniques which we presented in section 2.2, and for example we will employ dimensional regularization, evaluating the integrals in d generic spatial dimensions.

In particular in section C.1 and C.2 we evaluate 1-loop and 2-loop integral which appear when evaluating conservative diagrams; evaluating as well the needed Fourier integrals in section C.3. In section C.4 we compute the integral needed to evaluate radiation diagrams. Finally in section C.5 we show an explicit application of the multi-loop quantum field theory techniques which we presented in section 2.2.

C.1 | Evaluation of the scalar integral $I_S(d, a, b)$

We're interested in the computation of the following integral:

$$I_S(d, a, b)[\Delta] \equiv \int \frac{d^d \mathbf{k}}{(2\pi)^d} \frac{1}{|\mathbf{k}|^{2a} (|\mathbf{k}|^2 + \Delta)^b} \quad (\text{C.1})$$

where we're employing the euclidean metric for the d -dimensional spatial components, $|\mathbf{k}|^2 = \delta_{ij} k^i k^j$.

To evaluate such an integral we can proceed as in references [205, 225], first by performing a change of variables, from the cartesian \mathbf{k} system to the hyperspherical d -dimensional coordinates, in practice parameterizing the d components $\{k^1, \dots, k^d\}$ as a function of the radius $K \equiv |\mathbf{k}|$, $K \in [0, +\infty)$, of $d-2$ angles $\phi_1, \dots, \phi_{d-2}$ with domain $[0, \pi]$ radians, and of a last angle ϕ_{d-1} with domain $[0, 2\pi)$ radians; the integration measure hence becomes:

$$d^d \mathbf{k} = K^{d-1} dK d\Omega_{d-1} \quad (\text{C.2})$$

Performing the aforementioned operations on the I_S scalar integral defined in (C.1), and recalling

equation (2.20) to evaluate the hypersurface area $\Omega_{d-1} = \int d\Omega_{d-1}$, we obtain:

$$\begin{aligned}
I_S(d, a, b)[\Delta] &= \frac{1}{(2\pi)^d} \underbrace{\int d\Omega_{d-1}}_{=\Omega_{d-1}} \int_0^{+\infty} dK \frac{K^{d-1}}{K^{2a} (K^2 + \Delta)^b} = \frac{2^{1-d}}{(\pi)^{\frac{d}{2}} \Gamma(\frac{d}{2})} \int_0^{+\infty} dK \frac{K^{d-1}}{K^{2a} (K^2 + \Delta)^b} \\
&= \frac{2^{1-d}}{(\pi)^{\frac{d}{2}} \Gamma(\frac{d}{2})} \int_0^{+\infty} \left(\frac{1}{2} \sqrt{\Delta} u^{-\frac{1}{2}} \right) du \Delta^{\frac{d-1}{2} - a - b} \frac{u^{\frac{d-1}{2}}}{u^a (u+1)^b} \\
&= \frac{2^{-d}}{(\pi)^{\frac{d}{2}} \Gamma(\frac{d}{2})} \Delta^{\frac{d}{2} - a - b} \underbrace{\int_0^{+\infty} du \frac{u^{\frac{d}{2} - 1 - a}}{(u+1)^b}}_{=B(\frac{d}{2} - a, a + b - \frac{d}{2})} = \frac{2^{-d} \Delta^{\frac{d}{2} - a - b}}{(\pi)^{\frac{d}{2}} \Gamma(\frac{d}{2})} \frac{\Gamma(\frac{d}{2} - a) \Gamma(a + b - \frac{d}{2})}{\Gamma(b)}
\end{aligned} \tag{C.3}$$

where in the second line we performed the rescaling of the K coordinate $u = \frac{K^2}{\Delta}$, with measure $dK = \frac{1}{2} \sqrt{\Delta} u^{-\frac{1}{2}} du$, and in the third line we recognized the integral representation (B.12) of the beta function, which is briefly presented in appendix B.2.

Therefore the final result reads:

$$\begin{aligned}
I_S(d, a, b)[\Delta] &\equiv \int \frac{d^d \mathbf{k}}{(2\pi)^d} \frac{1}{|\mathbf{k}|^{2a} (|\mathbf{k}|^2 + \Delta)^b} \\
&= \frac{\Delta^{\frac{d}{2} - a - b}}{(4\pi)^{\frac{d}{2}}} \frac{\Gamma(\frac{d}{2} - a) \Gamma(a + b - \frac{d}{2})}{\Gamma(\frac{d}{2}) \Gamma(b)}.
\end{aligned} \tag{C.4}$$

C.2 | Evaluation of 1-loop and 2-loop scalar integrals $I_{S,1L}$

C.2.1 — Evaluation of the 1-loop master integral $I_{S,1L}(d, a, b)$

Some conservative diagrams will yield scalar integrals of the following kind, with \mathbf{p} an external momentum:

$$I_{S,1L}(d, a, b)[\mathbf{p}] \equiv \int \frac{d^d \mathbf{k}}{(2\pi)^d} \frac{1}{|\mathbf{k}|^{2a} |\mathbf{k} - \mathbf{p}|^{2b}} = \text{Diagram} \tag{C.5}$$

which may be associated to the massless 2-point bubble diagram with external momentum \mathbf{p} .

To solve them we can employ the Feynman parameters presented in section 2.2.5, in particular

imposing $A = |\mathbf{k} - \mathbf{p}|^2$ and $B = |\mathbf{k}|^2$ in formula (2.37):

$$\begin{aligned}
 I_{S,1L}(d, a, b)[\mathbf{p}] &= \frac{\Gamma(a+b)}{\Gamma(a)\Gamma(b)} \int_0^1 dx \int \frac{d^d \mathbf{k}}{(2\pi)^d} \frac{x^{a-1} (1-x)^{b-1}}{(|\mathbf{k} - x\mathbf{p}|^2 + x(1-x)|\mathbf{p}|^2)^{a+b}} \\
 &= \frac{\Gamma(a+b)}{\Gamma(a)\Gamma(b)} \int_0^1 dx x^{a-1} (1-x)^{b-1} \underbrace{\int \frac{d^d \mathbf{k}'}{(2\pi)^d} \frac{1}{(|\mathbf{k}'|^2 + \Delta(\mathbf{p}))^{a+b}}}_{=I_S(d,0,a+b)} \\
 &= \frac{\Gamma(a+b)}{\Gamma(a)\Gamma(b)} \int_0^1 dx x^{a-1} (1-x)^{b-1} \left((\Delta(\mathbf{p}))^{\frac{d}{2}-a-b} \frac{\Gamma(\frac{d}{2}) \Gamma(a+b-\frac{d}{2})}{(4\pi)^{\frac{d}{2}} \Gamma(\frac{d}{2}) \Gamma(a+b)} \right) \quad (\text{C.6}) \\
 &= \frac{\Gamma(a+b-\frac{d}{2})}{(4\pi)^{\frac{d}{2}} \Gamma(a)\Gamma(b)} |\mathbf{p}|^{d-2a-2b} \underbrace{\int_0^1 dx x^{\frac{d}{2}-b-1} (1-x)^{\frac{d}{2}-a-1}}_{=B(\frac{d}{2}-b, \frac{d}{2}-a)} \\
 &= \frac{\Gamma(a+b-\frac{d}{2})}{(4\pi)^{\frac{d}{2}} \Gamma(a)\Gamma(b)} |\mathbf{p}|^{d-2a-2b} \left(\frac{\Gamma(\frac{d}{2}-b) \Gamma(\frac{d}{2}-a)}{\Gamma(d-b-a)} \right),
 \end{aligned}$$

where in the second line we denoted $\Delta(\mathbf{p}) = x(1-x)|\mathbf{p}|^2$ and we performed the shift $\mathbf{k}' = \mathbf{k} - x\mathbf{p}$, which leaves the integration measure invariant, $d^d \mathbf{k}' = d^d \mathbf{k}$; in the third line we employed the previous result (C.4) we obtained for the scalar integral $I_S(d, a, b)$; while in the fourth line we recognized the integral representation (B.11) of the beta function (B.10).

Therefore finally we obtain the result:

$$\begin{aligned}
 I_{S,1L}(d, a, b)[\mathbf{p}] &\equiv \int \frac{d^d \mathbf{k}}{(2\pi)^d} \frac{1}{|\mathbf{k}|^{2a} |\mathbf{k} - \mathbf{p}|^{2b}} \\
 &= \frac{1}{(4\pi)^{\frac{d}{2}}} \frac{\Gamma(a+b-\frac{d}{2}) \Gamma(\frac{d}{2}-a) \Gamma(\frac{d}{2}-b)}{\Gamma(d-a-b) \Gamma(a) \Gamma(b)} |\mathbf{p}|^{d-2a-2b}. \quad (\text{C.7})
 \end{aligned}$$

C.2.2 — Evaluation of the 2-loop master integral $I_{S,2La}$

This 2-loop master integral is needed to evaluate diagrams first appearing at 2PN:

$$I_{S,2La}(d, a, b, c)[\mathbf{p}] \equiv \int \frac{d^d \mathbf{k}_1}{(2\pi)^d} \frac{d^d \mathbf{k}_2}{(2\pi)^d} \frac{1}{|\mathbf{k}_1|^{2a}} \frac{1}{|\mathbf{k}_2|^{2b}} \frac{1}{|\mathbf{k}_1 + \mathbf{k}_2 - \mathbf{p}|^{2c}} = \text{Diagram} \quad (\text{C.8})$$

and we can see that we regard this expression as coming from a the 2-point massless sunrise diagram. We can then solve it by recognizing that this expression is equivalent to nested 1-loop integrals:

$$\begin{aligned}
I_{S,2La}(d, a, b, c)[\mathbf{p}] &= \int \frac{d^d \mathbf{k}_1}{(2\pi)^d} \frac{1}{|\mathbf{k}_1|^{2a}} \underbrace{\int \frac{d^d \mathbf{k}_2}{(2\pi)^d} \frac{1}{|\mathbf{k}_2|^{2b}} \frac{1}{|\mathbf{k}_2 - (\mathbf{p} - \mathbf{k}_1)|^{2c}}}_{=I_{S,1L}(d,b,c)[\mathbf{p}-\mathbf{k}_1]} \\
&= \frac{\Gamma(b+c-\frac{d}{2}) \Gamma(\frac{d}{2}-c) \Gamma(\frac{d}{2}-b)}{(4\pi)^{\frac{d}{2}} \Gamma(d-b-c) \Gamma(b) \Gamma(c)} \int \frac{d^d \mathbf{k}_1}{(2\pi)^d} \frac{1}{|\mathbf{k}_1|^{2a}} \frac{1}{|\mathbf{k}_1 - \mathbf{p}|^{2b+2c-d}} \\
&= \frac{1}{(4\pi)^d} \frac{\Gamma(a+b+c-d) \Gamma(\frac{d}{2}-a) \Gamma(\frac{d}{2}-b) \Gamma(\frac{d}{2}-c)}{\Gamma(\frac{3}{2}d-a-b-c) \Gamma(a) \Gamma(b) \Gamma(c)} |\mathbf{p}|^{2(d-a-b-c)}. \tag{C.9}
\end{aligned}$$

The expression for this master integral therefore is given by:

$$\begin{aligned}
I_{S,2La}(d, a, b, c)[\mathbf{p}] &\equiv \int \frac{d^d \mathbf{k}_1}{(2\pi)^d} \frac{d^d \mathbf{k}_2}{(2\pi)^d} \frac{1}{|\mathbf{k}_1|^{2a}} \frac{1}{|\mathbf{k}_2|^{2b}} \frac{1}{|\mathbf{k}_1 + \mathbf{k}_2 - \mathbf{p}|^{2c}} \\
&= \frac{1}{(4\pi)^d} \frac{\Gamma(a+b+c-d) \Gamma(\frac{d}{2}-a) \Gamma(\frac{d}{2}-b) \Gamma(\frac{d}{2}-c)}{\Gamma(\frac{3}{2}d-a-b-c) \Gamma(a) \Gamma(b) \Gamma(c)} |\mathbf{p}|^{2(d-a-b-c)}. \tag{C.10}
\end{aligned}$$

C.2.3 — Evaluation of the 2-loop master integral $I_{S,2Lb}$

Also this 2-loop master integral is needed for the evaluation of diagrams first appearing at 2PN:

$$\begin{aligned}
I_{S,2Lb}(d, a, b, c, e)[\mathbf{p}] &\equiv \int \frac{d^d \mathbf{k}_1}{(2\pi)^d} \frac{d^d \mathbf{k}_2}{(2\pi)^d} \frac{1}{|\mathbf{k}_1|^{2a}} \frac{1}{|\mathbf{k}_2|^{2b}} \frac{1}{|\mathbf{k}_1 - \mathbf{p}|^{2c}} \frac{1}{|\mathbf{k}_2 - \mathbf{p}|^{2e}} \\
&= \begin{gathered} \begin{array}{c} \begin{array}{ccc} \overleftarrow{k_1 - p} & \overleftarrow{k_2 - p} & \\ \overrightarrow{p} & \text{---} & \overrightarrow{p} \\ \text{---} & \text{---} & \text{---} \\ \overrightarrow{k_1} & \overrightarrow{k_2} & \end{array} \end{array} \end{gathered} \tag{C.11} \\
&= \underbrace{\int \frac{d^d \mathbf{k}_1}{(2\pi)^d} \frac{1}{|\mathbf{k}_1|^{2a}} \frac{1}{|\mathbf{k}_1 - \mathbf{p}|^{2c}}}_{=I_{S,1L}(d,a,c)[\mathbf{p}]} \underbrace{\int \frac{d^d \mathbf{k}_2}{(2\pi)^d} \frac{1}{|\mathbf{k}_2|^{2b}} \frac{1}{|\mathbf{k}_2 - \mathbf{p}|^{2e}}}_{=I_{S,1L}(d,b,e)[\mathbf{p}]} \\
&= \frac{\Gamma(a+c-\frac{d}{2}) \Gamma(b+e-\frac{d}{2}) \Gamma(\frac{d}{2}-a) \Gamma(\frac{d}{2}-b) \Gamma(\frac{d}{2}-c) \Gamma(\frac{d}{2}-e)}{(4\pi)^d \Gamma(d-c-a) \Gamma(d-e-b) \Gamma(a) \Gamma(b) \Gamma(c) \Gamma(e)} |\mathbf{p}|^{2(d-a-b-c-e)}.
\end{aligned}$$

This master integral is equivalent to the integral arising from the computation of a massless double-bubble diagram, and is factorizable into the product of the 1-loop master integral $I_{S,1L}$.

C.3 | Evaluation of the scalar Fourier integral $I_F(d, a)$

While evaluating diagrams throughout this thesis work, a class of Fourier transform scalar integral, which we'll denote $I_F(d, a)$, often appears while evaluating the vacuum diagrams: assuming to be working in d -dimensional Euclidean space, so restricting ourselves to spatial components only with a metric given by $+\delta_{ij}$, these integrals generically have the following structure:

$$I_F(d, a)[\mathbf{x}] = \int \frac{d^d \mathbf{k}}{(2\pi)^d} e^{i\mathbf{k}\cdot\mathbf{x}} \frac{1}{|\mathbf{k}|^{2a}}. \tag{C.12}$$

To evaluate them we can initially retrace what has been done as done in references [205, 225]. Let us notice that, once we have parameterized the momentum space with a cartesian coordinate system, it is always possible to find a rotation which acts on the \mathbf{k} variable such that it will make the last k^d axis parallel to the \mathbf{x} vector, i.e. $\mathbf{k} \cdot \mathbf{x} = k^d |\mathbf{x}|$. Furthermore, the integration measure $d^d \mathbf{k}$ and the $|\mathbf{k}|$ term are invariant under generic rotations, and because we're integrating over all possible momentum components, the integration domain is mapped into itself. Therefore only the dot product in the exponential will be affected by such a rotation, yielding exactly $e^{ik^d |\mathbf{x}|}$, and as a consequence of this the result of the scalar integral will only depend on the modulus $|\mathbf{x}|$ of the \mathbf{x} vector.

The symmetry of the system then suggest a change of coordinate system: that is, we can parameterize the momenta space with a d -dimensional hypercylindrical coordinate system, aligned along the k^d variable. In practice we can reparameterize the $d-1$ coordinates $\{k^1, \dots, k^{d-1}\}$ employing an hyperspherical coordinate system, with radius $K \equiv \sqrt{(k^1)^2 + \dots + (k^{d-1})^2} \geq 0$, $d-3$ angles $\phi_1, \dots, \phi_{d-3}$ with domain $[0, \pi]$ radians, and another angle ϕ_{d-2} with domain $[0, 2\pi)$ radians; the integration measure then will read

$$d^d \mathbf{k} = d(k^d) K^{d-2} dK d\Omega_{d-1} \quad (\text{C.13})$$

and the scalar integral

$$I_F(d, a)[\mathbf{x}] = \frac{1}{(2\pi)^d} \int d\Omega_{d-1} d(k^d) dK K^{d-2} e^{i|\mathbf{x}|k^d} \frac{1}{((k^d)^2 + K^2)^a}. \quad (\text{C.14})$$

Below we proceed with the evaluation of the scalar integral: first, in equation (C.14), we consider as integration variables K^2 instead of K , which can be formally interpreted as a change of variable from K to K^2 , which nonetheless doesn't change the integration domain, as it was $K \in [0, +\infty)$. Then, in the second line of formula (C.15), we perform an additional change of variable from $(k^d, K^2) \in \mathbb{R} \times \mathbb{R}^+$ to (y, z) via $k^d = \frac{y}{|\mathbf{x}|}$ and $K^2 = \frac{y^2}{z|\mathbf{x}|^2}$, with the domain restricted to $K^2 > 0$. The Jacobian of the transformation is $\frac{y^2}{z^2|\mathbf{x}|^3}$, while the new integration domain is $(y, z) \in \mathbb{R} \times \mathbb{R}^+$. These manipulations explicitly yield:

$$\begin{aligned} I_F(d, a)[\mathbf{x}] &= \frac{\Omega_{d-1}}{(2\pi)^d} \int_{-\infty}^{+\infty} d(k^d) \int_0^{+\infty} \frac{d(K^2)}{2} (K^2)^{\frac{d-3}{2}} e^{i|\mathbf{x}|k^d} \frac{1}{((k^d)^2 + (K^2))^a} \\ &= \frac{\Omega_{d-1}}{(2\pi)^d} \frac{1}{2} \int \left(\frac{y^2}{z^2|\mathbf{x}|^3} \right) dy dz \left(\frac{y^2}{z|\mathbf{x}|^2} \right)^{\frac{d-3}{2}} e^{iy} \frac{z^a}{(1+z)^a} \left(\frac{y}{|\mathbf{x}|} \right)^{-2a} \\ &= \frac{2^{-d} \pi^{-\frac{d+1}{2}}}{\Gamma\left(\frac{d-1}{2}\right)} |\mathbf{x}|^{2a-d} \underbrace{\int_0^{+\infty} dz \frac{z^{a-\frac{d}{2}-\frac{1}{2}}}{(1+z)^a}}_{=B\left(a+\frac{1-d}{2}, \frac{d-1}{2}\right)} \int_{-\infty}^{+\infty} dy y^{d-2a-1} e^{iy} \\ &= \frac{2^{-d} \pi^{-\frac{d+1}{2}}}{\Gamma\left(\frac{d-1}{2}\right)} |\mathbf{x}|^{2a-d} \left(\frac{\Gamma\left(a+\frac{1-d}{2}\right) \Gamma\left(\frac{d-1}{2}\right)}{\Gamma(a)} \right) \int_{-\infty}^{+\infty} dy y^{d-2a-1} e^{iy} \\ &= 2^{-d} \pi^{-\frac{d+1}{2}} \frac{\Gamma\left(a+\frac{1-d}{2}\right)}{\Gamma(a)} |\mathbf{x}|^{2a-d} \underbrace{\int_{-\infty}^{+\infty} dy y^{d-2a-1} e^{iy}}_{\equiv L(d-2a-1)} \end{aligned} \quad (\text{C.15})$$

where in the third line we recalled formula (2.20) for the hypersurface area of a $(d-1)$ -sphere, and in the penultimate equality we recognized the integral representation (B.12) of the beta function (B.10).

Now we have to evaluate the remaining integral, which we define as:

$$L(\alpha) \equiv \int_{-\infty}^{+\infty} dy y^\alpha e^{iy} . \quad (\text{C.16})$$

To proceed let us first evaluate the following integral, which is reminiscent of the Schwinger trick shown in section 2.2.5:

$$\begin{aligned} \int_0^{+\infty} dx x^{-(1+\alpha)} e^{-t^2 x^2} &= \int_0^{+\infty} \frac{d(x^2)}{2} (x^2)^{-\frac{(2+\alpha)}{2}} e^{-t^2 x^2} = \int_0^{+\infty} \frac{1}{t^2} \frac{d(\bar{x}^2)}{2} (t^2)^{\frac{(2+\alpha)}{2}} (\bar{x}^2)^{-\frac{(2+\alpha)}{2}} e^{-\bar{x}^2} \\ &= \frac{t^\alpha}{2} \left(2 \int_0^{+\infty} d\bar{x} \bar{x}^{2(-\frac{\alpha}{2})-1} e^{-\bar{x}^2} \right) = \frac{t^\alpha}{2} \Gamma\left(-\frac{\alpha}{2}\right) ; \end{aligned} \quad (\text{C.17})$$

where we used the change of variables $\bar{x}^2 = t^2 x^2$ which is defined for $t \in \mathbb{R} \setminus \{0\}$, and where in the last equality we recalled the alternative definition (B.2) of the gamma function. Doing so we can recognize the relation:

$$y^\alpha = \frac{2}{\Gamma\left(-\frac{\alpha}{2}\right)} \int_0^{+\infty} d\xi \xi^{-(1+\alpha)} e^{-y^2 \xi^2} , \quad (\text{C.18})$$

which we can substitute in formula (C.16) to obtain:

$$L(\alpha) = \frac{2}{\Gamma\left(-\frac{\alpha}{2}\right)} \int_0^{+\infty} d\xi \xi^{-(1+\alpha)} \int_{-\infty}^{+\infty} dy e^{-y^2 \xi^2 + iy} . \quad (\text{C.19})$$

We can complete the squares in the exponential with respect to y , such that:

$$\begin{aligned} L(\alpha) &= \frac{2}{\Gamma\left(-\frac{\alpha}{2}\right)} \int_0^{+\infty} d\xi \xi^{-(1+\alpha)} \int_{-\infty}^{+\infty} dy e^{-\xi^2 \left(y - \frac{i}{2\xi^2}\right)^2 - \frac{1}{4\xi^2}} \\ &= \frac{2}{\Gamma\left(-\frac{\alpha}{2}\right)} \int_0^{+\infty} d\xi \xi^{-(2+\alpha)} e^{-\frac{1}{4\xi^2}} \int_{-\infty - \frac{i}{2\xi}}^{+\infty - \frac{i}{2\xi}} d\bar{y} e^{-\bar{y}^2} \end{aligned} \quad (\text{C.20})$$

where we performed the change of variable $\bar{y} = \xi \left(y - \frac{i}{2\xi^2}\right)$, with $\xi > 0$, under which the integration measure becomes $d\xi dy = \xi^{-1} d\xi d\bar{y}$; nonetheless such change of variable shifted the \bar{y} integration in the complex plane, along a path which doesn't lie anymore on the real \bar{y} axis.

So let us now focus our attention on this second integral, which we denote as:

$$J(\xi) \equiv \int_{-\infty - \frac{i}{2\xi}}^{+\infty - \frac{i}{2\xi}} d\bar{y} e^{-\bar{y}^2} = \lim_{R \rightarrow +\infty} \int_{\gamma_1} d\bar{y} e^{-\bar{y}^2} , \quad (\text{C.21})$$

where we defined the integration path γ_1 as shown in figure C.1, so $\gamma_1(s) = Rs - i\frac{1}{2\xi}$, with $s \in [-1, +1]$ and with $R > 0$ real constant; at the end the limit $R \rightarrow +\infty$ yields the initial integral.

We can notice that the integrand $e^{-\bar{y}^2}$ is an holomorphic function over the whole complex plane \mathbb{C} , i.e. it has no poles nor singularities. Therefore Cauchy's integral theorem implies that the contour integral of such a function over any simply closed contour $\tilde{\gamma}$ will be vanishing, that is:

$$\oint_{\tilde{\gamma}} d\bar{y} e^{-\bar{y}^2} = 0 . \quad (\text{C.22})$$

For such a closed path we can consider the counterclockwise contour $\tilde{\gamma} = \gamma_1 + \gamma_2 + \gamma_3 + \gamma_4$ shown in figure C.1; in particular we can parameterize them as $\gamma_2(s) = R - i\frac{1}{2\xi}(1-s)$ with $s \in [0, 1]$, $\gamma_3(s) = -Rs$ with $s \in [-1, +1]$ and $\gamma_4(s) = R - i\frac{1}{2\xi}s$ with $s \in [0, 1]$.

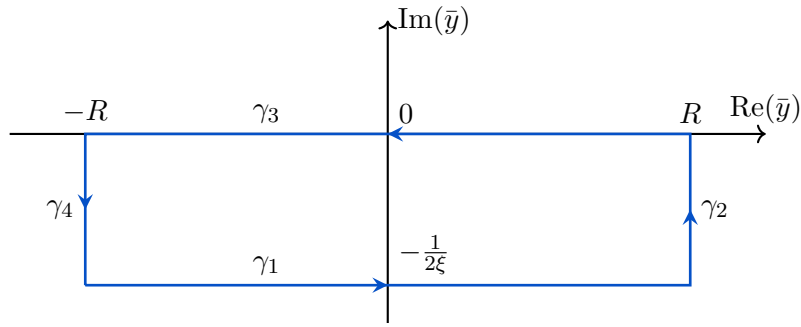


FIGURE C.1 — Complex integration contour employed for the evaluation of the integral $J(\xi)$.

We can recognize that the contour integration along the γ_3 path is equivalent to the integration along the real axis, from $+R$ to $-R$, in fact:

$$\int_{\gamma_3} d\bar{y} e^{-\bar{y}^2} = \int_{-1}^{+1} (-R) ds e^{-(Rs)^2} = \int_{+R}^{-R} du e^{-u^2}; \quad (\text{C.23})$$

and once we take the limit $R \rightarrow +\infty$ it holds:

$$\lim_{R \rightarrow +\infty} \int_{\gamma_3} d\bar{y} e^{-\bar{y}^2} = - \int_{-\infty}^{+\infty} du e^{-u^2} = -\sqrt{\pi}, \quad (\text{C.24})$$

where we employed the Gaussian integral result in the last equality.

Recalling the Darboux inequality $\left| \int_{\gamma} dz f(z) \right| \leq \int_{\gamma} |dz| |f(z)| \leq \sup_{z \in \gamma} |f(z)| \int_{\gamma} |dz|$ we can evaluate the contribution of the γ_2 and γ_4 paths to the contour integral:

$$\left| \int_{\gamma_2} d\bar{y} e^{-\bar{y}^2} \right| \leq \sup_{s \in [0,1]} \left| e^{-(R - \frac{i}{2\xi}(1-s))^2} \right| \int_0^1 \left| \frac{i}{2\xi} ds \right| = \sup_{s \in [0,1]} \left| e^{-R^2 + \frac{(1-s)^2}{4\xi^2} + \frac{iR}{\xi}(1-s)} \right| \frac{1}{2\xi} = \frac{e^{\frac{1}{4\xi^2}}}{2\xi} e^{-R^2} \quad (\text{C.25a})$$

$$\left| \int_{\gamma_4} d\bar{y} e^{-\bar{y}^2} \right| \leq \sup_{s \in [0,1]} \left| e^{-(R - \frac{i}{2\xi}s)^2} \right| \int_0^1 \left| \frac{-i}{2\xi} ds \right| = \sup_{s \in [0,1]} \left| e^{-R^2 + \frac{s^2}{4\xi^2} + \frac{iR}{\xi}s} \right| \frac{1}{2\xi} = \frac{e^{\frac{1}{4\xi^2}}}{2\xi} e^{-R^2}; \quad (\text{C.25b})$$

in particular we can notice that for any fixed $\xi > 0$ both integrals vanish in the limit $R \rightarrow +\infty$.

Hence taking the $R \rightarrow +\infty$ limit in formula (C.22) we obtain:

$$0 = \lim_{R \rightarrow +\infty} \left(\int_{\gamma_1} d\bar{y} e^{-\bar{y}^2} + \int_{\gamma_2} d\bar{y} e^{-\bar{y}^2} + \int_{\gamma_3} d\bar{y} e^{-\bar{y}^2} + \int_{\gamma_4} d\bar{y} e^{-\bar{y}^2} \right) = J(\xi) + 0 + (-\sqrt{\pi}) + 0 \quad (\text{C.26})$$

where we recalled the definition (C.21) and equation (C.24). Therefore we obtain the result we were looking for, that is:

$$J(\xi) \equiv \int_{-\infty - \frac{i}{2\xi}}^{+\infty - \frac{i}{2\xi}} d\bar{y} e^{-\bar{y}^2} = \sqrt{\pi}. \quad (\text{C.27})$$

We can now return to the main computation, so substituting formula (C.27) in equation (C.20) we obtain:

$$\begin{aligned} L(\alpha) &= \frac{2}{\Gamma(-\frac{\alpha}{2})} \int_0^{+\infty} d\xi \xi^{-(2+\alpha)} e^{-\frac{1}{4\xi^2}} J(\xi) = \frac{2\sqrt{\pi}}{\Gamma(-\frac{\alpha}{2})} \int_0^{+\infty} d\xi \xi^{-(2+\alpha)} e^{-\frac{1}{4\xi^2}} \\ &= \frac{2\sqrt{\pi}}{\Gamma(-\frac{\alpha}{2})} \int_{+\infty}^0 \left(-\frac{1}{2\eta^2} \right) d\eta 2^{2+\alpha} \eta^{2+\alpha} e^{-\eta^2} = \frac{2^{2+\alpha} \sqrt{\pi}}{\Gamma(-\frac{\alpha}{2})} \frac{1}{2} \underbrace{\left(2 \int_0^{+\infty} d\eta \eta^{2(\frac{\alpha}{2} + \frac{1}{2}) - 1} e^{-\eta^2} \right)}_{=\Gamma(\frac{\alpha}{2} + \frac{1}{2})} \end{aligned} \quad (\text{C.28})$$

where in the second line we performed the change of variables $\eta = \frac{1}{2\xi}$, and in the last equality we recalled again the alternative definition (B.2) of the gamma function. Therefore we obtain:

$$L(\alpha) = 2^{\alpha+1} \sqrt{\pi} \frac{\Gamma\left(\frac{\alpha}{2} + \frac{1}{2}\right)}{\Gamma\left(-\frac{\alpha}{2}\right)} = -2 \sin\left(\alpha \frac{\pi}{2}\right) \Gamma(\alpha + 1) \quad (\text{C.29})$$

Returning to the main computation of the scalar integral $I_F(d, a)[\mathbf{x}]$, we can resume from formula (C.15), substituting the result (C.29) we just obtained:

$$\begin{aligned} I_F(d, a)[\mathbf{x}] &= 2^{-d} \pi^{-\frac{d+1}{2}} \frac{\Gamma\left(a + \frac{1-d}{2}\right)}{\Gamma(a)} |\mathbf{x}|^{2a-d} L(d - 2a - 1) \\ &= 2^{-d} \pi^{-\frac{d+1}{2}} \frac{\Gamma\left(a + \frac{1-d}{2}\right)}{\Gamma(a)} |\mathbf{x}|^{2a-d} \left(2^{d-2a} \sqrt{\pi} \frac{\Gamma\left(\frac{d}{2} - a\right)}{\Gamma\left(a + \frac{1-d}{2}\right)} \right) \\ &= 2^{-2a} \pi^{-\frac{d}{2}} \frac{\Gamma\left(\frac{d}{2} - a\right)}{\Gamma(a)} |\mathbf{x}|^{2a-d} = \frac{\Gamma\left(\frac{d}{2} - a\right)}{(4\pi)^{\frac{d}{2}} \Gamma(a)} \left(\frac{|\mathbf{x}|}{2}\right)^{2a-d}. \end{aligned} \quad (\text{C.30})$$

Therefore the analytic result of the $I_F(d, a)[\mathbf{x}]$ scalar integral reads:

$$\begin{aligned} I_F(d, a)[\mathbf{x}] &\equiv \int \frac{d^d \mathbf{k}}{(2\pi)^d} e^{i\mathbf{k}\cdot\mathbf{x}} \frac{1}{|\mathbf{k}|^{2a}} \\ &= 2^{-2a} \pi^{-\frac{d}{2}} \frac{\Gamma\left(\frac{d}{2} - a\right)}{\Gamma(a)} |\mathbf{x}|^{2a-d}. \end{aligned} \quad (\text{C.31})$$

C.3.1 — Tensorial generalization of the integral $I_F(d, a)$

We can generalize the result (C.31) to the class of integrals with also tensorial quantities in the numerator, by taking derivatives with respect to the position \mathbf{x} , as suggested by references [224, 225]: in particular such calculations formally hold only as long as $2a \neq d$, nonetheless we can recover also this case via analytic continuation of the result.

Recalling that $\frac{\partial(|\mathbf{x}|^\alpha)}{\partial x^i} = \frac{\partial(\delta_{jk} x^j x^k)^{\frac{\alpha}{2}}}{\partial x^i} = \frac{\alpha}{2} (|\mathbf{x}|)^{\alpha-2} \delta_{jk} (\delta^j_i x^k + x^j \delta^k_i) = \alpha |\mathbf{x}|^{\alpha-2} x^i$, we obtain:

$$\begin{aligned} I_F(d, a)^i[\mathbf{x}] &\equiv \int \frac{d^d \mathbf{k}}{(2\pi)^d} e^{i\mathbf{k}\cdot\mathbf{x}} \frac{k^i}{|\mathbf{k}|^{2a}} \\ &= \int \frac{d^d \mathbf{k}}{(2\pi)^d} \frac{1}{|\mathbf{k}|^{2a}} \left(\frac{1}{i} \frac{\partial}{\partial x^i} \right) e^{i\mathbf{k}\cdot\mathbf{x}} = -i \frac{\partial(I_F(d, a)[\mathbf{x}])}{\partial x^i} \\ &= i(d - 2a) 2^{-2a} \pi^{-\frac{d}{2}} \frac{\Gamma\left(\frac{d}{2} - a\right)}{\Gamma(a)} |\mathbf{x}|^{2a-d-2} x^i \\ &= i 2^{1-2a} \pi^{-\frac{d}{2}} \frac{\Gamma\left(\frac{d}{2} - a + 1\right)}{\Gamma(a)} |\mathbf{x}|^{2a-d-2} x^i, \end{aligned} \quad (\text{C.32})$$

and also

$$\begin{aligned} I_F(d, a)^{ij}[\mathbf{x}] &\equiv \int \frac{d^d \mathbf{k}}{(2\pi)^d} e^{i\mathbf{k}\cdot\mathbf{x}} \frac{k^i k^j}{|\mathbf{k}|^{2a}} \\ &= \int \frac{d^d \mathbf{k}}{(2\pi)^d} \frac{1}{|\mathbf{k}|^{2a}} \left(-\frac{\partial^2}{\partial x^i \partial x^j} \right) e^{i\mathbf{k}\cdot\mathbf{x}} = -\frac{\partial^2(I_F(d, a)[\mathbf{x}])}{\partial x^i \partial x^j} \\ &= 2^{1-2a} \pi^{-\frac{d}{2}} \frac{\Gamma\left(\frac{d}{2} - a + 1\right)}{\Gamma(a)} |\mathbf{x}|^{2a-d-2} \left(\delta^{ij} + (2a - d - 2) \frac{x^i x^j}{|\mathbf{x}|^2} \right). \end{aligned} \quad (\text{C.33})$$

Yet to systematically evaluate Fourier integrals with a tensorial structure, and to implement it into a code, we found it more useful to perform a tensor decomposition of the integral, in order to reduce ourselves to work with a class of scalar integrals, which we present hereafter in section C.3.2.

C.3.2 — Generalization $I_{F,sp}(d, a, b)$ of the integral $I_F(d, a)$ with scalar products

Let us consider a generalization of the scalar integral (C.12), such that:

$$I_{F,sp}(d, a, b)[\mathbf{x}] \equiv \int \frac{d^d \mathbf{k}}{(2\pi)^d} e^{i\mathbf{k}\cdot\mathbf{x}} \frac{(\mathbf{k}\cdot\mathbf{x})^b}{|\mathbf{k}|^{2a}} ; \quad (\text{C.34})$$

in particular this class of integrals appears when we apply the tensor decomposition procedure in order to solve a Fourier integral with a tensorial structure at the numerator.

Let us define $j(a, b) \equiv I_{F,sp}(d, a, b)[\mathbf{x}]$ for convenience: in order to solve the integral above we'll apply the integration-by-parts identities to it. In particular, with $w^i = \alpha k^i + \beta x^i$, we obtain:

$$\begin{aligned} 0 &= \int \frac{d^d \mathbf{k}}{(2\pi)^d} \frac{\partial}{\partial k^i} \left((\alpha k^i + \beta x^i) e^{i\mathbf{k}\cdot\mathbf{x}} \frac{(\mathbf{k}\cdot\mathbf{x})^b}{|\mathbf{k}|^{2a}} \right) \\ &= d\alpha \int \frac{d^d \mathbf{k}}{(2\pi)^d} e^{i\mathbf{k}\cdot\mathbf{x}} \frac{(\mathbf{k}\cdot\mathbf{x})^b}{|\mathbf{k}|^{2a}} + \int \frac{d^d \mathbf{k}}{(2\pi)^d} (\alpha k^i + \beta x^i) \frac{\partial}{\partial k^i} \left(e^{i\mathbf{k}\cdot\mathbf{x}} \frac{(\mathbf{k}\cdot\mathbf{x})^b}{|\mathbf{k}|^{2a}} \right) \\ &= d\alpha j(a, b) + \int \frac{d^d \mathbf{k}}{(2\pi)^d} e^{i\mathbf{k}\cdot\mathbf{x}} \frac{(\mathbf{k}\cdot\mathbf{x})^b}{|\mathbf{k}|^{2a}} \left((b-2a)\alpha + i|\mathbf{x}|^2\beta + b\beta|\mathbf{x}|^2 \frac{1}{(\mathbf{k}\cdot\mathbf{x})} + i\alpha(\mathbf{k}\cdot\mathbf{x}) - 2a\beta \frac{(\mathbf{k}\cdot\mathbf{x})}{|\mathbf{k}|^2} \right) \\ &= ((d+b-2a)\alpha + i|\mathbf{x}|^2\beta) j(a, b) + b\beta|\mathbf{x}|^2 j(a, b-1) + i\alpha j(a, b+1) - 2a\beta j(a+1, b+1) ; \end{aligned} \quad (\text{C.35})$$

and imposing $\alpha = 1, \beta = 0$ before and then $\alpha = 0, \beta = 1$ we obtain the two independent conditions:

$$(d+b-2a)j(a, b) + i j(a, b+1) = 0 ; \quad (\text{C.36a})$$

$$i|\mathbf{x}|^2 j(a, b) + b|\mathbf{x}|^2 j(a, b-1) - 2a j(a+1, b+1) = 0 . \quad (\text{C.36b})$$

From formula (C.36a) follows directly

$$j(a, b+1) = i (d+b-2a) j(a, b) \quad (\text{C.37})$$

and therefore, as long as $b \in \mathbb{Z}$, using formula (C.65) we obtain:

$$\begin{aligned} j(a, b) &= \prod_{q=0}^{b-1} (i (d+q-2a)) j(a, 0) = \prod_{q=1}^b (i (q+d-1-2a)) j(a, 0) \\ &= i^b \frac{\Gamma(b+d-2a)}{\Gamma(d-2a)} j(a, 0) . \end{aligned} \quad (\text{C.38})$$

We may then impose $b = 0$ in relation (C.36b) and use equation (C.37) to reduce the integral $j(a, 0)$ down to $j(1, 0)$, nonetheless such a formula would hold only for $a \in \mathbb{N}$. However, during the evaluation of PN diagrams, some integrals will present $a \in \mathbb{R} - \mathbb{N}$, so we'll evaluate $j(a, 0)$ employ directly the result (C.31), which is valid for $a \in \mathbb{R}$. Doing so we obtain the full, exact result:

$$\begin{aligned} I_{F,sp}(d, a, b)[\mathbf{x}] &\equiv \int \frac{d^d \mathbf{k}}{(2\pi)^d} e^{i\mathbf{k}\cdot\mathbf{x}} \frac{(\mathbf{k}\cdot\mathbf{x})^b}{|\mathbf{k}|^{2a}} \\ &= i^b 2^{-2a} \pi^{-\frac{d}{2}} \frac{\Gamma(b+d-2a) \Gamma(\frac{d}{2}-a)}{\Gamma(d-2a) \Gamma(a)} |\mathbf{x}|^{2a-d} . \end{aligned} \quad (\text{C.39})$$

■ Discordant alternative evaluation of the integral

In order to evaluate the integral (C.34), we could have proceeded analogously to what we've done in section C.3, as the only difference is that we would have picked up a $(|\mathbf{x}|k^d)^b$ factor in formula (C.14), which then would have resulted in an additional y^b factor at the numerator of result (C.15), therefore yielding

$$\begin{aligned} I_{F,sp}(d, a, b)[\mathbf{x}] &= 2^{-d} \pi^{-\frac{d+1}{2}} \frac{\Gamma(a + \frac{1-d}{2})}{\Gamma(a)} |\mathbf{x}|^{2a-d} \underbrace{\int_{-\infty}^{+\infty} dy y^{d-2a+b-1} e^{iy}}_{\equiv L(d-2a+b-1)} \\ &= 2^{b-2a} \pi^{-\frac{d}{2}} \frac{\Gamma(a + \frac{1-d}{2}) \Gamma(\frac{(d+b)}{2} - a)}{\Gamma(a) \Gamma(a - \frac{(d+b-1)}{2})} |\mathbf{x}|^{2a-d}. \end{aligned} \quad (\text{C.40})$$

where we used the result (C.29). Nonetheless we can notice that the result above does not agree with result (C.39), and we have checked that only the latter equation yields the correct PN diagram evaluation, while formula (C.40) gives inconsistent results already for the tensor decomposition (C.32) with a single free index. Actually we have checked that, for the tensor decomposition with up to 4 free indices, formula (C.40) gives the correct result when the number of free spatial indices is even, like in (C.33), and instead is wrong by a factor $\frac{i}{\tan(\frac{\pi}{2}(2a-d))}$ when the number of indices is odd; however we couldn't trace back the reason for this inconsistency.

C.4 | Evaluation of the $I_R(d, a, b)$ scalar integral

We want to evaluate the scalar integral defined as

$$I_R(d, a, b)[f](t) = \int ds f(t+s) \int \frac{dk^0}{2\pi} e^{ik^0 s} \int \frac{d^d \mathbf{k}}{(2\pi)^d} \frac{1}{k^2 + i\epsilon} \frac{(k^0)^b}{|\mathbf{k}|^{2a}}, \quad (\text{C.41})$$

where the function f is a generic function of time that could eventually carry spatial indices.

First of all let us recall our notations, see (N12) and (N13), according to which the temporal Fourier transform $g(k)$ of a $g(t)$ function, and its inverse Fourier transform, are given respectively by:

$$g(k^0) = \int dt g(t) e^{ik^0 t}, \quad g(t) = \int \frac{dk^0}{2\pi} g(k^0) e^{-ik^0 t}; \quad (\text{C.42})$$

where we could denote k^0 also as ω . Hence, by performing the change of variable $u = t + s$, which amounts to a shift of s with t fixed, since it's an external parameter, we can recognize the Fourier transform $f(k^0)$ of the function $f(t)$ in equation (C.41), i.e.

$$I_R(d, a, b)[f](t) = \int \frac{dk^0}{2\pi} e^{-ik^0 t} (k^0)^b \underbrace{\int du f(u) e^{ik^0 u}}_{f(k^0)} \int \frac{d^d \mathbf{k}}{(2\pi)^d} \frac{1}{k^2 + i\epsilon} \frac{1}{|\mathbf{k}|^{2a}}. \quad (\text{C.43})$$

Afterwards we have to take care of the $+i\epsilon$ prescription due to the propagator $(k^2 + i\epsilon)^{-1} = ((k^0)^2 - |\mathbf{k}|^2 + i\epsilon)^{-1}$; in order to do so we can employ the *Plemelj-Sokhotski functional identity* [206, 312, 313]:

$$\lim_{\epsilon \rightarrow 0} \int dk^0 \frac{g(k^0)}{(k^0)^2 - |\mathbf{k}|^2 \pm i\epsilon} = P \int dk^0 \frac{g(k^0)}{(k^0)^2 - |\mathbf{k}|^2} \mp i\pi \int dk^0 g(k^0) \delta((k^0)^2 - |\mathbf{k}|^2); \quad (\text{C.44})$$

where the *Cauchy principal value* of an integral with a pole of order one in $x = a$ is defined as

$$P \int_{-\infty}^{+\infty} dx \frac{g(x)}{x-a} \equiv \lim_{\delta \rightarrow 0} \left(\int_{-\infty}^{a-\delta} dx \frac{g(x)}{x-a} + \int_{a+\delta}^{+\infty} dx \frac{g(x)}{x-a} \right) \quad (\text{C.45})$$

for a function $g(x)$ smooth and non-singular near $x = a$ which vanishes sufficiently fast on the boundaries.

Using this identities we can rewrite equation (C.41) as

$$\begin{aligned} I_R(d, a, b)[f](t) &= P \underbrace{\int \frac{dk^0}{2\pi} e^{-ik^0 t} (k^0)^b f(k^0) \int \frac{d^d \mathbf{k}}{(2\pi)^d} \frac{1}{(k^0)^2 - |\mathbf{k}|^2} \frac{1}{|\mathbf{k}|^{2a}}}_{\equiv I_{R,1}} \\ &\quad - i\pi \underbrace{\int \frac{dk^0}{2\pi} e^{-ik^0 t} (k^0)^b f(k^0) \int \frac{d^d \mathbf{k}}{(2\pi)^d} \frac{1}{|\mathbf{k}|^{2a}} \delta((k^0)^2 - |\mathbf{k}|^2)}_{\equiv I_{R,2}}. \end{aligned} \quad (\text{C.46})$$

Let us start by evaluating the first integral $I_{R,1}$ in (C.46), by recalling the result (C.4) for the scalar integral $I_S(d, a, b)[\Delta]$:

$$\begin{aligned} I_{R,1} &= P \int \frac{dk^0}{2\pi} e^{-ik^0 t} (k^0)^b f(k^0) \left(- \underbrace{\int \frac{d^d \mathbf{k}}{(2\pi)^d} \frac{1}{|\mathbf{k}|^2 - (k^0)^2} \frac{1}{|\mathbf{k}|^{2a}}}_{=I_S(d, a, 1)[-(k^0)^2]} \right) \\ &= \frac{i^{d-2a}}{(4\pi)^{\frac{d}{2}}} \frac{\Gamma(\frac{d}{2} - a) \Gamma(a + 1 - \frac{d}{2})}{\Gamma(\frac{d}{2})} P \int \frac{dk^0}{2\pi} e^{-ik^0 t} (k^0)^{b+d-2a-2} f(k^0) \\ &= - \frac{i^{b+2d-4a}}{(4\pi)^{\frac{d}{2}}} \frac{\Gamma(\frac{d}{2} - a) \Gamma(a + 1 - \frac{d}{2})}{\Gamma(\frac{d}{2})} \frac{d^{b+d-2a-2}}{dt^{b+d-2a-2}} \underbrace{\left(P \int \frac{dk^0}{2\pi} e^{-ik^0 t} f(k^0) \right)}_{=f(t)} \\ &= \frac{i^{b+2d-4a} 2^{-d} \pi^{1-\frac{d}{2}}}{\sin((2a-d)\frac{\pi}{2}) \Gamma(\frac{d}{2})} \frac{d^{b+d-2a-2} f(t)}{dt^{b+d-2a-2}}. \end{aligned} \quad (\text{C.47})$$

To proceed with the evaluation of the second integral $I_{R,2}$ in equation (C.46), we first recall the identity $\delta(g(x)) = \sum_k (|\frac{dg}{dx}(x_k)|)^{-1} \delta(x-x_k)$, where x_k are the zeroes of the function g , i.e. $g(x_k) = 0$, from which follows:

$$\delta((k^0)^2 - |\mathbf{k}|^2) = \delta((k^0 - |\mathbf{k}|)(k^0 + |\mathbf{k}|)) = \frac{1}{2|\mathbf{k}|} (\delta(k^0 + |\mathbf{k}|) + \delta(k^0 - |\mathbf{k}|)). \quad (\text{C.48})$$

Afterwards, to regularize the integral, we employ the fact that for what concerns our calculations (see chapter 5), the integral (C.41) is always integrated over $\int dt g(t)$ ($I_R(d, a, b)[f](t)$), with both $f(t)$ and $g(t)$ real functions, hence $f(-|\mathbf{k}|) = f^*(|\mathbf{k}|)$. Therefore we obtain:

$$\begin{aligned} I_{R,2} &= \frac{1}{2} \int \frac{dk^0}{2\pi} e^{-ik^0 t} (k^0)^b f(k^0) \int \frac{d^d \mathbf{k}}{(2\pi)^d} \frac{1}{|\mathbf{k}|^{2a+1}} (\delta(k^0 + |\mathbf{k}|) + \delta(k^0 - |\mathbf{k}|)) \\ &= \frac{1}{4\pi} \int \frac{d^d \mathbf{k}}{(2\pi)^d} \frac{1}{|\mathbf{k}|^{2a+1}} \left(e^{i|\mathbf{k}|t} (-|\mathbf{k}|)^b f(-|\mathbf{k}|) + e^{-i|\mathbf{k}|t} |\mathbf{k}|^b f(|\mathbf{k}|) \right) \\ &= \frac{1}{4\pi} \int \frac{d^d \mathbf{k}}{(2\pi)^d} |\mathbf{k}|^{b-2a-1} \left(e^{-i|\mathbf{k}|t} f(|\mathbf{k}|) + (-1)^b e^{i|\mathbf{k}|t} f^*(|\mathbf{k}|) \right) \end{aligned} \quad (\text{C.49})$$

Inserting the results (C.47) and (C.49) into (C.46), we obtain the final result:

$$\begin{aligned}
I_R(d, a, b)[f](t) &= \int ds f(t+s) \int \frac{d^d k^0}{2\pi} e^{ik^0 s} \int \frac{d^d \mathbf{k}}{(2\pi)^d} \frac{1}{k^2 + i\epsilon} \frac{(k^0)^b}{|\mathbf{k}|^{2a}} \\
&= \frac{2^{-d} \pi^{1-\frac{d}{2}}}{\Gamma\left(\frac{d}{2}\right)} \frac{i^{b+2d-4a}}{\sin\left((2a-d)\frac{\pi}{2}\right)} \frac{d^{b+d-2a-2} f(t)}{dt^{b+d-2a-2}} \\
&\quad - \frac{i}{4} \int \frac{d^d \mathbf{k}}{(2\pi)^d} |\mathbf{k}|^{b-2a-1} \left(e^{-i|\mathbf{k}|t} f(|\mathbf{k}|) + (-1)^b e^{i|\mathbf{k}|t} f^*(|\mathbf{k}|) \right).
\end{aligned} \tag{C.50}$$

C.5 | Example of scalar integral evaluation using multi-loop techniques

In this section we show explicitly the application of some of the multi-loop quantum field theory techniques which we have presented in section 2.2.

In particular as an example we'll show how these techniques could have been employed to evaluate an integral of the kind

$$I^{ij}(\mathbf{p}) \equiv \int \frac{d^d \mathbf{k}}{(2\pi)^d} \frac{k^i k^j}{|\mathbf{k}|^2 |\mathbf{k} - \mathbf{p}|^2}, \tag{C.51}$$

which we encountered in section 4.3, see equation (4.37). In that section we already applied the first step in the evaluation procedure, which is the tensor decomposition of the integrand, to find in equation (4.38)

$$I^{ij}(\mathbf{p}) = F_1(\mathbf{p}) \delta^{ij} + F_2(\mathbf{p}) p^i p^j \tag{C.52}$$

with form factors given in equations (4.39):

$$F_1(\mathbf{p}) = \frac{1}{(d-1)} \frac{1}{|\mathbf{p}|^2} \int \frac{d^d \mathbf{k}}{(2\pi)^d} \frac{(|\mathbf{k}|^2 |\mathbf{p}|^2 - (\mathbf{k} \cdot \mathbf{p})^2)}{|\mathbf{k}|^2 |\mathbf{k} - \mathbf{p}|^2}, \tag{C.53a}$$

$$F_2(\mathbf{p}) = \frac{1}{(d-1)} \frac{1}{|\mathbf{p}|^4} \int \frac{d^d \mathbf{k}}{(2\pi)^d} \frac{(d(\mathbf{k} \cdot \mathbf{p})^2 - |\mathbf{k}|^2 |\mathbf{p}|^2)}{|\mathbf{k}|^2 |\mathbf{k} - \mathbf{p}|^2}. \tag{C.53b}$$

Therefore in the following we will be concerned with the evaluation of the class of scalar integrals of the kind

$$\int \frac{d^d \mathbf{k}}{(2\pi)^d} \frac{1}{D_1^{\alpha_1} D_2^{\alpha_2}} \tag{C.54}$$

where we introduced the same basis given by the denominators (4.40a) and (4.40b):

$$D_1 \equiv |\mathbf{k}|^2, \tag{C.55a}$$

$$D_2 \equiv |\mathbf{k} - \mathbf{p}|^2; \tag{C.55b}$$

In fact evaluating by this class of integrals we will be able to evaluate the aforementioned form factors, since they can be opportunely recast in this basis, see equations (4.42).

C.5.1 — Reduction to master integrals using integration-by-parts identities

In fact in practice one does not evaluate each integral in equations (4.42) as we did there, but instead employs relations between such integrals, called *integration-by-parts identities*, which allows to simplify the problem to the evaluation of fewer integrals, known as *master integrals*; we already covered this topic in section 2.2.4.

In the following then we will denote this specific class of integrals (C.54) which we're interested in as

$$j(\alpha_1, \alpha_2) \equiv \int \frac{d^d \mathbf{k}}{(2\pi)^d} \frac{1}{D_1^{\alpha_1} D_2^{\alpha_2}} \quad (\text{C.56})$$

For the case of this example, we can consider then generic vector given by $w^i = a k^i + b p^i$, then formula (2.32) reads:

$$\begin{aligned} d a j(\alpha_1, \alpha_2) &= d a \int \frac{d^d \mathbf{k}}{(2\pi)^d} \frac{1}{D_1^{\alpha_1} D_2^{\alpha_2}} = - \int \frac{d^d \mathbf{k}}{(2\pi)^d} (a k^i + b p^i) \frac{\partial}{\partial k^i} \left(\frac{1}{D_1^{\alpha_1} D_2^{\alpha_2}} \right) \\ &= +2 \int \frac{d^d \mathbf{k}}{(2\pi)^d} \left(\frac{\alpha_1 (a |\mathbf{k}|^2 + b (\mathbf{k} \cdot \mathbf{p}))}{D_1^{\alpha_1+1} D_2^{\alpha_2}} + \frac{\alpha_2 (a (|\mathbf{k}|^2 - \mathbf{k} \cdot \mathbf{p}) + b (\mathbf{k} \cdot \mathbf{p} - |\mathbf{p}|^2))}{D_1^{\alpha_1} D_2^{\alpha_2+1}} \right) \\ &= +2 \int \frac{d^d \mathbf{k}}{(2\pi)^d} \left(\frac{\alpha_1 (a D_1 + \frac{b}{2} (D_1 - D_2 + |\mathbf{p}|^2))}{D_1^{\alpha_1+1} D_2^{\alpha_2}} \right. \\ &\quad \left. + \frac{\alpha_2 \left(a D_1 + \frac{(b-a)}{2} (D_1 - D_2 + |\mathbf{p}|^2) - b |\mathbf{p}|^2 \right)}{D_1^{\alpha_1} D_2^{\alpha_2+1}} \right) \end{aligned} \quad (\text{C.57})$$

which using the notation (C.56) also reads:

$$\begin{aligned} &(\alpha_1 (2a + b) + \alpha_2 (a - b) - d a) j(\alpha_1, \alpha_2) + \alpha_1 b |\mathbf{p}|^2 j(\alpha_1 + 1, \alpha_2) \\ &- \alpha_2 (a + b) |\mathbf{p}|^2 j(\alpha_1, \alpha_2 + 1) - \alpha_1 b j(\alpha_1 + 1, \alpha_2 - 1) + \alpha_2 (a + b) j(\alpha_1 - 1, \alpha_2 + 1) = 0 . \end{aligned} \quad (\text{C.58})$$

Now we may choose arbitrary values of a and b , to obtain up to two independent relations; in particular, considering first $a = 1, b = 0$ and then $a = -b = 1$:

$$(2\alpha_1 + \alpha_2 - d) j(\alpha_1, \alpha_2) - \alpha_2 |\mathbf{p}|^2 j(\alpha_1, \alpha_2 + 1) + \alpha_2 j(\alpha_1 - 1, \alpha_2 + 1) = 0 , \quad (\text{C.59a})$$

$$(\alpha_1 + 2\alpha_2 - d) j(\alpha_1, \alpha_2) - \alpha_1 |\mathbf{p}|^2 j(\alpha_1 + 1, \alpha_2) + \alpha_1 j(\alpha_1 + 1, \alpha_2 - 1) = 0 . \quad (\text{C.59b})$$

In this case we could also look for the Euclidean version of the Lorentz invariance identities, which follows from the fact that the scalar integrals are invariant under a generic rotation $R \in SO(d)$ of each of the external momenta; so we could consider the action of an infinitesimal rotation, proceeding analogously to what was done in section 2.2.4: we would then obtain that the antisymmetric tensor $\omega^{\mu\nu}$ which parametrizes the infinitesimal Lorentz transformation would be substituted by the antisymmetric matrix $\Omega^{ij} = R^{ij} - \delta^{ij} + O(\Omega^2)$ which describes the action of the infinitesimal rotation, thereby in the end obtaining a relation similar to equation (2.35). Nonetheless in this particular example, because we have only a single vector, we can only produce a symmetric matrix $p^i p^j$ to contract the antisymmetric $p_j \frac{\partial}{\partial p^i} - p_i \frac{\partial}{\partial p^j}$ operator: the contraction then is identically zero, thereby giving no identity.

Instead we can find one more equality by employing the symmetry relations, which have been outlined in section 2.2.4. In particular in formula (C.56) we may perform the change of variables $\mathbf{k} \rightarrow \mathbf{k}' = \mathbf{p} - \mathbf{k}$, which has a trivial Jacobian, to obtain:

$$j(\alpha_1, \alpha_2) = \int \frac{d^d \mathbf{k}}{(2\pi)^d} \frac{1}{|\mathbf{k}|^{2\alpha_1} |\mathbf{k} - \mathbf{p}|^{2\alpha_2}} = \int \frac{d^d \mathbf{k}'}{(2\pi)^d} \frac{1}{|\mathbf{k}' - \mathbf{p}|^{2\alpha_1} |\mathbf{k}'|^{2\alpha_2}} = j(\alpha_2, \alpha_1) . \quad (\text{C.60})$$

These relations already tell us that the $j(\alpha_1, \alpha_2)$ function vanishes if any of its two arguments is zero: in fact choosing $\alpha_2 = 0$ and $\alpha_1 = \alpha$ in (C.59a) we $(2\alpha - d)j(\alpha, 0) = 0$, which recalling also (C.60) yields

$$j(\alpha, 0) = j(0, \alpha) = 0 \quad (\alpha \neq \frac{d}{2}) ; \quad (\text{C.61a})$$

$$j(0, 0) = 0. \quad (\text{C.61b})$$

By manipulating the three identities (C.59a), (C.59b) and (C.60), we can find a recurrence relation between $j(\alpha_1, \alpha_2)$ functions whose arguments are a single integer apart. To do so we start by shifting $\alpha_1 \rightarrow \alpha_1 + 1$ and $\alpha_2 \rightarrow \alpha_2 - 1$ in equation (C.59a), and then substituting the result into equation (C.59b) multiplied by $(2\alpha_1 + \alpha_2 + 1 - d)$, we obtain:

$$(\alpha_1 + \alpha_2 + 1 - d)(2\alpha_1 + 2\alpha_2 - d)j(\alpha_1, \alpha_2) - \alpha_1(2\alpha_1 + 2 - d)|\mathbf{p}|^2 j(\alpha_1 + 1, \alpha_2) = 0 \quad (\text{C.62a})$$

$$j(\alpha_1 + 1, \alpha_2) = \underbrace{\frac{(\alpha_1 + \alpha_2 + 1 - d)(2\alpha_1 + 2\alpha_2 - d)}{\alpha_1(2\alpha_1 + 2 - d)}}_{\equiv c_{\alpha_1}} \frac{1}{|\mathbf{p}|^2} j(\alpha_1, \alpha_2) \quad (\alpha_1 \neq 0, \alpha_1 \neq \frac{d}{2} - 1) \quad (\text{C.62b})$$

We may then choose $\alpha_1 = -1$ and $\alpha_2 = \alpha$, to obtain

$$j(\alpha, -1) = j(-1, \alpha) = \frac{d}{(d - \alpha)(d + 2 - 2\alpha)} |\mathbf{p}|^2 j(0, \alpha) = 0 \quad (\alpha \neq \frac{d}{2}, \alpha \neq d, \alpha \neq 1 + \frac{d}{2}); \quad (\text{C.63})$$

where we recalled (C.60) and (C.61a).

We are now interested in integer values of α_1, α_2 ; we can then recall iteratively formula (C.62b) assuming $\alpha_1 \geq 1$ to obtain:

$$\begin{aligned} j(\alpha_1, \alpha_2) &= \left(\prod_{q=1}^{\alpha_1-1} c_q \right) j(1, \alpha_2) = \left(\frac{\left(\prod_{q=1}^{\alpha_1-1} (q + \alpha_2 + 1 - d) \right) \left(\prod_{q=1}^{\alpha_1-1} (2q + 2\alpha_2 - d) \right)}{\left(\prod_{q=1}^{\alpha_1-1} q \right) \left(\prod_{q=1}^{\alpha_1-1} (2q + 2 - d) \right) \left(\prod_{q=1}^{\alpha_1-1} |\mathbf{p}|^2 \right)} \right) j(1, \alpha_2) \\ &= \frac{\Gamma(\alpha_1 + \alpha_2 + 1 - d)}{\Gamma(\alpha_2 + 2 - d)} \frac{\Gamma(\alpha_1 + \alpha_2 - \frac{d}{2})}{\Gamma(\alpha_2 + 1 - \frac{d}{2})} \frac{1}{\Gamma(\alpha_1)} \frac{\Gamma(2 - \frac{d}{2})}{\Gamma(\alpha_1 + 1 - \frac{d}{2})} |\mathbf{p}|^{-2(\alpha_1-1)} j(1, \alpha_2). \end{aligned} \quad (\text{C.64})$$

In fact, assuming $\frac{b}{a} \in \mathbb{N}$, we have that:

$$\prod_{q=1}^n (aq + b) = a^n \prod_{q=1}^n \left(q + \frac{b}{a} \right) = a^n \prod_{q=1+\frac{b}{a}}^{n+\frac{b}{a}} q = a^n \frac{(n + \frac{b}{a})!}{(\frac{b}{a})!} = a^n \frac{\Gamma(n + \frac{b}{a} + 1)}{\Gamma(\frac{b}{a} + 1)}, \quad (\text{C.65})$$

where we recalled the gamma function relation (B.4): using this generalization of the factorial, also called *Pochhammer symbol* $(x)_n \equiv \frac{\Gamma(x+n)}{\Gamma(x)}$, the aforementioned identity then holds also for $\frac{b}{a} \notin \mathbb{N}$.

We can then use the relation (C.60) in (C.64) to obtain

$$j(1, \alpha_2) = j(\alpha_2, 1) = \frac{\Gamma(\alpha_2 + 2 - d)}{\Gamma(\alpha_2) \Gamma(3 - d)} |\mathbf{p}|^{-2(\alpha_2-1)} j(1, 1); \quad (\text{C.66})$$

and finally, from (C.64) and (C.66) follows

$$j(\alpha_1, \alpha_2) = \frac{\Gamma(\alpha_1 + \alpha_2 + 1 - d)}{\Gamma(\alpha_1 + 1 - \frac{d}{2}) \Gamma(\alpha_2 + 1 - \frac{d}{2})} \frac{\Gamma(\alpha_1 + \alpha_2 - \frac{d}{2})}{\Gamma(\alpha_1) \Gamma(\alpha_2)} \frac{\Gamma(2 - \frac{d}{2})}{\Gamma(3 - d)} |\mathbf{p}|^{-2(\alpha_1 + \alpha_2 - 2)} j(1, 1) \quad (\text{C.67})$$

for $\alpha_1, \alpha_2 \geq 1$ and $\alpha_1, \alpha_2 \neq \frac{d}{2} - 1$.

C.5.2 — Master integral evaluation using the differential equations method

To evaluate the master integral $j(1, 1)$, we may employ the method of differential equations, presented in section 2.2.5. In particular we may derive the master integral with respect to the only external kinematic quantity, which is $|\mathbf{p}|^2$, obtaining:

$$\begin{aligned}
\frac{\partial}{\partial |\mathbf{p}|^2} (j(1, 1)) &= \int \frac{d^d \mathbf{k}}{(2\pi)^d} \frac{1}{|\mathbf{k}|^2} \frac{\partial}{\partial |\mathbf{p}|^2} \left(\frac{1}{|\mathbf{k} - \mathbf{p}|^2} \right) \\
&= - \int \frac{d^d \mathbf{k}}{(2\pi)^d} \frac{1}{|\mathbf{k}|^2 |\mathbf{k} - \mathbf{p}|^4} \frac{\partial}{\partial |\mathbf{p}|^2} (|\mathbf{k}|^2 - 2(\mathbf{k} \cdot \mathbf{p}) + |\mathbf{p}|^2) \\
&= \int \frac{d^d \mathbf{k}}{(2\pi)^d} \frac{1}{D_1 D_2^2} \left(\frac{(D_1 - D_2 + |\mathbf{p}|^2)}{2|\mathbf{p}|^2} - 1 \right) \\
&= \frac{1}{2|\mathbf{p}|^2} j(0, 2) - \frac{1}{2|\mathbf{p}|^2} j(1, 1) - \frac{1}{2} j(1, 2) = \frac{(d-4)}{2} |\mathbf{p}|^{-2} j(1, 1).
\end{aligned} \tag{C.68}$$

where we used the fact that it holds $\frac{\partial}{\partial |\mathbf{p}|^2} (\mathbf{k} \cdot \mathbf{p}) = \frac{1}{2|\mathbf{p}|} \frac{\partial}{\partial |\mathbf{p}|} (|\mathbf{k}||\mathbf{p}| \cos(\theta_{\mathbf{k}, \mathbf{p}})) = \frac{|\mathbf{k}||\mathbf{p}| \cos(\theta_{\mathbf{k}, \mathbf{p}})}{2|\mathbf{p}|^2} = \frac{\mathbf{k} \cdot \mathbf{p}}{2|\mathbf{p}|^2}$, and we used the relations previously obtained with integration-by-parts identities which imply for $j(0, 2) = 0$.

We may then solve the differential equation (C.68) by using the method of the separation of variables, i.e. denoting $|\mathbf{p}|^2 = x$ and $j(1, 1) = y$:

$$\frac{dy}{dx} = \frac{(d-4)y}{2x} \implies \int_{y_i}^{y_f} \frac{dy}{y} = \frac{(d-4)}{2} \int_{x_i}^{x_f} \frac{dx}{x} \implies \log \left(\frac{y_f}{y_i} \right) = \log \left(\frac{x_f^{\frac{(d-4)}{2}}}{x_i^{\frac{(d-4)}{2}}} \right) \tag{C.69}$$

which once exponentiated and chosen $x_f = |\mathbf{p}|^2$, $y_f = j(1, 1)[\mathbf{p}]$, with initial values $x_i = |\mathbf{p}_i|^2$ and $y_i = j(1, 1)[\mathbf{p}_i]$, yields

$$j(1, 1)[\mathbf{p}] = C(d) |\mathbf{p}|^{(d-4)}, \quad C(d) = \frac{j(1, 1)[\mathbf{p}_i]}{|\mathbf{p}_i|^{(d-4)}}; \tag{C.70}$$

in particular let us notice that $C(d)$ is the integration constant, which doesn't depend on the arbitrary value \mathbf{p}_i we may choose, and neither depends on α_1 nor α_2 ; hence it may depend only on the dimension of the space d . Let us point out that actually we already know the exact results of $C(d)$, as it is proportional to the scalar integral (C.7) which we previously computed. However we will proceed with the evaluation, in order to show alternative strategies to compute such quantity.

If we only need the result of our scalar integral at leading order in the dimension of the space(-time) d , we may then evaluate $C(d)$ for that specific value, e.g. $d = 3$, which possibly results in a simpler evaluation: for the example at hand, using the Feynman parametrization result (2.38) in formula (C.70), we obtain

$$\begin{aligned}
C(d=3) &= |\mathbf{p}_i| \int \frac{d^3 \mathbf{k}}{(2\pi)^3} \frac{1}{|\mathbf{k}|^2 |\mathbf{k} - \mathbf{p}_i|^2} = \frac{|\mathbf{p}_i|}{(2\pi)^3} \int_0^1 dx \int d^3 \mathbf{k} \frac{1}{(|\mathbf{k}|^2 + (x(1-x)|\mathbf{p}_i|^2))^2} \\
&= \frac{1}{(2\pi)^3} (4\pi) \underbrace{\int_0^{+\infty} dK \frac{K^2}{(K^2 + 1)^2}}_{= \frac{1}{2} \left(\arctan(K) - \frac{K}{K^2 + 1} \right) \Big|_0^{+\infty}} \underbrace{\int_0^1 dx (x(1-x))^{-\frac{1}{2}}}_{= B(\frac{1}{2}, \frac{1}{2})} = \frac{1}{2\pi^2} \frac{\pi}{4} \frac{\sqrt{\pi} \sqrt{\pi}}{1} = \frac{1}{8}; \tag{C.71}
\end{aligned}$$

where $B(a, b)$ is the beta function (B.10).

■ Complementary approach based on asymptotic behavior

There is still another complementary approach one could employ to evaluate such $C(d)$ constant, possibly in arbitrary d dimensions, as long as one knows the *asymptotic behavior* of the scalar integral for some of its parameters; this approach then is particularly useful when it's not possible to exactly evaluate the corresponding integral. This method, pointed out by reference [55], is based on the fact that the constant $C(d)$ is independent on the other parameters, e.g. $|\mathbf{p}_i|$, α_1 or α_2 ; therefore, if we know the asymptotic behavior of the scalar integral for particular values of these parameters, and we have a formula which relates such scalar integral to the $C(d)$ constant, then we may be able to determine the value of the latter unknown quantity by relating the two expression for the scalar integral: finally, by taking an appropriate limit, the expression involving only an asymptotic behavior will yield an exact result for the value of $C(d)$.

Let us show the application of this approach to the evaluation of the $j(1, 1)$ scalar integral we were considering, assuming for example to know the asymptotic behavior of the scalar integral $j(\alpha_1, 1)$ as $\alpha_1 \rightarrow +\infty$. Noticing that equation (C.70) relates $C(d)$ with $j(1, 1)$ and that formula (C.67) establishes a relation, exact in d and α_1 , between $j(1, 1)$ and $j(\alpha_1, \alpha_2)$; choosing $\alpha_1 = \alpha - 1 \in \mathbb{N}$ and $\alpha_2 = 1$ it holds

$$j(\alpha - 1, 1) = \frac{1}{\Gamma(\alpha - 1)} \frac{\Gamma(\alpha + 1 - d)}{\Gamma(3 - d)} |\mathbf{p}|^{d-2\alpha} C(d) . \quad (\text{C.72})$$

We may then study the asymptotic behavior of the scalar integral $j(\alpha_1, 1)$, starting from its definition (C.56), and employing the Feynman parameters presented in section 2.2.5: imposing $A = |\mathbf{k} - \mathbf{p}|^2$ and $B = |\mathbf{k}|^2$ in formula (2.37) we obtain

$$\begin{aligned} j(\alpha - 1, 1) &= \int \frac{d^d \mathbf{k}}{(2\pi)^d} \frac{1}{|\mathbf{k}|^{2\alpha-2} |\mathbf{k} - \mathbf{p}|^2} \\ &= \frac{\Gamma(\alpha)}{\Gamma(\alpha - 1) \Gamma(1)} \int_0^1 dx x^{\alpha-2} \int \frac{d^d \mathbf{k}}{(2\pi)^d} \frac{1}{(|\mathbf{k} - x\mathbf{p}|^2 + x(1-x)|\mathbf{p}|^2)^\alpha} \\ &= (\alpha - 1) |\mathbf{p}|^{d-2\alpha} \underbrace{\int_0^1 dx x^{\frac{d}{2}-2} (1-x)^{\frac{d}{2}-\alpha}}_{=B(\frac{d}{2}-1, \frac{d}{2}-\alpha+1)} \underbrace{\int \frac{d^d \mathbf{k}'}{(2\pi)^d (|\mathbf{k}'|^2 + 1)^\alpha}}_{\equiv Y(d, \alpha)} \quad (\text{C.73}) \\ &= (\alpha - 1) \frac{\Gamma(\frac{d}{2} - \alpha + 1) \Gamma(\frac{d}{2} - 1)}{\Gamma(d - \alpha)} |\mathbf{p}|^{d-2\alpha} Y(d, \alpha) \end{aligned}$$

where in the third line we performed the change of variables $\mathbf{k}' = (x(1-x)|\mathbf{p}|^2)^{-\frac{1}{2}} (\mathbf{k} - x\mathbf{p})$ with $d^d \mathbf{k} = (x(1-x)|\mathbf{p}|^2)^{\frac{d}{2}} d^d \mathbf{k}'$ and we recognized the integral representation (B.11) of the beta function (B.10).

Let us now assume to not know the exact value of the $Y(d, \alpha)$ integral, but only its asymptotic behavior as $\alpha \rightarrow +\infty$, which in fact is given by:

$$Y(d, \alpha) = (4\pi\alpha)^{-\frac{d}{2}} + O\left(\frac{1}{\alpha}\right) ; \quad (\text{C.74})$$

then, equating the relations (C.72) and (C.73) we obtain

$$C(d) = \Gamma(\alpha) \frac{\Gamma(\frac{d}{2} - \alpha + 1)}{\Gamma(d - \alpha) \Gamma(\alpha + 1 - d)} \Gamma\left(\frac{d}{2} - 1\right) \Gamma(3 - d) Y(d, \alpha) , \quad (\text{C.75})$$

where the dependence on the external $|\mathbf{p}|$ momenta dropped out as expected, and so should also the α -dependency on the right-hand side, for $\alpha \in \mathbb{N}$. Applying twice the identity (B.7a) of the gamma function, we can rewrite equation (C.75) as

$$C(d) = -\frac{\sin((\alpha-d)\pi)}{\sin((\alpha-\frac{d}{2})\pi)} \Gamma\left(\frac{d}{2}-1\right) \Gamma(3-d) \frac{\Gamma(\alpha)}{\Gamma(\alpha-\frac{d}{2})} Y(d, \alpha). \quad (\text{C.76})$$

Under our assumption of $\alpha \in \mathbb{N}$, it holds $\sin(\alpha\pi - x) = (-1)^{\alpha+1} \sin(x)$, therefore $\frac{\sin((\alpha-d)\pi)}{\sin((\alpha-\frac{d}{2})\pi)} = \frac{\sin(d\pi)}{\sin(\frac{d}{2}\pi)} = 2 \cos(\frac{d}{2}\pi)$. Then we may employ Stirling's approximations (B.7c) to evaluate the asymptotic behavior of the gamma functions, as $\alpha \rightarrow +\infty$, noticing also that it holds $\Gamma(\alpha + c) = \Gamma(\alpha) e^{c \log(\alpha)} + O(\frac{1}{\alpha})$:

$$C(d) = -2 \cos\left(\frac{d}{2}\pi\right) \Gamma\left(\frac{d}{2}-1\right) \Gamma(3-d) e^{\frac{d}{2} \log(\alpha)} Y(d, \alpha) + O\left(\frac{1}{\alpha}\right); \quad (\text{C.77})$$

and furthermore we may use the information (C.74) about the asymptotic behavior of the $Y(d, \alpha)$ function, which results in:

$$\begin{aligned} C(d) &= -2 \cos\left(\frac{d}{2}\pi\right) \Gamma\left(\frac{d}{2}-1\right) \Gamma(3-d) e^{\frac{d}{2} \log(\alpha)} \left((4\pi)^{-\frac{d}{2}} e^{-\frac{d}{2} \log(\alpha)}\right) + O\left(\frac{1}{\alpha}\right) \\ &= -2 (4\pi)^{-\frac{d}{2}} \cos\left(\frac{d}{2}\pi\right) \Gamma\left(\frac{d}{2}-1\right) \Gamma(3-d) + O\left(\frac{1}{\alpha}\right) \end{aligned} \quad (\text{C.78})$$

Finally we may take the limit $\alpha \rightarrow +\infty$ to obtain the exact result of the $C(d)$ integration constant, which now doesn't depend on α anymore, as expected; in fact we obtain

$$C(d) = -\frac{2}{(4\pi)^{\frac{d}{2}}} \cos\left(\frac{d}{2}\pi\right) \Gamma\left(\frac{d}{2}-1\right) \Gamma(3-d) = -\frac{2^{3-2d} \pi^{\frac{3-d}{2}}}{\sin(\frac{d}{2}\pi) \Gamma(\frac{d-1}{2})}; \quad (\text{C.79a})$$

$$C(d \approx 3) = \frac{1}{8} + \frac{1}{16}(\gamma - \log(16\pi))\epsilon + \frac{1}{384}(5\pi^2 + 6(\gamma - \log(16\pi))^2)\epsilon^2 + O(\epsilon^3); \quad (\text{C.79b})$$

where in formula (C.79b) we expanded the exact result (C.79a) around $d \equiv 3 + \epsilon$ using the series expansion (B.8) of the gamma function, with γ the Euler-Mascheroni constant (B.9): we can notice that this result is consistent with the independent calculation (C.71) of $C(d=3)$ we performed before.

We can also compare result (C.79a) to the other exact value of $C(d)$ we could have obtained by directly computing it from formula (C.70), in fact recalling the exact result (C.7) and applying the gamma function properties (B.7a) and (B.7b) we would have obtained

$$C(d) = I_{S,1L}(d, 1, 1)[\mathbf{p}_i] \mathbf{p}_i^{4-d} = \frac{1}{(4\pi)^{\frac{d}{2}}} \Gamma\left(2 - \frac{d}{2}\right) \frac{(\Gamma(\frac{d}{2}-1))^2}{\Gamma(d-2)} = -\frac{2^{3-2d} \pi^{\frac{3-d}{2}}}{\sin(\frac{d}{2}\pi) \Gamma(\frac{d-1}{2})} \quad (\text{C.80})$$

which exactly agrees with formula (C.79a).

We can then compare also the full result (C.67) for $j(\alpha_1, \alpha_2)$ with the corresponding result $I_{S,1L}$ which we evaluated in equation (C.7): in this case we find them to agree only for integer values of α_1 and α_2 : this is however to be expected, since we evaluated the integration by parts identities (which relate exponents separated by integer values) only starting from the master integral $j(\alpha_1 = 1, \alpha_2 = 1)$.

In practice this multi-loop techniques are extremely useful, if not necessary, when evaluating integrals with multiple loops: in fact there the direct evaluation of the integral may not be possible at all.

C.5.3 — Fourier integrals evaluation using tensor decomposition

We argue that it is possible to evaluate in full generality the tensorial generalizations of the scalar integral (C.31), like formula (C.33) derived in section C.3.1, using the tensor decomposition procedure presented in section 2.2.2: for any number of tensorial indices we may perform such a tensor decomposition procedure, the only difference being that we have to consider $\{\mathbf{x}_i\}$ instead of $\{\mathbf{p}_i\}$ as the external vectors from which we'll build the ansatz tensors to which the form factor will be proportional to.

In fact in the `Mathematica` code we used for the evaluation of conservative diagrams we employed this method to programmatically evaluate any needed tensorial generalization of the I_F integral (C.31).

EXTRACTS FROM THE MATHEMATICA CODE

In the following we present a few extracts from the code which we developed in Mathematica to evaluate generic conservative diagrams, and which we outlined in section 4.4.

The high level function which can be called to evaluate a diagram , and which implements the procedure outlined in section 4.3, as presented also in section 4.4, reads as follows:

```

automaticEvaluateDiagram[listOfFeynmanRules_, positiveMultiplicitySymmetryFactor_, showOutputDynamically_ : False] := Module[
{listDiagramExpression, tempListOfDiagrams, resultListOfDiagrams, DynamicalOutputInitialText},
DynamicalOutputInitialText="===== ";
Monitor[
automaticEvaluateDiagramProgressIndicator=0.;
PrintTemporary[DynamicalOutputInitialText, "Constructing Diagram"];
listDiagramExpression=MultiplyDiagramByPositiveSymmetryFactor[JoinFeynmanRulesInternal[listOfFeynmanRules], positiveMultiplicitySymmetryFactor];
automaticEvaluateDiagramProgressIndicator=0.05;
If[showOutputDynamically===True, PrintTemporary[listDiagramExpression]; Input["Initial diagram, press enter to continue"], ];

PrintTemporary[DynamicalOutputInitialText, "Evaluating diagram temporal sector"];
tempListOfDiagrams=automaticSolveTemporalSector[listDiagramExpression];
automaticEvaluateDiagramProgressIndicator=0.20;
If[showOutputDynamically===True, PrintTemporary[tempListOfDiagrams]; Input["Solved temporal sector, press enter to continue"], ];

PrintTemporary[DynamicalOutputInitialText, "Summing over worldline indices in diagrams and simplifying expressions"];
tempListOfDiagrams=automaticDiagramOperationsOnTimeAndWorldlinesVariables[tempListOfDiagrams];
automaticEvaluateDiagramProgressIndicator=0.30;
If[showOutputDynamically===True, PrintTemporary[tempListOfDiagrams]; Input["Summed over worldline indices and simplified diagrams expressions, press enter to continue"], ];

PrintTemporary[DynamicalOutputInitialText, "Enforcing Dirac deltas of the spatial components of the bulk momenta"];
tempListOfDiagrams=Table[automaticEnforceBulkSpatialMomentaDiracSingleDiagram[tableTempDiagram], {tableTempDiagram, tempListOfDiagrams}];
automaticEvaluateDiagramProgressIndicator=0.31;
If[showOutputDynamically===True, PrintTemporary[tempListOfDiagrams]; Input["Enforced Dirac deltas of the spatial components of the bulk momenta, press enter to continue"], ];

PrintTemporary[DynamicalOutputInitialText, "Preparing evaluation IBP loop and Fourier integrals"];
tempListOfDiagrams=separateSpatialMomentaAndOtherQuantitiesListOfDiagrams[tempListOfDiagrams];

tempListOfDiagrams=separateLoopMomentaAndFourierMomentaListOfDiagrams[tempListOfDiagrams];
automaticEvaluateDiagramProgressIndicator=0.35;
If[showOutputDynamically===True, PrintTemporary[tempListOfDiagrams]; Input["Prepared IBP and Loop integrations, press enter to continue"], ];

PrintTemporary[DynamicalOutputInitialText, "Evaluating IBP loop integrals"];
tempListOfDiagrams=AutomaticEvaluationIBPsLoopIntegrals[tempListOfDiagrams];
automaticEvaluateDiagramProgressIndicator=0.75;
If[showOutputDynamically===True, PrintTemporary[tempListOfDiagrams]; Input["Evaluated IBP loop integration, press enter to continue"], ];

PrintTemporary[DynamicalOutputInitialText, "Evaluating Fourier integrals in diagrams"];
tempListOfDiagrams=AutomaticEvaluationFourierIntegralsNewer[tempListOfDiagrams];
automaticEvaluateDiagramProgressIndicator=0.95;
If[showOutputDynamically===True, PrintTemporary[tempListOfDiagrams]; Input["Evaluated Fourier integrals, press enter to continue"], ];

PrintTemporary[DynamicalOutputInitialText, "Finishing diagrams evaluation"];
tempListOfDiagrams=listOfDiagramsFinishCalculationsInternal[tempListOfDiagrams, False];

PrintTemporary[DynamicalOutputInitialText, "Finished diagrams evaluation!"];
automaticEvaluateDiagramProgressIndicator=1.0;
resultListOfDiagrams=tempListOfDiagrams;
, ProgressIndicator[automaticEvaluateDiagramProgressIndicator];
resultListOfDiagrams
]

```

In particular we report also the code corresponding to one of the functions called therein, which evaluates the temporal sectors (as explained in sections 4.3 and 4.4). That is, it performs the needed manipulations of the expressions by exchanging temporal Fourier momenta k^0 for time derivatives ∂_t , by applying these time derivatives to the expressions, by performing the integrals over the temporal Fourier components k^0 to obtain time Dirac deltas $\delta(t' - t)$, and finally by performing the integral over the relevant time variables in order to enforce these Dirac delta. The code reads:

```

automaticSolveTemporalSectorSingleDiagramInternal[diagram] :=
Module[{nBulkTemporalMomentaDiracInitialTemp, numberOfVarInBulkMomentaTemporalDiracsTemp, indexOfBulkTemporalDiracDeltaTemp,
tempDiagramBulk, expandedDiagram, listHomogeneousTemporalDiagrams, tempDiagram, scalingTemp, forTempIndex, forTempIndexInner, byPartsTemporalListTemp,
listOfTemporalMomentaTemp, listOfReturnDiagrams, numberOfVarInTemporalDiracsTemp, nTemporalDiracInitialTemp, indexOfDiracDeltaTemp},
tempDiagramBulk = diagram;
PrintTemporary["Enforcing Dirac deltas of the temporal components of the bulk momenta"];
nBulkTemporalMomentaDiracInitialTemp = Length[diagram["integrations", "temporalBulkDiracDelta"]];
For[forTempIndexInner = 1, forTempIndexInner ≤ nBulkTemporalMomentaDiracInitialTemp, forTempIndexInner++,
numberOfVarInBulkMomentaTemporalDiracsTemp = Table[{tableTempIndex,
Length[Select[tempDiagramBulk["integrations", "temporalBulkDiracDelta"], Not[FreeQ[#, tempDiagramBulk["integrations", "momentaTemporalIntegrationsVars", tableTempIndex]] &]],
{tableTempIndex, Length[tempDiagramBulk["integrations", "momentaTemporalIntegrationsVars"]]}];
numberOfVarInBulkMomentaTemporalDiracsTemp = SortBy[numberOfVarInBulkMomentaTemporalDiracsTemp, Last];
numberOfVarInBulkMomentaTemporalDiracsTemp = Select[numberOfVarInBulkMomentaTemporalDiracsTemp, Not[#[[2]] == 0] &];
indexOfBulkTemporalDiracDeltaTemp = FirstPosition[tempDiagramBulk["integrations", "temporalBulkDiracDelta"], SelectFirst[tempDiagramBulk["integrations", "temporalBulkDiracDelta"],
Not[FreeQ[#, tempDiagramBulk["integrations", "momentaTemporalIntegrationsVars", numberOfVarInBulkMomentaTemporalDiracsTemp[[1, 1]]] &]]];
If[indexOfBulkTemporalDiracDeltaTemp == Missing["Not Found"], Print["Error automaticSolveTemporalSectorSingleDiagramInternal: momenta temporal Dirac delta not found"].];
tempDiagramBulk = EnforceBulkTemporalMomentaDiracDeltaSingleDirac[tempDiagramBulk, numberOfVarInBulkMomentaTemporalDiracsTemp[[1, 1], indexOfBulkTemporalDiracDeltaTemp[[1]]];
];
expandedDiagram = diagramExpandSumInExpressionsKey[tempDiagramBulk, "momentaTemporalCoeff"];
listOfReturnDiagrams = {};
listHomogeneousTemporalDiagrams = groupIntoSeparateListofDiagramsHomogeneousScalingInIntegrationVariables[expandedDiagram, "momentaTemporalIntegrationsVars", "momentaTemporalCoeff"];
(* Now each diagram should scale homogeneously wrt temporal momenta components, so I can integrate by parts! *)
For[forTempIndex = 1, forTempIndex ≤ Length[listHomogeneousTemporalDiagrams], forTempIndex++,
PrintTemporary["Expression ", ToString[forTempIndex], " / ", ToString[Length[listHomogeneousTemporalDiagrams]], ": integrating by parts temporal momenta component"];
tempDiagram = listHomogeneousTemporalDiagrams[[forTempIndex];
scalingTemp = Table[Exponent[tempDiagram["expressions", 1, "momentaTemporalCoeff", 1], tableTempVar], {tableTempVar, tempDiagram["integrations", "momentaTemporalIntegrationsVars"]];
byPartsTemporalListTemp = Flatten[
Table[constantArray[tempDiagram["integrations", "momentaTemporalIntegrationsVars", tableTempIndex], Floor[scalingTemp[[tableTempIndex]/2], {tableTempIndex, Length[scalingTemp]}];
Table[tempDiagram = transformTwoMomentaTemporalIntoTimeDoubleDerivative[tempDiagram, tableTempVar], {tableTempVar, byPartsTemporalListTemp}];
byPartsTemporalListTemp = Flatten[Table[constantArray[tempDiagram["integrations", "momentaTemporalIntegrationsVars", tableTempIndex],
scalingTemp[[tableTempIndex] - 2 * Floor[scalingTemp[[tableTempIndex]/2], {tableTempIndex, Length[scalingTemp]}];
Table[tempDiagram = transformOneMomentaTemporalIntoTimeSingleDerivative[tempDiagram, tableTempVar], {tableTempVar, byPartsTemporalListTemp}];
tempDiagram = diagramSimplifyExpressionsInternal[tempDiagram, True];
PrintTemporary["Expression ", ToString[forTempIndex], " / ",
ToString[Length[listHomogeneousTemporalDiagrams]], ": converting temporal momenta components in exponential into temporal Dirac deltas"];
listOfTemporalMomentaTemp = tempDiagram["integrations", "momentaTemporalIntegrationsVars"];
Table[tempDiagram = convertExponentialLargTemporalToDiracDeltaSingle[tempDiagram, 1], {tableTempVar, Length[listOfTemporalMomentaTemp]}];
PrintTemporary["Expression ", ToString[forTempIndex], " / ", ToString[Length[listHomogeneousTemporalDiagrams]], ": enforcing temporal Dirac deltas"];
(* May be better to select Dirac delta which appear only once first*);
nTemporalDiracInitialTemp = Length[tempDiagram["integrations", "temporalDiracDelta"];
For[forTempIndexInner = 1, forTempIndexInner ≤ nTemporalDiracInitialTemp, forTempIndexInner++,
numberOfVarInTemporalDiracsTemp =
Table[{tableTempIndex, Length[Select[tempDiagram["integrations", "temporalDiracDelta"], Not[FreeQ[#, tempDiagram["integrations", "timeIntegrationsVars", tableTempIndex]] &]],
{tableTempIndex, Length[tempDiagram["integrations", "timeIntegrationsVars"]]}];
numberOfVarInTemporalDiracsTemp = SortBy[numberOfVarInTemporalDiracsTemp, Last];
numberOfVarInTemporalDiracsTemp = Select[numberOfVarInTemporalDiracsTemp, Not[#[[2]] == 0] &];
indexOfDiracDeltaTemp = FirstPosition[tempDiagram["integrations", "temporalDiracDelta"],
SelectFirst[tempDiagram["integrations", "temporalDiracDelta"], Not[FreeQ[#, tempDiagram["integrations", "timeIntegrationsVars", numberOfVarInTemporalDiracsTemp[[1, 1]]] &]]];
If[indexOfDiracDeltaTemp == Missing["Not Found"], Print["Error automaticSolveTemporalSectorSingleDiagramInternal: Dirac delta not found"].];
tempDiagram = EnforceTimeDiracDeltaSingleDirac[tempDiagram, numberOfVarInTemporalDiracsTemp[[1, 1], indexOfDiracDeltaTemp[[1]]];
];
AppendTo[listOfReturnDiagrams, tempDiagram];
];
listOfReturnDiagrams
]

```

As an example, the evaluation of diagram $\mathcal{A}_{(2g)}$, which is a diagram first contributing at 2PN, and which we evaluated explicitly in 4.3, can be performed with the following code:

```

In[ ] := ruleWorldPhi = precomputeWorldlineGravityVertex[{1, 0, 0}, {kt1}, {kt01}, "ruleWorldPhi"];
In[ ] := ruleWorldA = precomputeWorldlineGravityVertex[{0, 1, 0}, {kt1}, {kt01}, "ruleWorldA"];
In[ ] := SetDirectory[NotebookDirectory[]];
listOfNeededScalingsEvalNonZero = Get["listOfNeededScalingsEvalNonZero.dat.m"];
listOfNeededScalingsEvalNonZero = listOfNeededScalingsEvalNonZero //. {i → i3, A → A};
In[ ] := ruleBulkPhi2A = precomputeBulkFeynmanRule[listOfNeededScalingsEvalNonZero[[7, 6, 1],
{kt2, kt3}, {kt1}, {}], {{kt02, kt03}, {kt01}, {}}, {0, {ti1}}, {0}, "ruleBulkPhi2A"];
In[ ] := loadAllPrecomputedIBPs
In[ ] := loadPrecomputedTensorDecompositions

```


The above lines of code have to be computed just once (along with other initialization lines) in order to load the relevant Feynman rules and the precomputed integration-by-parts basis and tensor decompositions. Then the actual computation of the diagram is performed by simply specifying the relevant Feynman rules and the propagators, obtaining an expression exact in d and in v , which can then be expanded also to obtain the relevant contributions to the potential at any post-Newtonian order.

```

in|-> diagram2gRules = {specializePrecomputedBulkFeynmanRule[ruleBulkPhi2A, {k2, k3, k1}, {k02, k03, k01}, {}, {{i1}}, {}]},
  specializePrecomputedWorldlineFeynmanRule[ruleWorldA, a, 1, {-k1}, {-k01}, {i2}], specializePrecomputedWorldlineFeynmanRule[ruleWorldPhi, b, 2, {-k2}, {-k02}, {}],
  specializePrecomputedWorldlineFeynmanRule[ruleWorldPhi, c, 3, {-k3}, {-k03}, {}], APropagator[k1, k01, -i1, -i2, 0], phiPropagator[k2, k02, 0], phiPropagator[k3, k03, 0]
Out|->
{{{ruleBulkPhi2A, {integrations -> {timeIntegrationsVars -> {}, momentaSpatialIntegrationsVars -> {},
  momentaTemporalIntegrationsVars -> {}, temporalDiracDelta -> {}, spatialBulkDiracDelta -> {k1+k2+k3}, temporalBulkDiracDelta -> {k01+k02+k03}},
  informations -> {worldlineIndices -> {}, temporalIndices -> {}, symmetryFactor -> {1/2}, positiveSymmetryFactorImposed -> {False}, IBLoopMomenta -> {}, FourierLoopMomenta -> {}},
  expressions -> {{(scalarCoeff -> {-2 f cdd / A}, vectorCoeff -> {delta_{e11}^{i1}}, momentaSpatialCoeff -> {k2^{e11}}, momentaTemporalCoeff -> {k03}, exponentialArgSpatial -> {}, exponentialArgTemporal -> {}),
  (scalarCoeff -> {-2 f cdd / A}, vectorCoeff -> {delta_{e11}^{i1}}, momentaSpatialCoeff -> {k3^{e11}}, momentaTemporalCoeff -> {k02}, exponentialArgSpatial -> {}, exponentialArgTemporal -> {})}},
{ruleWorldA, {integrations -> {timeIntegrationsVars -> {t1}, momentaSpatialIntegrationsVars -> {}, momentaTemporalIntegrationsVars -> {},
  temporalDiracDelta -> {}, spatialBulkDiracDelta -> {}, temporalBulkDiracDelta -> {}},
  informations -> {worldlineIndices -> {a}, temporalIndices -> {1}, symmetryFactor -> {1}, positiveSymmetryFactorImposed -> {False}, IBLoopMomenta -> {}, FourierLoopMomenta -> {}},
  expressions -> {{(scalarCoeff -> {i m a / (A sqrt(1 - (v a1_{i2}^2 + v a1_{i2}^2))}), vectorCoeff -> {v a1^{i2}}, momentaSpatialCoeff -> {},
  momentaTemporalCoeff -> {1}, exponentialArgSpatial -> {-i (k1^{i2} x a1_{i2})}, exponentialArgTemporal -> {i k01 t1}})},
{ruleWorldPhi, {integrations -> {timeIntegrationsVars -> {t2}, momentaSpatialIntegrationsVars -> {}, momentaTemporalIntegrationsVars -> {},
  temporalDiracDelta -> {}, spatialBulkDiracDelta -> {}, temporalBulkDiracDelta -> {}},
  informations -> {worldlineIndices -> {b}, temporalIndices -> {2}, symmetryFactor -> {1}, positiveSymmetryFactorImposed -> {False}, IBLoopMomenta -> {}, FourierLoopMomenta -> {}},
  expressions -> {{(scalarCoeff -> {i m b (2 + (-2 + cdd) (v b2_{i1}^2 + v b2_{i1}^2)) / (2 A sqrt(1 - (v b2_{i1}^2 + v b2_{i1}^2))}), vectorCoeff -> {1}, momentaSpatialCoeff -> {},
  momentaTemporalCoeff -> {1}, exponentialArgSpatial -> {-i (k2^{i1} v b2_{i1})}, exponentialArgTemporal -> {i k02 t2}})},
{ruleWorldPhi, {integrations -> {timeIntegrationsVars -> {t3}, momentaSpatialIntegrationsVars -> {}, momentaTemporalIntegrationsVars -> {},
  temporalDiracDelta -> {}, spatialBulkDiracDelta -> {}, temporalBulkDiracDelta -> {}},
  informations -> {worldlineIndices -> {c}, temporalIndices -> {3}, symmetryFactor -> {1}, positiveSymmetryFactorImposed -> {False}, IBLoopMomenta -> {}, FourierLoopMomenta -> {}},
  expressions -> {{(scalarCoeff -> {i m c (2 + (-2 + cdd) (v c3_{i1}^2 + v c3_{i1}^2)) / (2 A sqrt(1 - (v c3_{i1}^2 + v c3_{i1}^2))}), vectorCoeff -> {1}, momentaSpatialCoeff -> {},
  momentaTemporalCoeff -> {1}, exponentialArgSpatial -> {-i (k3^{i1} x c3_{i1})}, exponentialArgTemporal -> {i k03 t3}})},
{propagator, {integrations -> {timeIntegrationsVars -> {}, momentaSpatialIntegrationsVars -> {k1}, momentaTemporalIntegrationsVars -> {k01},
  temporalDiracDelta -> {}, spatialBulkDiracDelta -> {}, temporalBulkDiracDelta -> {}},
  informations -> {worldlineIndices -> {}, temporalIndices -> {}, symmetryFactor -> {1}, positiveSymmetryFactorImposed -> {False}, IBLoopMomenta -> {}, FourierLoopMomenta -> {}},
  expressions -> {{(scalarCoeff -> {1/2}, vectorCoeff -> {delta_{i1 i2}}, momentaSpatialCoeff -> {1 / (k_{i1 i2} k_{i1 i2})}, momentaTemporalCoeff -> {1}, exponentialArgSpatial -> {}, exponentialArgTemporal -> {})}},
{propagator, {integrations -> {timeIntegrationsVars -> {}, momentaSpatialIntegrationsVars -> {k2}, momentaTemporalIntegrationsVars -> {k02},
  temporalDiracDelta -> {}, spatialBulkDiracDelta -> {}, temporalBulkDiracDelta -> {}},
  informations -> {worldlineIndices -> {}, temporalIndices -> {}, symmetryFactor -> {1}, positiveSymmetryFactorImposed -> {False}, IBLoopMomenta -> {}, FourierLoopMomenta -> {}},
  expressions -> {{(scalarCoeff -> {i / (2 cdd)}, vectorCoeff -> {1}, momentaSpatialCoeff -> {1 / (k_{2 i1}^2 k_{2 i1}^2)}, momentaTemporalCoeff -> {1}, exponentialArgSpatial -> {}, exponentialArgTemporal -> {})}},
{propagator, {integrations -> {timeIntegrationsVars -> {}, momentaSpatialIntegrationsVars -> {k3}, momentaTemporalIntegrationsVars -> {k03},
  temporalDiracDelta -> {}, spatialBulkDiracDelta -> {}, temporalBulkDiracDelta -> {}},
  informations -> {worldlineIndices -> {}, temporalIndices -> {}, symmetryFactor -> {1}, positiveSymmetryFactorImposed -> {False}, IBLoopMomenta -> {}, FourierLoopMomenta -> {}},
  expressions -> {{(scalarCoeff -> {i / (2 cdd)}, vectorCoeff -> {1}, momentaSpatialCoeff -> {1 / (k_{3 i1}^2 k_{3 i1}^2)}, momentaTemporalCoeff -> {1}, exponentialArgSpatial -> {}, exponentialArgTemporal -> {})}},
in|-> diagram2gResult = automaticEvaluateDiagram[diagram2gRules, 2]
Out|->
{{(integrations ->
  {timeIntegrationsVars -> {t}, momentaSpatialIntegrationsVars -> {}, momentaTemporalIntegrationsVars -> {}, temporalDiracDelta -> {}, spatialBulkDiracDelta -> {}, temporalBulkDiracDelta -> {}},
  informations -> {worldlineIndices -> {}, temporalIndices -> {}, symmetryFactor -> {1/2}, positiveSymmetryFactorImposed -> {True}, IBLoopMomenta -> {}, FourierLoopMomenta -> {}},
  expressions -> {{(scalarCoeff ->
  {-(i 2^{-7-d} m1 m2 pi^{3-d} Csc[d/2] Gamma[-2+d] spr[r], r]^{1-d} (-spr[r], r] (1 - spr[v1, v1] (1 - spr[v2, v2]) (2 + (-2 + cdd) spr[v2, v2]) ((5 - 2 d) Gamma[2 - d/2] (2 (1 - d) m1 (2 + (-2 + cdd) spr[v1, v1]) (spr[v1, v1] + spr[v1, v2])
  sqrt(1 - spr[v2, v2]) + (-2 + d) m2 sqrt(1 - spr[v1, v1]) spr[v1, v2] (2 + (-2 + cdd) spr[v2, v2]) - 2 Gamma[3 - d/2] (2 (1 - d) m1 (2 + (-2 + cdd) spr[v1, v1]) (spr[v1, v1] + spr[v1, v2]) sqrt(1 - spr[v2, v2]) +
  (-2 + d) m2 sqrt(1 - spr[v1, v1]) spr[v1, v2] (2 + (-2 + cdd) spr[v2, v2]) + (-1 + d) m2 sqrt(1 - spr[v1, v1]) spr[v1, v2] (2 + (-2 + cdd) spr[v2, v2]) + spr[r, v1] ((5 - 2 d) d Gamma[2 - d/2] (1 - spr[v1, v1]
  (1 - spr[v2, v2]) (2 + (-2 + cdd) spr[v2, v2]) (2 (1 - d) m1 (spr[r, v1] + spr[r, v2]) (2 + (-2 + cdd) spr[v1, v1]) sqrt(1 - spr[v2, v2]) + (-2 + d) m2 spr[r, v2] sqrt(1 - spr[v1, v1]) (2 + (-2 + cdd) spr[v2, v2]) -
  2 Gamma[3 - d/2] (1 - spr[v1, v1]) (1 - spr[v2, v2]) (2 + (-2 + cdd) spr[v2, v2]) (2 (1 - d) m1 (spr[r, v1] + spr[r, v2]) (2 + (-2 + cdd) spr[v1, v1]) sqrt(1 - spr[v2, v2]) + (-2 + d) m2 spr[r, v2] sqrt(1 - spr[v1, v1])
  (2 + (-2 + cdd) spr[v2, v2]) + (-1 + d)^2 Gamma[2 - d/2] spr[r, r] (2 m1 spr[a1, v1] (2 - 2 cdd + (-2 + cdd) spr[v1, v1]) (1 - spr[v2, v2])^{3/2} (2 + (-2 + cdd) spr[v2, v2]) - m1 spr[a2, v2] (1 - spr[v1, v1])
  (2 + (-2 + cdd) spr[v1, v1]) sqrt(1 - spr[v2, v2]) (2 - 2 cdd + (-2 + cdd) spr[v2, v2]) + 2 m2 spr[a2, v2] (1 - spr[v1, v1])^{3/2} (2 + (-2 + cdd) spr[v2, v2]) (2 - 2 cdd + (-2 + cdd) spr[v2, v2]) + m1 sqrt(1 - spr[v2, v2])
  (2 spr[a1, v1] (2 - 2 cdd + (-2 + cdd) spr[v1, v1]) (1 - spr[v2, v2]) (2 + (-2 + cdd) spr[v2, v2]) + spr[a2, v2] (2 + (-2 + cdd) spr[v1, v1]) (2 + (-2 + cdd) spr[v1, v1]) (2 - 2 cdd + (-2 + cdd) spr[v2, v2]))))},
  momentaTemporalCoeff -> {1}, exponentialArgSpatial -> {}, exponentialArgTemporal ->
  {})}},
in|-> saveListOfDiagrams[diagram2gResult, "Diagram2g.m"]
in|-> diagram2gPotential = automaticObtainPotentialFromEvaluatedListofDiagrams[diagram2gResult, 2]
Out|->
G^2 m1 m2 ((m1 + m2) spr[v1, v2] - 4 m1 spr[v1, v1]^2 - 3 (m1 + m2) spr[v1, v1] spr[v2, v2] + 2 (m1 v1^2 + m2 v2^2 - 2 m2 spr[v2, v2] r^2))

```


BIBLIOGRAPHY

- [1] B. P. Abbott et al., *Observation of Gravitational Waves from a Binary Black Hole Merger*, Phys. Rev. Lett. **116** (6 2016), 061102, DOI: [10.1103/PhysRevLett.116.061102](https://doi.org/10.1103/PhysRevLett.116.061102).
- [2] B. P. Abbott et al., *Properties of the Binary Black Hole Merger GW150914*, Physical Review Letters **116**.24 (2016), DOI: [10.1103/physrevlett.116.241102](https://doi.org/10.1103/physrevlett.116.241102).
- [3] B. P. Abbott et al., *GWTC-1: A Gravitational-Wave Transient Catalog of Compact Binary Mergers Observed by LIGO and Virgo during the First and Second Observing Runs*, Phys. Rev. X **9** (3 2019), 031040, DOI: [10.1103/PhysRevX.9.031040](https://doi.org/10.1103/PhysRevX.9.031040).
- [4] R. Abbott et al., *GWTC-2: Compact Binary Coalescences Observed by LIGO and Virgo during the First Half of the Third Observing Run*, Phys. Rev. X **11** (2 2021), 021053, DOI: [10.1103/PhysRevX.11.021053](https://doi.org/10.1103/PhysRevX.11.021053).
- [5] The LIGO Scientific Collaboration et al., *GWTC-3: Compact Binary Coalescences Observed by LIGO and Virgo During the Second Part of the Third Observing Run*, 2021, DOI: [10.48550/ARXIV.2111.03606](https://doi.org/10.48550/ARXIV.2111.03606).
- [6] *LIGO/Virgo/KAGRA Public Alerts*, URL: <https://gracedb.ligo.org/superevents/public/04/> (visited on).
- [7] B. Bertotti, *On gravitational motion*, Nuovo Cim. **4**.4 (1956), 898–906, DOI: [10.1007/bf02746175](https://doi.org/10.1007/bf02746175).
- [8] R. P. Kerr, *The Lorentz-covariant approximation method in general relativity I*, Nuovo Cim. **13**.3 (1959), 469–491, DOI: [10.1007/bf02732767](https://doi.org/10.1007/bf02732767).
- [9] B. Bertotti and J. Plebanski, *Theory of gravitational perturbations in the fast motion approximation*, Annals Phys. **11**.2 (1960), 169–200, DOI: [10.1016/0003-4916\(60\)90132-9](https://doi.org/10.1016/0003-4916(60)90132-9).
- [10] L. Bel, T. Damour, N. Deruelle, J. Ibanez, and J. Martin, *Poincaré-invariant gravitational field and equations of motion of two pointlike objects: The postlinear approximation of general relativity*, Gen. Rel. Grav. **13** (1981), 963–1004, DOI: [10.1007/BF00756073](https://doi.org/10.1007/BF00756073).
- [11] T. Damour, *Gravitational scattering, post-Minkowskian approximation, and effective-one-body theory*, Phys. Rev. D **94**.10 (2016), DOI: [10.1103/physrevd.94.104015](https://doi.org/10.1103/physrevd.94.104015).
- [12] A. Einstein, L. Infeld, and B. Hoffmann, *The Gravitational Equations and the Problem of Motion*, Annals of Mathematics **39**.1 (1938), 65–100, ISSN: 0003486X, URL: <http://www.jstor.org/stable/1968714> (visited on 2023).
- [13] H. A. Lorentz and J. Droste, *The Motion of a System of Bodies under the Influence of their Mutual Attraction, According to Einstein’s Theory, Collected Papers: Volume V*, Dordrecht: Springer Netherlands, 1937, 330–355, ISBN: 978-94-015-3445-1, DOI: [10.1007/978-94-015-3445-1_11](https://doi.org/10.1007/978-94-015-3445-1_11).
- [14] T. Damour, P. Jaranowski, and G. Schäfer, *Dynamical invariants for general relativistic two-body systems at the third post-Newtonian approximation*, Phys. Rev. D **62**.4 (2000), DOI: [10.1103/physrevd.62.044024](https://doi.org/10.1103/physrevd.62.044024).

-
- [15] L. Blanchet and G. Faye, *On the equations of motion of point-particle binaries at the third post-Newtonian order*, Physics Letters A **271**.1-2 (2000), 58–64, DOI: [10.1016/S0375-9601\(00\)00360-1](https://doi.org/10.1016/S0375-9601(00)00360-1).
- [16] T. Damour, P. Jaranowski, and G. Schäfer, *Dimensional regularization of the gravitational interaction of point masses*, Physics Letters B **513**.1-2 (2001), 147–155, DOI: [10.1016/S0370-2693\(01\)00642-6](https://doi.org/10.1016/S0370-2693(01)00642-6).
- [17] T. Damour, P. Jaranowski, and G. Schäfer, *Nonlocal-in-time action for the fourth post-Newtonian conservative dynamics of two-body systems*, Phys. Rev. D **89**.6 (2014), DOI: [10.1103/PhysRevD.89.064058](https://doi.org/10.1103/PhysRevD.89.064058).
- [18] P. Jaranowski and G. Schäfer, *Derivation of local-in-time fourth post-Newtonian ADM Hamiltonian for spinless compact binaries*, Phys. Rev. D **92**.12 (2015), DOI: [10.1103/PhysRevD.92.124043](https://doi.org/10.1103/PhysRevD.92.124043).
- [19] L. Bernard, L. Blanchet, A. Bohé, G. Faye, and S. Marsat, *Energy and periastron advance of compact binaries on circular orbits at the fourth post-Newtonian order*, Phys. Rev. D **95**.4 (2017), DOI: [10.1103/PhysRevD.95.044026](https://doi.org/10.1103/PhysRevD.95.044026).
- [20] D. Bini, T. Damour, and A. Gerialico, *Novel Approach to Binary Dynamics: Application to the Fifth Post-Newtonian Level*, Physical Review Letters **123**.23 (2019), DOI: [10.1103/PhysRevLett.123.231104](https://doi.org/10.1103/PhysRevLett.123.231104).
- [21] D. Bini, T. Damour, and A. Gerialico, *Sixth post-Newtonian nonlocal-in-time dynamics of binary systems*, Phys. Rev. D **102**.8 (2020), DOI: [10.1103/PhysRevD.102.084047](https://doi.org/10.1103/PhysRevD.102.084047).
- [22] D. Bini, T. Damour, and A. Gerialico, *Binary dynamics at the fifth and fifth-and-a-half post-Newtonian orders*, Phys. Rev. D **102**.2 (2020), DOI: [10.1103/PhysRevD.102.024062](https://doi.org/10.1103/PhysRevD.102.024062).
- [23] D. Bini, T. Damour, A. Gerialico, S. Laporta, and P. Mastrolia, *Gravitational scattering at the seventh order in G : Nonlocal contribution at the sixth post-Newtonian accuracy*, Phys. Rev. D **103**.4 (2021), DOI: [10.1103/PhysRevD.103.044038](https://doi.org/10.1103/PhysRevD.103.044038).
- [24] Y. Mino, M. Sasaki, and T. Tanaka, *Gravitational radiation reaction to a particle motion*, Phys. Rev. D **55**.6 (1997), 3457–3476, DOI: [10.1103/PhysRevD.55.3457](https://doi.org/10.1103/PhysRevD.55.3457).
- [25] T. C. Quinn and R. M. Wald, *Axiomatic approach to electromagnetic and gravitational radiation reaction of particles in curved spacetime*, Phys. Rev. D **56**.6 (1997), 3381–3394, DOI: [10.1103/PhysRevD.56.3381](https://doi.org/10.1103/PhysRevD.56.3381).
- [26] F. Pretorius, *Evolution of Binary Black-Hole Spacetimes*, Physical Review Letters **95**.12 (2005), DOI: [10.1103/PhysRevLett.95.121101](https://doi.org/10.1103/PhysRevLett.95.121101).
- [27] M. Campanelli, C. O. Lousto, P. Marronetti, and Y. Zlochower, *Accurate Evolutions of Orbiting Black-Hole Binaries without Excision*, Phys. Rev. Lett. **96** (11 2006), 111101, DOI: [10.1103/PhysRevLett.96.111101](https://doi.org/10.1103/PhysRevLett.96.111101).
- [28] J. G. Baker, J. Centrella, D.-I. Choi, M. Koppitz, and J. van Meter, *Gravitational-Wave Extraction from an Inspiral Configuration of Merging Black Holes*, Phys. Rev. Lett. **96** (11 2006), 111102, DOI: [10.1103/PhysRevLett.96.111102](https://doi.org/10.1103/PhysRevLett.96.111102).
- [29] M. Boyle et al., *The SXS collaboration catalog of binary black hole simulations*, Classical and Quantum Gravity **36**.19 (2019), 195006, DOI: [10.1088/1361-6382/ab34e2](https://doi.org/10.1088/1361-6382/ab34e2).
- [30] A. Buonanno and T. Damour, *Effective one-body approach to general relativistic two-body dynamics*, Phys. Rev. D **59**.8 (1999), DOI: [10.1103/PhysRevD.59.084006](https://doi.org/10.1103/PhysRevD.59.084006).
- [31] A. Buonanno and T. Damour, *Transition from inspiral to plunge in binary black hole coalescences*, Phys. Rev. D **62** (6 2000), 064015, DOI: [10.1103/PhysRevD.62.064015](https://doi.org/10.1103/PhysRevD.62.064015).
- [32] T. Regge and J. A. Wheeler, *Stability of a Schwarzschild Singularity*, Phys. Rev. **108** (4 1957), 1063–1069, DOI: [10.1103/PhysRev.108.1063](https://doi.org/10.1103/PhysRev.108.1063).

- [33] F. J. Zerilli, *Gravitational Field of a Particle Falling in a Schwarzschild Geometry Analyzed in Tensor Harmonics*, Phys. Rev. D **2** (10 1970), 2141–2160, DOI: [10.1103/PhysRevD.2.2141](https://doi.org/10.1103/PhysRevD.2.2141).
- [34] C. V. Vishveshwara, *Stability of the Schwarzschild Metric*, Phys. Rev. D **1** (10 1970), 2870–2879, DOI: [10.1103/PhysRevD.1.2870](https://doi.org/10.1103/PhysRevD.1.2870).
- [35] V. Moncrief, *Gravitational perturbations of spherically symmetric systems. I. The exterior problem*, Annals of Physics **88.2** (1974), 323–342, ISSN: 0003-4916, DOI: [https://doi.org/10.1016/0003-4916\(74\)90173-0](https://doi.org/10.1016/0003-4916(74)90173-0).
- [36] L. Blanchet, *Gravitational Radiation from Post-Newtonian Sources and Inspiralling Compact Binaries*, Living Rev. Relativ. **17.1** (2014), DOI: [10.12942/lrr-2014-2](https://doi.org/10.12942/lrr-2014-2).
- [37] A. Buonanno and B. S. Sathyaprakash, *Sources of Gravitational Waves: Theory and Observations*, 2014, DOI: [10.48550/ARXIV.1410.7832](https://doi.org/10.48550/ARXIV.1410.7832).
- [38] M. Levi, *Effective field theories of post-Newtonian gravity: a comprehensive review**, Reports on Progress in Physics **83.7** (2020), 075901, DOI: [10.1088/1361-6633/ab12bc](https://doi.org/10.1088/1361-6633/ab12bc).
- [39] A. Buonanno et al., *Snowmass White Paper: Gravitational Waves and Scattering Amplitudes*, 2022, DOI: [10.48550/ARXIV.2204.05194](https://doi.org/10.48550/ARXIV.2204.05194).
- [40] B. Bertotti and J. Plebanski, *Theory of gravitational perturbations in the fast motion approximation*, Annals of Physics **11.2** (1960), 169–200, ISSN: 0003-4916, DOI: [https://doi.org/10.1016/0003-4916\(60\)90132-9](https://doi.org/10.1016/0003-4916(60)90132-9).
- [41] N. D. H. Dass and V. Soni, *Feynman graph derivation of the Einstein quadrupole formula*, Journal of Physics A: Mathematical and General **15.2** (1982), 473, DOI: [10.1088/0305-4470/15/2/019](https://doi.org/10.1088/0305-4470/15/2/019).
- [42] T. Damour and G. Esposito-Farè se, *Testing gravity to second post-Newtonian order: A field-theory approach*, Phys. Rev. D **53.10** (1996), 5541–5578, DOI: [10.1103/physrevd.53.5541](https://doi.org/10.1103/physrevd.53.5541).
- [43] W. D. Goldberger and I. Z. Rothstein, *Effective field theory of gravity for extended objects*, Phys. Rev. D **73.10** (2006), DOI: [10.1103/physrevd.73.104029](https://doi.org/10.1103/physrevd.73.104029).
- [44] S. Foffa, P. Mastrolia, R. Sturani, and C. Sturm, *Effective field theory approach to the gravitational two-body dynamics at fourth post-Newtonian order and quintic in the Newton constant*, Phys. Rev. D **95.10** (2017), DOI: [10.1103/physrevd.95.104009](https://doi.org/10.1103/physrevd.95.104009).
- [45] K. Chetyrkin and F. Tkachov, *Integration by parts: The algorithm to calculate β -functions in 4 loops*, Nuclear Physics B **192.1** (1981), 159–204, ISSN: 0550-3213, DOI: [https://doi.org/10.1016/0550-3213\(81\)90199-1](https://doi.org/10.1016/0550-3213(81)90199-1).
- [46] F. Tkachov, *A theorem on analytical calculability of 4-loop renormalization group functions*, Physics Letters B **100.1** (1981), 65–68, ISSN: 0370-2693, DOI: [https://doi.org/10.1016/0370-2693\(81\)90288-4](https://doi.org/10.1016/0370-2693(81)90288-4).
- [47] Laporta, International Journal of Modern Physics A **15** (2000), 5087, DOI: [10.1016/s0217-751x\(00\)00215-7](https://doi.org/10.1016/s0217-751x(00)00215-7).
- [48] Laporta, International Journal of Modern Physics A **15** (2000), 5087, DOI: [10.1016/s0217-751x\(00\)00215-7](https://doi.org/10.1016/s0217-751x(00)00215-7).
- [49] S. Laporta, *Calculation of master integrals by difference equations*, Physics Letters B **504.1-2** (2001), 188–194, DOI: [10.1016/s0370-2693\(01\)00256-8](https://doi.org/10.1016/s0370-2693(01)00256-8).
- [50] A. Kotikov, *Differential equations method. New technique for massive Feynman diagram calculation*, Physics Letters B **254.1** (1991), 158–164, ISSN: 0370-2693, DOI: [https://doi.org/10.1016/0370-2693\(91\)90413-K](https://doi.org/10.1016/0370-2693(91)90413-K).
- [51] A. Kotikov, *Differential equations method: the calculation of vertex-type Feynman diagrams*, Physics Letters B **259.3** (1991), 314–322, ISSN: 0370-2693, DOI: [https://doi.org/10.1016/0370-2693\(91\)90834-D](https://doi.org/10.1016/0370-2693(91)90834-D).

- [52] A. Kotikov, *Differential equation method. The calculation of N -point Feynman diagrams*, Physics Letters B **267**.1 (1991), 123–127, ISSN: 0370-2693, DOI: [https://doi.org/10.1016/0370-2693\(91\)90536-Y](https://doi.org/10.1016/0370-2693(91)90536-Y).
- [53] E. Remiddi, *Differential equations for Feynman graph amplitudes*, Il Nuovo Cimento A **110**.12 (1997), 1435–1452, DOI: [10.1007/bf03185566](https://doi.org/10.1007/bf03185566).
- [54] T. Gehrmann and E. Remiddi, *Differential equations for two-loop four-point functions*, Nuclear Physics B **580**.1-2 (2000), 485–518, DOI: [10.1016/s0550-3213\(00\)00223-6](https://doi.org/10.1016/s0550-3213(00)00223-6).
- [55] M. Argeri and P. Mastrolia, *Feynman Diagrams and Differential Equations*, International Journal of Modern Physics A **22**.24 (2007), 4375–4436, DOI: [10.1142/s0217751x07037147](https://doi.org/10.1142/s0217751x07037147).
- [56] M. Argeri et al., *Magnus and Dyson series for Master Integrals*, Journal of High Energy Physics **2014**.3 (2014), DOI: [10.1007/jhep03\(2014\)082](https://doi.org/10.1007/jhep03(2014)082).
- [57] S. Foffa and R. Sturani, *Effective field theory calculation of conservative binary dynamics at third post-Newtonian order*, Phys. Rev. D **84**.4 (2011), DOI: [10.1103/physrevd.84.044031](https://doi.org/10.1103/physrevd.84.044031).
- [58] S. Foffa and R. Sturani, *Dynamics of the gravitational two-body problem at fourth post-Newtonian order and at quadratic order in the Newton constant*, Phys. Rev. D **87**.6 (2013), DOI: [10.1103/physrevd.87.064011](https://doi.org/10.1103/physrevd.87.064011).
- [59] S. Foffa, P. Mastrolia, R. Sturani, C. Sturm, and W. J. T. Bobadilla, *Static Two-Body Potential at Fifth Post-Newtonian Order*, Physical Review Letters **122**.24 (2019), DOI: [10.1103/physrevlett.122.241605](https://doi.org/10.1103/physrevlett.122.241605).
- [60] S. Foffa, R. A. Porto, I. Rothstein, and R. Sturani, *Conservative dynamics of binary systems to fourth post-Newtonian order in the EFT approach. II. Renormalized Lagrangian*, Phys. Rev. D **100**.2 (2019), DOI: [10.1103/physrevd.100.024048](https://doi.org/10.1103/physrevd.100.024048).
- [61] J. Blümlein, A. Maier, P. Marquard, and G. Schäfer, *Fourth post-Newtonian Hamiltonian dynamics of two-body systems from an effective field theory approach*, Nuclear Physics B **955** (2020), 115041, DOI: [10.1016/j.nuclphysb.2020.115041](https://doi.org/10.1016/j.nuclphysb.2020.115041).
- [62] S. Foffa, P. Mastrolia, R. Sturani, C. Sturm, and W. J. T. Bobadilla, *Calculating the static gravitational two-body potential to fifth post-Newtonian order with Feynman diagrams*, 2019, DOI: [10.48550/ARXIV.1912.04720](https://doi.org/10.48550/ARXIV.1912.04720).
- [63] S. Foffa, P. Mastrolia, R. Sturani, C. Sturm, and W. J. T. Bobadilla, *Static Two-Body Potential at Fifth Post-Newtonian Order*, Physical Review Letters **122**.24 (2019), DOI: [10.1103/physrevlett.122.241605](https://doi.org/10.1103/physrevlett.122.241605).
- [64] J. Blümlein, A. Maier, and P. Marquard, *Five-loop static contribution to the gravitational interaction potential of two point masses*, Physics Letters B **800** (2020), 135100, ISSN: 0370-2693, DOI: <https://doi.org/10.1016/j.physletb.2019.135100>.
- [65] J. Blümlein, A. Maier, P. Marquard, and G. Schäfer, *The fifth-order post-Newtonian Hamiltonian dynamics of two-body systems from an effective field theory approach*, Nuclear Physics B **983** (2022), 115900, DOI: [10.1016/j.nuclphysb.2022.115900](https://doi.org/10.1016/j.nuclphysb.2022.115900).
- [66] J. F. Donoghue, *General relativity as an effective field theory: The leading quantum corrections*, Phys. Rev. D **50**.6 (1994), 3874–3888, DOI: [10.1103/physrevd.50.3874](https://doi.org/10.1103/physrevd.50.3874).
- [67] D. Neill and I. Z. Rothstein, *Classical space-times from the S -matrix*, Nuclear Physics B **877**.2 (2013), 177–189, DOI: [10.1016/j.nuclphysb.2013.09.007](https://doi.org/10.1016/j.nuclphysb.2013.09.007).
- [68] N. Bjerrum-Bohr, P. H. Damgaard, G. Festuccia, L. Plantè, and P. Vanhove, *General Relativity from Scattering Amplitudes*, Physical Review Letters **121**.17 (2018), DOI: [10.1103/physrevlett.121.171601](https://doi.org/10.1103/physrevlett.121.171601).
- [69] C. Cheung, I. Z. Rothstein, and M. P. Solon, *From Scattering Amplitudes to Classical Potentials in the Post-Minkowskian Expansion*, Phys. Rev. Lett. **121** (25 2018), 251101, DOI: [10.1103/PhysRevLett.121.251101](https://doi.org/10.1103/PhysRevLett.121.251101).

- [70] D. A. Kosower, B. Maybee, and D. O’Connell, *Amplitudes, observables, and classical scattering*, Journal of High Energy Physics **2019.2** (2019), DOI: [10.1007/jhep02\(2019\)137](https://doi.org/10.1007/jhep02(2019)137).
- [71] G. Kälin and R. A. Porto, *From boundary data to bound states*, Journal of High Energy Physics **2020.1** (2020), DOI: [10.1007/jhep01\(2020\)072](https://doi.org/10.1007/jhep01(2020)072).
- [72] G. Kälin and R. A. Porto, *From boundary data to bound states. Part II. Scattering angle to dynamical invariants (with twist)*, Journal of High Energy Physics **2020.2** (2020), DOI: [10.1007/jhep02\(2020\)120](https://doi.org/10.1007/jhep02(2020)120).
- [73] G. Kälin and R. A. Porto, *Post-Minkowskian effective field theory for conservative binary dynamics*, Journal of High Energy Physics **2020.11** (2020), DOI: [10.1007/jhep11\(2020\)106](https://doi.org/10.1007/jhep11(2020)106).
- [74] Z. Bern et al., *Black hole binary dynamics from the double copy and effective theory*, Journal of High Energy Physics **2019.10** (2019), DOI: [10.1007/jhep10\(2019\)206](https://doi.org/10.1007/jhep10(2019)206).
- [75] P. D. Vecchia, C. Heissenberg, R. Russo, and G. Veneziano, *The eikonal approach to gravitational scattering and radiation at $O(G^3)$* , Journal of High Energy Physics **2021.7** (2021), DOI: [10.1007/jhep07\(2021\)169](https://doi.org/10.1007/jhep07(2021)169).
- [76] C. Dlapa, G. Kälin, Z. Liu, and R. A. Porto, *Conservative Dynamics of Binary Systems at Fourth Post-Minkowskian Order in the Large-Eccentricity Expansion*, Physical Review Letters **128.16** (2022), DOI: [10.1103/physrevlett.128.161104](https://doi.org/10.1103/physrevlett.128.161104).
- [77] J. Blümlein, A. Maier, P. Marquard, and G. Schäfer, *Testing binary dynamics in gravity at the sixth post-Newtonian level*, Physics Letters B **807** (2020), 135496, DOI: [10.1016/j.physletb.2020.135496](https://doi.org/10.1016/j.physletb.2020.135496).
- [78] J. Blümlein, A. Maier, P. Marquard, and G. Schäfer, *Gravity in binary systems at the fifth and sixth post-Newtonian order*, 2022, arXiv: [2208.04552](https://arxiv.org/abs/2208.04552) [[gr-qc](#)].
- [79] M. Levi and F. Teng, *NLO gravitational quartic-in-spin interaction*, Journal of High Energy Physics **2021.1** (2021), DOI: [10.1007/jhep01\(2021\)066](https://doi.org/10.1007/jhep01(2021)066).
- [80] M. K. Mandal, P. Mastrolia, R. Patil, and J. Steinhoff, *Gravitational Spin-Orbit Hamiltonian at NNNLO in the post-Newtonian framework*, 2022, DOI: [10.48550/ARXIV.2209.00611](https://doi.org/10.48550/ARXIV.2209.00611).
- [81] M. K. Mandal, P. Mastrolia, R. Patil, and J. Steinhoff, *Gravitational quadratic-in-spin Hamiltonian at NNNLO in the post-Newtonian framework*, JHEP **07** (2023), 128, DOI: [10.1007/JHEP07\(2023\)128](https://doi.org/10.1007/JHEP07(2023)128).
- [82] J.-W. Kim, M. Levi, and Z. Yin, *Quadratic-in-spin interactions at fifth post-Newtonian order probe new physics*, Physics Letters B **834** (2022), 137410, ISSN: 0370-2693, DOI: <https://doi.org/10.1016/j.physletb.2022.137410>.
- [83] M. K. Mandal, P. Mastrolia, H. O. Silva, R. Patil, and J. Steinhoff, *Gravitoelectric dynamical tides at second post-Newtonian order* (2023), arXiv: [2304.02030](https://arxiv.org/abs/2304.02030) [[hep-th](#)].
- [84] M. K. Mandal, P. Mastrolia, H. O. Silva, R. Patil, and J. Steinhoff, *Renormalizing Love: tidal effects at the third post-Newtonian order* (2023), arXiv: [2308.01865](https://arxiv.org/abs/2308.01865) [[hep-th](#)].
- [85] M. Punturo et al., *The Einstein Telescope: a third-generation gravitational wave observatory*, Classical and Quantum Gravity **27.19** (2010), 194002, DOI: [10.1088/0264-9381/27/19/194002](https://doi.org/10.1088/0264-9381/27/19/194002).
- [86] M. Maggiore et al., *Science case for the Einstein telescope*, J. Cosmol. Astropart. Phys. **2020.03** (2020), 050–050, DOI: [10.1088/1475-7516/2020/03/050](https://doi.org/10.1088/1475-7516/2020/03/050).
- [87] M. Branchesi et al., *Science with the Einstein Telescope: a comparison of different designs*, J. Cosmol. Astropart. Phys. **2023.07** (2023), 068, DOI: [10.1088/1475-7516/2023/07/068](https://doi.org/10.1088/1475-7516/2023/07/068).
- [88] D. Reitze et al., *Cosmic Explorer: The U.S. Contribution to Gravitational-Wave Astronomy beyond LIGO*, 2019, arXiv: [1907.04833](https://arxiv.org/abs/1907.04833) [[astro-ph.IM](#)].
- [89] M. Evans et al., *A Horizon Study for Cosmic Explorer: Science, Observatories, and Community*, 2021, arXiv: [2109.09882](https://arxiv.org/abs/2109.09882) [[astro-ph.IM](#)].

- [90] M. Evans et al., *Cosmic Explorer: A Submission to the NSF MPSAC ngGW Subcommittee*, 2023, arXiv: [2306.13745](https://arxiv.org/abs/2306.13745) [[astro-ph.IM](#)].
- [91] P. Amaro-Seoane et al., *Laser Interferometer Space Antenna*, 2017, DOI: [10.48550/ARXIV.1702.00786](https://doi.org/10.48550/ARXIV.1702.00786).
- [92] B. Abbott et al., *Tests of General Relativity with GW150914*, Physical Review Letters **116**.22 (2016), DOI: [10.1103/physrevlett.116.221101](https://doi.org/10.1103/physrevlett.116.221101).
- [93] B. Abbott et al., *Tests of General Relativity with GW170817*, Physical Review Letters **123**.1 (2019), DOI: [10.1103/physrevlett.123.011102](https://doi.org/10.1103/physrevlett.123.011102).
- [94] B. Abbott et al., *Tests of general relativity with the binary black hole signals from the LIGO-Virgo catalog GWTC-1*, Phys. Rev. D **100**.10 (2019), DOI: [10.1103/physrevd.100.104036](https://doi.org/10.1103/physrevd.100.104036).
- [95] R. Abbott et al., *Tests of general relativity with binary black holes from the second LIGO-Virgo gravitational-wave transient catalog*, Phys. Rev. D **103**.12 (2021), DOI: [10.1103/physrevd.103.122002](https://doi.org/10.1103/physrevd.103.122002).
- [96] The LIGO Scientific Collaboration and the Virgo Collaboration and the KAGRA Collaboration et al., *Tests of General Relativity with GWTC-3*, 2021, arXiv: [2112.06861](https://arxiv.org/abs/2112.06861) [[gr-qc](#)].
- [97] A. Einstein, *Die Feldgleichungen der Gravitation*, Sitzungsber. K. Preuss. Akad. Wiss. (1915), 844–847, URL: <https://ui.adsabs.harvard.edu/abs/1915SPAW.....844E>.
- [98] A. Einstein, *Die Grundlage der allgemeinen Relativitätstheorie*, Annalen der Physik **354**.7 (1916), 769–822, DOI: [10.1002/andp.19163540702](https://doi.org/10.1002/andp.19163540702).
- [99] S. Weinberg, *Gravitation and cosmology : principles and applications of the general theory of relativity*, eng, New York: Wiley, 1972, ISBN: 9780471925675.
- [100] S. M. Carroll, *Spacetime and Geometry: An Introduction to General Relativity*, Cambridge University Press, 2019, DOI: [10.1017/9781108770385](https://doi.org/10.1017/9781108770385).
- [101] M. P. Hobson, G. P. Efstathiou, and A. N. Lasenby, *General Relativity: An Introduction for Physicists*, Cambridge University Press, 2006, DOI: [10.1017/CB09780511790904](https://doi.org/10.1017/CB09780511790904).
- [102] E. D. Casola, S. Liberati, and S. Sonogo, *Nonequivalence of equivalence principles*, American Journal of Physics **83**.1 (2015), 39–46, DOI: [10.1119/1.4895342](https://doi.org/10.1119/1.4895342).
- [103] M. Maggiore, *Gravitational Waves: Volume 1: Theory and Experiments*, OUP Oxford, 2008, ISBN: 9780198570745, DOI: [10.1093/acprof:oso/9780198570745.001.0001](https://doi.org/10.1093/acprof:oso/9780198570745.001.0001).
- [104] C. W. Misner, K. S. Thorne, and J. A. Wheeler, *Gravitation*, eng, San Francisco: W. H. Freeman, 1973, ISBN: 0716703343.
- [105] E. Tiesinga, P. J. Mohr, D. B. Newell, and B. N. Taylor, *CODATA recommended values of the fundamental physical constants: 2018*, Rev. Mod. Phys. **93** (2 2021), 025010, DOI: [10.1103/RevModPhys.93.025010](https://doi.org/10.1103/RevModPhys.93.025010).
- [106] J. Isenberg, *The Initial Value Problem in General Relativity*, *Springer Handbook of Spacetime*, Springer Berlin Heidelberg, 2014, 303–321, DOI: [10.1007/978-3-642-41992-8_16](https://doi.org/10.1007/978-3-642-41992-8_16).
- [107] P. K. Townsend, *Black Holes*, 1997, DOI: [10.48550/ARXIV.GR-QC/9707012](https://doi.org/10.48550/ARXIV.GR-QC/9707012).
- [108] E. Kolb, *The Early Universe*, CRC Press, 1990, DOI: [10.1201/9780429492860](https://doi.org/10.1201/9780429492860).
- [109] D. H. Lyth and A. R. Liddle, *The Primordial Density Perturbation: Cosmology, Inflation and the Origin of Structure*, Cambridge University Press, 2009, DOI: [10.1017/CB09780511819209](https://doi.org/10.1017/CB09780511819209).
- [110] A. Einstein, *Näherungsweise Integration der Feldgleichungen der Gravitation*, Sitzungsber. K. Preuss. Akad. Wiss. (1916), 688–696.
- [111] A. Einstein, *Über Gravitationswellen*, Sitzungsber. K. Preuss. Akad. Wiss. (1918), 154–167.
- [112] J. Cervantes-Cota, S. Galindo-Uribarri, and G. Smoot, *A Brief History of Gravitational Waves*, Universe **2**.3 (2016), 22, DOI: [10.3390/universe2030022](https://doi.org/10.3390/universe2030022).

- [113] B. C. Barish and R. Weiss, *LIGO and the Detection of Gravitational Waves*, *Physics Today* **52.10** (1999), 44–50, DOI: [10.1063/1.882861](https://doi.org/10.1063/1.882861).
- [114] P. R. Saulson, *Josh Goldberg and the physical reality of gravitational waves*, *General Relativity and Gravitation* **43.12** (2011), 3289–3299.
- [115] J. Weber, *Detection and Generation of Gravitational Waves*, *Phys. Rev.* **117** (1 1960), 306–313, DOI: [10.1103/PhysRev.117.306](https://doi.org/10.1103/PhysRev.117.306).
- [116] J. Weber, *Evidence for Discovery of Gravitational Radiation*, *Phys. Rev. Lett.* **22** (24 1969), 1320–1324, DOI: [10.1103/PhysRevLett.22.1320](https://doi.org/10.1103/PhysRevLett.22.1320).
- [117] D. Lindley, *A fleeting detection of gravitational waves*, *Physics* **16** (2005), 19.
- [118] R. A. Hulse and J. H. Taylor, *Discovery of a pulsar in a binary system*. *Astrophys. J. Letters* **195** (1975), L51–L53, DOI: [10.1086/181708](https://doi.org/10.1086/181708).
- [119] J. H. Taylor, L. A. Fowler, and P. M. McCulloch, *Measurements of general relativistic effects in the binary pulsar PSR1913 + 16*, *Nature* **277.5696** (1979), 437–440, DOI: [10.1038/277437a0](https://doi.org/10.1038/277437a0).
- [120] B. P. Abbott et al., *GW170814: A Three-Detector Observation of Gravitational Waves from a Binary Black Hole Coalescence*, *Phys. Rev. Lett.* **119** (14 2017), 141101, DOI: [10.1103/PhysRevLett.119.141101](https://doi.org/10.1103/PhysRevLett.119.141101).
- [121] B. P. Abbott et al., *GW170817: Observation of Gravitational Waves from a Binary Neutron Star Inspiral*, *Phys. Rev. Lett.* **119** (16 2017), 161101, DOI: [10.1103/PhysRevLett.119.161101](https://doi.org/10.1103/PhysRevLett.119.161101).
- [122] M. Bailes et al., *Gravitational-wave physics and astronomy in the 2020s and 2030s*, *Nature Reviews Physics* **3.5** (2021), 344–366, DOI: [10.1038/s42254-021-00303-8](https://doi.org/10.1038/s42254-021-00303-8).
- [123] *KAGRA: 2.5 generation interferometric gravitational wave detector*, *Nat. Astron.* **3.1** (2019), 35–40, DOI: [10.1038/s41550-018-0658-y](https://doi.org/10.1038/s41550-018-0658-y).
- [124] LIGO scientific collaboration, *Observing Capabilities*, 2022, URL: <https://emfollow.docs.ligo.org/userguide/capabilities.html>.
- [125] European Space Agency, *LISA mission moves to final design phase*, 2022, URL: https://www.esa.int/Science_Exploration/Space_Science/LISA_mission_moves_to_final_design_phase.
- [126] P. Auclair et al., *Cosmology with the Laser Interferometer Space Antenna*, 2022, DOI: [10.48550/ARXIV.2204.05434](https://doi.org/10.48550/ARXIV.2204.05434).
- [127] N. Bartolo et al., *Science with the space-based interferometer LISA. IV: probing inflation with gravitational waves*, *J. Cosmol. Astropart. Phys.* **2016.12** (2016), 026–026, DOI: [10.1088/1475-7516/2016/12/026](https://doi.org/10.1088/1475-7516/2016/12/026).
- [128] M. C. Guzzetti, N. Bartolo, M. Liguori, and S. Matarrese, *Gravitational waves from inflation*, *La Rivista del Nuovo Cimento* **39.9** (2016), 399–495, ISSN: 0393697X, DOI: [10.1393/ncr/i2016-10127-1](https://doi.org/10.1393/ncr/i2016-10127-1).
- [129] Planck Collaboration et al., *Planck 2018 results - X. Constraints on inflation*, *A&A* **641** (2020), A10, DOI: [10.1051/0004-6361/201833887](https://doi.org/10.1051/0004-6361/201833887).
- [130] Particle Data Group et al., *Review of Particle Physics*, *Progress of Theoretical and Experimental Physics* **2022.8** (2022), 083C01, ISSN: 2050-3911, DOI: [10.1093/ptep/ptac097](https://doi.org/10.1093/ptep/ptac097).
- [131] A. H. Nitz, T. Dent, G. S. Davies, and I. Harry, *A Search for Gravitational Waves from Binary Mergers with a Single Observatory*, *Astrophys. J.* **897.2** (2020), 169, DOI: [10.3847/1538-4357/ab96c7](https://doi.org/10.3847/1538-4357/ab96c7).
- [132] M. Maggiore, *Gravitational Waves: Volume 2: Astrophysics and Cosmology*, Oxford University Press, 2018, ISBN: 9780198570899, DOI: [10.1093/oso/9780198570899.001.0001](https://doi.org/10.1093/oso/9780198570899.001.0001).

- [133] La Rivista del Nuovo Cimento **39.9** (2016), 399–495, ISSN: 0393697X, 0393697X, DOI: [10.1393/ncr/i2016-10127-1](https://doi.org/10.1393/ncr/i2016-10127-1).
- [134] The NANOGrav Collaboration, *The NANOGrav 15 yr Data Set: Evidence for a Gravitational-wave Background*, *Astrophys. J. Letters* **951.1** (2023), L8, DOI: [10.3847/2041-8213/acdac6](https://doi.org/10.3847/2041-8213/acdac6).
- [135] Y. Suwa, T. Yoshida, M. Shibata, H. Umeda, and K. Takahashi, *On the minimum mass of neutron stars*, *Monthly Notices of the Royal Astronomical Society* **481.3** (2018), 3305–3312, DOI: [10.1093/mnras/sty2460](https://doi.org/10.1093/mnras/sty2460).
- [136] R. Abbott et al., *Population Properties of Compact Objects from the Second LIGO–Virgo Gravitational-Wave Transient Catalog*, *Astrophys. J. Letters* **913.1** (2021), L7, DOI: [10.3847/2041-8213/abe949](https://doi.org/10.3847/2041-8213/abe949).
- [137] C. L. Fryer and V. Kalogera, *Theoretical Black Hole Mass Distributions*, *Astrophys. J.* **554.1** (2001), 548, DOI: [10.1086/321359](https://doi.org/10.1086/321359).
- [138] W. M. Farr et al., *The Mass Distribution of Stellar-Mass Black Holes*, *Astrophys. J.* **741.2** (2011), 103, DOI: [10.1088/0004-637X/741/2/103](https://doi.org/10.1088/0004-637X/741/2/103).
- [139] L. Rezzolla, E. R. Most, and L. R. Weih, *Using Gravitational-wave Observations and Quasi-universal Relations to Constrain the Maximum Mass of Neutron Stars*, *Astrophys. J.* **852.2** (2018), L25, DOI: [10.3847/2041-8213/aaa401](https://doi.org/10.3847/2041-8213/aaa401).
- [140] M. Volonteri, *Formation of supermassive black holes*, *The Astronomy and Astrophysics Review* **18.3** (2010), 279–315, DOI: [10.1007/s00159-010-0029-x](https://doi.org/10.1007/s00159-010-0029-x).
- [141] T. L. S. Collaboration et al., *The population of merging compact binaries inferred using gravitational waves through GWTC-3*, 2022, arXiv: [2111.03634](https://arxiv.org/abs/2111.03634) [[astro-ph.HE](https://arxiv.org/abs/2111.03634)].
- [142] T. E. H. T. Collaboration et al., *First M87 Event Horizon Telescope Results. I. The Shadow of the Supermassive Black Hole*, *Astrophys. J. Letters* **875.1** (2019), L1, DOI: [10.3847/2041-8213/ab0ec7](https://doi.org/10.3847/2041-8213/ab0ec7).
- [143] J. Bellovary et al., *Where are the Intermediate Mass Black Holes?*, arXiv preprint arXiv:1903.08144 (2019).
- [144] C. de Rham, J. T. Deskins, A. J. Tolley, and S.-Y. Zhou, *Graviton mass bounds*, *Reviews of Modern Physics* **89.2** (2017), DOI: [10.1103/revmodphys.89.025004](https://doi.org/10.1103/revmodphys.89.025004).
- [145] B. P. Abbott et al., *Gravitational Waves and Gamma-Rays from a Binary Neutron Star Merger: GW170817 and GRB 170817A*, *Astrophys. J. Letters* **848.2** (2017), L13, DOI: [10.3847/2041-8213/aa920c](https://doi.org/10.3847/2041-8213/aa920c).
- [146] B. Abbott et al., *Properties of the Binary Neutron Star Merger GW170817*, *Physical Review X* **9.1** (2019), DOI: [10.1103/physrevx.9.011001](https://doi.org/10.1103/physrevx.9.011001).
- [147] S. Babak et al., *Science with the space-based interferometer LISA. V. Extreme mass-ratio inspirals*, *Phys. Rev. D* **95.10** (2017), DOI: [10.1103/physrevd.95.103012](https://doi.org/10.1103/physrevd.95.103012).
- [148] C. J. Moore, R. H. Cole, and C. P. L. Berry, *Gravitational-wave sensitivity curves*, *Classical and Quantum Gravity* **32.1** (2014), 015014, DOI: [10.1088/0264-9381/32/1/015014](https://doi.org/10.1088/0264-9381/32/1/015014).
- [149] LIGO Scientific Collaboration et al., *Advanced LIGO*, *Classical and Quantum Gravity* **32.7**, 074001 (2015), 074001, DOI: [10.1088/0264-9381/32/7/074001](https://doi.org/10.1088/0264-9381/32/7/074001).
- [150] F. Acernese et al., *Advanced Virgo: a second-generation interferometric gravitational wave detector*, *Classical and Quantum Gravity* **32.2** (2014), 024001, DOI: [10.1088/0264-9381/32/2/024001](https://doi.org/10.1088/0264-9381/32/2/024001).
- [151] L. McCuller et al., *Frequency-Dependent Squeezing for Advanced LIGO*, *Phys. Rev. Lett.* **124** (17 2020), 171102, DOI: [10.1103/PhysRevLett.124.171102](https://doi.org/10.1103/PhysRevLett.124.171102).
- [152] E. steering committee, *ET design report update 2020*, Official document, Einstein Telescope, 2020, URL: <https://apps.et-gw.eu/tds/ql/?c=15418>.

- [153] B. P. Abbott et al., *A guide to LIGO–Virgo detector noise and extraction of transient gravitational-wave signals*, *Classical and Quantum Gravity* **37.5** (2020), 055002, DOI: [10.1088/1361-6382/ab685e](https://doi.org/10.1088/1361-6382/ab685e).
- [154] C. Cutler, *Angular resolution of the LISA gravitational wave detector*, *Phys. Rev. D* **57** (12 1998), 7089–7102, DOI: [10.1103/PhysRevD.57.7089](https://doi.org/10.1103/PhysRevD.57.7089).
- [155] C. Cutler and É. E. Flanagan, *Gravitational waves from merging compact binaries: How accurately can one extract the binary’s parameters from the inspiral waveform?*, *Phys. Rev. D* **49.6** (1994), 2658–2697, DOI: [10.1103/physrevd.49.2658](https://doi.org/10.1103/physrevd.49.2658).
- [156] L. Barack and A. Pound, *Self-force and radiation reaction in general relativity*, *Reports on Progress in Physics* **82.1** (2018), 016904, DOI: [10.1088/1361-6633/aae552](https://doi.org/10.1088/1361-6633/aae552).
- [157] P. Mastrolia, *EFT-Diagrammatic Approach to Compact Binary Dynamics*, presented at the workshop: ZPW2023: Recent highlights across phenomenology, 2023.
- [158] Z. Bern et al., *Scattering Amplitudes and Conservative Binary Dynamics at $O(G^4)$* , *Physical Review Letters* **126.17** (2021), DOI: [10.1103/physrevlett.126.171601](https://doi.org/10.1103/physrevlett.126.171601).
- [159] C. Dlapa, G. Kälin, Z. Liu, and R. A. Porto, *Dynamics of binary systems to fourth Post-Minkowskian order from the effective field theory approach*, *Physics Letters B* **831** (2022), 137203, ISSN: 0370-2693, DOI: <https://doi.org/10.1016/j.physletb.2022.137203>.
- [160] C. Dlapa, G. Kälin, Z. Liu, J. Neef, and R. A. Porto, *Radiation Reaction and Gravitational Waves at Fourth Post-Minkowskian Order*, *Phys. Rev. Lett.* **130** (10 2023), 101401, DOI: [10.1103/PhysRevLett.130.101401](https://doi.org/10.1103/PhysRevLett.130.101401).
- [161] G. U. Jakobsen, G. Mogull, J. Plefka, B. Sauer, and Y. Xu, *Conservative scattering of spinning black holes at fourth post-Minkowskian order*, 2023, arXiv: [2306.01714 \[hep-th\]](https://arxiv.org/abs/2306.01714).
- [162] B. Szilágyi et al., *Approaching the Post-Newtonian Regime with Numerical Relativity: A Compact-Object Binary Simulation Spanning 350 Gravitational-Wave Cycles*, *Phys. Rev. Lett.* **115** (3 2015), 031102, DOI: [10.1103/PhysRevLett.115.031102](https://doi.org/10.1103/PhysRevLett.115.031102).
- [163] V. Nedora et al., *Numerical Relativity Simulations of the Neutron Star Merger GW170817: Long-term Remnant Evolutions, Winds, Remnant Disks, and Nucleosynthesis*, *Astrophys. J.* **906.2** (2021), 98, DOI: [10.3847/1538-4357/abc9be](https://doi.org/10.3847/1538-4357/abc9be).
- [164] J. Blackman et al., *Fast and Accurate Prediction of Numerical Relativity Waveforms from Binary Black Hole Coalescences Using Surrogate Models*, *Phys. Rev. Lett.* **115** (12 2015), 121102, DOI: [10.1103/PhysRevLett.115.121102](https://doi.org/10.1103/PhysRevLett.115.121102).
- [165] V. Varma et al., *Surrogate model of hybridized numerical relativity binary black hole waveforms*, *Phys. Rev. D* **99.6** (2019), DOI: [10.1103/physrevd.99.064045](https://doi.org/10.1103/physrevd.99.064045).
- [166] J. Blackman et al., *Numerical relativity waveform surrogate model for generically precessing binary black hole mergers*, *Phys. Rev. D* **96.2** (2017), DOI: [10.1103/physrevd.96.024058](https://doi.org/10.1103/physrevd.96.024058).
- [167] M. M. Riva, *Gravitational Bremsstrahlung in the worldline effective field theory approach*, *Theses, Université Paris-Saclay*, 2022, URL: <https://theses.hal.science/tel-03895254>.
- [168] N. Warburton, A. Pound, B. Wardell, J. Miller, and L. Durkan, *Gravitational-Wave Energy Flux for Compact Binaries through Second Order in the Mass Ratio*, *Phys. Rev. Lett.* **127** (15 2021), 151102, DOI: [10.1103/PhysRevLett.127.151102](https://doi.org/10.1103/PhysRevLett.127.151102).
- [169] A. Buonanno, *Theory/Phenomenology of GW*, presented at the lecture series: The 2022 Onassis Lectures in Physics: Gravitational Waves, 2022.
- [170] K. D. Kokkotas and B. G. Schmidt, *Quasinormal modes of stars and black holes*, *Living Rev. Rel.* **2** (1999), 2, DOI: [10.12942/lrr-1999-2](https://doi.org/10.12942/lrr-1999-2).
- [171] T. Damour, *The Two-Body Problem in Classical General Relativity*, presented at the workshop: EFT methods from Bound States to Binary Systems, 2020.

- [172] C. García-Quiròs et al., *Multimode frequency-domain model for the gravitational wave signal from nonprecessing black-hole binaries*, Phys. Rev. D **102.6** (2020), DOI: [10.1103/physrevd.102.064002](https://doi.org/10.1103/physrevd.102.064002).
- [173] D. Bini, T. Damour, A. Geralico, S. Laporta, and P. Mastrolia, *Gravitational dynamics at $O(G^6)$: perturbative gravitational scattering meets experimental mathematics*, 2020, arXiv: [2008.09389 \[gr-qc\]](https://arxiv.org/abs/2008.09389).
- [174] S. Foffa, R. Sturani, and W. J. T. Bobadilla, *Efficient resummation of high post-Newtonian contributions to the binding energy*, Journal of High Energy Physics **2021.2** (2021), DOI: [10.1007/jhep02\(2021\)165](https://doi.org/10.1007/jhep02(2021)165).
- [175] L. Blanchet and T. Damour, *Hereditary effects in gravitational radiation*, Phys. Rev. D **46** (10 1992), 4304–4319, DOI: [10.1103/PhysRevD.46.4304](https://doi.org/10.1103/PhysRevD.46.4304).
- [176] L. Blanchet and T. Damour, *Radiative gravitational fields in general relativity I. general structure of the field outside the source*, Phil. Trans. Roy. Soc. Lond. A **320** (1986), 379–430, DOI: [10.1098/rsta.1986.0125](https://doi.org/10.1098/rsta.1986.0125).
- [177] R. Arnowitt, S. Deser, and C. W. Misner, *Republication of: The dynamics of general relativity*, General Relativity and Gravitation **40.9** (2008), 1997–2027, DOI: [10.1007/s10714-008-0661-1](https://doi.org/10.1007/s10714-008-0661-1).
- [178] G. L. Almeida, A. Müller, S. Foffa, and R. Sturani, *Conservative binary dynamics from gravitational tail emission processes*, 2023, arXiv: [2307.05327 \[gr-qc\]](https://arxiv.org/abs/2307.05327).
- [179] S. Foffa and R. Sturani, *Hereditary terms at next-to-leading order in two-body gravitational dynamics*, Phys. Rev. D **101** (6 2020), 064033, DOI: [10.1103/PhysRevD.101.064033](https://doi.org/10.1103/PhysRevD.101.064033).
- [180] G. L. Almeida, S. Foffa, and R. Sturani, *Gravitational radiation contributions to the two-body scattering angle*, Phys. Rev. D **107.2** (2023), DOI: [10.1103/physrevd.107.024020](https://doi.org/10.1103/physrevd.107.024020).
- [181] S. Foffa and R. Sturani, *Near and far zones in two-body dynamics: An effective field theory perspective*, Phys. Rev. D **104** (2 2021), 024069, DOI: [10.1103/PhysRevD.104.024069](https://doi.org/10.1103/PhysRevD.104.024069).
- [182] M. Levi and Z. Yin, *Completing the fifth PN precision frontier via the EFT of spinning gravitating objects*, Journal of High Energy Physics **2023.4** (2023), DOI: [10.1007/jhep04\(2023\)079](https://doi.org/10.1007/jhep04(2023)079).
- [183] L. Blanchet, *Post-Newtonian Theory and Dimensional Regularization*, AIP Conference Proceedings, AIP, 2006, DOI: [10.1063/1.2399575](https://doi.org/10.1063/1.2399575).
- [184] T. Futamase and B. F. Schutz, *Newtonian and post-Newtonian approximations are asymptotic to general relativity*, Phys. Rev. D **28** (10 1983), 2363–2372, DOI: [10.1103/PhysRevD.28.2363](https://doi.org/10.1103/PhysRevD.28.2363).
- [185] T. Binnington and E. Poisson, *Relativistic theory of tidal Love numbers*, Phys. Rev. D **80.8** (2009), DOI: [10.1103/physrevd.80.084018](https://doi.org/10.1103/physrevd.80.084018).
- [186] T. Hinderer, *Tidal Love Numbers of Neutron Stars*, Astrophys. J. **677.2** (2008), 1216–1220, DOI: [10.1086/533487](https://doi.org/10.1086/533487).
- [187] B. Abbott et al., *GW170817: Measurements of Neutron Star Radii and Equation of State*, Physical Review Letters **121.16** (2018), DOI: [10.1103/physrevlett.121.161101](https://doi.org/10.1103/physrevlett.121.161101).
- [188] M. Levi and J. Steinhoff, *Leading order finite size effects with spins for inspiralling compact binaries*, Journal of High Energy Physics **2015.6** (2015), DOI: [10.1007/jhep06\(2015\)059](https://doi.org/10.1007/jhep06(2015)059).
- [189] Y. Huang et al., *Statistical and systematic uncertainties in extracting the source properties of neutron star-black hole binaries with gravitational waves*, Phys. Rev. D **103** (8 2021), 083001, DOI: [10.1103/PhysRevD.103.083001](https://doi.org/10.1103/PhysRevD.103.083001).
- [190] M. D. Schwartz, *Quantum Field Theory and the Standard Model*, Cambridge University Press, 2013, DOI: [10.1017/9781139540940](https://doi.org/10.1017/9781139540940).

- [191] L. H. Ryder, *Quantum Field Theory*, 2nd ed., Cambridge University Press, 1996, DOI: [10.1017/CB09780511813900](https://doi.org/10.1017/CB09780511813900).
- [192] W. D. Goldberger, *Les Houches Lectures on Effective Field Theories and Gravitational Radiation*, 2007, DOI: [10.48550/ARXIV.HEP-PH/0701129](https://doi.org/10.48550/ARXIV.HEP-PH/0701129).
- [193] R. Penco, *An Introduction to Effective Field Theories*, 2020, DOI: [10.48550/ARXIV.2006.16285](https://doi.org/10.48550/ARXIV.2006.16285).
- [194] A. V. Manohar, *Effective field theories, Perturbative and Nonperturbative Aspects of Quantum Field Theory*, Springer Berlin Heidelberg, 1996, 311–362, DOI: [10.1007/bfb0104294](https://doi.org/10.1007/bfb0104294).
- [195] T. Appelquist and J. Carazzone, *Infrared singularities and massive fields*, Phys. Rev. D **11** (10 1975), 2856–2861, DOI: [10.1103/PhysRevD.11.2856](https://doi.org/10.1103/PhysRevD.11.2856).
- [196] S. Hartmann, *Effective Field Theories, Reductionism and Scientific Explanation*, Studies in History and Philosophy of Science Part B: Studies in History and Philosophy of Modern Physics **32.2** (2001), Spacetime, Fields and Understanding: Perspectives on Quantum Field, 267–304, ISSN: 1355-2198, DOI: [https://doi.org/10.1016/S1355-2198\(01\)00005-3](https://doi.org/10.1016/S1355-2198(01)00005-3).
- [197] R. Patil, *The Effective Field Theory Approach to Gravitation*, MA thesis, IISER Pune, 2020, URL: <http://dr.iiserpune.ac.in:8080/xmlui/handle/123456789/4705>.
- [198] S. Weinberg, *Effective Field Theory, Past and Future* (2009), DOI: [10.48550/ARXIV.0908.1964](https://doi.org/10.48550/ARXIV.0908.1964).
- [199] A. Falkowski, *Lectures on effective field theories*, Lecture notes for Saclay (2017).
- [200] H. Georgi, *Effective Field Theory*, Annual Review of Nuclear and Particle Science **43.1** (1993), 209–252, DOI: [10.1146/annurev.ns.43.120193.001233](https://doi.org/10.1146/annurev.ns.43.120193.001233).
- [201] S. Weinberg, *What is Quantum Field Theory, and What Did We Think It Is?*, 1997, DOI: [10.48550/ARXIV.HEP-TH/9702027](https://doi.org/10.48550/ARXIV.HEP-TH/9702027).
- [202] C. R. Galley and M. Tiglio, *Radiation reaction and gravitational waves in the effective field theory approach*, Phys. Rev. D **79.12** (2009), DOI: [10.1103/physrevd.79.124027](https://doi.org/10.1103/physrevd.79.124027).
- [203] C. R. Galley, *Classical Mechanics of Nonconservative Systems*, Physical Review Letters **110.17** (2013), DOI: [10.1103/physrevlett.110.174301](https://doi.org/10.1103/physrevlett.110.174301).
- [204] E. A. Calzetta and B.-L. B. Hu, *Nonequilibrium Quantum Field Theory*, Cambridge University Press, 2023, DOI: [10.1017/9781009290036](https://doi.org/10.1017/9781009290036).
- [205] G. Brunello, *Effective Field Theory Approach to General Relativity and Feynman Diagrams for Coalescing Binary Systems*, 2022, DOI: [10.48550/ARXIV.2211.01321](https://doi.org/10.48550/ARXIV.2211.01321).
- [206] M. M. Riva, *Effective Field Theory for Gravitational Radiation in General Relativity and beyond*, 2021, DOI: [10.48550/ARXIV.2111.07433](https://doi.org/10.48550/ARXIV.2111.07433).
- [207] R. D. Jordan, *Effective field equations for expectation values*, Phys. Rev. D **33** (2 1986), 444–454, DOI: [10.1103/PhysRevD.33.444](https://doi.org/10.1103/PhysRevD.33.444).
- [208] E. Calzetta and B. L. Hu, *Closed-time-path functional formalism in curved spacetime: Application to cosmological back-reaction problems*, Phys. Rev. D **35** (2 1987), 495–509, DOI: [10.1103/PhysRevD.35.495](https://doi.org/10.1103/PhysRevD.35.495).
- [209] J. Schwinger, *Brownian Motion of a Quantum Oscillator*, Journal of Mathematical Physics **2.3** (2004), 407–432, ISSN: 0022-2488, DOI: [10.1063/1.1703727](https://doi.org/10.1063/1.1703727).
- [210] P. Adshead, R. Easther, and E. A. Lim, *“In-in” formalism and cosmological perturbations*, Phys. Rev. D **80.8** (2009), DOI: [10.1103/physrevd.80.083521](https://doi.org/10.1103/physrevd.80.083521).
- [211] S. Weinzierl, *Feynman Integrals*, 2022, arXiv: [2201.03593 \[hep-th\]](https://arxiv.org/abs/2201.03593).
- [212] A. V. Manohar, *Introduction to Effective Field Theories*, 2018, arXiv: [1804.05863 \[hep-ph\]](https://arxiv.org/abs/1804.05863).
- [213] R. A. Porto, *The effective field theorist’s approach to gravitational dynamics*, Physics Reports **633** (2016), 1–104, DOI: [10.1016/j.physrep.2016.04.003](https://doi.org/10.1016/j.physrep.2016.04.003).

- [214] I. Z. Rothstein, *TASI Lectures on Effective Field Theories*, 2004, arXiv: [hep-ph/0308266](https://arxiv.org/abs/hep-ph/0308266) [[hep-ph](#)].
- [215] P. Breitenlohner and D. Maison, *Dimensional renormalization and the action principle*, Communications in Mathematical Physics **52** (1977), 11–38, DOI: [10.1007/BF01609069](https://doi.org/10.1007/BF01609069).
- [216] R. N. Lee, *Presenting LiteRed: a tool for the Loop InTEgrals REDuction*, 2012, arXiv: [1212.2685](https://arxiv.org/abs/1212.2685) [[hep-ph](#)].
- [217] R. N. Lee, *LiteRed 1.4: a powerful tool for reduction of multiloop integrals*, Journal of Physics: Conference Series **523** (2014), 012059, DOI: [10.1088/1742-6596/523/1/012059](https://doi.org/10.1088/1742-6596/523/1/012059).
- [218] A. G. GROZIN, *Integration by parts: An introduction*, International Journal of Modern Physics A **26.17** (2011), 2807–2854, DOI: [10.1142/s0217751x11053687](https://doi.org/10.1142/s0217751x11053687).
- [219] J. Chen, X. Jiang, C. Ma, X. Xu, and L. L. Yang, *Baikov representations, intersection theory, and canonical Feynman integrals*, Journal of High Energy Physics **2022.7** (2022), DOI: [10.1007/jhep07\(2022\)066](https://doi.org/10.1007/jhep07(2022)066).
- [220] A. Primo, *Cutting Feynman Amplitudes: from Adaptive Integrand Decomposition to Differential Equations on Maximal Cuts*, PhD thesis, Padua U., 2017, URL: <https://hdl.handle.net/11577/3426809>.
- [221] O. V. Tarasov, *Connection between Feynman integrals having different values of the space-time dimension*, Phys. Rev. D **54.10** (1996), 6479–6490, DOI: [10.1103/physrevd.54.6479](https://doi.org/10.1103/physrevd.54.6479).
- [222] P. Mastrolia and S. Mizera, *Feynman integrals and intersection theory*, Journal of High Energy Physics **2019.2** (2019), DOI: [10.1007/jhep02\(2019\)139](https://doi.org/10.1007/jhep02(2019)139).
- [223] H. Frellesvig et al., *Decomposition of Feynman integrals on the maximal cut by intersection numbers*, Journal of High Energy Physics **2019.5** (2019), DOI: [10.1007/jhep05\(2019\)153](https://doi.org/10.1007/jhep05(2019)153).
- [224] G. Brunello, *Diagrammatic approach to Gravitational Waves Physics: Theory and Phenomenology*, 2021.
- [225] A. Cristofoli, *An Effective Field Theory Approach to the Two-Body Problem in General Relativity*, MA thesis, Padua U., 2018, URL: <http://hdl.handle.net/20.500.12608/28924>.
- [226] P. Mastrolia and E. Remiddi, *Precise evaluation of the electron ($g-2$) at four loops: the algebraic way*, Nuclear Physics B - Proceedings Supplements **89.1** (2000), Loops and Legs in Quantum Field Theory, 76–81, ISSN: 0920-5632, DOI: [https://doi.org/10.1016/S0920-5632\(00\)00826-4](https://doi.org/10.1016/S0920-5632(00)00826-4).
- [227] K. G. Chetyrkin, J. H. Kühn, P. Mastrolia, and C. Sturm, *Heavy quark vacuum polarization: first two moments of the $O(\alpha_s^3 n_f^2)$ contribution*, The European Physical Journal C **40.3** (2005), 361–366, DOI: [10.1140/epjc/s2005-02151-y](https://doi.org/10.1140/epjc/s2005-02151-y).
- [228] R. Lee, *Group structure of the integration-by-part identities and its application to the reduction of multiloop integrals*, Journal of High Energy Physics **2008.07** (2008), 031, DOI: [10.1088/1126-6708/2008/07/031](https://doi.org/10.1088/1126-6708/2008/07/031).
- [229] S. Foffa and R. Sturani, *Effective field theory methods to model compact binaries*, Classical and Quantum Gravity **31.4** (2014), 043001, DOI: [10.1088/0264-9381/31/4/043001](https://doi.org/10.1088/0264-9381/31/4/043001).
- [230] W. Caswell and G. Lepage, *Effective lagrangians for bound state problems in QED, QCD, and other field theories*, Physics Letters B **167.4** (1986), 437–442, ISSN: 0370-2693, DOI: [https://doi.org/10.1016/0370-2693\(86\)91297-9](https://doi.org/10.1016/0370-2693(86)91297-9).
- [231] M. E. Luke, A. V. Manohar, and I. Z. Rothstein, *Renormalization group scaling in nonrelativistic QCD*, Phys. Rev. D **61.7** (2000), DOI: [10.1103/physrevd.61.074025](https://doi.org/10.1103/physrevd.61.074025).
- [232] N. Isgur and M. B. Wise, *Weak decays of heavy mesons in the static quark approximation*, Physics Letters B **232.1** (1989), 113–117, ISSN: 0370-2693, DOI: [https://doi.org/10.1016/0370-2693\(89\)90566-2](https://doi.org/10.1016/0370-2693(89)90566-2).

- [233] E. Eichten and B. Hill, *An effective field theory for the calculation of matrix elements involving heavy quarks*, Physics Letters B **234.4** (1990), 511–516, ISSN: 0370-2693, DOI: [https://doi.org/10.1016/0370-2693\(90\)92049-0](https://doi.org/10.1016/0370-2693(90)92049-0).
- [234] H. Georgi, *An effective field theory for heavy quarks at low energies*, Physics Letters B **240.3** (1990), 447–450, ISSN: 0370-2693, DOI: [https://doi.org/10.1016/0370-2693\(90\)91128-X](https://doi.org/10.1016/0370-2693(90)91128-X).
- [235] J. B. Gilmore and A. Ross, *Effective field theory calculation of second post-Newtonian binary dynamics*, Phys. Rev. D **78.12** (2008), DOI: [10.1103/physrevd.78.124021](https://doi.org/10.1103/physrevd.78.124021).
- [236] R. A. Porto and R. Sturani, *Scalar gravity: Post-Newtonian corrections via an effective field theory approach*, 2007, DOI: [10.48550/ARXIV.GR-QC/0701105](https://doi.org/10.48550/ARXIV.GR-QC/0701105).
- [237] V. Fock, *Three Lectures on Relativity Theory*, Rev. Mod. Phys. **29** (3 1957), 325–333, DOI: [10.1103/RevModPhys.29.325](https://doi.org/10.1103/RevModPhys.29.325).
- [238] W. D. Goldberger and I. Z. Rothstein, *Towers of Gravitational Theories*, General Relativity and Gravitation **38.11** (2006), 1537–1546, DOI: [10.1007/s10714-006-0345-7](https://doi.org/10.1007/s10714-006-0345-7).
- [239] R. A. Porto, *Post-Newtonian corrections to the motion of spinning bodies in nonrelativistic general relativity*, Phys. Rev. D **73.10** (2006), DOI: [10.1103/physrevd.73.104031](https://doi.org/10.1103/physrevd.73.104031).
- [240] R. A. Porto and I. Z. Rothstein, *Calculation of the First Nonlinear Contribution to the General-Relativistic Spin-Spin Interaction for Binary Systems*, Physical Review Letters **97.2** (2006), DOI: [10.1103/physrevlett.97.021101](https://doi.org/10.1103/physrevlett.97.021101).
- [241] M. Levi, *Effective Field Theory of Post-Newtonian Gravity Including Spins*, 2018, arXiv: [1705.07515 \[gr-qc\]](https://arxiv.org/abs/1705.07515).
- [242] W. D. Goldberger, *Effective field theories of gravity and compact binary dynamics: A Snowmass 2021 whitepaper*, 2022, DOI: [10.48550/ARXIV.2206.14249](https://doi.org/10.48550/ARXIV.2206.14249).
- [243] M. V. S. Saketh, J. Steinhoff, J. Vines, and A. Buonanno, *Modeling horizon absorption in spinning binary black holes using effective worldline theory*, Phys. Rev. D **107.8** (2023), DOI: [10.1103/physrevd.107.084006](https://doi.org/10.1103/physrevd.107.084006).
- [244] L. LANDAU and E. LIFSHITZ, *The Classical Theory of Fields: Volume 2*, Fourth Edition, **2**, Amsterdam: Pergamon, 1975, ISBN: 978-0-08-025072-4, DOI: <https://doi.org/10.1016/B978-0-08-025072-4.50005-8>.
- [245] B. Kol and M. Smolkin, *Classical effective field theory and caged black holes*, Phys. Rev. D **77.6** (2008), DOI: [10.1103/physrevd.77.064033](https://doi.org/10.1103/physrevd.77.064033).
- [246] B. Kol and M. Smolkin, *Non-relativistic gravitation: from Newton to Einstein and back*, Classical and Quantum Gravity **25.14** (2008), 145011, DOI: [10.1088/0264-9381/25/14/145011](https://doi.org/10.1088/0264-9381/25/14/145011).
- [247] B. Kol and M. Smolkin, *Einstein’s action and the harmonic gauge in terms of Newtonian fields*, Phys. Rev. D **85.4** (2012), DOI: [10.1103/physrevd.85.044029](https://doi.org/10.1103/physrevd.85.044029).
- [248] L. Blanchet and T. Damour, *Post-newtonian generation of gravitational waves*, en, Annales de l’I.H.P. Physique théorique **50.4** (1989), 377–408, URL: http://www.numdam.org/item/AIHPA_1989__50_4_377_0/.
- [249] M. Levi and J. Steinhoff, *EFTofPNG: a package for high precision computation with the effective field theory of post-Newtonian gravity*, Classical and Quantum Gravity **34.24** (2017), 244001, DOI: [10.1088/1361-6382/aa941e](https://doi.org/10.1088/1361-6382/aa941e).
- [250] M. Beneke and V. Smirnov, *Asymptotic expansion of Feynman integrals near threshold*, Nuclear Physics B **522.1-2** (1998), 321–344, DOI: [10.1016/s0550-3213\(98\)00138-2](https://doi.org/10.1016/s0550-3213(98)00138-2).
- [251] B. Jantzen, *Foundation and generalization of the expansion by regions*, Journal of High Energy Physics **2011.12** (2011), DOI: [10.1007/jhep12\(2011\)076](https://doi.org/10.1007/jhep12(2011)076).

- [252] G. L. Almeida, S. Foffa, and R. Sturani, *Tail contributions to gravitational conservative dynamics*, Phys. Rev. D **104** (12 2021), 124075, DOI: [10.1103/PhysRevD.104.124075](https://doi.org/10.1103/PhysRevD.104.124075).
- [253] U. Cannella, *Effective Field Theory Methods in Gravitational Physics and Tests of Gravity*, 2011, DOI: [10.48550/ARXIV.1103.0983](https://doi.org/10.48550/ARXIV.1103.0983).
- [254] W. D. Goldberger and A. Ross, *Gravitational radiative corrections from effective field theory*, Phys. Rev. D **81** (12 2010), 124015, DOI: [10.1103/PhysRevD.81.124015](https://doi.org/10.1103/PhysRevD.81.124015).
- [255] A. Ross, *Multipole expansion at the level of the action*, Phys. Rev. D **85** (12 2012), 125033, DOI: [10.1103/PhysRevD.85.125033](https://doi.org/10.1103/PhysRevD.85.125033).
- [256] L. Blanchet and B. R. Iyer, *Third post-Newtonian dynamics of compact binaries: equations of motion in the centre-of-mass frame*, Classical and Quantum Gravity **20.4** (2003), 755–776, DOI: [10.1088/0264-9381/20/4/309](https://doi.org/10.1088/0264-9381/20/4/309).
- [257] V. C. de Andrade, L. Blanchet, and G. Faye, *Third post-Newtonian dynamics of compact binaries: Noetherian conserved quantities and equivalence between the harmonic-coordinate and ADM-Hamiltonian formalisms*, Classical and Quantum Gravity **18.5** (2001), 753–778, DOI: [10.1088/0264-9381/18/5/301](https://doi.org/10.1088/0264-9381/18/5/301).
- [258] L. Landau and E. Lifshitz, *Mechanics: Volume 1*, Elsevier Science, 1976, ISBN: 9780750628969.
- [259] M. Levi and J. Steinhoff, *Equivalence of ADM Hamiltonian and Effective Field Theory approaches at next-to-next-to-leading order spin1-spin2 coupling of binary inspirals*, J. Cosmol. Astropart. Phys. **2014.12** (2014), 003–003, DOI: [10.1088/1475-7516/2014/12/003](https://doi.org/10.1088/1475-7516/2014/12/003).
- [260] V. Undheim, *First post-Newtonian correction to gravitational waves produced by compact binaries: How to compute relativistic corrections to gravitational waves using Feynman diagrams*, 2021, DOI: [10.48550/ARXIV.2110.15643](https://doi.org/10.48550/ARXIV.2110.15643).
- [261] José M. Martín-García, *xAct: Efficient tensor computer algebra for the Wolfram Language*, version 1.2.0, 2021, URL: <http://www.xact.es/>.
- [262] R. N. Lee and A. A. Pomeransky, *Critical points and number of master integrals*, Journal of High Energy Physics **2013.11** (2013), DOI: [10.1007/jhep11\(2013\)165](https://doi.org/10.1007/jhep11(2013)165).
- [263] D. Bini and A. Geralico, *Tutti-Frutti method: Recent developments in the PN/PM/SF treatment of the gravitational two-body problem*, 16th Marcel Grossmann Meeting on Recent Developments in Theoretical and Experimental General Relativity, Astrophysics and Relativistic Field Theories, 2023, DOI: [10.1142/9789811269776_0113](https://doi.org/10.1142/9789811269776_0113).
- [264] Z. Bern et al., *Scattering Amplitudes and the Conservative Hamiltonian for Binary Systems at Third Post-Minkowskian Order*, Phys. Rev. Lett. **122** (20 2019), 201603, DOI: [10.1103/PhysRevLett.122.201603](https://doi.org/10.1103/PhysRevLett.122.201603).
- [265] G. Kälin, Z. Liu, and R. A. Porto, *Conservative Dynamics of Binary Systems to Third Post-Minkowskian Order from the Effective Field Theory Approach*, Physical Review Letters **125.26** (2020), DOI: [10.1103/physrevlett.125.261103](https://doi.org/10.1103/physrevlett.125.261103).
- [266] G. Kälin and R. A. Porto, *From boundary data to bound states*, Journal of High Energy Physics **2020.1** (2020), DOI: [10.1007/jhep01\(2020\)072](https://doi.org/10.1007/jhep01(2020)072).
- [267] T. Damour, *High-energy gravitational scattering and the general relativistic two-body problem*, Phys. Rev. D **97** (4 2018), 044038, DOI: [10.1103/PhysRevD.97.044038](https://doi.org/10.1103/PhysRevD.97.044038).
- [268] A. Cristofoli, N. E. J. Bjerrum-Bohr, P. H. Damgaard, and P. Vanhove, *Post-Minkowskian Hamiltonians in general relativity*, Phys. Rev. D **100** (8 2019), 084040, DOI: [10.1103/PhysRevD.100.084040](https://doi.org/10.1103/PhysRevD.100.084040).
- [269] S. Foffa, *Gravitating binaries at the fifth post-Newtonian order in the post-Minkowskian approximation*, Phys. Rev. D **89.2** (2014), DOI: [10.1103/physrevd.89.024019](https://doi.org/10.1103/physrevd.89.024019).

- [270] N. E. J. Bjerrum-Bohr, P. H. Damgaard, L. Planté, and P. Vanhove, *The SAGEX review on scattering amplitudes Chapter 13: Post-Minkowskian expansion from scattering amplitudes*, Journal of Physics A: Mathematical and Theoretical **55.44** (2022), 443014, DOI: [10.1088/1751-8121/ac7a78](https://doi.org/10.1088/1751-8121/ac7a78).
- [271] L. Blanchet, T. Damour, and G. Esposito-Farè se, *Dimensional regularization of the third post-Newtonian dynamics of point particles in harmonic coordinates*, Phys. Rev. D **69.12** (2004), DOI: [10.1103/physrevd.69.124007](https://doi.org/10.1103/physrevd.69.124007).
- [272] A. Buonanno, B. R. Iyer, E. Ochsner, Y. Pan, and B. S. Sathyaprakash, *Comparison of post-Newtonian templates for compact binary inspiral signals in gravitational-wave detectors*, Phys. Rev. D **80.8** (2009), DOI: [10.1103/physrevd.80.084043](https://doi.org/10.1103/physrevd.80.084043).
- [273] L. Blanchet, G. Faye, Q. Henry, F. Larrouturou, and D. Trestini, *Gravitational-Wave Phasing of Compact Binary Systems to the Fourth-and-a-Half post-Newtonian Order*, 2023, arXiv: [2304.11185](https://arxiv.org/abs/2304.11185) [gr-qc].
- [274] A. K. Leibovich, B. A. Pardo, and Z. Yang, *Radiation Reaction for Non-Spinning Bodies at 4.5PN in the Effective Field Theory Approach*, 2023, arXiv: [2302.11016](https://arxiv.org/abs/2302.11016) [gr-qc].
- [275] L. Bernard, L. Blanchet, G. Faye, and T. Marchand, *Center-of-mass equations of motion and conserved integrals of compact binary systems at the fourth post-Newtonian order*, Phys. Rev. D **97.4** (2018), DOI: [10.1103/physrevd.97.044037](https://doi.org/10.1103/physrevd.97.044037).
- [276] T. Damour and G. Schäfer, *Lagrangians for n point masses at the second post-Newtonian approximation of general relativity*, General relativity and gravitation **17** (1985), 879–905.
- [277] T. Damour and G. Schäfer, *Redefinition of position variables and the reduction of higher-order Lagrangians*, Journal of mathematical physics **32.1** (1991), 127–134.
- [278] L. E. Kidder, *Coalescing binary systems of compact objects to (post) $^{\frac{5}{2}}$ -Newtonian order. V. Spin effects*, Phys. Rev. D **52.2** (1995), 821–847, DOI: [10.1103/physrevd.52.821](https://doi.org/10.1103/physrevd.52.821).
- [279] T. Damour, B. R. Iyer, and B. S. Sathyaprakash, *A Comparison of search templates for gravitational waves from binary inspiral*, Phys. Rev. D **63** (2001), [Erratum: Phys.Rev.D 72, 029902 (2005)], 044023, DOI: [10.1103/PhysRevD.63.044023](https://doi.org/10.1103/PhysRevD.63.044023).
- [280] M. Boyle et al., *High-accuracy numerical simulation of black-hole binaries: Computation of the gravitational-wave energy flux and comparisons with post-Newtonian approximants*, Phys. Rev. D **78.10** (2008), DOI: [10.1103/physrevd.78.104020](https://doi.org/10.1103/physrevd.78.104020).
- [281] E. Poisson and C. M. Will, *Gravitational waves from inspiraling compact binaries: Parameter estimation using second-post-Newtonian waveforms*, Phys. Rev. D **52.2** (1995), 848–855, DOI: [10.1103/physrevd.52.848](https://doi.org/10.1103/physrevd.52.848).
- [282] C. Bender and S. Orszag, *Advanced Mathematical Methods for Scientists and Engineers I: Asymptotic Methods and Perturbation Theory*, Springer, 1999, ISBN: 9780387989310, URL: <https://books.google.it/books?id=-yQXwhE6iWMC>.
- [283] C. M. Will, *The Confrontation between General Relativity and Experiment*, Living Rev. Relativ. **9.1** (2006), DOI: [10.12942/lrr-2006-3](https://doi.org/10.12942/lrr-2006-3).
- [284] E. Berti et al., *Testing general relativity with present and future astrophysical observations*, Classical and Quantum Gravity **32.24** (2015), 243001, DOI: [10.1088/0264-9381/32/24/243001](https://doi.org/10.1088/0264-9381/32/24/243001).
- [285] J. Baker et al., *The Laser Interferometer Space Antenna: Unveiling the Millihertz Gravitational Wave Sky*, 2019, arXiv: [1907.06482](https://arxiv.org/abs/1907.06482) [astro-ph.IM].
- [286] European Space Agency, *LISA factsheet*, 2023, URL: https://www.esa.int/Science_Exploration/Space_Science/LISA_factsheet.

- [287] M. Armano et al., *Sub-Femto- g Free Fall for Space-Based Gravitational Wave Observatories: LISA Pathfinder Results*, Phys. Rev. Lett. **116.23** (2016), 231101, DOI: [10.1103/PhysRevLett.116.231101](https://doi.org/10.1103/PhysRevLett.116.231101).
- [288] M. Armano et al., *Beyond the Required LISA Free-Fall Performance: New LISA Pathfinder Results down to 20 μ Hz*, Phys. Rev. Lett. **120.6** (2018), 061101, DOI: [10.1103/PhysRevLett.120.061101](https://doi.org/10.1103/PhysRevLett.120.061101).
- [289] LISA Science Study Team, *LISA Science Requirements Document*, tech. rep. ESA-L3-EST-SCI-RS-001, version 1.0, 2018, URL: <https://www.cosmos.esa.int/documents/678316/1700384/SciRD.pdf>.
- [290] C. Caprini et al., *Reconstructing the spectral shape of a stochastic gravitational wave background with LISA*, J. Cosmol. Astropart. Phys. **2019.11** (2019), 017–017, ISSN: 1475-7516, DOI: [10.1088/1475-7516/2019/11/017](https://doi.org/10.1088/1475-7516/2019/11/017).
- [291] L. J. Rubbo, N. J. Cornish, and O. Poujade, *Forward modeling of space-borne gravitational wave detectors*, Phys. Rev. D **69.8** (2004), DOI: [10.1103/physrevd.69.082003](https://doi.org/10.1103/physrevd.69.082003).
- [292] M. Vallisneri, *Use and abuse of the Fisher information matrix in the assessment of gravitational-wave parameter-estimation prospects*, Phys. Rev. D **77.4** (2008), DOI: [10.1103/physrevd.77.042001](https://doi.org/10.1103/physrevd.77.042001).
- [293] *CloudVeneto website*, URL: <https://cloudveneto.it/>.
- [294] L. Sampson, N. Cornish, and N. Yunes, *Gravitational wave tests of strong field general relativity with binary inspirals: Realistic injections and optimal model selection*, Phys. Rev. D **87.10** (2013), DOI: [10.1103/physrevd.87.102001](https://doi.org/10.1103/physrevd.87.102001).
- [295] J. Meidam et al., *Parametrized tests of the strong-field dynamics of general relativity using gravitational wave signals from coalescing binary black holes: Fast likelihood calculations and sensitivity of the method*, Phys. Rev. D **97.4** (2018), DOI: [10.1103/physrevd.97.044033](https://doi.org/10.1103/physrevd.97.044033).
- [296] C.-J. Haster, *Pi from the sky – A null test of general relativity from a population of gravitational wave observations*, 2020, arXiv: [2005.05472 \[gr-qc\]](https://arxiv.org/abs/2005.05472).
- [297] N. Aghanim et al., *Planck 2018 results. VI. Cosmological parameters*, Astronomy & Astrophysics **641** (2020), A6, DOI: [10.1051/0004-6361/201833910](https://doi.org/10.1051/0004-6361/201833910).
- [298] L. E. Kidder, *Coalescing binary systems of compact objects to (post)^{5/2}-Newtonian order. V. Spin effects*, Phys. Rev. D **52** (2 1995), 821–847, DOI: [10.1103/PhysRevD.52.821](https://doi.org/10.1103/PhysRevD.52.821).
- [299] R. Abbott et al., *Constraints on the Cosmic Expansion History from GWTC-3*, Astrophys. J. **949.2** (2023), 76, DOI: [10.3847/1538-4357/ac74bb](https://doi.org/10.3847/1538-4357/ac74bb).
- [300] N. Seto and K. Kyutoku, *How many extragalactic stellar mass binary black holes will be detected by space gravitational-wave interferometers?*, Monthly Notices of the Royal Astronomical Society **514.4** (2022), 4669–4675, DOI: [10.1093/mnras/stac1561](https://doi.org/10.1093/mnras/stac1561).
- [301] S. Babak et al., *Stochastic gravitational wave background from stellar origin binary black holes in LISA*, 2023, arXiv: [2304.06368 \[astro-ph.CO\]](https://arxiv.org/abs/2304.06368).
- [302] A. Sesana, M. Volonteri, and F. Haardt, *The imprint of massive black hole formation models on the LISA data stream*, Monthly Notices of the Royal Astronomical Society **377.4** (2007), 1711–1716, ISSN: 0035-8711, DOI: [10.1111/j.1365-2966.2007.11734.x](https://doi.org/10.1111/j.1365-2966.2007.11734.x).
- [303] J. R. Gair, I. Mandel, M. C. Miller, and M. Volonteri, *Exploring intermediate and massive black-hole binaries with the Einstein Telescope*, General Relativity and Gravitation **43.2** (2010), 485–518, DOI: [10.1007/s10714-010-1104-3](https://doi.org/10.1007/s10714-010-1104-3).
- [304] R. Abbott et al., *GW190521: A Binary Black Hole Merger with a Total Mass of 150 solar masses*, Physical Review Letters **125.10** (2020), DOI: [10.1103/physrevlett.125.101102](https://doi.org/10.1103/physrevlett.125.101102).

-
- [305] R. Abbott et al., *Properties and Astrophysical Implications of the 150 solar masses Binary Black Hole Merger GW190521*, *Astrophys. J.* **900**.1 (2020), L13, DOI: [10.3847/2041-8213/aba493](https://doi.org/10.3847/2041-8213/aba493).
- [306] I. Martinez, *Modeling Compact Objects with EFT II: The Post-Newtonian Expansion*, 2023, arXiv: [2201.00937](https://arxiv.org/abs/2201.00937) [[hep-th](https://arxiv.org/archive/hep)].
- [307] A. Kuntz, F. Piazza, and F. Vernizzi, *Effective field theory for gravitational radiation in scalar-tensor gravity*, *J. Cosmol. Astropart. Phys.* **2019**.05 (2019), 052–052, DOI: [10.1088/1475-7516/2019/05/052](https://doi.org/10.1088/1475-7516/2019/05/052).
- [308] H. Sanctuary and R. Sturani, *Effective field theory analysis of the self-interacting chameleon*, *General Relativity and Gravitation* **42**.8 (2010), 1953–1967, DOI: [10.1007/s10714-010-0974-8](https://doi.org/10.1007/s10714-010-0974-8).
- [309] S. Endlich, V. Gorbenko, J. Huang, and L. Senatore, *An effective formalism for testing extensions to General Relativity with gravitational waves*, *Journal of High Energy Physics* **2017**.9 (2017), DOI: [10.1007/jhep09\(2017\)122](https://doi.org/10.1007/jhep09(2017)122).
- [310] N. Sennett, R. Brito, A. Buonanno, V. Gorbenko, and L. Senatore, *Gravitational-wave constraints on an effective-field-theory extension of general relativity*, *Phys. Rev. D* **102**.4 (2020), DOI: [10.1103/physrevd.102.044056](https://doi.org/10.1103/physrevd.102.044056).
- [311] J. Huang, M. C. Johnson, L. Sagunski, M. Sakellariadou, and J. Zhang, *Prospects for axion searches with Advanced LIGO through binary mergers*, *Phys. Rev. D* **99**.6 (2019), DOI: [10.1103/physrevd.99.063013](https://doi.org/10.1103/physrevd.99.063013).
- [312] V. Cardoso, O. J. C. Dias, and P. Figueras, *Gravitational radiation in $d > 4$ from effective field theory*, *Phys. Rev. D* **78**.10 (2008), DOI: [10.1103/physrevd.78.105010](https://doi.org/10.1103/physrevd.78.105010).
- [313] A. Zee, *Quantum field theory in a nutshell*, **7**, Princeton university press, 2010, ISBN: 9780691140346.